

ISSN 2602-2575 • EISSN 2618-6144

EUROPEAN JOURNAL OF BIOLOGY

OFFICIAL JOURNAL OF ISTANBUL UNIVERSITY'S SCIENCE FACULTY

Volume: 81 • Issue: 2 • December 2022

<https://iupress.istanbul.edu.tr/en/journal/ejb/home>



Indexing and Abstracting

SCOPUS

TUBITAK ULAKBIM TR Index

Zoological Record - Clarivate Analytics

CAB Abstracts

DOAJ

CABI

- AgBiotechNet Database

- Animal Science Database

- VetMed Resource

- Environmental Impact Database

- Horticultural Science Database

- Nutrition and Food Sciences Database

Chemical Abstracts Service (CAS)

EBSCO Central & Eastern European Academic Source

SOBIAD

EUROPEAN JOURNAL OF BIOLOGY

Owner

Prof. Dr. Tansel AK

Istanbul University, Istanbul, Turkiye

Responsible Manager

Prof. Dr. Sehnaz BOLKENT

Istanbul University, Istanbul, Turkiye

sbolkent@istanbul.edu.tr

Correspondence Address

Istanbul University, Faculty of Science,
Department of Biology,

34134 Vezneciler, Fatih, Istanbul, Turkiye

Phone: +90 (212) 455 57 00 (Ext. 20318)

Fax: +90 (212) 528 05 27

E-mail: ejb@istanbul.edu.tr

<https://iupress.istanbul.edu.tr/en/journal/ejb/home>

Publisher

Istanbul University Press

Istanbul University Central Campus,

34452 Beyazit, Fatih, Istanbul, Turkiye

Phone: +90 (212) 440 00 00

Printed by

İlbey Matbaa Kağıt Reklam Org. Mc. San. Tic. Ltd. Őti.

2. Matbaacılar Sitesi 3NB 3 Topkapı / Zeytinburnu,

Istanbul, Turkiye

www.ilbeymatbaa.com.tr

Certificate No: 51632

Authors bear responsibility for the content of their published articles.

The publication language of the journal is English.

This is a scholarly, international, peer-reviewed and open-access journal published biannually in June and December.

Publication Type: Periodical

EDITORIAL MANAGEMENT BOARD

Editor-in-Chief

Prof. Dr. Sehnaz BOLKENT

Istanbul University, Faculty of Science, Department of Biology, Istanbul, Turkiye – sbolkent@istanbul.edu.tr

Co-Editor-in-Chief

Prof. Dr. Fusun OZTAY

Istanbul University, Faculty of Science, Department of Biology, Istanbul, Turkiye – fusoztay@istanbul.edu.tr

Guest Editor

Prof. Dr. Elif Damla ARISAN

Gebze Technical University, Institute of Biotechnology, Kocaeli, Turkiye – d.arisan@gtu.edu.tr

Editorial Management Board Members

Prof. Dr. Fusun OZTAY

Istanbul University, Faculty of Science, Department of Biology, Istanbul, Turkiye – fusoztay@istanbul.edu.tr

Prof. Dr. Gulriz BAYCU KAHYAOGU

Istanbul University, Faculty of Science, Department of Biology, Istanbul, Turkiye – gulrizb@istanbul.edu.tr

Assoc. Prof. Dr. Aysegul MULAYIM

Istanbul University, Faculty of Science, Department of Biology, Istanbul, Turkiye – aysegulm@istanbul.edu.tr

Section Editors

Prof. Dr. Filiz GUREL

University of Maryland, Department of Plant Science & Landscape Architecture, Maryland, USA – filiz@umd.edu

Prof. Dr. Gulriz BAYCU KAHYAOGU

Istanbul University, Faculty of Science, Department of Biology, Istanbul, Turkiye – gulrizb@istanbul.edu.tr

Prof. Dr. Bekir KESKIN

Ege University, Faculty of Science, Department of Biology, Izmir, Turkey – bekir.keskin@ege.edu.tr

Assoc. Prof. Dr. Aysegul MULAYIM

Istanbul University, Faculty of Science, Department of Biology, Istanbul, Turkiye – aysegulm@istanbul.edu.tr

Assoc. Prof. Dr. Pinar CAGLAYAN

Marmara University, Department of Biology, Istanbul, Turkiye – pinar.caglayan@marmara.edu.tr

Language Editors

Elizabeth Mary EARL

Istanbul University, School of Foreign Languages (English), Istanbul, Turkiye – elizabeth.earl@istanbul.edu.tr

Alan James NEWSON

Istanbul University, School of Foreign Languages (English), Istanbul, Turkiye – alan.newson@istanbul.edu.tr

Statistics Editor

Prof. Dr. Ahmet DIRICAN

Istanbul University-Cerrahpasa, Faculty of Cerrahpasa Medicine, Department of Biostatistics, Istanbul, Turkiye – adirican@iuc.edu.tr

Publicity Manager

Dr. Ozgecan KAYALAR

Koç University, Research Center for Translational Medicine, Istanbul, Turkiye – okayalar@ku.edu.tr

Editorial Assistant

Oykum GENÇ

Istanbul University, Faculty of Science, Department of Biology, Istanbul, Turkiye – oykumgenc@istanbul.edu.tr

EDITORIAL BOARD

Hafiz AHMED

University of Maryland, Maryland, USA – *hahmed@som.umaryland.edu*

Elif Damla ARISAN

Gebze Technical University, Istanbul, Turkiye – *d.arisan@gtu.edu.tr*

Ahmet ASAN

Trakya University, Edirne, Turkiye - *ahasan@trakya.edu.tr*

Meral BIRBIR

Marmara University, Istanbul, Turkiye – *mbirbir@marmara.edu.tr*

Ricardo Antunes DE AZEVEDO

Universidade de Sao Paulo, Sao Paulo, Brazil – *raa@usp.br*

Kasim BAJROVIC

University of Sarajevo, Sarajevo, Bosnia – *kasim.bajrovic@ingeb.unsa.ba*

Levent BAT

Sinop University, Sinop, Turkiye – *leventb@sinop.edu.tr*

Mahmut CALISKAN

Istanbul University, Istanbul, Turkiye – *mahmut.caliskan@istanbul.edu.tr*

Carmela CAROPPO

Institute for Coastal Marine Environment, Rome, Italy – *carmela.caroppo@iamc.cnr.it*

Cihan DEMIRCI

Istanbul University, Istanbul, Turkiye – *cihan@istanbul.edu.tr*

Mustafa DJAMGOZ

Imperial College, London, United Kingdom – *m.djamgoz@imperial.ac.uk*

Mehmet Haluk ERTAN

The University of New South Wales (UNSW), Sydney, Australia – *hertan@unsw.edu.au*

Rafael Ruiz De La HABA

University of Sevilla, Sevilla, Spain – *rrh@us.es*

Onder KILIC

Istanbul University, Istanbul, Turkiye – *okilic@istanbul.edu.tr*

Ayten KIMIRAN

Istanbul University, Istanbul, Turkiye – *kimiran@istanbul.edu.tr*

Armagan KOCER

University of Twente, Enschede, The Netherlands – *a.kocer@utwente.nl*

Domenico MORABITO

Université d'Orléans, Orléans, France – *domenico.morabito@univ-orleans.fr*

Michael MOUSTAKAS

Aristotle University, Thessaloniki, Greece – *moustak@bio.auth.gr*

Gokhan M. MUTLU

University of Chicago, Chicago, USA – *gmutlu@medicine.bsd.uchicago.edu*

Maxim NABOZHENKO

Dagestan State University, Dagestan, Russia – *nalassus@mail.ru*

EDITORIAL BOARD

Selda OKTAYOGLU

Istanbul University, Istanbul, Turkiye – *selgez@istanbul.edu.tr*

Nesrin OZOREN

Bogazici University, Istanbul, Turkiye – *nesrin.ozoren@boun.edu.tr*

Majeti Narasimha VARA PRASAD

University of Hyderabad, Hyderabad, India – *mnvsl@uohyd.ernet.in*

Thomas SAWIDIS

Aristotle University, Thessaloniki, Greece – *sawidis@bio.auth.gr*

Jaswinder SINGH

McGill University, Quebec, Canada – *jaswinder.singh@mcgill.ca*

Lejla PAŠIĆ

University Sarajevo School of Science and Technology, Sarajevo, Bosnia and Herzegovina – *lejla.pasic@sst.edu.ba*

Nico M. Van STRAALEN

Vrije Universiteit, Amsterdam, The Netherlands – *n.m.van.straalen@vu.nl*

Ismail TURKAN

Ege University, Izmir, Turkiye - *ismail.turkan@ege.edu.tr*

Refiye YANARDAG

Istanbul University-Cerrahpasa, Istanbul, Turkiye – *yanardag@iuc.edu.tr*

Argyro ZENETOS

Hellenic Centre for Marine Research, Anavyssos, Greece – *zenetos@hcmr.gr*

Aims and Scope

European Journal of Biology (Eur J Biol) is an international, scientific, open access periodical published in accordance with independent, unbiased, and double-blinded peer-review principles. The journal is the official publication of Istanbul University Faculty of Science and it is published biannually on June and December. The publication language of the journal is English. European Journal of Biology has been previously published as IUFS Journal of Biology. It has been published in continuous publication since 1940.

European Journal of Biology aims to contribute to the literature by publishing manuscripts at the highest scientific level on all fields of biology. The journal publishes original research and review articles, and short communications that are prepared in accordance with the ethical guidelines in all fields of biology and life sciences.

The scope of the journal includes but not limited to; animal biology and systematics, plant biology and systematics, hydrobiology, ecology and environmental biology, microbiology, cell and molecular biology, biochemistry, biotechnology and genetics, physiology, toxicology, cancer biology, developmental and stem cell biology.

The target audience of the journal includes specialists and professionals working and interested in all disciplines of biology.

The editorial and publication processes of the journal are shaped in accordance with the guidelines of the International Committee of Medical Journal Editors (ICMJE), World Association of Medical Editors (WAME), Council of Science Editors (CSE), Committee on Publication Ethics (COPE), European Association of Science Editors (EASE), and National Information Standards Organization (NISO). The journal is in conformity with the Principles of Transparency and Best Practice in Scholarly Publishing (doaj.org/bestpractice).

European Journal of Biology is currently indexed by Web of Science Zoological Record, CAB Abstracts (CABI), Chemical Abstracts Service (CAS), TUBITAK-ULAKBIM TR Index, Scopus, DOAJ, EBSCO Central & Eastern European Academic Source and SOBIAD.

Processing and publication are free of charge with the journal. No fees are requested from the authors at any point throughout the evaluation and publication process. All manuscripts must be submitted via the online submission system, which is available at dergipark.gov.tr/iufsjb. The journal guidelines, technical information, and the required forms are available on the journal's web page.

All expenses of the journal are covered by the Istanbul University.

Statements or opinions expressed in the manuscripts published in the journal reflect the views of the author(s) and not the opinions of the Istanbul University Faculty of Science, editors, editorial board, and/or publisher; the editors, editorial board, and publisher disclaim any responsibility or liability for such materials.

All published content is available online, free of charge at <https://dergipark.org.tr/tr/pub/iufsjb>. Printed copies of the journal are distributed free of charge.



Editor in Chief: Prof. Dr. Sehnaz BOLKENT

Address: Istanbul University, Faculty of Science, Department of Biology, 34134 Vezneciler, Fatih, Istanbul, Turkiye

Phone: +90 212 4555700 (Ext. 20318)

Fax: +90 212 5280527

E-mail: sbolkent@istanbul.edu.tr

Instructions to Authors

European Journal of Biology (Eur J Biol) is an international, scientific, open access periodical published in accordance with independent, unbiased, and double-blinded peer-review principles. The journal is the official publication of Istanbul University Faculty of Science and it is published biannually on June and December. The publication language of the journal is English. European Journal of Biology has been previously published as IUFS Journal of Biology. It has been published in continuous publication since 1940.

European Journal of Biology aims to contribute to the literature by publishing manuscripts at the highest scientific level on all fields of biology. The journal publishes original research and review articles, and short communications that are prepared in accordance with the ethical guidelines in all fields of biology and life sciences.

The scope of the journal includes but not limited to; animal biology and systematics, plant biology and systematics, hydrobiology, ecology and environmental biology, microbiology, cell and molecular biology, biochemistry, biotechnology and genetics, physiology, toxicology, cancer biology, developmental and stem cell biology.

The editorial and publication processes of the journal are shaped in accordance with the guidelines of the International Council of Medical Journal Editors (ICMJE), the World Association of Medical Editors (WAME), the Council of Science Editors (CSE), the Committee on Publication Ethics (COPE), the European Association of Science Editors (EASE), and National Information Standards Organization (NISO). The journal conforms to the Principles of Transparency and Best Practice in Scholarly Publishing (doaj.org/bestpractice).

Originality, high scientific quality, and citation potential are the most important criteria for a manuscript to be accepted for publication. Manuscripts submitted for evaluation should not have been previously presented or already published in an electronic or printed medium. Manuscripts that have been presented in a meeting should be submitted with detailed information on the organization, including the name, date, and location of the organization.

Manuscripts submitted to European Journal of Biology will go through a double-blind peer-review process. Each submission will be reviewed by at least three external, independent peer reviewers who are experts in their fields in order to ensure an unbiased evaluation process. The editorial board will invite an external and independent editor to manage the evaluation processes of manuscripts submitted by editors or by the editorial board members of the journal. The Editor in Chief is the final authority in the decision-making process for all submissions.

An approval of research protocols by the Ethics Committee in accordance with international agreements (World Medical Association Declaration of Helsinki "Ethical Principles for Medical Research Involving Human Subjects," amended in October

2013, www.wma.net) is required for experimental, clinical, and drug studies. If required, ethics committee reports or an equivalent official document will be requested from the authors.

For manuscripts concerning experimental research on humans, a statement should be included that shows the written informed consent of patients and volunteers was obtained following a detailed explanation of the procedures that they may undergo. Information on patient consent, the name of the ethics committee, and the ethics committee approval number should also be stated in the Materials and Methods section of the manuscript. It is the authors' responsibility to carefully protect the patients' anonymity. For photographs that may reveal the identity of the patients, signed releases of the patient or of their legal representative should be enclosed.

European Journal of Biology requires experimental research studies on vertebrates or any regulated invertebrates to comply with relevant institutional, national and/or international guidelines. The journal supports the principles of Basel Declaration (basel-declaration.org) and the guidelines published by International Council for Laboratory Animal Science (ICLAS) (iclas.org). Authors are advised to clearly state their compliance with relevant guidelines.

European Journal of Biology advises authors to comply with IUCN Policy Statement on Research Involving Species at Risk of Extinction and the Convention on the Trade in Endangered Species of Wild IUCN Policy Statement on Research Involving Species at Risk of Extinction and the Convention on the Trade in Endangered Species of Wild Fauna and Flora.

All submissions are screened by a similarity detection software (iThenticate by CrossCheck).

In the event of alleged or suspected research misconduct, e.g., plagiarism, citation manipulation, and data falsification/fabrication, the Editorial Board will follow and act in accordance with COPE guidelines.

Each individual listed as an author should fulfil the authorship criteria recommended by the International Committee of Medical Journal Editors (ICMJE - www.icmje.org). The ICMJE recommends that authorship be based on the following 4 criteria:

- 1 Substantial contributions to the conception or design of the work; or the acquisition, analysis, or interpretation of data for the work; AND
- 2 Drafting the work or revising it critically for important intellectual content; AND
- 3 Final approval of the version to be published; AND
- 4 Agreement to be accountable for all aspects of the work in ensuring that questions related to the accuracy or integrity of any part of the work are appropriately investigated and resolved.

In addition to being accountable for the parts of the work he/she has done, an author should be able to identify which co-authors are responsible for specific other parts of the work. In addition, authors should have confidence in the integrity of the contributions of their co-authors.

All those designated as authors should meet all four criteria for authorship, and all who meet the four criteria should be identified as authors. Those who do not meet all four criteria should be acknowledged in the title page of the manuscript.

European Journal of Biology requires corresponding authors to submit a signed and scanned version of the authorship contribution form (available for download through the journal's web page) during the initial submission process in order to act appropriately on authorship rights and to prevent ghost or honorary authorship. If the editorial board suspects a case of "gift authorship," the submission will be rejected without further review. As part of the submission of the manuscript, the corresponding author should also send a short statement declaring that he/she accepts to undertake all the responsibility for authorship during the submission and review stages of the manuscript.

European Journal of Biology requires and encourages the authors and the individuals involved in the evaluation process of submitted manuscripts to disclose any existing or potential conflicts of interests, including financial, consultant, and institutional, that might lead to potential bias or a conflict of interest. Any financial grants or other supports received for a submitted study from individuals or institutions should be disclosed to the Editorial Board. To disclose a potential conflict of interest, the ICMJE Potential Conflict of Interest Disclosure Form should be filled and submitted by all contributing authors. Cases of a potential conflict of interest of the editors, authors, or reviewers are resolved by the journal's Editorial Board within the scope of COPE and ICMJE guidelines.

The Editorial Board of the journal handles all appeal and complaint cases within the scope of COPE guidelines. In such cases, authors should get in direct contact with the editorial office regarding their appeals and complaints. When needed, an ombudsperson may be assigned to resolve cases that cannot be resolved internally. The Editor in Chief is the final authority in the decision-making process for all appeals and complaints.

When submitting a manuscript to European Journal of Biology, authors accept to assign the copyright of their manuscript to Istanbul University Faculty of Science. If rejected for publication, the copyright of the manuscript will be assigned back to the authors. European Journal of Biology requires each submission to be accompanied by a Copyright Transfer Form (available for download at the journal's web page). When using previously published content, including figures, tables, or any other material in both print and electronic formats, authors must obtain permission from the copyright holder. Legal, financial and criminal liabilities in this regard belong to the author(s).

Statements or opinions expressed in the manuscripts published in European Journal of Biology reflect the views of the author(s) and not the opinions of the editors, the editorial board, or the publisher; the editors, the editorial board, and the publisher disclaim any responsibility or liability for such materials. The final responsibility in regard to the published content rests with the authors.

MANUSCRIPT SUBMISSION

European Journal of Biology endorses ICMJE-Recommendations for the Conduct, Reporting, Editing, and Publication of Scholarly Work in Medical Journals (updated in December 2015 - <http://www.icmje.org/icmje-recommendations.pdf>). Authors are required to prepare manuscripts in accordance with the CONSORT guidelines for randomized research studies, STROBE guidelines for observational original research studies, STARD guidelines for studies on diagnostic accuracy, PRISMA guidelines for systematic reviews and meta-analysis, ARRIVE guidelines for experimental animal studies, TREND guidelines for non-randomized public behaviour, and COREQ guidelines for qualitative research.

Manuscripts can only be submitted through the journal's online manuscript submission and evaluation system, available at the journal's web page. Manuscripts submitted via any other medium will not be evaluated.

Manuscripts submitted to the journal will first go through a technical evaluation process where the editorial office staff will ensure that the manuscript has been prepared and submitted in accordance with the journal's guidelines. Submissions that do not conform to the journal's guidelines will be returned to the submitting author with technical correction requests.

During the initial submission, authors are required to submit the following:

- Copyright Agreement Form,
- Author Contributions Form, and

ICMJE Potential Conflict of Interest Disclosure Form (should be filled in by all contributing authors). These forms are available for download at the journal's web page.

Preparation of the Manuscript

Title page: A separate title page should be submitted with all submissions and this page should include:

- The full title of the manuscript as well as a short title (running head) of no more than 50 characters,
- Name(s), affiliations, and highest academic degree(s) of the author(s),
- Grant information and detailed information on the other sources of support,
- Name, address, telephone (including the mobile phone number) and fax numbers, and email address of the corresponding author,
- Acknowledgment of the individuals who contributed to the preparation of the manuscript but who do not fulfil the authorship criteria.

Abstract: Abstract with subheadings should be written as structured abstract in submitted papers except for Review Articles and Letters to the Editor. Please check Table 1 below for word count specifications (250 words).

Keywords: Each submission must be accompanied by a minimum of three to a maximum of six keywords for subject indexing at the end of the abstract. The keywords should be listed in full without abbreviations.

Manuscript Types

Original Articles: This is the most important type of article since it provides new information based on original research. A structured abstract is required with original articles and it should include the following subheadings: Objective, Materials and Methods, Results and Conclusion. The main text of original articles should be structured with Introduction, Materials and Methods, Results, Discussion, and Conclusion subheadings. Please check Table 1 for the limitations of Original Articles.

Statistical analysis to support conclusions is usually necessary. Statistical analyses must be conducted in accordance with international statistical reporting standards. Information on statistical analyses should be provided with a separate subheading under the Materials and Methods section and the statistical software that was used during the process must be specified.

Units should be prepared in accordance with the International System of Units (SI).

Short Communications: Short communication is for a concise, but independent report representing a significant contribution to Biology. Short communication is not intended to publish preliminary results. But if these results are of exceptional interest and are particularly topical and relevant will be considered for publication.

Short Communications should include an abstract and should be structured with the following subheadings: "Introduction", "Materials and Methods", "Results and Discussion".

Editorial Comments: Editorial comments aim to provide a brief critical commentary by reviewers with expertise or with high reputation in the topic of the research article published in the journal. Authors are selected and invited by the journal to provide such comments. Abstract, Keywords, and Tables, Figures, Images, and other media are not included.

Review Articles: Reviews prepared by authors who have extensive knowledge on a particular field and whose scientific background has been translated into a high volume of publications with a high citation potential are welcomed. These authors may even be invited by the journal. Reviews should describe, discuss, and evaluate the current level of knowledge of a topic in clinical practice and should guide future studies. The main text should contain Introduction, Experimental and Clinical Research Consequences, and Conclusion sections. Please check Table 1 for the limitations for Review Articles.

Letters to the Editor: This type of manuscript discusses important parts, overlooked aspects, or lacking parts of a previously published article. Articles on subjects within the scope of the journal that might attract the readers' attention, particularly educative cases, may also be submitted in the form of a "Letter to the Editor." Readers can also present their comments on the published manuscripts in the form of a "Letter to the Editor." Abstract, Keywords, and Tables, Figures, Images, and other media should not be included. The text should be unstructured. The manuscript that is being commented on must be properly cited within this manuscript.

Tables

Tables should be included in the main document, presented after the reference list, and they should be numbered consecutively in the order they are referred to within the main text. A descriptive title must be placed above the tables. Abbreviations used in the tables should be defined below the tables by footnotes (even if they are defined within the main text). Tables should be created using the "insert table" command of the word processing software and they should be arranged clearly to provide easy reading. Data presented in the tables should not be a repetition of the data presented within the main text but should be supporting the main text.

Figures and Figure Legends

Figures, graphics, and photographs should be submitted as separate files (in TIFF or JPEG format with 1200 dpi for graphic and 600 dpi for colour images) through the submission system. The files should not be embedded in a Word document or the main document. When there are figure subunits, the subunits should be labeled merged to form a single image. Each subunit should be submitted separately through the submission system. Images

Table 1. Limitations for each manuscript type

Type of manuscript	Word limit	Abstract word limit	Reference limit	Table limit	Figure limit
Original Article	4500	250 (Structured)	No limit	6	Maximum 10
Short Communication	2500	200	30	3	4
Review Article	5500	250	No limit	5	6
Letter to the Editor	500	No abstract	5	No tables	No media

should be labeled (a, b, c, etc.) to indicate figure subunits. Thick and thin arrows, arrowheads, stars, asterisks, and similar marks can be used on the images to support figure legends. Like the rest of the submission, the figures too should be blind. Any information within the images that may indicate an individual or institution should be blinded. The minimum resolution of each submitted figure should be 300 DPI. To prevent delays in the evaluation process, all submitted figures should be clear in resolution and large in size (minimum dimensions: 100 × 100 mm). Figure legends should be listed at the end of the main document.

All acronyms and abbreviations used in the manuscript should be defined at first use, both in the abstract and in the main text. The abbreviation should be provided in parentheses following the definition.

When a drug, chemical, product, hardware, or software program is mentioned within the main text, product information, including the name of the product, the producer of the product, and city and the country of the company (including the state if in USA), should be provided in parentheses in the following format: "Discovery St PET/CT scanner (General Electric, Milwaukee, WI, USA)".

All references, tables, and figures should be referred to within the main text, and they should be numbered consecutively in the order they are referred to within the main text.

Limitations, drawbacks, and the shortcomings of original articles should be mentioned in the Discussion section before the conclusion paragraph.

References

While citing publications, preference should be given to the latest, most up-to-date publications. If an ahead-of-print publication is cited, the DOI number should be provided. Authors are responsible for the accuracy of references. Journal titles should be abbreviated in accordance with the journal abbreviations in Index Medicus/ MEDLINE/PubMed. When there are six or fewer authors, all authors should be listed. If there are seven or more authors, the first six authors should be listed followed by "et al." In the main text of the manuscript, references should be cited using Arabic numbers in parentheses. The reference styles for different types of publications are presented in the following examples.

Journal Article: Rankovic A, Rancic N, Jovanovic M, Ivanović M, Gajović O, Lazić Z, et al. Impact of imaging diagnostics on the budget – Are we spending too much? *Vojnosanit Pregl* 2013; 70: 709-11.

Book Section: Suh KN, Keystone JS. Malaria and babesiosis. Gorbach SL, Barlett JG, Blacklow NR, editors. *Infectious Diseases*. Philadelphia: Lippincott Williams; 2004.p.2290-308.

Books with a Single Author: Sweetman SC. *Martindale the Complete Drug Reference*. 34th ed. London: Pharmaceutical Press; 2005.

Editor(s) as Author: Huizing EH, de Groot JAM, editors. *Functional reconstructive nasal surgery*. Stuttgart-New York: Thieme; 2003.

Conference Proceedings: Bengissson S, Sothemin BG. Enforcement of data protection, privacy and security in medical infor-

matics. In: Lun KC, Degoulet P, Piemme TE, Rienhoff O, editors. *MEDINFO 92. Proceedings of the 7th World Congress on Medical Informatics*; 1992 Sept 6-10; Geneva, Switzerland. Amsterdam: North-Holland; 1992. pp.1561-5.

Scientific or Technical Report: Cusick M, Chew EY, Hoogwerf B, Agrón E, Wu L, Lindley A, et al. Early Treatment Diabetic Retinopathy Study Research Group. Risk factors for renal replacement therapy in the Early Treatment Diabetic Retinopathy Study (ETDRS), *Kidney Int*: 2004. Report No: 26.

Thesis: Yılmaz B. Ankara Üniversitesindeki Öğrencilerin Beslenme Durumları, Fiziksel Aktiviteleri ve Beden Kitle İndeksleri Kan Lipidleri Arasındaki İlişkiler. H.Ü. Sağlık Bilimleri Enstitüsü, Doktora Tezi. 2007.

Epub Ahead of Print Articles: Cai L, Yeh BM, Westphalen AC, Roberts JP, Wang ZJ. Adult living donor liver imaging. *Diagn Interv Radiol*. 2016 Feb 24. doi: 10.5152/dir.2016.15323. [Epub ahead of print].

Manuscripts Published in Electronic Format: Morse SS. Factors in the emergence of infectious diseases. *Emerg Infect Dis* (serial online) 1995 Jan-Mar (cited 1996 June 5): 1(1): (24 screens). Available from: URL: [http:// www.cdc.gov/ncidod/EID/cid.htm](http://www.cdc.gov/ncidod/EID/cid.htm).

REVISIONS

When submitting a revised version of a paper, the author must submit a detailed "Response to the reviewers" that states point by point how each issue raised by the reviewers has been covered and where it can be found (each reviewer's comment, followed by the author's reply and line numbers where the changes have been made) as well as an annotated copy of the main document. Revised manuscripts must be submitted within 30 days from the date of the decision letter. If the revised version of the manuscript is not submitted within the allocated time, the revision option may be cancelled. If the submitting author(s) believe that additional time is required, they should request this extension before the initial 30-day period is over.

Accepted manuscripts are copy-edited for grammar, punctuation, and format. Once the publication process of a manuscript is completed, it is published online on the journal's webpage as an ahead-of-print publication before it is included in its scheduled issue. A PDF proof of the accepted manuscript is sent to the corresponding author and their publication approval is requested within 2 days of their receipt of the proof.

Editor in Chief: Prof. Dr. Sehnaz BOLKENT

Address: Istanbul University, Faculty of Science, Department of Biology, 34134 Vezneciler, Fatih, Istanbul, Türkiye

Phone: +90 212 4555700 (Ext. 20318)

Fax: +90 212 5280527

E-mail: sbolkent@istanbul.edu.tr

Contents

Research Articles

- 117 Investigation the Cytotoxic and Anti-Proliferative Effects of Crude Venom of *Euscorpis mingrelicus* (Scorpiones: Euscorpiidae) Scorpion**
Nazife Yigit Kayhan, Ilkay Corak Ocal, Mustafa Akdeniz
- 125 In Silico Analysis of BMAL1 and CLOCK SNPs in the Ensembl Database**
Seref Gul
- 136 Inflammation Parameters, Xanthine Oxidase and Anti-Xanthine Oxidase Antibodies in Synovial Fluid of Patients Suffering from Arthritis**
Nadjet Hanachi, Lekhmici Arrar
- 144 New Records for Microalgae Species of the Turkish Seas Under the Effect of Intense Mucilage in the Sea of Marmara**
Turgay Durmus, Neslihan Balkis-Ozdelice, Seyfettin Tas, Fatma Bayram-Partal, Muharrem Balci, Cem Dalyan, Mustafa Sari 144
- 163 Phenolic Extracts of *Zizyphus lotus* L. (Rhamnaceae) and *Ruta chalepensis* L. (Rutaceae) as Alternatives to Antibiotics and their Antimicrobial Effects on Clinical Multidrug-Resistant Pathogens**
Nour El Houda Bekkar, Boumediene Meddah, Yavuz Selim Cakmak, Bahadir Keskin, Pascal Sonnet
- 184 The Role of Gamma-Amino Butyric Acid in Short-Term High Temperature Acclimation in Lichen *Pseudevernia furfuracea***
Nihal Goren-Saglam, Fazilet Ozlem Albayrak, Dilek Unal
- 190 Strigolactone and Auxin Applications on Cotyledon Senescence in Sunflower Seedlings under Salt Stress**
Humeyra Ozel, Serap Saglam
- 197 The Role of rs4626 and rs7221352 Polymorphisms on the *TOB1* Gene in Turkish Relapsing-Remitting Multiple Sclerosis Patients**
Fulya Basoglu Koseahmet, Candan Eker, Musa Ozturk, Sebnem Ozdemir, Ayhan Koksall, Sevim Baybas, Tuba Gunel
- Review Article**
- 206 Emergence, Evolution and Economics of Coronaviruses**
Sidhant Jain, Meenakshi Rana, Pooja Jain

Contents

Theme: The aspects of cellular signalling pathways of different disease models

Research Articles

217 *Myrtus communis* L. Extract Ameliorates High Fat Diet Induced Kidney and Bladder Damage by Inhibiting Oxidative Stress and Inflammation

Fatma Kanpalta Mustafaoglu, Busra Ertas, Ali Sen, Dilek Akakin, Goksel Sener, Feriha Ercan

231 Effects of Apocynin against Monosodium Glutamate-Induced Oxidative Damage in Rat Kidney

Merve Acikel Elmas, Gokcen Ozgun, Ozlem Bingol Ozakpinar, Zozan Guleken, Serap Arbak

240 Epibrassinolide Triggers Apoptotic Cell Death in SK-N-AS Neuroblastoma Cells by Targeting GSK3 β in a ROS Generation-Dependent Way

Pinar Obakan Yerlikaya, Shafaq Naxmedova²⁴⁰

251 Anti-Cancer Effects of *Trigonella foenum* in Neuroblastoma Cell Line

Irem Urkmez, Hatice Ilayhan Karahan Coven, Asli Eldem, Melek Pehlivan

257 *In silico* Evaluation of WWC1 in Melanoma Using Bioinformatic Analyses

Dilara Kamer Colak, Ufuk Unal, Sema Bolkent

Review Articles

267 Personalized Medicine: A Solution for Today and Tomorrow

Basak Dalbayrak, Mustafa Dogukan Metiner

274 Thioredoxin-Interacting Protein: The Redoxosome Complex in Glomerular Lesion

Gabriel Pereira, Emily Pereira dos Santos, Maria Augusta Ruy-Barbosa, Sofia Tomaselli Arioni, Thabata Caroline de Oliveira Santos, Débora Tavares de Resende e Silva, Juan Sebastian Henao Agudelo, Maria do Carmo Pinho Franco, Ricardo Fernandez, Rafael Luiz Pereira, Danilo Cândido de Almeida

Investigation the Cytotoxic and Anti-Proliferative Effects of Crude Venom of *Euscorpis mingrelicus* (Scorpiones: Euscorpiidae) Scorpion

Nazife Yigit Kayhan¹ , Ilkay Corak Ocal² , Mustafa Akdeniz³ 

¹Kırıkkale University, Faculty of Science and Arts, Department of Biology, Kırıkkale, Türkiye

²Çankırı Karatekin University, Faculty of Science, Department of Biology, Çankırı, Türkiye

³Kırıkkale University, Institute of Science, Department of Biology, Kırıkkale, Türkiye

ORCID IDs of the authors: N.Y.K. 0000-0002-8731-3362; I.C.O. 0000-0003-1479-2697; M.A. 0000-0001-9344-0184

Please cite this article as: Yigit Kayhan N, Corak Ocal I, Akdeniz M. Investigation the Cytotoxic and Anti-Proliferative Effects of Crude Venom of *Euscorpis mingrelicus* (Scorpiones: Euscorpiidae) Scorpion. Eur J Biol 2022; 81(2): 117-124. DOI: 10.26650/EurJBiol.2022.1105838

ABSTRACT

Objective: Since they contain various toxins that may influence various biological events, scorpion venoms raise new hopes for cancer treatments. It is thought that the bioactive compounds contained in scorpion venom could be used in cancer treatments in near future.

Materials and Methods: In this study, different cytotoxic, apoptotic, necrotic, and anti-proliferative effects of crude venom obtained from *Euscorpis mingrelicus* (Kessler, 1874) scorpions species were tested on human breast cancer cells (MCF-7), human lung carcinoma cells (H1299), and mice fibroblast cells (L929).

Results: It was determined that the crude venom had cytotoxic and anti-proliferative effects on MCF-7 and fibroblast cells even when at low concentrations and the effect on H1299 was half of the effect on MCF-7 and fibroblast. It was observed that, as the dilution rate increased, the venom effect decreased, apoptosis and necrosis rates on H1299 decreased, and it had no effect on cell proliferation. With regards to the MCF-7 cells, apoptosis and necrosis rates were similar in H1299 cells.

Conclusion: It was found that crude venom of *E. mingrelicus* scorpion played an effective role in decreasing the proliferation of MCF-7 cells, and more comprehensive studies are needed in order to determine the toxin that is responsible for this effect.

Keywords: Scorpion Venom, Cancer, Anti-Proliferative, Apoptosis, Necrosis

INTRODUCTION

Given the death statistics of developed countries, it can be seen that, following cardiovascular diseases, cancer is the second-most lethal disease. Cancer manifests itself as an uncontrolled proliferation of cells with an invasive character and metastasis, and is hard to cure. While radiotherapy, chemotherapy, and surgical methods are widely used in cancer treatment, target-specific treatments, biological treatment methods, and hormone therapies are less frequently used. These methods are used either separately or in combination (1).

In addition to their treatment characteristics, methods with the potential to cure may also have adverse effects, i.e., negative effects on healthy cells. The medications used in chemotherapy are artificial chemicals and it is known that they have many side effects. One of the factors limiting the efficiency of anti-cancer medications in treatment is the resistance mechanism that tumor cells develop, sometimes on their own in certain cancer types and sometimes after chemotherapy in some other types of cancer (2). The objective of cancer treatment is to destroy all the cells until there is no remaining malignant cell in the body. However, at this moment,



Corresponding Author: Nazife Yigit Kayhan

E-mail: naz_yigit2@hotmail.com

Submitted: 20.04.2022 • **Revision Requested:** 09.05.2022 • **Last Revision Received:** 29.07.2022 •

Accepted: 03.08.2022 • **Published Online:** 09.09.2022

Content of this journal is licensed under a Creative Commons Attribution-NonCommercial 4.0 International License.



such a treatment is not possible, with a couple of exceptions (3). Researchers have focused on natural sources, since chemotherapeutic agents have adverse effects and they cause the development of resistance to multiple drugs. Nowadays, it is thought that *biotoxins* may be useful in cancer treatment.

Scorpion, snake, and spider venoms are mixtures that are rich in protein, polypeptide, and various biogenic amines. The venoms of these creatures have started to be used directly and indirectly in cancer treatment. Scorpion venom, in particular, comes to the forefront in cancer research because of its high protein content. Scorpions are found everywhere on earth, except for New Zealand and ocean islands, and they are more widespread in tropical and subtropical climate zones (4,5). Scorpions combine many bioactive compounds in their venoms and use them in catching their prey and protecting themselves (6). Scorpion venoms are complex mixtures containing more than 100 compounds, including mucosa, oligopeptide, nucleotide, amino acid, various ions and salts, neurotransmitter, water, low molecular weight materials, and phospholipase, hyaluronidase, lipase, alkaline phosphatase, and proteolytic enzyme (7,8).

There are numerous techniques and methods to carry out the extraction of venom from scorpions (9-12). An early method was to remove the venom glands and telsons and macerate them, followed by extracting the venom in normal saline or water. The main problem with this method was that the scorpions had to be sacrificed after the removal of the telson, and thousands of scorpions had to be sacrificed to obtain sufficient quantities of venom for research purposes (9-11). Another method was to puncture the venom gland through the chitinous covering with a sharp, hypodermic needle and suck out the venom. Again, the amount of venom that could be obtained was very limited and the process caused serious damage to the scorpion. In the widely used electro-stimulation technique, a 20-25 V electric current is applied to the scorpion's telson and the venom is collected directly from the tip of the sting. The toxicity of the venom obtained with this technique is found to be higher, a higher amount of venom is obtained, and there are no permanent injuries to the scorpions. Within 2-3 weeks, the same scorpions can be used for venom milking again (11,12).

Scorpion venoms are toxic for humans. They cause severe reactions that may result in central nervous system damage, allergic reactions, tissue necrosis, and even death (6). Moreover, they are reported to have hemolytic, antibacterial, antifungal, insecticide, antitumor, analgesic, and (on several cells) apoptotic effects (13,14). Although scorpion venoms have very severe effects on humans, which can result in death, certain toxins found in scorpion venoms are used in central nervous system disease treatments in particular (15,16). In humans, scorpion venoms can be used in the treatment of rheumatism, pancreatic inflammation, skin cancer, breast cancer, prostate cancer, kidney tumors, male impotency, brain tumors, leukemia, epilepsy, HIV, tetanus, cardiovascular diseases, and sub-

cutaneous nodules, and in acute and chronic convulsion therapies (17).

Scorpion venoms are classified by different channel and channel structures, binding sites, and effects. Scorpion venoms are classified as long- or short-chain peptides by molecular length, insect-, mammal-, or crustacean-specific toxins by effect groups, neurotoxins or cytotoxins by effect mechanism, and disulfide bridge peptides (DBPs) or non-disulfide bridge peptides (NDBPs) by the presence of disulfide bridge (18). DBPs are generally the ion channels showing neurotoxin activity and are bound to the membrane. They contain 3-4 disulfide bridges. These channels play important roles in arranging the cellular physiology among many mammals. After the scorpion stings, the functions of these channels deteriorate and sting causes remarkable changes (19). NDBPs are anti-carcinogenic, anti-inflammatory, antimicrobial, hemolytic, and immunomodulator (19).

The sodium channel toxins (NaTx) in scorpion venoms prefer different sodium channels in cells of mammals and insects. These toxins bind to different receptor zones and target these channels by creating pores (20). The long-chain toxins affecting the sodium channels are divided mainly into two subtypes: α -toxin and β -toxin. Scorpion α -toxins bind to Na⁺ channels in mammals and suddenly inactivate the sodium channel receptor affinity. Hence, they prolong the nerve-muscle potential. In mammals, β -toxins bind to the 4th zone as sodium channel receptor and cause a sudden change in the direction of membrane potential or a more negative membrane potential (21,22). The potassium channel toxins (KTx) that scorpion venom contains function as various potassium channel blockers. The scorpion toxins targeting the potassium channels are the short-chain peptides cross-linked with 3 or 4 disulfide bridges, and it was reported that they might be used in treatment of various diseases, such as cancer, inflammation, neuropathy, and autoimmune diseases (23). Calcium channel ions play an important role in organizing functions such as regulation of gene expression, intracellular mechanism, release of neurotransmitters, and cellular stimulation. Calcium channels generally spread over the body in the form of endocrine cells, smooth muscles, skeletal muscle, cardiac muscle, and neurons. Many calcium channel toxins (CaTx) that scorpion venom contains affect the functions of Ca⁺⁺ ion channels and their activities by modulating them. Since these peptides have pharmacological and physiological properties, they have been investigated in various studies (24,25).

Scorpion venoms show their effects by influencing the movement of ions causing lethal depolarization by disintegrating the cellular membrane. The contents of the venom create pores on the cellular membrane and cause the cell content to leak outside. Moreover, some peptides contained in venom composition include hydrolases that cause the disintegration of the cellular membrane. Hydrolases distort the membrane function by causing the distribution of membrane lipids (26).

In the present study, the effects of the venom of *Euscorpis mingrelicus*, which does not have a venom that is intense enough to affect humans, was examined on two different cancer types and normal fibroblast cell lines. The effect of *E. mingrelicus* venom was examined on human breast cancer cells (MCF-7), human large cell lung carcinoma cells (H1299), and mice fibroblast cells (L929) via cytotoxic and apoptosis properties.

MATERIALS AND METHODS

Obtaining the Scorpions and Venoms

The *Euscorpis mingrelicus* (Scorpiones: Euscorpiidae) scorpions used in the present study were collected from nature (under stones) in Çamlidere and Çamkoru Forests in Ankara province (33°E, 40°N, Ankara, Turkey) between 15th July and 15th September 2015. The scorpions, which were released into individual habitats that we specially prepared for them in the laboratory, were not given any food for a week in order to prevent a decrease in the amount of their venom, and venom collection was performed using electrostimulation method. Using an electrostimulator, 15-20 volts of current were applied to the tail of the scorpion through two electrodes. The crude venom was collected using the injector from the sting at the tip of telson. The crude venom was dissolved in double distilled water and centrifuged at +4°C and 15,000 g for 15 min. After the centrifuge, the supernatant containing peptide toxins was transferred to a new tube and the protein concentration was measured using the Bradford method at 405 nm wavelength (27). The protein concentration of resultant crude venom was found to be 3290 µg/µl. The crude venom was stored at -20°C until the experiment day. The venom was diluted at the ratios 1/30, 1/60, 1/120, 1/240, 1/480, 1/960, 1/1920, and 1/3840.

Cell Culture

H1299, MCF-7, and L929 cell lines were obtained from the cell collection of Kırıkkale University's Central Research Laboratory (KUBTAL). The procedures were conducted in the same laboratory in accordance with the standards. These cell lines were incubated in 25cm³ flasks and 15 ml medium with Dulbecco's Modified Eagle Media containing 0.1 mM L-glutamine and 10% heat-activated fetal calf serum at 37°C in an incubator with 5% CO₂.

WST-1 Cytotoxicity Test

Using a cell counting device on the cell lines that we had cultivated, we achieved cell counts of 4.5x10⁵ for MCF-7, 1.7x10⁵ for H1299 cells, and 3.4x10⁵ for L929 cells. A WST-1 cytotoxicity test was performed using a 96-well plate by placing 5,000 cells in each well, using 2 wells for control, and leaving the rest empty. Then, DMEM containing 1% penicillin-streptomycin and 10% fetal bovine serum was added to RPMI (L-glutamine, without sodium bicarbonate) for L929, MCF-7, and H1299 cells. Cells were incubated for 24 h at 37°C in an incubator with 5% CO₂. After the 24 h incubation, 40µl of venom was diluted to 1200 µl using double distilled water. Then, it was equally distributed to the first 6 wells (100 µl). The resting portion was diluted by ½ and divided equally into the next 6 wells (100 µl). This process

was continued up to the last well, and the venom doses of 1/30, 1/60, 1/120, 1/240, 1/480, 1/960, and 1/1920 µg/µl were achieved. Then, another 24 h incubation was performed. After the incubation, the cell media were removed from the wells and 100 µl media containing no phenol red were added. 10 µl WST-1 solution was added to each well, and then they were incubated for 4 hours. After the incubation, the absorbance measurement was performed at 440 nm wavelength using a spectrophotometer with a microplate scanner.

Determining the Apoptosis and Necrosis by Using Double Staining

This process was performed using a 96-well plate. MCF-7, H1299, and L929 cells were divided into 16 wells each (5,000 cells in each well). Two wells were used as control for each. DMEM containing 1% penicillin and 10% fetal bovine serum were added to RPMI for L929, MCF-7, and H1299 cells. Cells were incubated at 37°C for 24 h with an incubator having 5% CO₂. After the 24 h incubation, 40 µl of venom was diluted to 1200 µl using double distilled water. Then, it was equally distributed to the first 6 wells (100 µl). The resting portion was diluted by ½ and divided equally into the next 6 wells (100 µl). This process was continued until the last well and the venom doses of 1/30, 1/60, 1/120, 1/240, 1/480, 1/960, and 1/1920 dilutions were achieved. Then, another 24 h incubation was performed. After the incubations, the media were removed and 70 µl double staining solution was added to each well. They were incubated for 15 minutes in darkness. After the incubation, the examinations were performed using FITC and DAPI filter with a microscope with a fluorescent attachment. For each well, the total number of living cells, the total number of apoptotic cells, and the total number of necrotic cells were manually counted.

Monitoring Cell Proliferation Using Real-Time Cell Analysis System (xCELLigence RTCA)

After determining that the number of cells in flux reached an adequate number using a microscope, the medium was removed and 1 ml trypsin-EDTA was added. The flux was kept in an incubator for 3-4 min. After the incubation, flux was microscopically checked to see if the cells were detached from the surface of flux. After confirming microscopically that the cells were detached, medium was added into flux, and the cells were put into a vial and centrifuged at 2,500g for 2 min. The supernatant portion was removed after the centrifuging and the resting cell pellet at the bottom of the tube was suspended by adding 1 ml mem-α medium. Cell counting was performed. Then, 100 µl medium was added to each well of the e-plate. After the plate in the oven was placed in xCELLigence. There was a 5 min waiting period for the plate and device to reach the same temperature. After 1 min of background scanning in the device, the e-plate was removed and MCF-7 and H1299 cell lines (100 µl 3x10³ cells) were added to each well. The e-plate was placed into the drying oven again and reading was initiated at the end of the 10min period. There was a 24 h waiting period for the cell proliferation. Moreover, venom doses of 1/30, 1/60, 1/120, and 1/240 were applied and the proliferation was monitored for 120 h.

Statistical Analysis

All experiments in this study were performed in triplicate. The data shown are representative results. Values were calculated as the mean and standard error. Owing to the fact that the data from vitality experiments did not meet the normality assumptions, statistical comparisons of results from control and venom application groups were made non-parametrically using the Mann-Whitney U test. Statistical package program (version 7) was utilized.

RESULTS

WST-1 Test Results

Since the scorpions examined here are small creatures, the amount of venom they provide is also very small. Hence, the dilution rates were kept high. At the dilution rate of 1/30, it was found that venom affected the vitality of MCF-7 and L929 cell lines by 50% and the effect on H1299 was found to be 27%. It was determined that the effect of venom decreased as the dilution rate increased and the cell vitality exceeds the beginning level after a specific dilution rate (Table 1).

In the study, when the viability percentages of the non-cancer cell (L929), which we used as a control, and the venom cancer

cells (MCF-7 and H1299) are compared, it is seen that MCF-7 and L929 are similar, while H1299 is statistically different (Table 2).

Double Staining Results

As a result of the double staining test, it was determined that, for MCF-7 cells for which the vitality results were in corroboration with WST-1 test, $13.88 \pm 0.5\%$ of all dead cells died of apoptosis and $12.5 \pm 1.5\%$ died of necrosis at the dilution level of 1/30 (Table 3). Apoptosis and necrosis rates gradually decreased as the dilution rate increased (Figures 1A, B). After the dilution rate of 1/240, the decrease in necrotic deaths became sharper. While the apoptosis and necrosis rates were close to each other at the dilution rates of 1/30 and 1/60, it was determined that apoptosis rate was higher than the rate of necrosis at other doses. In H1299 cell line and at the dilution level of 1/30, apoptosis rate was found to be $10.52 \pm 0.4\%$ and necrosis rate to be $5.26 \pm 0.5\%$ (Table 3). Apoptosis/necrosis rates ranged between 1.41 and 4.0 at other dilution rates (Figures 1C, D).

In L929 fibroblast and at a dilution rate of 1/30, the rate of apoptosis was found to be approximately 30% and the rate of necrosis to be half of it. This ratio varied as the dilution ratio increased (Table 3).

Table 1. WST 1 test absorbance results. The cell viability (%) based on mean absorbance values at 440 nm is presented. Data are expressed as mean±standard error as calculated from 3 separate experiments.

Venom Doses	MCF-7 Vitality (%)	H1299 Vitality (%)	L929 Vitality (%)
1/30	52.69±0.2	72.96±1.0	49.12±1.0
1/60	76.27±1.5	119.45±0.7	81.33±0.1
1/120	83.12±0.8	127.33±0.8	85.79±1.1
1/240	100.59±0.7	133.34±1.1	90.36±1.4
1/480	118.80±2.0	131.81±1.4	96.30±0.5
1/960	131.36±0.5	129.54±2.1	97.82±1.0
1/1920	129.03±0.7	123.98±2.0	97.27±1.1
1/3840	122.12±0.4	124.14±0.1	100.54±0.5
Negative Control	100.59±0.1	110.45±0.5	100.54±0.1

Table 2. Paired comparisons of vitalities between L929 (control group) and each venom application (MCF and H1299) by nonparametric Mann-Whitney U test. Tests shown in bold are significant at $p < 0.05$. (n=8).

Groups	Rank Sum L929	Rank Sum MCF	z	p-level
L929 x MCF-7	60.00	76.00	-0.84	0.40
L929 x H1299	44.00	92.00	-2.52	0.01
MCF-7 x H1299	53.00	83.00	-1.58	0.12

Table 3. Apoptosis and necrosis indexes. Data are expressed as mean \pm standard error as calculated from 3 separate experiments.

Venom	MCF-7		H1299		L929	
	% apoptosis	% necrosis	% apoptosis	% necrosis	% apoptosis	% necrosis
1/30	13.88 \pm 0.5	12.5 \pm 1.5	10.52 \pm 0.4	5.26 \pm 0.5	30.55 \pm 0.7	16.6 \pm 0.1
1/60	9.09 \pm 0.4	10.38 \pm 1.0	8.23 \pm 0.5	5.83 \pm 0.5	25 \pm 0.5	14.77 \pm 0.5
1/120	8.88 \pm 0.2	7.5 \pm 0.7	6.29 \pm 1.0	1.57 \pm 1.0	21.42 \pm 1.0	14.28 \pm 0.5
1/240	8.49 \pm 0.1	4.71 \pm 0.5	6.36 \pm 0.7	1.91 \pm 0.7	18.91 \pm 0.7	10.81 \pm 1.0
1/480	7.95 \pm 0.3	4.54 \pm 0.5	3.94 \pm 0.8	1.49 \pm 1.0	14.63 \pm 0.5	9.75 \pm 0.7
1/960	6.38 \pm 0.5	4.25 \pm 0.8	3.33 \pm 0.7	1.25 \pm 0.5	11.89 \pm 0.6	8.64 \pm 0.5
1/1920	6.73 \pm 0.5	2.32 \pm 0.6	3.48 \pm 0.7	1.24 \pm 0.8	11.25 \pm 0.7	7.5 \pm 0.1
1/3840	5.31 \pm 0.4	2.12 \pm 0.5	2.32 \pm 1.0	1.16 \pm 0.1	9.89 \pm 0.5	4.39 \pm 0.1

Determining Cell Proliferation Using Real-Time Cell Analysis System (xCELLigence RTCA)

During the 120-h proliferation monitoring, it was determined that the proliferation of MCF-7 and H1299 cells proportionally increased within the first 24 h. After the 24th h, when the venom was applied, proliferation stopped and even the number of living cells decreased. Then, because the effect of venom

decreased, cells entered into the proliferation process again. Proliferation was found to be at the minimum level at the dilution rate of 1/30 (the highest amount of venom). It was observed that the effect of venom lasted longer (Figures 2,3). At the dilution rate of 1/30, the proliferation of MCF-7 is faster than H1299. Similar results were achieved after the 24th hour (Figure 4).

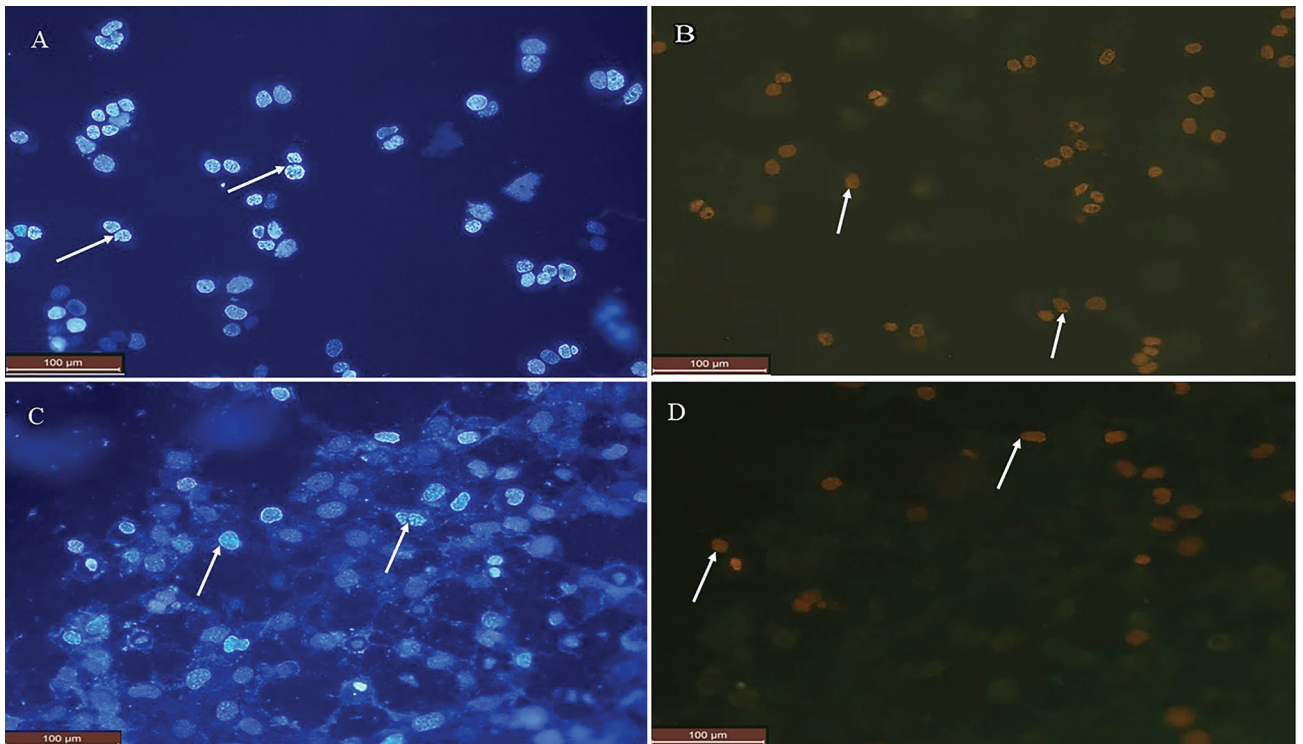


Figure 1. Inverted microscope image of MCF-7 cells at the dilution rate of 1/30; apoptosis (A) and necrosis (B), H1299 cells at the dilution rate of 1/30; apoptosis (C) and necrosis (D). Apoptotic and necrotic cells are shown with arrows.

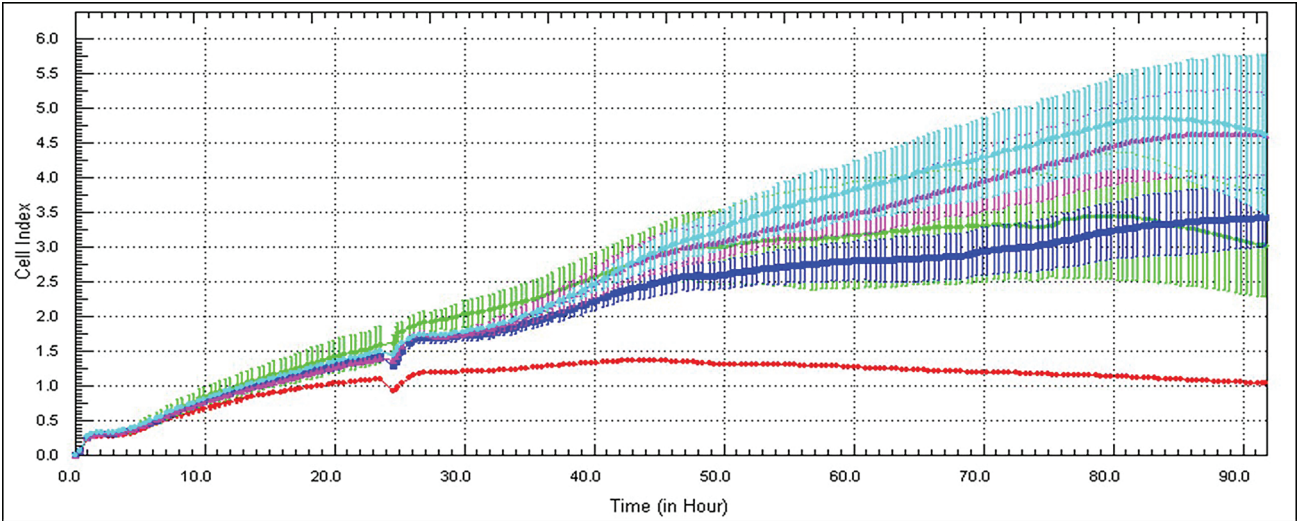


Figure 2. 24-h cell proliferation for MCF-7 cell line (Red 1/30, Blue 1/60, Pink 1/120, Turquoise 1/240, Green control).

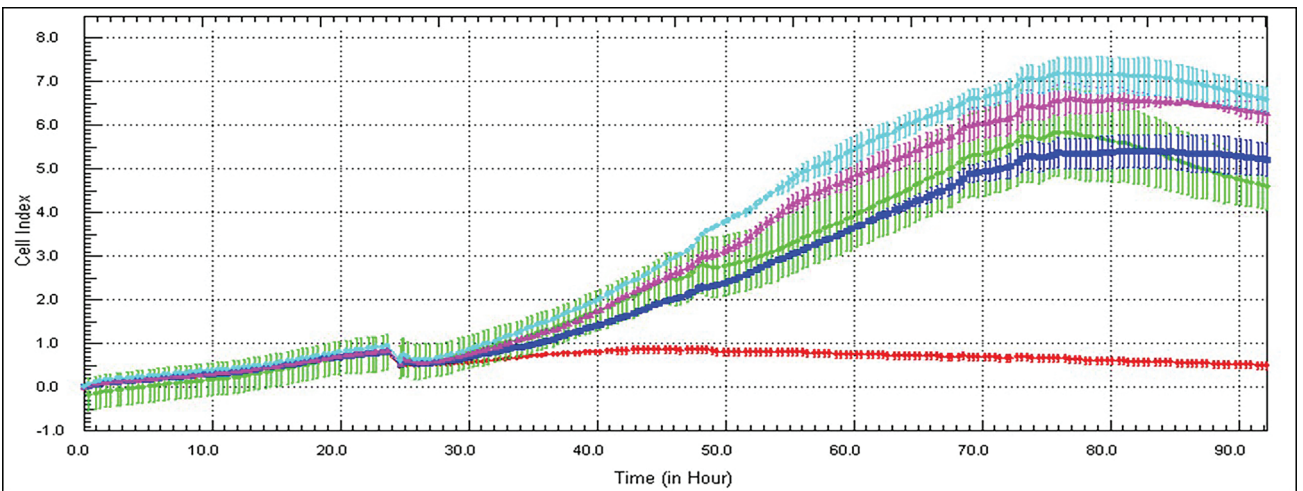


Figure 3. 24-h cell proliferation for H1299 cell line (Red 1/30, Blue 1/60, Pink 1/120, Turquoise 1/240, Green control).

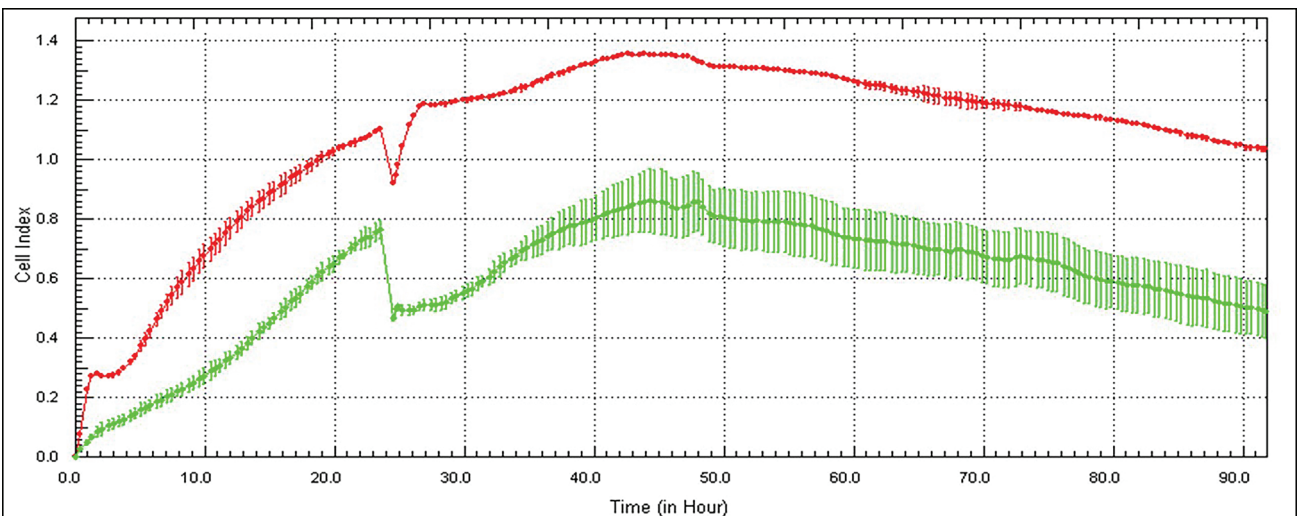


Figure 4. Comparison of proliferation curves of MCF-7 and H1299 cells at the dose of 1/30 (Red MCF-7, Green H1299).

DISCUSSION

Radiotherapy, chemotherapy, and surgical interventions are used in cancer treatment. Although they have curative potential, their negative effects on healthy cells limit the treatment potential. Because of their low side effects, biotoxins have drawn attention as a new hope for cancer treatment in recent years. Cytolytic and cytotoxic activities of peptides that venom contains show their effects by strengthening the immune system of the body. It is thought that biotoxins could replace the anti-neoplastic in the near future (1).

It was reported that ion channels and potassium channels associated with voltage-related the human ether-à-go-go-related gene decelerated the DNA synthesis and cellular proliferation in tumor cells (28). Çalıřkan et al. (29) purified Ac8, Ac9, and Ac10 peptides from *Androctonus crassicauda* species using High performance liquid chromatographic analysis and determined that these peptides had a cytotoxic effect on BC3H1 (mouse brain tumor cell) cells. It was stated that these peptides would have an antitumor effect in humans. A peptide consisting of 36 amino acids was isolated from the *Leiurus quinquestriatus* species. Blocking the chlorine channels, this peptide is named chlorotoxin (CITx). It was found to have an apoptotic and necrotic effect on the human embryonic renal cells and mouse myoblast cells (30). Chlorotoxin is specifically sensitive to glioma cells. It was found to prevent proliferation in human glioma cells and have a therapeutic effect on brain cancer (31-33). Chlorotoxin is a noninvasive scanning tool for the early diagnosis of colon, esophageal, cervical, lung, and skin cancers. Binding with ferrous oxide nanoparticles, chlorotoxin forms a polyethylene glycol binder. This structure successfully binds to ligands targeted via the medications. These ligands preferably accumulate on tumor cells and increase the cytotoxicity in tumor cells. This multifunctional nanoparticle system is believed to be potentially useful in cancer diagnosis and treatment (34). *Buthus martensii* Karsch antitumor-analgesic peptide isolated from *Buthus martensi* Karsch species is a sodium channel neurotoxin. This peptide was reported to stimulate apoptosis by influencing the ion channels in malignant glioma cells (35). It was observed that the crude venom of *E. mingrelicus*, which we used in the present study, decreased the proliferation of MCF-7 cancer cell line. However, further studies are needed to elucidate this mechanism of action.

The venom called bengaline and isolated from *Heterometrus bengalensis* was reported to inhibit cellular proliferation by stimulating the apoptosis in human leukemia cells (36,37). The polypeptide extract from scorpion venom (PESV) is a peptide consisting of 50-60 amino acids isolated from *Buthus martensi* Karsch scorpions and it was determined to have anti-proliferative, cytotoxic, and (for human belly vein cells) apoptotic effects. It was revealed that polypeptide extract from scorpion venom was found to be effective against the androgen-dependent prostate cancer cell line. Hormone-resistance prostate cancer (HRPC) remains a problem (38). Breast cancer is a

cancer that might originate from any point in breast tissue. The death that is most frequently seen among breast cancer patients is due to the metastatic spread of cancer cells invading the angiogenic blood vessels growing within the tumor. A hyaluronidase (BmHYA1) was purified from the venom of *Buthus martensii*. The human breast cancer line (MDA-MB-231) contains many hyaluronidases. Hyaluronidase constitutes a new class for anti-cancer treatment without therapeutic and toxic side effects (39,40). It was reported that protease isolated from *Mesobuthus gibbosus* scorpion venom yielded a significant decrease in human lung adenocarcinoma cell lines. These peptides show very strong gelatinolytic and cytotoxic effects against human lung adenocarcinoma (41). TRAIL peptide (TNF-related apoptosis-inducing ligand) obtained from scorpion venom is used for inducing apoptosis in melanoma cells. While normal cells are not affected, these peptides target only the cancer cells. In melanoma cancer cells, TRAIL initiates proapoptotic Bcl-2 and caspase. Resulting in the release of mitochondrial factors such as TRAIL, SMAC (secondary mitochondrial caspase activator), and AIF (apoptosis-inducing factor), it causes depolarization and permeabilization of the external membrane of mitochondria. These factors inhibit the proliferation of cancer cells and induce apoptotic death (42). In literature, the scorpion venoms that have been examined are those that are strong enough to intoxicate humans. In this study, the crude venom of *E. mingrelicus*, a scorpion species that does not have enough venom to intoxicate humans, was tested on two different cancer types and normal fibroblast cell lines. This venom reduced proliferation of mcf-7 cancer cell line. This showed that there are agents that can affect cancer cells in the venom of scorpions, which do not cause intoxication in humans.

CONCLUSION

In the present study, it was observed that the scorpion venom used reduced the proliferation of the MCF-7 cancer cell line. Since the amount of venom was limited, dilution rates were set to be high. By carrying out further studies determining the protein content of venom and increasing the venom concentration, it is thought that this scorpion venom can be used as a biotherapy agent in the treatment of human breast cancer.

Peer-review: Externally peer-reviewed.

Author Contributions: Conception/Design of study- N.Y.K., I.C.O.; Data Acquisition- N.Y.K., I.C.O., M.A.; Data Analysis/Interpretation- N.Y.K., I.C.O., M.A.; Drafting Manuscript- N.Y.K., I.C.O., M.A.; Critical Revision of Manuscript- N.Y.K., I.C.O.; Final Approval and Accountability- N.Y.K., I.C.O.

Conflict of Interest: The authors declare that they have no conflicts of interest to disclose.

Financial Disclosure: There are no funders to report for this submission.

REFERENCES

- Lipps BV. Novel snake venom protein cytolytic to cancer cells *in vitro* and *in vivo* systems. *J Venom Anim Toxins* 1999; 5: 172-83.
- Szakacs G, Paterson JK, Ludwig JA, Genthe CB, Gottesman MM. Targeting multidrug resistance in Cancer. *Nat Rev Drug Discov* 2006; 5: 219-34.
- Kocdogan K. Meme Kanserli Hastalarda Glutasyon S-Trensferaz Izozimlerin Coklu Ilac Direnc Mekanizmasındaki Proteinlerle Olan İlişkilerin İncelenmesi. K.Ü. Fen Bilimleri Enstitüsü, Yüksek Lisans Tezi. 2016.
- Cheng D, Dattaro JA, Yakobi R, Bush SP, Gerardo CJ. Scorpion envenomation. *Medscape* 2011 Sep. Available from: URL: <http://emedicine.medscape.com/article/168230-overview>.
- Ozkan O, Carhan A. The neutralizing capacity of *Androctonus crassicauda* antivenom against *Mesobuthus eupeus* scorpion venom. *Toxicon* 2008; 52: 375-9.
- Gurevitz M, Karbat I, Cohen L, Ilan N, Kahn R, Turkov M, Stankiewicz M, Stühmer W, Dong K, Gordon D. The insecticidal potential of scorpion β -toxins. *Toxicon* 2007; 49: 473-89.
- Park J, Cho SY, Choi SJ. Purification and characterization of hepatic lipase from *Todarodes pacificus*. *BMB reports* 2008; 41: 254-8.
- Rapôso C. Scorpion and spider venoms in cancer treatment: state of the art, challenges, and perspectives. *J Clin Transl Res* 2017; 24: 233-49.
- Gopalakrishnakone P, Cheah J, Gwee MCE. Black scorpion (*Heterometrus longimanus*) as a laboratory animal: maintenance of a colony of scorpion for milking of venom for research, using a restraining device. *Lab Anim* 1995; 29: 456-8.
- Oukkache N, Chgoury F, Lalaoui M, Cano A A, Ghalim N. Comparison between two methods of scorpion venom milking in Morocco. *J Venom Anim Toxins Incl Trop Dis* 2013; 19: 5-8.
- Tobassum S, Tahir HM, Zahid MT, Gardner QA, Ahsan MM. Effect of milking method, diet, and temperature on venom production in scorpions. *J Insect Sci* 2018; 18: 19-21.
- du Plessis JL. Collection of venom from southern African scorpions. *Toxicon* 2005; 45: 681-2.
- Diniz CR. Chemical and pharmacological aspects of Tityinae venoms. *Arthropod venoms*. Berlin: Springer-Verlag, 1978, 379-94.
- Willems J, Noppe W, Moerman L, Van der WJ, Verdonck F. Cationic peptides from scorpion venom can stimulate and inhibit polymorphonuclear granulocytes. *Toxicon* 2002; 40: 1679-83.
- Xiong Y, Lan Z, Wang M, Liu B, Liu X, Fei H, et al. Molecular characterization of new excitatory insect neurotoxin with an analgesic effect on mice from the scorpion *Buthus martensii* Karsch. *Toxicon* 1999; 37: 1165-80.
- Mortari MR, Cunha AOS, Ferreira LB, Ferreira dos Santos W. Neurotoxins from invertebrates as anticonvulsants: From basic research to therapeutic application. *Pharmacol Ther* 2007; 114: 171-83.
- Chen Y, Cao L, Zhong M, Zhang Y, Han C, Li Q, et al. Anti-HIV-1 activity of a new scorpion venom peptide derivative Kn2-7. *PLoS One* 2012; 7: e34947.
- Zhijian C, Feng L, Yingliang W, Xin M, Wenxin L. Genetic mechanisms of scorpion venom peptide diversification. *Toxicon* 2006; 47: 348-55.
- Ammar A, Qosay A. Scorpion venom peptides with no disulfide bridges: A review. *Peptides* 2014; 51: 35-45.
- Yu FH, Catterall WA. Overview of the voltage-gated sodium channel family. *Genome Biol* 2003; 4(3): 1-7.
- Possani LD, Merino E, Corona M, Bolivar F, Becerril B. Peptides and genes coding for scorpion toxins that affect ion-channels. *Biochimie* 2000; 82(9): 861-8.
- Cestele S, Catterall WA. Molecular mechanisms of neurotoxin action on voltage-gated sodium channels. *Biochimie* 2000; 82(9): 883-92.
- Shieh CC, Coghlan M, Sullivan JP, Gopalakrishnan M. Potassium channels: molecular defects, diseases, and therapeutic opportunities. *Pharmacol Rev* 2000; 52 (4): 557-94.
- Catterall WA. Cellular and molecular biology of voltage-gated sodium channels. *Physiol Rev* 1992; 72(4): 15-48.
- Cid-Urbe JI, Veytia-Bucheli JI, Romero-Gutierrez T, Ortiz E, Possani LD. Scorpion venomomics: a 2019 overview. *Expert Rev Proteomics* 2020; 7(1): 67-83.
- Tossi A, Sandri L, Giangaspero A. Amphipathic, α -helical antimicrobial peptides. *Biopolymers* 2000; 55: 4-30.
- Bradford MM. Rapid and sensitive method for the quantitation of microgram quantities of protein utilizing the principle of protein-dye binding. *Anal Biochem* 1976; 72: 248-54.
- Kelle I. Terapötik potansiyele sahip venom peptidleri. *Dicle Med J* 2006; 33: 113 - 26.
- Çalışkan F, Sivas H, Şahin Y. Purification of Ac8, Ac9 and Ac10 peptides from *Androctonus crassicauda* crude venom with cytotoxic effect on Bc3h1 cells. *Anadolu Univ J of Sci and Technology – A – Appl Sci and Eng* 2009;10(2): 515-24.
- Omran MAA. Cytotoxic and apoptotic effects of scorpion *Leiurus quinquestriatus* venom on 293T and C2C12 eukaryotic cell lines. *J Venom Anim Toxins Incl Trop Dis* 2003; 9:255-76.
- Fu YJ, Yin LT, Liang AH, Zhang CF, Wang W, Chai BF, et al. Therapeutic potential of chlorotoxin-like neurotoxin from the Chinese scorpion for human gliomas. *Neurosci Lett* 2007; 412 (1): 62-7.
- Veiseh M, Gabikian P, Bahrami SB. Tumor paint: a chlorotoxin: L Cy5.5 bioconjugate for intraoperative visualization of cancer foci. *Cancer Research* 2007; 67: 6882-8.
- Kesavan K, Ratliff J, Johnson EW, Dahlberg W, Asara JM, Misra P. Annexin A2 is a molecular target for TM601, a peptide with tumor-targeting and anti-angiogenic effects. *J Biol Chem* 2010; 285: 4366-74.
- Sun C, Stephen Z, Veiseh O, Harisen S, Lee D, Ellenbogen RG, et al. Tumor targeted drug delivery and MRI contrast enhancement by chlorotoxin conjugated iron oxide nanoparticle. *Nanomed* 2008; 3: 495-505.
- Wang WX, Ji YH. Scorpion venom induces glioma cell apoptosis *in vivo* and inhibits glioma tumor growth *in vitro*. *J Neuro-Oncol* 2005; 73(1): 1-7.
- Gupta SD, Gomes A, Debnath A, Saha A, Gomes A. Apoptosis induction in human leukemic cells by a novel protein bengalin, isolated from Indian black scorpion venom: through mitochondrial pathway and inhibition of heat shock proteins. *Chem Biol Interact* 2010; 183(2): 293-303.
- Hayden MS, West AP, Ghosh S. NF-kappaB and the immune response. *Oncogene* 2006; 25: 6758-80.
- Zhang YY, Wu LC, Wang ZP, Wang ZX, Jia Q, Jiang GS, et al. Anti-proliferation effect of polypeptide extracted from scorpion venom on human prostate cancer cells *in vitro*. *J Clin Med Res* 2009; 1(1): 24-3.
- Feng L, Gao R, Gopalakrishnakone P. Isolation and characterization of a hyaluronidase from the venom of Chinese red scorpion *Buthus martensii*. *Comp Biochem Physiol C Toxicol Pharmacol* 2008; 148: 250-7.
- Sariego J. Breast cancer in the young patient. *Am Surg* 2010; 76:1397-401.
- Pessini AC, Takao TT, Cavalheiro EC, Vichnewski W, Sampaio SV, Giglio JR, et al. A hyaluronidase from *Tityus serrulatus* scorpion venom: isolation, characterization and inhibition by flavonoids. *Toxicon* 2001; 39: 1495-504.
- Norberg E, Orrenius S, Zhivotovsky B. Mitochondrial regulation of cell death: Processing of apoptosis-inducing factor (AIF). *Biochem Biophys Res Comm* 2010; 396: 95-100.

In Silico Analysis of BMAL1 and CLOCK SNPs in the Ensembl Database

Seref Gul¹ 

¹Istanbul University, Faculty of Science, Department of Biology, Biotechnology Division, Istanbul, Turkiye

ORCID IDs of the authors: S.G. 0000-0002-5613-1339

Please cite this article as: Gul S. In Silico Analysis of BMAL1 and CLOCK SNPs in the Ensembl Database. Eur J Biol 2022; 81(2): 125-135. DOI: 10.26650/EurJBiol.2022.1164864

ABSTRACT

Objective: A circadian rhythm in mammals controls the sleep-wake cycle, blood pressure, hormone secretion, metabolism and many other physiological processes. The circadian clock mechanism is regulated by four genes: *Bmal1*, *Clock*, *Cry*, and *Per*. Mutations in these regulatory genes are associated with sleep and mood disorders, obesity, and cancer. Several PER2 and CRY2 SNPs are associated with advanced sleep phase syndrome. It is, therefore, critical to understand the effect of clock genes' SNPs on the circadian clock. In this study, we determined "pathogenic" BMAL1 and CLOCK SNPs in the Ensembl database for biochemical characterization.

Materials and Methods: BMAL1 and CLOCK SNPs in the Ensembl database were filtered out for only missense mutations. Among the missense mutations, pathogenic ones were determined according to SIFT, PolyPhen, and CADD scores, REVEL, MetalR, Mutation Assessor, I-Mutant, PROVEAN, and FireDock programs. BMAL1 and CLOCK SNPs were visualized by using PyMol.

Results: Thousands of BMAL1 and CLOCK missense SNP mutations were reported in the Ensembl database. After the classification of those SNPs according to their SIFT, PolyPhen, and CADD pathogenicity, twelve SNPs for each protein remained as pathogenic. A further analysis with all in silico tools revealed that BMAL1 SNPs causing Ala154Val, Arg166Gln, and Val440Gly mutations; and CLOCK SNPs causing Gly120Val, Asp119Val, Gly120Ser, Ala117Val, and Cys371Gly mutations were predicted as the most "pathogenic" ones.

Conclusion: Overall, by using in silico tools, we provided a starting point for experimental studies for determining the effect of pathogenic BMAL1 and CLOCK SNPs on the circadian clock mechanism.

Keywords: Circadian clock, Ensembl, BMAL1, CLOCK, SNP

INTRODUCTION

The circadian clock is an endogenous biological system that generates 24-hour rhythmic changes in the physiology and behavior of organisms according to environmental factors such as light-dark and eating-fasting cycles or social interactions. The circadian clock mechanism is found in a wide variety of organisms from cyanobacteria to drosophila to mammals (1). The circadian clock determines the correct timing of various biochemical processes in mammals such as the sleep-wake cycle, metabolism, body temperature, hormone

secretion, detoxification, sexual functions, DNA repair and apoptosis (2-5). Factors such as the night-day cycle, mealtime, social interaction, emotional mood, and temperature synchronize the circadian clock to exactly 24 hours (6,7). Among those, light turned out to be the most dominant *zeitgeber* (time-giver) (8).

Throughout the body, each tissue has a clock known as the peripheral clock; however, the master clock located in the suprachiasmatic nucleus synchronizes all peripheral clocks to generate a unified gene transcription oscillation around a day, 24 hours (9,10). At the cellular



Corresponding Author: Seref Gul

E-mail: serefgul@istanbul.edu.tr

Submitted: 21.08.2022 • **Revision Requested:** 26.09.2022 • **Last Revision Received:** 05.10.2022 •

Accepted: 20.10.2022 • **Published Online:** 23.11.2022

Content of this journal is licensed under a Creative Commons Attribution-NonCommercial 4.0 International License.



level, the circadian clock mechanism is regulated by intertwined transcriptional-translational feedback loops (TTFLs). In mammals, the positive arm of the feedback loop is composed of two transcriptional factors *Bmal1* (Brain-muscle-arnt-like protein 1) and *Clock* (Circadian Locomotor Output Cycles Kaput) (11-13). The negative feedback loop is generated by the *Cry* (*Cry1*, *Cry2*) and *Per* (*Per1*, *Per2*, *Per3*) genes in which their transcriptions are under the control of the BMAL1 and CLOCK activity (14-16). BMAL1 and CLOCK form a heterodimer and bind to E-box sequences found in the promoter regions of the target genes and initiate their transcription (17). After *Cry* and *Per* are translated, they form a heterodimer at the cytoplasm, then translocate to the nucleus and repress the BMAL1/CLOCK dependent transcription (9,16). This mechanism controls nearly 40% of protein-coding genes in mice (18). Post-translational modifications play important roles to regulate the activity, stability, half-life, and subcellular localization of these core clock proteins (19). An auxiliary TTFL helps to maintain precise clock ticking. The retinoic acid receptor-related orphan receptors (RORs) and REV-ERBs whose transcriptions are under the control of the circadian clock bind to the ROR enhancer element to initiate and repress the *Bmal1* transcription, respectively (20,21).

When the circadian clock mechanism is disturbed or misaligned with the light-dark cycle, organisms have difficulty coping with the changes in the environment. Organisms, therefore, become more prone to diseases or syndromes. For example, cancer, depression, obesity, and some metabolic diseases are associated with the disrupted circadian clock function (5,22,23). More interestingly, some single nucleotide polymorphisms (SNPs) found in the coding region of core clock genes that change the amino acid are linked to diseases. A *PER2* SNP (p.Ser662Gly), located on a phosphorylation site, was detected in people suffering from advanced sleep phase syndrome (ASPS) (24). Another SNP, found in *CRY2* (rs201220841) changing p.Ala260Thr, caused better interaction with *CRY2*'s E3 ligase that led to its rapid degradation, was associated as well with ASPS (24). Two *CRY1* exon

skipping variants (*CRY1* without exon 11 and exon 6) detected in the population were associated with familial delayed phase sleep syndrome and attention deficit hyperactivity disorder, respectively (25,26). Molecular characterizations showed that the exon 6 of *CRY1* encodes amino acids near the CLOCK binding region, hence the absence of amino acids around this region abolished *CRY1*-CLOCK interaction, and mutant *CRY1* (without exon 6) could not rescue the circadian rhythm at the cellular level (26). Similar characterization for *CRY1* without exon 11 showed that mutant *CRY1* had a higher affinity to CLOCK and BMAL1, and lengthened the period of the circadian rhythm (25). In addition to understanding the role of SNPs in human disorders, their molecular characterization may contribute to the understanding of the circadian clock mechanism better. In one of our recent studies, the characterization of a rare *CRY1* SNP (p.Arg293His) showed that two pockets of *CRY1* were allosterically regulated (27). Another recent study, that analyzed rare *CRY2* SNPs, showed that amino acids around the secondary pocket are important for nuclear localization and its stability (28). It is, therefore, essential to understand how SNPs have an impact on the molecular circadian clock mechanism.

CLOCK and BMAL1 are composed of basic helix-loop-helix (bHLH) and PER-ARNT-SIM (PAS) domains. Co-crystal of BMAL1-CLOCK showed that PAS-A and PAS-B domains of these proteins interact with each other to form a heterodimer (29). PAS domains are mainly interacting with each other via hydrophobic amino acids. Leu159, Thr285, Tyr287, Val315 and Ile317 on PAS-A of BMAL1 interact with Phe104, Leu105 and Leu113 of CLOCK. PAS-B domains bind to each other in a parallel mode. Additionally, Phe423, Trp427 and Val 435 on PAS-B of BMAL1 are found to be critical for interacting with CLOCK (29). In both the BMAL1 and CLOCK, two flexible linker loops connect PAS-A and PAS-B domains. Positively charged bHLH domains of BMAL1 and CLOCK interact with each other and then are bound to the negatively charged DNA backbone (Figure 1) (30). The bHLH domains have critical hydrophobic core amino acids. For

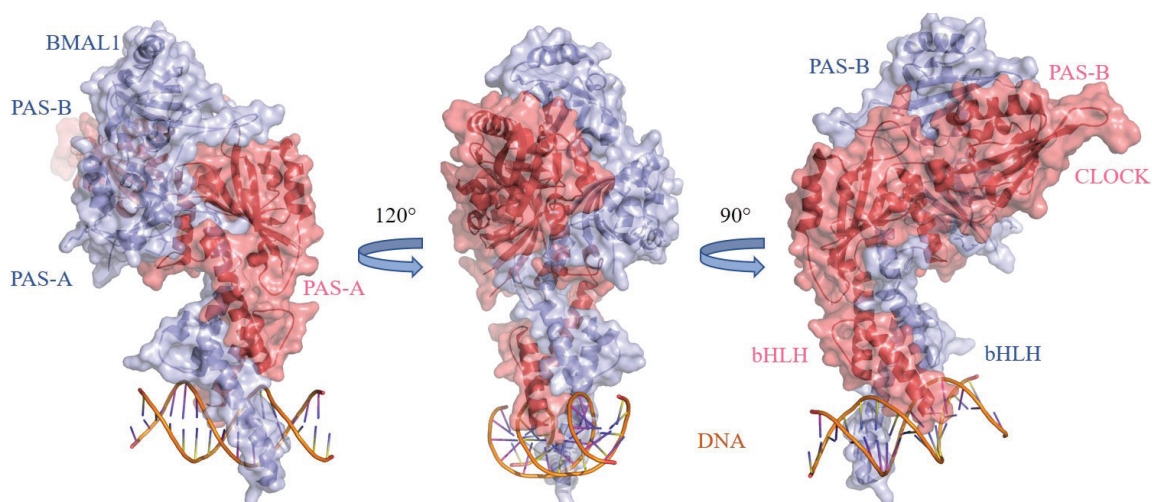


Figure 1. Superimposed crystal structures of BMAL1-CLOCK-E-Box complex (PDB id: 4f3l and 4h10). BMAL1 is shown in blue, CLOCK is shown in red. Backbone of DNA is shown in orange.

example, Leu57, Leu74 of BMAL1 and Leu95, Leu115 of CLOCK were determined as critical hydrophobic amino acids in which mutating to glutamate diminished the transactivation property of BMAL1/CLOCK. In addition to the transactivation, these core hydrophobic amino acids are critical for heterodimer formation (29).

BMAL1 and CLOCK are two main transcriptional factors driving the circadian clock, therefore, determining and understanding the effect of these two proteins' SNPs in the population will advance the relationship between the circadian clock and disease; and help elucidate the molecular mechanism details of the circadian clock. While core clock genes have some paralogs (i.e., *Cry1* and *Cry2*; *Per1-Per2-Per3*; *Clock* and *Npas*), *Bmal1* has no such paralog. It is, therefore, expected that any disruption in the BMAL1 function or stability may disrupt the clock mechanism. So, the characterization of BMAL1 SNPs is of great importance. In this report, we analyzed thousands of SNPs deposited in the Ensembl database by using multiple computational tools. According to the pathogenicity criteria of various in silico analyses in the Ensembl, we ended up with twelve CLOCK and twelve BMAL1 SNPs. We expanded our calculations by using other computational tools and determined the most pathogenic SNPs by giving them pathogenicity scores. Although in silico analyses, per se, are not enough to conclude the effect of SNPs on any biological system, they provide a rational perspective for choosing a manageable number of SNPs for wet-lab experiments. By reporting pathogenic CLOCK and BMAL1 SNPs, we provided a starting point for experimental studies to analyze the effect of deleterious CLOCK and BMAL1 SNPs on the circadian clock mechanism.

MATERIALS AND METHODS

SNPs studied in this manuscript were retrieved from the Ensembl databank. Explanation of various in silico methods used to determine the effect of SNPs on BMAL1, CLOCK or BMAL1/CLOCK heterodimer are given below.

SIFT uses multiple sequence alignment approaches to determine the effect of mutations on a protein sequence (31). SIFT works in the following way: i) similar sequences are searched, ii) sequences that can show similar functions to the query sequence are selected, iii) multiple sequence alignments among selected sequences are determined, iv) normalized amino acid probability for each amino acid position is calculated. If the probability of normalized tolerability is less than 0.05, the mutation is classified as "Deleterious", if the probability is more than 0.05, it is classified as "Benign."

PolyPhen (version 2) predicts the effect of a mutation on the function of the protein by using empirical rules (32). Values larger than 0.908 were evaluated as "Probably Damaging," and values 0.446-0.908 were evaluated as "Possibly Damaging".

CADD integrates multiple parameters to one by comparing naturally selected variants and simulated mutations. The C-scores were related to the allelic variations, the pathogenicity of cod-

ing and non-coding variants, the regulating effects are determined experimentally, and a high level of pathogenic variants among individual genome sequences. CADD qualitatively prioritize functional, benign, and deleterious mutations among various functional categories, and the impact and genetic architectures (33). CADD scores larger than 30 are evaluated as "Deleterious".

REVEL is an ensemble method used to predict the pathogenicity of mutation that integrates MutPred, FATHMM, VEST, PolyPhen, SIFT, PROVEAN, MutationAssesor, MutationTaster, LRT, GERP, SiPhy, phyloP and phastCons (34). Values larger than 0.5 are classified as "Likely Disease Causing."

MetalR predicts the pathogenicity of missense mutations by integrating nine independent pathogenic scores and allele frequency using the logistic regression method. Variants are scored between 0 and 1, and the higher scored ones have a higher risk of being deleterious (35).

Mutation Assesor predicts the functional effect of amino acids by using evolutionary conservation of amino acids among homologous proteins. The program scores mutations between 0 and 1, then, classifies them as neutral, low, intermediate, or high. The higher the scores, the higher the risk of pathogenicity (36). Values greater than 0.93 are classified at high risk of pathogenicity.

I-Mutant is a neural network that calculates the protein stability change upon a single mutation. A protein sequence is given to the program in the FASTA format. I-Mutant can calculate the free-energy change ($\Delta\Delta G$) between mutant and wild-type proteins with the help of the FoldX program (37). According to the program output, if $\Delta\Delta G < 0$ then the mutation destabilizes the protein, and if $\Delta\Delta G > 0$ then the mutation stabilizes the protein.

PROVEAN predicts the effect of a single missense or indel mutation on the function of a protein. The program uses a fast algorithm, that allows calculations of all possible mutations of amino acids in mouse and human proteins (38). If the score is < 2.5 , it destabilizes the protein and its function.

FoldX is an algorithm that qualitatively predicts the interaction and stability of proteins upon mutation(s). The program enables a comparison between wild-type and mutant protein in the form of van der Waals interaction and reports a free energy change ($\Delta\Delta G$) (39). If $\Delta\Delta G$ reported by the program > 0 , the mutation destabilizes the protein or interaction and if $\Delta\Delta G < 0$, the mutation stabilizes the protein or interaction.

FireDock is a web server that allows a refinement of protein-protein interaction by calculating binding energies via the molecular docking approach (40). The program performs local and global minimization by letting side chains find the optimum conformation and then calculates the binding energy of docked proteins. The more negative the binding energy, the more stable structure was.

Multiple sequence alignment was performed by using EMBL Multiple Sequence Comparison by the Log-Expectation (MUSCLE) server (41). Jalview software was used to visualize the sequence alignment results (42).

Open source Pymol software was used to visualize and generate protein figures (43).

RESULTS

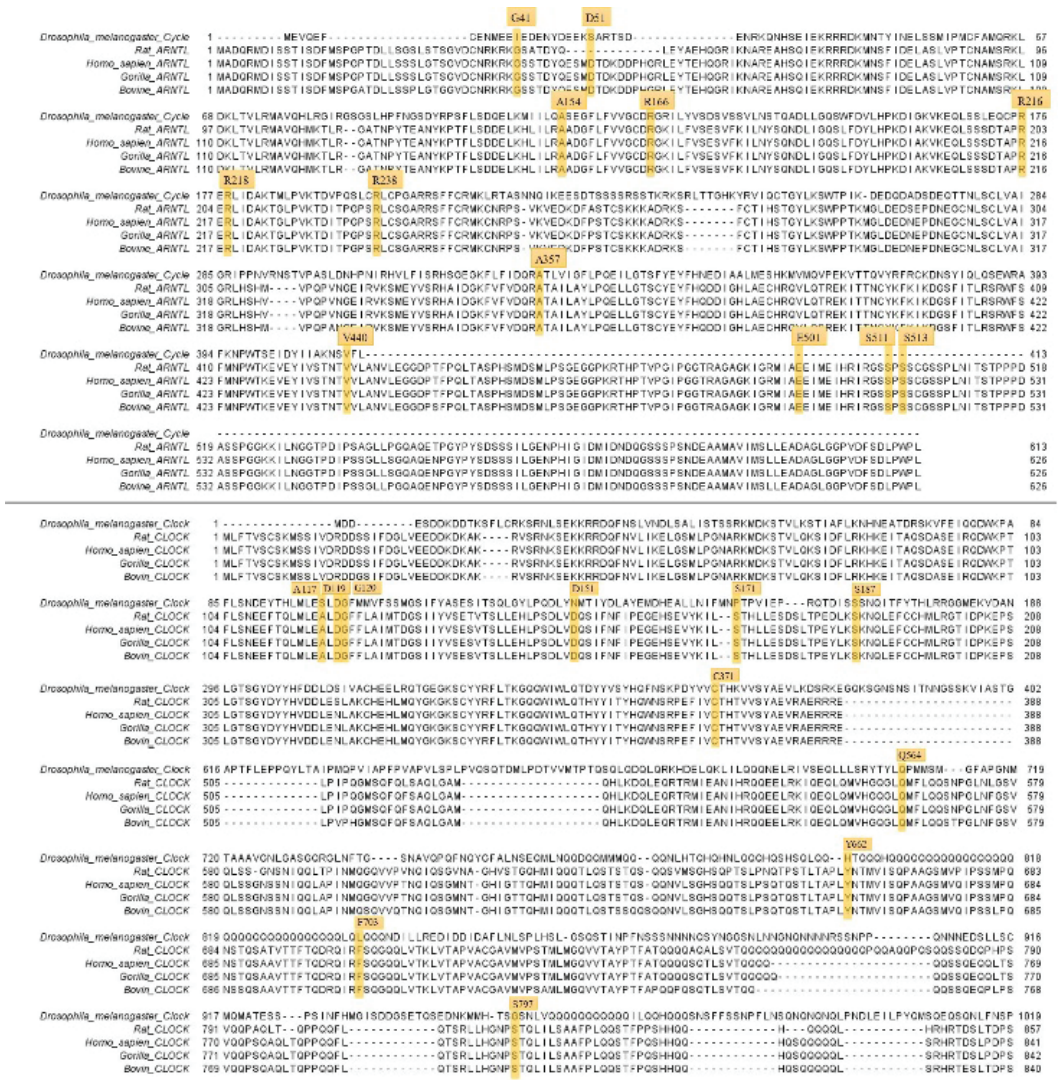
Initially, all CLOCK and BMAL1 SNPs were searched through the Ensembl database. For this purpose, we searched "CLOCK" and "ARNTL" (BMAL1) genes, one by one, in the "Human" species. Then, CLOCK (Human Gene) or ARNTL (Human Gene) were selected on the next page. "Variant table" on the left was selected and the "Filters" option appears. The following criteria were used to select SNPs: Class=SNP; Consequences=missense variant; SIFT=0-0.05; PolyPhen=0.9-1; CADD>30. More options can be found under the "Filter Other Columns" option. As a result, 71 variants for BMAL1 and 42 variants for CLOCK were obtained from the databank. Since BMAL1 is expressed in several isoforms, in the Ensembl database the same SNPs could be seen multiple times because the SNP was reported in different transcripts. We, therefore, selected ENST00000389707.8 transcripts (NP_001025443.1) for the sake of unifying the amino acid numbers in SNPs. A similar approach was used for CLOCK SNPs and ENST00000309964.8 transcript (NP_001254772.1) was selected. After eliminating the variants reported multiple times, we end up with 12 variants for BMAL1 and 12 variants for CLOCK. Multiple sequence alignment of BMAL1 and CLOCK among some vertebrates (e.g. bovin, gorilla, and rat) and *Drosophila melanogaster* which has a strong circadian clock system showed that almost all selected amino acids are conserved in these species (Figure 2). Since some in silico tools take advantage of available protein structures, we also classified variants as "structural" for those that are available on the crystal structures (PDB id: 4h10, 4f3l) and "non-structural" for those that were not resolved on the crystal. To determine "structural" variants we superimposed two crystal structures. Functional PAS and bHLH domains, and E-Box (DNA) were labeled on the aligned structures (Figures 1 and 3). Out of 12 BMAL1 variants, five of them were "structural" and seven of them were "non-structural". CLOCK had eight "structural," and four "non-structural" variants (Table 1).

The "Structural" SNPs of BMAL1 and CLOCK are shown on the BMAL1-CLOCK complex (Figure 3). Arg166 and Val440 are located on the surface of BMAL1 and are exposed to solvent. Ala154 and Arg238 are found on the BMAL1 PAS-A domain and both are interacting with CLOCK. Ala357 is found on the PAS-B domain and buried inside the BMAL1 (Figure 3A). Asp151, Ser171 and Ser187 are located on the surface of CLOCK and the PAS-A domain. Ala117, Asp 119 and Gly120 are also found on the PAS-A domain, however, located inside the CLOCK and interact with BMAL1. Cys371 is found in the CLOCK PAS-B domain and is located in a hydrophobic region (Figure 3B). The SNPs found on the BMAL1-CLOCK interaction site are shown with an asterisk (*) in Tables 2 and 3.

All SNPs SIFT, Poly-Phen, CADD, REVEL, MetaR, Mutation Assessor, and PhD-SNP values were evaluated. In addition, I-Mutant, PROVEAN, Dynamut, and FireDock software/web-servers were used for "structural" variants to evaluate the effect of mutations on BMAL1-CLOCK binding or change in the stability of proteins. Results are shown in Tables 2 and 3 for CLOCK and BMAL SNPs.

If the SIFT score is less than 0.05, it is classified as "Deleterious." If the Poly-Phen value is larger than 0.908, then it is evaluated as "Probably Damaging." If the CADD score is larger than 30, it is evaluated as "Deleterious". At the beginning of the SNP selection from the Ensembl database we used these three scores to select "Deleterious" mutations. All BMAL1 and CLOCK mutations were deleterious according to SIFT, Poly-Phen and CADD (Tables 2 and 3). Although there was no certain cut-off value for REVEL, scores larger than 0.5 are classified as "disease causing." Three structural BMAL1 SNPs (Arg166Gln, Val440Gly and Ala154Val) and six structural CLOCK SNPs (Cys371Gly, Ser171Phe, Gly120Val, Gly120Ser, Asp119Val and Ala117Val) were disease causing according to their REVEL values. The PhD-SNP probability score is calculated between 0 and 1; scores more than 0.5 are evaluated as pathogenic. One non-structural BMAL1 SNP (Asp51Tyr), and four structural BMAL1 SNPs (Arg166Gln, Val440Gly, Ala357Thr and Ala154Val) were evaluated as pathogenic by PhD-SNP (Table 2). All CLOCK SNPs, non-structural Ser797Leu and structural Asp151His, were classified as pathogenic by the same program (Table 3). I-Mutant calculated the free energy change ($\Delta\Delta G$) upon mutation in which mutants causing $\Delta\Delta G < 0$ are evaluated as destabilizing. All BMAL1 SNPs were determined as destabilizing by I-Mutant (Figure 4A). The same calculation for CLOCK SNPs showed that all except non-structural Tyr662Cys and structural Ser171Phe were destabilizing mutants (Table 3). PROVEAN is a useful tool to predict the effect of a single missense mutation on the stabilization and function of a protein. If the PROVEAN score is < 2.5 , it can destabilize the protein and its function (38). All BMAL1 SNPs except two non-structural Glu501Lys and Gly41Arg SNPs turned out to be deleterious by the PROVEAN. The same analysis for CLOCK SNPs showed that all but one non-structural Ser797Leu and one structural Ser187Pro SNPs were deleterious. Finally, FireDock server was used to calculate the binding energy between wild-type BMAL1 and CLOCK, and between BMAL1-CLOCK variants found in the interaction site. Since FireDock calculates physical binding energy, lower binding energy means a stronger interaction. We calculated $\Delta\Delta G$ binding energy by subtracting the binding energy of wild-type BMAL1-CLOCK from the binding energy of SNPs ($\Delta\Delta G_{\text{binding energy}} = \Delta G_{\text{SNP}} - \Delta G_{\text{WT}}$). $\Delta\Delta G < 0$ means stabilized interaction between proteins. Interestingly, all SNPs found in the BMAL1-CLOCK interface stabilized the interaction. While both BMAL1 interface SNPs showed a strong effect (> 1 kcal/mol) on BMAL1-CLOCK binding energy, two out of four CLOCK interface SNPs showed a similar but less potent effect than BMAL1 SNPs on the binding energy (Figure 4B).

A



B

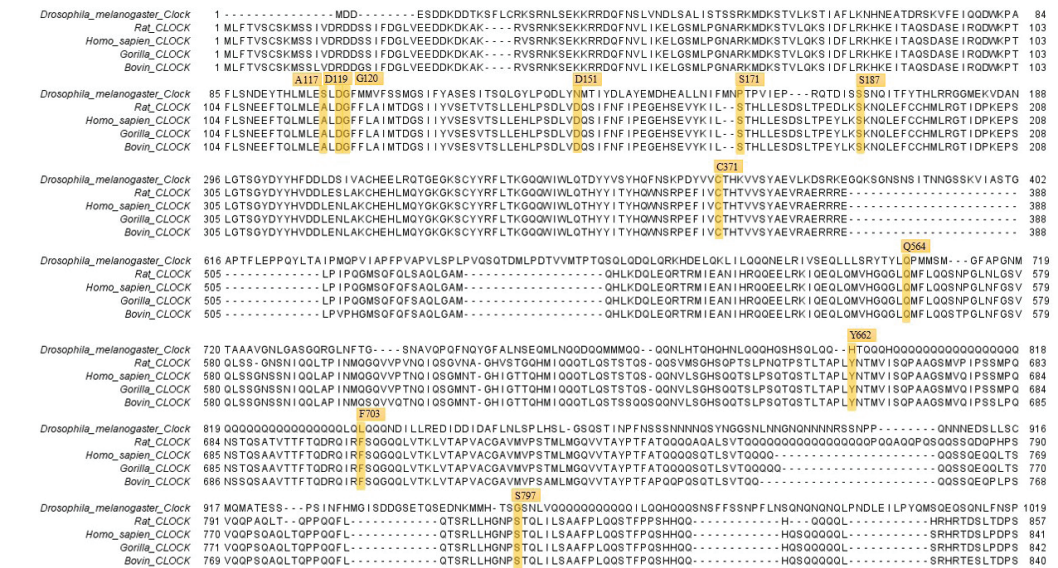


Figure 2. Multiple sequence alignment of A) BMAL1, B) CLOCK from human, *Drosophila melanogaster*, gorilla, bovine, and rat.

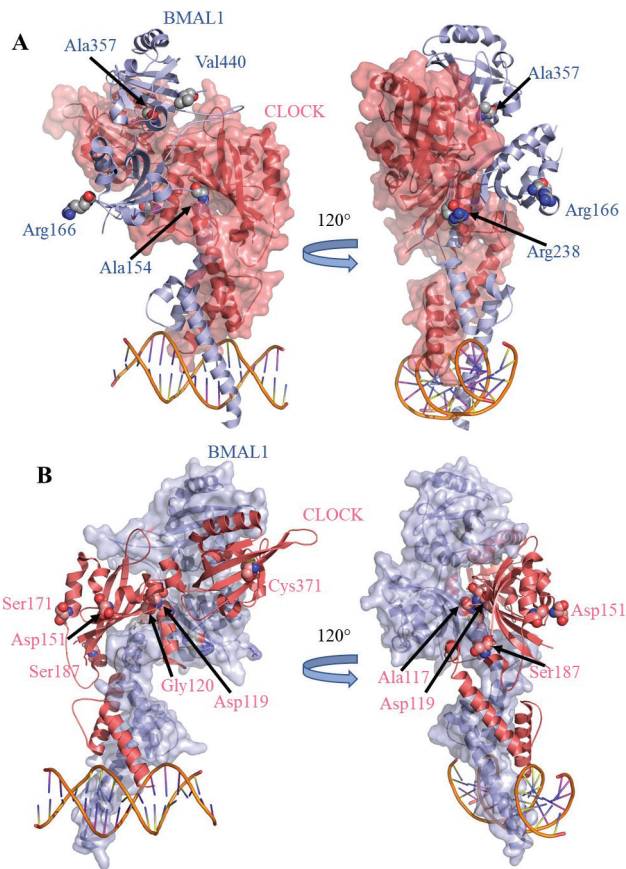


Figure 3. Position of “structural” SNPs of A) BMAL1 and B) CLOCK. In A) BMAL1 is shown in blue cartoon, SNPs are shown in sticks, CLOCK is shown in red surface representations. In B) CLOCK is shown in red cartoon, SNPs are shown in sticks, BMAL1 is shown in blue surface representations.

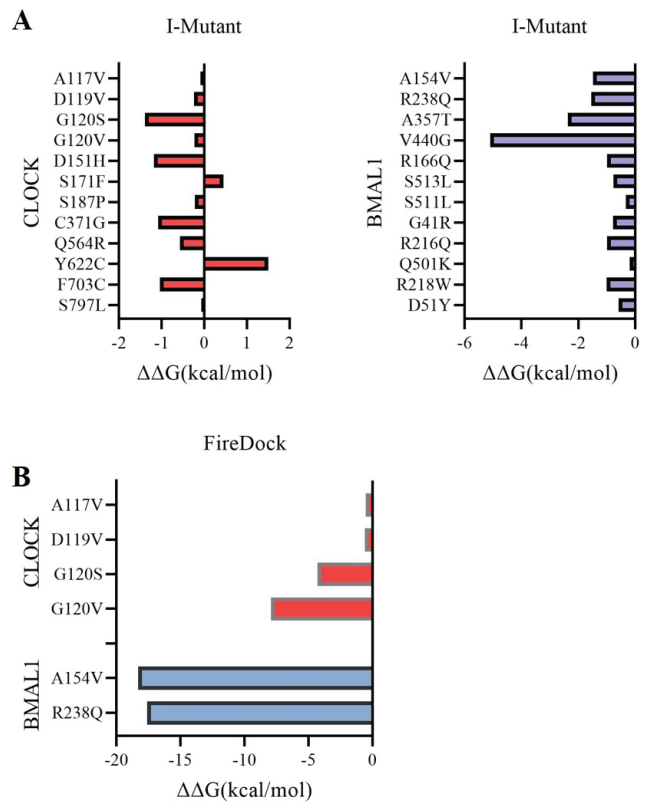


Figure 4. $\Delta\Delta G$ (kcal/mol) values calculated by A) I-Mutant for all SNPs, B) FireDock program for BMAL1-CLOCK interacting amino acids.

Table 1. List of all single nucleotide polymorphisms (SNPs) selected from the Ensembl database

	Structural		Non-structural	
	SNP ID	Amino acid change	SNP ID	Amino acid change
BMAL1	rs1226276621	Arg166Gln	rs1163932326	Asp51Tyr
	rs1450371323	Val440Gly	rs757010873	Arg218Trp
	rs746713814	Ala357Thr	rs146679326	Glu501Lys
	rs1434856001	Arg238Gln	rs368050146	Arg216Gln
	rs768337963	Ala154Val	rs771438108	Gly41Arg
			rs762595978	Ser511Leu
CLOCK			rs1316220783	Ser513Leu
	rs1406765260	Cys371Gly	rs953927923	Ser797Leu
	rs1204057040	Ser187Pro	rs1178386174	Phe703Cys
	rs768013881	Ser171Phe	rs763646149	Tyr662Cys
	rs375936156	Asp151His	rs752522729	Gln564Arg
	rs767225278	Gly120Val		
	rs1445208701	Gly120Ser		
	rs1289814329	Asp119Val		
	rs999814126	Ala117Val		

Table 2. Brain and muscle ARNT-Like 1 (BMAL1) single nucleotide polymorphisms (SNPs) and scores of in silico prediction tools.

	SNP ID	Amino acid change	SIFT	PolyPhen	CADD	REVEL	MetaLR	Mutation Assessor	PROVEAN
Non-Structural	rs1163932326	Asp51Tyr	0	0.912	32	0.305	0.269	0.472	Disease -3.02
	rs757010873	Arg218Trp	0	0.999	32	0.401	0.11	0.883	Neutral -6.79
	rs146679326	Glu501Lys	0	0.991	32	0.25	0.24	0.819	Neutral -2.1
	rs368050146	Arg216Gln	0	0.989	32	0.478	0.091	0.612	Neutral -3.83
	rs771438108	Gly41Arg	0	0.999	30	0.379	0.179	0.535	Neutral -2.11
	rs762595978	Ser511Leu	0.02	0.99	31	0.187	0.285	0.805	Neutral -2.92
	rs1316220783	Ser513Leu	0.02	0.978	32	0.267	0.162	0.831	Neutral -2.72
Structural	rs1226276621	Arg166Gln	0	0.996	31	0.521	0.26	0.745	Disease -3.74
	rs1450371323	Val440Gly	0	0.971	30	0.702	0.16	0.695	Disease -4.78
	rs746713814	Ala357Thr	0.01	0.998	33	0.371	0.14	0.800	Disease -3.82
	rs1434856001*	Arg238Gln*	0.03	0.994	32	0.431	0.102	0.330	Neutral -2.83
	rs768337963*	Ala154Val*	0.04	0.997	32	0.576	0.377	0.869	Disease -3.11

Table 3. Circadian locomotor output cycles kaput (CLOCK) single nucleotide polymorphisms (SNPs) and scores of in silico prediction tools.

	SNP ID	Amino acid change	SIFT	PolyPhen	CADD	REVEL	MetaLR	Mutation Assessor	PROVEAN
Non-Structural	rs953927923	Ser797Leu	0	0.966	32	0.339	0.069	0.480	Neutral -1.83
	rs1178386174	Phe703Cys	0	0.962	31	0.495	0.062	0.700	Disease -2.98
	rs763646149	Tyr662Cys	0.02	0.96	31	0.205	0.055	0.700	Disease -3.31
	rs752522729	Gln564Arg	0	0.999	33	0.373	0.118	0.753	Disease -2.703
Structural	rs1406765260	Cys371Gly	0	0.998	31	0.661	0.107	0.420	Disease -10.831
	rs1204057040	Ser187Pro	0.02	0.932	32	0.142	0.043	0.385	Disease -2.362
	rs768013881	Ser171Phe	0.01	0.969	31	0.639	0.163	0.906	Disease -3.984
	rs375936156	Asp151His	0	0.976	31	0.431	0.088	0.237	Neutral -4.39
	rs767225278*	Gly120Val*	0	0.999	32	0.705	0.249	0.950	Disease -8.11
	rs1445208701*	Gly120Ser*	0	0.983	32	0.642	0.147	0.809	Disease -5.34
	rs1289814329*	Asp119Val*	0	0.996	33	0.762	0.217	0.934	Disease -8.24
	rs999814126*	Ala117Val*	0	0.99	32	0.678	0.107	0.898	Disease -3.74

Table 4. Pathogenic score of all single nucleotide polymorphisms (SNPs). Pathogenic predictions are highlighted.

		SNP ID	Amino acid change	SIFT	PolyPhen	CADD	REVEL	Mutation Assessor	PhD-SNP	Provean	I-Mutant	Pathogenicity Score		
BMAL1	Non-Structural	rs1163932326	Asp51Tyr	0	0.912	32	0.305	0.472	Disease	Deleterious	-0.59	6		
		rs757010873	Arg218Trp	0	0.999	32	0.401	0.883	Neutral	Deleterious	-1.00	5		
		rs146679326	Glu501Lys	0	0.991	32	0.25	0.819	Neutral	Neutral	-0.20	4		
		rs368050146	Arg216Gln	0	0.989	32	0.478	0.612	Neutral	Deleterious	-0.99	5		
		rs771438108	Gly41Arg	0	0.999	30	0.379	0.535	Neutral	Neutral	-0.78	4		
		rs762595978	Ser511Leu	0.02	0.99	31	0.187	0.805	Neutral	Deleterious	-0.33	5		
		rs1316220783	Ser513Leu	0.02	0.978	32	0.267	0.831	Neutral	Deleterious	-0.76	5		
	Structural	rs1226276621	Arg166Gln	0	0.996	31	0.521	0.745	Disease	Deleterious	-0.99	7		
		rs1450371323	Val440Gly	0	0.971	30	0.702	0.695	Disease	Deleterious	-5.10	7		
		rs746713814	Ala357Thr	0.01	0.998	33	0.371	0.800	Disease	Deleterious	-2.37	6		
		rs1434856001*	Arg238Gln*	0.03	0.994	32	0.431	0.330	Neutral	Deleterious	-1.54	5		
		rs768337963*	Ala154Val*	0.04	0.997	32	0.576	0.869	Disease	Deleterious	-1.48	7		
		CLOCK	Non-Structural	rs953927923	Ser797Leu	0	0.966	32	0.339	0.480	Neutral	Neutral	-0.07	4
				rs1178386174	Phe703Cys	0	0.962	31	0.495	0.700	Disease	Deleterious	-1.04	6
				rs763646149	Tyr662Cys	0.02	0.96	31	0.205	0.700	Disease	Deleterious	1.50	5
rs752522729	Gln564Arg			0	0.999	33	0.373	0.753	Disease	Deleterious	-0.57	6		
Structural	rs1406765260		Cys371Gly	0	0.998	31	0.661	0.420	Disease	Deleterious	-1.08	7		
	rs1204057040		Ser187Pro	0.02	0.932	32	0.142	0.385	Disease	Neutral	-0.22	5		
	rs768013881		Ser171Phe	0.01	0.969	31	0.639	0.906	Disease	Deleterious	0.45	6		
	rs375936156		Asp151His	0	0.976	31	0.431	0.237	Neutral	Deleterious	-1.18	5		
rs767225278*	Gly120Val*	0	0.999	32	0.705	0.950	Disease	Deleterious	-0.23	8				
rs1445208701*	Gly120Ser*	0	0.983	32	0.642	0.809	Disease	Deleterious	-1.39	7				
rs1289814329*	Asp119Val*	0	0.996	33	0.762	0.934	Disease	Deleterious	-0.24	8				
rs999814126*	Ala117Val*	0	0.99	32	0.678	0.898	Disease	Deleterious	-0.09	7				

DISCUSSION

The SNP is a single nucleotide difference among gene sequences of the canonical population. SNPs causing missense mutation to change an amino acid to a different one. Some SNPs and exon skipping mutations of core circadian clock genes are related to sleep and mood disorders (24-26,44,45). Specifically, a PER2 SNP (Ser662Gly) was detected in the population having ASPS (24). Similarly, a CRY2 SNP causing Ala260Thr mutation was also associated with ASPA (45). In common, both PER2 and CRY2 mutations destabilized the protein and changed the timing of the circadian clock. In addition to understanding the disease mechanism, characterization of rare SNPs helps to understand the clock mechanism better. A recent study, analyzing the effect of CRY1 SNPs on the clock mechanism, showed that

CRY1 is an allosterically regulated protein (27). Another study dealing with the effect of CRY2 SNPs showed that secondary pocket amino acids are important for nuclear localization and stability of CRY2 (28). Thus, understanding the effect of clock genes' SNPs on the circadian clock is an active research field.

For this purpose, we identified pathogenic missense SNPs in the Ensembl database by using various in silico tools. Our initial analysis by using pathogenicity criteria of SIFT, PolyPhen, and CADD showed that there were 12 SNPs for both BMAL1 and CLOCK in the Ensembl database (Table 1). Since some software used protein structures for analysis, we classified SNPs as "structural" and "non-structural" according to the presence of amino acids available on crystal structures (pdb id: 4f3l, 4h10) (Table 1). As a result, seven non-structural and five structural SNPs for

BMAL1; and four structural and eight non-structural SNPs for CLOCK were determined (Table 1) (Figure 3). Multiple sequence alignment revealed that in vertebrates all analyzed amino acids of BMAL1 were conserved except Asp51 in rat (Figure 2A). In *Drosophila*, Gly41 and Asp51 are replaced with isoleucine and serine, respectively. In addition to these two amino acids, *Cycle* protein has a lack of C-terminal and only 413 amino acids; Glu501, Ser511, and Ser513 of human BMAL1 do not exist in the fly *Cycle* protein. Among CLOCK proteins analyzed in Figure 2B, all studied SNP amino acids are conserved in vertebrates. However, only Asp119, Gly120, Ser187, Cys371, and Gln564 amino acids are conserved in the *Clock* protein of *Drosophila melanogaster* (Figure 2B). Other than Ala117 of fly *Clock*, all SNPs found on the BMAL1-CLOCK interaction interface are conserved among the analyzed species (Figure 2).

The REVEL program predicted only three structural Arg166Gln, Val440Gly and Ala154Val BMAL1 SNPs, and six structural Cys371Gly, Ser171Phe, Gly120Val, Gly120Ser, Asp119Val and Ala117Val CLOCK SNPs as disease-causing. The PhD-SNP software predicted that one non-structural Asp51Tyr, and four structural Arg166Gln, Val440Gly, Ala357Thr and Ala154Val BMAL1 SNPs as pathogenic (Table 2). The same program classified all CLOCK SNPs other than non-structural Ser797Leu and structural Asp151His as pathogenic (Table 3). The MetaR program uses multiple in silico prediction programs and scores the mutation. Although there is no certain cut-off score to evaluate mutations as pathogenic by the MetaR program, a larger score means a higher risk of being pathogenic. PROVEAN predicts that all BMAL1 SNPs except two non-structural Glu501Lys and Gly41Arg were deleterious. The same program predicted all but one non-structural Ser797Leu and one structural Ser187Pro SNPs of CLOCK as deleterious. The mutation assessor classified only two structural CLOCK SNPs Asp119Val and Gly120Val as pathogenic.

According to I-Mutant, if the free energy change ($\Delta\Delta G$) upon mutation < 0 , it is a destabilizing mutation. The I-Mutant predicted that all BMAL1 SNPs were destabilizing (Figure 4A). Similarly, all CLOCK SNPs, other than Ser171Phe and Tyr622Cys were destabilizing mutants (Figure 4A). To better understand the I-Mutant results we analyzed proteins according to the hydrophobicity of amino acids. Ala357 and Val440 of BMAL1 are buried in a hydrophobic region. Since glycine and threonine are less hydrophobic than valine and alanine, respectively, disruption of these hydrophobic cores might destabilize the protein. Ala154 is remarkably close to a region rich in basic amino acids. Thus, the Ala154Val mutation that introduced a more hydrophobic amino acid may destabilize the protein. The side chains of Ala117 and Gly120 of CLOCK are located near a hydrophobic region. Therefore, Ala117Val and Gly120Val mutations which are also hydrophobic amino acids did not destabilize the protein. However, Gly120Ser mutation which introduced a polar amino acid destabilized the protein. When Asp151 is exposed to solvent and because of its negative charge, it can be found in H-bond interactions with surrounding water molecules. Asp151His mutation may decrease the number and strength of H-bond interactions since histidine

is mostly neutral around the physiological pH. Therefore, Asp151His mutation is a destabilizing mutation.

To predict the binding energy change in BMAL1-CLOCK interaction upon introducing SNPs, we used the FireDock server. The server calculates physical binding energy and if $\Delta\Delta G$ after mutation < 0 , it means a stabilized energy (in contrast to I-Mutant). FireDock predicted that all SNPs found on the interaction interface were stabilizing the BMAL1-CLOCK interaction (Figure 4B). It showed that a gain of function mutation on BMAL1 and CLOCK caused a stronger interaction between them, but it did not affect the circadian rhythm in cell-based circadian assays. Similarly, the same mutations had a subtle effect on BMAL1-CLOCK dependent transactivation (29). On the other hand, loss of function mutations that weakened the BMAL1-CLOCK binding significantly abolished the transactivation (29). Since the FireDock analysis predicted that all SNPs had a better binding energy than the wild-type, these mutants should not have a detrimental effect on the BMAL1-CLOCK transactivation.

Finally, we generated a table that collectively gives a score for each analysis. If an SNP was predicted as pathogenic or destabilizing by a program, the SNP gets a score of 1. A higher overall score means a higher risk of pathogenicity. For this, we used results from the SIFT, PolyPhen, CADD, REVEL, PhD-SNP, PROVEAN, Mutation Assessor and I-Mutant analysis. So, an SNP could get the highest score of 8. Our results showed that structural CLOCK SNPs: Gly120Val and Asp119Val got the highest score of 8; Cys371Gly, Gly120Ser, and Ala117Val got 7; BMAL1 structural SNPs Arg166Gln, Val440Gly, and Ala154Val also got 7 (Table 4). The highest scored SNPs can have a significant effect on the BMAL1-CLOCK activity and may disrupt the robust ticking of the circadian clock mechanism.

Despite the fact that Gly41Arg SNP got a pathogenicity score of 4, the amino acid is at the end of the nuclear localization signal sequence which is important for nuclear translocation of BMAL1 and CLOCK (46). Since BMAL1 carries CLOCK to the nucleus, if BMAL1 cannot translocate to the nucleus neither can CLOCK. So, if this SNP interferes with BMAL1 translocation, it may disrupt the clock mechanism.

Cys371Gly obtained a pathogenicity score of 7 and should be analyzed in detail. Recently, it was found that the side chain of Cys195 (-SH) of CLOCK can be oxidized to sulfenic acid (-SOH) depending on the amount of H_2O_2 (47). As a result, oxidized Cys195 stabilized the CLOCK-BMAL1 interaction and enhanced the transactivation. Since all cysteine amino acids can be oxidized, this possibility should be considered while experimentally analyzing the effect of Cys371Gly.

Heme can bind to CLOCK and may interfere with CLOCK binding to E-Box and regulate the circadian clock (48,49). His141 was critical for Heme binding. In the CLOCK amino acids we studied, Ala117, Asp119, Gly120, and Asp151 surrounded His141 in the crystal structure. These SNPs can affect the orientation of the His141 side chain and heme binding.

CONCLUSION

Among the thousands of SNPs in the Ensemble database, we filtered out only missense mutation with high pathogenic probability. After applying pathogenic criteria of SIFT, PolyPhen, and CADD, we studied 12 SNPs using various in silico tools. In spite of the fact that these in silico tool analysis were not adequate to make general conclusions about the effect of SNPs on biological systems, they are useful to narrow down the number of SNPs for experimental studies. Thus, the in silico analysis help to save time and budget. Researchers aiming to experimentally analyze the effect of CLOCK and BMAL1 SNPs on the clock mechanism should give priority to those highlighted in this study.

Peer Review: Externally peer-reviewed.

Conflict of Interest: Author declared no conflict of interest.

Financial Disclosure: Author declared no financial support.

REFERENCES

1. Dunlap JC. Molecular bases for circadian clocks. *Cell* 1999; 96(2): 271-90.
2. Panda S, Antoch MP, Miller BH, Su AI, Schook AB, Straume M, et al. Coordinated transcription of key pathways in the mouse by the circadian clock. *Cell* 2002; 109(3): 307-20.
3. Sancar G, Brunner M. Circadian clocks and energy metabolism. *Cell Mol Life Sci* 2014; 71(14): 2667-80.
4. Turek FW, Joshu C, Kohsaka A, Lin E, Ivanova G, McDearmon E, et al. Obesity and metabolic syndrome in circadian Clock mutant mice. *Science* 2005; 308(5724): 1043-45.
5. Nernpermpisooth N, Qiu SQ, Mintz JD, Suvitayavat W, Thirawarapan S, Rudic DR, et al. Obesity Alters the Peripheral Circadian Clock in the Aorta and Microcirculation. *Microcirculation* 2015; 22(4): 257-66.
6. Damiola F, Le Minh N, Preitner N, Kornmann B, Fleury-Olela F, Schibler U. Restricted feeding uncouples circadian oscillators in peripheral tissues from the central pacemaker in the suprachiasmatic nucleus. *Gene Dev* 2000; 14(23): 2950-61.
7. Mohawk JA, Takahashi JS. Cell autonomy and synchrony of suprachiasmatic nucleus circadian oscillators. *Trends Neurosci* 2011; 34(7): 349-58.
8. Kavakli IH, Sancar A. Circadian photoreception in humans and mice. *Mol Interv* 2002; 2(8): 484-92.
9. Ko CH, Takahashi JS. Molecular components of the mammalian circadian clock. *Hum Mol Genet* 2006; 15: R271-R77.
10. Welsh DK, Logothetis DE, Meister M, Reppert SM. Individual Neurons Dissociated from Rat Suprachiasmatic Nucleus Express Independently Phased Circadian Firing Rhythms. *Neuron* 1995; 14(4): 697-706.
11. King DP, Zhao YL, Sangoram AM, Wilsbacher LD, Tanaka M, Antoch MP, et al. Positional cloning of the mouse circadian Clock gene. *Cell* 1997; 89(4): 641-53.
12. Vitaterna MH, King DP, Chang AM, Kornhauser JM, Lowrey PL, Mcdonald JD, et al. Mutagenesis and Mapping of a Mouse Gene Clock, Essential for Circadian Behavior. *Science* 1994; 264 (5159): 719-25.
13. Bunger MK, Wilsbacher LD, Moran SM, Clendenin C, Radcliffe LA, Hogenesch JB, et al. Mop3 is an essential component of the master circadian pacemaker in mammals. *Cell* 2000; 103(7): 1009-17.
14. Shearman LP, Zylka MJ, Weaver DR, Kolakowski LF, Reppert SM. Two period homologs: Circadian expression and photic regulation in the suprachiasmatic nuclei. *Neuron* 1997; 19(6): 1261-69.
15. Griffin EA, Staknis D, Weitz CJ. Light-independent role of CRY1 and CRY2 in the mammalian circadian clock. *Science* 1999; 286(5440): 768-71.
16. Kume K, Zylka MJ, Sriram S, Shearman LP, Weaver DR, Jin XW, et al. mCRY1 and mCRY2 are essential components of the negative limb of the circadian clock feedback loop. *Cell* 1999; 98(2): 193-205.
17. Hao HP, Allen DL, Hardin PE. A circadian enhancer mediates PER-dependent mRNA cycling in *Drosophila melanogaster*. *Mol Cell Biol* 1997; 17(7): 3687-93.
18. Zhang R, Lahens NF, Ballance HI, Hughes ME, Hogenesch JB. A circadian gene expression atlas in mammals: Implications for biology and medicine. *P Natl Acad Sci USA* 2014; 111(45): 16219-24.
19. Hirano A, Fu YH, Ptacek LJ. The intricate dance of post-translational modifications in the rhythm of life. *Nat Struct Mol Biol* 2016; 23(12): 1053-60.
20. Preitner N, Damiola F, Molina LL, Zakany J, Duboule D, Albrecht U, et al. The orphan nuclear receptor REV-ERB alpha controls circadian transcription within the positive limb of the mammalian circadian oscillator. *Cell* 2002; 110(2): 251-60.
21. Sato TK, Panda S, Miraglia LJ, Reyes TM, Rudic RD, McNamara P, et al. A functional genomics strategy reveals rora as a component of the mammalian circadian clock. *Neuron* 2004; 43(4): 527-37.
22. Kelleher FC, Rao A, Maguire A. Circadian molecular clocks and cancer. *Cancer Lett* 2014; 342(1): 9-18.
23. Scheer FAJL, Hilton MF, Mantzoros CS, Shea SA. Adverse metabolic and cardiovascular consequences of circadian misalignment. *P Natl Acad Sci USA* 2009; 106(11): 4453-58.
24. Fu Y, Jones CR, Toh K, Virshup D, Ptacek LJ. An hPer2 phosphorylation site mutation in familial Advanced Sleep-Phase Syndrome. *Am J Hum Genet* 2001; 69(4): 597-97.
25. Patke A, Murphy PJ, Onat OE, Krieger AC, Ozcelik T, Campbell SS, et al. Mutation of the Human Circadian Clock Gene CRY1 in Familial Delayed Sleep Phase Disorder. *Cell* 2017; 169(2): 203-15.
26. Onat OE, Kars ME, Gul S, Bilguvar K, Wu YM, Ozhan A, et al. Human CRY1 variants associate with attention deficit/hyperactivity disorder. *J Clin Invest* 2020; 130(7): 3885-900.
27. Gul S, Aydin C, Ozcan O, Gurkan B, Surme S, Baris I, et al. The Arg-293 of Cryptochrome1 is responsible for the allosteric regulation of CLOCK-CRY1 binding in circadian rhythm. *J Biol Chem* 2020; 295(50): 17187-99.
28. Parlak GC, Camur BB, Gul S, Ozcan O, Baris I, Kavakli IH. The secondary pocket of Cryptochrome 2 is important for the regulation of its stability and localization. *J Biol Chem* 2022; 102334.
29. Huang NA, Chelliah Y, Shan YL, Taylor CA, Yoo SH, Partch C, et al. Crystal Structure of the Heterodimeric CLOCK:BMAL1 Transcriptional Activator Complex. *Science* 2012; 337(6091): 189-94.
30. Wang ZX, Wu YL, Li LF, Su XD. Intermolecular recognition revealed by the complex structure of human CLOCK-BMAL1 basic helix-loop-helix domains with E-box DNA. *Cell Res* 2013; 23(2): 213-24.
31. Ng PC, Henikoff S. SIFT: predicting amino acid changes that affect protein function. *Nucleic Acids Res* 2003; 31(13): 3812-14.
32. Ramensky V, Bork P, Sunyaev S. Human non-synonymous SNPs: server and survey. *Nucleic Acids Res* 2002; 30(17): 3894-900.
33. Kircher M, Witten DM, Jain P, O'Roak BJ, Cooper GM, Shendure J. A general framework for estimating the relative pathogenicity of human genetic variants. *Nat Genet* 2014; 46(3): 310.
34. Ioannidis NM, Rothstein JH, Pejaver V, Middha S, McDonnell SK, Baheti S, et al. REVEL: An Ensemble Method for Predicting the Pathogenicity of Rare Missense Variants. *Am J Hum Genet* 2016; 99(4): 877-85.

35. Dong CL, Wei P, Jian XQ, Gibbs R, Boerwinkle E, Wang K, et al. Comparison and integration of deleteriousness prediction methods for nonsynonymous SNVs in whole exome sequencing studies. *Hum Mol Genet* 2015; 24(8): 2125-37.
36. Li C, Zhi D, Wang K, Liu X. MetaRNN: Differentiating Rare Pathogenic and Rare Benign Missense SNVs and InDels Using Deep Learning. *bioRxiv* 2021.
37. Capriotti E, Fariselli P, Casadio R. I-Mutant2.0: predicting stability changes upon mutation from the protein sequence or structure. *Nucleic Acids Res* 2005; 33: W306-W10.
38. Choi Y, Chan AP. PROVEAN web server: a tool to predict the functional effect of amino acid substitutions and indels. *Bioinformatics* 2015; 31(16): 2745-47.
39. Schymkowitz J, Borg J, Stricher F, Nys R, Rousseau F, Serrano L. The FoldX web server: an online force field. *Nucleic Acids Res* 2005; 33: W382-W88.
40. Mashiach E, Schneidman-Duhovny D, Andrusier N, Nussinov R, Wolfson HJ. FireDock: a web server for fast interaction refinement in molecular docking. *Nucleic Acids Res* 2008; 36: W229-W32.
41. Madeira F, Pearce M, Tivey ARN, Basutkar P, Lee J, Edbali O, et al. Search and sequence analysis tools services from EMBL-EBI in 2022. *Nucleic Acids Res* 2022; 50(W1): W276-W79.
42. Waterhouse AM, Procter JB, Martin DMA, Clamp M, Barton GJ. Jalview Version 2-a multiple sequence alignment editor and analysis workbench. *Bioinformatics* 2009; 25(9): 1189-91.
43. Schrodinger L. The PyMOL Molecular Graphics System. 2010.
44. Hua P, Liu WG, Chen DH, Zhao YY, Chen L, Zhang N, et al. Cry1 and Tef gene polymorphisms are associated with major depressive disorder in the Chinese population. *J Affect Disorders* 2014; 157: 100-03.
45. Hirano A, Shi G, Jones CR, Lipzen A, Pennacchio LA, Xu Y, et al. A Cryptochrome 2 mutation yields advanced sleep phase in humans. *Elife* 2016; 5.
46. Kwon I, Lee J, Chang SH, Jung NC, Lee BJ, Son GH, et al. BMAL1 shuttling controls transactivation and degradation of the CLOCK/BMAL1 heterodimer. *Mol Cell Biol* 2006; 26(19): 7318-30.
47. Pei JF, Li XK, Li WQ, Gao Q, Zhang Y, Wang XM, et al. Diurnal oscillations of endogenous H2O2 sustained by p66(Shc) regulate circadian clocks. *Nat Cell Biol* 2019; 21(12): 1553-64.
48. Shimizu T, Huang D, Yan F, Stranova M, Bartosova M, Fojtikova V, et al. Gaseous O2, NO, and CO in signal transduction: structure and function relationships of heme-based gas sensors and heme-redox sensors. *Chem Rev* 2015; 115(13): 6491-533.
49. Freeman SL, Kwon H, Portolano N, Parkin G, Venkatraman Girija U, Basran J, et al. Heme binding to human CLOCK affects interactions with the E-box. *Proc Natl Acad Sci U S A* 2019; 116(40): 19911-16.

Inflammation Parameters, Xanthine Oxidase and Anti-Xanthine Oxidase Antibodies in Synovial Fluid of Patients Suffering from Arthritis

Nadjet Hanachi¹ , Lekhmici Arrar¹ 

¹Ferhat Abbas University of Setif, Faculty of Nature and Life Sciences, Laboratory of Applied Biochemistry, Setif, Algeria

ORCID IDs of the authors: N.H. 0000-0002-0019-3127; L.A. 0000-0003-3822-1469

Please cite this article as: Hanachi N, Arrar L. Inflammation Parameters, Xanthine Oxidase and Anti-Xanthine Oxidase Antibodies in Synovial Fluid of Patients Suffering from Arthritis. Eur J Biol 2022; 81(2): 136-143.
DOI: 10.26650/EurJBiol.2022.1097938

ABSTRACT

Objective: Rheumatoid arthritis (RA) is an autoimmune disease where sera and synovial fluid (SF) of suffering patients contain immune complexes formed from autoantibodies to several proteins. SF from humans with joint diseases was examined for the presence of some inflammatory parameters and autoantibodies.

Materials and Methods: Antibodies in their free and complex forms were assayed by indirect ELISA. The immunoprecipitation technique was used to evaluate total IgG and IgM and complement.

Results: The results showed that most RA SF was anti-ASLO negative, but they were CRP positive. Levels of complement components (C3 and C4) were highest in the group of mono-/oligo-arthritis and lowest in RA. The results showed that xanthine oxidase (XO) presence and activity were important in SF of RA patients. Moreover, free and complex anti-XO antibodies were detected in all SF with different titers throughout the groups of patients where IgG was lower than IgM.

Conclusion: The studied parameters of inflammation and auto-antibodies especially against XO could serve as an evaluation of the severity of joint inflammation and in RA pathogenesis understanding.

Keywords: Autoantibodies, joint inflammation, streptolysin, Rheumatoid arthritis, xanthine oxidase, complement

INTRODUCTION

Rheumatoid arthritis (RA) is the most severe and destructive of all joint diseases affecting approximately 1% of the worldwide adult population and more often women than men. In the Western world more than 50% of RA patients are older than 65 years at diagnosis (1). The main pathological changes that occur in RA are of an autoimmune nature, chronic synovitis, cartilage destruction and bone erosion (2,3). It is also the most common systemic autoimmune disease and is characterized by the presence of various autoantibodies in serum and synovial fluid (SF) (4,5). This distinguishes RA from other joint diseases (6) where autoimmune phenomena are rarely observed. The immunological

process is a crucial factor in the pathophysiology of RA with the presence of immune cells like lymphocytes, phagocytes and plasma cells in the pannus (7,8), whereas SF encloses immunoglobulins, complement, and anti- γ -globulins (9,10). Serologically, RA is known by the existence of a variety of autoantibodies like anti-citrullinated protein, anti-carbamylated protein, peptidylarginine deiminase (PAD4) etc., which possess great roles in RA pathogenesis and diagnosis (6). Synovitis is thought to be caused by the action of interleukin-1, tumor necrosis factor-alpha, prostaglandin E2, matrix metalloproteinases and nitric oxide (11). In addition, xanthine oxidase generates reactive oxygen species (ROS), which lead to chronic damage in joints of RA and osteoarthritis patients (12,13). We have pre-



Corresponding Author: Lekhmici Arrar

E-mail: lekharar@univ-setif.dz, lekharar@hotmail.com

Submitted: 04.04.2022 • **Revision Requested:** 09.08.2022 • **Last Revision Received:** 26.09.2022 •

Accepted: 04.10.2022 • **Published Online:** 24.11.2022

Content of this journal is licensed under a Creative Commons Attribution-NonCommercial 4.0 International License.



viously described the presence of active xanthine oxidase and anti-xanthine oxidase antibodies in synovial fluids of patients suffering from different joint inflammations (10,14). The present study aims to evaluate inflammatory parameters in the SF of patients suffering from RA and other joint illness. For this reason, free and complexed anti-xanthine oxidase (XO) antibodies, Anti-Streptolysin antibodies (ASLO), C-reactive protein (CRP), complement factors (C3, C4), and total immunoglobulins (IgG and IgM) were examined. In addition to their diagnostic use, the presence of autoantibodies should give deeper understanding of the mechanism of joint inflammations.

MATERIALS AND METHODS

SF samples were collected from adult volunteers during regular medical examinations in Dr. Zenoun, Dr. Benouar, Dr. Lebani and Dr. Ait Majbar's clinics. Patients and volunteers have signed an informed consent following a detailed explanation of the undertaken procedures. Samples (n=137) were divided into five groups as shown in Table 1: rheumatoid arthritis group (RAG), mono/oligo arthritis group (MOA), a group suffering from gonarthrosis of the knee (GKG), hemarthrosis and mechanical inflammations group (HMI) and with other types of joint inflammations (OJI). Approval was obtained from the ethics local committee (NrECA/003/22). Collected samples were centrifuged at 3000 x g (Hettich Universal centrifuge) for 15 min, then distributed to small aliquots and kept at -20°C until use. To reduce viscosity, an aliquot of each SF was incubated with Hyaluronidase enzyme (Sigma, Germany) at 20 µg/ml of SF, for 3 h at 37°C then centrifuged (15) with modifications, and the supernatant was used in various estimations, in parallel to non-treated SF.

Inclusion and exclusion criteria of RA samples were the same as previously explained by Arrar et al. (10). Human sera, pooled as a standard serum, were obtained from the Centre of blood of Setif. Latex positive sera were collected from Central Laboratory of the University Hospital of Setif, Dr Latri and Dr Messai laboratories (Setif).

Xanthine Oxidase Preparation and Activity

Xanthine oxidase (XO) was purified from human milk, kindly provided by volunteers, according to Baghiani et al. (16) and

Abadeh et al. (17). It was supplemented with 2.5 mM dithioerythritol, 1 mM EDTA and 1.25 mM sodium salicylate. It was centrifuged at 3000 × g for 20 min and the cream was collected. An equal volume of 0.2 M K₂HPO₄, containing 2.5 mM dithioerythritol, 1 mM EDTA and 1.25 mM sodium salicylate was added to the cream, followed by slow addition of cold (-20°C) butanol to give 15% (v/v) and then 15% (w/v) solid (NH₄)₂SO₄ with constant stirring. The resultant slurry was stirred for 1 h and then centrifuged at 13,000 × g for 20 min. The aqueous lower phase was separated and 20% (w/v) solid (NH₄)₂SO₄ was added, with stirring. The suspension was allowed to stand at 4°C for 2 h, after which the separated top phase was collected and centrifuged at 10,000 × g for 30 min. The top phase was again collected and suspended in a small volume of buffer A (0.2 M Na₂HPO₄, containing 2.5 mM dithioerythritol, 1 mM EDTA and 1.25 mM sodium salicylate, pH 6.0) and dialyzed against the same buffer overnight. The precipitate was removed by centrifugation at 40,000 g for 1 h. The supernatant was applied to a column (1 cm/8 cm) of heparin-agarose (Sigma, type 1) equilibrated with heparin buffer. The column was washed with 0.1 M NaCl in buffer A and xanthine oxidase was then eluted by using buffer A, containing, additionally, 5% (w/v) (NH₄)₂SO₄. Protein-containing fractions were combined and dialyzed overnight against 50 mM sodium bicine, pH 8.3 (3L) buffer aliquoted (0.5 ml) and stored at -20°C. The purity of the enzyme was based on protein/flavin ratio (PFR = A₂₈₀/A₄₅₀), and SDS-PAGE using vertical slab gels. XO activity was determined by measuring the generation of uric acid at 295 nm (16).

Anti-XO Antibodies Preparation

Antibodies against XO enzyme were obtained by immunizing New Zealand white rabbits (18). After obtaining IgG by precipitation with 18% sodium sulphate the purity and the immune reactivity were tested by SDS-PAGE and indirect ELISA, respectively (10).

Indirect ELISA Protocol

To determine titers of rabbit immune-serum, normal or latex positive human sera or synovial liquids against XO, 5 µg/ml of human xanthine oxidase (HXO) in NaHCO₃/Na₂CO₃ solution (50 mM, pH 9.6) were coated on well microtitration plates (100 µl).

Table 1. Repartition of sample among different groups of patients

	Group of patients	Number	Age
Synovial fluids	Rheumatoid arthritis (RAG)	26	52±15
	Mono-/oligo-arthritis (MOA)	22	61±19
	Gonarthrosis of the knee (GKG)	24	63±4
	Hemarthrosis/mechanical inflammations (HMI)	30	39±5
	Other joint inflammations (OJI)	35	49±11
Sera	Healthy donors	65	38±13
	Latex positive patients	69	42±12

After overloading of the free sites by casein, series of serum or SF dilutions were added and incubated for 1 h 30 min. at 37°C, then goat anti-rabbit IgG or anti-human IgG/IgM antibodies labeled with horse radish peroxidase diluted in PBS-Tween were added and incubated for 1 h at 37°C. The revelation of the interaction was done by the substrate solution containing orthophenylene diamine (Sigma, Germany) and H₂O₂ (0.07%, v/v) in sodium citrate (0.1 M) Na₂HPO₄ (0.2 M), pH6. After an incubation during 10 to 15 min in the dark, the reaction was stopped with 50 µl/well of H₂SO₄ (1N) and the absorbance measured at 492 nm with a microplate reader (Diagnostics Pasteur LP200), (10).

For XO-anti-XO immune-complex estimation, rabbit anti-HXO serum (diluted 40 times in NaHCO₃/Na₂CO₃, 50mM, pH 9.6) was coated on the microplates then serum or SF was added; after that the same steps as above were followed.

The same steps of ELISA for the titration of antibody, in their free and complex forms, were followed to calibrate standard human serum according to Arrar et al. (10).

Detection of Xanthine Oxidase

For the detection of XO enzyme in SF, the microplates were coated with diluted SF (100 times in NaHCO₃/Na₂CO₃, pH 9.6, 50 mM), and then incubated with a series of dilutions of rabbit anti-XO for 90 min at 37°C. The immune reaction was detected using peroxidase-labeled anti-rabbit IgG.

Determination of Rheumatoid Factor

The detection of RF was conducted using a hemagglutination method according to the manufacturer (Spinreact, Spain). The presence of visible agglutination of erythrocytes indicates a RF concentration equal or greater than 8 IU/ml.

Determination of C-reactive Protein Level

The samples were tested for the detection of CRP by an agglutination test (RapiTex[®] CRP), by dispensing 40 µl of undiluted patient sample and 40 µl of each CRP positive and negative control serum, each onto a different field of a test plate. Absorption solution (40 µl) was dispensed alongside each sample or control sera. A volume of 40 µl of RapiTex-CRP was added to the absorption solution. After thoroughly mixing each set of drops with stirring rods for 2 min., agglutination was checked for 2 min. The sensitivity of the test is approximately 6mg/ml for a sample volume of 40µl when the test is read after 2 min.

Determination of Anti-streptolysin and Complement Components

To detect ASLO antibodies, an agglutination test was used according to the manufacturer's instructions (RapiTex[®]ASLO, 2003). Samples with an ASLO content of ≥200 IU/ml ± 20%, exhibit clear agglutination. Samples with an ASLO content of <200 IU/ml show no agglutination. Also, complement factors (C3c, C4) were assayed following the protocol assigned by the manufacture (Turbiquant[®]). The results are directly given as g/l. The measurement range valid for the TurbiTime System when using 1:21 diluted samples is C3c (0.3- 4.5 g/l) and C4 (0.045- 1.17 g/l).

Determination of Total Immunoglobulins G and M

Turbiquant[®]Immunoglobuline test was used to determine IgG and IgM antibodies in SF and sera. Samples were diluted 1/21 with isotonic saline solution. The vial reagent was placed in the reagent receptacle of the TurbiTime System. Volumes of 20 µl (IgG) and 200 µl (IgM) of the diluted samples were placed in a cuvette. The quantification, given as g/l, is automatically performed after adding the reagent. The measurement range valid for the TurbiTime System when using 1:21 diluted samples is IgG (0.85- 145 g/l) and IgM (0.17- 33.5 g/l).

Statistical Analysis

All results were calculated as three or more determinations and expressed as mean±standard deviation (SD). Statistical analyses were carried out by using SigmaStat. Comparison of groups was carried out with Student's *t* test. P values less than 0.05 were considered statistically significant.

RESULTS

Total IgG and IgM Immunoglobulins in SF

The results obtained show that total IgG and IgM are present in the SF in most cases. IgG are the most represented with the highest concentrations in patients with mono or oligo-arthritis (between 8.41 and 18.60 mg/l) and less in patients with RA, while almost equal in the other samples. For IgM-type antibodies, concentrations are much lower than IgG and the highest percentage was recorded in patients OJI (2.21 mg/l), and the lowest percentage in the GKG samples (Figure 1).

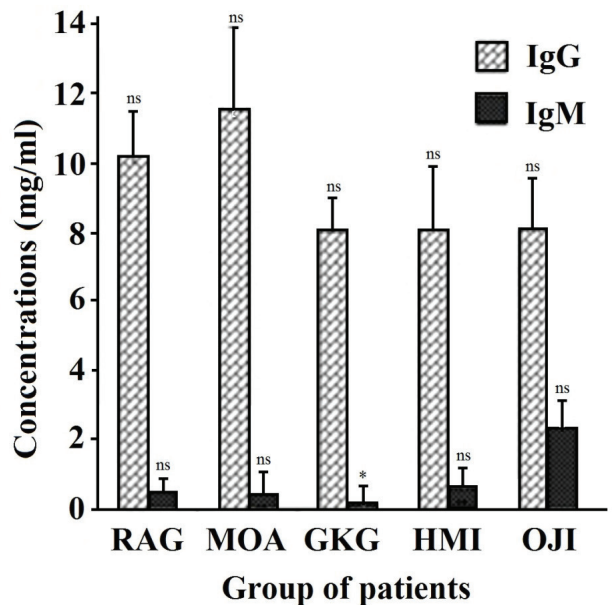


Figure 1. Total IgG and IgM in synovial fluid, using Turbiquant technique.

RAG: Rheumatoid arthritis group, MOA: mono/oligo-arthritis, GKG: gonarthrosis of the knee group, HMI: hemarthrosis/mechanical inflammations, OJI: Other joint inflammations. ns: non-significant, *p<0.05, compared to normal serum.

Inflammation Parameters

Only SF of patients with Rheumatoid arthritis (92.3%) and HMI (50%) were positive for IgM-RF by Latex agglutination test, except a sample of a 20-year-old girl and another of a 57-year-old woman with RA, who were negative (<8 IU/ml; Figure 2). ELISA revealed that SF of all patients was positive except for the group OJI, with the highest percentage in SF from the RAG group.

Results of the detection of CRP are plotted in Figure 2. Samples of subject RAG were mostly positive CRP. This confirms that the incidence was of inflammatory origin. While in the category of mono-/oligo-arthritis (MOA), only 27.27% of the samples were CRP-positive, as well as in the case of HMI (23.33%) and of GKG (18.18%). In the category of OJI, only samples with gout and rheumatoid popliteal cyst were CRP positive.

The test of ASLO antibodies is classified among the rheumatologic markers (19). The results revealed that only two SF from the mono-/oligo-arthritis group were positive (a 44-year-old man with mono-arthritis, and a 68-year-old woman with oligo-arthritis). Also, in GKG only two SF were positive (a 60-year-old woman and an 80-year-old man). In the group with hemarthrosis and mechanical inflammations only one sample was positive (a 40-year-old man with post traumatic injury) (Figure 2).

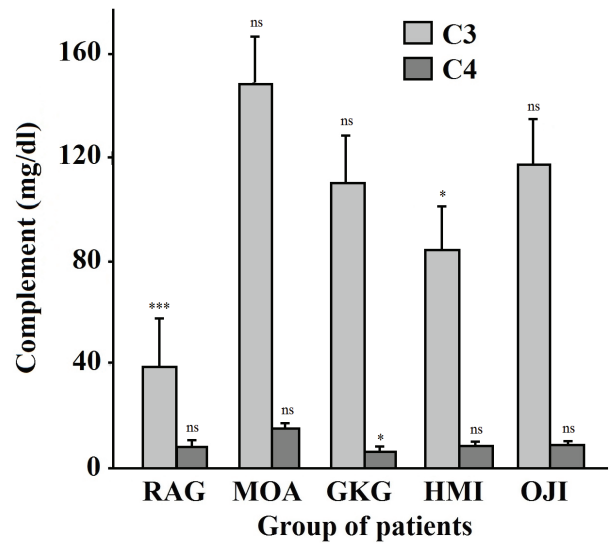


Figure 3. Estimation of C3 and C4 concentrations in SF.
 RAG: Rheumatoid arthritis group, MOA: mono/oligo-arthritis, GKG: gonarthrosis of the knee group, HMI: hemarthrosis/mechanical inflammations, OJI: Other joint inflammations. ns: non-significant, *p<0.05, ***p<0.001, compared to normal serum.

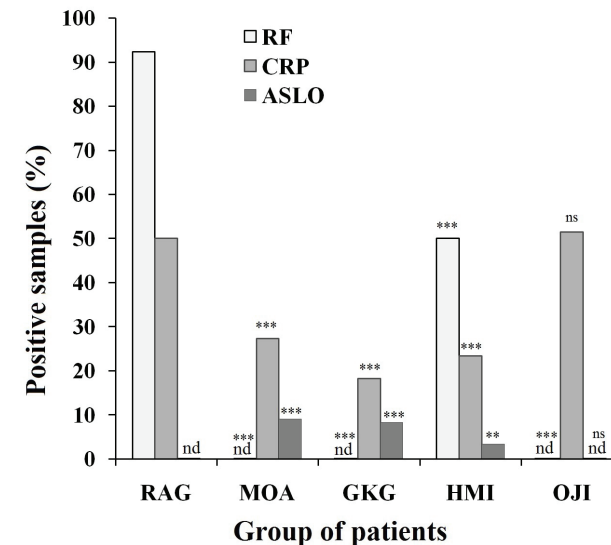


Figure 2. Detection of inflammation markers.
 RF: rheumatoid factor, CRP: c-reactive protein and ASLO: anti-streptolysin antibodies. RAG: Rheumatoid arthritis group, MOA: mono/oligo-arthritis, GKG: gonarthrosis of the knee group, HMI: hemarthrosis/mechanical inflammations, OJI: Other joint inflammations. nd: not detected, ns: non-significant, **p<0.01, ***p<0.001, compared to the most severe disease (RAG).

The levels of C3 and C4 can serve as important factors linked to infectious and immune complex diseases (20). For this reason, the concentrations of these two components were evaluated in SF. Results presented in Figure 3 showed that in the category

of RA patients (RAG), the concentration of C₃ factor was less than 30 mg/dl in most samples and reached 70.9 mg/dl in a sample where detected C₄ factor was absent, and 59.4 mg/dl in the sample that contained the greatest concentration of C₄ (24.8 mg/dl). In SF from the rest of the samples, C₄ concentrations ranged between 4.5 and 8.17 mg/dl. On the whole, C₃ and C₄ concentrations were much lower than their concentration in the serum, which ranged between 70 to 180 g/l for C₃ and between 10 to 80 mg/dl for C₄ (21). As for the category with MOA, values of C₃ factor ranged between 33.1 mg/dl to concentrations greater than 450 mg/dl, at an average of 148.86 mg/dl, where most values were beyond the concentration of this factor in normal serum. While the concentration of C₄ factor was weakly compared with C₃ factor, concentrations ranged from traces in one of the samples to 25.6 mg/dl, and at a mean of 15.67 mg/dl.

The concentration of C₃ factor in the group with GKG was 110.581 mg/dl. However, most of values were above the natural level of this factor in normal serum and some of them were less than the normal concentration (less than 30 mg/dl). The concentration of C₄ factor in four samples was less than 4.5 mg/dl, while in the remaining samples it ranged between 5.06 and 13.2 mg/dl at a rate of 7.037 mg/dl. The highest concentration of C₃ that exceeds 450 mg/dl was observed in a sample of a patient suffering from gout, where the concentration of C₄ was found to be equal to 10.5 mg/dl.

Presence and Activity of Xanthine Oxidase

The presence of XO in SF was detected using indirect ELISA. All studied synovial fluids were XO-positive. The interactions varied

between 320 and 5120 titers. The highest recorded titers were in the RA groups (RAG, MOA).

The presence of XO in SF was detected by using spectrophotometric technique (16). XO activity in SF was estimated by adding 50 µl of each SF into reaction medium, and reading was performed within 10 min due to the viscosity of the liquid and the slow reaction (Figure 4). XO activity in samples of the RA group ranged between 0 and 5 mIU/ml. For the group with mono-/oligo-arthritis, enzymatic activity is concentrated around 1.43 mIU/ml. Gonarthrosis samples showed no enzymatic activity in 75% of samples. In most samples, we obtained different activities of XO enzyme; the highest rate was recorded in the two samples which have gout disease, and joint chondrocalcinosis. A lower rate was registered in the two cases of hemarthrosis and sprained knee. The activity was completely absent in ankylosing spondylitis, hygroma and rheumatoid popliteal cyst samples.

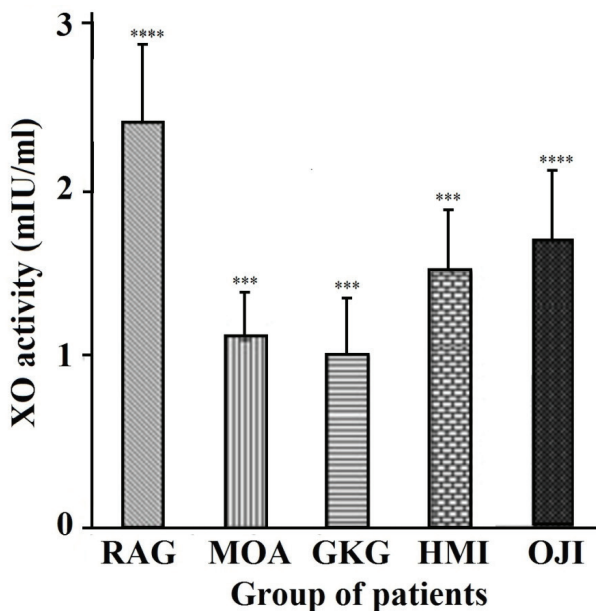


Figure 4. Total xhantine oxidase (XO) activities in synovial fluid.

RAG: Rheumatoid arthritis group, MOA: mono/oligo-arthritis, GKG: gonarthrosis of the knee group, HMI: hemarthrosis/mechanical inflammations, OJI: Other joint inflammations. *** $p < 0.001$, **** $p < 0.0001$ compared to standard serum.

The results of enzymatic activity indicate that in more than 96% of SF, XO exist as oxidase form; the XO activity was completely inhibited with allopurinol as a specific inhibitor for XO.

Unexpectedly, we noticed a significant decrease in the activity after treatment of the samples with hyaluronidase. This decrease is probably due to the impact of the active center of the enzyme by centrifugation and the length of the time of incubation during the treatment of the samples with hyaluronidase.

Anti-xanthine Oxidase Antibodies

The results showed that in the RAG, the treatment with hyaluronidase enhanced anti-XO IgM percentage both in free and complex forms, while there was no change in IgG level. IgG antibodies were lower than IgM in the two forms (Figure 5B).

Most of the anti-XO antibodies in the SF of patients in the MOA category were present as IgM class, but with levels lower than those in the RA group (Figure 5A). After the treatment of the SF with hyaluronidase, the levels of IgM antibodies slightly increased while those of IgG type decreased (Figure 5B).

Unlike SF in the RA group, the largest proportion of anti-XO antibodies within GKG was IgG, either in free or immune complexed form (Figure 5A). After treatment of the SF with hyaluronidase enzyme, no change in proportion of free antibodies was detected, but that of immune complexes declined (Figure 5B).

In the HMI group, most of the anti-XO antibodies were IgM in the two forms (Figure 5A). Treatment of the SF with hyaluronidase enzyme led to a slight increase in the proportion of IgM

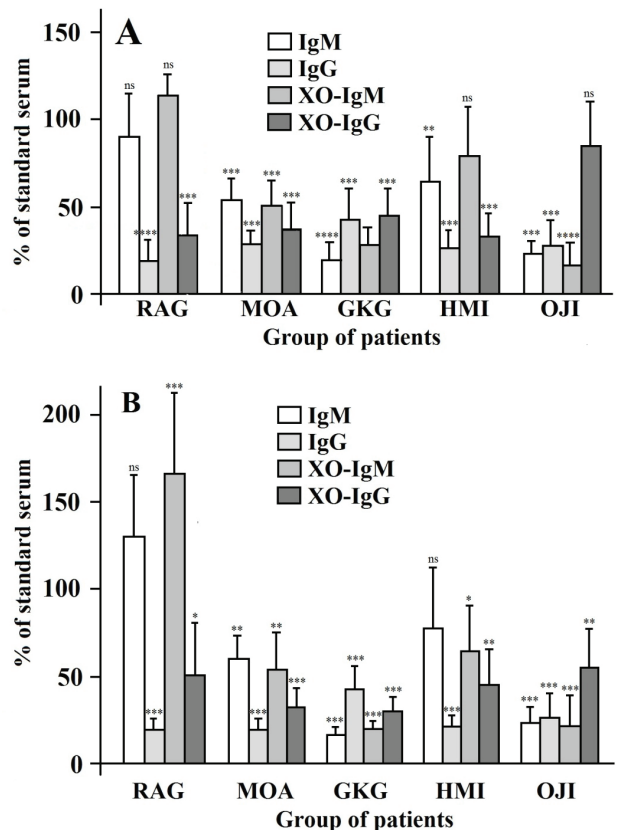


Figure 5. Free and complex anti-XO IgG and IgM represented as % of standard serum \pm SD in SF of patients. A and B: SF without and with hyaluronidase, respectively.

RAG: Rheumatoid arthritis group, MOA: mono/oligo-arthritis, GKG: gonarthrosis of the knee group, HMI: hemarthrosis/mechanical inflammations, OJI: Other joint inflammations. ns: non-significant, * $p < 0.05$, ** $p < 0.01$, *** $p < 0.001$, **** $p < 0.0001$ compared to standard serum.

ti-XOR antibodies and IgG-XO immune complexes and a slight decrease in the proportion of IgM-XO immune complexes (Figure 5B).

The OJI group includes patients with joint pain with inflammatory origin. The levels of antibodies were close in all types of anti-XO antibodies, except for immune-complexes containing IgG that exceed four times the value of the rest of other antibodies (Figure 5A). Treatment of SF with hyaluronidase did not affect the level of antibodies, either in free or complexes form containing IgM, while it led to a significant decrease (about 30%) in the proportion of immune complexes containing IgG (Figure 5B).

DISCUSSION

The highest levels of total IgG and IgM titers were registered in the SF of patients with arthritis (RAG and MOA) and other joint inflammations (OJI) compared to the levels in the control serum, and are in agreement with previous studies (10, 22). These high levels are due to the auto-immune nature of the diseases.

The presence of CRP found in this study indicates the presence of inflammation in the SF of patients. CRP levels increase in response to tissue damaging processes (up to 1000 fold), (23) and in inflammatory arthropathies like RA (24). In RA serum there is a good correlation between CRP levels and disease severity.

Rheumatoid factor is an important biomarker in RA. However, a positive test for RF is a diagnostic and prognostic indicator of RA (25, 26). The serum levels of RF do not reflect disease activity since they are found in patients with other autoimmune and non-autoimmune diseases, as well as in healthy subjects (27). In the current study, the presence of RF was greater in RA patients with high activity. Using ELISA, all SF were positive due to the high sensitivity of this technique.

The most widely used oropharyngeal culture in clinical practice includes the detection of anti-streptococcal antibodies such as ASLO and anti-deoxyribonuclease B. Of these two tests, ASLO was the first developed and is the most commonly used test (28, 29). In the present study no correlation of ASLO and the severity of the rheumatic inflammation was found. This finding agrees with the results previously obtained by Geerts et al. (19), who concluded that little or no scientific evidence was found for the use of ASLO in patients with pharyngitis, post-streptococcal glomerulonephritis and in adults with rheumatoid arthritis.

Complement activation participates in the pathogenesis of several autoimmune and inflammatory diseases including RA (30). The evidence of complement activation in the SF of RA patients is probably due to the presence of immune complexes. Levels of complement components are generally depressed in the SF of patients with RA, reflecting their consumption. On the other hand, elevated levels of cleavage products have been observed in SF. TNF α -inhibitor effectiveness in arthritis is exerted by the reduction of complement activation. Complement could be an attractive therapeutic target both in RA and in PsA (31).

The presence of active XO is significantly higher in the SF of patients with RAG compared to the other groups. This result agrees with the finding of Blake et al. (32) who showed that XO concentration is significantly raised up to 60 times in the synovium of patients with RA. This could be due to the up-regulation of the enzyme by high levels of cytokines, hypoxic nature and the symptoms of radical attack present in rheumatoid synovium (33). The roles of XOR in cytokine induced bone erosion promoting vasculitis were well documented by Miesel and Zuber (34). As we have previously found (14), more than 50% of XO is in its oxidase form. This finding indicates that XOR is liberated from the pannus (33) and correlates well with the severity of RA.

Anti-XO antibodies of IgM class were found to be higher in RA, followed by mechanical origin infections, hemarthrosis, and mono-/oligo-arthritis, then by other joint inflammation and gonarthrosis. A greater proportion of immune complexes IgM-XOR were recorded in the RA group, followed by mechanical infections and hemarthrosis; the lowest levels were recorded in patients with other joint inflammations. The highest percentage of immune complexes IgG-XOR was recorded in mechanical infections and the hemarthrosis category, and was close to the rest of the groups. These results confirm our previous study (10, 35) where the presence of these antibodies was well discussed. Al Muhtaseb et al. (35) indicated that anti-XO antibodies in SF possess a protective role in inflammatory arthritis, where they play a role in eliminating XOR from SF. However, immune complexes could activate complement and participate in propagating the inflammatory cycle. Treatment of SF with hyaluronidase gives variable effects either in free or complexed antibodies (IgG and IgM). Similar effects were observed by Brouwers et al. (36) in the case of cytokines. In contrast, these authors found that the treatment with this enzyme resulted in a lower coefficient of variation for IgG measurements.

IgM anti-XOR antibodies titers and IgM-containing XORICs in the SF of RAG patients were significantly higher than in joint pathologies. It is noteworthy that XOR activity was detectable; even it could be in part affected by immune complex formation (36).

CONCLUSION

The current study suggests that XOR may play a negative role in arthritis by generating ROS which causes self-maintenance of the disease. Furthermore, anti-XO antibodies in sera and SF may participate in eliminating the enzyme and stop its negative action. However, XORIC formation could activate complement which has a crucial role in the self-maintenance of the illness.

Acknowledgements: Authors acknowledge the Algerian Ministry of Higher Education and Scientific Research (MESRS) and General Directory of Scientific Research and Technologic Development (DGRSDT) for the financing of this work.

Ethics Committee Approval: This study was approved by the ethics local committee (NrECA/003/22).

Informed Consent: Written consent was obtained from the participants.

Peer Review: Externally peer-reviewed.

Author Contributions: Conception/Design of Study- L.A.; Data Acquisition- N.H.; Data Analysis/Interpretation- N.H., L.A.; Drafting Manuscript- N.H.; Critical Revision of Manuscript- L.A.; Final Approval and Accountability- L.A., N.H.

Conflict of Interest: Authors declared no conflict of interest.

Financial Disclosure: This work is financed by the Algerian Ministry of Higher Education and Scientific Research (MESRS) and General Directory of Scientific Research and Technologic Development (DGRSDT).

REFERENCES

- Nilsson J, Andersson MLE, Hafström I, Svensson B, Forslind K, Ajeganova S, et al. Influence of age and sex on disease course and treatment in rheumatoid arthritis. *Open Access Rheumatol: Res Reviews* 2021; 13: 123-38.
- Lu S, Carlsen S, Hansson AS, Holmdahl R. Immunization of rats with homologous type XI collagen leads to chronic and relapsing arthritis with different genetics and joint pathology than arthritis induced with homologous type II collagen. *J Autoimmunity* 2002; 18: 199-211.
- Backlund J, Treschow A, Firan M, Malmstrom V, Issazadeh-Navikas S, Ward ES, et al. Reversal of tolerance induced by transplantation of skin expressing the immunodominant T cell epitope of rat type II collagen entitles development of collagen-induced arthritis but not graft rejection. *Eur J Immunol* 2002; 32: 1773-83.
- Jilani AA, Mackworth-Young CG. The role of citrullinated protein antibodies in predicting erosive disease in rheumatoid arthritis: a systematic literature review and meta-analysis. *Int JRheumatol* 2015; 2015: 728610.
- Panagopoulos PK, Lambrou GI. Bone erosions in rheumatoid arthritis: recent developments in pathogenesis and therapeutic implications. *J Musculoskelet Neuronal Interact* 2018; 18(3): 304-19.
- Rocha SdB, Baldo DC, Andrade LEC. Clinical and athophysiological relevance of autoantibodies in rheumatoid arthritis. *Adv Rheumatol* 2019; 59:1-13.
- Smith M. The Normal Synovium. *Open Rheumatol J* 2011; 5(Suppl 1:M2): 100-6.
- Chang MH, Levescot A, Nelson-Maney N, Blaustein RB, Winden KD, Morris A, et al. Arthritis flares mediated by tissue-resident memory T cells in the joint. *Cell Reports* 2021;37: 109902.
- Polgar A, Falus A, Koo´ E, Ujfalussy I, Seszták M, Szűts I, et al. Elevated levels of synovial fluid antibodies reactive with the small proteoglycans biglycan and decorin in patients with rheumatoid arthritis or other joint diseases. *Rheumatology* 2003; 42:522-7.
- Arrar L, Hanachi N, Rouba K, Charef N, Khenouf S, Baghiani A. Anti-xanthine oxidase antibodies in sera and synovial fluid of patients with rheumatoid arthritis and other joint inflammations; *Saudi Med J* 2008; 29(6): 803-7.
- Nakamura H, Masuko K, Yudoh K, Kato T, Kamada T, Kawahara T. Effects of glucosamine administration on patients with rheumatoid arthritis. *Rheumatol Int* 2007; 27: 213-8.
- Valko M, Leibfritz D, Moncol J, Cronin MT, Mazur M, Telser J. Free radicals and antioxidants in normal physiological functions and human disease. *Int J Biochem Cell Biol* 2007; 39: 44-84.
- Nasi S, Castelblanco M, Chobaz V, Ehrichiou D, So A, Bernabei I, Kusano T, et al. Xanthine oxidoreductase is involved in chondrocyte mineralization and expressed in osteoarthritic damaged cartilage. *Front Cell Dev Biol* 2021; 9: 612440.
- Hanachi N, Charef N, Baghiani A, Khenouf S, Derradji Y, Boumerfeg S, et al. Comparison of xanthine oxidase levels in synovial fluid from patients with rheumatoid arthritis and other joint inflammations. *Saudi Med J* 2009; 30(11): 1422-5
- Boere J, van de Lest CHA, Libregts SFWM, Arkesteijn GJA, Geerts WJC, Hoen ENMN, et al. Synovial fluid pretreatment with hyaluronidase facilitates isolation of CD₄₄⁺ extracellular vesicles. *J Extracell Vesicles* 2016; 5: 1-16
- Baghiani A, Harrison R, Benboubetra M. Purification and partial characterisation of camel milk xanthine oxidoreductase. *Arch Physiol Biochem* 2003; 111: 407-14.
- Abadeh S, Killackey J, Benboubetra M, Harrison R. Purification and partial characterization of xanthine oxidase from human milk. *Biochim Biophys Acta* 1992; 1117: 25-32.
- Rousseaux-Prevost R, De Almeida M, Arrar L, Hublau P, Rousseaux J. Antibodies to sperm basic nuclear proteins detected in infertile patients by dot-immunobinding assay and by enzyme-linked immunosorbent assay. *Am J Reprod Immunol* 1989; 20: 17-20.
- Geerts I, De Vos N, Frans J, Mewis A. The clinical diagnostic role of antistreptolysin O antibodies. *Acta Clin Belgica* 2011; 66: 411-5.
- Zinellu A, Mangoni AA. Serum complement C3 and C4 and COVID-19 severity and mortality: A systematic review and meta-analysis with meta-regression. *Front Immunol* 2021; 12: 96085.
- Hebert LA, Cosio FG, Neff JC. Diagnostic significance of hypocomplementemia. *Kidney Int* 1991; 39: 811-21.
- Ng YL and Lewis WH. Circulating immune complexes of xanthine oxidase in normal subjects. *Br J Biomed Sci* 1994; 51: 124-7.
- Pepys MB, Baltz ML. Acute phase proteins with special reference to C-reactive protein and related proteins (pentaxins) and serum amyloid A protein. *Adv Immunol* 1983; 34: 141-212.
- Mallya RK, de Beer FC, Berry H, Hamilton EDB, Mace BEW & Pepys MB. Correlation of clinical parameters of disease activity in rheumatoid arthritis with serum concentrations of C-reactive protein and erythrocyte sedimentation rate. *J Rheum* 1982; 9: 224-8.
- Sihvonen S, Korpela M, Mustila A and Mustonen J. The predictive value of rheumatoid factor isotypes, anti-cyclic citrullinated peptide antibodies, and antineutrophil cytoplasmic antibodies for mortality in patients with rheumatoid arthritis. *J Rheum* 2005; 32: 2089-94.
- Westwood OMR, Nelson PN and Hay FC. Rheumatoid factors: What's new? *Rheum* 2006; 45: 379-85.
- Ingegnoli F, Castelli R, Gualtierotti R. Rheumatoid factors: clinical applications. *Disease Markers* 2013; 35(6): 727-34.
- Johnson DR, Kaplan EL, Sramek J, Bicova R, Havlicek J, Havlickova H et al. Laboratory diagnosis of group A streptococcal infections. Geneva (Switzerland): World Health Organization; 1996.
- Massell BF. Confirmation of haemolytic streptococcus hypothesis. In: Massell BF, ed. *Rheumatic Fever and Streptococcal Infection. Unravelling the mysteries of a dread disease.* Boston: Harvard University Press; 1997: p. 93-110.
- Okroj M, Heinegård D, Holmdahl R, Blom AM. Rheumatoid arthritis and the complement system. *Ann Med* 2007; 39(7): 517-30.
- Ballanti E, Perricone C, di Muzio G, Kroegler B, Chimenti MS, Graceffa D, et al. Role of the complement system in rheumatoid arthritis and psoriatic arthritis: Relationship with anti-TNF inhibitors. *Autoimmun Rev* 2011;10: 617-23.

32. Blake DR, Stevens CR, Sahinoglu T, Ellis G, Gaffney K, Edmonds S et al. Xanthine oxidase; four roles for the enzyme in rheumatoid pathology. *Biochem Soc Trans* 1997; 25: 812-6.
33. Stevens CR, Benboubetra M, Harrison R, Sahinoglu T, Smith EC, Blake DR. Localization of xanthine oxidase to synovial endothelium. *Ann Rheum Dis* 1991; 199750: 760-2.
34. Miesel R, Zuber M. Elevated levels of xanthine oxidase in serum of patients with inflammatory and autoimmune rheumatic diseases. *Inflammation* 1993; 17(5): 551-61.
35. Al-Muhtaseb N, Al-Kaissi E, Thawaini AJ, Eldeen ZM, Al-Muhtaseb, Al-Saleh B. The role of human xanthine oxidoreductase (HXOR), anti-HXOR antibodies, and microorganisms in synovial fluid of patients with joint inflammation. *Rheumatol Int* 2012; 32: 2355-62.
36. Brouwers H, von Hegedus JH, van der Linden E, Mahdad R, Klop-penburg M, Toes R et al. Hyaluronidase treatment of synovial fluid is required for accurate detection of inflammatory cells and soluble mediators. *Arthritis Res Ther* 2022; 24(18): 1-18.

New Records for Microalgae Species of the Turkish Seas Under the Effect of Intense Mucilage in the Sea of Marmara

Turgay Durmus¹ , Neslihan Balkis-Ozdelice¹ , Seyfettin Tas² , Fatma Bayram-Partal³ ,
Muharrem Balci¹ , Cem Dalyan¹ , Mustafa Sari⁴ 

¹Istanbul University, Faculty of Science, Department of Biology, Istanbul, Turkiye

²Istanbul University, Institute of Marine Sciences and Management, Istanbul, Turkiye

³TUBITAK-Marmara Research Center, Environment and Cleaner Production Institute, Kocaeli, Turkiye

⁴Bandırma Onyedi Eylül University, Maritime Faculty, Department of Maritime Business Administration, Balıkesir, Turkiye

ORCID IDs of the authors: T.D. 0000-0002-8242-1823; N.B.O. 0000-0001-8030-7480; S.T. 0000-0002-4660-3937; F.B.P. 0000-0002-5661-1439; M.B. 0000-0001-9373-6647; C.D. 0000-0002-7386-5641; M.S. 0000-0003-2733-3254

Please cite this article as: Durmus T, Balkis-Ozdelice N, Tas S, Bayram-Partal F, Balci M, Dalyan C, Sari M. New Records for Microalgae Species of the Turkish Seas Under the Effect of Intense Mucilage in the Sea of Marmara. Eur J Biol 2022; 81(2): 144-162. DOI: 10.26650/EurJBiol.2022.1195227

ABSTRACT

Objective: New records of microalgae species for Turkish seas taking into account the species lists published to date have been reported in this study conducted in the Sea of Marmara and the Aegean Sea. Furthermore, new records of microalgae species for the Sea of Marmara and the Aegean Sea were listed.

Materials and Methods: New record species for Turkish seas were described by their morphological and ecological features and also their images were taken under a light microscope with epifluorescence attachment, and also some of them were photographed on a scanning electron microscope.

Results: A total of 66 new record species were identified in this study. A total of 25 microalgae taxa belonging to 11 taxonomic classes were recorded for the first time for Turkish seas. Two taxa were freshwater or brackish water form, which is known from the lakes. The class Prymnesiophyceae had seven taxa that were recorded for the first time, followed by Bacillariophyceae and Dinophyceae with four taxa and the other classes. Furthermore, a total of 65 taxa belonging to 16 taxonomic classes were recorded for the first time for the Sea of Marmara. Twelve taxa were freshwater or brackish water form, which is known from the lakes. Among these, Dinophyceae had 24 taxa, followed by Prymnesiophyceae with 11 taxa, and Bacillariophyceae with 9 taxa and the other classes. In addition, one new record taxon was detected for the Aegean Sea.

Conclusion: New records of microalgae detected in the Sea of Marmara during this study period will provide an important contribution to both the microalgae checklist of Turkish seas, the Sea of Marmara and the Aegean Sea.

Keywords: Mucilage, new records, phytoplankton, biodiversity, Turkish coastal waters

INTRODUCTION

The phytoplankton studies in Turkish seas began in 1950's, and its number increased, especially since 1980's and 1990's. The first detailed checklist of phytoplankton species of Turkish seas was prepared by Koray (1). Furthermore, the first detailed checklist of phytoplankton species of the Sea of Marmara was prepared by Balkis (2).

New records of species have been added to this checklist in the studies in the following years (3-9).

Turkish seas contain the southern Black Sea, Sea of Marmara, eastern Aegean Sea and northeastern Mediterranean Sea, each of which has different ecological features. The Sea of Marmara (SoM), where this study was conducted, is a semi-enclosed inland sea and transition



Corresponding Author: Turgay Durmus

E-mail: turgay.durmus@istanbul.edu.tr

Submitted: 31.10.2022 • **Revision Requested:** 07.11.2022 • **Last Revision Received:** 08.11.2022 •

Accepted: 14.11.2022 • **Published Online:** 20.12.2022

Content of this journal is licensed under a Creative Commons Attribution-NonCommercial 4.0 International License.



zone between Mediterranean Sea and Black Sea, with a surface area of 11,500 km² and a maximum depth of 1390 m. It connects to the Black Sea by the İstanbul Strait and to the Aegean Sea by the Çanakkale Strait. The SoM has a two-layer water system; the upper layer water with low salinity (~18) coming from the Black Sea with nutrient-rich water and lower layer water with high salinity (~38) coming from the Mediterranean Sea, and it has a strong intermediate layer at a depth of ~25m. The vertical mixing in the SoM is limited as a result of two-layered system. The oceanographic conditions in the SoM are controlled by the two straits (10-13). Oxygen consumption increases in the lower layer due to the decomposition of organic particles coming from the upper layer, the oxygen level is regulated by the Mediterranean water content which has a rich oxygen level (13). However, the organic material on the surface has been carried to the benthic region with time. This case led to a decrease in dissolved oxygen in the bottom layer. It is determined that the mucilage material is rich in terms of carbohydrate and protein in the intense mucilage period (14), and the dominant microalgae responsible for the formation were reported (7, 15).

This study presents a list of the microalgae species recorded for the first time for Turkish seas with their descriptions during the studies conducted in the Sea of Marmara in 2021, when intense mucilage was observed, and also 2022, when mucilage formation disappeared. In addition, new records of microalgae species also for the Sea of Marmara and the Aegean Sea were listed in this study. It is considered that new records in microalgae during this study period will provide an important

contribution for both the microalgae checklists of Turkish seas and the Sea of Marmara.

MATERIALS AND METHODS

In this study, which was carried out at 16 sampling stations (Sts. 1-16) in the Sea of Marmara and one station in the Aegean Sea (St. 17), samples were collected from different depths (especially 0.5 m) during and after an intense mucilage period from March 2021 to June 2022 (Figure 1). For identifications and enumerations of microalgae species, samples were taken from mucilage aggregates at stations that have dense mucilage and also were collected with plankton nets with 20 and 40 µm mesh sizes, and Niskin bottles at stations that have less mucilage.

The net samples collected for qualitative analysis of microalgae species were fixed with a neutral formaldehyde solution (2-4%) and examined under the Olympus BX51 bright-field microscope at magnifications of 100, 200, 400 and 1000× (with immersion oil). The water samples collected for quantitative analysis of microalgae species were fixed with an acidic Lugol-iodine solution (2%) (16) and the samples were sedimented in accordance with the Utermohl sedimentation technique (17). After the sedimentation, upper water was removed and the sample was concentrated up to 10 mL (18). The homogenized subsample of one ml was taken and counted under the "Olympus CK2" model phase-contrast inverted microscope using the Sedgewick-Rafter counting chamber (19).

Furthermore, microalgae species were also examined with an FEI Versa 3D model scanning electron microscope (SEM). Samples

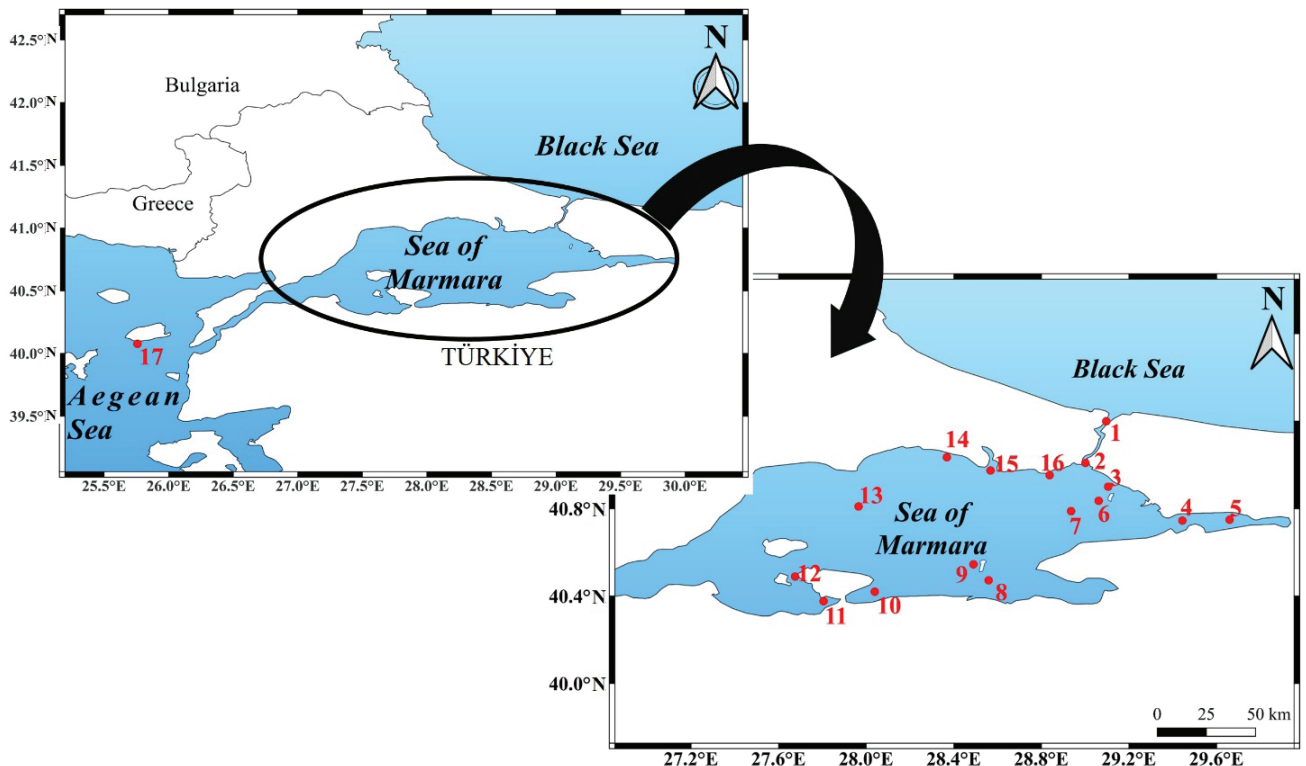


Figure 1. Sampling stations in the Sea of Marmara and Aegean Sea.

were digested with acids (HCl and H₂O₂) for Bacillariophyceae members (20, 21). In the classes, except for Bacillariophyceae, SEM imaging was performed after the fixation of samples with osmium tetroxide (OsO₄). For this, the samples were fixed with OsO₄ at a final volume of 2% during the field and kept at +4°C in the dark until analysis. Afterwards, the samples, which were desalted by washing several times with distilled water, were passed through various volumes of ethanol series (20, 40, 60, 80, and 95%) for dehydration (22) and transferred to stubs which had carbon bands on them. They were left to dry for half an hour in an oven at 50°C. The stubs were kept in desiccators for 30 minutes to remove moisture, then coated with platinum for 90 seconds.

Taxonomic classifications were made as Heimdal (23), Thronsen (24), Hasle & Syvertsen (25) Steidinger & Tangen (26) and World Register of Marine Species (27) and Algaebase (28) were used for the current nomenclatures of species. For the identifications of species, the sources used were as follows: Cleve (29), Schmidle (30), Hustedt (31), Gantt & Conti (32), Bukry (33), Fukuyo (34), Vørs (35), Heimdal (23), Thronsen (24), Hasle &

Syvertsen (25), Steidinger & Tangen (26) 1997, Young et al. (36), Haywood et al. (37), Fresnel & Probert (38), Hoppenrath et al. (39), Takano & Matsuoka (40), Idei et al. (41), Hardardóttir et al. (42), Han et al. (43), Young et al. (44).

RESULTS

Group Composition

Phytoplankton biodiversity obtained from the water and net samples examined during this study showed that a total of 25 taxa belonging to 13 taxonomic classes were recorded for the first time for Turkish seas. Seven taxa among them were at the genus level. Two taxa among them were freshwater or brackish water form. The distribution of the new record taxa by classes is as follows: Bacillariophyceae and Dinophyceae with four taxa, Prymnesiophyceae with seven taxa and each of other classes (Chrysophyceae, Xanthophyceae, Pelagophyceae, Raphidophyceae, Euglenophyceae, Pyramimonadophyceae, Ulvophyceae, Zygnematophyceae, Florideophyceae and Porphyridiophyceae) included one taxon (Table 1; Figures 2-9).

Table 1. The list of new record taxon in the Turkish coastal waters, the Sea of Marmara and Aegean Sea. (*indicates the potentially toxic species, ** indicates harmful species, and ^{*} indicates freshwater species)

No	TAXON	New Record for Turkish Coastal Waters	New Record for Sea of Marmara	New Record for Aegean Sea
CYANOPHYTA				
Cyanophyceae				
1	[*] <i>Aphanocapsa delicatissima</i> West & G.S.West, 1912		✓	
2	[*] <i>Glaucospira</i> sp.		✓	
3	<i>Richelia intracellularis</i> Schmidt, 1901		✓	
4	<i>Stigonema</i> sp.		✓	
Total Number of Cyanophyceae		0	4	0
CHROMOPHYTA				
Bacillariophyceae				
1	<i>Auricula</i> sp.	✓	✓	
2	[*] <i>Craticula cuspidata</i> (Kützinger) D.G.Mann, 1990		✓	
3	<i>Cyclophora</i> sp.		✓	
4	<i>Diploneis</i> cf. <i>papula</i> (A.W.F.Schmidt) Cleve, 1894			✓
5	<i>Donkinia</i> sp.	✓	✓	
6	<i>Eucampia</i> cf. <i>groenlandica</i> Cleve, 1896	✓	✓	
7	[*] <i>Fragilaria crotonensis</i> Kitton, 1869		✓	
8	<i>Licmophora</i> cf. <i>inflata</i> Mereschkowsky, 1901	✓	✓	
9	[*] <i>Synedra famelica</i> Kützinger, 1844= <i>Fragilaria famelica</i>		✓	

Table 1. The list of new record taxon in the Turkish coastal waters, the Sea of Marmara and Aegean Sea. **(continued)**
 (*indicates the potentially toxic species, ** indicates harmful species, and [†] indicates freshwater species)

No	TAXON	New Record for Turkish Coastal Waters	New Record for Sea of Marmara	New Record for Aegean Sea
10	<i>Triceratium antediluvianum</i> (Ehrenberg) Grunow, 1868= <i>Biddulphia antediluviana</i>		✓	
Total Number of Bacillariophyceae		4	9	1
Dinophyceae				
1	<i>Amoebophrya ceratii</i> (Koeppen) J.Cachon, 1964	✓	✓	
2	* <i>Amphidinium carterae</i> Hulburt, 1957		✓	
3	<i>Amphidinium crassum</i> Lohmann, 1908		✓	
4	* <i>Amphidinium operculatum</i> Claparède & Lachmann, 1859		✓	
5	* <i>Coolia monotis</i> Meunier, 1919		✓	
6	<i>Diplopelta asymmetrica</i> (Mangin) M.Lebour ex Balech 1988= <i>Dissodium asymmetricum</i>		✓	
7	<i>Heterocapsa minima</i> A.J.Pomroy, 1989		✓	
8	<i>Heterocapsa niei</i> (Loeblich III) Morrill & Loeblich III, 1981		✓	
9	<i>Heterocapsa pygmaea</i> Loeblich III, R.J.Schmidt & Sherley, 1981		✓	
10	* <i>Karenia cf. brevis</i> (Davis) Hansen & Moestrup, 2000		✓	
11	* <i>Karenia cf. mikimotoi</i> (Oda) Hansen & Moestrup, 2000		✓	
12	* <i>Karenia cf. selliformis</i> Haywood, Steidinger & MacKenzie, 2004	✓	✓	
13	* <i>Ostreopsis</i> sp.		✓	
14	<i>Oxytoxum caudatum</i> Schiller, 1937		✓	
15	<i>Oxytoxum cf. longum</i> Schiller, 1937		✓	
16	<i>Oxytoxum mediterraneum</i> Schiller, 1937		✓	
17	<i>Prorocentrum cf. emarginatum</i> Fukuyo, 1981	✓	✓	
18	<i>Prorocentrum shikokuense</i> Hada, 1975	✓	✓	
19	<i>Pyrocystis cf. fusiformis</i> Thomson, 1876		✓	
20	<i>Pyrocystis pseudonociluca</i> Wyville-Thompson, 1876		✓	
21	<i>Spatulodinium pseudonociluca</i> (Pouchet) J.Cachon & M.Cachon, 1968		✓	
22	<i>Tripos azoricus</i> (Cleve) F.Gómez, 2013		✓	
23	<i>Tripos hexacanthus</i> (Gourret) F.Gómez, 2013		✓	
24	<i>Tripos vultur</i> (Cleve) Hallegraeff & Huisman, 2020		✓	
Total Number of Dinophyceae		4	24	0
Raphidophyceae				
1	<i>Olisthodiscus</i> sp.	✓	✓	

Table 1. The list of new record taxon in the Turkish coastal waters, the Sea of Marmara and Aegean Sea. (continued)
 (*indicates the potentially toxic species, ** indicates harmful species, and [†] indicates freshwater species)

No	TAXON	New Record for Turkish Coastal Waters	New Record for Sea of Marmara	New Record for Aegean Sea
Total Number of Raphidophyceae		1	1	0
Chrysophyceae				
1	** <i>Chrysophaeum taylorii</i> Lewis & Bryan, 1941		✓	
2	<i>Kephyrion</i> sp.		✓	
3	<i>Ollicola</i> cf. <i>vangoorii</i> (W.Conrad) Vørs, 1992= <i>Calycomonas wulfii</i>	✓	✓	
Total Number of Chrysophyceae		1	3	0
Xanthophyceae				
1	<i>Meringosphaera mediterranea</i> Lohmann, 1903	✓	✓	
Total Number of Xanthophyceae		1	1	0
Pelagophyceae				
1	<i>Sarcinochrysis marina</i> Geitler, 1930	✓	✓	
Total Number of Pelagophyceae		1	1	0
Prymnesiophyceae				
1	* <i>Chrysochromulina</i> sp.		✓	
2	<i>Corisphaera</i> sp.	✓	✓	
3	<i>Dicrateria</i> sp.	✓	✓	
4	<i>Discosphaera tubifer</i> (G.Murray & V.H.Blackman) Ostenfeld, 1900		✓	
5	<i>Gephyrocapsa oceanica</i> Kamptner, 1943	✓	✓	
6	<i>Hayaster perplexus</i> (Bramlette & Riedel) Bukry, 1973	✓	✓	
7	<i>Helladosphaera cornifera</i> (J.Schiller) Kamptner, 1937= <i>Syrachosphaera cornifera</i>	✓	✓	
8	* <i>Ochrosphaera neapolitana</i> Schussnig, 1930	✓	✓	
9	* <i>Phaeocystis globosa</i> Scherffel, 1899		✓	
10	<i>Scyphosphaera apsteinii</i> Lohmann, 1902		✓	
11	<i>Umbilicosphaera sibogae</i> (Weber Bosse) Gaarder, 1970	✓	✓	
Total Number of Prymnesiophyceae		7	11	0
CHLOROPHYTA				
Euglenophyceae				
1	<i>Astasia</i> sp.	✓	✓	
2	* <i>Lepocinclis acus</i> (O.F.Müller) B.Marin & Melkonian, 2003= <i>Euglena acusformis</i>		✓	
3	* <i>Trachelomonas</i> sp.		✓	

Table 1. The list of new record taxon in the Turkish coastal waters, the Sea of Marmara and Aegean Sea. (continued)
 (*indicates the potentially toxic species, ** indicates harmful species, and ^{*} indicates freshwater species)

No	TAXON	New Record for Turkish Coastal Waters	New Record for Sea of Marmara	New Record for Aegean Sea
Total Number of Euglenophyceae		1	3	0
Pyramimonadophyceae				
1	<i>Pyramimonas</i> cf. <i>discoicola</i> Hardardóttir, N.Lundholm, Moestrup & T.G.Nielsen, 2014	✓	✓	
Total Number of Pyramimonadophyceae		1	1	0
Trebouxiophyceae				
1	[*] <i>Crucigenia</i> sp.		✓	
Total Number of Trebouxiophyceae		0	1	0
Chlorophyceae				
1	[*] <i>Scenedesmus acuminatus</i> (Lagerheim) Chodat, 1902= <i>Tetradesmus lagerheimii</i>		✓	
Total Number of Chlorophyceae		0	1	0
Ulvophyceae				
1	<i>Binuclearia lauterbornii</i> = <i>Planctonema lauterbornii</i> (Schmidle) Proshkina-Lavrenko, 1966	✓	✓	
Total Number of Ulvophyceae		1	1	0
CHAROPHYTA				
Zygnematophyceae				
1	[*] <i>Cosmarium</i> sp.		✓	
2	[*] <i>Staurastrum tetracerum</i> Ralfs ex Ralfs, 1848	✓	✓	
Total Number of Zygnematophyceae		1	2	0
RHODOPHYTA				
Florideophyceae				
1	[*] <i>Batrachospermum</i> sp.	✓	✓	
Total Number of Florideophyceae		1	1	0
Porphyridiophyceae				
1	<i>Porphyridium purpureum</i> (Bory) K.M.Drew & R.Ross, 1965	✓	✓	
Total Number of Porphyridiophyceae		1	1	0
Total Number of Phytoplankton Species		25	65	1

Furthermore, a total of 65 taxa belonging to 14 taxonomic classes were recorded for the first time for the Sea of Marmara. In addition, one new record taxon (*Diploneis* cf. *papula*) was detected for the Aegean Sea. Sixteen taxa were at the genus level. Twelve taxa among these were freshwater or brackish water form.

The distribution of the new record taxa by classes is as follows: Cyanophyceae with four taxa (Figure 5), Bacillariophyceae with nine taxa (Figures 2, 8), Dinophyceae with 24 taxa (Figures 3, 4), Chrysophyceae with three taxa (Figure 5), Prymnesiophyceae with 11 taxa (Figures 6, 9), Euglenophyceae with three taxa (Figure

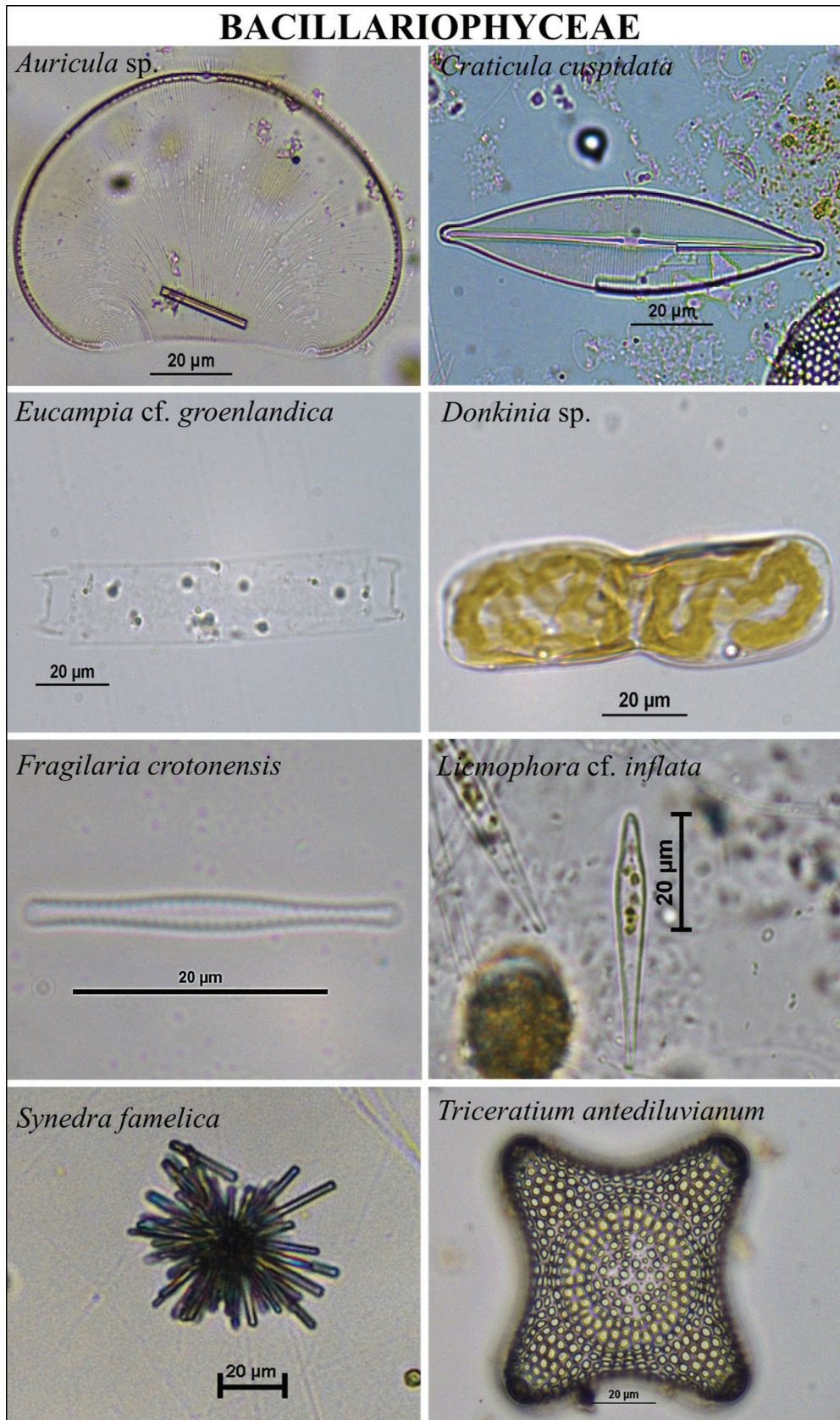


Figure 2. The images of new record Bacillariophyceae species were taken with a bright-field microscope.

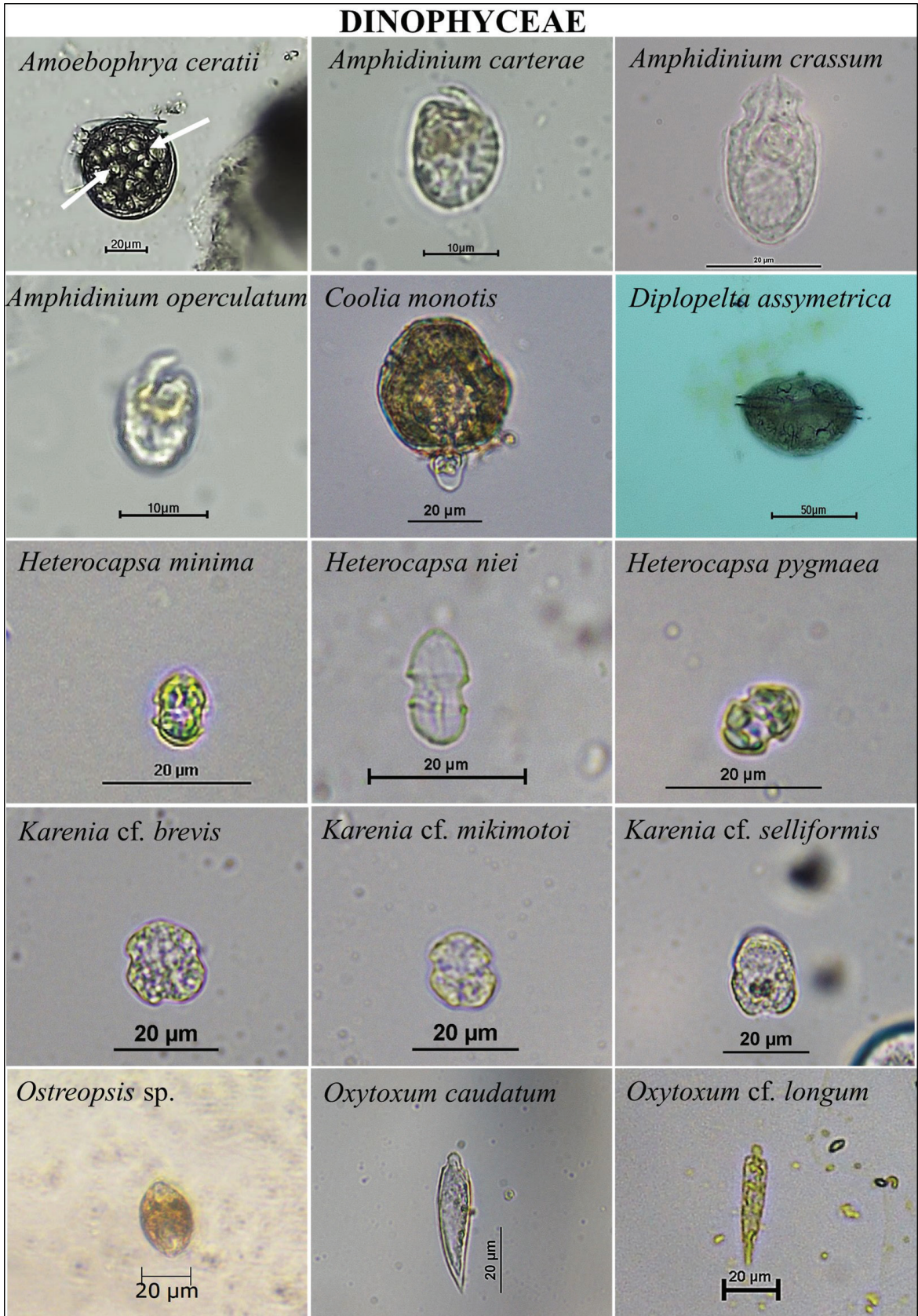


Figure 3. The images of new record some Dinophyceae species were taken with a bright-field microscope (arrows indicate the cells of the species).

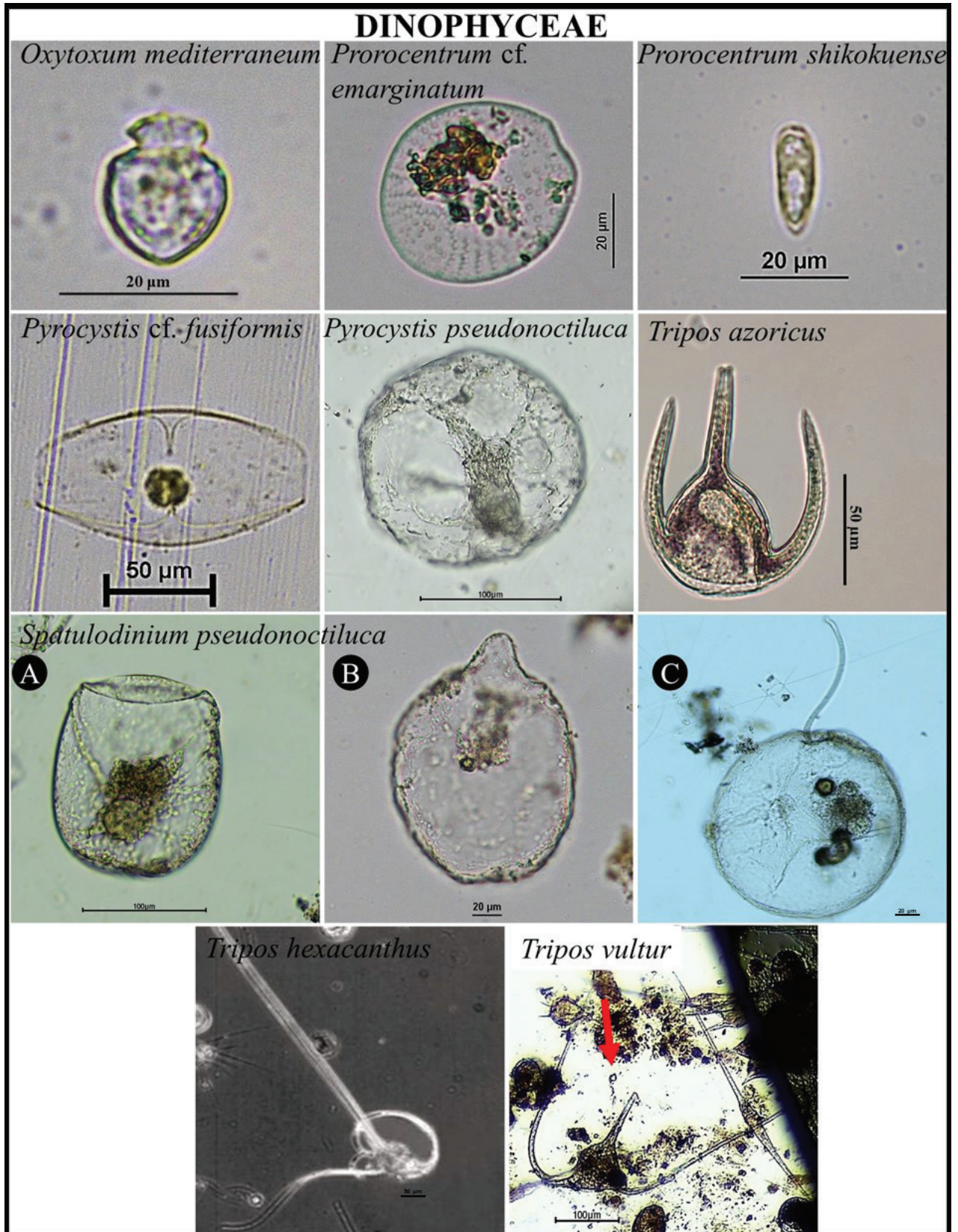


Figure 4. The images of new record other Dinophyceae species were taken with a bright-field microscope (arrow indicates the species; A-C show the different morphological stages of *S. pseudonociluca*).

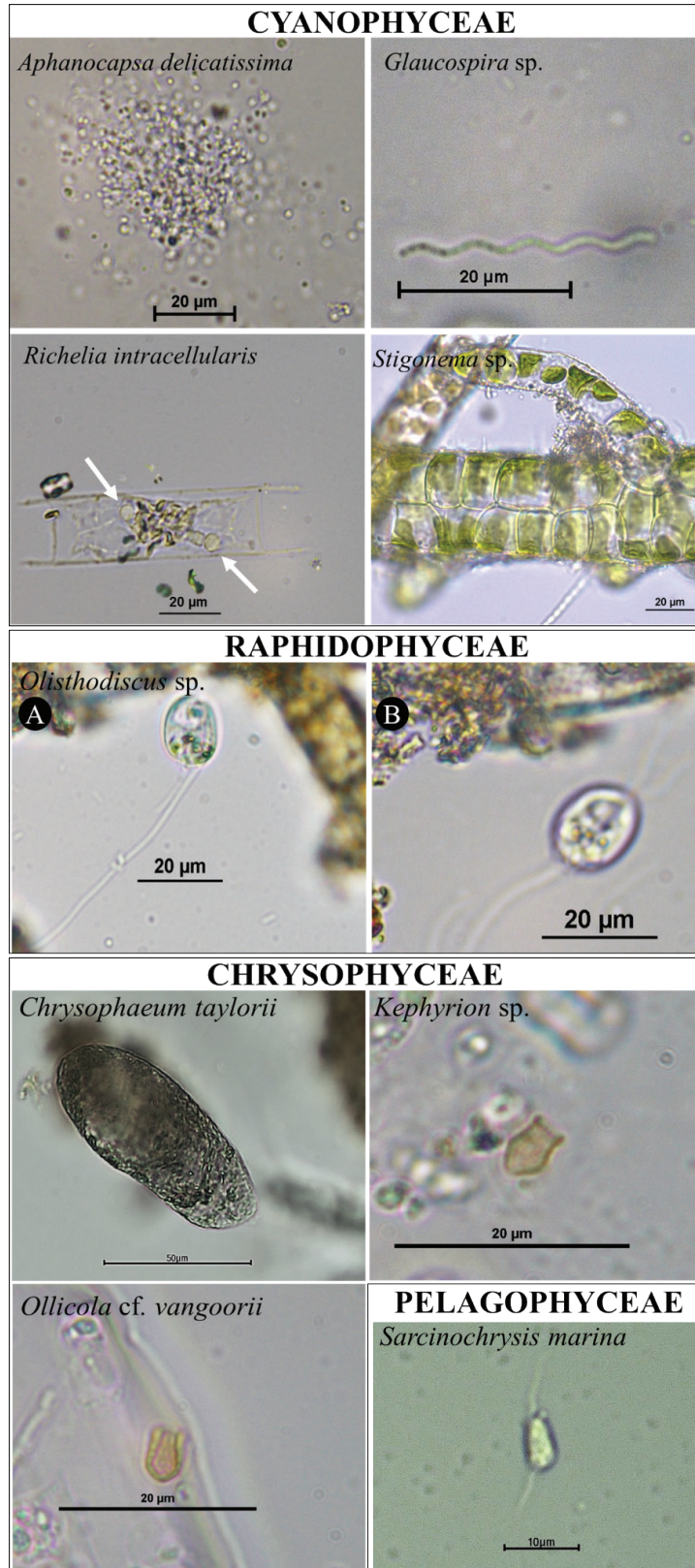
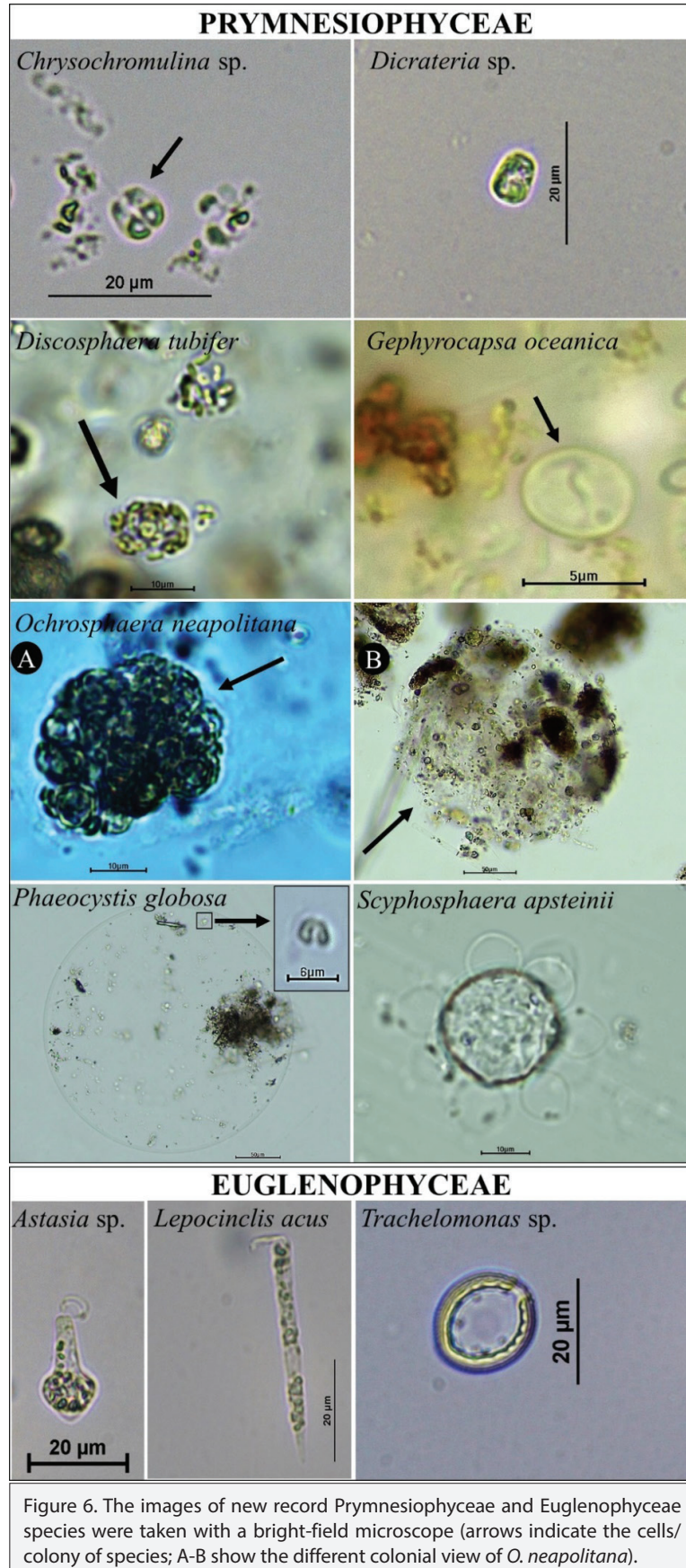


Figure 5. The images of new record Cyanophyceae, Raphidophyceae, Chrysophyceae and Pelagophyceae species were taken with a bright-field microscope (arrows indicate the heterocysts of *R. intracellularis*; A-B show the different images of *Olisthodiscus* sp.).



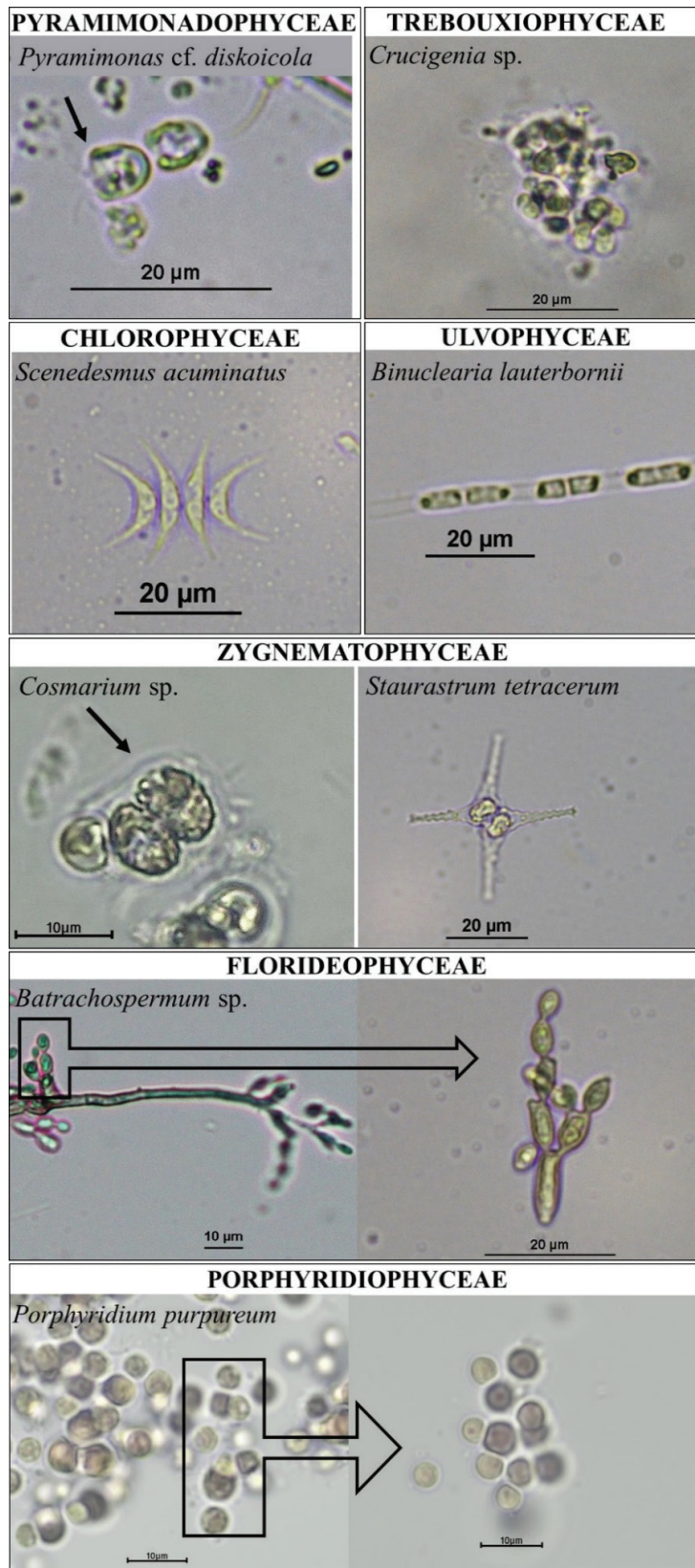
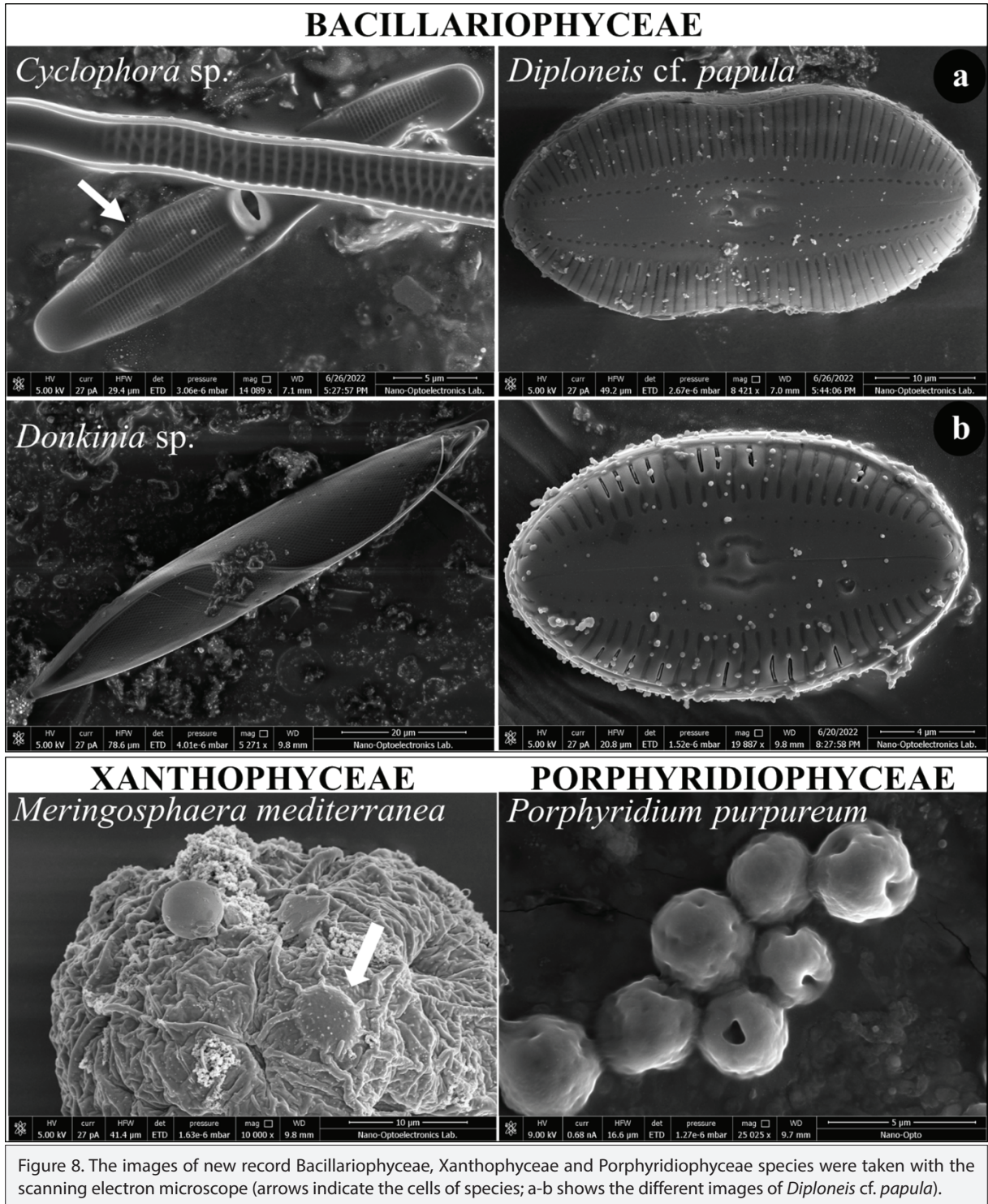


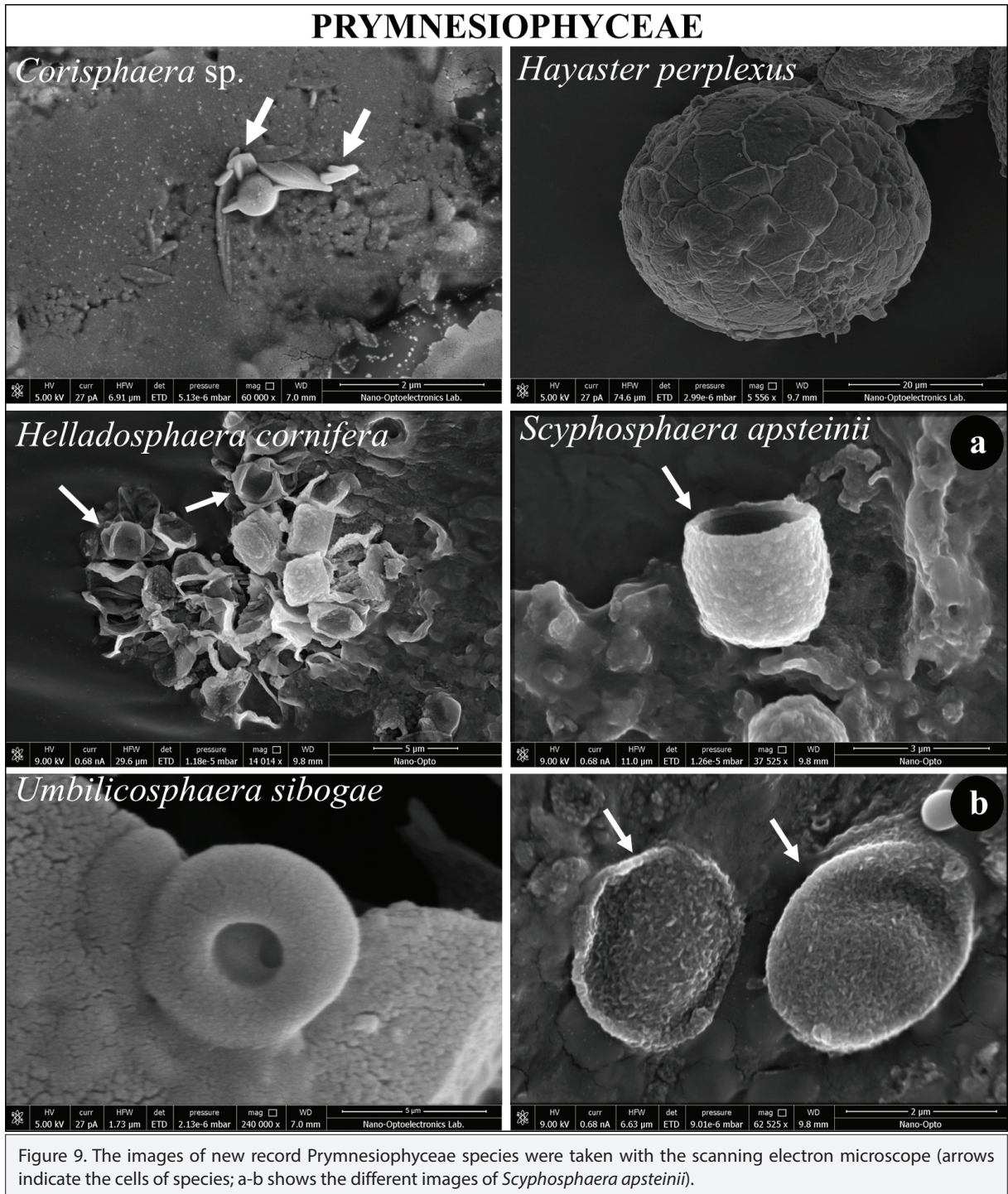
Figure 7. The images of new record other microalgae species were taken with a bright-field microscope (arrows indicate the cells/colony of species).



6), Zygnematophyceae with two taxa (Figure 7) and each of other classes (Xanthophyceae, Pelagophyceae, Raphidophyceae, Pyramimonadophyceae, Trebouxiophyceae, Chlorophyceae, Ulvophyceae, Florideophyceae and Porphyridiophyceae; Figures 5-8) included one taxon (Table 1).

Eleven species among these 66 new record taxa were potentially toxic and/or harmful microalgae (45-49). These toxic

species (*Amphidinium carterae*, *A. operculatum*, *Coolia monotis*, *Karenia* cf. *brevis*, *K. cf. mikimotoi*, *K. cf. selliformis*, *Ostreopsis* sp., *Chrysophaeum taylorii*, *Chrysochromulina* sp., *Ochrosphaera neapolitana* and *Phaeocystis globosa*) should be monitored carefully. Among these, *Karenia* cf. *selliformis* and *Ochrosphaera neapolitana* were recorded for the first time from Turkish coastal waters.



Species Descriptions

The descriptive features of the species reported as new records for Turkish coastal waters are given below (species at genus level were not described).

CHROMOPHYTA Christensen (1962); Bourrelly (1968); Hibberd (1972)

Class: BACILLARIOPHYCEAE Haeckel, 1878

Order: Hemialales Round & Crawford, 1990

Family: Hemialaceae Heiberg, 1863

Genus: *Eucampia* Ehrenberg, 1839

Eucampia cf. groenlandica Cleve, 1896

Cells are silicified, curved or straight, spiral chains occasional. Apical length of cells varied between 16.5-18.7 µm and perivalvar axis were 95.6-100.0 µm, as in the literature (25).

Locality: This species was found only in the St.9 (August 2021) and its abundance was 1500 cells L⁻¹.

Order: Licmophorales Round, 1990
Family: Licmophoraceae Kützing, 1844
Genus: *Licmophora* Agardh, 1827

Licmophora cf. inflata Mereschkowsky, 1901
Cells are narrow in girdle view, linear-wedge shaped with slightly rounded upper corners as mentioned in Hustedt (31). The cell size was 42.9 µm in length and 6.1 µm in width.
Locality: The cells of this species were found only in plankton net samples in the St.5 (May 2021, the Sea of Marmara).
Class: DINOPHYCEAE Fritsch, 1927
Order: Syndiniales Loeblich III, 1982
Family: Amoebophryaceae Cachon ex Loeblich III
Genus: *Amoebophrya* Koeppen, 1894

Amoebophrya ceratii (Koeppen) Cachon, 1964
Synonym: *Hyalosaccus ceratii* Koeppen, 1899
Endocyttoplasmic parasitic dinoflagellates which they do not have chloroplasts (39). Their cells were found into the dinoflagellate *Phalacroma rotundatum*. The diameters of these specimens varied between 4.5-8.5 µm.
Locality: The cells of this species were found only in plankton net samples in the Sts.2, 4, and 15 (June 2022, Sea of Marmara).
Order: Gymnodiniales Lemmermann, 1910
Family: Kareniacea Bergholtz, Daugbjerg, Moestrup & Fernández-Tejedor 2005
Genus: *Karenia* Hansen & Moestrup, 2000

Karenia cf. selliformis Haywood, Steidinger & MacKenzie, 2004
Epitheca hemispherical flattened or slightly conical and generally smaller than hypotheca; thin oval outline in longitudinal section. The size of cells was 20-32 µm long, and 16-32 µm wide as mentioned in Haywood et al. (37).
Locality: The cells of this species were found only in plankton net samples in the St.5 (May 2021).
Order: Procoentrales Lemmermann, 1910
Family: Procoentrales Stein, 1883
Genus: *Prorocentrum* Ehrenberg, 1834

Prorocentrum cf. emarginatum Fukuyo, 1981
An anterior margin is broadly excavated in the valve view of the small and oval cells. There are tiny pores, which are postmedian arranged radially similar to the literature (26). The size of cells was 46-50 µm in length and 43-46 µm in width.
Locality: The cells of this species were found only in plankton net samples in the St.7 (June 2022) and St.9 (August 2021).

Prorocentrum shikokuense Hada, 1975
Synonym: *Prorocentrum donghaiense* Lu, 2001
Cells are asymmetric, vary in shape, and are elongated, narrowing toward the posterior ends. Cells were 20.4-22.9 µm long and 7.6-8.1 µm wide, as mentioned in Takano & Matsuoka (40).
Locality: This species was observed in the St.7 (August 2021), and St.16 (June 2021). Its maximum abundance was determined as 2400 cells L⁻¹ in the St.16.
Class: CHRYSOPHYCEAE Pascher, 1914

Order: Chromulinales Pascher, 1910
Family: Dinobryaceae Ehrenberg 1834
Genus: *Ollicola* Vørs, 1992

Ollicola cf. vangoorii (Conrad) Vørs, 1992
Synonyms: *Calycomonas wulfii* Conrad, 1938; *Calycomonas vangoorii* (Conrad) Lund, 1960; *Codonomonas vangoorii* W.Conrad, 1938
Description: Cells are tiny and have one chloroplast and a lorica. The size of lorica was 6 µm in length and 3 µm in width as mentioned in Vørs (35).
Locality: This species was just recorded in the St.8 (April 2021), and its abundance was 200 cells L⁻¹.
Class: XANTHOPHYCEAE Allorge ex Fritsch, 1935
Order: Mischococcales Fritsch, 1927
Family: Pleurochloridaceae Pascher, 1937
Genus: *Meringosphaera* Lohmann, 1903

Meringosphaera mediterranea Lohmann, 1903
Synonym: *Meringosphaera baltica* Lohmann
Cells spherical, there are long spines and radiating in all directions. The size of cell was 6.2 µm in diameter, and it has six long spines similar to the literature (24).
Locality: The cells of this species were found only in plankton net samples in the St.6 (May 2022).
Class: PELAGOPHYCEAE Andersen & Saunders in Andersen, Saunders & Paskind, 1993
Order: Sarcinochrysidales Gayral & Billard, 1977
Family: Sarcinochrysidaceae Gayral & Billard, 1977
Genus: *Sarcinochrysis* Geitler, 1930

Sarcinochrysis marina Geitler, 1930
There are two flagella which are two different directions and they are longer than cell length similar to the literature (24). The cells were 7.2-7.9 µm long and 4.7-5.8 µm wide as mentioned in Han et al. (43).
Locality: The cells of this species were observed in the St.7 (August 2021), and St.13 (August 2021), and its maximum abundance was recorded as 400 cells L⁻¹ in the St.13.

Class: PRYMNESIOPHYCEAE Hibbert, 1976
Order: Isochrysidales Pascher, 1910
Family: Noelaerhabdaceae Jerkovic, 1970
Genus: *Gephyrocapsa* Kamptner, 1943

Gephyrocapsa oceanica Kamptner, 1943
Synonym: *Crenalithus daronicooides* P.H.Roth, 1973
Cells are spherical, and the size of the central area and the development of a collar around the distal opening of the central canal may vary (23). The cell was 4.7 µm in length and 3.8 µm in width
Locality: There was just a specimen in the St.14.
Order: Coccolithales Schwarz, 1932
Family: Calcidiscaceae Young & Bown, 1997
Genus: *Hayaster* Bukry, 1973

Hayaster perplexus (Bramlette & Riedel) Bukry, 1973
Synonym: *Discoaster perplexus* Bramlette & Riedel 1954

The coccoliths are polygonal and thin. The distal shield is straight and larger than the proximal one. Crystallites radiate from a simple centre point and are essentially equant (33). The size of coccoliths was between 8.1 and 11.8 µm in diameter as mentioned in Young et al. (44).

Locality: There was just a specimen in the St.6 (May 2022).

Genus: *Umbilicosphaera* Lohmann, 1902

Umbilicosphaera sibogae (Weber Bosse) Gaarder, 1970

Synonyms: *Coccolithus sibogae* (Weber Bosse) Schiller; *Coccosphaera sibogae* Weber Bosse, 1901; *Cyclococcolithus sibogae* (Weber Bosse) Gaarder, 1959; *Umbilicosphaera mirabilis* (Lohmann) Lohmann, 1902

The coccoliths are circular, and the centre is open and broad. The size of the cell was 6.4 µm in diameter and central aperture was 2.3 µm similar to the literature (36).

Locality: There was just one coccolith in the St.1

Family: Calyptosphaeraceae Boudreaux & Hay, 1969

Genus: *Helladosphaera* Kamptner, 1937

Helladosphaera cornifera (Schiller) Kamptner, 1937

Synonym: *Syracosphaera cornifera* Schiller, 1913

The coccoliths are helladololiths consisting of an oval tube, about 1.5 µm long and 1.0 µm wide, with a thin bridge on each coccolith as mentioned in Heimdal (23). The size of cells was between 2.5-2.7 µm in length and 2.0-2.1 µm in width.

Locality: There was just a specimen in the St.4 (May 2022).

Family: Hymenomonadaceae Senn, 1900

Genus: *Ochrosphaera* Schussnig, 1930

Ochrosphaera neapolitana Schussnig, 1930

Synonym: *Ochrosphaera verrucosa* Schussnig, 1940

Cells are surrounded by a single layer of tremaliths and are circular in the distal view. Cells are 5-12 µm in diameter (38). The size of our samples were between 6.8-7.2 µm in diameter.

Locality: The coccoliths of this species were observed in the St.2 and St.15 (May 2022).

CHLOROPHYTA Reichenbach, 1834

Class: PYRAMIMONADOPHYCEAE Moestrup & Daugbjerg, 2019

Order: Pyramimonadales Chadefaud, 1950

Family: Pyramimonadaceae Korshikov, 1938

Genus: *Pyramimonas* Schmarida, 1849

Pyramimonas cf. diskoicola Hardardóttir, Lundholm, Moestrup & Nielsen, 2014

The cells elongate with parallel sides and are distinctly longer than wide. The four flagella are equal, slightly longer than the body, and located in the apical area. The cells were 6.2-7.3 µm in length and 4.9-5.2 µm in width similar to the literature (42).

Locality: This species was observed only in the St.9 (April 2021), and its abundance was 500 cells L⁻¹.

Class: ULVOPHYCEAE Mattox & Stewart, 1978

Order: Ulotrichales Borzi, 1895

Family: Gloeotilaceae Ettl & Gärtner, 1995

Genus: *Binuclearia* Wittrock, 1886

Binuclearia lauterbornii (Schmidle) Proshkina-Lavrenko, 1966
Synonym: *Planctonema lauterbornii* Schmidle, 1903

This species has a multicellular unbranched filament. Cells are cylindrical, and the chloroplasts are usually band-shaped and parietal positioned. The size of cells was 11.2-12.7 µm in length, and 3.1 µm in width similar to the literature (30).

Locality: This species was observed in the St.8 (April 2021), 10 (April 2021), 12 (May 2021), and 15 (June 2022). The maximum abundance was detected in the St.12 as 5000 cells L⁻¹.

CHAROPHYTA Migula, 1889

Class: ZYGNEMATOPHYCEAE Round ex Guiry, 2013

Order: Desmidiaceae Bessey, 1907

Family: Desmidiaceae Ralfs, 1848

Genus: *Staurastrum* Meyen ex Ralfs, 1848

Staurastrum tetracerum Ralfs ex Ralfs, 1848

Cell was deeply constricted and sinus V- or U-shaped. The semi-cell body was usually bowl-shaped to rectangular. The cell body had some spines on it as mentioned in Coesel & Meesters (50). The length of cell was 20 µm in length and 5 µm in width

Locality: This species was only observed in the plankton net sample of St.10 (April 2021).

RHODOPHYTA, Wettstein, 1901

Class: PORPHYRIDIOPHYCEAE Shameel, 2001

Order: Porphyridiales Kylin, 1937

Family: Porphyridiaceae Kylin, 1937

Genus: *Porphyridium* Nägeli, 1849

Porphyridium purpureum (Bory) K.M.Drew & R.Ross, 1965

Synonym: *Aphanocapsa cruenta* (Smith) Hansgirg, 1885; *Byssus purpurea* Lamarck, 1778; *Chaos sanguinari* Bory ex Desmazières, 1823; *Coccolithis cruenta* (Smith) Sprengel, 1827; *Merrettia purpurea* (Bory) Trevisan, 1848; *Olivia cruenta* Gray, 1821; *Palmella cruenta* (Smith) Agardh, 1824; *Phytoconis cruenta* (Smith) Trevisan, 1842; *Phytoconis purpurea* Bory de Saint-Vincent, 1797; *Porphyridium cruentum* (Gray) Nägeli, 1849; *Porphyridium marinum* Kylin, 1937; *Sarcoderma sanguineum* Ehrenberg; *Tremella cruenta* Smith, 1807

The cells could be single or irregular colonies and circular-shaped. The cells include a single chloroplast. The size of cells was 3.4-5.0 µm in diameter, as showed in Gantt & Conti (32).

Locality: This species was only observed in the plankton net samples of St.11 (December 2021).

DISCUSSION

Phytoplankton are primary producers in the food chain and their biodiversity is important for a healthy functioning of marine ecosystem. The number of microalgae species of a certain region can give us some important information about its ecological status. So, it may be said that an increase in biodiversity in the microalgae community in the marine environment will have a positive effect on its water quality. Therefore, the revealing of phytoplanktonic biodiversity has a very importance meaning in the marine ecosystem.

The most comprehensive check-list of microalgae of Turkish seas was created in 2001 (1). Koray (1) listed 7 prokaryotic and 485 eukaryotic microalgae taxa in his study. It is considered that this number of microalgae taxa has increased significantly in the studies carried out in the Sea of Marmara in the last two decades. In the present study conducted in the Sea of Marmara and the Aegean Sea, 25 microalgae taxa were recorded for the first time for Turkish seas. The addition of these new record taxa will provide an important contribution to the check-list of microalgae of Turkish seas.

The most detailed check-list study covered the Sea of Marmara with the Turkish Straits System and was achieved by Balkis & Tas (3), and at total of 333 microalgae taxa were reported. The new record taxa continued to be reported also after 2016 (4-6, 8). With the contribution of these studies, the number of microalgae known to exist in the Sea of Marmara increased to 348. Four more taxa were recorded for the first time during the mucilage event in the Sea of Marmara in 2021 (7, 9). With the addition of 65 more taxa identified in the present study, the recorded number of taxa in the Sea of Marmara increased to 417. In addition, a total of 452 benthic diatom species was reported in a study conducted in the Sea of Marmara (51). However, the researchers (51) have not been provided any descriptive information and images on the new recorded species for the Turkish seas and the Sea of Marmara.

The increase of the number of taxa for Turkish seas including the Sea of Marmara will provide an important contribution. In addition, it should be taken into account that there were some potentially toxic and/or harmful species among the new recorded species. Among the new recorded taxa during this study period, 2 of 25 taxa for Turkish seas and 9 taxa within 65 taxa for the Sea of Marmara were detected as potentially toxic and/or harmful. Among these, *Phaeocystis globosa*, *Chrysophaeum taylorii*, *Ochrosphaera neopolitana*, *Coolia monotis* and *Ostreopsis* spp. are species that are able to produce mucilage, and it was suggested that other species belonging the genus *Phaeocystis* (*P. pouchettii*) were responsible from mucilage on the surface (7). It has been reported that *Chrysophaeum taylorii*, observed for the first time in the Aegean Sea in 2011, was a new record for Turkish coastal waters (47). This species is known to cause the mucilage phenomenon in benthic regions, especially in the Atlantic and Western Pacific coasts. *Ochrosphaera neopolitana* is observed frequently in the littoral zones of seas, and it is a known species from especially the North Atlantic, Indian Ocean and Mediterranean Sea (38). Along with this species, some coccolithophores are able to produce TEP (Transparent Exopolymer Particulate) and DMSP (Dimethylsulfoniopropionate). These species are able to produce TEP at the growth phase stage in haploid and diploid life stages and in a viral infection (48, 52). *Ostreopsis* sp., one of the toxic species among them, is an epiphytic/epibenthic species and displays a distribution in a coastal area (53). One of the toxic species of this genus is *Ostreopsis ovata* and it was reported for the first time in Turkish coastal areas from the Aegean Sea (54). *Coolia monotis*, a benthic species, can form bloom and excretes mucilage in different amounts in certain environmental conditions (55). This species produces a polyether toxin (a mono-sulphated polyether

compounds; Cooliatoxin) from a monosulfate polyether from bioactive compounds (56). Moreover, it has been detected that *Coolia monotis* with *Amphidinium carterae*, are other harmful algal bloom species recorded in a previous study (57). Considering their possible negative effects on the marine ecosystem, these harmful microalgae should be monitored carefully with the main environmental factors.

CONCLUSION

The observation of the new microalgae species in the present study carried out in the Sea of Marmara indicates that microalgae species may be used as indicator organisms depending on the various environmental conditions. The remarkable changes in the phytoplankton composition indicate the probable effect of climate change. The increase of freshwater inflows, carried by streams after terrestrial runoffs following the precipitation, causes an increase in the freshwater microalgae species in marine ecosystems. It is considered that the changes in the phytoplankton composition in the study area were a result of the effect of the environmental conditions. Furthermore, potentially toxic and/or harmful species detected among the new recorded taxa during this study should be monitored carefully accompanied by the environmental factors affecting their abundance.

Acknowledgments: This study has been supported by TUBITAK 1001-121G116 & 1001-121G028 projects and the "Integrated Marine Pollution Monitoring 2020-2022 Programme" carried out by the Ministry of Environment and Urbanization/General Directorate of EIA, Permit and Inspection/Department of Laboratory, Measurement and coordinated by TUBITAK-MRC ECPI. Also, the authors are thankful to Istanbul University, Nano & Optoelectronics Research Laboratory staff for their valuable assistance in taking the SEM pictures of the species.

Peer Review: Externally peer-reviewed.

Author Contributions: Conception/Design of Study- T.D., N.B.O., S.T.; Data Acquisition- T.D., N.B.O., S.T., F.B.P., M.B., C.D., M.S.; Data Analysis/Interpretation- T.D., N.B.O., S.T., F.B.P., M.B.; Drafting Manuscript- T.D., N.B.O., S.T., F.B.P., M.B., C.D., M.S.; Critical Revision of Manuscript- T.D., N.B.O., S.T.; Final Approval and Accountability- T.D., N.B.O., S.T., F.B.P., M.B., C.D., M.S.

Conflict of Interest: Authors declared no conflict of interest.

Financial Disclosure: This study was supported by TÜBİTAK with Project Number 121G116.

REFERENCES

1. Koray T. A check-list for phytoplankton of Turkish seas. EgeJFAS 2001; 18(1-2): 1-23.
2. Balkis N. List of phytoplankton of the Sea of Marmara. J Black Sea/ Medit Environ 2004; 10: 123-41.
3. Balkis N, Tas S. Phytoplankton of the Sea of Marmara: A review. Özsoy, E., Çağatay, M. N., Balkis, N., Balkis, N., Öztürk, B., editors. The Sea of Marmara: Marine Biodiversity, fisheries, conservation and governance. Istanbul: Turkish Marine Research Foundation (TUDAV), Istanbul; 2016.p.326-43.

4. Tas S, Hernández-Becerril DD. Diversity and distribution of planktonic diatom genus *Chaetoceros* (Bacillariophyceae) in the Golden Horn Estuary (Sea of Marmara). *Diatom Res* 2017; 32(3): 309-23.
5. Balci M, Balkis N. Assessment of phytoplankton and environmental variables for water quality and trophic state classification in the Gemlik Gulf, Marmara Sea (Turkey)". *Mar Pollut Bull* 2017; 115: 172-89.
6. Balkis-Ozdelice N, Durmus T, Toklu-Alicli B, Balci M. Phytoplankton composition related to the environmental conditions in the coastal waters of the Gulf of Erdek. *Indian J Mar Sci* 2020; 49(9): 1545-59.
7. Balkis-Ozdelice N, Durmus T, Balci M. A preliminary study on the intense pelagic and benthic mucilage phenomenon observed in the Sea of Marmara. *Int J Environ Geoinformatics* 2021; 8(4): 414-22.
8. Kayadelen Y, Balkis-Ozdelice N, Durmus T. Determination of seasonal changes in phytoplankton community of the coastal waters of Burgaz Island (the Sea of Marmara). *J Mar Biolog Assoc UK* 2022; 102(3-4): 1-13.
9. Eker-Develi E, Kideys AE. First record of the diatom *Nitzschia navisvaringica* in the Sea of Marmara. *Mar Sci Tech Bull* 2022; 11(2): 231-35.
10. Yüce H. Investigation of the Mediterranean water in the Black Sea. *Bülten* 1988; 5: 121-57.
11. Yüce H, Türker A. Marmara Denizi'nin fiziksel oşinografik özellikleri ve Akdeniz suyunun Karadeniz'e girişi. Uluslararası çevre sorunları sempozyumu tebliğleri. İstanbul: Türkiye; 1991.p.284-303.
12. Beşiktepe ŞT, Sur Hİ, Özsoy E, Abdullatif MA, Oğuz T, Ünlüata Ü. The circulation and hydrography of the Marmara Sea. *Prog Oceanogr* 1994; 34: 285-334.
13. Beşiktepe Ş, Özsoy E, Latif MA, Oğuz T. Marmara Denizi'nin hidrografisi ve Dolaşımı, (Hydrography and Circulation of the Marmara Sea). *Marmara Sea 2000 Symposium*; 2000 Nov 11-2; İstanbul: Türkiye.p.1-14.
14. Aksu A, Caglar-Balkis N, Taskin Ö. Müsilajın çevresel şartlarda değişen kimyasal karakterizasyonunun incelenmesi (in Turkish). Ozturk İ, Seker M, editors. *Marmara Denizi'nin Ekolojisi: Deniz Salyası Oluşumu, Etkileşimleri ve Çözüm Önerileri*. Ankara: TÜBA; 2021.p.127-35.
15. Ergül H, Balkis-Ozdelice N, Koral M, Aksan S, Durmuş T, Kaya M, Kayal M, Ekmekçi F, Oltan C. The early stage of mucilage formation in the Marmara Sea during spring 2021. *J Black Sea/Medit Environ* 2021; 27(2): 232-57.
16. Thronsen J. Preservation and storage. Sournia A, editor. *Phytoplankton Manual*. Paris: UNESCO; 1978.p.69-74.
17. Utermöhl H. Zur vervollkommnung der quantitativen phytoplankton methodik. *Mitt - Int Ver Theor Angew Limnol* 1958; 9: 1-38.
18. Sukhanova IN. Settling without the inverted microscope. Sournia A, editor. *Phytoplankton Manual*. Paris: UNESCO; 1978.p.97.
19. Semina HJ. Treatment of an aliquot sample. Sournia A, editor. *Phytoplankton Manual*. Paris: UNESCO; 1978.p.181.
20. Hendeby NI. A revised check-list of British marine diatoms. *J Mar Biol Assoc UK* 1974; 54(2): 277-300.
21. Battarbee RW, Cameron NG, Golding P, Brooks SJ, Switsur R, Harkness D, McGovern A. Evidence for holocene climate variability from the sediments of a Scottish remote mountain lake. *J Quat Sci* 2001; 16(4): 339-46.
22. Perez-Lopez H, Duran-Riveroll L, Gomez-Lizarraga L, Mendoza-Garfias M. Simple method for preparing delicate dinoflagellate of the genus *Amphidinium* for scanning electron microscopy. *Microsc Microanal* 2020; 26(2): 1366-9.
23. Heimdal BR. Modern Coccolithophorids. Tomas CR, editor. *Marine Phytoplankton*. California: Academic Press; 1993.p.147-236.
24. Thronsen J. The planktonic marine flagellates. Tomas CR, editor. *Marine Phytoplankton*. California: Academic Press; 1993. p. 7-146.
25. Hasle GR, Syvertsen EE. Marine diatoms. Tomas CR, editor. *Identifying Marine Phytoplankton*. California: Academic Press; 1997. p. 5-385.
26. Steidinger KA, Tangen K. Dinoflagellates. Tomas CR, editor. *Identifying Marine Phytoplankton*. California: Academic Press; 1997.p.387-570.
27. World Register of Marine Species. Chromista. Accessed at: <https://www.marinespecies.org/aphia.php?p=taxdetails&id=7>. Accessed on 1 Oct 2022.
28. Algaebase. World-wide electronic publication, National University of Ireland, Galway. <https://www.algaebase.org>. Accessed on 1 Oct 2022.
29. Cleve PT. Synopsis of the Naviculoid diatoms (Part I). *K Sven Vetensk Akad Handl* 1894; 26(2): 1-194.
30. Schmidle W. Bemerkungen zu einigen Süßwasserragen. *Ber Deutsch Bot Ges* 1903; 21: 346-55.
31. Hustedt F. Bacillariophyta (Diatomeae). In: *Die Süßwasser-Flora Mitteleuropas* (Ed: Pascher A, 2nd edition). Jena: Verlag von Gustav Fischer; 1930.
32. Gantt E, Conti SF. The ultrastructure of *Porphyridium cruentum*. *J Cell Biol* 1965; 26(2): 365-81.
33. Bukry D. Phytoplankton stratigraphy, deep sea drilling project leg 20, Western Pacific Ocean. *Initial Rep Deep Sea Drill Proj* 1973; 20: 307-17.
34. Fukuyo Y. Taxonomical study on benthic dinoflagellates collected in coral reefs. *Bull Japan Soc Sci Fish* 1981; 47(8): 967-78.
35. Vørs N. Heterotrophic amoebae, flagellates and heliozoa from the Tvärminne area, Gulf of Finland, in 1988-1990. *Ophelia* 1992; 36: 1-109.
36. Young JR, Geisen M, Cros L, Kleijne A, Sprengel C, Probert I, Ostergaard JB. A guide to extant coccolithophore taxonomy. *Journal of Nannoplankton Research* 2003; Special Issue 1: 1-125.
37. Haywood AJ, Steidinger KA, Truby EW, Bergquist PR, Bergquist PL, Adamson J, MacKenzie L. Comparative morphology and molecular phylogenetic analysis of three new species of the genus *Karenia* (Dinophyceae) from New Zealand. *J Phycol* 2004; 40: 165-79.
38. Fresnel J, Probert I. The ultrastructure and life cycle of the coastal coccolithophorid *Ochrosphaera neapolitana* (Prymnesiophyceae). *Eur J Phycol* 2005; 40(1): 105-22.
39. Hoppenrath M, Elbrachter M, Drebes G. *Marine phytoplankton*. Stuttgart: E. Schweizerbart'sche Verlagsbuchhandlung; 2009.
40. Takano Y, Matsuoka K. A comparative study between *Prorocentrum shikokuense* and *P. donghaiense* (Prorocentrales, Dinophyceae) based on morphology and DNA sequences. *Plankton Benthos Res* 2011; 6(4): 179-86.
41. Idei M, Sato S, Watanabe T, Nagumo T, Mann DG. Sexual reproduction and auxospore structure in *Diploneis papula* (Bacillariophyta). *Phycologia* 2013; 52(3): 295-308.
42. Hardardottir S, Lundholm N, Moestrup OE, Nielsen TG. Description of *Pyramimonas diskoicola* sp. nov. and the importance of the flagellate *Pyramimonas* (Prasinophyceae) in Greenland sea ice during the winter-spring transition. *Polar Biol* 2014; 37: 1479-94.
43. Han Y, Graf L, Reyes CP, Melkonian B, Andersen RA, Yoon HS, Melkonian M. A Re-investigation of *Sarcinochrysis marina* (Sarcinochrysidales, Pelagophyceae) from its type locality and the descriptions of *Arachnochrysis*, *Pelagospilus*, *Sargassococcus* and *Sungminbooa* genera nov. *Protist* 2018; 169(1): 79-106.

44. Young JR, Bown PR, Lees JA. International Nannoplankton Association. www.mikrotax.org/Nannotax3. Accessed on 12 Oct 2022.
45. Holmes MJ, Lewis RJ, Jones A, Hoy AW. Cooliatoxin, the first toxin from *Coolia monotis* (Dinophyceae). *Nat Toxins* 1995;3(5):355-62.
46. Faust, MA, Gullede RA. Identifying harmful marine dinoflagellates. *Contributions from the United States National Herbarium, National Museum of Natural History*, 2002; 42: 1-144.
47. Aktan Y, Topaloğlu B. First record of *Chrysophaeum taylorii* Lewis & Bryan and their benthic mucilaginous aggregates in the Aegean Sea (Eastern Mediterranean). *J Black Sea/Medit Environ* 2011; 17(2): 159-70.
48. Pedrotti ML, Fiorini S, Kerros ME, Middelburg JJ, Gattuso JP. Variable production of transparent exopolymeric particles by haploid and diploid life stages of coccolithophores grown under different CO₂ concentrations. *J Plankton Res* 2012; 34(5): 388-98.
49. Lundholm N, Churro C, Fraga S, Hoppenrath M, Iwataki M, Larsen J, Mertens K, Moestrup Ø, Zingone A (Eds) (2009 onwards). IOC-UNESCO Taxonomic Reference List of Harmful Micro Algae. <https://www.marinespecies.org/hab>. Accessed on 7 Nov 2022.
50. Coesel PFM, Meesters KJ. *European Flora of the Desmid Genera Staurastrum and Staurodesmus*. Utrecht: KNNV Publishing; 2014.
51. Akcaalan R, Kaleli A, Koker L. Distribution of marine benthic diatoms on the coasts of the Sea of Marmara and their responses to environmental variables. *J Mar Syst* 2022; 234: 103780.
52. Nissimov JI, Vandzura R, Johns CT, Natale F, Haramaty L, Bidle KD. Dynamics of transparent exopolymer particle production and aggregation during viral infection of the coccolithophore, *Emiliania huxleyi*. *Environ Microbiol* 2018; 20(8): 2880-97.
53. Rhodes L. World-wide occurrence of the toxic dinoflagellate genus *Ostreopsis schmidt*. *Toxicon* 2011; 57: 400-7.
54. Bizsel N, Aligizaki K. Detection of *Ostreopsis cf ovata* in coastal waters of Turkey (Eastern Aegean Sea). *International Conference on Ostreopsis Development*; April 2011; Villefranche: France.
55. Lewis NI, Wolny JL, Achenbach JC, Ellis L, Pitula JS, Rafuse C, Rosales DS, McCarron P. Identification, growth and toxicity assessment of *Coolia Meunier* (Dinophyceae) from Nova Scotia, Canada. *Harmful Algae* 2018; 75: 45-56.
56. Holmes MJ, Lewis RJ, Jones A, Hoy AWW. Cooliatoxin, the first toxin from *Coolia monotis* (Dinophyceae). *Nat Toxins* 1995; 3: 355-62.
57. Aquino-Cruz A, Okolodkov YB. Impact of increasing water temperature on growth, photosynthetic efficiency, nutrient consumption, and potential toxicity of *Amphidinium cf. carterae* and *Coolia monotis* (Dinoflagellata). *Rev Biol Mar Oceanogr* 2016; 51(3): 565-80.

Phenolic Extracts of *Zizyphus lotus* L. (Rhamnaceae) and *Ruta chalepensis* L. (Rutaceae) as Alternatives to Antibiotics and their Antimicrobial Effects on Clinical Multidrug-Resistant Pathogens

Nour El Houda Bekkar¹ , Boumediene Meddah¹ , Yavuz Selim Cakmak² ,
Bahadır Keskin³ , Pascal Sonnet⁴ 

¹Mustapha Stambouli University, Faculty of Life and Nature Sciences, Microbiological Engineering and Health Safety, Laboratory of Bioconversion, Mascara, Algeria

²Aksaray University, Faculty of Science and Letters, Department of Biotechnology and Molecular Biology, Aksaray, Turkiye

³Yildiz Technical University, Faculty of Arts & Science, Department of Chemistry, Istanbul, Turkiye

⁴Picardie Jules Verne University, AGIR Laboratory: Infectious Agents, Resistance and Chemotherapy, EA4294 UFR of Pharmacy, Amiens, France

ORCID IDs of the authors: NEH.B. 0000-0002-1194-3472; B.M. 0000-0001-7946-012X; Y.S.C. 0000-0001-8954-5485; B.K. 0000-0001-8502-8982; P.S. 0000-0003-0118-9151

Please cite this article as: Bekkar NEH, Meddah B, Cakmak YS, Keskin B, Sonnet P. Phenolic Extracts of *Zizyphus lotus* L. (Rhamnaceae) and *Ruta chalepensis* L. (Rutaceae) as Alternatives to Antibiotics and their Antimicrobial Effects on Clinical Multidrug-Resistant Pathogens. Eur J Biol 2022; 81(2): 163-183. DOI: 10.26650/EurJBiol.2022.1129558

ABSTRACT

Objective: The phytochemical composition and the antibacterial and antifungal properties of *Zizyphus lotus* L. (ZL) leaves and *Ruta chalepensis* L. (RC) aerial parts harvested from Oran in northwest Algeria were assessed against multidrug-resistant (MDR) clinical pathogens.

Materials and Methods: The phenolic compounds identification in the hydromethanolic (MeOH.E) and the aqueous extracts (Aq. E) was done by HPLC-DAD analysis, while the phenolic, flavonoid and tannin contents were determined using quantitative methods. The antibacterial and antifungal activities were also determined. The synergistic effect between both plants was elucidated using the checkerboard dilution test.

Results: An important phenolic content was determined with higher concentrations in *Z. lotus* leaves extracts than *R. chalepensis*. The HPLC-DAD analysis allowed us to identify benzoic acid as the major phenolic compound in *Z. lotus* extracts, while catechin, quercetin and epicatechin were the major compounds identified in *R. chalepensis*. Important antimicrobial activity was observed against all the clinical pathogen strains. The most potent effect was estimated against MDR *Salmonella enterica* sp. *arizonae* with 20 ± 0.1 mm of growth inhibition zone diameter using RC^{MeOH.E}, while a diameter of 35.03 ± 0.06 mm was measured using ZL^{MeOH.E}. Also, important anti-Candida activity was estimated. No synergistic interaction against the different microbial strains was determined by applying the combinations of both plants' extracts, with a fractional inhibitory concentration index superior to 4 ($FIC_{index} > 4$).

Conclusion: *Z. lotus* and *R. chalepensis* can be exploited in the medical field as a potential source of antimicrobial components.

Keywords: Antibiotic alternatives, antimicrobial activity, multidrug-resistant pathogens, phenolic compounds, *R. chalepensis*, *Z. lotus*



Corresponding Author: Nour El Houda Bekkar

E-mail: bekkarnour8@gmail.com; nourelhouda.bekkar@univ-mascara.dz

Submitted: 12.06.2022 • **Revision Requested:** 29.08.2022 • **Last Revision Received:** 14.10.2022 •

Accepted: 20.10.2022 • **Published Online:** 28.12.2022

Content of this journal is licensed under a Creative Commons Attribution-NonCommercial 4.0 International License.



INTRODUCTION

The increase of food-borne illnesses or collective food poisoning (CFP) and nosocomial infections transmitted in reanimation services and hospitals are considered a global health concern. The majority of the responsible microorganisms are multidrug-resistant (MDR) bacteria and microscopic fungi, germs with high pathogenicity expressed by the presence of genes for virulence and resistance to the various antibiotics commonly used in the medical field, which makes the therapeutic application of these drugs less efficient for the treatment of microbial infections, whatever food-borne disease or nosocomial infection. In addition, patients suffer from considerable side effects from antibiotic consumption, like vomiting, nausea, abdominal pain, loss of appetite and development of other microbial infections. Some antibiotic treatments induce the development of other infectious germs, such as candidiasis induced after therapeutic consumption of an antibiotics association for the treatment of gastric ulcers caused by *Helicobacter pylori* (1).

Furthermore, the most important side effect is the dysbiosis phenomenon. Antibiotics exert a noteworthy adverse effect on the gut microbial balance (*Bifidobacterium*, *Lactobacillus*, *Streptococcus*, and against *Enterobacteriaceae*). Thus, the immune system is stimulated by the attack of a broad spectrum of pathogenic microbes (barrier effect) and the penetration of foreign agents (chemicals or microbials) at the level of the gastrointestinal mucosa (2).

Therefore, there is increasing interest in the study of biomolecules that have a stronger antimicrobial effect than antibiotics, but do not pose any danger to the health of the organism. Phenolic extracts of medicinal plants have been reported to possess potent antioxidant and antimicrobial effects in the literature.

In Algeria, three species of the family Rhamnaceae are widely used as food and folk medicine: *Zizyphus spina-christi* (L.) Desf., *Zizyphus lotus* (L.) and *Zizyphus jujuba* Mill. (3). Studies have allowed the isolation of flavonoids (4,5), triterpenes (6), alkaloids (7), indole derivatives (8) and fatty acids in the genus *Zizyphus* (9). The sedative and hypnotic effects of saponins, flavonoids and fatty acids of *Zizyphus* species have also been demonstrated (10).

The health-promoting effects of the genus *Zizyphus* in various diseases such as respiratory problems, scabies, pimples, mouth and gums inflammation or in memory enhancement have been indicated due to its bioactive compounds. This plant is also utilized in the cosmetic sector due to its efficient properties for bleaching the face and neck, and in hair growth (11,12).

Z. lotus is popularly called "Sedra" in Algeria and its delicious fruits known as "Nbeg," are consumed fresh. *Z. lotus* is widely used in the field of nutrition, cosmetics and healthcare. It is consumed in Algeria as infusions and decoctions to treat a variety of diseases, including urinary tract infections and digestive dis-

orders, and also acts as a hypoglycemic, hypotensive, antidiarrheal, and anti-ulcer agent (13-15).

Also, the fruit parts of this plant are used for the treatment of several illnesses: diarrhea, intestinal diseases and digestive problems, liver disorders, insomnia, skin infections and abscess (16-18). Various studies have reported that the plant has antibacterial, anti-inflammatory, anticancer, antifungal and antiulcerogenic activity, as well as analgesic and gastroprotective effects (19-24). *Z. lotus* fruits contain significant concentrations of health-promoting compounds: minerals, vitamins, amino acids, fatty acids and phenolic compounds (25).

Moreover, the bark, fruit, leaves, roots and seeds of *Z. lotus* have been reported to possess antimicrobial effects, antioxidant activity and antispasmodic and litholytic effects (26-30). In their recent study, Bencheikh et al. (31) demonstrated the nephroprotective effect of *Z. lotus* fruits in a gentamicin-induced acute kidney injury model in rats.

R. chalepensis (Rutaceae) is popularly called "Fidjel," This plant species is of particular interest in traditional medicine due to its potential therapeutic effect against various human pathogens. *R. chalepensis* is known for its richness of secondary metabolites, such as essential oils, alkaloids (0.4-1.4%), flavonoids, coumarins (chalepensine), furocoumarines, phenols, tannins and saponins (32).

The biological properties of *R. chalepensis* extracts have been studied by several researchers. In their study, Loizzo et al. (33) showed that the leaf extracts of this plant exhibited important antioxidant and hypoglycemic activities. In another study, antimicrobial efficacy against *Streptococcus mutans*, a major etiological pathogen in dental caries was demonstrated for chalepensin extracted from *R. chalepensis* (34).

Szewczyk et al. (35) have demonstrated antioxidant and antimicrobial properties of phenolic extracts of *R. chalepensis* phenolic extracts. Khadhri et al. (36) and Adsersen et al. (37) determined the antiacetylcholinesterase (AChE) activities of ethanol extracts obtained from the leaf parts of this plant. *R. chalepensis* is also used in traditional medicine for the treatment of rheumatism, fever, mental disorders, dropsy, menstrual problems, anxiety and epilepsy disorders (38).

To the best of our knowledge, there have been no reports on the antibacterial and antifungal effects against multidrug-resistant clinical pathogens of phenolic components isolated from *Z. lotus* and *R. chalepensis* harvested from Oran-Taфраoui region in northwest Algeria. Thus, the objective of this work was to determine the quantitative contents of total phenolic compounds, flavonoids and tannins from the methanol and aqueous extracts of *Z. lotus* and *R. chalepensis*. The determination of qualitative and quantitative variation of polyphenolic compounds was performed using colorimetric methods and HPLC-DAD analysis. In addition, the antimicrobial activities against test bacteria and fungi were examined.

MATERIALS AND METHODS

Plant Sample Collection

Fresh samples of *Z. lotus* leaves were collected during the month of July 2017 and *R. chalepensis* aerial parts (leaves, flowers and small stems) during April 2017 from northwest Algeria's Oran-Taфраoui region. The collected plant parts were identified by a botanist from the Department of Biology of Mascara University, Algeria.

Microbial Strains: Isolation and Identification

The antimicrobial effect was assessed on pathogenic clinical isolates including Gram-positive bacteria (*Staphylococcus aureus*, *Streptococcus pyogenes* and *Enterococcus faecalis*), Gram-negative bacteria (Enteropathogenic *Escherichia coli*, *Salmonella enterica* sp. *Arizonae*, *Proteus mirabilis*, *Hafnia alvei*) and pathogenic microscopic fungi (*Candida albicans*). All these microbial strains were isolated from different clinical samples (n=25): stool specimens of gastroenteritis patients of both sex (n=15; man and women), samples from the oral cavity and the periodontal pocket of periodontal disease patients (n=4) and urine of patients with urinary tract infections (n=6). The microbial identification was carried out using commercial kits (API STAPH, API 20E and API CANDIDA) that were administered according to the BioMerieux manual and adopting standard procedures. The coagulase and blood hemolysin tests were also performed (39,40).

Antibiotics Susceptibility Test

To complete the identification of the various isolated clinical strains, antibiotic susceptibility testing is necessary for the determination of antibiotic resistance profiles for each microbial strain. For that, susceptibility to different antibiotics was evaluated using the agar diffusion method and carried out according to the Clinical and Laboratory Standards Institute guidelines (41). The results were interpreted following the critical diameters mentioned by the FMS-AC (42) and the FMS-AC/EUCAST (43). After that, only the microbial strains presenting a multidrug-resistance were selected for the antimicrobial activity assays. The antibiotics tested were Spiramycin, Amoxicillin, Pristinamycin, Nitroxolin, Neomycin, Oxacillin, Colistin, Penicillin-G and Fluconazole.

Phenolic Compounds Extraction

Preparation of Hydromethanolic and Aqueous Extracts

For the preparation of hydromethanolic extracts (MeOH.E), powdered fresh leaves of *Z. lotus* and leaf, small stem and flower parts of *R. chalepensis* (50 g) were macerated in 500 mL of hydromethanolic solution of 80% concentration at room temperature (20°C) and in shaded glass vials that inhibit light penetration. The filtrates were then evaporated to dryness under vacuum using a rotary evaporator at 40°C. The aqueous extracts (Aq.E) of the tested materials were prepared by decoction procedure. 50 g of each plant material were boiled in 500 mL of distilled water at 100°C/30 min (44, 45). The prepared polyphenolic extracts (PPEs) were stored in small shaded vials at 4°C until use. The extraction yields (%) for each PPE were calculated as

the ratio between the plant weights (m_1 ; g) and the dry extract weight (m_2).

Phytochemical Screening

The qualitative phytochemical analysis was done to identify the main chemical groups of bioactive substances contained in the leaves of *Z. lotus* and the aerial parts of *R. chalepensis*. Phenolic compounds, flavonoids, tannins, saponosides, anthocyanins, glycosides, terpenes and coumarins were analyzed in this study (46).

Phenolic Compounds

The detection of polyphenolic compounds was carried out by a test with ferric perchloride (FeCl_3) at 10%. To each 5 mL of the hydromethanolic extract and the aqueous extract, 1 to 2 drops of FeCl_3 were added to observe the appearance of an intense black-green precipitate.

Flavonoids

The detection of flavonoids was carried out by a magnesium test. A few drops of concentrated HCl (2N) and a small amount of magnesium (Mg) were added to each 2 mL of the MeOH.E and Aq.E extracts with agitation for 3 minutes. The appearance of an orange or red color indicated the presence of flavonoids (cherry red color: flavonols; orange color: flavones; purplish red color: flavanones).

Tannins

1 mL of the MeOH.E and 10% of the Aq.E were mixed with 1 mL of distilled water and 1 to 2 drops of 10% diluted FeCl_3 solution. The test is considered positive by the appearance of a dark green color for catechic tannins (condensed tannins). The appearance of a dark blue color indicates the presence of gallic tannins.

Saponins

2 mL of the extract was added to 2 mL of a 1% lead acetate solution. The test is considered positive by the formation of a white precipitate. Thus, the presence of saponosides was determined qualitatively by the appearance, after agitation, of persistent foam for more than 15 min.

Anthocyanins

5 mL of each extract was added to 4 mL of 30% concentrated ammonia hydroxide (NH_4OH). The appearance of a red color indicates the presence of anthocyanins.

Glycosides

The demonstration of glycosides was carried out using concentrated sulfuric acid solution (96%). 150 mg of the MeOH.E and the Aq.E dissolved in 2 mL of methanol and distilled water respectively was mixed with a few drops of sulfuric acid solution (96%). The appearance of a blue-red color indicates the presence of glycosides.

Terpenes

The detection of terpenes in all extracts was performed by mixing 5 mL of phosphomolybdic acid and 5 mL of concentrated

sulfuric acid (96%) with each 5 mL of 10% MeOH.E and Aq.E solutions. The appearance of a blue color reveals the presence of terpenes.

Coumarins

The detection of coumarins was carried out using 2 g of the plant powder mixed with 20 mL of ethanol. The mixture was boiled for 15 min under reflux. After cooling and filtering, 10 drops of potassium hydroxide (KOH) and a few drops of 10% hydrogen chloride (HCl) were added to the extracts solutions. The formation of turbidity indicates the presence of coumarins.

Determination of Total Phenolic, Flavonoid and Tannin Contents

The total phenolic content (TPC), total flavonoid content (TFC) and total tannin content (TTC) were determined according to the methods described by Boizot and Charpentier (47) using Folin Ciocalteu as reagent, Samatha et al. (48) using the 2% aluminum trichloride solution ($AlCl_3$) and Ba et al. (49) using vanillic acid, respectively. The concentrations of these phenolic contents were calculated after the absorbance measurements using a spectrophotometer (JENWAY model, 6400 spectrophotometer). All the determinations were performed in triplicate.

Chromatographic Analysis

Thin Layer Chromatography (TLC)

The qualitative determination and detection of the different bioactive components in the MeOH.E and Aq.E extracts were carried out by applying thin layer chromatography (TLC), as described by Sanogo et al. (50). In-brief, 5 μ L of plant extracts solutions at a concentration of 20 mg/mL was applied on silica gel plates of the Silicagel 60 F₂₅₄ type (Merck, Darmstadt, Germany). The plates were then deposited in a mobile phase, which consists of a solvents mixture (Butanol/ acetic acid/water (60/15/35) (v/v/v)). After the phenolic components' migration and separation, the different spots observed in the silica gel plates were detected under UV light at 254 and 366 nm, and the relative migration rates (R_m), were estimated using the following formula: $R_m = d/D$, where d: Migration distance of the substance, D: Migration distance of the solvents mixture. Gallic acid, catechin, quercetin, rutin and vanillin were used as control.

High Performance Liquid Chromatography (HPLC-DAD)

The chemical composition of the MeOH.E and Aq.E extracts was determined according to the method described by Caponio et al. (51), with slight modifications. It was performed using an HP-Agilent 1290 Infinity HPLC equipped with a C₁₈ column and diode array detector (DAD).

Antimicrobial Activity Assessment

Agar Diffusion Method

The agar-disc diffusion method was applied to determine the antimicrobial potency of the MeOH.E and Aq.E extracts of *Z. lotus* and *R. chalepensis* collected from the Tafraoui region in Oran against the MDR clinical strains previously isolated and identified. Briefly, sterile discs were impregnated in MeOH.E and Aq.E

solutions at a concentration of 200 mg.mL⁻¹ then aseptically deposited on the previously inoculated Muller-Hinton plates with 0.5 McFarland of bacterial and fungal cultures in their exponential growth kinetics. The antimicrobial potency against all the clinical pathogens, determined as resistant strain, sensitive, very sensitive or extremely sensitive, was established according to the criteria of Poncé et al. (52).

Determination of the Antimicrobial Parameters

The microdilution titration method was done to determine the most important parameters in the antimicrobial effect evaluation: the minimum inhibitory concentrations (MIC) and the minimum bactericidal concentrations (MBC). The assays were done according to the method described by Chandrasekaran et al. (53), with slight modifications. After the plants' extracts concentrations and the adjusted microbial suspensions were blended out in equal volumes, the sterile 96-well microplates were aseptically incubated at 37°C and the microbial growth kinetics were measured after optical density lecture at 620 nm for bacteria and 450 nm for fungi at different time-kill kinetics: 0, 4, 18, 48 and 72 hours, using a Microplate Absorbance Reader (Tecan Spectra II Microplate Reader). The results were expressed as log germs/mL for each plant extract concentration. The minimum bactericidal and fungicidal concentrations (MBCs) were determined after inoculating a microbial suspension from each dilution that represented the MIC values on MHA agar. After incubation at 37°C /24 h, the viable bacteria and fungi cells were counted. The dilution for which no bacterial or fungal colony was counted represents the MBC and the MFC. Reports of MBC/MIC were calculated to determine the efficiency of PPEs as bactericidal or bacteriostatic.

Dilution Checkerboard Method

The microdilution checkerboard method was used to evaluate the interaction between *Z. lotus* and *R. chalepensis* phenolic extracts against MDR clinical pathogens. So this technique allowed us to have an idea whether a medicinal plant extract is more effective when used alone or in combination, in order to broaden its action spectrum on pathogenic microorganisms and to induce many more bactericidal and fungicidal effects.

During this study, we evaluated the synergistic, additive or antagonistic effect using the following combinations between the prepared extracts of both studied plants: $ZL^{MeOH.E}/RC^{MeOH.E}$ and $ZL^{Aq.E}/RC^{Aq.E}$.

The association interaction of both antimicrobial extracts was quantified after the determination of the MIC values for each PPE (previously determined) and by calculating the index of fractional inhibitory concentrations (FICI or Σ FIC) which are the lowest concentrations of the antimicrobial extracts in combination, completely inhibiting the microbial growth. A volume of 50 μ L of Mueller Hinton broth was distributed in all the sterile cupules of the microplates. The first extract solution of *Z. lotus* was serially diluted along the abscissa, while the extracts of *R. chalepensis* were diluted along the ordinate. Subsequently, each solution was inoculated with 50 μ L of the bacterial or fun-

gal cultures and the microplates were incubated at 37°C for 18 hours. The value of the combination is calculated using the FIC in the cupules where no microbial growth is observed, and considered effective MIC for the combination (54).

The FICs were measured as follows: $FICI = FIC_A + FIC_B$, where FIC_A is the MIC of drug A (MeOH.E or Aq.E of *Z. lotus*) in the combination / MIC of drug A alone, and $FIC_B = MIC$ of drug B (MeOH.E or Aq.E of *R. chalepensis*) in the combination / MIC of drug B alone. The combination is considered synergistic when the FICI is ≤ 0.5 , additive: $0.5 < FICI \leq 1$, indifference: $1 < FICI \leq 4$ and antagonism: $FICI > 4$ (55).

Statistical Analysis

The statistical analyses were performed using the SPSS software for comparing between the averages using the one-way and multivariate analysis of variance (ANOVA). Significant differences were also mentioned: $p < 0.05$.

RESULTS

Clinical Strains Isolation and Identification

Results of the different bacterial and fungal strains isolation and identification are shown in Table 1.

Antibiotics Susceptibility Testing

The antibiogram profile for each microbial strain is shown in Table 2. Based on the critical diameters of antibiotic susceptibility stated by the French Society of Microbiology, the FSM-AC. (2013) and the FMS-AC/EUCAST. (2018), the results showed that only 8 clinical isolates among the 41 microbial strains were multidrug-resistant.

Extraction Yield, Qualitative and Quantitative Determination of Polyphenols

Results of the extraction yields, the phytochemical screening and quantification of the polyphenols, flavonoids and tannins in the polyphenolic extracts of *Z. lotus* and *R. chalepensis* are shown in Table 3.

The results showed that aqueous extracts represented the highest yield: $23.97 \pm 0\%$ for *Z. lotus* and $30.83 \pm 0.0057\%$ for *R. chalepensis*, followed by the crude methanolic extract where the proportions were about $17.68 \pm 0.015\%$ for *Z. lotus* and $14.73 \pm 0.03\%$ for *R. chalepensis*. No significant differences were determined between the yields of both plants PPE, whereas the highest yields among the different PPE were registered for RC^{Aq.E} followed by ZL^{Aq.E} (Table 3).

The phytochemical examination revealed the presence of seven biochemical groups: phenols, flavonoids, condensed tannins, glycosides, terpenes, coumarins and saponosides. We noted the richness in polyphenols, catechin tannins and terpenes in both tested plants with positive reactions of the phytochemical tests. In addition, abundant flavonoids were noted in the aqueous extract and hydromethanolic extract of *R. chalepensis* compared to *Z. lotus* extracts. However, a very abundant presence of saponosides was found in *Z. lotus* extracts compared to

Table 1. Microbial strains isolated from different biological samples.

Biological sample	N*	
Gastroenteritis	15	S ₁ SP _{1-M} <i>S. aureus</i>
		S ₂ SP _{1-M} <i>E. coli</i>
		S ₃ SP _{1-M} <i>P. mirabilis</i>
		S ₄ SP _{1-M} <i>C. albicans</i>
		S ₅ SP _{2-W} <i>S. enterica</i> sp. <i>arizonae</i>
		S ₆ SP _{2-W} <i>C. albicans</i>
		S ₇₋₈ SP _{3-4-M} <i>E. coli</i>
		S ₉ SP _{5-W} <i>E. coli</i>
		S ₁₀ SP _{5-W} <i>S. enterica</i> sp. <i>arizonae</i>
		S ₁₁ SP _{6-M} <i>E. coli</i>
		S ₁₂ SP _{7-M} <i>S. enterica</i> sp. <i>arizonae</i>
		S ₁₃₋₁₄ SP _{8-9-W} <i>E. coli</i>
		S ₁₅ SP _{10-M} <i>E. coli</i>
		S ₁₆ SP _{11-W} <i>S. enterica</i>
		S ₁₇ SP _{11-W} <i>H. alvei</i>
Urinary tract infections	06	S ₁₈ SP _{12-M} <i>P. mirabilis</i>
		S ₁₉ SP _{12-M} <i>H. alvei</i>
		S ₂₀ SP _{12-M} <i>E. faecalis</i>
		S ₂₁ SP _{13-W} <i>E. coli</i>
		S ₂₂ SP _{14-M} <i>E. coli</i>
		S ₂₃ SP _{15-M} <i>E. coli</i>
		S ₂₄ SP _{16-W} <i>S. aureus</i>
		S ₂₅ SP _{17-W} <i>S. aureus</i>
		S ₂₆ SP _{18-W} <i>E. coli</i>
		S ₂₇ SP _{19-W} <i>S. aureus</i>
S ₂₈₋₂₉ SP ₂₀₋₂₁ <i>E. coli</i>		
Periodontitis	04	S ₃₀ SP _{22-W} <i>S. pyogenes</i>
		S ₃₁ SP _{22-W} <i>Streptococcus</i> sp.
		S ₃₂ SP _{22-W} <i>E. faecalis</i>
		S ₃₃ SP _{23-M} <i>S. pyogenes</i>
		S ₃₄ SP _{23-M} <i>Streptococcus</i> sp.
		S ₃₅ SP _{23-M} <i>S. aureus</i>
		S ₃₆ SP _{24-W} <i>Streptococcus</i> sp.
		S ₃₇ SP _{24-M} <i>E. faecalis</i>
		S ₃₈ SP _{25-W} <i>S. aureus</i>
		S ₃₉ SP _{25-W} <i>Streptococcus</i> sp.
S ₄₀ SP _{25-W} <i>E. faecalis</i>		
S ₄₁ SP _{25-W} <i>C. albicans</i>		

*N: Number of samples, S: Strain, SP: Sample, M: Man, W: Women.

Table 2. Antibiotic resistance profiles of the pathogenic clinical isolates.

Microbial strains code	Clinical isolates	SP	AMX	PT	NI	N	OX	CT	P	P-G	FCA
S ₁ SP ₁	S ₁ / <i>S. aureus</i>	0 ^R	12 ^R	0 ^R	18 ^I	15 ^I	0 ^R	12 ^R	10 ^R	0 ^R	/
S ₃₃ SP ₂₃	S ₂ / <i>S. pyogenes</i>	0 ^R	15 ^R	0 ^R	22 ^I	15 ^I	0 ^R	12 ^R	0 ^R	0 ^R	/
S ₂₀ SP ₁₂	S ₃ / <i>E. faecalis</i>	23 ^S	19 ^I	20 ^I	12 ^I	0 ^R	0 ^R	0 ^R	21 ^I	0 ^S	/
S ₈ SP ₄	S ₄ / <i>E. coli</i> (EPEC)	0 ^R	0 ^R	0 ^R	20 ^I	15 ^R	0 ^R	11 ^R	0 ^R	0 ^R	/
S ₃ SP ₁	S ₅ / <i>P. mirabilis</i>	0 ^R	15 ^R	0 ^R	14 ^I	16 ^R	0 ^R	0 ^R	10 ^R	0 ^R	/
S ₁₀ SP ₅	S ₆ / <i>S. enterica</i> sp. <i>arizonae</i>	0 ^R	0 ^R	0 ^R	22 ^I	18 ^S	0 ^R	13 ^R	0 ^R	0 ^R	/
S ₁₇ SP ₁₁	S ₇ / <i>H. alvei</i>	0 ^R	0 ^R	0 ^R	20 ^I	20 ^S	0 ^R	13 ^R	0 ^R	0 ^R	/
S ₄ SP ₁	S ₈ / <i>C. albicans</i>	0 ^R	0 ^R	0 ^R	0 ^R	0 ^R	0 ^R	0 ^R	0 ^R	0 ^R	0 ^R

S: Strain, SP: Sample, SP: Spiramycin, AMX: Amoxycillin, PT: Pristinamycin, NI: Nitroxolin, N: Neomycin, OX: Oxacillin, CT: Colistin, P: Penicillin-G, FCA: Fluconazole, R: Resistant, S: Sensitive, I: Intermediate sensitivity.

Table 3. Polyphenolic compounds extraction yields, phytochemical screening and quantitative determination of polyphenols (mg/g DE) in *Z. lotus* and *R. chalepensis* harvested from Tafraoui region in Oran.

Plant Extracts	Yield (%)	TP	F	T	A _t	G	T _r	I	C	S/Fl	TPC	TFC	TTC
ZL ^{MeOH.E}	17.68±0.015*	+++	++	+++	-	+	+++	-	-	+++/500	268.65±7*	109.45±2.87*	94.18±4.84*
ZL ^{Aq.E}	23.97±0*	+++	++	+++	-	+	+++	-	-	+++/500	222.85±5.99*	71.51±2.34*	113.87±0.79*
RC ^{MeOH.E}	14.73±0.03*	+++	+++	+++	-	+++	+++	-	++	+/125	214.06±4.71*	81.16±4.42*	18.97±1.79*
RC ^{Aq.E}	30.83±0.0057*	+++	+++	+++	-	+++	+++	-	++	+/125	224.18±6.28*	59.83±1.96*	20.76±0*

TP: Total polyphenols, F: Flavonoids, T: Tannins, A_t: anthocyanins, G: Glycosides, T_r: terpenes, I: Iridoid, C: coumarins, S: saponins, Fl: Foam index, TPC: Total phenol content, TFC: Total flavonoid content, TTC: Total tannin content. Measurements were performed in triplicate. Results are expressed as means± SD. *p*<0.05: Significant*.

R. chalepensis, which was illustrated by a marked foam index: IM=500. We also noted the presence of glycosides with a positive test reaction for *R. chalepensis* compared to *Z. lotus*.

The quantitative analysis of the methanolic and aqueous extracts was carried out by dosage of the main bioactive components: total polyphenols (PPT), flavonoids (TFC) and tannins (TTC). The contents of these phenolic compounds are shown in Table 3. We quantified variable important concentrations of the main chemical groups per gram of the dry extract. Both plants were detected to have higher doses of PPT (ZL^{MeOH.E}=268.65±7 mg GAE/g DE, RC^{MeOH.E}=214.06±4.71 mg GAE/g DE, RC^{Aq.E}=224.18±6.28 mg GAE/g DE), of flavonoids (RC^{MeOH.E}=81.16±4.42 mg QE/g DE, RC^{Aq.E}=59.83±1.96 mg QE/g DE) and tannins (ZL^{Aq.E}=113.87±0.79 mg CE/g DE, RC^{Aq.E}=20.76±0 mg CE/g DE) (Table 3).

The aqueous extract of *Z. lotus* showed a PPT content of 222.85±5.996 mg GAE/g DE, while the concentration in the MeOH.E extract was 268.65±7 mg GAE/g DE (Table 3).

The methanolic extract of *R. chalepensis* represented TPC, TFC and TTC of 214.06±0.053 mg GAE/g DE, 81.16±0.06 mg QE/g DE and 18.97±0.002 mg QE/g DE, respectively (Table 3).

Thin Layer Chromatography Analysis (TLC)

Results of the TLC analysis of the different PPE, as well as the standard phenols used: gallic acid, quercetin, catechin, rutin and vanillin are cited in Figure 1 and Table 4. The appearance of numerous spots after molecules' migration on the different TLC plates enabled us to conclude that both plant PPE are richer in various biological substances. Each spot is characterized by its frontal ratio and its color under UV light, at a wavelength of 254 and 366 nm (Figure 1).

Each spot gave a specific color or fluorescence under UV light, which indicates the separated chemical substance identity. Thirteen substances were migrated along the TLC plate of ZL^{MeOH.E}, while 8 substances were detected in ZL^{Aq.E} (Table 4). However, for *R. chalepensis*, the large numbers of molecules were detected in the aqueous extract, of which 14 spots were observed in the TLC plate, while 10 molecule spots were detected for RC^{MeOH.E} (Table 4; Figure 1).

High Performance Liquid Chromatography (HPLC-DAD)

The results of chromatogram profiles and phenolic compounds concentrations are shown in Figure 3 and Table 5. Various phe-

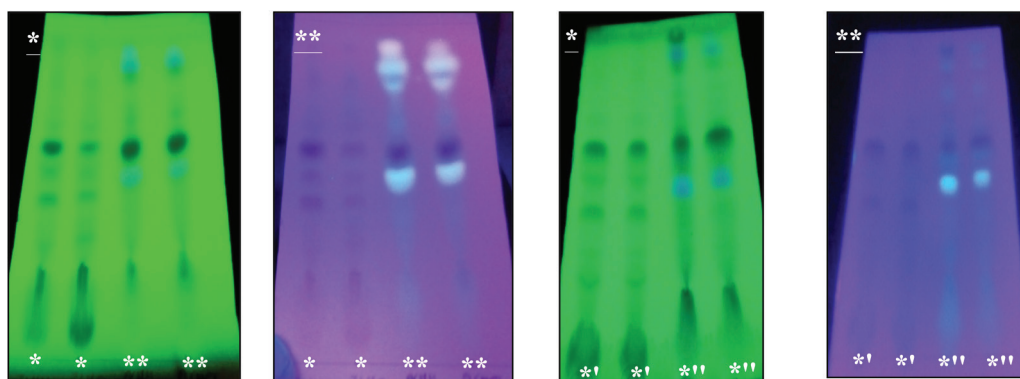


Figure 1. TLC profiles after UV revelation of the methanolic and aqueous extracts of *Z. lotus* and *R. chalepensis* harvested from Tafraoui region, in Oran (North-west Algeria). (*) 254 nm, (**) 366 nm, *: ZL^{MeOH.E}, **: RC^{MeOH.E}, *!: ZL^{Aq.E}, **: RC^{Aq.E}.

Table 4. Frontal ratios (F_R) of polyphenol spots obtained by TLC.

F_R of substances migrating along the TLC plates		
Solvent system used		Eluent E1: butanol/acetic acid/water (60:15:35 ; v/v/v)
Control substance	Gallic acid	0.84*
	Catechin	0.91
	Quercetin	0.94*
	Rutin	0.52*
	Vanillin	0.92
PPE	ZL ^{MeOH.E}	0.07; 0.19; 0.21; 0.33; 0.39; 0.46; 0.52*; 0.57; 0.61; 0.68; 0.72; 0.77; 0.84*
	ZL ^{Aq.E}	0.08; 0.23; 0.29; 0.39; 0.48; 0.57; 0.67; 0.84*
	RC ^{MeOH.E}	0.21; 0.26; 0.42; 0.46; 0.52*; 0.59; 0.66; 0.71; 0.76; 0.84*
	RC ^{Aq.E}	0.17; 0.26; 0.36; 0.45; 0.52*; 0.58; 0.62; 0.66; 0.69; 0.74; 0.78; 0.84*; 0.89; 0.94*

* F_R : Frontal Ratio.

Table 5. Phenolic compounds ($\mu\text{g/g DE}$) identified in the methanolic and aqueous extracts of *Z. lotus* leaves and *R. chalepensis* aerial parts collected from Oran-Taфраoui region, in western Algeria.

Plant Extracts	A	B	C	D	E	F	G	H	I	J	K	L	M	N	O
R_t (min)	5.400	12.430	15.745	18.336	18.917	19.165	21.250	26.385	31.265	33.416	38.571	54.719	59.326	68.506	71.045
ZL^{MeOH.E}	3.54	3.90	2.01	NI	NI	NI	NI	NI	NI	NI	431.34	NI	NI	0.90	2.32
ZL^{Aq.E}	0.88	NI	NI	NI	NI	NI	NI	NI	NI	NI	50.56	NI	NI	NI	NI
RC^{MeOH.E}	1.39	78.38	35.38	6.18	4.29	55.47	1.06	3.76	NI	3.76	NI	NI	NI	NI	129.54
RC^{Aq.E}	7.15	24.42	0.98	0.61	NI	NI	1.57	NI	NI	NI	NI	NI	NI	NI	3.39

A: Gallic acid, B: Catechin, C: Chlorogenic acid, D: Caffeic acid, E: Hydroxybenzoic acid, F: Epicatechin, G: Syringic acid, H: Coumaric acid, I: Trans-ferrulic acid, J: Sinapic acid, K: Benzoic acid, L: Hesperidin, M: Rosmarinic acid, N: Cinnamic acid, O: Quercetin, R_t: Retention time in minutes (min), NI: Not identified.

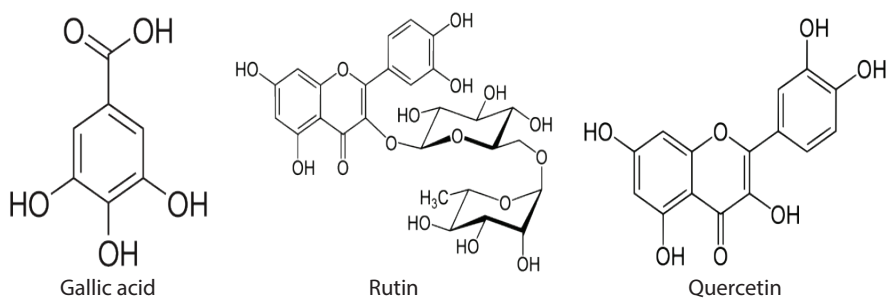


Figure 2. Chemical structure of bioactive compounds containing *Z. lotus* and *R. chalepensis* extracts.

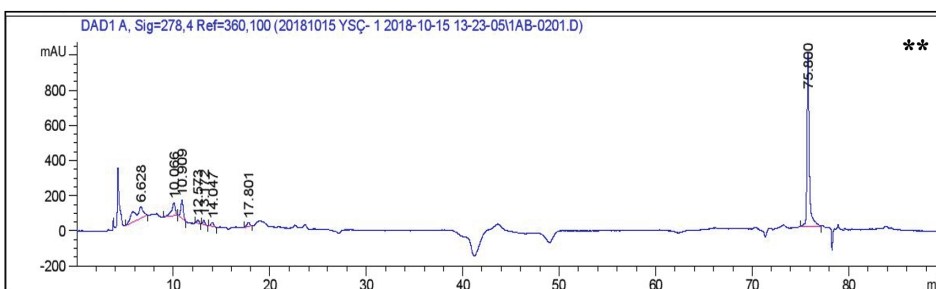
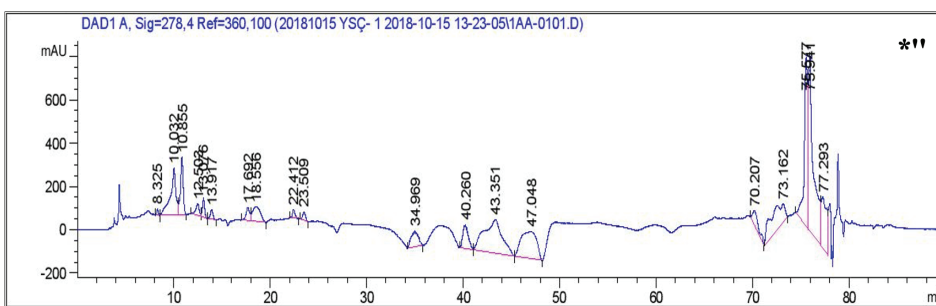
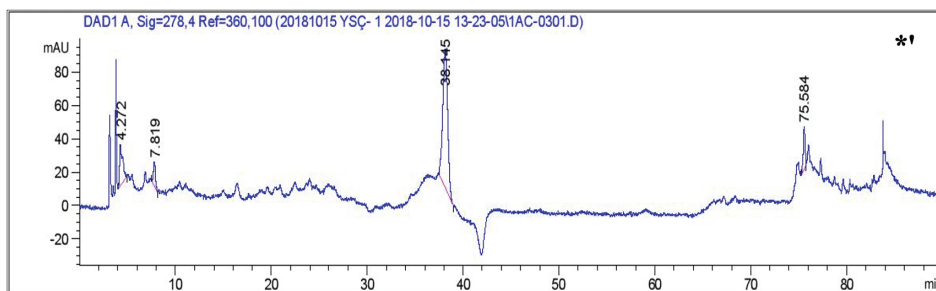
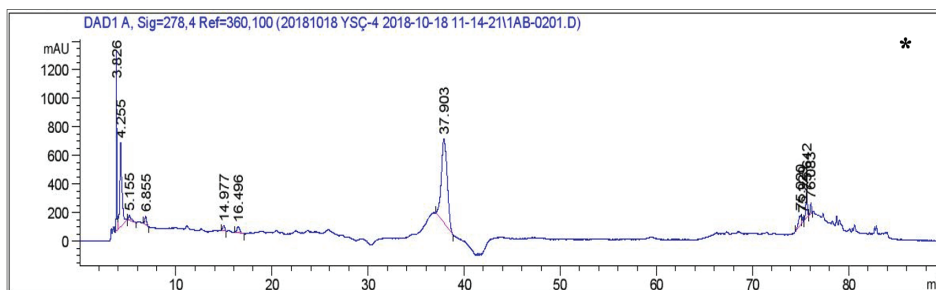


Figure 3. HPLC-DAD phenolic profiles of *Z. lotus* and *R. chalepensis* phenolic extracts detected at 278 nm. *: ZL^{MeOH:E}, **: ZL^{Aq:E}, ***: RC^{MeOH:E}, ****: RC^{Aq:E}.

nolic components were identified and quantified in *Z. lotus* and *R. chalepensis* extracts using the HPLC-DAD analysis, including phenolic acids and flavonoids.

The HPLC results of *Z. lotus* polyphenolic extracts showed the presence of benzoic acid as a major phenolic component in methanolic and aqueous extracts. The highest concentration was quantified in the hydromethanolic extract of the plant (431.34 $\mu\text{g/g}$ DE), while the lower content of this compound was determined in the aqueous extract (50.56 $\mu\text{g/g}$ DE) (Table 5; Figure 3).

Other phenolic acids: Chlorogenic acid, gallic acid, cinnamic acid and flavonoids: Catechin and quercetin were also quantified in ZL^{MeOH.E} and ZL^{Aq.E} extracts with lower concentrations. Quercetin, catechin and chlorogenic acid were quantified only in the methanolic extract of *Z. lotus*.

Furthermore, ten phenolic compounds were identified in RC^{MeOH.E}. These bioactive components included seven phenolic acids (Chlorogenic acid, gallic acid, caffeic acid, hydroxybenzoic acid, syringic acid, coumaric acid and sinapic acid) and three flavonoids (Catechin, epicatechin and quercetin). Quercetin was

qualified as the major phenolic compound in the hydromethanolic extract (129.54 $\mu\text{g/g}$), followed by catechin (78.38 $\mu\text{g/g}$ DE) and chlorogenic acid (35.38 $\mu\text{g/g}$ DE). For RC^{Aq.E}, catechin was identified as a major component, with a concentration of 24.42 $\mu\text{g/g}$ DE, followed by gallic acid (7.15 $\mu\text{g/g}$ DE) and quercetin (3.39 $\mu\text{g/g}$ DE) (Table 5; Figure 3). The chemical structure of the main phenolic compounds identified and quantified in *Z. lotus* and *R. chalepensis* extracts is given in Figure 4.

Antimicrobial Activity

The results of the antimicrobial tests are shown in Tables 6 and 7 and in Figures 5-8. A potent antimicrobial effect was recorded on all bacterial strains using *R. chalepensis* and *Z. lotus* extracts, as well as significant antifungal activity on *C. albicans*, with diameters of the microbial growth inhibition zones exceeding 10 mm. The largest inhibition diameters were recorded using ZL^{MeOH.E} (19.13 \pm 0.23 mm) on *C. albicans* (Table 6).

The MeOH.E and Aq.E of both plants were effective against different MDR Gram-positive and Gram-negative bacteria, as well as against *C. albicans*. In contrast, *S. pyogenes*, *E. faecalis*, *P. mirabilis*, *S. enterica* sp *arizonae* and *H. alvei* were the most sensitive isolates to the extracts of *Z. lotus* and *R. chalepensis*,

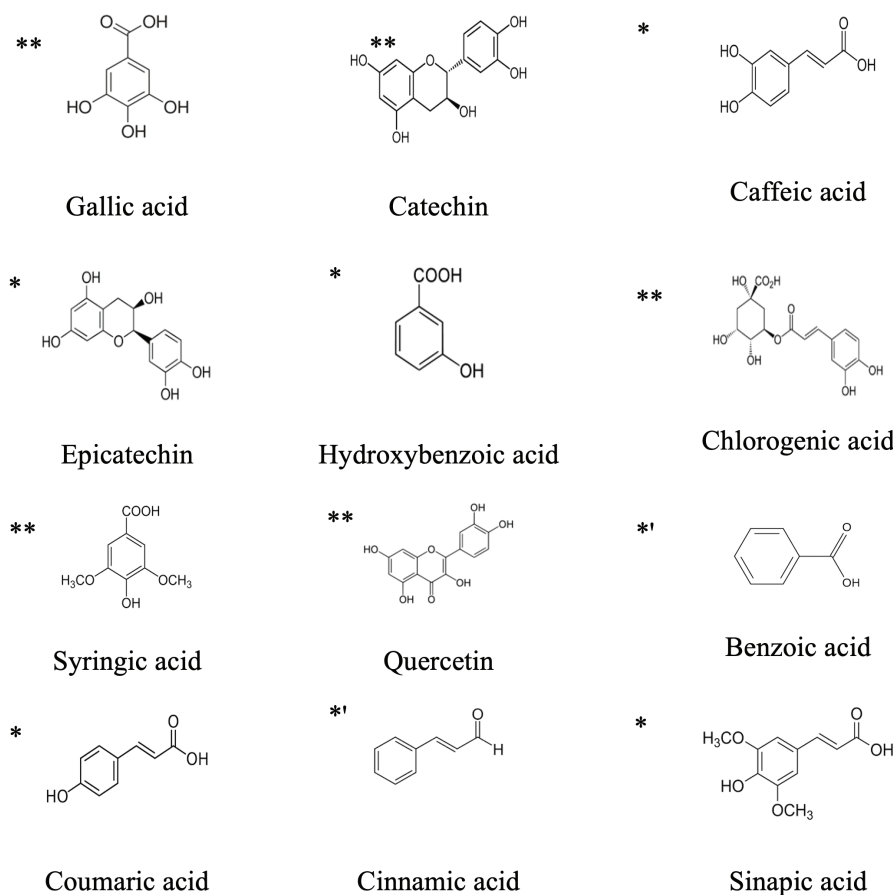


Figure 4. Main phenolic compounds containing *Z. lotus* and *R. chalepensis* extracts. **: Compounds quantified in both plant extracts, *: Compounds quantified only in *R. chalepensis* extracts, *': compounds quantified only in *Z. lotus* extracts.

Table 6. Antimicrobial activity of phenolic extracts of *Z. lotus* and *R. chalepensis* harvested in Tafraoui region-Oran (western Algeria), against pathogenic clinical germs.

Clinical isolates	Diameters of growth inhibition zones (Ø mm)			
	ZL ^{MeOH.E}	ZL ^{Aq.E}	RC ^{MeOH.E}	RC ^{Aq.E}
S ₁	11.13 ±0.23 ^{S*}	11.03 ±0.06 ^{S*}	10.13 ±0.15 ^{S*}	8.97 ±0.06 ^{S*}
S ₂	24.03 ±0.06 ^{EHS*}	24.03 ±0.06 ^{EHS*}	NE	NE
S ₃	24.06 ±0.12 ^{EHS*}	21.03 ±0.06 ^{EHS*}	15.13 ±0.23 ^{HS*}	NE
S ₄	16.03 ±0.06 ^{HS*}	NE	9.03 ±0.06 ^{S*}	11.07 ±0.12 ^{S*}
S ₅	22.06 ±0.12 ^{EHS*}	18.03 ±0.06 ^{HS*}	12.06 ±0.12 ^{S*}	10.1 ±0.17 ^{S*}
S ₆	35.03 ±0.06 ^{EHS*}	25.06 ±0.12 ^{EHS*}	20 ±0.1 ^{EHS*}	NE
S ₇	34.06 ±0.12 ^{EHS*}	33.03 ±0.06 ^{EHS*}	NE	NE
S ₈	19.13 ±0.23 ^{HS*}	15 ±0 ^{HS*}	12.03 ±0.06 ^{S*}	9.16 ±0.2 ^{S*}

Ø (mm): Diameters of growth inhibition zone in millimeter, S₁: *S. aureus*, S₂: *S. pyogenes*, S₃: *E. faecalis*, S₄: *E. coli* (EPEC), S₅: *P. mirabilis*, S₆: *S. enterica* sp. *arizonae*, S₇: *H. alvei*, S₈: *C. albicans*, NE: No effect, R: Resistance (Ø < 8mm), S: Sensitivity (9 mm < Ø < 14 mm), HS: High susceptibility (15 mm < Ø < 19 mm), EHS: Extremely high susceptibility (Ø > 20 mm). The values are presented as the mean of three replicates ± the standard deviation. p < 0.05: Significant*.

Table 7. Quantitative analysis of the antimicrobial parameter: The minimum inhibitory and bactericidal concentrations (MICs, MBCs) against the clinical microbial isolates.

Clinical strains	MIC; MBC; MBC/MIC (mg/mL)			
	ZL ^{MeOH.E}	ZL ^{Aq.E}	RC ^{MeOH.E}	RC ^{Aq.E}
S ₁	100; 200; 2	100; 100; 1	50; 100; 2	200; 200; 1
S ₂	100; 200; 2	50; 200; 4	100; 200; 2	100; 200; 2
S ₃	100; 200; 2	50; 100; 2	50; 100; 2	100; 200; 2
S ₄	100; 200; 2	100; 200; 2	100; 200; 2	200; 200; 1
S ₅	100; 100; 1	200; 200; 1	100; 200; 2	200; 200; 1
S ₆	100; 100; 1	50; 200; 4	50; 100; 2	100; 100; 1
S ₇	100; 100; 1	25; 100; 4	100; 200; 2	100; 200; 2
S ₈	100; 100	50; 100; 2	50; 100; 2	50; 100; 2

with inhibition diameters of 24.03±0.06 mm against *S. pyogenes*, 24.06±0.12 mm and 21.03±0.06 mm against *E. faecalis*, 22.06±0.12 mm, 18.03±0.06 mm, and 24.06±0.12 mm against *P. mirabilis*, 34.06±0.12 mm and 33.03±0.06 mm against *H. alvei* using ZL^{MeOH.E} and ZL^{Aq.E} extracts, respectively.

The diameters of 35.03±0.06 mm, 25.06±0.12 mm and 20±0.1 mm against *S. enterica* sp. *arizonae* were determined using ZL^{MeOH.E}, ZL^{Aq.E} and RC^{MeOH.E}, respectively (Table 6). However, the extracts ZL^{Aq.E}, RC^{MeOH.E} and RC^{Aq.E} did not exert antibacterial effect on *E. coli* and *S. pyogenes*, respectively (Table 6).

All these qualitative results were completed by the quantitative determination of the antimicrobial effect by determining

the most important antimicrobial parameter, the minimum inhibitory concentration (MIC) for all the clinical microbial strains tested during this study. The results of the MIC values are shown in Table 7. Thus, an important decrease in microbial cells concentration was detected after the first 4 hours of direct contact between the plant extracts and the microbial strains, expressed by the decrease in log germs.mL⁻¹ number as a function of microbial kill kinetics time (Figure 5-8).

The inhibitory properties of the MeOH.E and the Aq.E extracts of both plants on the different microbial strains were determined with the lowest MIC values of 25 mg/mL against *E. faecalis*, *H. alvei* and *C. albicans* using *Z. lotus* aqueous extracts (Table 7).

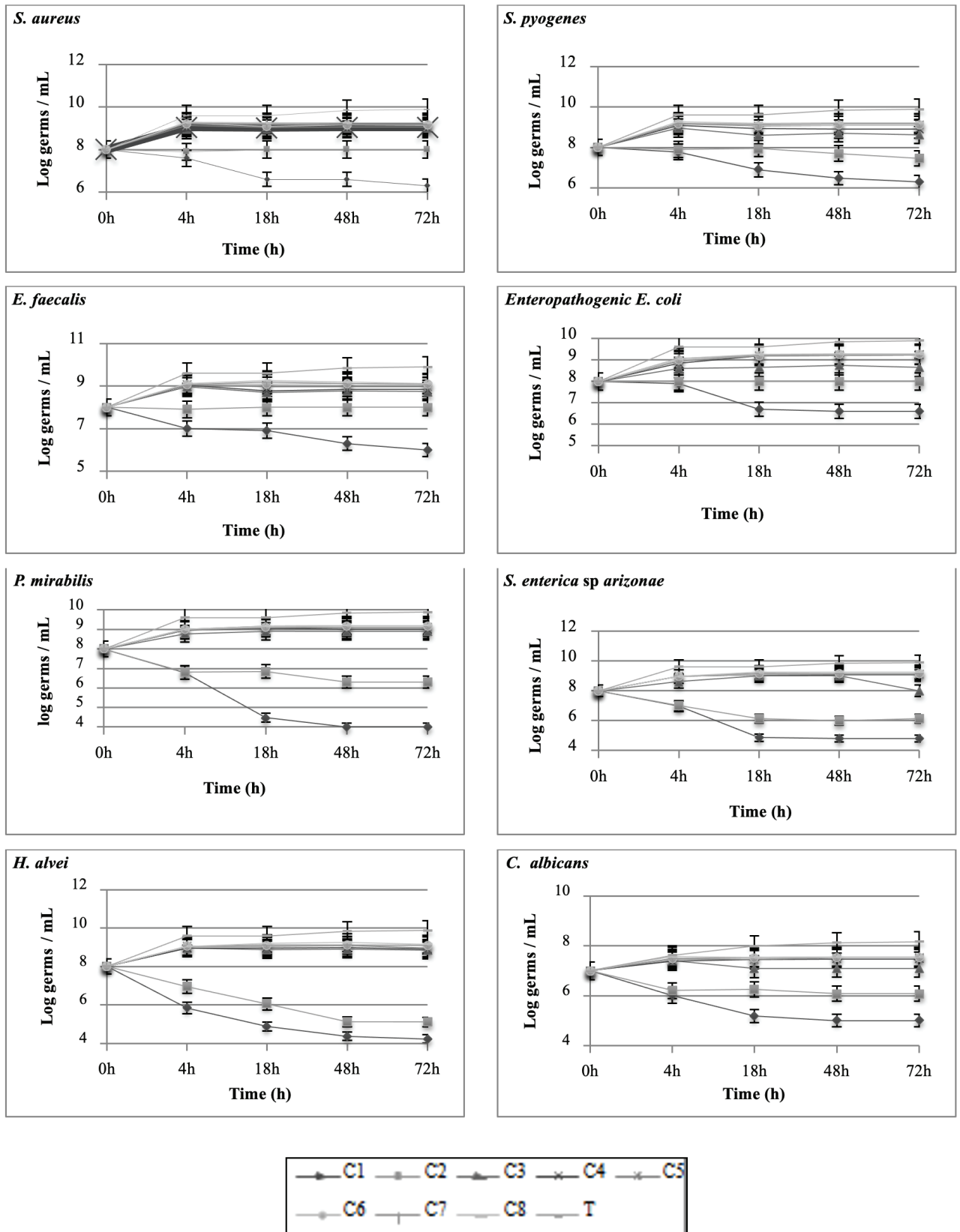


Figure 5. Microbial-kill kinetics of *Zizyphus lotus* hydromethanolic extract ($p < 0.05$). T: Control test. C1: 200 mg/mL, C2: 100mg/mL, C3: 50 mg/mL, C4: 25 mg/mL, C5: 12.5 mg/mL, C6: 6.25 mg/mL, C7: 3.13 mg/mL, C8: 1.56 mg/mL.

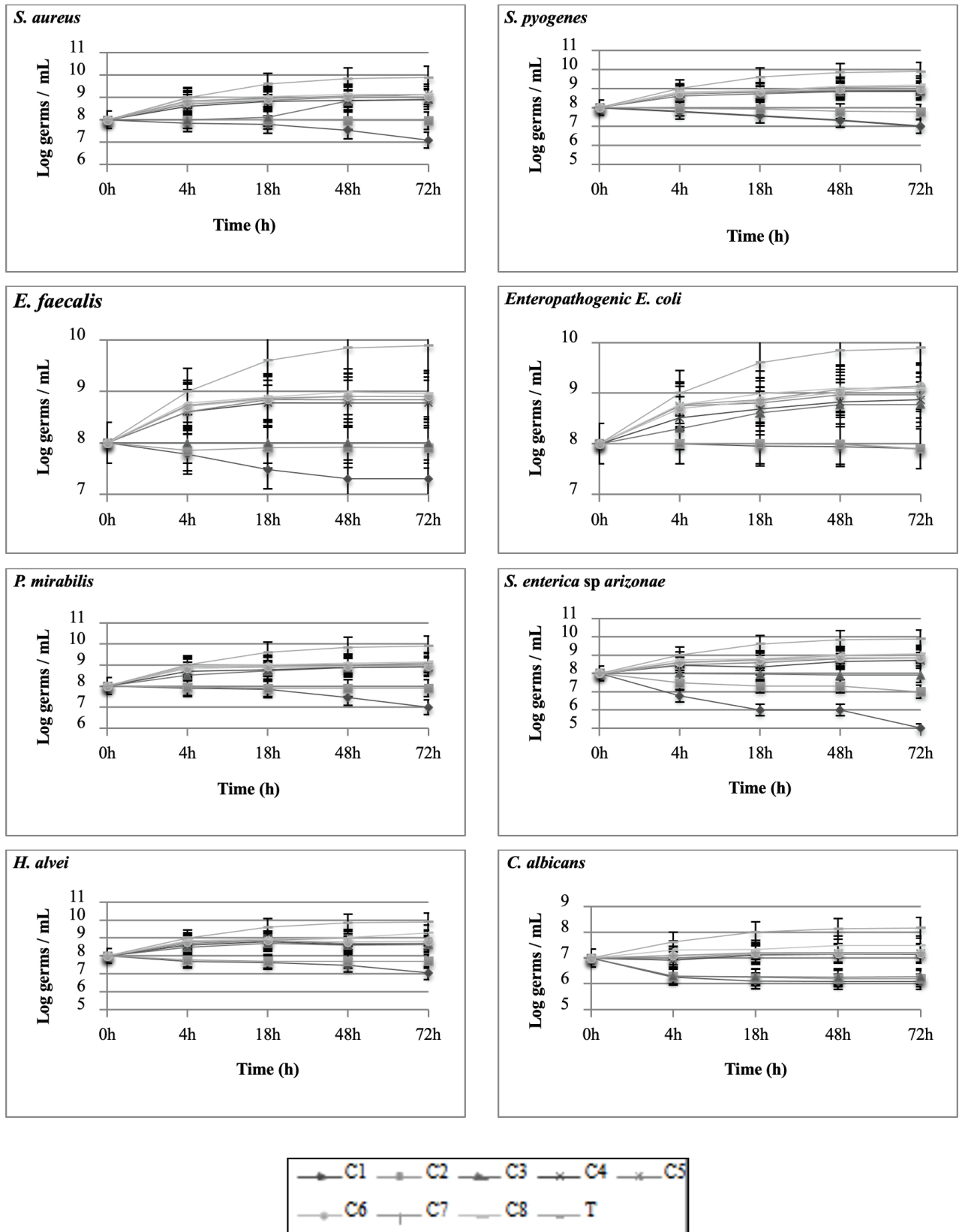


Figure 6. Microbial-kill kinetics of *Zizyphus lotus* aqueous extract ($p < 0.05$). T: Control test. C1: 200 mg/mL, C2: 100mg/mL, C3: 50 mg/mL, C4: 25 mg/mL, C5: 12.5 mg/mL, C6: 6.25 mg/mL, C7: 3.13 mg/mL, C8: 1.56 mg/mL.

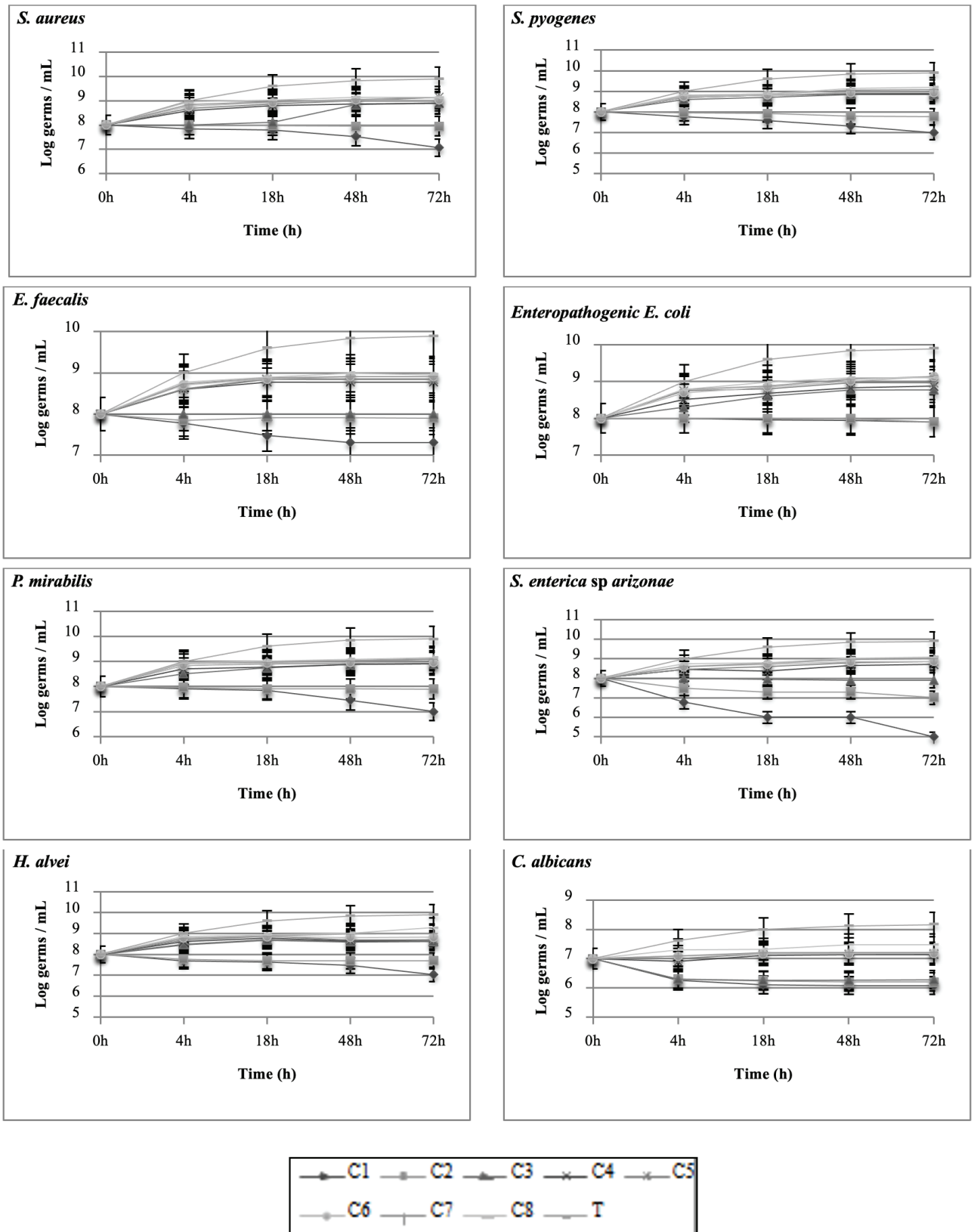


Figure 7. Microbial-kill kinetics of *R. chalepensis* hydromethanolic extract ($p < 0.05$). T: Control test. C1: 200 mg/mL, C2: 100mg/mL, C3: 50 mg/mL, C4: 25 mg/mL, C5: 12.5 mg/mL, C6: 6.25 mg/mL, C7: 3.13 mg/mL, C8: 1.56 mg/mL.

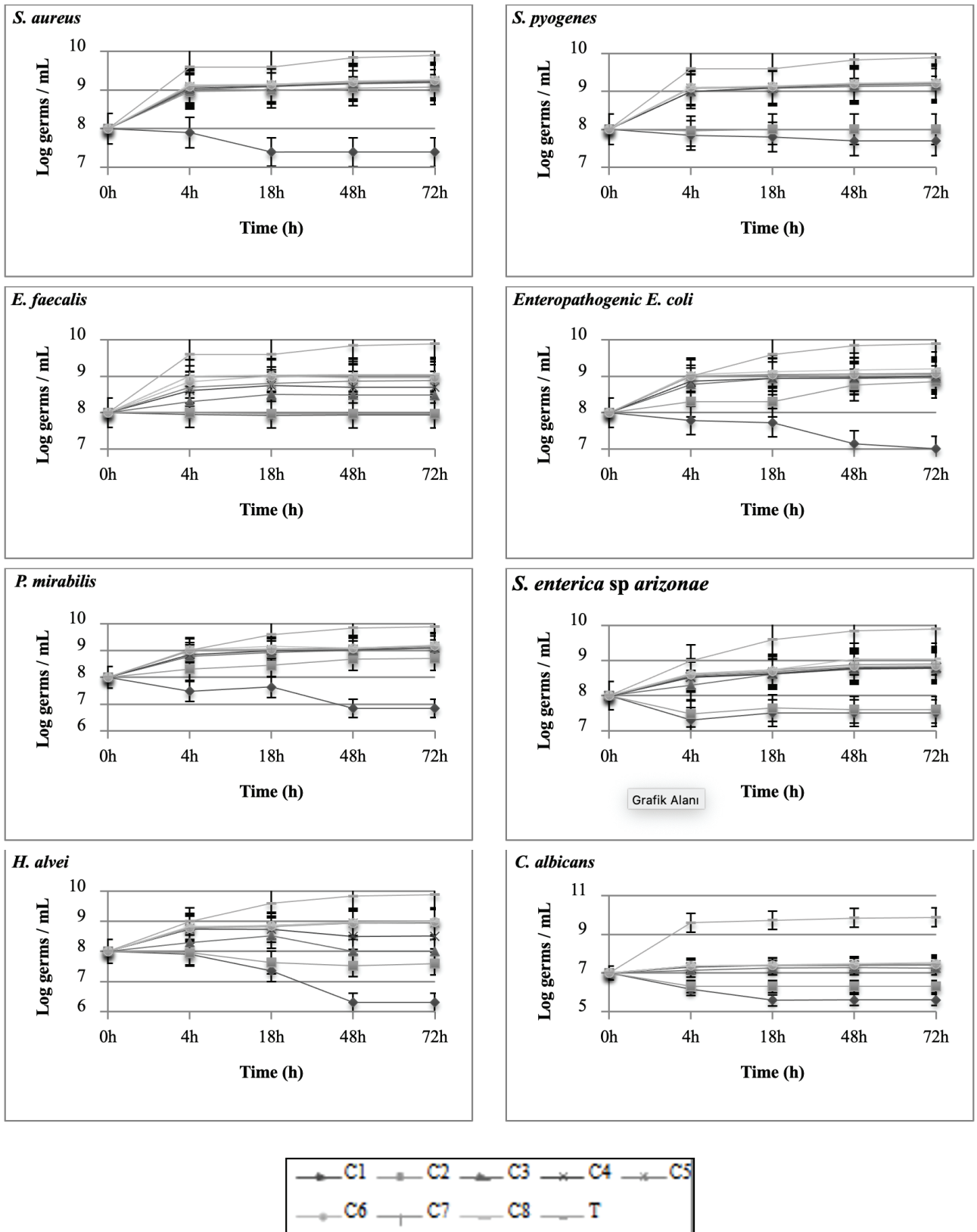


Table 8. FIC_{index} of the different combinations between *Z. lotus* and *R. chalepensis* phenolic extracts on the different microbial strains tested.

Clinical strains	ZL ^{MeOH.E} /RC ^{MeOH.E}			ZL ^{Aq.E} /RC ^{Aq.E}		
	MIC _{Cb}	FIC _{Id}	FIC _{index}	MIC _{Cb}	FIC _{Id}	FIC _{index}
<i>S. aureus</i>	200/200	2/4	6 ^a	200/200	2/1	3 ⁱ
<i>S. pyogenes</i>	200/200	2/2	4 ⁱ	200/200	4/2	6 ^a
<i>E. faecalis</i>	200/200	2/4	6 ^a	200/200	4/2	6 ^a
<i>E. coli</i>	200/200	2/2	4 ⁱ	200/200	2/1	3 ⁱ
<i>P. mirabilis</i>	200/200	2/2	4 ⁱ	200/200	1/1	2 ⁱ
<i>S. enterica</i>	200/200	2/4	6 ^a	200/200	4/2	6 ^a
<i>H. alvei</i>	100/100	1/1	2 ⁱ	100/100	2/1	3 ⁱ
<i>C. albicans</i>	200/200	2/4	6 ^a	200/200	4/4	8 ^a

a: antagonism, i: indifference, Cb: combination, Id: individual.

Also, the results of MBC/MIC reports allowed us to qualify both plants' extracts as bactericidal and fungicidal.

Checkerboard Test: Determination of the Fractional Inhibitory Concentrations (FIC test)

The checkerboard titration method was used to determine the FIC index of both plants' PPEs against MDR pathogenic bacteria and yeast. The results of the checkerboard assays are shown in Table 8. FIC_{index} values of the combination of *R. chalepensis* and *Z. lotus* extracts were greater than 0.5 (Table 8).

Therefore, the results demonstrated that *Z. lotus* extracts in combination with *R. chalepensis* showed no synergistic interaction. These combinations exerted antagonistic interactions on the microbial strains tested, with FIC index values greater than 4 (FIC_{index} >4). However, indifference interactions were recorded on *S. pyogenes*, *E. coli*, *P. mirabilis* and *H. alvei* by applying ZL^{MeOH.E} and RC^{MeOH.E} combination, and against *S. aureus*, *E. coli*, *P. mirabilis* and *H. alvei* using the combination of ZL^{Aq.E} and RC^{Aq.E}, with an inhibitory fractional concentration index greater than 2 (FIC_{index} >2) (Table 8).

DISCUSSION

A total of 41 clinical strains were isolated during this study from the different biological samples (Table 1). The performance of antibiotics susceptibility testing is important to assure and confirm susceptibility to chosen empirical antimicrobial agents for particular infections, or to detect resistance in clinical microbial isolates. Results enabled us to entitle the eight selected microbial strains as multidrug-resistant pathogens, which carries in its genetic material several antimicrobial resistance genes.

According to Cheurfa et al. (56), the aqueous extract yield of *Z. lotus* roots is about 9.49% and 7.91% for the methanolic extract, which is incongruent with the results of our study, in which very

interesting yields using the leaves of the plant were obtained. Thus, the study carried out by Zoughlache (57) showed that the extraction yields of the methanol extract and the aqueous extract of *Z. lotus* fruits were about 6.4% and 40.4%, respectively. This indicates that the polyphenolic extract content differs according to the plant part used. We found that the methanolic extract of *Z. lotus* leaves record higher yields compared to other parts of the plant, as shown by various studies.

The results obtained during this study are more interesting, because we obtained higher amounts of PPEs than those obtained by Mansour El-Said et al. (58), who obtained a lower yield of *Z. lotus* crude extracts (3.75%), and which may be explained by the use of high temperatures applying the Soxhlet extraction method. Thus, the content of polyphenolic compounds in *Z. lotus* was much higher compared to the yield obtained by Loizzo et al. (59), who found that the ultrasound extraction technique gives a content of 4.84% leaf methanolic extract. These results confirm that the technique used also influences the extraction yield of polyphenolic compounds.

The crude extract content differs from one specific plant part to another, which is confirmed by Attou (60), who recorded higher yields in *R. chalepensis* flowers harvested from Ain-Temouchent (32.15%), followed by leaves and stems, with a richness of the plant in methanol-soluble substances. So, during this study, in which we used the aerial part of the plant, we also obtained the highest yields of methanolic and aqueous extracts (RC^{MeOH.E} = 14.73%, RC^{Aq.E} = 30.83%) (Table 3).

These results allowed us to conclude that the harvest area has an immense influence on the extraction yields and chemical composition on bioactive compounds. Each harvest region is characterized by its climatic conditions (rain and outside temperature), which have an influence on the physical qualities of

medicinal plants (61). Other ecological factors can intervene in the development of the plant species: the altitude, the harvest period, the plant part harvested (leaves, flowers or stems, roots or aerial parts), the bioactive substances extraction technique, as well as the extraction time period, which influences not only the yield, but also the plant extract composition (62-64).

With regard to the obtained results of the phytochemical screening of the various PPEs, the presence of polyphenols, flavonoids, catechic tannins, coumarins, terpenes and saponins in the *R. chalepensis* aerial part was evident, which is in accordance with the study results demonstrated by Khadri et al. (65), while the results obtained by Alotaibi et al. (66) indicate that saponins were absent in the *R. chalepensis* extracts. Thus, the phytochemical tests performed by ZL^{MeOH.E} and ZL^{Aq.E} revealed the abundant presence of flavonoids: the orange color appearing in the extract solutions designates the presence of flavonoids of the flavone type, and the presence of catechin tannins.

All these results were in accordance with different recent studies by Borgi et al. (67), Chetibi and Diab (68) and Chelli et al. (69), who determined the presence of flavonoid and tannin components with high intensity in the methanolic and aqueous extracts prepared from different parts of *Z. lotus*.

In addition, the absence of gallic tannins, anthocyanins and iridoids (monoterpenes) was recorded in the leaves of *Z. lotus* and the aerial part of *R. chalepensis*. Thus, an absence of coumarins was observed in the *Z. lotus* leaves, which conforms to the results obtained by Saiah et al. (70). Moreover, our results are not in agreement with those of Belkadi and Hadj-Ali (71), who demonstrated an abundant richness of anthocyanins in *Z. lotus* leaves and fruits harvested from different regions of southern Algeria (Laghouat and Ghardaïa).

Phytochemical screening showed that *Z. lotus* contains tannins, terpenes and saponins as the main bioactive chemical compounds. These results are in agreement with those obtained by recent studies (72). Tannins are among the bioactive compounds of great interest in the medical field due to their potent anti-ulcer and gastroprotective properties (73). According to Ghazghazi et al. (74) and Borgi et al. (75), the *Z. lotus* leaves are rich in flavonoids, tannins and saponins of the dammarane type: jujuboside B, jujubogenin glycoside, as well as an important source of polyphenols, which is confirmed by the results of our study.

According to Gonzalez Trujano et al. (76), *R. chalepensis* is known for its greater richness in flavonoids, coumarins (chalepensisin), phenols, tannins and saponins. This abundance of bioactive compounds allows these medicinal plants to have various pharmacological properties, which could justify their multiple indications or therapeutic uses in traditional medicine, including anti-inflammatory, analgesic, anti-ulcerogenic, antidiabetic, antioxidant and antimicrobial properties, and in treatment of intestinal disorders (77-79).

For both plants, it was noticed that the MeOH.E extracts contain higher concentrations of polyphenols, tannins and flavonoids

compared to the aqueous extracts. The present study results revealed that *Z. lotus* is richer in polyphenolic compounds compared to *R. chalepensis*. This may be due to the plants' natures, each of which is characterized by its own composition and content of bioactive compounds. *R. chalepensis* harvested in Mascara is richer in polyphenol, with high levels compared with the plant harvested in Oran, which indicate that the harvest region has a great influence on the composition in secondary metabolite content of medicinal plants.

According to Neffati et al. (80), *Z. lotus* expressed significant levels on TPC, about 211 and 201.66 mg. Thus, Abdoul Azize et al. (81) reported significant amounts of polyphenols in *Z. lotus* extracts. According to Rsaissi et al. (82), *Z. lotus* fruits harvested from the El Brouj-Chaouia region in Morocco contain approximately 82.62 mg/kg, 46.21 mg/kg and 336.24 mg/kg, respectively of TPC, TFC and TTC. Comparing this with our results, we can conclude that *Z. lotus* leaves harvested in western Algeria are richer in polyphenols than other plant parts from other harvesting regions.

Saiah et al. (83) determined phenolic content ranging from 207.52±1.92 mg GAE/g DE and 21.91±0.31 mg QE/g DE on polyphenols and flavonoids, respectively, in *Z. lotus* harvested in Chlef. In our study, we determined higher content from the extracts (268.65±7 mg GAE/g DE and 109.45±2.87 mg EQ/g DE in ZL^{MeOH.E}). This difference in phenolic compound content may be related not only to the variety, but also to the influences of the extraction methods and conditions, maturity stage of the plant and the harvest region, biogenetic and environmental factors, the reagents used in the quantitative determination of polyphenol contents and spectrophotometer type used (84,85).

The hydromethanolic and aqueous extracts of *R. chalepensis* aerial part showed a TPC with values (Table 3) exceeding those demonstrated by Khadri et al. (86). They have determined a TPC in the ethanolic extract of 2.73±0.5 mg/g, and 3.90±0.3 mg/g in the Aq.E of *R. chalepensis* harvested from northern Tunisia. Therefore, as mentioned by Loizzo et al. (87), the hydromethanolic extract of *Ruta* harvested from Italy exhibited TPC, TFC and TTC contents with concentrations of 6.22 mg GAE/g DE, 6.59 mg QE /g DE and 0.72 mg epigallocatechin gallate equivalents/g DE, respectively. Comparing this with our results, we concluded that the Algerian medicinal plants we tested contain more bioactive substances than those collected from other harvest regions of other countries.

The literature analysis revealed a TPC in *R. chalepensis* ethanolic and Aq.E extracts of 54.13 and 51.28 mg/g, respectively (88). Kacem et al. (89,90) showed that *R. chalepensis* phenolic extracts are richer in total phenols, around 178 mg/g in the ethanol extracts and 152.09 mg/g in the Me.E extracts of the plant, with rutin as the main abundant flavonoid. Thus, Gali and Bedjou (91) determined the polyphenol and flavonoid contents of 12.2±0.84 µg AEG/mg DE and 3.43±0.13 µg QE/mg DE, respectively, in *R. chalepensis* aqueous extract. In addition, it has been

shown that the polyphenol content is much higher in both plants' hydromethanolic and aqueous extracts, which indicates that the polyphenolic extracts may be alternative plant-based drugs representing a rich and a potent reservoir of bioactive molecules. The highest content of polyphenols, flavonoids and tannins quantified in the different prepared extracts indicated that these plants were harvested during the optimal development stage and the harvest period when secondary metabolites production is much greater.

Comparing the TLC profiles of both plants' phenolic extracts, it can be observed that *Z. lotus* and *R. chalepensis* are richer in chemical substances based on the spot numbers on silica gel. The use of standard molecules in the phenolic compounds identification allowed us to determine the presence of gallic acid, which is a phenolic acid, in both plants' methanolic and aqueous extracts. For $ZL^{MeOH.E}$, the frontal ratios measurement for each of the spots revealed the presence of gallic acid with an $F_R=0.84$ and rutin: $F_R=0.52$ (Table 4; Figure 2). This is in agreement with the results obtained by Zoughlache (92) and Tlili et al. (93), who showed the presence of polyphenols and rutin in *Z. lotus* methanolic extract.

In addition, we detected the presence of coumarins and phenols in *R. chalepensis* extracts. According to Wagner and Bladt (94), any fluorescence detected at 366 nm on the TLC plates expresses the presence of hydroxycoumarines. Thus, the presence of quercetin was detected in $RC^{Aq.E}$: $R_F=0.94$, whereas it was absent in the methanolic extract (Table 4).

The different TLC plates visualized under UV at 254 nm presented colored spots including purple, brown, blue, red and green, which may correspond to several secondary metabolite classes. According to Markham (95), a black-violet color spot indicates the flavones' and flavonols' presence, a blue color spot indicates flavone or flavanone, a yellowish color indicates flavanol, an orange color indicates isoflavones, a yellow green color spot indicates aurones, a green color spot indicates chalcones and a blue green color spot reveals the presence of flavanone.

Based on the literature, we can conclude that *Z. lotus* extracts are rich in steroids, triterpenes, flavones, flavanones and chalcones. The absence of blue color spots in the chromatographic profile of *Z. lotus* extracts indicates the absence of coumarins, which is consistent with the qualitative analysis results of *Z. lotus* extracts obtained during this study. Thus, *R. chalepensis* extracts are rich in flavones, flavanones, steroids, chalcones and coumarins. These results are in agreement with those of Fasla (96), who showed the presence of flavonoids in *R. chalepensis* extracts.

The HPLC results revealed that *R. chalepensis* extracts exhibited higher flavonoid contents than *Z. lotus*. According to Bekkar et al. (97), the methanolic and aqueous extracts of *Z. lotus* harvested in Mascara-western Algeria had higher polyphenolic composition when compared with the results of the present research, using the same medicinal plant collected from other regions, which confirms the influence of the harvest region and

geographical area in the plants' bioactive substance composition. High phenolic compound contents from *Z. lotus* were determined by Cacciola et al. (98), as well, as in our study.

Thus, our results were congruent with those described in the study by Marmouzi et al. (99), who detected the presence of gallic acid, catechin and chlorogenic acid in *Z. lotus* aqueous extract.

Z. lotus used in this study is characterized by a very abundant richness in benzoic acid, many studies have mentioned the antimicrobial properties of this chemical substance (100, 101). According to Mkadmini Hammi et al. (102), *Z. lotus* fruits "Nbeg" collected in Southern Tunisia are rich in flavonoid compounds. Our results suggest that *Z. lotus* leaves and *R. chalepensis* leaves, small stems and flowers can confer potent sources of natural antimicrobials

The results of the antimicrobial activity indicated that the phenolic extracts of *Z. lotus* and *R. chalepensis* are more effective in inhibiting the growth of *C. albicans*, which may justify its uses in the treatment of candidiasis.

With reference to antibiotic susceptibility testing, the PPEs of both plants were more active on the clinical strains, however, the inhibitory potency of *Z. lotus* was higher than *R. chalepensis*.

Some MDR strains have been found to be highly sensitive to antibiotics compared to other strains, as mentioned in Table 6. *P. mirabilis*, *S. enterica* and *H. alvei* were determined to be the strains most sensitive to *Z. lotus* extracts, with potent growth inhibition expressed by very large diameters compared to the antibacterial potency of *R. chalepensis*.

The potent bactericidal and fungicidal effects of *Z. lotus* could be elucidated by the abundance of major phenolic components, particularly the benzoic acid known as a potent antimicrobial. In addition, the phenolic compounds identified in the phenolic extracts of *R. chalepensis* are appreciated as vigorous antibacterial and antifungal.

Our findings were more interesting than those obtained by Tukue and Karismala (103), who showed that the aqueous extract of *R. chalepensis* exerts an antibacterial effect with an inhibition growth diameter of 5 mm against *S. aureus*, while as a result of the antibacterial effect, the extracts used in this study gave diameters exceeding 10 mm with bactericidal and fungicidal effects (Table 7).

In comparison with the findings of Hamza and Meziani (104), the *Z. lotus* leaves used in our study exerted highly effective antimicrobial activity. Furthermore, the present results are found to be consistent with those of Chelli Chentouf et al. (105), who indicated that the Me.E extract of the plant harvested from the Mascara region in western Algeria exerts potent antibacterial effects on *S. aureus* and *E. coli* at a concentration of 200 mg/mL.

Our results are in agreement with those of Elaloui et al. (106) and Lahmer and Messai (107), who showed that the leaf ex-

tracts of *Z. lotus* exert an important antibacterial effect on *S. aureus* and *E. coli*.

In the present study, the most potent microbial growth inhibitory effect was obtained by *Z. lotus* when compared with *R. chalepensis*. This could be described by the abundance of secondary metabolites in *Z. lotus* leaf extracts, in particular phenols known for their antimicrobial activities (108). This activity was related to the high level not only of monoterpene hydrocarbons, but also of tannins that bind to bacterial cell walls (109,110).

Naili et al. (111) demonstrated that the Me.E extract of *Z. lotus* harvested from Libya was less effective against Gram-negative bacterial strains, while the results of our study indicated that the PPEs of this plant, harvested from Oran in western Algeria, were effective on both Gram-negative and Gram-positive strains. All these results justified the therapeutic applications of these medicinal plants as antimicrobials (112-115).

Previous studies have shown the effectiveness of plant extract combinations in the expression of a synergistic effect against pathogenic bacteria. Amirouche and Belkolai (116) demonstrated that a combination of sage and tea tree essential oils had a synergistic effect against *S. aureus*.

In addition, medicinal plants show their most important synergistic effect not only for antimicrobial activity but also on other biological activities. Ghali and Rafed (117) reported the synergistic effects of the aqueous extracts of *Allium ursinum* and *A. porrum* with an important anti-hemolytic activity. On the other hand, it was determined during this study that the effect of the combinations of both plants' phenolic extracts is lower compared to the effect exerted by each plant extract alone.

Therefore, *Z. lotus* and *R. chalepensis* extracts cannot be used in combination, due to the antagonism effect exerted on the different microbial strains tested, and therefore, the combination of these extracts can limit and reduce the bactericidal and fungicidal effect on MDR pathogens.

CONCLUSION

Research on natural bioactive substances extracted from medicinal plants is of particular interest, as it contributes to the national effort to conserve medicinal plants and to promote local traditional medicine. Our work was carried out to determine the phytochemical profiles and *in vitro* antimicrobial activity of *Z. lotus* and *R. chalepensis* collected from Oran in northwest Algeria. This study demonstrated that phenolic compounds extracted from the leaves of *Zizyphus lotus* and the leaves, small stems and flowers of *R. chalepensis* exhibited antibacterial activities on the MDR clinical isolates, as well an important antifungal effect against the MDR *C. albicans* strain. According to our study results, both plants' PPEs could be used in the medical field to tackle the emergence of antimicrobial resistance due to their potent antimicrobial activities on the MDR bacteria and fungi.

Acknowledgement: The authors would like to thank the Department of Biology, Mustapha Stambouli University, Algeria for financial support supplied to achieve this work and the Laboratory of Bioconversion, Microbiological Engineering and Health Safety for providing research facilities. Authors are grateful to Meslem Taib Hospital, the team research of Microbiology for facilitating collection of the clinical bacterial isolates used in this study.

Peer Review: Externally peer-reviewed.

Author Contributions: Conception/Design of Study- N.E.H.B., B.M.; Data Acquisition- N.E.H.B., B.M.; Data Analysis/Interpretation- N.E.H.B., B.M., B.K., Y.S.C., P.S.; Drafting Manuscript- N.E.H.B.; Critical Revision of Manuscript- N.E.H.B., B.M., B.K., Y.S.C., P.S.; Final Approval and Accountability- N.E.H.B., B.M., B.K., Y.S.C., P.S.

Conflict of Interest: Authors declared no conflict of interest.

Financial Disclosure: Authors declared no financial support.

REFERENCES

- Karczewska E, Wojtas I, Sito E, Trojanowska D, Budak A, zwolinska-Wcislo M, Wilk A. Assessment of Co-Existence of *Helicobacter pylori* and Candida Fungi in Diseases of the upper Gastrointestinal Tract. *J Physiol Pharmacol* 2009; 60(6): 33-9.
- Barbut F, Joly F. The intestinal microbiota: balance and dysbiosis. Pierre and Marie Curie University, Paris-France. 2017.
- Guo S, Duan JA, Li Y, Wang R, Yan H, Qian D, et al. Comparison of the bioactive components in two seeds of *Ziziphus* species by different analytical approaches combined with chemometrics. *Front Pharmacol* 2017; 8: 609.
- Zhang J, Wu Y, Chen M, Yu B, Wang D, Liu JG. C-glucosyl flavones from *Ziziphus jujuba* var. *spinosa*. *Chem Nat Compd* 2015; 51: 247-51.
- Hamood A, Hossain A, Humaid MT. Comparative evaluation of total phenols, flavonoids content and antioxidant potential of leaf and fruit extracts of Omani *Ziziphus jujuba* L. *Nat Sci Eng* 2015; 18: 78-83.
- Wu Y, Zhang J, Wang D, Liu JG, Hu Y. Triterpenoid saponins from *Ziziphus jujuba* var. *spinosa*. *Chem Nat Compd* 2013; 49: 677-81.
- Kang KB, Jang DS, Kim JW, Sung SH. UHPLC-ESI-qTOF-MS analysis of cyclopeptide alkaloids in the seeds of *Ziziphus jujuba* var. *spinosa*. *MSL* 2016; 7: 45-9.
- Li M, Wang Y, Tsoi B, Jin XJ, He RR, Yao XJ. Indoleacetic acid derivatives from the seeds of *Ziziphus jujuba* var. *spinosa*. *J Fitote* 2014; 99: 48-55.
- Zhao J, Li SP, Yang FQ, Li P, Wang YT. Simultaneous determination of saponins and fatty acids in *Ziziphus jujuba* (Suanzaoren) by high performance liquid chromatography-evaporative light scattering detection and pressurized liquid extraction. *J Chromatogr A* 2006; 11: 188-94.
- Xie J, Zhang Y, Wang L, Qi W, Zhang M. Composition of fatty oils from Semen *Ziziphus spinosae* and its cardioprotective effect on isolated toad hearts. *Nat Prod Res* 2012; 26: 479-83.
- Zhang Y, Qiao L, Song M, Wang L, Xie J, Feng H. HPLC-ESI-MS/MS analysis of the water-soluble extract from *Ziziphi spinosae* semen and its ameliorating effect of learning and memory performance in mice. *Pharmacogn Mag* 2014; 10: 509-16.
- Chen J, Liu X, Li Z, Qi A, Yao P, Zhou Z, et al. A review of dietary *Ziziphus jujuba* fruit (Jujube): Developing health food supplements for brain protection. *Evid Based Complement Alternat Med* 2017; 24: 1-10.

13. Benammar C, Baghdad C, Belarbi M, Subramaniam S, Hichami A, Khan NA. Antidiabetic and antioxidant activities of *Zizyphus lotus* L. aqueous extracts in Wistar rats. *J Nutr Food Sci* 2014; 8: 1-6.
14. Bnouham M, Mekhfi H, Legssy A, Ziyat A. Ethnopharmacology Forum: Medicinal plants used in the treatment of diabetes in Morocco. *Int J Diabetes Metab* 2002; 10: 33-50.
15. Borgi W, Ghedira K, Chouchane N. Anti-inflammatory and analgesic activities of *Zizyphus lotus* root barks. *J fitote* 2007; 78: 16-9.
16. Abdoul-Azize S. Potential Benefits of Jujube (*Zizyphus lotus* L.) Bioactive Compounds for Nutrition and Health. *J Nutr Metab* 2016; 2867470.
17. Mrabti HN, Jaradat N, Kachmar MR, Ed-Dra A, Ouahbi A, Cherrah Y, El Abbas Faouzi M. Integrative Herbal Treatments of Diabetes in Beni Mellal Region of Morocco. *J Integr Med* 2019; 17: 93-9.
18. Hammi KM, Jdey A, Abdely C, Majdoub H, Ksouri R. Optimization of ultrasound-assisted extraction of antioxidant compounds from Tunisian *Zizyphus lotus* fruits using response surface methodology. *Food Chem* 2015; 184: 80-9.
19. Bencheikh N, Bouhrim M, Kharchoufa L, Mohamed Al Kamaly O, Mechchate H, Es-safi I, et al. The Nephroprotective Effect of *Zizyphus lotus* L. (Desf.) Fruits in a Gentamicin-Induced Acute Kidney Injury Model in Rats: A Biochemical and Histopathological Investigation. *Molecules* 2021; 26(16): 4806.
20. El-Hachimi F, Alfaiz C, Bendriss A, Cherrah Y, Alaoui K. Anti-inflammatory activity of *Zizyphus lotus* seed oil (L.). *J Phyto* 2016; 1-8.
21. Borgi W, Recio MC, Ríos JL, Chouchane N. Anti-inflammatory and analgesic activities of flavonoid and saponin fractions from *Zizyphus lotus* (L.) Lam. *J SAJB* 2008; 74: 320-24.
22. Benammar. C, Hichami A, Yessoufou A, Simonin AM, Belarbi M, Allali H, et al. *Zizyphus lotus* L. (Desf.) modulates antioxidant activity and human T-cell proliferation. *BMC Complement Altern Med* 2010; 10: 54.
23. Wahida B, Abderrahman B, Nabil C. Antiulcerogenic Activity of *Zizyphus lotus* (L.) Extracts. *J Ethnopharmacol* 2007; 112: 228-31.
24. Bakhtaoui FZ, Lakmichi H, Megraud F, Chait A, Gadhi CEA. Gastro-Protective, Anti-*Helicobacter Pylori* and, Antioxidant Properties of Moroccan *Zizyphus lotus* L. *J Appl Pharm Sci* 2014; 4: 81-7.
25. Hossain MA. A phytopharmacological review on the Omani medicinal plant: *Zizyphus jujube*. *J King Saud Univ Sci* 2018; 31(4): 1352-7.
26. Marmouzi I, Kharbach M, El-Jemli M, Bouyahya A, Cherrah Y, Bouklouze A, et al. Antidiabetic, Dermatoprotective, Antioxidant and Chemical Functionalities in *Zizyphus lotus* Leaves and Fruits. *Ind Crops Prod* 2019; 132: 134-9.
27. Khouchlaa A, Talbaoui A, El-Yahyaoui EIA, Bouyahya A, Ait-Lahsen S, Kahouadjji A, Tijane M. Determination of phenolic compounds and evaluation of *in vitro* litholytic activity on urinary lithiasis of *Zizyphus lotus* L. extract of Moroccan origin. *J Phyto* 2017; 1-6.
28. Ghalem M, Merghache S, Belarbi M. Study on the antioxidant activities of root extracts of *Zizyphus lotus* from the western region of Algeria. *Pharmacogn J* 2014; 6: 32-42.
29. Ghedira K. *Zizyphus lotus* (L.) Desf. (Rhamnaceae): jujubier sauvage. *J Phyto* 2013; 11: 149-53.
30. Borgi W, Chouchane N. Anti-spasmodic effects of *Zizyphus lotus* (L.) Desf. extracts on isolated rat duodenum. *J Ethnopharmacol* 2009; 126: 571-7.
31. Bencheikh N, Bouhrim M, Kharchoufa L, Mohamed Al-Kamaly O, Mechchate H, Essafi I, et al. The Nephroprotective Effect of *Zizyphus lotus* L. (Desf.) Fruits in a Gentamicin-Induced Acute Kidney Injury Model in Rats: A Biochemical and Histopathological Investigation. *Molecules* 2021; 26: 4806.
32. Gonzalez-Trujano ME, Carrera D, Ventura-Martinez A, Cedillo-Portugal E, Navarrete A. Neuropharmacological profile of an ethanol extract *Ruta chalepensis* L. in mice. *J Ethnopharmacol* 2006; 106: 129-35.
33. Loizzo MR, Falco T, Bonesi M, Sicari V, Tundis R, Bruno M. *Ruta chalepensis* L. (Rutaceae) leaf extract: chemical composition, antioxidant and hypoglycaemic activities. *Nat Prod Res* 2017; 32.
34. Gomez-Flores R. Antimicrobial effect of chalepensis against *Streptococcus mutans*. *J Med Plant Res* 2016; 10(36): 631-4.
35. Szweczyk A, Marino A, Molinari J, Ekiert H, Miceli N. Phytochemical Characterization, and Antioxidant and Antimicrobial Properties of Agitated Cultures of Three Rue Species: *Ruta chalepensis*, *Ruta corsica*, and *Ruta graveolens*. *Antiox* 2022; 11: 592.
36. Khadhri A, Bouali I, Belkhir S, Mokded R, Smiti S, Falé P. et al. *In vitro* digestion, antioxidant and antiacetylcholinesterase activities of two species of *Ruta: Ruta chalepensis* and *Ruta montana*. *Pharmacoeutic Biol* 2016; 55: 101-7.
37. Adrsersen A, Gauguin B, Gudiksen L, Jäger AK. Screening of plants used in Danish folk medicine to treat memory dysfunction for acetylcholinesterase inhibitory activity. *J Ethnopharmacol* 2006; 104: 418-22.
38. González-Trujano ME, Urbina-Trejo E, Santos-Valencia F, Villasana-Salazar B, Carmona-Aparicio L, Martínez-Vargas D. Pharmacological and toxicological effects of *Ruta chalepensis* L. on experimentally induced seizures and electroencephalographic spectral power in mice. *J Ethnopharmacol* 2021; 271.
39. Kloss WE, Wolfshohl JF. Identification of *Staphylococcus* species with the API STAPH-IDENT system. *J Clin Microbiol* 1982; 16(3): 509-16.
40. Beutin L, Montenegro MA, Orskov I, Orskov F, Prada J, Zimmermann S, Stephan R. Close association of verotoxin (Shiga-like toxin) production with enterohemolysin production in strains of *Escherichia coli*. *J Clin Microbiol* 1989; 27(11): 2559-64.
41. CLSI: Clinical and Laboratory Standards Institute. Performance standards for Antimicrobial Disk Susceptibility Tests. 364 Approved Standard Twelfth Edition. Clinical and Laboratory Standards Institute, 365 Wayne, PA: 2015.
42. FSM-AC: French Society of Microbiology-Antibiogram Committee. Antibiotics to be tested, concentrations, critical diameters and specific interpretative reading rules. 2013.
43. FMS-AC/EUCAST: French Society of Microbiology-Antibiogram Committee/European Committee on Antimicrobial Susceptibility Testing. Antibiogram Committee of the French Society of Microbiology: 2018.
44. Romani A, Pinelli P, Cantini C, Cimato A, Heimler D. Characterization of Violetto di Toscana, a typical Italian variety of artichoke (*Cynara scolymus* L.). *J Food Chem* 2006; 95: 221-5.
45. Chavan UD, Shahidi F, Nacz M. Extraction of condensed tannins from beach pea (*Lathyrus maritimus* L.) as affected by different solvents. *J Food Chem* 2001; 75(4): 509-12.
46. Harborne JB. Phytochemical methods: A guide to modern techniques of plant analysis. 3rd ed. Chapman & Hall Thomson Science(UK); 1998. p.203-34.
47. Boizot N, Charpentier JP. Méthode rapide d'évaluation du contenu en composés phénoliques des organes d'un arbre forestier. *Cah Tech INRA* 2006; 79-82.
48. Samatha T, Shyamsundarachary R, Srinivas P, Swamy NR. Quantification of total phenolic and total flavonoid contents in extracts of *Oroxylum indicum* L. Kurz. *Asian J Pharmaceut Clin Res* 2012; 5(4): 177-9.
49. Ba K, Tine E, Destain J, Cisse N, Thonart P. Comparative study of phenolic compounds, antioxidant potency of different varieties of *Senegalese sorghum* and amylolytic enzymes of their malt. *Bio-technol Agro Soc Environ* 2010; 14(1): 131-9.
50. Sanogo Y, Guessennd NK, Tra-Bi HF, Kouadio NJ, Konan FK, Bamba M, Danho N, Bakayoko A, Ya K, Dosso M. Evaluation *in vitro* de l'activité des écorces de tige de *Anogeissus leiocarpus* (DC) Guill. et Perr. (Combretaceae) sur des bactéries responsables de maladies courantes en Afrique et criblage phytochimique. *Int J Biol Chem Sci* 2016; 10(3): 1139-52.

51. Caponio F, Alloggio V, Gomes T. Phenolic compounds of virgin olive oil: Influence of paste preparation techniques. *Food Chem* 1999; 64(2): 203-9.
52. Ponce AG, Fritz R, Del-Valle CE, Roura SI. Antimicrobial activity of essential oils on the native microflora of organic Swiss chard. 2003; 36(7): 679-84.
53. Chandrasekaran M, Venkatesalu V. Antibacterial and antifungal activity of *Syzygium jambolanum* seeds. *J Ethnopharmacol* 2004; 91(1): 105-8.
54. Orhan G, Bayram A, Zer Y, Balci I. Synergy Tests by E Test and Checkerboard Methods of Antimicrobial Combinations against *Brucella melitensis*. *J Clin Microbiol* 2005; 43(1): 140-3.
55. Mulyaningsih S, Sporer F, Zimmermann S, Reichling J, Wink M. Synergistic properties of the terpenoids aromadendrene and 1,8-cineole from the essential oil of *Eucalyptus globulus* against antibiotic-susceptible and antibiotic-resistant pathogens. *Phytomed* 2010; 17: 1061-6.
56. Cheurfa M, Allem R, Zabel K, Aichouni W, Medjkane M. Study of the effects of extracts from the roots of *Glycyrrhiza glabra* L. and *Zizyphus lotus* L. on some human pathogenic bacteria. *J Phyto* 2017. <https://doi.org/10.1007/s10298-017-1116-1>.
57. Djemai-Zoughlache S, Yahia M, Hambaba L, Abdeddaim M, Aberkan MC, Ayachi A. Study of the biological activity of extracts from the fruit of *Zizyphus lotus* L. *TJMPNP* 2009; 2: 10-23.
58. Mansour El-Said S. Studies on *Ruta chalepensis*, an ancient medicinal herb still used in traditional medicine. *J Ethnopharmacol* 1990; 28: 305-12.
59. Loizzo MR, Falco T, Bonesi M, Sicari V, Tundis R, Bruno M. *Ruta chalepensis* L. (Rutaceae) leaf extract: chemical composition, antioxidant and hypoglycaemic activities. *Nat Prod Res* 2017; 32.
60. Attou A. Contribution to the phytochemical study and biological activities of the extracts of the plant *Ruta chalepensis* (Fidjel) from the region of Ain Témouchent. Abou Bekr Belkaid-Tlemcen University. 2011.
61. WHO: World Health Organization. WHO Guidelines on Good Agricultural Practices and Good Harvesting Practices (GAPs) for medicinal plants. 2003.
62. Zouari N, Ayadi I, Fakhfakh , Rebai A, Zouari S. Variation of chemical composition of essential oils in wild populations of *Thymus algeriensis* Boiss. and Reut., a North African endemic Species. *LHD* 2012; 11: 28-39.
63. Pinto E, Pina-Vaz C, Salgueiro L, Gonçalves MJ, Costa-De-Oliveira S, Cavaleiro C, Palmeira , Rodrigues A, Martinez-De-Oliveira J. Antifungal activity of the essential oil of *Thymus pulegioides* on *Candida*, *Aspergillus* and dermatophyte species. *J Med Microbiol* 2006;55: 1367-73.
64. Lucchesi ME. Microwave-Assisted Solvent-less Extraction: Design and Application to Essential Oil Extraction. Faculty of Science and Technology, University of Reunion. 2005.
65. Khadri A, Bouali I, Belkhir S, Mokded R, Smiti S, Falé P, Eduarda M, Araújo M, Luisa M, Serralheiro M. *In vitro* digestion, antioxidant and antiacetylcholinesterase activities of two species of *Ruta: Ruta chalepensis* and *Ruta montana*. *Pharmaceutic Biol* 2016; 55: 101-7.
66. Alotaibi SM, Saleem MS, Al-humaidi JG. Phytochemical contents and biological evaluation of *Ruta chalepensis* L. growing in Saudi Arabia. *SPJ* 2018; 26(4): 504-8.
67. Borgi W, Bouraoui A, Chouchane N. Antiulcerogenic activity of *Zizyphus lotus* (L.) extracts. *J Ethnopharmacol* 2007; 12: 228-31.
68. Chetibi C, Diab S. Study of the biological activity *in vitro* and *in vivo* of the methanolic and aqueous extracts of the bark of the roots of *Zizyphus lotus* L. Frères Mentouri University, Constantine. 2016.
69. Chelli-Chentouf N, Tir-Touil Meddah A, Belgharbi A, Benfreha-Temouri H, Meddah B. Phytochemical and antimicrobial screening of fruits and leaves of *Zizyphus lotus* L. collected in North West of Algeria. *Maghr. J Pure & Appl Sci* 2018; 4(1): 50-8.
70. Saiah H, Allem R, El-Kebir FZ. Antioxidant and antibacterial activities of six Algerian medicinal plants. *Int J Pharm Pharm Sci* 2016; 8(1): 367-74.
71. Belkadi N, Hadj-Ali I. Morphometric study and germination test of jujube seeds (*Zizyphus lotus*) from southern Algeria. Extraction and dosage of 3 classes of flavonoids and estimation of the effect of fruit powder against *Tribolium castaneum* Herbst (Coleoptera: Tenebrionidae). Mouloud Mammeri University of Tizi-Ouzou, Master's thesis in Biology. 2016.
72. El-Maaiden E, El-Kharrassi Y, Moustaid K, Essamadi AK, Nasser B. Comparative study of phytochemical profile between *Zizyphus spina christi* and *Zizyphus lotus* from Morocco. *JFMC* 2018.
73. Bensal VK, Goel K. Gastroprotective effect of *Acacia nilotica* young seed less pod extract: Role of polyphenolic constituents. *Asian Pac J Trop Med* 2012; 5: 523-8.
74. Ghazghazi H, Aouadhi C, Riahi L, Maaroui A, Hasnaoui B. "Fatty acids composition of Tunisian *Zizyphus lotus* L. (Desf.) fruits and variation in biological activities between leaf and fruit extracts". *Nat Prod Res* 2014; 28(14): 1106-10.
75. Borgi W, Recio MC, Rios JL, Chouchane N. Anti-inflammatory and analgesic activities of flavonoid and saponin fractions from *Zizyphus lotus* (L.) Lam. *SAJB* 2008; 74(2): 320-4.
76. Gonzalez-Trujano ME, Carrera D, Ventura-Martinez A, Cedillo-Portugal E, Navarrete A. Neuropharmacological profile of an ethanol extract *Ruta chalepensis* L. in mice. *J Ethnopharmacol* 2006; 106: 129-35.
77. Esameldin E, Joslyn T, Annemarie V. Screening of medicinal plants used in South African traditional medicine for genotoxic effects. *Toxicol Lett* 2003; 143(2): 195-207.
78. Benammar CH, Benkada D, Benammar F. GC/MS analysis of the essential oil of *Ruta chalepensis* (Fidjel) from Tlemcen. 2nd Symposium on Aromatic and Medicinal Plants, 2006; Marrakech.
79. Bouajaj S, Romane A, Benyamna A, Amri I, Hanana M, Hamrouni L, Romdhane M. Essential oil composition, phytotoxic and antifungal activities of *Ruta chalepensis* L. leaves from High Atlas Mountains (Morocco). *Nat Prod Res* 2014; 28(21): 1910-4.
80. Neffati N, Aloui Z, Karoui H, Guizani I, Boussaid M, Zaouali Y. Phytochemical composition and antioxidant activity of medicinal plants collected from the Tunisian flora. *Nat Prod Res* 2017; 31(13): 1583-8.
81. Abdoul-Azize S, Bendahmane M, Hichami A, Dramane G, Simonin AM, Benammar C, Sadou H, Akpona S, El-Boustani ES, Khan NA. Effects of *Zizyphus lotus* L. (Desf.) polyphenols on Jurkat cell signaling and proliferation. *Int Immunopharmacol* 2013; 15: 364-71.
82. Rsaissi N, El-Kamili Bencharki B, Hillali L, Bouhache M. Antimicrobial activity of fruits extracts of the wild jujube "*Zizyphus Lotus* (L.) Desf. *IJSER* 2013; 4(9): 1521-8.
83. Saiah H, Allem R, El-Kebir FZ. Antioxidant and antibacterial activities of six Algerian medicinal plants. *Int J Pharm Pharm Sci* 2016; 8(1): 367-74.
84. N'guessan AHO, Deliko CED, Bekro JAM, Beko YY. Contents of phenolic compounds of 10 medicinal plants used in the traditional therapy of arterial hypertension, an emerging pathology in Côte d'Ivoire. 2011; 6: 55-61.
85. Pawlowska AM, Camangi F, Bader A, Braca A. Flavonoids of *Zizyphus jujuba* L. and *Zizyphus spina-christi* (L.) Willd (Rhamnaceae) fruits. *Food Chem* 2009; 112(4): 858-62.
86. Khadri A, Bouali I, Belkhir S, Mokded R, Smiti S, Falé P, Eduarda M, Araújo M, Luisa M, Serralheiro M. *In vitro* digestion, antioxidant and antiacetylcholinesterase activities of two species of *Ruta: Ruta chalepensis* and *Ruta montana*. *Pharmaceutic Biol* 2016; 55: 101-7.
87. Loizzo MR, Falco T, Bonesi M, Sicari V, Tundis R, Bruno M. *Ruta chalepensis* L. (Rutaceae) leaf extract: chemical composition, antioxidant and hypoglycaemic activities. *Nat Prod Res* 2017; 32(5): 521-8.

88. Fakhfakh N, Zouari S, Zouari M, Loussayef C, Zouari N. Chemical composition of volatile compounds and antioxidant activities of essential oil, aqueous and ethanol extracts of wild Tunisian *Ruta chalepensis* L. (Rutaceae). *J Med Plants Res* 2012; 6: 593-600.
89. Kacem M, Kacem I, Simon G, Mansour AB, Chaabouni S, Elfeki A, Bouaziz M. Phytochemicals and biological activities of *Ruta chalepensis* L. growing in Tunisia. *Food Biosci* 2015; 12: 73-83.
90. Kacem M, Simo G, Leschiera R, Misery L, Elfeki A, Lebonvallet N. Antioxidant and antiinflammatory effects of *Ruta chalepensis* L. extracts on LPS-stimulated RAW 264.7 cells. *In Vitro Cell Dev Biol Anim* 2015; 51: 128-41.
91. Gali L, Bedjou F. Antioxidant and anticholinesterase effects of the ethanol extract, ethanol extract fractions and total alkaloids from the cultivated *Ruta chalepensis*. *SAJB* 2019; 120: 163-9.
92. Zoughlache S. Study of the biological activity of the fruit extracts of *Zizyphus lotus* L. El-Hadj Lakhdar University, Batna. 2009.
93. Tlili H, Hanen N, Ben-Arfa A, Neffati M, Boubakri A, Buonocore D, Dossena M, Verri M, Doria D. Biochemical properties and *in vitro* biological activities of extracts from seven folk medicinal 2 plants growing wild in southern Tunisia. 2019.
94. Wagner H, Bladt S. Plant drug analysis, a thin layer chromatography atlas. 2nd ed. Berlin: Springer-Verlag; 1996.
95. Markham KR. Techniques of flavonoids identification. Ed. London. Academic Press; 1982.
96. Fasla B. Evaluation of the antimitotic and genotoxic potential of medicinal plants and phytochemical analysis. Es-Senia University, Oran. 2009.
97. Bekkar NEH, Meddah B, Cakmak YS, Keskin B. Phenolic Composition, Antioxidant And Antimicrobial Activities of *Zizyphus lotus* L. and *Ruta chalepensis* L. Growing in Mascara (Western Algeria). *JMBFS* 2021; 10(5): e3004-e3004.
98. Cacciola A, D'Angelo V, Raimondo FM, Germanò MP, Braca A, De Leo M. *Zizyphus lotus* (L.) Lam. as a Source of Health Promoting Products: Metabolomic Profile, Antioxidant and Tyrosinase Inhibitory Activities. *Chem & Biodiver* 2022; e202200237.
99. Marmouzi I, Kharbach M, El-Jemli M, Bouyahya A, Cherrah Y, Bouklouze A, Heyden YV, Faouzi ME. Antidiabetic, dermatoprotective, antioxidant and chemical functionalities in *Zizyphus lotus* leaves and fruits. *Industrial Crops & Products* 2019; 132: 134-9.
100. Dracea O, Larion C, Chifiriuc MC, Raut I, Limban C, Nitulescu GM, Badiceanu CD, Israil AM. New thiourea derivatives of 2-(4-methylphenoxymethyl) benzoic acid with antimicrobial activity. *Roum Arch Microbiol Immunol* 2008; 3(4): 92-7.
101. Wei Q, Wang X, Cheng JH, Zeng G, Sun DW. Synthesis and antimicrobial activities of novel sorbic and benzoic acid amide derivatives. *Food Chem* 2018; 268: 220-32.
102. Mkadmini hammi K, Jdey A, Abdelly C, Majdou H, Ksouri R. Optimization of ultrasound-assisted extraction of antioxidant compounds from Tunisian *Zizyphus lotus* fruits using response surface methodology. *Food Chem* 2015; 184: 80-9.
103. Tukue M, Karismala MB. Phytochemical screening and antibacterial activity of two common terrestrial medicinal plants *Ruta chalepensis* & *Rumex nervosus*. *Carib J Sci Tech* 2014; 2: 634-41.
104. Hamza K, Meziani A. Study of the biological activity of the aqueous extract of *Zizyphus lotus* leaves. Frères-Mentouri University, Constantine. 2015.
105. Chelli Chentouf N, Tir-Touil Meddah A, Belgharbi A, Benfreha Temmouri H, Meddah B. Phytochemical and antimicrobial screening of fruits and leaves of *Zizyphus lotus* L. collected in North West of Algeria. *Maghr J Pure & Appl Sci* 2018; 4(1): 50-8.
106. Elaloui M, Ennajah A, Ghazghazi H, Ben-Youssef I, Ben-Othman N, Hajlaoui MR, Khouja A, Laamouri A. Quantification of total phenols, flavonoides and tannins from *Zizyphus jujuba* (mill.) and *Zizyphus lotus* (L.) (Desf). Leaf extracts and their effects on antioxidant and antibacterial activities. *Int J Sec Metabolite* 2017; 4(1): 18-26.
107. Lahmer N, Messai S. Phytochemical and biological study of aqueous and methanolic extracts of *Zizyphus lotus* root bark (L). Frères-Mentouri University, Constantine. 2017.
108. García-Lafuente A, Guillamón E, Villares A, Mauricio A, Jose R, Martinez A. Flavonoids as anti-inflammatory agents: implications in cancer and cardiovascular disease. *Inflamm Res* 2009; 58: 537.
109. Amri I, Hamrouni L, Hanana M, Gargouri S, Fezzani T, Jamoussi B. Chemical composition, physicochemical properties, antifungal and herbicidal activities of *Pinus halepensis* Miller essential oils. *Biol Agric Hort* 2013; 29: 91-106.
110. Bukar AM, Kyari MZ, Gwaski M, Gudusu FS, Kuburi PA, Abadam YI. Evaluation of phytochemical and potential antibacterial activity of *Zizyphus spina-christi* L. against some medically important pathogenic bacteria obtained from University of Maiduguri Teaching Hospital, Maiduguri, Borno State-Nigeria. *J Pharmacogn Phytochem* 2015; 3: 98-101.
111. Naili MB, Alghazeer RO, Saleh NA, Al-Najjar AY. Evaluation of antibacterial and antioxidant activities of *Artemisia campestris* (Asteraceae) and *Zizyphus lotus* (Rhamnaceae). *Arab J Chem* 2010; 3: 79-84.
112. Zazouli S, Chigr M, Ramos PA, Rosa D, Castro MM, Jouaiti A, et al. Chemical profile of lipophilic fractions of different parts of *Zizyphus lotus* L. by GC-MS and evaluation of their antiproliferative and antibacterial activities. *Molecules* 2022; 27(2): 483.
113. Hammi KM, Jdey A, Abdelly C, Majdou H, Ksouri R. "Optimization of ultrasound-assisted extraction of antioxidant compounds from Tunisian *Zizyphus lotus* fruits using response surface methodology". *Food Chem* 2015; 184: 80-9.
114. Ben-Bnina E, Hammami S, Daamii Remadi M, Ben-Jannet H, Mighri Z. Chemical composition and antimicrobial effects of Tunisian *Ruta chalepensis* L. essential oils. *J Soc Chim Tunisie* 2010; 12: 1-9.
115. Haddouchi F, Chaouche TM, Zaouali Y, Ksouri R. Chemical composition and antimicrobial activity of the essential oils from four *Ruta* species growing in Algeria. *Food Chem* 2013; 141: 253-8.
116. Amirouche R, Belkola F. *In vitro* effect of the association of essential oils of *Salvia officinalis*, *Melaleuca alternifolia* and two major compounds on bacteria. Faculty of Nature and Life Sciences, University of Mira A, Bejaia. 2013.
117. Ghali A, Rafed S. Phytochemical screening and anti-hemolytic activity of two medicinal plants: *Allium ursinum* and *Allium porrum*. University of Bouira. 2019.

The Role of Gamma-Amino Butyric Acid in Short-Term High Temperature Acclimation in Lichen *Pseudevernia furfuracea*

Nihal Goren-Saglam¹ , Fazilet Ozlem Albayrak² , Dilek Unal³ 

¹Istanbul University, Faculty of Science, Department of Biology, Istanbul, Turkiye

²Aksaray University, Faculty of Science and Letters, Department of Biology, Aksaray, Turkiye

³Seyh Edebali University, Faculty of Science and Letter, Department of Molecular Biology, Bilecik, Turkiye

ORCID IDs of the authors: N.G.S. 0000-0003-1255-5188; F.O.A. 0000-0002-5434-0081; D.U. 0000-0002-6915-9699

Please cite this article as: Goren-Saglam N, Albayrak FO, Unal D. The Role of Gamma-Amino Butyric Acid in Short-Term High Temperature Acclimation in Lichen *Pseudevernia furfuracea*. Eur J Biol 2022; 81(2): 184-189.
DOI: 10.26650/EurJBiol.2022.1155582

ABSTRACT

Objective: Global warming causes many different stresses for plants. High-temperature stress is one of the important problems caused by global warming. Plants develop various tolerance mechanisms to protect themselves against these stresses. γ -Aminobutyric acid (GABA) metabolism has a critical role in various biological processes in plants. GABA plays a critical role in the acclimation to different stress conditions in plants. Lichens can grow in environments exposed to severe abiotic stresses such as drought and extreme heat. The major aim of this study was to identify whether GABA accumulation could improve short-term, high-temperature tolerance in lichen *Pseudevernia furfuracea*.

Materials and Methods: For this aim, *P. furfuracea* samples were kept in petri dishes in an incubator at $45 \pm 2^\circ\text{C}$ for 24 and 48 h. We analyzed the chlorophyll a/b ratio, GABA content, glutamate decarboxylase (GAD) and glutamate dehydrogenase (GDH) activities, which are important enzymes involved in the GABA shunt, and also peroxidase (POD) and catalase (CAT) activities of the antioxidant metabolism.

Results: Our study indicated that the chlorophyll a/b ratio was not changed significantly under 45°C within 48 h. POD and CAT activities were significantly decreased in lichen thalli under 45°C , however; GABA accumulation was approximately enhanced by 1.5-fold depending on the time exposure. GAD and GDH activities were significantly increased under high temperature conditions.

Conclusions: The acclimation of *P. furfuracea* to high temperatures may be related to the increase in GAD and GDH activities. Our findings provided evidence that the GABA shunt could help lichen *P. furfuracea* to acclimate to high temperatures.

Keywords: Acclimation, antioxidant mechanism, GABA, high temperature, lichen, *Pseudevernia furfuracea*

INTRODUCTION

Many researchers suggest that increases in global temperature will be the biggest problem in the future (1,2). Understanding the factors that regulate high temperatures and tolerance mechanisms which belong to different organisms are very important subjects for the scientific community. Besides, lichens are symbiotic organisms and have a high adaptation capacity to various environmental conditions including high temperatures

(2,3). Previous studies demonstrated that some lichen species have remarkable thermotolerance and they can survive between $35\text{-}46^\circ\text{C}$ (2,3). It is known that lichens include first- and second-line protection systems such as producing phytochelatins, lichen acids, non-thiol compounds and activated antioxidant systems under different stress conditions, especially metal toxicity (4). The antioxidant defense mechanism, including enzymatic and non-enzymatic systems, is a fundamental reactive oxygen scavenger system to deal with oxidative stress



Corresponding Author: Nihal Goren Saglam

E-mail: goren@istanbul.edu.tr

Submitted: 04.08.2022 • **Accepted:** 18.10.2022 • **Published Online:** 30.12.2022



in fungi, animal and plant systems, as well as lichen. In higher plants and lichens, antioxidant capacity determines the ability of plants to acclimate or survive against high temperatures (4-6). In addition, γ -aminobutyric acid (GABA) metabolism could be included in tolerance mechanisms to high temperatures (7-9). However, the physiological mechanisms of thermotolerance in lichens have not been clearly understood yet.

GABA has critical roles in the acclimation to different stress conditions in plants and animals (10-12). Previous researches have also shown that GABA could have important roles in the metabolism of plants such as amino acid metabolism, nitrogen repartition, and the signalling and development processes due to the close link to the Tricarboxylic acid cycle (13,14). Besides, GABA biosynthesis occurs in animals, plants, algae and lichens (14,15). Glutamate decarboxylase (GAD; EC 4.1.1.15), GABA transaminase (GABA-T; EC 2.6.1.19), and succinic semialdehyde dehydrogenase (SSADH; EC 1.2.1.16) have important roles in the metabolic pathway of GABA. Recent studies have indicated that GAD participates in the regulation of metabolism and can play a considerable role in signal transduction under abiotic stress (15,16). Although an increase in content of GABA by abiotic stress factors such as high temperatures, chilling, drought, salt and heavy metal stresses were shown in the previous studies (8,17-20), GABA metabolism in lichens under different abiotic stress conditions, especially high temperature, is not well known. We tried to figure out the function of GABA metabolism and antioxidant enzyme activity in lichens exposed to high temperature acclimation. For this purpose, we indicated the activities of GAD and GDH and the change in GABA accumulation in *Pseudevernia furfuracea*.

MATERIALS AND METHODS

Plant Materials

P. furfuracea (including *Trebouxia*, green algae as photobiont) were carefully collected from an unpolluted location in Bilecik Center Forest, Turkey (N 40° 11.526', E 029° 57.962'). The collected lichen thalli were cleaned and washed with dH₂O until their surfaces were cleared of dust. All of the lichen thalli were incubated at 23 ± 2°C, 16 h light/8 h under 100 $\mu\text{mol m}^{-2}\text{s}^{-1}$ light intensity for 48 h in a growth cabinet. Experimental conditions were designed according to the laboratory environment. *P. furfuracea* samples were kept in petri dishes in an incubator (100 $\mu\text{mol m}^{-2}\text{s}^{-1}$ light intensity, 16 h light/8 h dark, 45 ± 2°C) for 24 and 48 h. The lichen thallus was watered once a day. The data presented are means of three independent experiments. Each treatment was comprised of three replicates.

Chlorophyll Content Analysis

The lichen thalli (20 mg) were extracted in the dark in 3.0 mL dimethyl sulfoxide (DMSO) with polyvinylpyrrolidone for 1 h at 65°C to minimize the chlorophyll degradation (21). The chlorophyll content was measured at 665.1 and 649.1 nm.

Analysis of GABA Content

Measurement of GABA content was performed via HPLC (Agilent 1200) (18). The lichen samples (0.1 g of *P. furfuracea*) were

homogenized in a water:chloroform:methanol solution, and then centrifuged for 10 min at 4°C. After that, and we dried the supernatants and then dissolved them in an ultra-pure H₂O, borax buffer solution with 2-hydroxynaphthaldehyde and then incubated at 80°C for 30 min. We analyzed the samples at 330 nm by reversed-phase column (250x4.6 mm², 5 μm , Supelco LC18) and the mobile phase was methanol:water (62:38 ratio). While calculating, GABA standard peak areas were taken into consideration.

GAD and GDH Analysis

The lichen extracts were mixed with a reaction mixture ((NH₄)₂SO₄, α -ketoglutarate, NADPH and CaCl₂ in Tris-HCl buffer). The activity of GDH was analyzed spectrophotometrically at 340 nm according to Akihiro et al. (22) and Yolcu et al. (14).

GAD activity was measured by Bartyzel et al. (17) and Yolcu et al. (14). 100 μL of sample was added to an assay mixture (L-glutamate, pyridoxal phosphate and potassium phosphate), mixed, and for the decarboxylation process, we kept it at 30°C for 1 h. To stop the reaction we added HCl to the mixture. Then we centrifuged the mixture for 10 min at 12,500 x g. All of the samples were derivatized with ninhydrin solution. We calculated GAD activity by comparison with the GABA standards.

MDA Content

We analyzed malondialdehyde (MDA) content by the TBA (thio-barbituric acid) method (23). For the calculation of the MDA content, we used the differences in absorbances at 532 and 600 nm.

Antioxidant Enzyme Analysis

20 mg of the thalli were homogenized in liquid nitrogen with pestle and mortar. We resuspended the pellet with 4 mL of homogenization buffer (50 mM phosphate buffer, 1 mM EDTA, 2% TritonX-100 and 2% polyvinylpyrrolidone, pH 7.5). The pellet continued to homogenize with pestle and mortar. Afterwards, the sample was centrifuged at 12,000 g for 20 min at 4°C and then transferred to new Eppendorf tubes. Obtained total protein extracts used as the enzyme extract immediately and kept on ice during experiments.

Catalase (CAT) (EC 1.11.1.6) activity was analyzed in the reaction mixture (100 mM phosphate buffer, the extract and 6 mM H₂O₂). The breakdown of H₂O₂ was measured at 240 nm. Calculation of the CAT activity was made according to Bergmeyer (24) by using an extinction coefficient of 39.4 mM⁻¹ cm⁻¹.

The ascorbate peroxidase (APX) (EC 1.11.1.11) activity was analyzed at 290 nm in accordance with the decrease in the absorbance of the substrate (25). The oxidized ascorbate's concentration was calculated by using an extinction coefficient of 2.8 mM⁻¹ cm⁻¹. One unit of APX activity was described as the $\mu\text{mol mL}^{-1}$ oxidized ascorbate per min and APX content was defined as unit. mg⁻¹ total soluble protein.

The peroxidase (POD) (EC 1.11.1.7) activity was analyzed spectrophotometrically at 470 nm according to (26). The reaction

solution was formed by mixing the guaiacol (0.25%) in a sodium phosphate buffer (0.1 mol/L, pH 7.0, 0.1% hydrogen peroxide). The crude enzyme extract (60 μ L) was added to initiate the reaction, which is based on the oxidation of guaiacol. POD activity was defined as $\Delta A/g \cdot Fr \cdot W \cdot x \cdot Min$.

The protein amount was measured according to the Bradford method (27).

Statistical Analysis

All the data obtained in the study were subjected to one-way ANOVA and we also used Pearson's correlation test. The comparisons between ($p < 0.01$ and $p < 0.05$) were regarded as significantly different.

RESULTS

GABA accumulation was increased under heat treatments with time exposures (Figure 1). It was found that the highest increase in GABA content was in *P. furfuracea* after 48 h heat application ($p < 0.001$). In this study, the activities of GAD and GDH were determined in order to understand whether GABA was enhanced in the lichen thalli. The activity of GAD was increased under heat treatments *P. furfuracea* compared to the control group, significantly (Figure 2a). In *P. furfuracea*, GAD activity increased approximately by 1.5-fold under high temperatures at 48 h. Similarly, GDH activity significantly increased in comparison with the control group ($p < 0.05$, Figure 2b). GDH

activity of *P. furfuracea* thalli at 45°C increased approximately 1.4- and 1.3-fold respectively, in the 24 h comparison with the control ($P < 0.05$).

We found that chlorophyll a and chlorophyll a+b contents were significantly decreased under high temperatures at 48 h (Table 1). However, the chlorophyll a/b ratio was not markedly changed under high temperatures at 24 and 48 h.

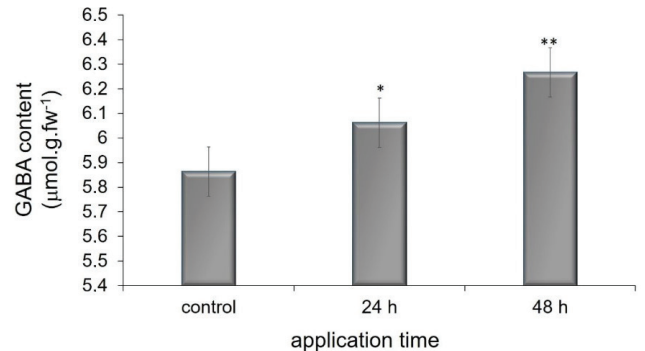


Figure 1. The GABA content of *P. furfuracea* exposed to high temperature (45°C) for 0 (as a control), 24 and 48 h.*Represents a statistically significant difference of $p < 0.05$ when compared with the control, **represents a statistically significant difference of $p < 0.01$ when compared with the control.

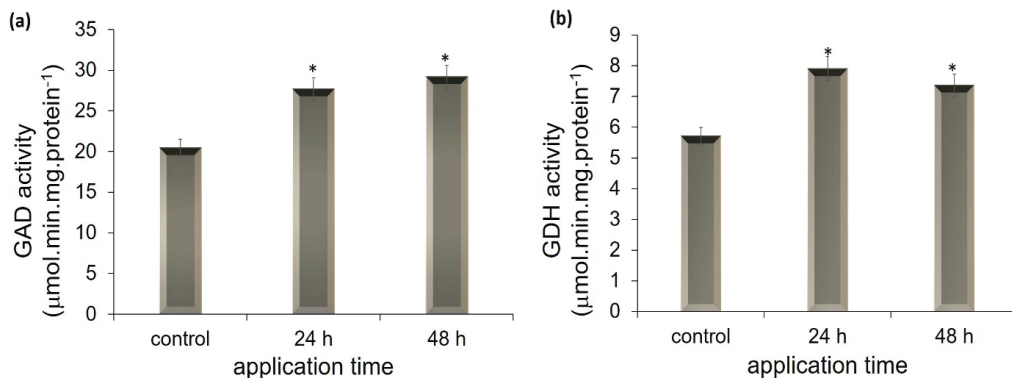


Figure 2. GABA biosynthesis enzymes activities in *P. furfuracea* exposed to high temperature (45°C) for 0 (as a control), 24 and 48 h. (a) GAD activity; (b) GDH activity *Represents a statistically significant difference of $p < 0.05$ when compared with the control.

Table 1. Chlorophyll a, b and a+b content and Chlorophyll a/b ratio in thalli of *P. furfuracea* under high temperature for 0 (as a control), 24 and 48 h.

Groups	n	Chla (μ g/mg fw)	Chlb (μ g/mg fw)	Chla+b (μ g/mg fw)	Chla/b (μ g/mg fw)
Control (0 h)	3	1.58 \pm 0.02	0.516 \pm 0.04	2.096 \pm 0.02	3.06 \pm 0.02
24 h	3	1.518 \pm 0.04	0.502 \pm 0.06	2.023 \pm 0.03	3.02 \pm 0.04
48 h	3	1.471\pm0.03*	0.478 \pm 0.06	1.949\pm0.03*	3.08 \pm 0.06

*Represents a statistically significant difference of $p < 0.05$ when compared with the control.

Figure 3 indicates the MDA content after the high-temperature treatment for 0, 24 and 48 h exposure. In the thallus of *P. furfuracea*, the MDA content was increased significantly ($p < 0.05$) at 24 and 48 h under high temperatures (Figure 3).

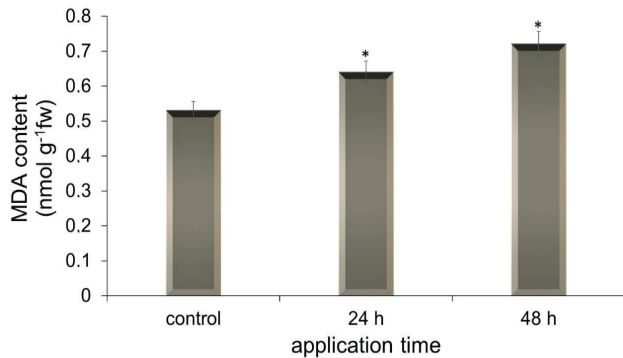


Figure 3. Malondialdehyde (MDA) content of *P. furfuracea* exposed to high temperature (45°C) for 0 (as a control), 24 and 48 h. *Represents a statistically significant difference of $p < 0.05$ when compared with the control

The effects of high temperatures on the enzyme activities of *P. furfuracea* is shown in Figures 4a–c. As shown in Figures 4a and b, the POD and CAT activities gradually decreased due to high temperatures at 24 and 48 h. However, APX activity of *P. furfuracea* was 1.51-fold higher than the control group at 24 h ($p < 0.05$, Figure 4c). Besides, APX activity of *P. furfuracea* was significantly reduced at 48 h comparison with the control group ($p < 0.05$).

Pearson’s correlation results indicated that lipid peroxidation rate as an oxidative stress marker was related to the GABA metabolic pathway (Table 2). MDA level was strongly positively correlated with GABA content and GAD activity (Table 2). In contrast, GDH activity indicated a moderate positive correlation with lipid peroxidation. MDA content also had a strongly positive correlation with CAT activity. In addition, the antioxidant enzyme activity, especially POD activity, showed a strong negative correlation with GAD activity. POD activity also had a strong positive correlation with CAT and APX activities (Table 2).

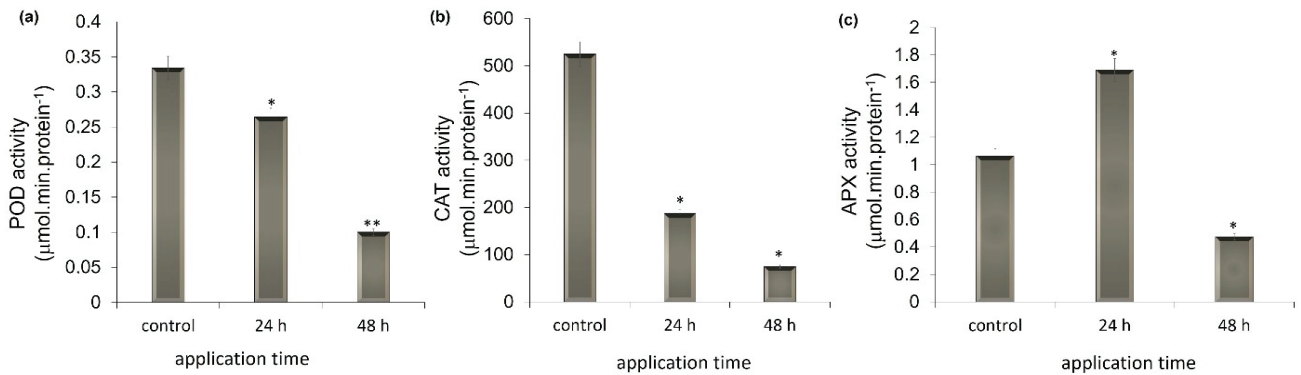


Figure 4. The antioxidant enzymes activities of *P. furfuracea* exposed to high temperature (45°C) for 0 (as a control), 24 and 48 h. (a) peroxidase (POD) activity; (b) catalase (CAT) activity; (c) ascorbate peroxidase (APX) activity. *Represents a statistically significant difference of $p < 0.05$ when compared with the control, **represents a statistically significant difference of $p < 0.01$ when compared with the control.

Table 2. Pearson’s correlation test results (R^2 value) about physiological parameters under high temperature. * $p < 0.05$, ** $p < 0.01$

	MDA	GABA	GDH	GAD	POD	APX	CAT
MDA	-	0.9231**	0.5129	0.7439*	-0.963**	-0.6192	-0.8376**
GABA	0.9231**	-	0.5583	0.8877**	-0.4009	-0.4423	-0.8848**
GDH	0.5129	0.5583	-	0.7138*	-0.5114	0.1109	-0.702
GAD	0.7439*	0.8877**	0.7138*	-	-0.6722*	-0.1648	-0.8449**
POD	-0.963**	-0.4009	-0.5114	-0.6722*	-	0.6739*	0.8171**
APX	-0.6192	-0.4423	0.1109	-0.1648	0.6739*	-	0.1826
CAT	-0.8376**	-0.8848**	-0.702*	-0.8449**	0.8171**	0.1826	-

DISCUSSION

High temperatures negatively affect photosynthetic organisms via inhibition of photosynthesis, distribution of cell membrane integrity and structure, though it causes damage to or inhibits many biological processes such as carbon metabolism (5,8,28). Chlorophyll is also a molecule sensitive to altered environmental conditions and chlorophyll content is frequently used for the determination of physiological conditions of lichen thalli (29-32). Many lichen researchers have demonstrated that chlorophyll a/b ratio is a more sensitive marker than chlorophyll a+b value (29,30). Previous studies have reported that high temperatures cause decreased chlorophyll content in higher plants (8,9). However, chlorophyll content of some lichen species was not significantly changed under high temperatures (2,32). In the present study, chlorophyll a+b content significantly decreased in *P. furfuracea* thalli at 48 h. In contrast, the chlorophyll a/b ratio was not significantly changed in *P. furfuracea* thalli at 45°C for 24 and 48 h. These results suggest that the photobiont of *P. furfuracea* could acclimate to high temperatures.

GABA metabolism could play a remarkable role for acclimation to high temperatures (7-9). Our previous work demonstrated that GABA content increased under high temperatures in *Evernia prunastri* thalli and this increase could be related to high-temperature tolerance (32). Similarly, in the present study, GABA accumulation was observed under high-temperature condition (Figure 1).

In higher plants, GABA is mainly produced from glutamate via cytosolic GAD enzyme activity (16,33). For glutamate to convert to GABA, glutamate needs deamination from the mitochondrial GDH enzyme (34,35). Yolcu et al. (14) demonstrated that *P. furfuracea* had the lowest GDH activity under normal conditions. In the present study, the GAD and GDH enzyme activities increased under high-temperature stress (Figure 2). These results demonstrated that GABA accumulation could occur in a short time and it could be synthesized via GAD activity as in higher plants. In yeast and higher plants, rapid GABA acclimation also occurred in response to heat stress (7,8,20). Similarly, Sadowsky et al. (36) reported that GABA content was increased during desiccation in the strains of green algal photobionts (*Trebouxia*). In both photosynthetic and non-photosynthetic regimes, TCA-related amino acids could have important roles in various metabolic processes (37). Yolcu et al. (14) also indicated that in *P. furfuracea* GABA could be one of the prepotent amino acids, which is in agreement with our findings. Moreover, the enzymes of GABA shunt, especially GAD activity, has a critical role in reducing the effect of oxidative stress (20,38). In our study, GAD could have also a special role under high-temperature stress.

Lipid peroxidation rate is a good indicator for understanding oxidative damage in cells. In the present study, the lipid peroxidation rate increased depending on the time of exposure to high temperatures (Figure 3). Interestingly, lipid peroxidation rate and GAD activity showed a positive correlation (Table 2). While in plants the role of GABA as a signal molecule has been proven,

in lichens, further studies should be done to identify the role of GABA metabolism. Moreover, GABA content in different parts of plants could indicate the impacts of atmospheric pollution (39), and different parts of the lichens should be well evaluated.

Antioxidant mechanisms provide for the scavenging of reactive oxygen species (ROS) and acclimation to environmental stress conditions (5,9,38). Previous studies have demonstrated that high temperatures caused a decrease in CAT and POD activities (9) and increased APX activity (8,9). Similarly, in this study, APX activity enhanced within 24 h, while CAT and POD activities decreased (Figure 4). In addition, there is much information in the literature that exogenous GABA may enhance CAT, POD and APX activities under different stress conditions in higher plants (8,40). However Li et al. (9) demonstrated that the application of GABA did not stimulate CAT and POD activities. In our study, CAT and POD activities indicated a negative correlation with GABA accumulation and its biosynthetic enzymes (Table 2). Moreover, APX activity did not show any positive correlation with GABA metabolism. On the other hand, increased APX activity in 24 h could result in acclimation to high temperatures.

CONCLUSION

In summary, physiological analysis of thalli of *P. furfuracea* under short time high temperatures demonstrated that GABA could improve high-temperature acclimation through multiple physiological processes including protection of photosynthesis, and the improvement of some antioxidant enzyme activities. Lichens have a high tolerance to climate change, and the increase in GABA content may trigger some metabolic pathways in the mycobiont or photobiont sides. Our results demonstrated that GABA metabolism could have a role in lichen acclimating to temperature stress. However, future research should focus on the role of GABA shunt as a stress signaling molecule on different metabolic pathways in lichen under short- and long-term different stress conditions.

Peer Review: Externally peer-reviewed.

Author Contributions: Conception/Design of Study- N.G.S., F.O.A., D.U.; Data Acquisition- N.G.S., F.O.A., D.U.; Data Analysis/ Interpretation- N.G.S., F.O.A., D.U.; Drafting Manuscript- N.G.S., D.U.; Critical Revision of Manuscript- N.G.S., F.O.A., D.U.; Final Approval and Accountability- N.G.S., F.O.A., D.U.

Conflict of Interest Disclosure: This manuscript has not been published before and is not under consideration for publication anywhere else. All authors approved the publication of this article.

REFERENCES

1. Karl TR, Kukla G, Razuvayev VN, Changery MJ, Quayle RG, Heim RR, Easterlinf DR, Fu CB. Global warming: evidence for asymmetric diurnal temperature change. *Geophys Res Lett* 1991; 18: 2253-6.
2. Pisani T, Paoli L, Gaggi C, Pirtosos SA, Loppi S. Effects of high temperature on epiphytic lichens: Issues for consideration in a changing climate scenario. *Plant Biosyst* 2007; 141: 164-9.

3. Dyakov MY, Insarova ID, Kharabadze DE, Ptushenko VV, Shtae OV. Influence of extreme ambient temperatures and anaerobic conditions on *Peltigera aphthosa* (L.) Wild. viability. *Life Sci Space Res* 2015; 7: 66-72.
4. Sanita di Toppi BL, Pawlik-Skowronska E, Vurro Z, Vattuone R, Kalinowska FM. First and second line mechanisms of cadmium detoxification in the lichen photobiont *Trebouxia impressa* (Chlorophyta). *Environ Pollut* 2008; 151: 280-6.
5. Xu S, Li J, Zhang X, Wei H, Cui L. Effects of heat acclimation pretreatment on changes of membrane lipid peroxidation, antioxidant metabolites, and ultrastructure of chloroplast in two-season turfgrass species under heat stress. *Environ Exp Bot* 2006; 56: 274-85.
6. Sen G, Kutlu E, Ozakca D. The effect of aluminium and exogenous spermidine on chlorophyll degradation, glutathione reductase activity and the photosystem II D1 protein gene (psbA) transcript level in lichen *Xanthoria parietina*. *Phytochemistry* 2014; 98: 54-9.
7. Youn YS, Park JK, Jang HD, Rhee YW. Sequential hydration with anaerobic and heat treatment increases GABA (γ -aminobutyric acid) content in wheat. *Food Chem* 2011; 129: 1631-5.
8. Nayyar H, Kaur, R, Kaur S, Singh R. γ -aminobutyric acid (GABA) imparts partial protection from heat stress injury to rice seedlings by improving leaf turgor and upregulating osmoprotectants and antioxidants. *J Plant Growth Regul* 2014; 33: 408-19.
9. Li Z, Yu J, Peng Y, Huang B. Metabolic pathways regulated by γ -aminobutyric acid (GABA) contributing to heat tolerance in creeping bentgrass (*Agrostis stolonifera*). *Sci Rep* 2016; 6: 1-6.
10. Kinnersley AM, Turano FJ. Gamma Aminobutyric Acid (GABA) and Plant Responses to Stress. *Crit Rev Plant Sci* 2000; 19: 479-509.
11. Sharma SS, Dietz KJ. The significance of amino acids and amino acid-derived molecules in plant responses and adaptation to heavy metal stress. *J Exp Bot* 2006; 57: 28711-26.
12. Chand N, Muhammad S, Khan RU, Alhidary IA, Rehman ZU. Ameliorative effect of synthetic γ -aminobutyric acid (GABA) on performance traits, antioxidant status and immune response in broiler exposed to cyclic heat stress. *Environ Sci Pollut Res* 2016; 23: 23930-5.
13. Fait A, Fromm H, Walter D, Galili G, Fernie AR. Highway or byway: the metabolic role of the GABA shunt in plants. *Trends Plant Sci* 2008; 13: 14-9.
14. Yolcu S, Ozdemir F, Bor M. Gamma-amino butyric acid, glutamate dehydrogenase and glutamate decarboxylase levels in phylogenetically divergent plants. *Plant Syst. Evol* 2013;299: 403-12.
15. Bouché N, Fromm H. GABA in plants : just a metabolite ? *Trends Plant Sci* 2004;9:110-15.
16. Bouché N, Fait A, Bouchez D, Moller SG, Fromm H. Mitochondrial succinic-semialdehyde dehydrogenase of the gamma-aminobutyrate shunt is required to restrict levels of reactive oxygen intermediates in plants. *Proc Natl Acad Sci U.S.A* 2003; 100: 6843-8.
17. Bartyzel I, Pelczar K, Paszkowski A. Functioning of the gammaaminobutyrate pathway in wheat seedlings affected by osmotic stress. *Biol Plant* 2003; 47: 221-5.
18. Bor M, Seckin B, Ozgur R, Yilmaz O, Ozdemir F, Turkan I. Comparative effects of drought, salt, heavy metal and heat stresses on gamma-aminobutyric acid levels of sesame. *Acta Physiol Plant* 2009; 31: 655-9.
19. Al-Quraan NA, Locy RD, Singh NK. Implications of paraquat and hydrogen peroxide-induced oxidative stress treatments on the GABA shunt pathway in *Arabidopsis thaliana* calmodulin mutants. *Plant Biotechnol Rep* 2011; 5: 225-34.
20. Cao J, Barbosa JM, Singh N, Locy RD. GABA shunt mediates thermotolerance in *Saccharomyces cerevisiae* by reducing reactive oxygen production. *Yeast* 2013; 30: 129-44.
21. Wellburn AR. The spectral determination of chlorophylls a and b, as well as total carotenoids, using various solvents with spectrophotometers of different resolution. *J Plant Physiol* 1994; 144: 307-13.
22. Akihiro T, Koike S, Tani R, Tominaga T, Watanabe S, Iijima Y, et al. Biochemical mechanism on GABA accumulation during fruit development in tomato. *Plant Cell Physiol* 2008; 49: 1378-89.
23. Heath RL, Packer L. Photoperoxidation in isolated chloroplast: 1. Kinetics and stoichiometry of fatty acid peroxidation. *Arch Biochem Biophys* 1968; 125: 189-98.
24. Bergmeyer, N. Methoden der enzymatischen analyse. Akademie Verlag, Berlin 1970; 1: 636-64.
25. Nakano Y, Asada K. Hydrogen peroxide is scavenged by ascorbate specific peroxidase in spinach chloroplasts. *Plant Cell Physiol* 1981; 22: 867-80.
26. Birecka H, Briber KA, Catalfamo JL. Comparative studies on tobacco pith and sweet potato root isoperoxidases in relation to injury, indoleacetic acid, and ethylene effects. *Plant Physiol* 1973; 52: 43-9.
27. Bradford MM. Rapid and sensitive method for quantitation of microgram quantities of protein utilizing principle of protein dye binding. *Anal Biochem* 1976; 72: 248-54.
28. Karim MA, Fracheboud Y, Stamp P. Photosynthetic activity of developing leaves of *Zea mays* is less affected by heat stress than that of development leaves. *Physiol Plant* 1999; 105: 685-93.
29. Chettri MK, Cook CM, Vardaka E, Sawidis T, Lanaras T. The effect of Cu, Zn, and Pb on the chlorophyll content of lichens *Cladonia convolute* and *Cladonia rangiformis*. *Environ Exp Bot* 1998; 39: 1-10.
30. Bačkor M, Zetková J. Effects of copper, cobalt and mercury on the chlorophyll content of lichens *Centraria islandica* and *Flavocetraria cucullata*. *J Hattori Bot Lab* 2003; 93: 175-87.
31. Unal D, Tuney I, Sukatar A. The role of external polyamines on photosynthetic responses, lipid peroxidation, protein and chlorophyll a content under the UV-A (352 nm) stress in *Physcia semipinnata*. *J Photochem Photobiol B, Biol* 2008; 90: 64-8.
32. Cekic FO, Goren-Saglam N, Torun H, Yiğit E, Unal D. Gamma-Amino Butyric acid metabolism under high temperature stress in two lichen species. *Appl Ecol Environ Res* 2018; 16: 5529-38.
33. Cao S, Cai Y, Yang Z, Zheng Y. MeJA induces chilling tolerance in loquat fruit by regulating proline and γ -aminobutyric acid contents. *Food Chem* 2012; 133: 1466-70.
34. Andersson JO, Roger AJ. Evolution of GDH genes: evidence for lateral gene transfer within and between prokaryotes and eukaryotes. *BMC Evol Biol* 2003; 3: 14.
35. Forde BG, Lea PJ. Glutamate in plants: metabolism, regulation and signalling. *J Exp Bot* 2007; 58: 2339-58.
36. Sadowsky A, Mettler-Altman T, Ott S. Metabolic response to desiccation stress in strains of green algal photobionts (*Trebouxia*) from two Antarctic lichens of southern habitats. *Phycologia* 2016; 55: 703-14.
37. Cowan DA, Wilson AT, Green TGA. Lichen metabolism: 2. Aspects of light and dark physiology. *New Phytol* 1979; 83: 761-9.
38. Bouché N, Fait A, Zik M, Fromm H. The root-specific glutamate decarboxylase (GAD1) is essential for sustaining GABA levels in *Arabidopsis*. *Plant Mol Biol* 2004; 55: 315-25.
39. Xu Y, Xiao H, Guan H, Wang Y, Long C, Zhao J. Variations in free amino acid concentrations in mosses and different parts of *Cinnamomum camphora* along an urban-to-rural gradient. *Ecol Indic* 2018; 93: 813-21.
40. Baek KH, Skinner DZ. Alteration of antioxidant enzyme gene expression during cold acclimation of near-isogenic wheat lines. *Plant Sci* 2003; 165: 1221-7.

Strigolactone and Auxin Applications on Cotyledon Senescence in Sunflower Seedlings under Salt Stress

Humeyra Ozel¹ , Serap Saglam¹ 

¹Istanbul University, Faculty of Science, Department of Biology, Division of Botany, Vezneciler, Istanbul, Turkey

ORCID IDs of the authors: H.O. 0000-0003-0941-8529; S.S. 0000-0002-4245-8031

Please cite this article as: Ozel H, Saglam S. Strigolactone and Auxin Applications on Cotyledon Senescence in Sunflower Seedlings under Salt Stress. Eur J Biol 2022; 81(2): 190-196. DOI: 10.26650/EurJBiol.2022.1187517

ABSTRACT

Objective: Senescence is a programmed cell death process and is important in the growth, development and flowering process of the plant. Delaying senescence has a very important effect on agriculture in terms of product yield. Indole-3-acetic acid (IAA) and strigolactone (GR24) are growth regulators that affect plant development and senescence. Salt stress accelerates the senescence process. The aim of this study is to increase crop yield by delaying senescence by the application of auxin and GR24 under stress conditions, because the delay of senescence causes the prolongation of the vegetative process and the formation of more apical tips. In this case, the seedling produces more fruit.

Materials and Methods: In this study, senescent cotyledons of sunflower seedlings were used as experimental material. Half of the developing sunflower seedlings were irrigated with Hoagland solution, and the other half was irrigated with 150 mM sodium chloride (NaCl) solution. IAA and GR24 were applied by spraying on seedlings that are grown both in Hoagland solution and under salt stress.

Results: The degree of senescence of the cotyledons of the plants was determined in terms of the percentage of green area. When the green area percentage of cotyledons of seedlings grown in Hoagland solution was 50, all cotyledons were harvested. After that, fresh weight, pigment contents, total protein, malondialdehyde, and proline levels, peroxidase enzyme activities of cotyledons were determined. The application of IAA and GR24 to the cotyledons of seedlings grown in the salt medium significantly delayed the senescence.

Conclusion: This study was conducted in the plant growth chamber under controlled conditions. Results showed that the application of IAA and GR24 to leaves can ameliorate the adverse effects of salt stress and delay senescence due to the activation of chlorophyll components and modulation of photosynthesis as well as antioxidant defense capacity. The effect of IAA is more precise when all analyzes are considered. More importantly, showed that all findings (except MDA and Proline) IAA and GR24 promote senescence in Hoagland in this research. Delaying senescence contributes to basic science. It is desired to increase fruit and vegetable yield by delaying senescence. It is suggested that this information can be used practically in the field of agriculture. On the other hand in this study, we can say that IAA and relatively GR24 can play an important role in the protection of plants in agricultural areas in salt stress.

Keywords: Green area percentage, *Helianthus annuus* L., Hoagland, NaCl, Plant growth substance, Senescence

INTRODUCTION

Plants need optimum conditions for growth. When plants are suddenly exposed to an unexpected condition, their development and lifespan are affected (1). The factors that create all these conditions are defined as "stress". Stress conditions affecting plants include biotic conditions are created by living things such as animals, plants, and microorganisms, and abiotic con-

ditions are created by environmental conditions such as water, minerals, gases, temperature, and radiation (2). Increasing land areas rich in salt (NaCl) poses a serious threat to plants and ecosystems, agriculture is endangered, and agricultural products are restricted with population increase.

Senescence is an important active process involving serious catabolic changes in gene expression and hor-



Corresponding Author: Serap Saglam

E-mail: sercag@istanbul.edu.tr

Submitted: 11.10.2022 • **Revision Requested:** 04.11.2022 • **Last Revision Received:** 08.11.2022 •

Accepted: 17.11.2022 • **Published Online:** 29.12.2022

Content of this journal is licensed under a Creative Commons Attribution-NonCommercial 4.0 International License.



monal signaling (3). Senescence is an indicator characterized by the yellowing of cotyledons and leaves, and multiple signals, such as various plant hormones can regulate this process. Senescence seen at the level of the whole organism causes the death of the plant in the last stage of plant ontogenetic development. Senescence, the last stage of plant development, has an important impact, especially in agriculture. The senescence process speeds up in seedlings exposed to salt stress. Delaying senescence causes the growth period to be extended in an organized manner, thus increasing the product yield (4).

Endogenous factors such as phytohormone levels, high-order epigenetic mechanisms, and expression of specific environment-dependent genes and environmental factors such as day length, drought, freezing, and insufficient light cause senescence. Plant hormones are metabolic regulators that control plant growth, development and many more processes. Hormones regulate plant growth and provide the necessary energy in plant life by affecting the metabolism.

Strigolactones (SLs) have recently been identified as new phytohormones that regulate plant growth and development by influencing plant metabolism (5). Strigolactones are derived from carotenoids and are involved in seed germination, photomorphogenesis, regulation of plant morphology (inhibition of bud growth and shoot branching) and physiological reactions to abiotic factors. SLs are synthesized in roots and stems and transported through the xylem (6). Although the effect of strigolactones in regulating leaf senescence is known (7), information on the molecular mechanism of the action is still insufficient. SL deficient or SL insensitive mutants show senescence delay (8). Some studies have shown that leaf senescence is accelerated by strigolactone (GR24). To investigate these effects, GR24 was applied to the leaves of *Arabidopsis* and rice (9,10). Exogenous application of GR24 increased leaf senescence in both *Arabidopsis* and SL-deficient mutants of rice (11,12). Auxin is an important hormone for plant growth and development. IAA can coordinate growth under stressful conditions by managing the plant's response to stress (13). The senescence delaying effect of auxin has been reported for many years in scientific studies (14). When the sources of auxins are examined, it is seen that the role of this phytohormone in regulating senescence by auxin is complex. Auxins and SLs link with each other in the feedback loop (15). Auxins play an important role in strigolactone biosynthesis through gene expression and are involved in developmental processes with strigolactone (16,17). Strigolactones promote auxin transport in seedling stems (18). It has been noted that SLs affect and regulate auxin pathways by facilitating auxin transport and stimulating transcription of the auxin receptor TIR1 (19).

In summary, the aim of this study was to investigate the effects of indole-3-acetic acid and strigolactone on cotyledon senescence in sunflower seedlings due to salt stress. At the end of this study, it was determined that the application of IAA and GR24 played a beneficial role in accelerating the salt-induced senescence process in the sunflower.

MATERIALS AND METHODS

Plant Material, Growth Conditions and Treatments

Seedlings of sunflower [*Helianthus annuus* L. (Tar-San 1018 TR.00.00.1024.0265)] were grown in a plant growth chamber (6000-lux light intensity, 16 h light, 8 h dark photoperiod and $25\pm 2^\circ\text{C}$, 59% humidity). 10^{-5} M IAA (Sigma-Aldrich) and 10^{-8} M GR24 (rac-GR24 from Chiralix) were applied to the seedlings grown in Hoagland solution for Control groups and Hoagland+150 mM NaCl (NaCl-CAS No: 7647-14-5) solution for salt stress groups. The IAA concentration used in this study was obtained from the results of our previous studies. The GR24 concentration was determined after several applications based on the article information. The cotyledons of all plants were harvested on the day when the cotyledons of the seedlings in the salt group causing early senescence were 50%.

Determination of Senescence Degree

The degree of senescence in the cotyledons of plants was determined by a method developed by Lindoo and Noodén (20) for soybeans and then successfully used by modification. According to this method, the senescence degree of cotyledons of the sunflower plant was determined considering the green area percentage of cotyledons.

Determination of Total Chlorophyll and Carotenoid Amount

Chlorophyll and carotenoid amounts of the extracts obtained from fresh samples were determined according to Parsons and Strickland's method (21). The Elisa reader device was used in all experiments in which absorbance values were measured.

Determination of Soluble Total Protein Amount

The determination of soluble total protein amount was made by the Bradford method (22) in which homogenates were taken into Eppendorf tubes and centrifuged at $+4^\circ\text{C}$ for 30 min at $13,000 \times g$. The samples were measured at 595 nm wavelength, and the protein amount calculations were made by comparing them with the previously prepared BSA standard.

Determination of Peroxidase (POD) Activity

In order to determine the differences in POD activity in sunflower cotyledons, Birecka et al.'s method (23) was used. The samples, which were homogenized with phosphate buffer (pH: 7), were centrifuged for 30 min at $13,000 \times g$. Phosphate buffer at pH: 5.8 was used for measurement. After all procedures were completed, it was placed in the device for measurement, and the kinetic absorbance was measured with a total of 13 measurements, 10 sec apart for 2 min.

Malondialdehyde (MDA) Determination

MDA measurement was made according to the Heath and Packer method (24). The prepared extracts were centrifuged at $10,000 \times g$ for 15 min. The supernatants taken were incubated in a 96°C water bath for 30 min, then taken into the refrigerator and cooled to terminate the reaction, then centrifuged at $10,000 \times g$ for 10 min. After centrifugation, samples were measured at 532 nm and 600 nm.

Proline Determination

Proline measurement was made according to the Bates et al. method (25). The extracts were obtained at $12,000 \times g$ for 7 min.

After centrifugation, necessary materials were added to the supernatant and left for 1 h to be incubated in a 98°C water bath. Later, after the procedure was applied to the samples that were cooled in the refrigerator, 518 nm absorbance value was measured with an Elisa reader.

Statistical Analysis

Each treatment included six replicates and each experiment was carried out at least five times. The data obtained as a result of the analysis were analyzed by one-way analysis of variance (ANOVA) included in the Statistical Package for Social Sciences (SPSS for Windows 10.0) package program. The differences between the means were determined as significant with $p < 0.05$ according to Duncan's new multiple range test.

RESULTS

Change in Average Green Area (A.G.A.) Percentage of the Cotyledons

The cotyledons of the seedlings grown in Hoagland and salt solutions and treated with IAA and GR24 were observed. The A.G.A. percentages of cotyledons were determined at regular intervals for 30 days. While the cotyledons of all groups were 100% green, the senescence process started from the 19th

day. The differences between the Hoagland and salt groups increased day by day. Most of the cotyledons of the seedlings treated with IAA completed the senescence process on the 30th day. IAA caused faster senescence than GR24. While cotyledons in the salt medium experienced rapid senescence, the application of GR24 slowed down the senescence process a little but accelerated it in the next process. On the other hand, IAA had a retarding effect on the senescence and healing effect on salt toxicity under NaCl stress.

Analyses of the harvested cotyledons were carried out when the average percentage of the green area of the Hoagland group was approximately 50% (Figure 1).

Changes in Total Chlorophyll and Carotenoid Amount

In the Hoagland solution, the chlorophyll content in cotyledons of the seedlings treated with IAA and GR24 decreased by 50% and 48%, and the carotenoid content decreased by 68% and 50%, respectively. On the other hand, the amount of chlorophyll in seedlings grown in the salt medium increased by 185% and 178%, and the carotenoid content by 99% and 36%, respectively, with the application of IAA and GR24 (Table 1). This indicates that IAA and GR24 in Hoagland's solution encourage senescence but delay senescence in salt stress.

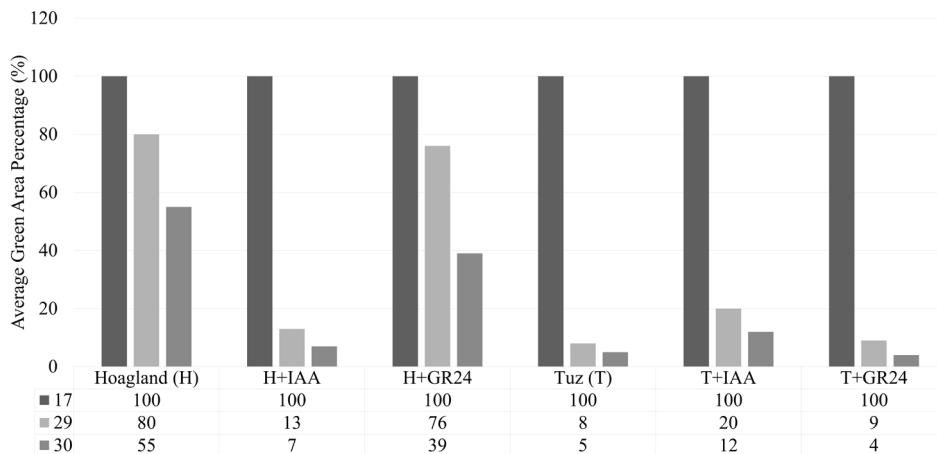


Figure 1. Average Green Area (A.G.A.) percentage of senescence occurring in cotyledons of *Helianthus annuus* L. (sunflower) seedlings grown in Hoagland solution and salt solution for 30 days.

Table 1. Comparison of total chlorophyll ($p < 0.05$) and carotenoid ($p < 0.05$) amount in cotyledons of *Helianthus annuus* L. seedlings grown in Hoagland and salt medium and treated with 10^{-5} M IAA and 10^{-8} M strigolactone (GR24) at approximately 50% senescence point of Hoagland group.

Treatment Groups	Total Chlorophyll Amount ($\mu\text{g/g fr wt}$)	Carotenoid Amount ($\mu\text{g/g fr wt}$)
Hoagland	126.2129 \pm 2.1157 ^a	0.8570 \pm 0.0270 ^a
Hoagland+IAA	64.1296 \pm 3.5607 ^b	0.2746 \pm 0.0378 ^b
Hoagland+GR24	66.4460 \pm 0.7634 ^b	0.4282 \pm 0.0338 ^c
Hoagland+NaCl	64.6257 \pm 1.6693 ^b	0.5799 \pm 0.0429 ^d
Hoagland+NaCl+IAA	120.0975 \pm 5.5115 ^c	1.1546 \pm 0.0252 ^e
Hoagland+NaCl+GR24	116.7482 \pm 5.3101 ^d	0.7866 \pm 0.0485 ^f

Data are means \pm standard deviations (SD) of least five independent experiments with six replicates. Different letters indicate values that differ significantly from the control and strigolactone-indoleacetic acid treatments, respectively at $P < 0.05$ according to Duncan's new multiple range test.

Changes in the Amount of Soluble Total Protein

While the total amount of protein in the cotyledons of the seedlings treated with 10^{-5} M IAA decreased by 41% compared to the cotyledons of the Hoagland group, it was determined that there was no difference in the 10^{-8} M GR24 application (Figure 2). As a result, it was found that IAA application decreased the amount of protein due to early senescence in cotyledons and increased salt stress with a healing effect.

Changes in POD Activity

POD activity in cotyledons of seedlings grown in Hoagland solution increased 2.1 times with IAA application and 1.4 times with GR24 application (Table 2). The POD activity in cotyledons of seedlings exposed to salt stress increased 2.2 times when compared to Hoagland group cotyledons. In addition, it was determined that IAA and GR24 application increased POD activity by 31% in cotyledons of seedlings

grown in Hoagland solution compared to cotyledons of seedlings in salt.

Changes in the MDA Ratio

Compared to cotyledons harvested at 50% senescence of seedlings grown in Hoagland solution, MDA content in cotyledons of seedlings treated with IAA and GR24 decreased approximately 1.8 times and 1.16 times, respectively (Table 2). The amount of MDA in cotyledons of seedlings grown in salt solution decreased by 1.6 and 1.2 times, respectively, with IAA and GR24 application.

Changes in the Proline Rate

Proline in cotyledons of the seedlings treated with IAA and GR24 reduced by 70% and 10% in Hoagland solution (Table 2). In cotyledons of seedlings grown in the salt solution, the amount of proline decreased by 47% and 28% with IAA and GR24 application, respectively.

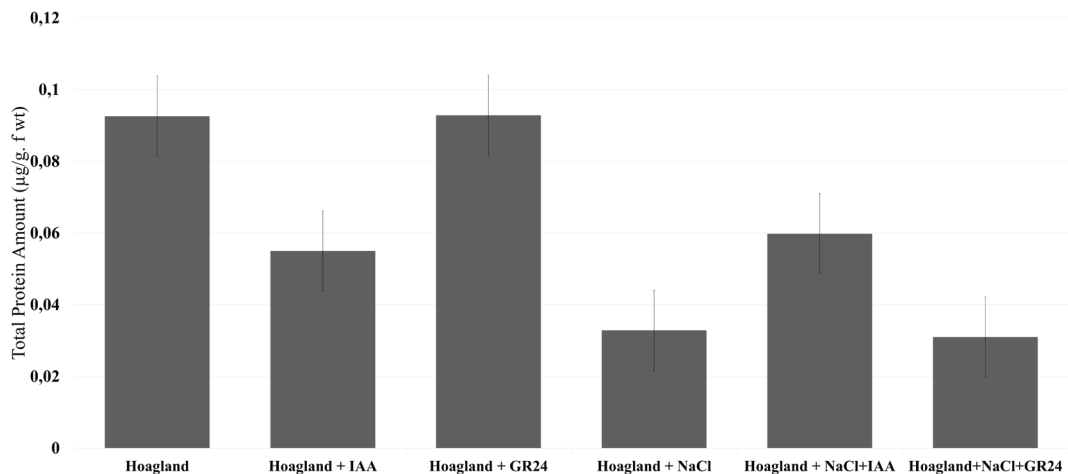


Figure 2. Comparison of the total protein amount in cotyledons of *Helianthus annuus* L. seedlings grown in Hoagland and salt medium and treated with 10^{-5} M IAA and 10^{-8} M GR24 at 50% senescence time ($p < 0.05$).

Table 2. Comparison of peroxidase (POD) enzyme activity, the amount of MDA and proline in cotyledons of *Helianthus annuus* L. seedlings grown in Hoagland and salt medium and treated with 10^{-5} M IAA and 10^{-8} M GR24 at 50% senescence time of Hoagland group ($p < 0.05$).

Treatment Groups	POD Activity ($\Delta A/g$ fr wt. min)	MDA Amount ($\mu\text{mol/g. f wt}$)	Proline Amount ($\mu\text{mol/g. f wt}$)
Hoagland	0.0547 \pm 0.0039 ^a	12.9301 \pm 0.7366 ^a	33.1518 \pm 4.6258 ^a
Hoagland+IAA	0.1165 \pm 0.0059 ^b	7.1640 \pm 0.8871 ^b	9.9066 \pm 1.0937 ^b
Hoagland+GR24	0.0773 \pm 0.0069 ^c	11.1290 \pm 0.9140 ^c	29.8773 \pm 2.3791 ^c
Hoagland+NaCl	0.1227 \pm 0.0069 ^d	39.7446 \pm 1.3817 ^d	165.9861 \pm 7.0719 ^d
Hoagland+NaCl+IAA	0.0806 \pm 0.0045 ^e	24.9651 \pm 1.6667 ^e	88.0193 \pm 6.3961 ^e
Hoagland+NaCl+GR24	0.0629 \pm 0.0005 ^a	34.2204 \pm 2.5806 ^f	119.0541 \pm 3.1777 ^f

Data are means \pm standard deviations (SD) of least five independent experiment with six replicates. Different letters indicate values that differ significantly from the control and strigolactone-indoleacetic acid treatments, respectively at $P < 0.05$ according to Duncan's new multiple range test.

DISCUSSION

The role of auxins in the senescence process has been discussed for a long time. While some researchers state that auxins delay senescence (26,27), some recent studies have shown that auxins accelerate senescence. Noh and Amasino (28) found a link between auxin gene expression and senescence. In this study, IAA and a synthetic strigolactone analog GR24 were sprayed to the foliage to evaluate the response of sunflower to the application of GR24 with IAA in optimum and salt conditions. According to the findings, the fact that it encourages senescence in the presence of IAA in the Hoagland medium is in line with the previous findings. Zn is known to provide IAA stabilization (29,30). Some researchers found that auxin was effective in the speed of the senescence process by establishing a link between Zn and IAA (31). In their study, Saglam-Cag and Okatan (31) applied C¹⁴ to the apical end, preventing IAA from reaching cotyledons, and found that senescence does not occur in these cotyledons. Technological advances in plant molecular biology will help unravel the mystery between auxin and senescence. In recent research on senescence and auxin-related genes, information about current molecular regulatory senescence patterns has been obtained (27).

In this study, parallel to the acceleration of the senescence observed in cotyledons of the seedlings grown in Hoagland solution and treated with IAA, a decrease in fresh weight, chlorophyll, carotenoid contents, total protein amount, MDA and proline, and an increase in peroxidase activity were detected. Our results show that IAA practice increases senescence in Hoagland solution. Similarly, Hou et al. (26) stated that auxin increases the expression of the SAUR 36 gene, which is a positive regulator of the senescence process. Moreover, some researchers stated that auxin measurements in senescing leaves have shown that the abundance of free, bioactive IAA increased two fold, which correlates with an increased expression of key enzymes involved in IAA biosynthesis during age-dependent leaf senescence (32). Looking at the average green area percentage, the increase in the senescence rate observed in the cotyledons of the seedlings grown in Hoagland solution and treated with GR24 also decreased in fresh weight, chlorophyll, and carotenoid contents similar to the IAA effect. In recent years, it has been reported that SL accelerates leaf senescence, which is also regulated by sugar signals and ethylene (3,33,34). On the other hand, there are studies that GR24 delays senescence (35). It was reported that sugar suppresses SL-induced leaf senescence in the dark. But there was no difference in the total protein amount compared to the control of the untreated seedlings. This difference may have affected the transcription stability of the enzyme proteins that controlled the anabolic and catabolic degradation processes in those days of the application of GR24 to the cotyledons of the seedlings grown in the Hoagland solution. Since senescence occurred earlier and faster during IAA application, a significant difference was observed in the amount of protein. The fact that IAA and GR24 applications also cause an increase in peroxidase activity indicates that the application of IAA and GR24 promotes senescence. Proline in cotyledons treated with IAA and GR24 was reduced by 70% and 10% in Hoagland solution (Table 2). According to this

result, it is obvious that IAA and GR24 promote senescence. These results are parallel to some sources (32). Indeed, it is known that proline is also protective under normal conditions and is important in preventing cell death. It is known that chlorophyll and total soluble proteins are degraded and proteolytic activity is increased during the senescence process. Most findings in this study indicate that IAA promotes senescence. However, it has been stated that proline accumulation in barley plays no role in salinity tolerance, but rather represents a sensitivity symptom (36). On the other hand, in this research, MDA and proline contents were found to be high in rapidly senescent cotyledons under salt conditions (Table 2). Indeed, MDA activity reaches high levels in the NaCl environment, and this is a sign that the cell membrane is damaged by the effect of salinity (37). MDA, which increased as a result of the damage of salt, decreased with the application of IAA to the seedlings. This result suggests that IAA plays a curative role in salt stress by following a different path. In recent years, many researchers have stated that IAA applications to seedlings can be effective in developing resistance to salt stress (38,39). However, there is limited information about the ameliorating role of IAA in salt stress. Some researchers (40,41) have determined that synthetic GR24 treated plants showed higher MDA content by different stress when compared to the control.

In our study, GR24 application under salt stress conditions decreased the amount of MDA, proline and activity of POD (Table 2), whereas increased the content of chlorophyll and carotenoids (Table 1). This result may suggest that GR24 delays senescence and exerts a curative effect. The same researchers found higher chlorophyll content and photosynthesis rate in synthetic GR24 treated plants under drought stress. Lu et al. (42) found low MDA content and POD activity in low light stress.

To summarize, senescence occurs earlier in seedlings grown under abiotic stress conditions. It has been shown that in seedlings exposed to stress conditions, auxin may at least partially participate in the positive regulation of stress resistance by affecting the expression of abscisic acid response genes and reactive oxygen species metabolism (43). As a matter of fact, in this study, it was determined that the senescence of the cotyledons of sunflower seedlings grown in a salt environment accelerated significantly compared to the cotyledons of seedlings grown in the Hoagland environment. However, IAA application to grown seedlings in a salt environment had a delayed effect on senescence. The GR24 application, on the other hand, accelerated the senescence at the end of the process. Although the causes of proline accumulation in salt stress are not fully explained, it is accepted as an important indicator of salt tolerance (44). In many studies, it was stated that lipid peroxidation and consequently MDA increased with salt stress (45,46). In this study, a statistically significant increase was found in the proline and MDA content in the cotyledons of the seedlings grown in a salt environment compared to the proline content in the cotyledons of the seedlings grown in optimum conditions. These findings are in agreement with scientific sources (47-50). In our study, it was revealed that IAA and partially GR24 regulate salinity positively (51) and delay senescence. However, Mina et

al. (41) reported that GR24 application decreased the level of IAA in roots and leaves under stress. Briefly, when we consider the average percentage of green area, during the delay of the senescence observed in cotyledons of the seedlings grown in Hoagland+NaCl solution and treated with IAA, chlorophyll and carotenoid contents increased in total protein amount. A decrease in the peroxidase activity, MDA and proline amounts of cotyledons under the same conditions was detected. These results proved that IAA application reduced lipid peroxidation, preserved membrane structure, and delayed senescence, and the toxic effect created by salt stress had a healing effect. Considering the average green area percentages, the senescence rate observed in the cotyledons of the seedlings grown in a salty environment and treated with GR24 is not as strong as the IAA effect. GR24 application in salt stress caused an increase in chlorophyll, carotenoid and a decrease in POD enzyme activity, MDA and proline amount. It is thought that the GR24 application has a delaying effect on senescence. Little is known about the regulation of leaf senescence by strigolactone. Ueda and Kusaba (10) showed that SL promotes leaf senescence in a study they did. Moreover, their results showed that both ethylene synthesis and SL synthesis were induced during the effective progression of leaf senescence caused by darkness. Yamada and Umehara (11) stated that the production of strigolactones is stimulated in response to nitrogen and phosphorus deficiency and accelerates leaf senescence. Agusti et al. (52) showed that strigolactone signaling is necessary for promoting vascular cambium formation and strongly interacts with the auxin signaling pathway. This information supports our views put forward in our study that effectively the IAA and GR24 encourage senescence. If the receptors associated with the senescence process are not yet present in a cell, it is out of the question for that cell to perceive the senescence signal. Therefore, in order for IAA to function as a senescence signal, receptors that will perceive IAA as a senescence signal must be synthesized in the cells of target organs that will undergo senescence. In a study, two different receptor proteins that bind IAA and occur at a different time from the other were detected in the plasma membrane. The first of these proteins are related to growth, and the role of the second is still not determined (53,54). The possibility that the second protein that binds IAA is the receptor that detects the senescence signal can be considered.

As a result, this study was conducted in the plant growth chamber under controlled conditions. Results showed that the application of IAA and GR24 to leaves can ameliorate the adverse effects of salt stress and delay senescence due to the activation of chlorophyll components and modulation of photosynthesis as well as antioxidant defense capacity. The effect of IAA is more precise when all analyses are considered. More importantly, most of the findings showed that IAA and GR24 encourage senescence in Hoagland (control/without salt) in this research. Delaying senescence contributes to basic science. It is suggested that this information can be used practically in the field of agriculture. In this study, our aim is to delay senescence with various applications under stress condition, to extend the vegetative period and to increase the yield of the crop. IAA and

relatively, GR24 can play an important role in the protection of plants in agricultural areas in salt stress.

CONCLUSION

This study was conducted in a plant growth chamber under controlled conditions. According to our results, while IAA and partially GR24 promote senescence under optimum conditions, these delay senescence under salt stress. The mechanism of the effect of auxin and GR24 on senescence has not been determined yet. Further studies are needed to obtain sufficient information on this subject. The results showed that IAA and GR24 delay senescence in salt stress. If senescence is delayed in salty conditions, fruit yield will increase. This research will support overcoming plant development problems related to global warming.

Peer Review: Externally peer-reviewed.

Author Contributions: Conception/Design of Study- S.S.; Data Acquisition- S.S.; Data Analysis/Interpretation- S.S., H.O.; Drafting Manuscript- S.S., H.O.; Critical Revision of Manuscript- S.S.; Final Approval and Accountability- S.S., H.O.

Conflict of Interest: Authors declared no conflict of interest.

Financial Disclosure: The present work was supported by the Research Fund of Istanbul University. Project No. FYL-2017-25661

REFERENCES

1. Shao HB, Chu LY, Jaleel CA, Zhao CX. Water-deficit stress-induced anatomical changes in higher plants. *C R Biol* 2008; 331(3): 215-25.
2. Larcher W. *Physiological Plant Ecology*. New York: Published by Springer, ISBN 0-387-09795-3, 1995.p.506.
3. Guo Y, Ren G, Zhang K, Li Z, Miao Y, Guo H. Leaf senescence: progression, regulation, and application. *Mol Horticult* 2021; 1:1-25.
4. Havé M, Marmagne A, Chardon F, Masclaux-Daubresse C. Nitrogen remobilization during leaf senescence. Lessons from Arabidopsis to crops. *J Exp Bot* 2017; 68: 2513-29.
5. Huang P, Li Z, Guo H. New advances in the regulation of leaf senescence by classical and peptide hormones. *Front Plant Sci (Sec. Plant Physiol)* 2022; 13:1-17.
6. Kohlen W, Charnikhova T, Liu Q, Bours R, Domagalska MA, Beguerie S, et al. Strigolactones are transported through the xylem and play a key role in shoot architectural response to phosphate deficiency in nonarbuscular mycorrhizal host Arabidopsis. *Plant Physiol* 2011; 155(2): 974-87.
7. Woo HR, Chung KM, Park JH, Oh SA, Ahn T, Hong SH, et al. ORE9, an F-box protein that regulates leaf senescence in Arabidopsis. *Plant Cell* 2001; 13:1779-90.
8. Hamiaux C, Drummond RS, Janssen BJ, Ledger SE, Cooney JM, Newcomb RD, et al. DAD2 is an α/β hydrolase likely to be involved in the perception of the plant branching hormone, strigolactone. *Curr Biol* 2012; 22(21): 2032-6.
9. Tsuchiya Y, Vidaurre D, Toh S, Hanada A, Nambara E, Kamiya Y, et al. A small-molecule screen identifies new functions for the plant hormone strigolactone. *Nat Chem Biol* 2010; 6: 741-9.
10. Ueda H, Kusaba M. Strigolactone regulates leaf senescence in concert with ethylene in Arabidopsis. Strigolactone and ethylene in leaf senescence. *Plant Physiol* 2015; 169: 138-47.

11. Yamada Y, Umehara M. Possible roles of strigolactones during leaf senescence. *Plants (Basel)* 2015; 4(3): 664-77.
12. Joshi N, Nautiyal P, Papnai G. Unravelling diverse roles of strigolactones in stimulating plant growth and alleviating various stress conditions: A review. *J Pharmaco Phytochem* 2019; 8(5): 396-04.
13. Rhaman MS, Imran S, Rauf F, Khatun M, Baskin CC, Murata Y., et al. Seed priming with phytohormones: An effective approach for the mitigation of abiotic stress. *Plants* 2021; 10(37): 1-17.
14. Thimann KV. *Senescence in plants*. Florida, USA: CRC Press; 2000.
15. Hayward A, Stirnberg P, Beveridge C, Leyser O. Interactions between auxin and strigolactone in shoot branching control. *Plant Physiol* 2009; 151(1): 400-12.
16. Johnson X, Brcich T, Dun EA, Goussot M, Haurogne K, Beveridge CA, et al. Branching genes are conserved across species: genes controlling a novel signal in pea are coregulated by other long-distance signals. *Plant Physiol* 2006; 142: 1014-26.
17. Crawford S, Shinohara N, Sieberer T, Williamson L, George G, Hepworth J, et al. Strigolactones enhance competition between shoot branches by dampening auxin transport. *Development* 2010; 137: 2905-13.
18. Domagalska MA, Leyser O. Signal integration in the control of shoot branching. *Nat Rev Mol Cell Biol* 2011; 12: 211-21.
19. Bouwmeester HJ, Matusova R, Zhongkui S. Beale MH. Secondary metabolite signalling in host-parasitic plant interactions. *Curr Opin Plant Biol* 2003; 6: 358-64.
20. Lindoo SS, Noodén LD. The interrelation of fruit development and leaf senescence in anoka soybeans. *Bot Gaz* 1976; 137: 218-23.
21. Parsons TR, Strickland JDH. Discussion of spectrophotometric determination of marine plant pigments, with revised equations for ascertaining chlorophylls and carotenoids. *J Mar Res* 1963; 21(3): 115-63.
22. Bradford MM. A rapid and sensitive method for the quantitation of microgram quantities of protein utilizing the principle of protein-dye binding. *Anal Biochem* 1976; 72: 248-54.
23. Birecka H, Briber KA, Catalfamo JL. Comparative studies on tobacco pith and sweet potato root isoperoxidases in relation to injury, indoleacetic acid, and ethylene effects. *Plant Physiol* 1973; 52(1): 43-9.
24. Heath RL, Packer L. Photoperoxidation in isolated: I. Kinetics and stoichiometry of fatty acid peroxidation. *Arch Biochem Biophys* 1968; 1: 189-98.
25. Bates LS, Waldren R.P, Teare ID. Rapid determination of free proline for waterstress studies. *Plant and Soil* 1973; 39(1): 205-07.
26. Hou K, Wu W, Gan SS. SAUR36, a small auxin up RNA gene, is involved in the promotion of leaf senescence in *Arabidopsis*. *Plant Physiol* 2013; 16(2): 1002-09.
27. Mueller-Roeber B, Balazadeh S. 2014. Auxin and Its Role in Plant Senescence. *J Plant Growth Regul* 2014; 33(1): 21-33.
28. Noh Y, Amasino R. Identification of a promoter region responsible for the senescence specific expression of SAG12. *Plant Mol Biol* 1999; 41: 181-94.
29. Skoog F. Relationships between zinc and auxin in the growth of higher plants. *Am J Bot* 1940; 27: 939-51.
30. Takaki H, Kushizaki M. Accumulation of free triptophan and triptamine in zinc deficient maize seedlings. *Plant Cell Physiol* 1970; 11: 793-04.
31. Saglam-Cag S, Okatan Y. The effects of zinc (Zn) and C14- indoleacetic acid (IAA) on leaf senescence in *Helianthus annuus* L. *Int J Plant Physiol Biochem* 2014; 6: 28-33.
32. Khan M, Rozhon W, Poppenberger B. The role of hormones in the aging of plants—A mini-review. *Gerontology* 2014; 60: 49-55.
33. Barna B. Manipulation of senescence of plants to improve biotic stress resistance. *Life* 2022; 12:1496. doi.org/10.3390/life12101496.
34. Hu Q, Ding F, Li M, Zhang X, Huang B. Strigolactone ethylene inhibitor suppressing dark-induced leaf senescence in perennial ryegrass involving transcriptional downregulation of chlorophyll degradation. *J Amer Soc Hort Sci* 2021; 146(2): 79-86.
35. Takahashi I, Jiang K, Asami T. Counteractive effects of sugar and strigolactone on leaf senescence of rice in darkness. *Agronomy* 2021; 1044: 1-11.
36. Kishor, PBK, Sreenivasulu N. Is proline accumulation per se correlated with stress tolerance or is proline homeostasis a more critical issue? *Plant Cell Environ* 2014; 37: 300-11.
37. Ayaz M, Varol N, Yolcu S, Pelvan A, Kaya U, Aydogdu E. Three (Turkish) olive cultivars display contrasting salt stress-coping mechanisms under high salinity. *Trees* 2021; 35: 1283-98.
38. Iqbal N, Umar S, Khan NA, Khan MIR. A new perspective of phytohormones in salinity tolerance: Regulation of proline metabolism. *Environ Exp Bot* 2014; 100:34-42.
39. Kirecci OA. The effects of salt stress, SNP, ABA, IAA and GA applications on antioxidant enzyme activities in *Helianthus annuus* L. *Fresen Environ Bull* 2018; 27: 3783-8.
40. Javid MG, Sorooshzadeh A, Moradi F, Sanavy SAMM, Allahdadi I. The role of phytohormones in alleviating salt stress in crop plants. *Aust J Crop Sci* 2011; 5: 726-34.
41. Mina Z, Li R, Chen L, Zhang Y, Li Z, Liu M, et al. Alleviation of drought stress in grapevine by foliar-applied strigolactones. *Plant Physiol Bioch* 2019; 135: 99-110.
42. Lu T, Yu H, Li Q, Chai L, Jiang W. Improving plant growth and alleviating photosynthetic inhibition and oxidative stress from low-light stress with exogenous GR24 in tomato (*Solanum lycopersicum* L.) seedlings. *Front Plant Sci* 2019; 10: 1-13.
43. Shi H, Chen L, Ye T, Liu X, Ding K, Chan Z. Modulation of auxin content in *Arabidopsis* confers improved drought stress resistance. *Plant Physiol Bioch* 2014; 82: 209-17.
44. Lutts S, Kinet JM, Bouharmont J. NaCl induced senescence in leaves of rice (*Oryza sativa* L.) cultivars differing in salinity resistance. *Ann Bot* 1996; 78: 389-98.
45. Baran A, Dogan M. Tuz Stresi uygulanan soyada (*Glycine max* L.) salisilik asidin fizyolojik etkisi. *J Nat App Sci* 2014; 18(1): 78-4.
46. Dogan M, Tıpırdamaz R, Demir Y. Effective salt criteria in callus-cultured tomato genotypes. *J Bioscience* 2010; 65: 613-8.
47. Ali B, Hayat S, Fariduddin Q, Ahmad A. 24-Epibrassinolide protects against the stress generated by salinity and nickel in *Brassica juncea*. *Chemosphere* 2008; 72(9): 1387-92.
48. Hayat S, Maheshwari P, Wani AS, Irfan M, Alyemeni MN, Ahmad A. Comparative effect of 28 homobrassinolide and salicylic acid in the amelioration of NaCl stress in *Brassica juncea* L. *Plant Physiol Biochem* 2012; 53: 61-8.
49. Sharma P, Jha AB, Dubey RS, Pessarakli M. Reactive oxygen species, oxidative damage, and antioxidative defense mechanism in plants under stressful conditions. *J Bot* 2012; 2012: 1-26.
50. Chawla S, Jain S, Jain V. Salinity induced oxidative stress and antioxidant system in salt-tolerant and salt-sensitive cultivars of rice (*Oryza sativa* L.). *J Plant Biochem Biotechnol* 2013; 22: 27-4.
51. Cetin ES, Canbay HS, Daler S. The roles of strigolactones: Mineral compounds, indole-3 acetic acid and GA3 content in grapevine on drought stress. *J Plant Stress Physiol* 2022; 8: 1-7.
52. Agusti J, Herold S, Schwarz M, Sanchez P, Ljung K, Dun EA. Strigolactone signaling is required for auxin-dependent stimulation of secondary growth in plants. *Proc Natl Acad Sci USA* 2011; 50(108): 20242-7.
53. Jones AM, Lamerson P, Venis MA. Comparison of site I auxin-binding and a 22-kilodalton auxin-binding protein maize. *Planta* 1989; 179: 409-13.
54. Jones AM. Auxin binding proteins. *Ann Rew Plant Physiol Plant Mol Biol* 1994; 45: 393-20.

The Role of rs4626 and rs7221352 Polymorphisms on the *TOB1* Gene in Turkish Relapsing-Remitting Multiple Sclerosis Patients

Fulya Basoglu Koseahmet^{1*} , Candan Eker^{2*} , Musa Ozturk¹ , Sebnem Ozdemir³ ,
Ayhan Koksal¹ , Sevim Baybas¹ , Tuba Gunel² 

¹University of Health Sciences, Bakirkoy Prof. Dr. Mazhar Osman Research and Training Hospital for Psychiatry, Neurology and Neurosurgery, Department of Neurology, Istanbul, Turkiye

²Istanbul University, Faculty of Science, Department of Molecular Biology and Genetics, Istanbul, Turkiye

³Istinye University, Faculty of Economics, Administrative and Social Sciences, Department of Management Information Systems, Istanbul, Turkiye

ORCID IDs of the authors: F.B.K. 0000-0002-9277-6644; C.E. 0000-0001-9049-6131; M.O. 0000-0001-9652-384X; S.O. 0000-0001-6668-6285; A.K. 0000-0003-4664-2167; S.B. 0000-0003-1724-9577; T.G. 0000-0003-3514-5210

Please cite this article as: Basoglu Koseahmet F, Eker C, Ozturk M, Ozdemir S, Koksal A, Baybas S, et al. The Role of rs4626 and rs7221352 Polymorphisms on the *TOB1* Gene in Turkish Relapsing-Remitting Multiple Sclerosis Patients. Eur J Biol 2022; 81(2): 197-205. DOI: 10.26650/EurJBiol.2022.1191215

ABSTRACT

Objective: Multiple sclerosis often causes neurological disability and reduced quality of life. Genetic biomarkers are important tools for the diagnosis and prognosis of diseases. This study has been conducted to explore the haplotype frequencies formed by rs4626 and rs7221352 single-nucleotide polymorphisms (SNPs) in the coding region variant (rs4626) and 5' upstream region intron variant (rs7221352) of the transducer of the *ERBB2.1* (*TOB1*) gene in individuals with relapsing-remitting multiple sclerosis.

Materials and Methods: Thirty patients with an Expanded Disability Status Scale (EDSS) score <3, 30 patients with EDSS ≥5, and 30 healthy controls participated in the study. The *TOB1* rs4626 T/C and rs7221352 G/A single-base variations were applied using the quantitative real-time polymerase chain reaction method in accordance with the TaqMan SNP Genotyping Assays instructions.

Results: The genotype frequencies of *TOB1* rs4626 TT/TC/CC were respectively 3.3%, 53.3%, and 43.3% in the EDSS <3 cases and 10%, 53.3%, and 36.7% in the EDSS ≥5 cases. The genotype frequencies of *TOB1* rs7221352 GG/AG/AA were respectively 3.3%, 86.7%, and 10% in the EDSS <3 cases and 10%, 70%, and 20% in the EDSS ≥5 cases. With respect to the estimated values in the study cohort, allelic variant frequency was higher in the patient group for both SNP variants ($p < 0.001$).

Conclusion: The presence of variant alleles in the rs4626 and rs7221352 polymorphisms in *TOB1* may have a role in the disease immunopathogenesis. Further investigations involving larger groups are required to understand the effects of *TOB1*.

Keywords: *TOB1*, multiple sclerosis, single-nucleotide polymorphisms, allelic variation, quantitative real-time PCR

INTRODUCTION

Multiple sclerosis (MS) is mainly defined by the disruption of myelin sheaths and inflammation of the central nervous system (CNS) neurons. The most frequent clinical subtype is called relapsing-remitting

MS (RRMS). Patients with RRMS experience distinct attacks of disease resulting either in recovery or neurological disability. MS is considered to be an autoimmune disease, and recent data have shown genetic, immunological, and environmental factors to be able to contribute to disease complexity, causing

*Equal contributors



Corresponding Author: Fulya Basoglu Koseahmet E-mail: fbasoglu_crh@hotmail.com

Submitted: 18.10.2022 • **Revision Requested:** 05.12.2022 • **Last Revision Received:** 06.12.2022 •

Accepted: 13.12.2022 • **Published Online:** 30.12.2022

Content of this journal is licensed under a Creative Commons Attribution-NonCommercial 4.0 International License.



a different onset and course for each individual (1). Therefore, discovering reliable biomarkers is important for identifying susceptible individuals, diagnosing the disease, and predicting prognosis. Although no ideal marker has been defined so far, genetic biomarkers would potentially be invaluable as they are not strongly affected by environmental conditions and may be studied via blood samples instead of more invasive procedures.

TOB1 is considered a promising biomarker of MS (2) and occurs in the anti-proliferative Tob/Btg-1 protein family, which possesses a regulatory role in cellular growth and proliferation (3). *TOB1* is located on chromosome 17 at the 17q21 cytogenetic location. It has two exons, with transcription occurring in the 5'-3' direction on the reverse strand of DNA. Promoter and enhancer sequences regulate transcription on the upstream side of the coding exon (4). The synonymous variant rs4626 is located in the Chr 17: 50863061 (forward strand) within the promoter region, providing an initial binding site for transcription factors and RNA polymerase. Additionally, the intron variant (non-coding transcript variant) rs7221352 (Chr 17: 50869864) is found within the promoter flanking sequences in the 5' upstream sequence region of *TOB1*. Although many transcription binding sites reside in the upstream region of the rs7221352 variant, the rs4626 single-nucleotide polymorphism (SNP) is positioned in the CCCTC-binding factor site (5,6).

The transcriptional CCCTC-binding factor is involved in many cellular processes and plays a repressor role in cellular pathways regarding chromatin architecture regulation, V(D)J recombination, dielectric activity, and transcriptional regulation. The V(D)J somatic recombination mechanism that contributes to the formation of various macromolecules such as antibodies, immunoglobulins, and T cell receptors in B and T cells has been observed in the early stages of lymphocytes (6,7). Active or inactive forms of *TOB1* in T cells and brain tissue have been explored using the Genes and Regulation Database (7).

TOB1 encodes a 45-kDa protein (Tob1) with modulatory roles in mitosis and cytokine production (4). Its expression decreases during the G1/S phase to proceed to mitosis. Furthermore, it binds to erbB2 receptors and acts as a negative regulator of erbB2-related pathways (3). These findings and other data from the past two decades imply that *TOB1* acts as a tumor suppressor gene (3,8-13).

TOB1 also interferes with T-cell activation and cytokine production in lymphocytes. Increased expression of Tob1 in T cells has been demonstrated to inhibit CD3⁺ and anti-CD28-related proliferation (14). Removal of endogenous Tob1 decreases the T-cell activation threshold and enhances the T cell receptor engagement response (14). Furthermore, the Tob1 protein inhibits T cell proliferation by decreasing the levels of pro-inflammatory cytokines such as interleukin-2, interleukin-4, interferon gamma, cyclins A, and cyclin E (14-16).

Previous studies have observed the Tob1 protein in the cytoplasm of T cells and implicated this in the mRNA stability and translational degradation of interleukin-2 (14-16). *TOB1*

was later revealed to also be effective in post-transcriptional modifications. These observations suggest Tob1 to be involved in actively maintaining lymphocyte quiescence and to maybe even set a threshold for T-cell activation. Therefore, its role in autoimmune diseases and potential as a biomarker should be evaluated (17).

Experimental studies on humans suggest a possible relationship to exist between the downregulation of *TOB1* expression and the progression of MS. Corvol et al. (18) investigated a biomarker to foresee which clinically isolated syndrome (CIS) patients were more prone to progress to clinical definite MS and observed that the patients who had decreased expression of *TOB1* RNA and therefore decreased protein levels had significantly elevated rates of progressing to clinical definite MS within 1 year. Corvol et al. performed SNP analyses for five selected regions (rs11079937, rs9905480, rs9303568, rs4626, and rs7221352) within and near the gene in clinically mild MS patients (Expanded Disability Status Scale, EDSS<3, n=62) and severe MS patients (EDSS>6, n=74) to evaluate the role of *TOB1* in disease progression. Their results identified two markers: rs4626 in the coding and rs7221352 in the non-coding areas of *TOB1*, indicating these markers to possibly be related to the progression of MS (18).

Thus, changes in the structure of *TOB1* can cause inadequate functioning and create a tendency toward inflammation and autoimmunity. Therefore, its clinical effects should be evaluated in terms of disease initiation and progression. The current study examines two previously identified SNPs in *TOB1* with regard to patients diagnosed with mild (EDSS<3) and severe (EDSS≥5) MS in comparison to healthy individuals.

The study also evaluates the following patient information: age at disease onset, localization at onset, number of attacks in the first year of diagnosis, cerebrospinal fluid immunoglobulin G (IgG) index, and oligoclonal band (OCB) results (where available). The study additionally investigates whether a possible relationship exists between genotype status and these parameters. The study's aim is to investigate the possible genetic associations between rs4626 and rs7221352 polymorphisms in *TOB1* in terms of RRMS susceptibility and/or severity.

MATERIALS AND METHODS

Ethical Approval

This study was approved by the Ethics Committee of Bakirkoy Dr. Sadi Konuk Training and Research Hospital (Istanbul, Turkey; Project no: 2016-152). The study was carried out in accordance with the Declaration of Helsinki and the review board-approved protocols of Istanbul University. Study participants provided written informed consent.

Study Population

Two SNPs within (rs4626) and 5' upstream (rs7221352) of *TOB1* were designated for genotyping in 60 individuals with MS and 30 healthy control subjects. The patient subgroups are composed of 30 patients with EDSS<3.0 (mild RRMS) and 30

patients with EDSS \geq 5 (severe RRMS) and at least 5 years since disease onset. Of the patients in the EDSS \geq 5 group, 25 had reached an EDSS=5 within 5 years of disease onset, while the remaining five patients had reached an EDSS=3 within 5 years and reached or exceeded an EDSS=5 within 6–10 years after disease onset. These were considered to experience a more severe course of the disease. The patient groups had no history of cancer or autoimmune disease other than MS. All subjects were followed up at the outpatient clinics of the Bakirkoy Research and Training Hospital for Psychiatry, Neurology and Neurosurgery (Istanbul, Turkiye). The study also included 30 healthy volunteers matched for age and sex who were biologically unrelated to the patients and had no history of autoimmune diseases or cancer as the control group.

Genotyping the rs4626 and rs7221352 Polymorphisms

Peripheral blood samples were drawn from all the subjects and collected in EDTA tubes. Genomic DNA were isolated from the peripheral blood lymphocytes using the Quick Blood Genomic DNA Extraction Kit (Hilbrigen Biotechnology, Istanbul, Turkiye). The amount and quality of the samples were measured by the NanoPhotometer P330 (Implen, GmbH, Munchen, Germany). TaqMan[®] SNP Genotyping Assays, human (Applied Biosystems, Foster City, CA, USA) were used for genotyping the *TOB1* rs4626 and rs7221352 polymorphisms on the Stratagene Mx3005P[™] Multiplex Quantitative PCR System (Agilent Technologies, Santa Clara, CA, USA). FAM[™] and VIC[™] dye-labeled TaqMan minor groove binder (MGB) probes were used for allele discrimination. The presence of two probes in each reaction allowed the genotyping of two possible variant alleles at the polymorphic site of the *TOB1* DNA sequence (Table 1). Genotyping assays were performed by adding approximately 20–25 ng of purified genomic DNA for a total volume of 25 μ L. Quantitative real-time polymerase chain reactions (qPCR) were carried out under the following conditions: 95°C for 10 min (denaturation cycle), followed by 40 cycles at 95°C for 15 s, then at 60°C for 60 s (annealing/extension). The results were analyzed using the software Stratagene MxPro[™] QPCR (v. 4.10). For quality control, qPCR analysis for genotyping was repeated using randomly selected samples.

Statistical Analysis

The programs SPSS (v. 20.0; SPSS, Inc., Chicago, IL, USA) and RGui in R-3.4.1 (i386, 32-bit, R Computing Group, Vienna, Austria) were used to conduct the statistical analyses. The direct gene counting method was implemented to calculate the genotype and allele frequencies. The chi-square test of independence was used to evaluate the significance of the distributions for each subgroup. All *p* values are two-sided, with estimated values of *p*<0.05 being accepted as statistically significant.

Pearson's chi-square (χ^2) test was applied to estimate and compare both the allele and genotype frequencies of the groups, with Fisher's exact test and Yates's correction for continuity being used where appropriate. Odds ratios (ORs) at a 95% confidence interval (CI) were assessed using logistic regression analyses (19). Haplotype analyses were carried out by calculating the co-occurrence of each allele for the rs4626 (T/C) and rs7221352 (G/A) polymorphisms. Individuals carrying the T-G, C-A, T-A, C-G genotypes were identified in each study group (EDSS<3, EDSS \geq 5, control), with the haplotype frequencies and *p* values being calculated according to Pearson's chi-square test.

Hardy-Weinberg Equilibrium (HWE) was applied to assess genotype frequencies among the patient and healthy control groups. The observed and expected number of genotypes and their compliance to the Hardy-Weinberg principle were calculated using the Gene-Calc portal website (20). In addition, expression quantitative trait loci (eQTLs) values for rs4626 and rs7221352 were obtained from the Genotype-Tissue Expression (GTEx) Analysis Portal (dbGaP Accession phs000424.v8.p2) (21).

RESULTS

Patient Demographics and Clinical Parameters

The groups' mean ages were 44.1 \pm 9.45 years for the EDSS<3 patient group, 47.2 \pm 9.84 years for the EDSS \geq 5 patient group, and 48.13 \pm 12.51 years for the healthy control group. The female-to-male ratios are 19:11 for the EDSS<3 group, 20:10 for the EDSS \geq 5, and 20:10 for the healthy controls. No statistically significant difference was found in terms of the distributions of age or gender (*p*>0.05). Table 2 summarizes the laboratory

Table 1. TaqMan SNP Genotyping Assay design details for *TOB1* rs4626 and rs7221352 polymorphisms.

SNP ID / Assay ID	SNP Type / Cytogenetic location	Reporter / Quencher	Forward and Reverse Primer Concentration (μ M)	Context Sequence
rs4626 C-159174_10	Silent Mutation 17q21.33	Allele 1: VIC/MGB-NFQ Allele 2: FAM/MGB-NFQ	Forward primer: 36 μ M Reverse primer: 36 μ M	TAAAATTCAAGCCATCTACAAAAGA [C/T] TTCTCATTGAGGCCTCCATAGGCTG
rs7221352 C-31810760_10	NA 17q21.33	Allele 1: VIC/MGB-NFQ Allele 2: FAM/MGB-NFQ	Forward primer: 36 μ M Reverse primer: 36 μ M	TTACTTTGGAATTGTGCAGGGGAGT [A/G] GAGGGCTAACTGCTAATTGTGCAGG

NA: Not applicable or not available, MGB: Minor-Groove Binder, NFQ: Non-Fluorescent Quencher, Ftable FAM and VIC: Dye-labeled probe (FAM Emission spectra: ~517 nm, VIC Emission spectra: ~551 nm). A: Adenine, T: Thymine, C: Cytosine, G: Guanine.

Table 2. Clinical and CSF parameters of patient groups.

	EDSS<3	EDSS≥5
Age of onset (years)	32.07 ± 10,14	32.83 ± 11.77
Disease duration (years)	12.7± 6.4	14.9 ± 5.5
Last EDSS	0.65 ± 0.82	6.48 ± 1.01
Number of attacks at the first year:		
1	24	19
2	4	9
3	1	1
4	1	1
IgG Index (mean)	1.01 ± 0.76	1.075 ± 0.95
CSF OCB positive (n/N)	18/21	14/16

EDSS: Extended Disability Status Scale, CSF: Cerebrospinal Fluid, n: Number of patients with positive results for CSF parameters, N: Number of patients with available CSF results, IgG: Immunoglobulin G, OCB: Oligoclonal Band.

results and clinical features. Statistically significant differences were not present between the patient groups in terms of age of onset, mean disease duration, number of attacks in the first year, mean IgG index values, or OCB positivity ($p>0.05$).

The sensory system onset ratio was higher in the EDSS<3 group, whereas the spinal and cerebellar localizations ratios were higher in the EDSS≥5 group. However, the differences in these distributions are not statistically significant ($p>0.05$). Optic neuritis, brainstem, and pyramidal system onsets were similar between the two groups. Compared to the EDSS<3 group, the EDSS≥5 group had a higher IgG positivity (IgG index >0.6) ($P=0.023$).

The distributions regarding rs4626 and rs7221352 SNPs for each subgroup were calculated and found statistically significant (Table 3).

Allelic Frequencies of rs4626 and rs7221352 in MS Patients with EDSS<3, EDSS≥5 and Healthy Controls

When considering the genotype TT as a reference for the rs4626 polymorphism, the genotype TC prevalence was found to be equal for the patients with MS in the EDSS<3 and EDSS≥5 subgroups. When compared to the healthy subjects, the patient

groups showed a higher prevalence for the TC genotype ($p=0.001$ for EDSS<3, $p=0.030$ for EDSS≥5; Table 4). Additionally, the frequency of the rs4626 genotype CC was found to be higher in the patient groups than in the control group ($p=0.005$ for EDSS<3, $p=0.018$ for EDSS≥5; Table 4).

No significant difference was found between the EDSS<3 (30%) and the EDSS≥5 subgroups (36.7%) for the allele T of rs4626, which was more prevalent in the healthy control group (51.7%) than in patient groups (30% for EDSS<3, 36.7% for EDSS≥5; Table 4). However, the rs4626 allele C was more frequent in the patient groups than in the healthy control group, although this was solely significant for the EDSS<3 patients ($p=0.016$), not for the EDSS≥5 ($p=0.099$; Table 4).

For the rs7221352 polymorphism, the genotype AG prevalence in patients with EDSS<3 (86.7%) and EDSS≥5 (70.0%) was greater than in the control group (13.3%, $p=0.000$). Although the difference in prevalence of the rs7221352 genotype AA between the EDSS<3 patients and the control group was not significant ($p=0.069$), the EDSS≥5 patients showed a significantly higher frequency than in the control group ($p=0.038$; Table 4).

Table 3. Statistical significance of rs4626 and rs7221352 distributions among groups.

	rs4626			rs7221352		
	Value	df	Asymp. Sig. (2-sided)	Value	df	Asymp.Sig. (2-sided)
Pearson Chi-Square	19.361a	4	0.001	44.097a	4	0.000
Likelihood ratio	19.238	4	0.001	47.312	4	0.000
N of Valid cases	90			90		

* 0 cells (0.0%) have expected count less than 5. The minimum expected count is 5.00. Asymp. Sig.: Asymptotic Significance; df: degrees of freedom, N: Number

Table 4. Genotype and allele frequencies of rs4626 and rs7221352 polymorphisms in MS patients with EDSS<3, EDSS≥5 and healthy controls.

TOB1 polymorphism	Patients (EDSS<3) (n=30)		Patients (EDSS≥5) (n=30)		Controls (n=30)		EDSS<3 Patients vs Controls		EDSS≥5 Patients vs Controls	
	Genotype Frequency	Patients (EDSS<3) (n=30)	Genotype Frequency	Patients (EDSS≥5) (n=30)	Genotype Frequency	Controls (n=30)	OR (95%)	Test Values	OR (95%)	Test Values
rs4626 - Genotype										
TT	1	% 3.3	3	% 10	13	% 43.3	Reference	Reference	Reference	Reference
TC	16	% 53.3	16	% 53.3	5	% 16.7	41.6 (1.036-13.383)	11.038**	13.866 (1.026-6.286)	4.693**
CC	13	% 43.3	11	% 36.7	12	% 40	14.083 (1.035-12.098)	7.721**	3.972 (1.024-5.548)	5.590**
rs4626- Allele										
T	18	% 30	22	% 36.7	31	% 51.7	Reference	Reference	Reference	Reference
C	42	% 70	38	% 63.3	29	% 48.3	2.494 (1.012-2.355)	5.716*	1.846 (1.011-2.302)	2.71*
rs7221352- Genotype										
GG	1	3.3%	3	10%	20	66.7%	Reference	Reference	Reference	Reference
AG	26	86.7%	21	70%	4	13.3%	130 (1.036-13.371)	30.056**	35 (1.026-6.357)	21.370**
AA	3	10%	6	20%	6	20%	10 (1.039-16.289)	-	6.666 (1.026-6.669)	-
rs7221352- Allele										
G	28	46.7%	27	45%	44	73.3%	Reference	Reference	Reference	Reference
A	32	53.3%	33	55%	16	26.7%	3.142 (1.012-2.397)	8.602*	3.361 (1.012-2.40)	9.627*

A: adenine, T: thymine, C: cytosine, G: guanine, * χ^2 (Chi-square), **Continuity Correction (Yates Correction), *** Fisher Exact Significance

Table 5. Haplotype frequencies of *TOB1* rs4626 and rs7221352 polymorphisms in patients with EDSS<3, EDSS≥5 and healthy controls.

TOB1 polymorphism	Patients (EDSS<3) (n=30)	Patients (EDSS<3) Genotype frequencies	Patients (EDSS≥5) (n=30)	Patients (EDSS≥5) Genotype frequencies	Controls (n=30)	Controls Genotype frequencies	EDSS<3 Patients vs Controls		EDSS≥5 Patients vs Controls			
							OR (95%CI)	χ^2	P	OR (95%CI)	χ^2	P
Haplotype (rs4626-rs7221352)												
T-G	16	18.4%	17	21.5%	17	42.5%	Reference					
C-A	28	32.2%	24	30.4%	7	17.5%	4.25	6.98	0.0082	3.43	5.02	0.025
							(1.017-3.412)			(1.017-3.428)		
T-A	17	19.5%	17	21.5%	4	10%	4.52	5.29	0.0214	4.25	4.90	0.026
							(1.02-4.349)			(1.02-4.322)		
C-G	26	29.9%	21	26.6%	12	30%	2.30	2.85	0.091	1.75	1.26	0.261
							(1.015-3.019)			(1.015-3.057)		

A: adenine, T: thymine, C: cytosine, G: guanine. EDSS: Extended Disability Status Scale

Allelic frequencies of the rs7221352 polymorphism were similar for the patients with EDSS<3 and EDSS≥5 (respectively, 46.7% vs. 45% for the rs7221352 allele G and 53.3% vs. 55% for the rs7221352 allele A). However, the allele G in the rs7221352 region was more frequent in the healthy control group (73.3%) than in the patient groups (46.7% for EDSS<3 and 45% for EDSS≥5), whereas the allele A frequency was significantly lower in the healthy control group compared to either the EDSS<3 group ($p=0.003$) or the EDSS≥5 group ($p=0.001$; Table 4).

Haplotype Association of the rs4626 and rs7221352 Polymorphisms in the EDSS<3 and EDSS≥5 MS Patient Groups and the Healthy Control Group

Table 5 shows the haplotype frequency results for the *TOB1* rs4626 and rs7221352 polymorphisms. With regard to the rs4626-rs7221352 haplotype analyses, haplotype T-G was considered as the reference, with no significant differences being observed for haplotype C-G between the control group and either the EDSS<3 ($p=0.091$) or EDSS≥5 ($p=0.261$) groups (Table 5). Haplotype C-A was significantly more frequent in individuals with MS than in the control group ($p=0.0082$ for the EDSS<3 comparison, and $p=0.025$ for the EDSS≥5 comparison; Table 5). Haplotype T-A was less frequent in the control group than in either the EDSS<3 ($p=0.0214$) or EDSS≥5 ($p=0.026$) patient groups (Table 5). Comparing the haplotype frequency of the rs4626-rs7221352 polymorphisms between patients with mild (EDSS<3) and severe (EDSS≥5) RRMS showed no significant differences ($p>0.05$).

Genetic Association of rs4626 and rs7221352 Polymorphisms in the Subjects

The χ^2 test of independence for comparatively analyzing the presence of the rs4626 and rs7221352 polymorphisms between patients with EDSS<3 and those with EDSS≥5 showed no significant difference. However, a statistical significance was found in the relationship of the presence of rs4626 and rs7221352 polymorphisms between the RRMS patients and the healthy controls (Table 6).

Table 6. Chi-square (χ^2) test for independence results.

	χ^2 independence	df	p
rs4626			
EDSS≥5, EDSS<3, Control (n=90)	21.22	4	0.000285
EDSS≥5 vs. Control (n=60)	12.05	2	0.002417
EDSS<3 vs. Control (n=60)	11.8	2	0.002739
EDSS<3 vs. EDSS≥5 (n=60)	1.16	2	0.558221
rs7221352			
EDSS≥5, EDSS<3, Control (n=90)	44.09	4	6.14 e-9
EDSS≥5 vs. Control (n=60)	24.12	2	5.78 e-6
EDSS<3 vs. Control (n=60)	34.32	2	3.52 e-8
EDSS<3 vs. EDSS≥5 (n=60)	2.53	2	0.282

df: degrees of freedom, EDSS: Extended Disability Status Scale

Hardy-Weinberg Equilibrium Analysis

Table 7 shows the observed and expected genotype distributions according to the Hardy-Weinberg principle. The distributions of rs4626 in the EDSS<3 and EDSS≥5 compared to the distributions of rs7221352 in the EDSS≥5 groups were found to be consistent with the Hardy-Weinberg principle at a significance value of 0.05 (Table 8).

eQTL Analysis

eQTL analysis was obtained from the GTEx Analysis Portal (dbGaP Accession phs000424.v8.p2; <https://www.gtexportal.org/>). Different parts of brain tissue and whole blood (relevant immune cell type investigation) samples were analyzed separately for the eQTL identification of the rs4626 and rs7221352 SNP variants. The whole blood sample analysis revealed a significant eQTL $p=0.00067$ for the rs4626 and $p=0.000015$ for the rs7221352 SNPs in the *TOB1* expression, with $p\leq 0.0045$ being accepted as statistically significant. Figure 1 presents the eQTL genotype-normalized *TOB1* expression plots.

DISCUSSION

MS is a multifactorial disease, and research on its genetic aspects has rapidly accelerated within the past two decades. MS's tendency to cluster in families and certain ethnic groups supports the genetic aspects of MS. First-degree relatives of MS patients have a 30-40 times greater risk of MS compared

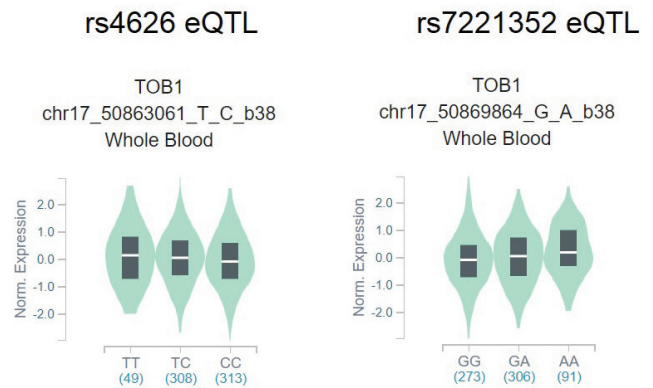


Figure 1: eQTL plots of rs4626 and rs7221352 SNP variants for whole blood.

to the normal population (22). The HLA-DRB1*1501 locus is known to have the strongest relationship, with more than 200 MS-predisposed genes having so far been identified in genome wide association studies (GWAS). Still much remains to be achieved (23-25). Researchers hope to reveal all the responsible genes and individualize risk assessment. These data may ultimately help the early identification of susceptible individuals and develop individualized targeted therapies for MS in the future (24-26).

Table 7. Expected Hardy-Weinberg Equilibrium (HWE) distribution and observed results.

rs4626	rs7221352				
	HWE distribution	Observed Results	HWE distribution	Observed Results	
TT	0.156	0.188	GG	0.302	0.267
CT	0.239	0.412	AG	0.247	0.167
CC	0.367	0.400	AA	0.202	0.567

A: adenine, T: thymine, C: cytosine, G: guanine, HWE: Hardy-Weinberg Equilibrium

Table 8. The compliance analysis between observed and expected number of genotypes based on Hardy-Weinberg law.

	p	Chi-square	Yates's chi-square	Yates's p	Status
rs4626, EDSS<3	0.335	2.184	1.298	0.522	*Distribution consistent
rs4626, EDSS≥5	0.718	0.660	0.270	0.873	*Distribution consistent
rs4626, Control	0.0012	13.318	-	-	**fis= 0.666
rs7221352, EDSS<3	0.0002	16.475	14.323	0.0007	**fis= -0.741
rs7221352, EDSS≥5	0.076	5.145	3.971	0.137	*Distribution consistent
rs7221352, Control	0.0014	13.032	10.474	0.0053	**fis= 0.659

*Distribution consistent with Hardy-Weinberg's principle at a level of significance of 0.05, **Distribution not consistent with Hardy-Weinberg's principle at a level of significance of 0.05, fis: inbreeding coefficient value

This study has assessed the rs4626 and rs7221352 SNPs of *TOB1* regarding their possible relationships to MS onset and/or prognosis. According to Corvol et al. (18), despite 975 differentially expressed transcripts being observed in CD4⁺ T cells among CIS patients and healthy subjects, only 108 genes exhibited variable expression levels in higher-risk patients with MS. *TOB1* showed the largest expression difference (a 7-fold downregulation) compared to other downregulated and upregulated genes involved in pro-apoptotic processes and cellular cycle regulation. The majority of CD4⁺ T cells from subjects with a high risk of disease activity were prone to progressing to a proliferative state and experiencing new clinical attacks. Researchers have also suggested *TOB1* to be an important biomarker of MS progression (18, 27) and also identified five SNPs positioned within or near *TOB1*, with the allelic frequencies of rs4626 (significant) and rs7221352 (not significant) among them showing differences when comparing mild and severe cases (18). The current research found no other studies in the literature to have evaluated these two SNPs together for each individual.

This study has investigated the possible relationships between different haplotypes formed by the rs4626 and rs7221352 polymorphisms in EDSS<3 and EDSS≥5 RRMS patient groups, as well as in healthy subjects. The frequencies of the genotype TC, CC, and allele C of rs4626 were found to occur more frequently in MS patient groups compared to the healthy subject group (statistically significant for all except allele C in the EDSS≥5 vs. control group comparison). Additionally, genotype AG and allele A of rs7221352 occur more frequently in the patient groups than in the healthy controls. The rs7221352 genotype AA occurred significantly more frequently in the EDSS≥5 patient subgroup compared to in the healthy subjects. Healthy controls had higher frequencies of the reference genotypes (TT for rs4626 and GG for rs7221352) compared to the patients.

Haplotype T-G (reference) of the rs4626-rs7221352 polymorphisms was observed less frequently in both the EDSS<3 and EDSS≥5 patient groups compared to in the control group. Additionally, rs4626-rs7221352 haplotype C-A and haplotype T-A were significantly more frequent in patients with EDSS<3 and EDSS≥5 than in the controls. No significant differences were found in the rs4626-rs7221352 haplotype C-G frequencies between the MS patient groups and the healthy control group.

In summary, the study has found more variant genotypes (not significant for the EDSS<3 vs. controls for genotype AA of rs7221352) and variant alleles (not significant for EDSS≥5 for rs4626) in the MS patient groups than in the control group. The haplotype analyses showed the control group to have significantly more wild-type haplotypes. These findings suggest these two SNPs to be involved in MS immunopathogenesis.

No statistically significant differences were found among the patient subgroups regarding either of the SNP markers, which differs from the results from Corvol et al. (18).

In the current study, the variant allele (represented by C [cytosine] on the forward strand) frequency in all participants was approximately 48% with regard to rs4626. Population studies observed a 50% variant allele frequency in East Asians and a 70% in Europeans (28), while the current study found a variant allele (A) frequency for rs7221352 of 27%, which is between those found in European (41%) and East Asian (15%) populations (29). However, larger population studies will be required in order to obtain more accurate results for the Turkish population.

A number of SNPs were identified as potential risk factors for MS. A recent study by Gresle et al. described MS risk eQTL associations for more than a 100 genes (24,30). The current study could find no other study that had evaluated eQTL specifically for the *TOB1* gene with regard to MS. However, data from the GTEx Analysis Portal blood analysis showed a significant eQTL effect for rs4626 and rs7221352 SNPs in the *TOB1* gene (21), which could imply a possible relationship to MS pathogenesis. However, further research is still needed.

Treatment status may have been a possible intervening factor in this study. Two patients with EDSS<3 did not consent to therapy, while four had not initially consented but only did so a few years after disease onset. Because they showed good prognosis regardless of late treatment, the study results were not affected. One patient in the EDSS≥5 group never consented to therapy, while three patients from this group consented during their disease course rather than at the beginning. Although these patients underwent late or no treatment, they were included in the study based on their aggressive clinical course and radiological lesion load since disease onset. All the patients were followed up and treated by an MS specialist in accordance with the latest available guidelines. On limitation of the study involves the impossibility of following up on all the patients who do not receive treatment.

The sample sizes of the patient and control groups were small, which is another important limitation. However, this was a preliminary study analyzing polymorphisms in the *TOB1* region in the Turkish population. This is the first study in the published literature to have analyzed these two SNPs together with respect to both RRMS patients and healthy subjects.

CONCLUSION

The presence of variant alleles in the rs4626 and rs7221352 polymorphisms of the *TOB1* gene may play a role in MS immunopathogenesis. Further studies over larger populations will be required to clarify the role of *TOB1* polymorphisms in MS.

Acknowledgments: We thank Dr. Ozlem Ulucan Acan (Assist. Prof., Istanbul Bilgi University, Genetics and Bioengineering Department) for her support with statistical analysis.

Ethics Committee Approval: This study was approved by the Ethics Committee of Bakirkoy Dr. Sadi Konuk Training and Research Hospital (Istanbul, Turkey; Project no: 2016-152).

Informed Consent: Written consent was obtained from the participants.

Peer Review: Externally peer-reviewed.

Author Contributions: Conception/Design of Study- T.G., C.E.; Data Acquisition- F.B.K., M.O., A.K., S.B.; Data Analysis/Interpretation- C.E., S.O., F.B.K.; Drafting Manuscript- F.B.K., C.E.; Critical Revision of Manuscript- C.E., F.B.K., T.G., M.O., S.O., A.K., S.B.; Final Approval and Accountability- F.B.K., C.E., M.O., S.O., A.K., S.B., T.G.

Conflict of Interest: Authors declared no conflict of interest.

Financial Disclosure: This study was financially supported by the Non-Profit Bakirkoy Mental Health Hospital Foundation [project number 2016-152].

REFERENCES

1. Daroff RB, Fenichel GM, Jankovic, J. *Bradley's Neurology in Clinical Practice*. 6th ed. Philadelphia: Elsevier Saunders Publishing; 2012. p.693-7.
2. Katsavos S, Anagnostouli M. Biomarkers in Multiple Sclerosis: An Up-to-Date Overview. *Mult Scler Int* 2013; 2013: 1-20.
3. Lin S, Zhu Q, Xu Y, Liu H, Zhang J, Xu J, et al. The role of the *TOB1* gene in growth suppression of hepatocellular carcinoma. *Oncol Lett* 2012; 4: 981-7.
4. Salerno F, van Lier RAW, Wolkers MC. Better safe than sorry: *TOB1* employs multiple parallel regulatory pathways to keep Th17 cells quiet. *Eur J Immunol* 2014; 44: 646-9.
5. NCBI (2022) Variation Viewer database [online] <https://www.ncbi.nlm.nih.gov/variation/view> [accessed on October, 2022].
6. Ensembl (Release 107-2022). Ensembl database, Human (GRCh38.p13) build [online] https://www.ensembl.org/Homo_sapiens/Variation, [accessed on October, 2022].
7. Ensembl (Release 107-2022). Ensembl database, Human (GRCh38.p13) build [online] https://m.ensembl.org/info/genome/funcgen/regulatory_build.html, [accessed on October, 2022].
8. O'Malley S, Su H, Zhang T, Ng C, Ge H, Tang CK. *TOB* suppresses breast cancer tumorigenesis. *Int J Cancer* 2009; 125: 1805-13.
9. Park GT, Seo EY, Lee KM, Yang JM. *Tob* is a potential marker gene for the basal layer of the epidermis and is stably expressed in human primary keratinocytes. *Br J Dermatol* 2006; 154: 411-8.
10. Iwanaga K, Sueoka N, Sato A, Sakuragi T, Sakao Y, Tominaga M, et al. Alteration of expression or phosphorylation status of *tob*, a novel tumor suppressor gene product, is an early event in lung cancer. *Cancer Lett* 2003; 202: 71-9.
11. Jiao Y, Sun KK, Zhao L, Xu JY, Wang LL, Fan SJ. Suppression of human lung cancer cell proliferation and metastasis in vitro by the transducer of *ErbB-2.1* (*TOB1*). *Acta Pharmacol Sin* 2012; 33: 250-60.
12. Kundu J, Wahab SMR, Kundu JK, Choi YL, Erkin OC, Lee HS, et al. *Tob1* induces apoptosis and inhibits proliferation, migration and invasion of gastric cancer cells by activating *Smad4* and inhibiting β -catenin signaling. *Int J Oncol* 2012; 41: 839-48.
13. Gebauer M, Saas J, Haag J, Dietz U, Takigawa M, Bartnik E, et al. Repression of anti-proliferative factor *Tob1* in osteoarthritic cartilage. *Arthritis Res Ther* 2005; 7: R274-84.
14. Tzachanis D, Freeman GJ, Hirano N, van Puijenbroek AAFL, Delfs MW, Berezovskaya A, et al. *Tob* is a negative regulator of activation that is expressed in anergic and quiescent T cells. *Nat Immunol* 2001; 2: 1174-82.
15. Ikematsu N, Yoshida Y, Kawamura-Tsuzuku J, Ohsugi M, Onda M, Hirai M, et al. *Tob2*, a novel anti-proliferative *Tob/BTG1* family member, associates with a component of the *CCR4* transcriptional regulatory complex capable of binding cyclin-dependent kinases. *Oncogene* 1999; 18: 7432-41.
16. Schulze-Topphoff U, Casazza S, Varrin-Doyer M, Pekarek K, Sobel RA, Hauser SL, et al. *Tob1* plays a critical role in the activation of encephalitogenic T cells in CNS autoimmunity. *J Exp Med* 2013; 210: 1301-9.
17. Tzachanis D, Boussiotis VA. *Tob*, a member of the *APRO* family, regulates immunological quiescence and tumor suppression. *Cell Cycle* 2009; 8: 1019-25.
18. Corvol JC, Pelletier D, Henry RG, Caillier SJ, Wang J, Pappas D, et al. Abrogation of T cell quiescence characterizes patients at high risk for multiple sclerosis after the initial neurological event. *Proc Natl Acad Sci USA* 2008; 105: 11839-44.
19. Woolf B. On estimating the relation between blood group and disease. *Ann Hum Genet* 1955; 19: 251-3.
20. Gene Calc-Szymon Mijs, Jan Binkowski portal website, (2022), <https://gene-calc.pl/hardy-weinberg-page>, [accessed on November, 2022].
21. GTE Portal website (2022), <https://www.gtportal.org/>, [accessed on November, 2022].
22. Nielsen NM, Westergaard T, Rostgaard K, Frisch M, Hjalgrim H, Wohlfahr J, et al. Familial risk of multiple sclerosis: a nationwide cohort study. *Am J Epidemiol* 2005; 162: 774-8.
23. Baranzini SE, Oksenberg JR. The Genetics of Multiple Sclerosis: From 0 to 200 in 50 Years. *Trends Genet* 2017; 33: 960-70.
24. Patsopoulos NA, Baranzini SE, Santaniello A, Shoostari P, Cotsapas C, Wong G, et al. Multiple sclerosis genomic map implicates peripheral immune cells and microglia in susceptibility. *Science* 2019; 365: 1-25.
25. Mansilla MJ, Presas-Rodríguez S, Teniente-Serra A, González-Larreategui I, Quirant-Sánchez B, Fondelli F, et al. Paving the way towards an effective treatment for multiple sclerosis: advances in cell therapy. *Cell Mol Immunol* 2021; 18: 1353-74.
26. Beecham AH, Patsopoulos NA, Xifara DK, Davis MF, Kempainen A, Cotsapas C, et al. Analysis of immune-related loci identifies 48 new susceptibility variants for multiple sclerosis. *Nat Genet* 2013; 45: 1353-60.
27. Baranzini SE. The role of antiproliferative gene *Tob1* in the immune system. *Clin Exp Neuroimmunol* 2014; 5: 132-6.
28. Ensembl (Release 107-2022), rs4626 SNP ensemble genome browser information page, http://www.ensembl.org/Homo_sapiens/Variation/Explore?r=17:50862561-50863561;v=rs4626;vdb=variation;vf=87138538 [accessed on October, 2022].
29. Ensembl (Release 107-2022), rs7221352 SNP ensemble genome browser information page, http://www.ensembl.org/Homo_sapiens/Variation/Explore?r=17:50869364-50870364;v=rs7221352;vdb=variation;vf=88123893 [accessed on October, 2022].
30. Gresle MM, Jordan MA, Stankovich J, Spelman T, Johnson LJ, Laverick L, et al. Multiple sclerosis risk variants regulate gene expression in innate and adaptive immune cells. *Life Sci Alliance* 2020; 3: 1-11.

Emergence, Evolution and Economics of Coronaviruses

Sidhant Jain^{1,2} , Meenakshi Rana³ , Pooja Jain⁴ 

¹University of Delhi, Department of Zoology, North Campus, Delhi, India

²Institute for Globally Distributed Open Research and Education (IGDORE), India

³University of Delhi, Department of Zoology, Dyal Singh College, Delhi, India

⁴Bhagwati Hospital, Department of Obstetrics and Gynaecology, Sector-13, Delhi, India

ORCID IDs of the authors: S.J. 0000-0003-2596-9566; M.R. 0000-0002-4465-4298; P.J. 0000-0002-3380-5492

Please cite this article as: Jain S, Rana M, Jain P. Emergence, Evolution and Economics of Coronaviruses. Eur J Biol 2022; 81(2): 206-216. DOI: 10.26650/EurJBiol.2022.1113847

ABSTRACT

Viruses are the most abundant biological entities on our planet. On the basis of parameters like capsid structure, morphology, genetic material, etc., they are classified into different families. The *Coronaviridae* family of viruses includes a diverse group of positive strand RNA viruses and a subset of these viruses infects humans. Though some of these human-infecting coronaviruses cause minor respiratory ailments in healthy adults but three of them are responsible for major pandemics of the 21st century. These pandemics claimed thousands to several hundred thousands of human lives and have plunged the regional economies and even the global economy into an abyss. This work highlights the current research on human coronaviruses involving their diversity, evolution, clinical, and zoonotic attributes. An economic impact analysis of major coronaviruses is also presented to point out how these pathogens have claimed billions of dollars.

Keywords: ACE-2 receptor, *Coronaviridae*, Coronaviruses, COVID-19, Evolution, MERS, SARS

INTRODUCTION

Viruses are sub-microscopic, infectious agents which require a living cell as a host for their replication. In most well-studied habitats, they significantly outnumber the cellular forms and infect all known cellular life forms (1). Origin of viruses is nothing less than a biological enigma. Though many hypotheses are proposed but none of them can individually explain the emergence of all viruses. As per the 'virus-first' hypothesis, viruses originated in primordial pool even before the origin of cellular forms (1,2). The two other hypotheses (Escape hypothesis and Reduction hypothesis), generally termed as 'cell-first' hypothesis, believe in the origin of cells prior to viruses (3,4).

Major families of RNA virus families having medical importance are shown in Table 1. Coronaviruses belong to the family *Coronaviridae*. These viruses are enveloped

and have a single stranded RNA genome (positive strand). These genomes are made up of around 30,000 nucleotides. Human coronaviruses (HCoVs) can cause a range of health issues from minor complications like common colds to serious diseases like pneumonia, bronchitis, or bronchiolitis (5). Members of coronavirus family are solely responsible for three major pandemics recorded in the 21st century, namely Severe Acute Respiratory syndrome (SARS), Middle East Respiratory syndrome (MERS) (6), and Coronavirus Disease 2019 (COVID-19). Though certain researchers shy away from using the term 'pandemic' for SARS and MERS but as these outbreaks have infected people in multiple countries, it is accurate to term both of them as pandemics (7).

The aim of this review is multi-directional. First, it talks briefly about the diversity and evolution of coronaviruses. Second, it summarizes the information available on



Corresponding Author: Sidhant Jain

E-mail: jain.sidhant482@gmail.com

Submitted: 10.05.2022 • **Revision Requested:** 27.06.2022 • **Last Revision Received:** 28.07.2022 •

Accepted: 29.07.2022 • **Published Online:** 09.09.2022

Content of this journal is licensed under a Creative Commons Attribution-NonCommercial 4.0 International License.



Table 1. Major families of RNA viruses having a medical impact.

Family (RNA viruses)	Examples
<i>Picornaviridae</i>	Poliovirus, Human Rhino virus, Hepatitis A virus
<i>Caliciviridae</i>	Hepatitis E virus
<i>Flaviviridae</i>	Yellow fever virus, Hepatitis C virus, Zika Virus, Dengue virus
<i>Togaviridae</i>	Rubella virus
<i>Reoviridae</i>	Reovirus, Human Rotavirus
<i>Orthomyxoviridae</i>	Influenza virus A, B, C
<i>Paramyxoviridae</i>	Mumps virus, Measles virus, Nipah Virus
<i>Rhabdoviridae</i>	Rabies virus
<i>Bunyaviridae</i>	Hantavirus
<i>Coronaviridae</i>	Human Coronaviruses
<i>Arenaviridae</i>	Lymphocytic choriomeningitis virus (LCMV)
<i>Retroviridae</i>	Human Immunodeficiency Virus (HIV)
<i>Filoviridae</i>	Marburg virus

HCoVs, especially taking into account the novel coronavirus. Finally, it tries to shed light on the impact that members of *Coronaviridae* have on humans both medically and economically. Though many reviews are available in this field (6,8-10), a broad review highlighting the economic and medical impacts of coronaviruses is not available, especially covering the COVID-19 pandemic and other aspects like CoVs infecting poultry animals.

DIVERSITY AND EVOLUTION

In animals, CoV was first reported in 1931 in chickens (11,12), whereas HCoVs were first reported in 1965 in patients having a common cold (13). Based upon the available genetic sequences, all human-infecting coronaviruses seem to have animal origins (Table 2). This observation highlights the zoonotic attribute of these viruses. *Coronaviridae* family involves a sub-family *Coronavirinae*, which has four major genera, namely *Alphacoronavirus*, *Betacoronavirus*, *Gammacoronavirus*, and *Deltacoronavirus*. The former two exclusively infect mammals, especially bats, whereas the latter two mainly infect birds. Yet some can have mammalian hosts as well (14).

Coronaviruses seem to be the viruses of ancient lineage. The time of the most recent common ancestor (tMRCA) for the four above mentioned genera was reported to be 10,100 years (14). However, another study (15) questioned this time estimation of tMRCA as it contradicted with the co-evolution hypothesis of coronaviruses and natural hosts (bats/birds). Using tMRCA extrapolation methodology, they concluded that the last tMR-

Table 2. CoVs which infect humans or have a major impact on agriculture. *possible natural hosts of origin.

HCoVs	Origin	Genus	Reference
HCoV-229E	Bats	<i>Alphacoronavirus</i>	(9,23)
HCoV-OC43	Rodents*	<i>Betacoronavirus</i>	(9-10)
HCoV-HKU1	Rodents*	<i>Betacoronavirus</i>	(9-10)
HCoV-NL63	Bats	<i>Alphacoronavirus</i>	(9, 23)
SARS-CoV	Bats	<i>Betacoronavirus</i>	(8, 40)
MERS-CoV	Bats	<i>Betacoronavirus</i>	(9, 48)
SARS-CoV-2	Bats	<i>Betacoronavirus</i>	(18)
Animal CoVs	Origin	Genus	Reference
PEDV	Bats	<i>Alphacoronavirus</i>	(16)
PDCoV	Avian*	<i>Deltacoronavirus</i>	(100,101)
SADS-CoV	Bats	<i>Alphacoronavirus</i>	(102)
IBV	Avian*	<i>Gammacoronavirus</i>	(14)

(HCoV: Human Coronavirus, SARS: Severe Acute Respiratory Syndrome, MERS: Middle East Respiratory Syndrome, PEDV: Porcine Epidemic Diarrhoea Virus, PDCoV: Porcine Delta Coronavirus, SADS-CoV: Swine Acute Diarrhoea Syndrome Coronavirus, IBV: Avian Infectious Bronchitis Virus)

CA for these four genera would at least be around 55.8 million years, but as per them (15) it is highly possible that these genera separated 300 million years ago, which allowed the co-evolution of viruses and hosts (9,15).

Many studies (8-9,14,16-18) have analysed the genomes of coronaviruses to understand the origin, genetic recombination, and molecular evolution of these viruses. A study proposed a model for diversification and cross-transmission of these viruses. As per them (14), there exists a huge diversity of bat CoVs in *Alphacoronavirus* and *Betacoronavirus* but not in the rest two genera. Similarly, a huge diversity of bird CoVs is found in *Gammacoronavirus* and *Deltacoronavirus*, but not in the previous two genera, hence pointing bats and birds as gene sources for *Alpha-Betacoronavirus* and *Gamma-Deltacoronavirus* respectively (Figure 1) (14).

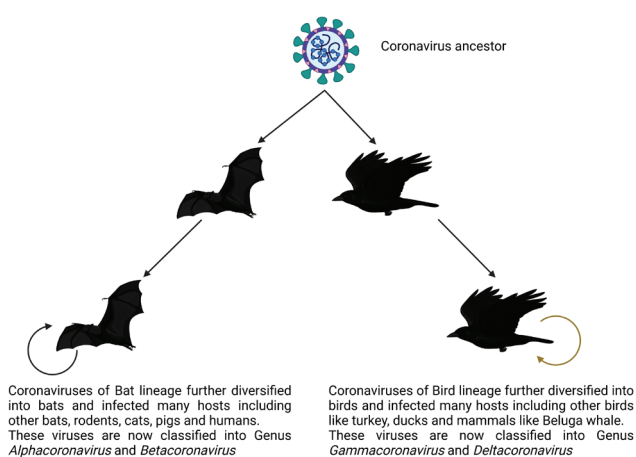


Figure 1. Diversification and cross-transmission of coronaviruses ("created with BioRender.com")

After having jumped between species of bats and given rise to *Alpha-Beta* coronaviruses, bat lineage CoV further jumped to other mammalian species, including species of other bats, pigs, giraffes, rats, and humans, and each jump to different species evolved dichotomously. Similarly, the bird lineage CoV jumped to other species of birds, generating *Gamma-Delta* coronaviruses, which further jumped to other birds and occasionally entered certain mammalian species like beluga whale or pigs, and, like bat lineage CoV, each jumping event evolved dichotomously (8-9,14). Estimated time and region of emergence of HCoVs are shown in Table 3.

HUMAN CoVs

There are seven members of the corona family which are known to infect humans. Four of them cause relatively minor ailments whereas three of them became medical emergencies either in specific regions of the world or even globally as described below.

HCoV-229E

HCoV-229E was first isolated from medical students having respiratory illness who were enrolled in University of Chicago (19). Adults infected with the virus showed common cold-like symptoms (20). However, nosocomial viral respiratory infections among high-risk infants are also linked with it (21). In a recent study, this virus has been detected in infection of lower respiratory tract in an adult individual having acute respiratory distress syndrome with no co-morbidities (22). It appears that HCoV-229E has different clinical manifestations in different patients and the reason for these different manifestations is still not clear.

It is speculated that this virus originated in bats, which might be the primary host, as sequences closely related to this virus were found in a study in bats in Kenya (23). HCoV-229E related

Table 3. Time and area of emergence of Human CoVs.

HCoVs	Estimated time of emergence (year)	Area of origin or first report	Reference
HCoV-229E	~220-330 years ago (1686-1800)	Isolated from students of Chicago University	(19, 103)
HCoV-OC43	~130 years ago (1890s)	Isolated in viral diseases lab. in Maryland, USA	(33, 36)
HCoV-HKU1	~70 years ago (1950s)	Isolated in Hong Kong in late 2004	(39, 104)
HCoV-NL63	~563-822 years ago	Isolated from a 7-month old in the Netherlands	(27, 105)
SARS-CoV	~20 years ago (4 years before outbreak)	Originated in the Guangdong province of China	(42, 106)
	~35 years ago (17 years before outbreak)		(107)
MERS-CoV	~10 years ago (2010)	Originated in Arabian Peninsula	(42, 108)
SARS-CoV-2	Not defined	First reported in Wuhan city of China	(62)

(HCoV: Human Coronavirus, SARS: Severe Acute Respiratory Syndrome, MERS: Middle East Respiratory Syndrome)

viruses have been isolated from dromedaries where anti-HCoV-229E antibodies from human sera are found to neutralise dromedary-derived virus *in-vitro* (24). A potential role of camels in transmission of this virus to humans can be hence speculated. This role of camels can be of very high significance as they have been an important link in the chain of transmission of MERS-CoV from dromedaries to humans, which is discussed ahead (25).

HCoV-229E uses human aminopeptidase N as its receptor, which is a cell surface metalloprotease present on epithelial cells of lung, kidney, and intestine (26). After infecting an individual, this virus, like others, replicates and gets transmitted to other individuals. Transmission between individuals occurs via respiratory droplets or coming in contact with contaminated objects (20,21).

HCoV-NL63

HCoV-NL63 was first isolated from a seven-month old child suffering from bronchiolitis in the Netherlands (27). This virus is associated with respiratory tract illnesses involving both the upper and lower respiratory tract (28). The virus mostly affects the young children, adults, and immune-compromised individuals (29), and its symptoms involve fever, rash, bronchiolitis, bronchitis, sore throat, congestion, and malaise (30).

It has been demonstrated that HCoV-NL63 is a recombinant between viruses similar to NL63 circulating in *Triaenops* bats and 229E like viruses circulating in *Hipposideros* bats (23). The bats might be the primary hosts; however, the intermediate host remains unidentified (31). HCoV-NL63 uses angiotensin-converting enzyme 2 (ACE2) as its receptor for cellular entry (32). The mode of transmission is the same as that of HCoV-229E.

HCoV-OC43

HCoV-OC43 was first isolated in laboratory of viral diseases in Maryland (33). Infected individuals demonstrate common cold-like symptoms (34). This virus is majorly involved in upper respiratory tract infections. However, in cases of children and individuals co-infected with other respiratory viruses, lower respiratory tract infections are common (35).

Rodents are speculated to be the natural or primary host of this virus (9-10), whereas a recent zoonotic transmission is suggested which involved bovines (36), suggesting that bovines are its intermediate hosts.

The protein receptor for the virus still remains unknown, but N-acetyl-9-O-acetylneuraminic acid is identified as the receptor determinant (37). OC43 utilises endocytic route for entry inside the cells and this entry is caveolin-1 dependent. After entering the cell via caveolae, the virus is transported through actin cytoskeleton. There are also other entry pathways to the cells; however, they do not lead to productive infection (38).

HCoV-HKU1

HCoV-HKU1 was isolated in late 2004 in Hong Kong (39). Similar to the three previously described HCoVs, this virus leads to common cold-like symptoms. As compared to other HCoVs, rel-

atively less information is available about this virus. Like HCoV-OC43, rodents are speculated to be its primary host; however, the intermediate host still remains elusive (10,31). Though the protein receptor is still not identified but O-acetylated sialic acid is identified as a receptor determinant (37,39).

SARS-CoV

SARS-CoV emerged about 20 to 35 years ago in the Guangdong province of China (Table 3). SARS-CoV is responsible for the first pandemic of the 21st century, which broke out at the end of February 2003, though no outbreak or transmission has been reported since May 2004 (40). This virus causes SARS, which is characterized by severe pneumonia and diffuse alveolar damage (41-43).

SARS-CoV originated in horseshoe bats by recombination events in SARS related CoVs (41). A study proposed that after its origin, SARS-CoV was transmitted to farmed civet (or another mammal), which got transmitted to other civets (intermediary host) by oral-fecal mode of transmission. These 'virus-carrying' civets were then transported to Guangdong market, leading to the spread of the virus there. The virus acquired more mutations and finally spilled over to humans (10). The mode of transmission from animals to humans remains mysterious; however, contacts with intermediary host in the form of uncooked meat or urine are some of the main suppositions. Respiratory secretions, like droplets, can transmit this virus by direct person to person contact (42).

Upon exposure to the host, the virus binds to the virus receptors, expressed by the target cells (43). ACE2 is the main functional receptor for SARS-CoV (44), whereas it also binds to an alternative receptor, CD209L, but with a greatly reduced affinity (44). ACE2 is widely distributed in respiratory tract epithelium, alveolar monocytes, and macrophages, whereas CD209L is expressed in human type II alveolar cells and endothelial cells (42,45). The virus infects these target cells and multiplies. ACE2 is a surface receptor which provides the virus with an advantage of infecting diverse range of cells. As ACE2 is also expressed in arterial and venous endothelia, arterial smooth muscle, cells of small intestine, cerebral neurons, epithelial cells of the distal renal tubules (46). Hence, virus can infect all these cells.

Atypical pneumonia sets in along with respiratory deterioration, which can lead to respiratory failure. These virus particles can be found in urine, faeces and sweat as the virus has the potential to infect kidneys, intestines, and sweat glands, thereby providing the virus with additional means of spreading along with the respiratory droplets (46,47). A total of 27 nations (including Russian Federation and Taiwan) and two administrative regions of China (Macao and Hong Kong) were affected by SARS-CoV. In total, 8096 individuals were infected, out of which 774 died, leading to a high mortality rate of 9.60% (48).

MERS-CoV

MERS-CoV possibly emerged around 2010 in the Arabian Peninsula (Table 3). The second pandemic of this century is attributed to MERS-CoV. This virus leads to life-threatening MERS disease,

which first broke out in 2012 in Saudi Arabia. Certain cases are reported every year highlighting the fact that virus still remains in circulation (49). MERS-CoV can lead to highly lethal pneumonia and renal dysfunction, though certain individuals infected with it might remain asymptomatic (50).

MERS related CoVs (MERSr-CoVs) have been reported in 14 species of bats, but as the S protein of these MERSr-CoVs is significantly different from MERS-CoV, none of these can be identified as a direct progenitor of MERS-CoV (51,52). Emergence of this virus involved an exchange(s) of genetic elements between different viral ancestors which might have taken place either in bat ancestors or dromedaries (intermediate hosts) which acted as 'mixing vessels' for viruses thriving in different hosts (51,53). All the known MERSr-CoVs bat strains, though, suggest that MERS-CoV originated in bats. But as there exists a phylogenetic gap between MERSr-CoVs and MERS-CoV isolated from humans and camels, some 'yet-to-be identified' viruses must be present in the environment, which led to emergence of MERS-CoV of human and camels (10).

As in the case of SARS, the animal to human mode of transmission could not be fully understood even for MERS. Customs involving consuming uncooked meat, milk and urine might have led to animal to human transfers (43). However, human to human transmission is reported. Reports suggest that unless there is a close contact between two persons, like a healthcare worker providing unprotected care to patient, the virus does not easily pass (54,55). "Simple proximity" and "casual contact" are not generally associated with MERS transmission, but close contact like sharing or sleeping in the room of infected patient or direct patient contact increases this risk (56). Many of the MERS infections were nosocomial in nature (57,58). Further, a study found that the spread of virus by an asymptomatic individual is highly unlikely. However, the study itself calls for more data collection to reach a definitive conclusion (59).

The virus receptor in the case of MERS is dipeptidyl peptidase 4 (DPP4, alternatively known as CD 26), a multi-functional surface protein of cell (Table 4), which is expressed in lower respiratory

tract in humans including type-1 and 2 alveolar cells of lung parenchyma, endothelial cells, and macrophages, whereas the expression in nasal cavity and conducting airways is weak and scattered (60,61). On the contrary, in the case of camels, this receptor is expressed in the upper respiratory tract (61).

DPP4 is also expressed on endothelium of venules as well as in the venous part of capillary bed. It is also expressed in kidney cortex, small intestine (especially ileum) and prostate gland (62). Further, what makes MERS-CoV more dangerous is its ability to efficiently infect the T cells in peripheral blood as well as the T cells of lymphoid organs like tonsils and spleen. The virus induces both intrinsic and extrinsic pathways of apoptosis in T cells leading to its death (63). As a result of virus receptor expression, MERS-CoV leads to pneumonia and renal dysfunction as well as immune system deregulation, which gives rise to a life threatening situation requiring immediate medical care. Owing to the receptor distribution, it is possible that along with respiratory droplets, virus particles may also be found in the urine, stool, and semen of an infected individual. As on 8th May, 2022, a total of 2494 MERS cases have been reported from 27 countries out of which 858 people died, leading to a high mortality rate of 34.40% (64).

SARS-CoV-2

SARS-CoV-2 virus is responsible for the latest pandemic of the 21st century to date. It has brought the human civilisation at a partial halt. Humans are discouraged or even blocked from gathering outside or travelling. Partial or complete lockdowns are in force in many places. Owing to the possibility of more infection waves, it is a great emerging threat for most countries (65).

SARS-CoV-2 was first reported in Wuhan, China in December 2019. As this is an emerging virus, relatively little is known about it. Similar to SARS-CoV, SARS-CoV-2 has 29903 nucleotides in its RNA genome (GenBank: NC_045512.2). This virus causes COVID-19 in humans, and its clinical manifestations range from mild pneumonia to respiratory failure, septic shock, and multiple organ dysfunction (66).

Table 4. Cellular receptors of Human CoVs.

HCoV	Receptor on human cells
HCoV-229E	Aminopeptidase N (AP-N)
HCoV-OC43	Unknown; N-acetyl-9-O-acetylneuraminic acid (receptor determinant)
HCoV-HKU1	Unknown; O-acetylated sialic acid (receptor determinant)
HCoV-NL63	Angiotensin-converting enzyme 2 (ACE2)
SARS-CoV	Angiotensin-converting enzyme 2 (ACE2); CD209L (another receptor with reduced affinity)
MERS-CoV	Dipeptidyl peptidase 4 (DPP4, also known as CD 26)
SARS-CoV-2	Angiotensin-converting enzyme 2 (ACE2)

(HCoV: Human Coronavirus, SARS: Severe Acute Respiratory Syndrome, MERS: Middle East Respiratory Syndrome)

SARS-CoV-2 has about 80% sequence similarity with SARS-CoV and is more than 96% similar to that of bat CoVs RaTG13 and BANAL-52 on whole genome level, suggesting bats to be its natural hosts (18,67,68). Another study showed that Malayan Pangolins associated CoVs have 85.5 to 92.4% similarity to SARS-CoV-2, suggesting these to be the intermediate host (69,70). Other studies have also suggested snakes and turtles as intermediate hosts (71,72), but this possibility has been ruled out by another study which advocates for screening of rodents and bovine animals as potential intermediate hosts (73). Owing to its recent emergence, little is known about animal to human transfer of the virus, but WHO recommends to avoid eating raw or uncooked animal products.

Human to human transmission through droplets, fomites and contaminated frozen meat and seafood is widely documented (74). In contrast to what was observed for MERS-CoV, asymptomatic individuals infected from SARS-CoV-2 have a high potential to transmit the virus to healthy individuals (75,76). Interestingly, human to animal transmissions of SARS-CoV-2 are reported. A tigress in the Bronx Zoo in New York appears to be the first such case where it has tested positive for COVID-19, and it seems that she acquired the infection from an asymptomatic care taker. A study carried out in this regard showed that cats are highly susceptible to this air born infection (77). Human to animal transmissions have also been reported in dogs, cats, minks, lions, and puma (78).

SARS-CoV-2, like SARS-CoV, uses ACE2 as the virus receptor (67) as a result of which all the cellular types (expressing ACE2), which were susceptible to SARS-CoV infection, can be infected by SARS-CoV-2 as well. Though COVID-19 might only cause flu-like symptoms in some individuals but in critical cases, it can lead to respiratory distress, respiratory failure, multiple organ dysfunction, and multiple organ failure, which may finally lead to death. The virus can be detected in oral and anal swabs as well as the blood of the patients indicating the presence of multiple shedding routes (79).

As on 8th May, 2022, 226 countries and territories of the world have been affected by SARS-CoV-2. A total of 517,095,499 cases have been reported worldwide, out of which 6,276,097 individuals have died of the disease and 471,780,006 individuals have recovered with the rest being currently infected (Table 5). This

brings the mortality to 1.21% (80). However, this percentage will change depending upon the reports of new cases and the death of currently infected individuals who are in critical state.

Various pharmaceutical companies distributed worldwide have been working hard for development, trials and safety assessment and mass production of Covid-19 vaccines. About 300 vaccine projects are in development with a significant number of them under trials (81). Regulatory bodies of many countries have now approved few vaccines for mass administration like Covaxin, Covishield, Sputnik V, CoronaVac, and others.

ECONOMIC IMPACT OF CoVs

Members of coronavirus family have made a huge dent in regional as well as global economies. A standardised system or a set of rules/guidelines to calculate the projected or actual economic loss incurred as result of an epidemic or a pandemic is not available. Hence, an array of parameters and methodologies are used by different economists in different studies to reach a figure. Here, we try to give a sense of the economic losses that nations incurred due to these minute pathogenic 'creatures'.

Human CoVs

The four HCoVs (namely 229E, OC43, NL63, HKU1) are not life-threatening, and once they infect the host, the symptoms are very much similar to common colds along with fever, cough, headache, and sore throat (8). Owing to such clinical presentations, the economic impact of these CoVs in terms of providing medical support and health care is relatively miniscule. On the other hand, the rest three HCoVs caused global pandemics of varying severity and hence led to massive economic losses (82-85).

The SARS outbreak initiated in Guangdong and as a result of it, the major economic blow was faced by China and Hong Kong. Other countries also bear the burnt; however, the impact was relatively less. The global macroeconomic impact of SARS was estimated at USD 3-10 million per case (USD 30-100 billion in total). 1% of Chinese GDP declined as an outcome of SARS (82). However, in Hong Kong, the impact of SARS on tourism, travel, and consumption was short-lived, and as soon as the outbreak came under control, the panic and fear subsided quickly (83).

Table 5. Description of HCoVs that caused pandemics. (A: Animal, H: Human, '}' shows transmission direction).

HCoV	Disease	Mode of transmission	Cases reported (as on 8 th May, 2022)	Mortality (as on 8 th May, 2022)
SARS-CoV	SARS	A} H H} H	8,096	09.60%
MERS-CoV	MERS	A} H H} H	2,494	34.40%
SARS-CoV-2	COVID-19	A} H H} H H} A	517,095,499	01.21%

(SARS: Severe Acute Respiratory Syndrome, MERS: Middle East Respiratory Syndrome)

In the case of MERS, the average cost of managing each MERS case in the Saudi Arabia's hospital was around USD 12,947.03 ± 19,923.14 (84). The major industrial sectors of the Republic of Korea faced a loss of USD 3.61 billion (85).

SARS-CoV-2, which is still emerging as a medical and economic emergency, has led to a global economic crisis. As it is an emerging virus, it is extremely difficult to assess the size of the final impression it will leave on global economy, not to mention its adverse effects on different cultures and society. Some initial figures of this pandemic are dismaying. COVID-19 has the potential to bring a global recession and plunge world economies into a chasm (86). As this virus seems to be highly contagious, has led to hospitalization in many cases and has created a fear among the masses, most nations are either facing a partial or complete lockdown or some other form of restrictions to avoid the spread and to avert an exponential burden on the health care machinery.

As a result, sectors like manufacturing and sales, hospitality and tourism, entertainment and others are shut at various levels. A sector wise impact analysis of COVID-19 has been done in a recent study (87). Poor and under developed nations, which lack basic medical facilities, are badly hit. The International Monetary Fund has said that the cumulative loss of COVID-19 pandemic will range around USD 9 trillion. This figure is greater than the sum of economies of Japan and Germany (88).

ANIMAL CoVs

Porcine Epidemic Diarrhoea Virus (PEDV)

The PEDV outbreak was first reported in the 1970s in Europe and since then, sporadic occurrences have been observed in many countries including major ones in China (2010) and the USA (2015). PEDV is responsible for causing lethal diarrhoea in pigs at neonatal stage whereas weight reduction is observed in hogs (89). In suckling piglets in China, a death rate of 80-100% was reported (90). PEDV led to a decrease of USD 900 million to USD 1.8 billion for the U.S. economic welfare. Similarly, there was an annual reduction in income of pork packers, and as a result of declined supply, pork consumers not only had to pay more for limited supply of pork, but also for other meats as well, as prices strengthened due to PEDV (91).

Porcine Delta Coronavirus (PDCoV)

PDCoV was first detected in Hong Kong in 2012 and since then, it has reached Canada, the USA, Laos, Vietnam, Thailand, South Korea, and China. Though the clinical severity is less than PEDV, it still causes serious diseases (89). It causes vomiting, dehydration and diarrhoea in neonatal piglets which can be lethal and has a 40% mortality rate (92). The economic impacts are somewhat similar to that of PEDV albeit low in nature owing to its low mortality rate. However, as it is a new and emerging virus, more studies are required to exactly estimate the economic losses happening as a result of it.

Apart from these two porcine coronaviruses, there are many more porcine coronaviruses, like Transmissible gastroenteritis

virus (TGEV), porcine respiratory coronavirus (PRCoV), porcine hemagglutinating encephalomyelitis virus (HEV), and swine acute diarrhoea syndrome (SADS-CoV), and they have a huge impact on agricultural returns.

Avian Infectious Bronchitis Virus (IBV)

IBV mainly causes a respiratory infection in chickens, but it can have multiple clinical infestations including reproductive disease, and nephritis along with respiratory disorders. IBV was first reported in the 1930s, but all countries having intensive poultry industries are affected by it. Though a morbidity of 100% is reported but mortality is around 20-30% and almost always occur as a result of co-infection with a bacterium or mycoplasma (93). As a result of morbidity and mortality, agricultural economy is significantly impacted. A study conducted in Brazil with breeders and broilers showed that with breeders of about 6 months of age, a total loss of USD 3567.40 per 1000 birds was incurred. The same statistic became USD 4210.80 per 1000 birds in 10 months old breeders, showing an increase in loss with increased age of birds. In the case of 48 days old broilers, the loss per 1000 birds was estimated at USD 266.30 (94).

Turkey Coronavirus (TCoV)

Another coronavirus which infects turkeys is commonly known as TCoV. It causes severe diarrhoea in young turkey poults. Though a direct estimate of economic loss from TCoV couldn't be found but a high field-prevalence ranging between 60-74% among different turkey classes like meat turkeys and breeders was reported (95).

CoVs are also reported from other animals used in agriculture like Pheasant CoV, Duck CoV, Goose CoV, and Pigeon CoV. Though it seems impossible to estimate all the economic losses which occur as a result of CoVs, but the examples cited above give a clear picture about how badly these CoVs impact economies and hence warrant extensive research to prevent human lives, animal lives as well as the agriculture industry.

CURRENT STATUS AND FUTURE PROSPECTS

HCoVs like 229E, OC43, NL63, HKU1 never lead to life-threatening manifestations alone, whereas SARS-CoV, MERS-CoV and SARS-CoV-2 not only threaten life but also have serious economic manifestations. However, infections with the former CoVs can be fatal if patients have low haemoglobin concentration, serum albumin levels or other such issues (96). Similarly, infants, immune-compromised individuals, and people with co-morbidities or those in old age are at high risk of developing serious clinical manifestations if infected with the former four HCoVs (22,29).

Three of these seven HCoVs, namely HCoV-NL63, SARS-CoV, and SARS-CoV-2 use similar receptor-ACE2; however, not only do these viruses have different infection potential, but the mortality rates are also very different (Tables 4 and 5). Mortality with NL63 is rarely reported, SARS-CoV has about 10% mortality, whereas around 1.21% mortality is currently observed for SARS-CoV-2. Similarly, the number of infected individuals also

varies greatly, where SARS-CoV infected about 8100 individuals, SARS-CoV-2 has globally infected 517.10 million people as on 8th May, 2022 (Table 5). This indicates that mere use of the similar receptor doesn't define the capacity or severity of infection and mortality rates. Possible factors for these observed differences probably involve varying demographic structures as mortality is skewed towards older people (97), prevalent climatic conditions, population density, and access to medical care among many.

All the three diseases i.e. SARS, MERS, and COVID-19 can be lethal; however, the contagiousness of all the three viruses seems to be different. The SARS-CoV-2 seems to be highly contagious (98), whereas MERS-CoV requires a close contact between the infected and healthy person to get transmitted (54, 58). Further, transmission of SARS-CoV-2 is reported from asymptomatic individual, which is not the case in the case of MERS (59,75,76).

It is possible that the absence of MERS-CoV receptor, DPP4, in the upper respiratory tract of humans (60,61) is a major reason for this restricted human to human contact, hence requiring close proximity for transmission. As MERS had a high mortality rate (35%), one cannot even imagine the kind of calamity the human civilisation would have faced if MERS-CoV could have transmission rates as that of SARS-CoV-2 and if it could have been transmitted by asymptomatic individuals. On the contrary, it is also possible that SARS-CoV-2 has a high transmission rate as it has a relatively low mortality rate and it causes milder symptoms.

Acts like consumption of raw meat and sea food, wild life trade not only give a chance to newly evolved viruses to spill over but also brings these viruses in close contact with humans and other animals, which can lead to calamities as evident in the case of SARS-CoV-2. Live animals were on sale in Huanan seafood wholesale market in China, from where SARS-CoV-2 seems to have reached humans (74). Owing to the rich diversity of coronaviruses in bats and presence of wet markets in Asian countries, evolution and spillover of a more deadly virus than SARS-CoV-2 cannot be denied.

A high diversity of SARS and MERS related coronaviruses exists in primary and intermediate hosts (41,99), as a result of which evolution and emergence of new coronaviruses are very much possible in the near future. One study (6) showed that there existed a high probability of emergence of a SARS- and MERS-CoV like coronavirus in China itself, and in less than a year, it became true. It is of utmost importance to fill the phylogenetic gaps among the evolutionary stages of coronaviruses which will help in understanding the dynamics between primary and intermediate hosts, further helping in preventing the transmission of newly evolved coronaviruses in the future.

The COVID-19 crisis highlights the need for every country to fund research institutions as well as the need for scientific temperament among the masses. Similarly, it also emphasises the need for robust healthcare and pharmaceutical sectors along with equipping the medical staff, even in remote areas, to deal with highly contagious infectious agents.

CONCLUSION

Coronaviruses are the viruses of ancient lineage. Though the tMRCA is debated, it is highly possible that it originated about 300 million years ago and diversified further. HCoV infections manifest in a variety of ways, ranging from common cold-like symptoms in some cases to life-threatening concerns with others despite the fact that many of these HCoVs use the same receptors and infect the same cell types.

The primary and intermediary hosts play an extremely crucial role in virus propagation because they help the viruses to 'jump' between different species. Owing to this zoonotic potential of these viruses, more research is needed to understand the dynamics among the hosts as well as the urgency to fill the phylogenetic gaps which can allow to break the transmission chain of coronaviruses among humans in the future. The ramifications of HCoV propagation also call for an urgent regulation of wet markets in order to avoid further spill over of deadly viruses.

The economic impact of both HCoVs and animal CoVs is daunting. Not only do the animal CoVs have an impact on the agricultural aspects, but also the economic shutdown, especially due to SARS-CoV-2, will have far reaching consequences. COVID-19 forced countries to go into lockdown, causing various sectors such as tourism, sales, entertainment, manufacturing, and other businesses to suffer. The GDP growth of many major economies is projected to be negative. All these have been happening because of a sub-microscopic RNA particle enclosed in an envelope, demonstrating the need of allocation of bigger chunks of GDP to education, research, and healthcare.

As the emergence of new viruses is inevitable, human civilisation must learn from the current crisis not only to prevent deaths, but also to take care of the economy.

Peer Review: Externally peer-reviewed.

Author Contributions: Conception/Design of Study- S.J.; Data Acquisition- S.J.; Data Analysis/Interpretation- S.J., M.R., P.J.; Drafting Manuscript- S.J.; Critical Revision of Manuscript- S.J., M.R., P.J.; Final Approval and Accountability- S.J., M.R., P.J.

Conflict of Interest: Authors declared no conflict of interest.

Financial Disclosure: Authors declared no financial support.

REFERENCES

1. Koonin EV, Dolja VV. A virocentric perspective on the evolution of life. *Curr Opin Virol* 2013; 3(5): 546-57.
2. Koonin EV, Senkevich TG, Dolja VV. Compelling reasons why viruses are relevant for the origin of cells. *Nat Rev Microbiol* 2009;7(8):615.
3. Wessner DR. The origins of viruses. *Nature Education* 2010; 3(9): 37.
4. Durzyńska J, Goździcka-Józefiak A. Viruses and cells intertwined since the dawn of evolution. *Virol J* 2015; 12: 169.
5. Geller C, Varbanov M, Duval RE. Human coronaviruses: insights into environmental resistance and its influence on the development of new antiseptic strategies. *Viruses* 2012; 4(11): 3044-68.
6. Fan Y, Zhao K, Shi ZL, Zhou, P. Bat coronaviruses in China. *Viruses* 2019; 11(3).

7. LeDuc JW, Barry MA. SARS, the first pandemic of the 21st Century. *Emerg Infect Dis* 2004; 10(11): e26.
8. Su S, Wong G, Shi W, Liu J, Lai ACK, Zhou J, et al. Epidemiology, genetic recombination, and pathogenesis of coronaviruses. *Trends Microbiol* 2016; 24(6): 490-502.
9. Forni D, Cagliani R, Clerici M, Sironi M. Molecular evolution of human coronavirus genomes. *Trends Microbiol* 2017; 25(1): 35-48.
10. Cui J, Li F, Shi ZL. Origin and evolution of pathogenic coronaviruses. *Nat Rev Microbiol* 2019; 17(3): 181-92.
11. Schalk AF, Hawn MC. An apparently new respiratory disease of baby chicks. *J. Amer. vet. med. Ass* 1931; 78: 413-22.
12. McIntosh K. Coronaviruses: a comparative review. *Curr Top Microbiol Immunol* 1974; 63: 85-129.
13. Tyrrell DA, Bynoe ML. Cultivation of a novel type of common-cold virus in organ cultures. *Br med J* 1965; 1(5448): 1467-70.
14. Woo PC, Lau S K, Lam CS, Lau CC, Tsang AK, Lau JH, et al. Discovery of seven novel Mammalian and avian coronaviruses in the genus *deltacoronavirus* supports bat coronaviruses as the gene source of *alphacoronavirus* and *betacoronavirus* and avian coronaviruses as the gene source of *gammacoronavirus* and *deltacoronavirus*. *J Virol* 2012; 86(7): 3995-4008.
15. Wertheim JO, Chu DK, Peiris JS, Kosakovsky Pond S L, Poon LL. A case for the ancient origin of coronaviruses. *J Virol* 2013; 87(12): 7039-45.
16. Huang YW, Dickerman AW, Piñeyro P, Li L, Fang L, Kiehne R. Origin, evolution, and genotyping of emergent porcine epidemic diarrhea virus strains in the United States. *mBio* 2013; 4(5): e00737-13.
17. Ma Y, Zhang Y, Liang X, Lou F, Oglesbee M, Krakowka S, et al. Origin, evolution, and virulence of porcine *deltacoronaviruses* in the United States. *mBio* 2015; 6(2): e00064.
18. Guo Y, Cao Q, Hong Z, Tan Y, Chen S, Jin H. The origin, transmission and clinical therapies on coronavirus disease 2019 (COVID-19) outbreak – an update on the status. *Military Med Res* 2020; 7: 11.
19. Hamre D, Procknow JJ. A new virus isolated from the human respiratory tract. *Proc Soc Exp Biol Med* 1966; 121(1): 190-3.
20. Bradburne AF, Bynoe ML, Tyrrell DA. Effects of a “new” human respiratory virus in volunteers. *Br Med J* 1967; 3(5568): 767-9.
21. Gagneur A, Vallet S, Talbot PJ, Legrand-Quillien M, Picard B, Payan C, et al. Outbreaks of human coronavirus in a pediatric and neonatal intensive care unit. *Eur J Pediatr* 2018; 167(12): 1427-34.
22. Vassilara F, Spyridaki A, Pothitos G, Deliveliotou A, Papadopoulos A. A rare case of human coronavirus 229E associated with acute respiratory distress syndrome in a healthy adult. *Case Rep Infect Dis* 2018.
23. Tao Y, Shi M, Chommanard C, Queen K, Zhang J, Markotter W, et al. Surveillance of bat coronavirus in Kenya identifies relatives of human coronaviruses NL63 and 229E and their recombination history. *J Virol* 2017; 91(5): e01953-16.
24. Corman VM, Eckerle I, Memish ZA, Liljander AM, Dijkman R, Jonsdottir H, et al. Link of a ubiquitous human coronavirus to dromedary camels. *Proc Natl Acad Sci U S A* 2016; 113(35): 9864-9.
25. Li Z, Tomlinson AC, Wong AH, Zhou D, Desforges M, Talbot PJ, et al. The human coronavirus HCoV-229E S-protein structure and receptor binding. *Elife* 2019; 8: 51230.
26. Yeager CL, Ashmun RA, Williams RK, Cardellicchio CB, Shapiro LH, Look AT, et al. Human aminopeptidase N is a receptor for human coronavirus 229E. *Nature* 1992; 357(6377): 420-2.
27. Van der Hoek L, Pyrc K, Jebbink MF, Vermeulen-Oost W, Berkhout RJ, Wolthers KC, et al. Identification of a new human coronavirus. *Nat Med* 2004; 10(4): 368-73.
28. Van der Hoek L, Pyrc K, Berkhout B. Human coronavirus NL63, a new respiratory virus. *FEMS Microbiol Rev* 2006; 30(5): 760-73.
29. Abdul-Rasool S, Fielding BC. Understanding human coronavirus HCoV-NL63. *Open Virol J* 2010; 4: 76-84.
30. Bastien N, Anderson K, Hart L, Van Caesele P, Brandt K, Milley D, et al. Human coronavirus NL63 infection in Canada. *J Infect Dis* 2005; 191(4): 503-6.
31. Ye ZW, Yuan S, Yuen KS, Fung SY, Chan CP, Jin DY. Zoonotic origins of human coronaviruses. *Int J Biol Sci* 2020; 16(10): 1686-97.
32. Hofmann H, Pyrc K, Van der Hoek L, Geier M, Berkhout B, Pöhlmann S. Human coronavirus NL63 employs the severe acute respiratory syndrome coronavirus receptor for cellular entry. *Proc Natl Acad Sci USA* 2005; 102(22): 7988-93.
33. McIntosh K, Becker W, Chanock R. Growth in suckling-mouse brain of “IBV-Like” viruses from patients with upper respiratory tract disease. *Proc Natl Acad Sci USA* 1967; 58(6): 2268-73.
34. Wevers BA, Van der Hoek L. Recently discovered human coronaviruses. *Clin Lab Med* 2009; 29(4): 715-24.
35. Jean A, Quach C, Yung A, Semret M. Severity and outcome associated with human coronavirus OC43 infections among children. *Pediatr Infect Dis J* 2013; 32(4): 325-9.
36. Vijgen L, Keyaerts E, Moës E, Thoelen I, Wollants E, Lemey P, et al. Complete genomic sequence of human coronavirus OC43: molecular clock analysis suggests a relatively recent zoonotic coronavirus transmission event. *J Virol* 2005; 79(3): 1595-1604.
37. Jonsdottir HR, Dijkman R. Coronaviruses and the human airway: a universal system for virus-host interaction studies. *Virol J* 2016; 13: 24.
38. Owczarek K, Szczepanski A, Milewska A, Baster Z, Rajfur Z, Sarna M, et al. Early events during human coronavirus OC43 entry to the cell. *Sci Rep* 2018; 8(1): 7124.
39. Woo PC, Lau SK, Chu CM, Chan KH, Tsoi HW, Huang Y, et al. Characterization and complete genome sequence of a novel coronavirus, coronavirus HKU1, from patients with pneumonia. *J Virol* 2005; 79(2): 884-95.
40. WHO: https://who.int/csr/don/2004_05_18a/en/ (Last accessed: 3rd Nov., 2021)
41. Hu B, Zeng LP, Yang XL, Ge XY, Zhang W, Li B, et al. Discovery of a rich gene pool of bat SARS-related coronaviruses provides new insights into the origin of SARS coronavirus. *PLoS Pathog* 2017; 13(11): e1006698.
42. Yin Y, Wunderink RG. MERS, SARS and other coronaviruses as causes of pneumonia. *Respirology* 2018; 23(2): 130-7.
43. Song Z, Xu Y, Bao L, Zhang L, Yu P, Qu Y, et al. From SARS to MERS, thrusting coronaviruses into the spotlight. *Viruses* 2019; 11(1): 59.
44. Li W, Moore MJ, Vasilieva N, Sui J, Wong SK, Berne MA, et al. Angiotensin-converting enzyme 2 is a functional receptor for the SARS coronavirus. *Nature* 2003; 426(6965): 450-4.
45. Jeffers SA, Tusell SM, Gillim-Ross L, Hemmila EM, Achenbach JE, Babcock GJ, et al. CD209L (L-SIGN) is a receptor for severe acute respiratory syndrome coronavirus. *Proc Natl Acad Sci U S A* 2004; 101(44): 15748-53.
46. Guo Y, Korteweg C, McNutt MA, GU J. Pathogenetic mechanisms of severe acute respiratory syndrome. *Virus Res* 2008; 133(1): 4-12.
47. Ding Y, He L, Zhang Q, Huang Z, Che X, Hou J, et al. Organ distribution of severe acute respiratory syndrome (SARS) associated coronavirus (SARS-CoV) in SARS patients: implications for pathogenesis and virus transmission pathways. *J Pathol* 2004; 203(2): 622-30.
48. WHO: https://www.who.int/csr/sars/country/table2004_04_21/en/ (Last accessed: 3rd March, 2022).
49. WHO: <https://www.who.int/emergencies/mers-cov/en/> (Last accessed: 3rd March, 2022).
50. Chan JF, Lau SK, To KK, Cheng VC, Woo PC, Yuen KY. Middle East respiratory syndrome coronavirus: another zoonotic *betacoronavirus* causing SARS-like disease. *Clin. Microbiol Rev* 2005; 28(2): 465-522.

51. Corman VM, Ithete NL, Richards LR, Schoeman MC, Preiser W, Drosten C, et al. Rooting the phylogenetic tree of Middle east respiratory syndrome coronavirus by characterization of a conspecific virus from an African bat. *J Virol* 2014; 88(19): 11297-303.
52. Yang L, Wu Z, Ren X, Yang F, Zhang J, He G, et al. MERS-related *betacoronavirus* in *Vespertilio superans* bats, China. *Emerg Infect Dis* 2014; 20(7): 1260-2.
53. Haagmans BL, Al Dhahiry SH, Reusken CB, Raj VS, Galiano M, Myers R, et al. Middle East respiratory syndrome coronavirus in dromedary camels: an outbreak investigation. *Lancet Infect Dis* 2014; 14(2): 140-5.
54. Hijawi B, Abdallat M, Sayaydeh A, Alqasrawi S, Haddadin A, Haarour N, et al. Novel coronavirus infections in Jordan, April 2012: epidemiological findings from a retrospective investigation. *East Mediterr Health J* 2013; 19(1): S12-18.
55. Assiri A, Al-Tawfiq JA, Al-Rabeeh AA, Al-Rabiah FA, Al-Hajjar S, Al-Barrak A, et al. Epidemiological, demographic, and clinical characteristics of 47 cases of Middle east respiratory syndrome coronavirus disease from Saudi Arabia: a descriptive study. *Lancet Infect Dis* 2013; 13(9): 752-61.
56. Arwady MA, Alraddadi B, BaslerC, Azhar EI, Abuelzein E, Sindy AI, et al. Middle east respiratory syndrome coronavirus transmission in extended family, Saudi Arabia, 2014. *Emerg Infect Dis* 2016; 22(8): 1395-402.
57. Korean Centres for Disease Control and Prevention. Middle east respiratory syndrome coronavirus outbreak in the Republic of Korea. *Osong Public Health Res Perspect* 2015; 6(4): 269-78.
58. Hunter J, Nguyen D, AdenB, Al Bandar Z, Al Dhaheri W, Abu Elkheir K. Transmission of middle east respiratory syndrome coronavirus infections in healthcare settings, Abu Dhabi. *Emerg Infect Dis* 2016; 22(4): 647-56.
59. Moon SY, Son JS. Infectivity of an asymptomatic patient with middle east respiratory syndrome coronavirus infection. *Clin Infect Dis* 2017; 64(10): 1457-8.
60. Meyerholz DK, Lambertz AM, McCray PB. Dipeptidyl Peptidase 4 Distribution in the human respiratory tract: Implications for the middle east respiratory syndrome. *Am J Pathol* 2016; 186(1): 78-86.
61. Widagdo W, Raj VS, Schipper D, Kolijn K, Leenders GJLH, Bosch BJ, et al. Differential expression of the middle east respiratory syndrome coronavirus receptor in the upper respiratory tracts of humans and dromedary camels. *J Virol* 2016; 90: 4838-42.
62. Lambeir AM, Durinx C, Scharpé S, De Meester I. Dipeptidyl-peptidase IV from bench to bedside: an update on structural properties, functions, and clinical aspects of the enzyme DPP IV. *Crit Rev Clin Lab Sci* 2003; 40(3): 209-94.
63. Chu H, Zhou J, Wong BH, Li C, Chan JF, Cheng ZS, et al. Middle east respiratory syndrome coronavirus efficiently infects human primary T lymphocytes and activates the extrinsic and intrinsic apoptosis pathways. *J Infect Dis* 2016; 213(6): 904-14.
64. WHO: <https://www.who.int/emergencies/mers-cov/en/> (Last accessed: 8th May, 2022).
65. Engelbrecht FA, Scholes RJ. Test for Covid-19 seasonality and the risk of second waves. *One Health* 2021; 12: 100202.
66. Wu Z, McGoogan JM. Characteristics of and important lessons from the coronavirus disease 2019 (COVID-19) outbreak in China: summary of a report of 72314 cases from the Chinese center for disease control and prevention. *JAMA* 2020; 323(13): 1239-42.
67. Zhou P, Yang XL, Wang XG, Hu B, Zhang L, Zhang W, et al. A pneumonia outbreak associated with a new coronavirus of probable bat origin. *Nature* 2020; 579(7798): 270-3.
68. Temmem S, Vongphayloth K, Salazar EB, Munier S, Bonomi M, Regnault B, et al. Coronaviruses with a SARS-CoV-2-like receptor-binding domain allowing ACE2-mediated entry into human cells isolated from bats of Indochinese peninsula. Pre-print. 2021. DOI: 10.21203/rs.3.rs-871965/v1
69. Lam TT, Jia N, Zhang YW, Shum MH, Jiang JF, Zhu HC, et al. Identifying SARS-CoV-2-related coronaviruses in Malayan pangolins. *Nature* 2020; 583(7815), 282-5.
70. Xiao K, Zhai J, Feng Y, Zhou N, Zhang X, Zou JJ, et al. Isolation of SARS-CoV-2-related coronavirus from Malayan pangolins. *Nature* 2020; 583(7815): 286-9.
71. Liu X, Xiao X, Wei X, Li J, Yang J, Tan H, et al. Composition and divergence of coronavirus spike proteins and host ACE2 receptors predict potential intermediate hosts of SARS-CoV-2. *J. Med. Virol* 2020; 92(6): 595-60.
72. Ji W, Wang W, Zhao X, Zai J, Li X. Cross-species transmission of the newly identified coronavirus 2019-nCoV. *J Med Virol* 2020; 92(4): 433-40.
73. Luan J, Jin X, Lu Y, Zhang L. SARS-CoV-2 spike protein favors ACE2 from Bovidae and Cricetidae. *J Med Virol* 2020; 92(9): 1649-56.
74. Zheng J. SARS-CoV-2: an Emerging coronavirus that causes a global threat. *Int J Biol Sci* 2020; 16(10): 1678-85.
75. Bai Y, Yao L, Wei T, Tian F, Jin DY, Chen L, et al. Presumed asymptomatic carrier transmission of COVID-19. *JAMA* 2020; 323(14): 1406-7.
76. Rothe C, Schunk M, Sothmann P, Bretzel G, Froeschl G, Wallrauch C, et al. Transmission of 2019-nCoV Infection from an asymptomatic contact in Germany. *N Engl J Med* 2020; 382(10): 970-1.
77. Shi J, Wen Z, Zhong G, Yang H, Wang C, Huang B, et al. Susceptibility of ferrets, cats, dogs, and other domesticated animals to SARS-coronavirus 2. *Science* 2020; 368(6494): 1016-20.
78. Do Vale B, Lopes AP, Fontes M, Silvestre M, Cardoso L, Coelho AC. Bats, pangolins, minks and other animals - villains or victims of SARS-CoV-2? *Vet Res Commun* 2021; 45(1): 1-19.
79. Zhang W, Du RH, Li B, Zheng XS, Yang XL, Hu B, et al. Molecular and serological investigation of 2019-nCoV infected patients: implication of multiple shedding routes. *Emerg Microbes Infect* 2020; 9(1): 386-9.
80. Worldometer: <https://www.worldometers.info/coronavirus/> (Last accessed: 8th May, 2022).
81. Forni G, Mantovani A, COVID-19 Commission of Accademia Nazionale dei Lincei, Rome. COVID-19 vaccines: where we stand and challenges ahead. *Cell Death Differ* 2021; 28(2): 626-39.
82. Qiu W, Chu C, Mao A, Wu J. The impacts on health, society, and economy of SARS and H7N9 outbreaks in China: A case comparison study. *J Environ Public Health* 2018; 2710185.
83. Siu A, Richard Wong YCR. Economic impact of SARS: The case of Hong Kong. *Asian Economic Papers* 2004; 3(1): 62-83.
84. AlRuthia Y, Somily AM, Alkhamali AS, Bahari OH, AlJuhani RJ, Alsenaidy M, et al. Estimation of direct medical costs of middle east respiratory syndrome coronavirus infection: A single-center retrospective chart review study. *Infect Drug Resist* 2019; 12: 3463-73.
85. Joo H, Maskery BA, Berro AD, Rotz LD, Lee YK, Brown CM. Economic Impact of the 2015 MERS Outbreak on the Republic of Korea's tourism-related industries. *Health Secur* 2019; 17(2): 100-8.
86. Aljazeera: <https://www.aljazeera.com/ajimpact/imf-covid-19-global-recession-2020-200323231228113.html> (Last accessed: 3rd Nov., 2021).
87. Nicola M, Alsaifi Z, Sohrabi C, Kerwan A, Al-Jabir A, Iosifidis C, et al. The socio-economic implications of the coronavirus pandemic (COVID-19): A review. *Int J Surg* 2020; 78: 185-93.
88. IMF: <https://blogs.imf.org/2020/04/14/the-great-lockdown-worst-economic-downturn-since-the-great-depression/> (Last accessed: 3rd Nov., 2021).

89. Koonpaew S, Teeravechyan S, Frantz PN, Chailangkarn T, Jongkaewwattana A. PEDV and PDCoV Pathogenesis: The interplay between host innate immune responses and porcine enteric coronaviruses. *Front Vet Sci* 2019; 6: 34.
90. Sun RQ, Cai RJ, Chen YQ, Liang PS, Chen DK, Song CX. Outbreak of porcine epidemic diarrhea in suckling piglets, China. *Emerg Infect Dis* 2012; 18(1): 161-3.
91. Paarlberg PL. Updated estimated economic welfare impacts of porcine epidemic diarrhea virus (PEDV). Purdue University, Department of Agricultural Economics, Working Papers 2014; 14: 1-38.
92. Jung K, Hu H, Saif LJ. Porcine *deltacoronavirus* infection: Etiology, cell culture for virus isolation and propagation, molecular epidemiology and pathogenesis. *Virus Res* 2016; 226: 50-9.
93. Ignjatović J, Sapats S. Avian infectious bronchitis virus. *Rev Sci Tech* 2000; 19(2): 493-508.
94. Colvero LP, Villarreal LY, Torres CA, Brañdo PE. Assessing the economic burden of avian infectious bronchitis on poultry farms in Brazil. *Rev Sci Tech* 2015; 34(3): 993-9.
95. Goma MH, Yoo D, Ojkic D, Barta JR. Seroprevalence of turkey coronavirus in North American turkeys determined by a newly developed enzyme-linked immunosorbent assay based on recombinant antigen. *Clin Vaccine Immunol* 2008; 15(12): 1839-44.
96. Woo PC, Lau SK, Yuen KY. Clinical features and molecular epidemiology of coronavirus-HKU1-associated community-acquired pneumonia. *Hong Kong Med J* 2009; 15(9): 46-7.
97. Petersen E, Koopmans M, Go U, Hamer DH, Petrosillo N, Castelli C. Comparing SARS-CoV-2 with SARS-CoV and influenza pandemics. *Lancet Infect Dis* 2020; 20(9): e238-44.
98. Sanche S, Lin YT, Xu C, Romero-Severson E, Hengartner N, Ke R. High contagiousness and rapid spread of severe acute respiratory syndrome coronavirus 2. *Emerg Infect Dis* 2020; 26(7).
99. Chu DKW, Hui KPY, Perera RAPM, Miguel E, Niemeyer D, Zhao J, et al. MERS coronaviruses from camels in Africa exhibit region-dependent genetic diversity. *Proc Natl Acad Sci U S A* 2018; 115(12): 3144-9.
100. Wang L, Byrum B, Zhang Y. Porcine coronavirus HKU15 detected in 9 US states, 2014. *Emerg Infect Dis* 2014; 20(9): 1594-5.
101. Zhai SL, Wei WK, Li XP, Wen XH, Zhou X, Zhang H, et al. Occurrence and sequence analysis of porcine *deltacoronaviruses* in southern China. *Virology* 2016; 13: 136.
102. Zhou P, Fan H, Lan T, Yang XL, Shi WF, Zhang W. Fatal swine acute diarrhoea syndrome caused by an HKU2-related coronavirus of bat origin. *Nature* 2018; 556(7700): 255-8.
103. Pfeifferle S, Oppong S, Drexler JF, Gloza-Rausch F, Ipsen A, Seebens A, et al. Distant relatives of severe acute respiratory syndrome coronavirus and close relatives of human coronavirus 229E in bats, Ghana. *Emerg Infect Dis* 2009; 15(9): 1377-84.
104. Al-Khannaq MN, Ng KT, Oong XY, Pang YK, Takebe Y, Chook JB. Molecular epidemiology and evolutionary histories of human coronavirus OC43 and HKU1 among patients with upper respiratory tract infections in Kuala Lumpur, Malaysia. *Virology* 2016; 13: 33.
105. Huynh J, Li S, Yount B, Smith A, Sturges L, Olsen JC, et al. Evidence supporting a zoonotic origin of human coronavirus strain NL63. *J Virol* 2012; 86(23): 12816-25.
106. Hon CC, Lam TY, Shi ZL, Drummond A J, Yip CW, Zeng F. Evidence of the recombinant origin of a bat severe acute respiratory syndrome (SARS)-like coronavirus and its implications on the direct ancestor of SARS coronavirus. *J Virol* 2008; 82(4): 1819-26.
107. Vijaykrishna D, Smith GJ, Zhang JX, Peiris JS, Chen, H Guan, Y. Evolutionary insights into the ecology of coronaviruses. *J Virol* 2007; 81(8): 4012-20.
108. Zhang Z, Shen L, Gu, X. Evolutionary Dynamics of MERS-CoV: Potential recombination, positive selection and transmission. *Sci Rep* 2016; 6: 25049.

***Myrtus communis* L. Extract Ameliorates High Fat Diet Induced Kidney and Bladder Damage by Inhibiting Oxidative Stress and Inflammation**

Fatma Kanpalta Mustafaoglu¹ , Busra Ertas² , Ali Sen³ , Dilek Akakin¹ , Goksel Sener⁴ , Feriha Ercan¹ 

¹Marmara University, School of Medicine, Department of Histology and Embryology, İstanbul, Türkiye

²Marmara University, School of Pharmacy, Department of Pharmacology, İstanbul, Türkiye

³Marmara University, School of Pharmacy, Department of Pharmacognosy, İstanbul, Türkiye

⁴Fenerbahçe University, School of Pharmacy, İstanbul, Türkiye

ORCID IDs of the authors: F.K.M. 0000-0001-9832-6938; B.E. 0000-0001-8374-1098; A.Ş. 0000-0002-2144-5741; D.A. 0000-0002-1781-3708; G.Ş. 0000-0001-7444-6193; F.E. 0000-0003-2339-5669

Please cite this article as: Kanpalta Mustafaoglu F, Ertas B, Sen A, Akakin D, Sener G, Ercan F. *Myrtus communis* L. Extract Ameliorates High Fat Diet Induced Kidney and Bladder Damage by Inhibiting Oxidative Stress and Inflammation. Eur J Biol 2022; 81(2): 217-230. DOI: 10.26650/EurJBiol.2022.1111191

ABSTRACT

Objective: Obesity is associated with many diseases, including urinary system disorders such as chronic kidney disease and overactive bladder syndrome. *Myrtus communis* L. (MC) extract has been reported to have antioxidant and anti-inflammatory effects. The aim of this study was to investigate the protective effects of MC extract on high-fat diet (HFD)-induced kidney and bladder damage.

Materials and Methods: Wistar albino male rats were divided into three experimental groups: control, HFD and HFD+MC. Experimental groups were fed a standard diet (control group) or HFD (HFD and HFD+MC groups) for 16 weeks. MC extract (100 mg/kg) was administered to the HFD+MC group orally during the last 4 weeks (5 days/week) of the experiment. High-density lipoprotein, total cholesterol, triglyceride and leptin levels were measured in blood serum. Tissue malondialdehyde (MDA), glutathione (GSH), 8-hydroxy-2'-deoxyguanosine (8-OHdG) and myeloperoxidase (MPO) levels were evaluated biochemically. Kidney and bladder morphology, NADPH oxidase-2 (NOX-2) and nuclear factor-kappa B (NF-κB)-positive and apoptotic cells were evaluated histologically.

Results: Lipid profiles altered and leptin levels increased in blood serum. MDA, 8-OHdG and MPO levels increased and GSH level decreased in kidney and bladder in the HFD group. Moreover, degenerated kidney and bladder morphology, increased NOX-2 and NF-κB-positive and apoptotic cells were observed in this group. All of these biochemical and histological parameters were ameliorated in the HFD+MC group.

Conclusion: HFD-induced obesity causes kidney and bladder damage by oxidative and inflammatory processes. MC extract may reduce oxidative stress and inflammation and play a protective role in obesity-related kidney and bladder damage.

Keywords: High fat diet, *Myrtus communis* L. extract, kidney, bladder, oxidative stress, inflammation

INTRODUCTION

The number of overweight and obese individuals is rising in the world. Obesity has a complex etiology, with various factors to consider, including changes in eating

habits, such as high-fat diet (HFD) consumption (1,2). HFDs, mainly involving high saturated fatty acid consumption, affect weight gain and finally lead to obesity (3). Obesity is associated with the development of many diseases, including cardiovascular diseases, type



Corresponding Author: Feriha Ercan

E-mail: eferiha@hotmail.com; fercan@marmara.edu.tr

Submitted: 29.04.2022 • **Accepted:** 17.08.2022 • **Published Online:** 02.12.2022



2 diabetes, metabolic disorders, chronic kidney disease (CKD), overactive bladder syndrome and bladder cancer (2,4-7). Obesity has been shown to increase reactive oxygen species (ROS) (6,8,9). Gradual mitochondrial damage in the kidney and the bladder due to HFD feeding causes loss of efficiency of the electron transport chain, further increasing ROS production, decreasing ATP production, and causing cell dysfunction (9,10). Therefore, oxidative stress, including various reactive oxygen and nitrogen species, has an important role in the pathophysiology of HFD-induced urinary tract damage (9). An increase in NADPH oxidase (NOX), as a major source of the ROS, has been demonstrated to trigger renal inflammation (11) and transforming growth factor (TGF)- β 1 mediated fibrosis (12).

Long-term hyperlipidemia due to HFD causes tissue damage in a variety of organs and systems, often resulting in significant diseases and production of ROS (13). In the course of HFD-induced obesity progression, perirenal fat accumulation directly affects renal function with the increased numbers of macrophages in adipose tissue that cause higher levels of the secretion of proinflammatory cytokines, such as tumor necrosis factor- α (TNF- α) and interleukin-6 (IL-6) (14-16). Hypertrophy of adipose tissue causes inflammation, oxidative stress and insulin resistance through numerous adipokines such as leptin, which causes inflammation in the kidney and the bladder (17,18). Studies have shown that leptin-mediated oxidative damage and mesangial cell inflammation develop in the kidney when HFD has been established (11), together with the detrusor muscle hypertrophy, collagen deposition and epithelial hypertrophy that occur in the bladder (17,19). Lower urinary tract dysfunctions associated with obesity have been shown in both experimental animals and humans (20,21). Neuronal alterations are also mentioned in addition to urothelial and detrusor smooth muscle changes for the obesity related bladder dysfunctions (22).

Herbal medicine including flavonoids and essential oils via the antioxidative and anti-inflammatory activity may have many positive effects for the prevention and treatment of the many diseases associated with obesity, including CKD (23). *Myrtus communis* L. subsp. *communis* (MC), a plant of the Myrtaceae family, has been utilized for antihypertensive, antitussive, antiemetic, diuretic, antidiarrheic, cardiostimulant, antidiabetic, antioxidant and anti-inflammatory purposes (24-26). MC fruits and leaves contain phenolic acids, flavonoids, essential oils, alkaloids, lignans and vitamins (27,28). In several experimental studies, such as on colonic inflammation, hepatic and pulmonary fibrosis and renovascular hypertension, myrtucommulone and semimyrtucommulone extracted from MC leaves were demonstrated to exhibit antioxidant and anti-inflammatory activities (29-33).

Based on the above findings, we aimed to investigate the possible protective effects of MC on kidney and bladder damage caused by HFD-induced obesity via biochemical and histological analysis. Lipid profile and leptin level in the blood serum and oxidative damage parameters in the renal and bladder ho-

mogenates were measured using biochemical methods. Renal and bladder morphology, apoptotic, NOX-2 and nuclear factor kappa B (NF- κ B)-positive cells were evaluated using histological and immunohistochemical methods.

MATERIALS AND METHODS

Animals and Experimental Groups

Wistar albino male rats (8-week-old, 250–300 g), taken from the Marmara University Animal Center (DEHAMER) were kept in a laboratory environment with a standard light/dark (12/12 hour) cycle, temperature (22 \pm 2°C) and humidity (65-70%) for the duration of this study. The animals drank tap water *ad libitum*. This study was approved by The Animal Care and Ethical Committee for Experimental Animals at Marmara University (10.2020.mar). Three experimental groups (n=8, in each) were set up in the study: control, HFD and HFD+MC groups. The rats in the control group were fed with standard lab chow. The rats in HFD and HFD+MC groups were fed with HFD (45%) for 4 months. Saline or MC extract (dissolved in saline, 100 mg/kg/day) was given orally by gavage five days a week for the last month of the experiment to the animals in HFD and HFD+MC groups. The MC dose was chosen according to the previous studies (34, 35). The rats' weight was measured weekly during the experiment. The rats were decapitated under light ether anesthesia and trunk blood and kidney and bladder samples were obtained at the end of the 4th month. Serum, kidney and bladder samples were kept at -20°C until biochemical analyses were performed.

Preparation of MC Extract

MC leaves were collected from the Turgutlu region of Manisa, Turkey and defined by botanist Dr. Gizem Bulut. Voucher specimens were kept in the herbarium in the Herbarium of the School of Pharmacy, Marmara University (MARE No: 13006). MC extract was prepared according to a previous study (35). MC leaves (100 g) were dried in the shade at room temperature. The dried powdered leaves were extracted with 96% ethanol using the Soxhlet device. After filtration, the extract was concentrated using a rotary evaporator. The MC extract powder obtained with a yield of 28.56% was kept in a dark glass bottle at 4°C until use.

Measurement of Serum High-Density Lipoprotein, Total Cholesterol, Triglyceride and Leptin Levels

High-density lipoprotein (HDL), total cholesterol, triglyceride and leptin levels were analyzed using enzyme-linked immunosorbent assay (ELISA) kits (Elabscience, Wuhan, China) in the serum. The results were given as ng/ml for HDL, triglyceride and leptin and mmol/L for total cholesterol.

Measurement of Malondialdehyde, Glutathione, 8-Hydroxy-2'-Deoxyguanosine Levels and Myeloperoxidase Activity

The malondialdehyde (MDA), glutathione (GSH) and 8-hydroxy-2'-deoxyguanosine (8-OHdG) levels and myeloperoxidase (MPO) activity were measured in kidney and bladder homogenates using commercial ELISA kits (MyBioSource, Southern California, San Diego USA). The results were given as nmol/g for MDA and GSH, ng/mg for 8-OHdG and U/ml for MPO.

Light Microscopic Preparation

The kidney and bladder samples were fixed with 10% formalin, dehydrated in ascending alcohol series, cleared in toluene and embedded in paraffin. Paraffin sections (5 µm-thick) were stained using hematoxylin and eosin (H&E) for histopathological evaluation, picrosirius red for collagen distribution and acidified toluidine blue (pH 2.5, TB) for mast cell distribution. All stained sections were examined under a photomicroscope (Olympus BX51, Tokyo, Japan). For both samples at least 5 similar microscopical areas were evaluated semi quantitatively in H&E stained sections according to a histopathological scoring system. Scores were given as 0 – none, 1 – mild, 2 – moderate and 3 – severe for each criterion, using a semiquantitative scale as follows. In the renal tissue, (a) degeneration of glomerular structure and dilatation of Bowman's space, (b) degeneration of proximal and distal tubuli, (c) vascular congestion, interstitial edema and inflammatory cell infiltration; and in the urinary bladder (a) damage in urothelium, (b) inflammatory cell infiltration in mucosa, (c) inflammatory cell infiltration in mucosa and muscular layers (36,37). The maximum score was 9 for each tissue. Collagen distribution in picrosirius red-stained sections of both kidney and bladder and mast cell count in TB-stained sections of bladder were evaluated in five non-overlapping pictures from each section using ImageJ Software (version 1.52a, Wayne Rasband, National Institutes of Health, USA).

NOX-2 and NF-κB Immunohistochemistry

Paraffin sections were immersed in 3% hydrogen peroxide to block endogenous peroxidase activity, then microwaved in 10 mM sodium citrate (pH 6.0) for antigen retrieval. The sections were washed in phosphate buffered saline (PBS) and treated with protein blocking solution (EXPOSE Rabbit specific HRP/DAB Detection IHC Kit, Abcam, Cambridge, UK). The sections were then incubated with primary antibodies (NOX-2, 1:200, Bioss; NF-κB, 1:1000, Cell Signalling Technology, Massachusetts, USA) at 4 °C overnight. After washing in PBS, the sections were treated with a biotinylated secondary antibody (20 min, ScyTek, USA) and HRP-conjugated streptavidin (20 min, Santa Cruz, USA) at room temperature. The slides were washed and then treated with 3.30-diaminobenzidine chromogen (5 min) and then stained with hematoxylin. Five similar, randomly chosen areas were photographed in the NOX-2 and NF-κB were measured by using ImageJ Software (version 1.52a, Wayne Rasband, National Institutes of Health, USA).

Terminal Deoxynucleotidyl Transferase dUTP Nick End Labelling Analysis

A terminal deoxynucleotidyl transferase dUTP nick end labelling (TUNEL) kit (ApopTag Plus, In Situ Apoptosis Detection Kit, S7101, Millipore) was used for determination of apoptotic cells. TUNEL-positive cells were counted by examining five randomly chosen similar areas in the sections using ImageJ Software (version 1.52a, Wayne Rasband, National Institutes of Health, USA).

Statistical Analysis

Analysis was evaluated by an instant statistical analysis pack-

age (Prism 6.0 GraphPad Software, San Diego, CA, USA). All parameters were analyzed using a one-way analysis of variance (ANOVA). Tukey's multiple comparisons test was used for the determination of differences between groups. The data were conveyed as mean ± standard error of the mean (SEM). Significance was accepted at the $p < 0.05$ level.

RESULTS

Body weight results

The body weight of rats in the experimental groups was higher in the HFD group ($p < 0.001$) than the control and HFD+MC groups at the end of the study (Figure 1).

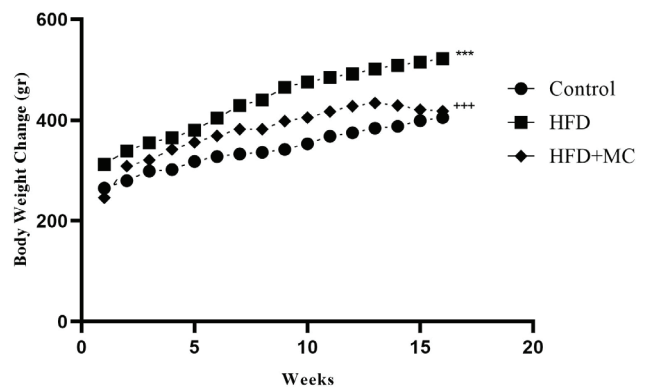


Figure 1. Weekly body weight results of the experimental groups.

*** $p < 0.001$ compared to the control group, +++ $p < 0.001$ compared to HFD group.

Serum HDL, Cholesterol, Triglyceride and Leptin Level Results

Serum HDL level decreased in the HFD group ($p < 0.001$) compared to the control group and decreased in the HFD+MC group ($p < 0.01$) compared to the HFD group. However, total cholesterol ($p < 0.001$) and triglyceride ($p < 0.001$) levels increased in the HFD group compared to the control group and total cholesterol ($p < 0.001$) and triglyceride ($p < 0.001$) levels reduced in the HFD+MC group compared to the HFD group. Moreover, leptin level was higher in the HFD group than the control group and lower in the HFD+MC group ($p < 0.001$) compared to the HFD group (Figure 2).

MDA, GSH, 8-OHdG and MPO Level Results

Kidney MDA ($p < 0.001$), 8-OHdG ($p < 0.001$) and MPO ($p < 0.01$) levels were higher and GSH ($p < 0.01$) level was lower in the HFD group than the control group. However, MDA ($p < 0.001$), 8-OHdG ($p < 0.001$) and MPO ($p < 0.01$) levels were lower and GSH level ($p < 0.01$) was higher in the HFD+MC group than the HFD group in kidney homogenates. Additionally, bladder MDA ($p < 0.001$), 8-OHdG ($p < 0.001$) and MPO ($p < 0.001$) levels elevated and GSH ($p < 0.001$) level reduced in the HFD group compared to the control group. However, MDA ($p < 0.001$), 8-OHdG ($p < 0.01$) and MPO ($p < 0.01$) levels were significantly re-

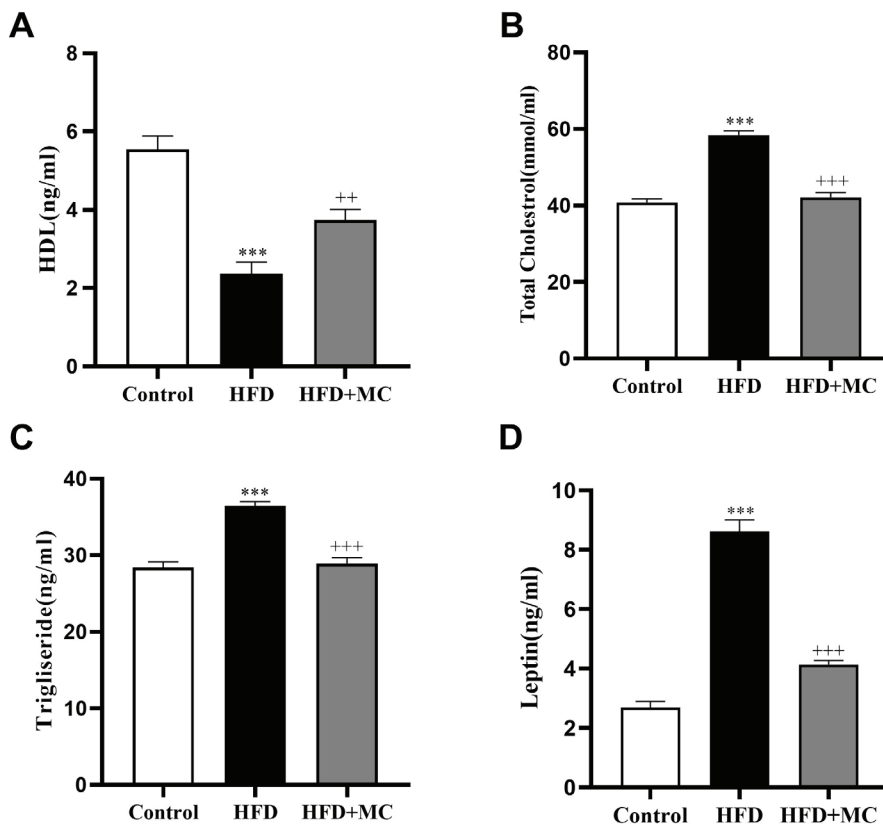


Figure 2. Serum HDL (A), total cholesterol (B), triglyceride (C) and leptin (D) levels of the experimental groups.

***p<0.001 compared to the control group, **p<0.01 and +++p<0.001 compared to the HFD group.

duced and GSH level ($p<0.001$) was elevated in the HFD+MC group compared to the HFD group in bladder homogenates (Figure 3).

Histopathological Findings

Histological evaluation of the kidney showed that regular renal corpuscles, proximal and distal tubuli and interstitial connective tissue with collagen distribution were present in the control group. However, degenerated renal corpuscles with dilatation of Bowman space, glomerular and vascular congestion, degenerated proximal and distal tubuli with luminal cellular debris and increase of collagen deposition were observed in the HFD group. All these histopathological findings decreased in HFD+MC group. Renal histopathological score and collagen deposition were significantly elevated in the HFD group ($p<0.001$) compared to the control group. Both histopathological score ($p<0.001$) and collagen deposition ($p<0.01$) were significantly reduced in the HFD+MC group compared to the HFD group (Figure 4).

Histological evaluation of the bladder showed that regular mucosa with urothelium and muscular layer, collagen distribution in both mucosa and muscular layers and a small number of mast cells in mucosa were present in the control group. Degenerated urothelium in the local area, vascular congestion and inflamma-

tory cell infiltration in mucosa, increase of collagen deposition in both mucosa and the muscular layer and increased number of mast cells were observed in the HFD group. All these histological alterations were ameliorated in the MC applied HFD group. Bladder histopathological score ($p<0.001$), collagen deposition ($p<0.001$) and mast cell number ($p<0.05$) increased in the HFD group compared to the control group. Histopathological score ($p<0.001$), collagen deposition ($p<0.01$) and mast cell number ($p<0.05$) decreased in the HFD+MC group compared to the HFD group (Figure 5).

NOX-2 and NF κ B Immunohistochemistry Results

In the kidney, NOX-2 and NF κ B-immunopositive cells were present in glomerular and tubular cells in the control group. Although NOX-2 and NF κ B-immunopositive glomerular and tubular cells increased in the HFD group, they were decreased in MC treated HFD-fed rats. The percentage of NOX-2 ($p<0.05$), and NF κ B ($p<0.001$) immunostained area increased in the kidney of the HFD group compared to the control group. However, the percentage of NOX-2 ($p<0.01$) and NF κ B ($p<0.05$) immunoreactive (ir) area decreased in the kidney of the HFD+MC group compared to the HFD group (Figure 6).

In bladder samples, NOX-2 and NF κ B-immunopositive cells were present in urothelium, blood vessels and smooth muscle

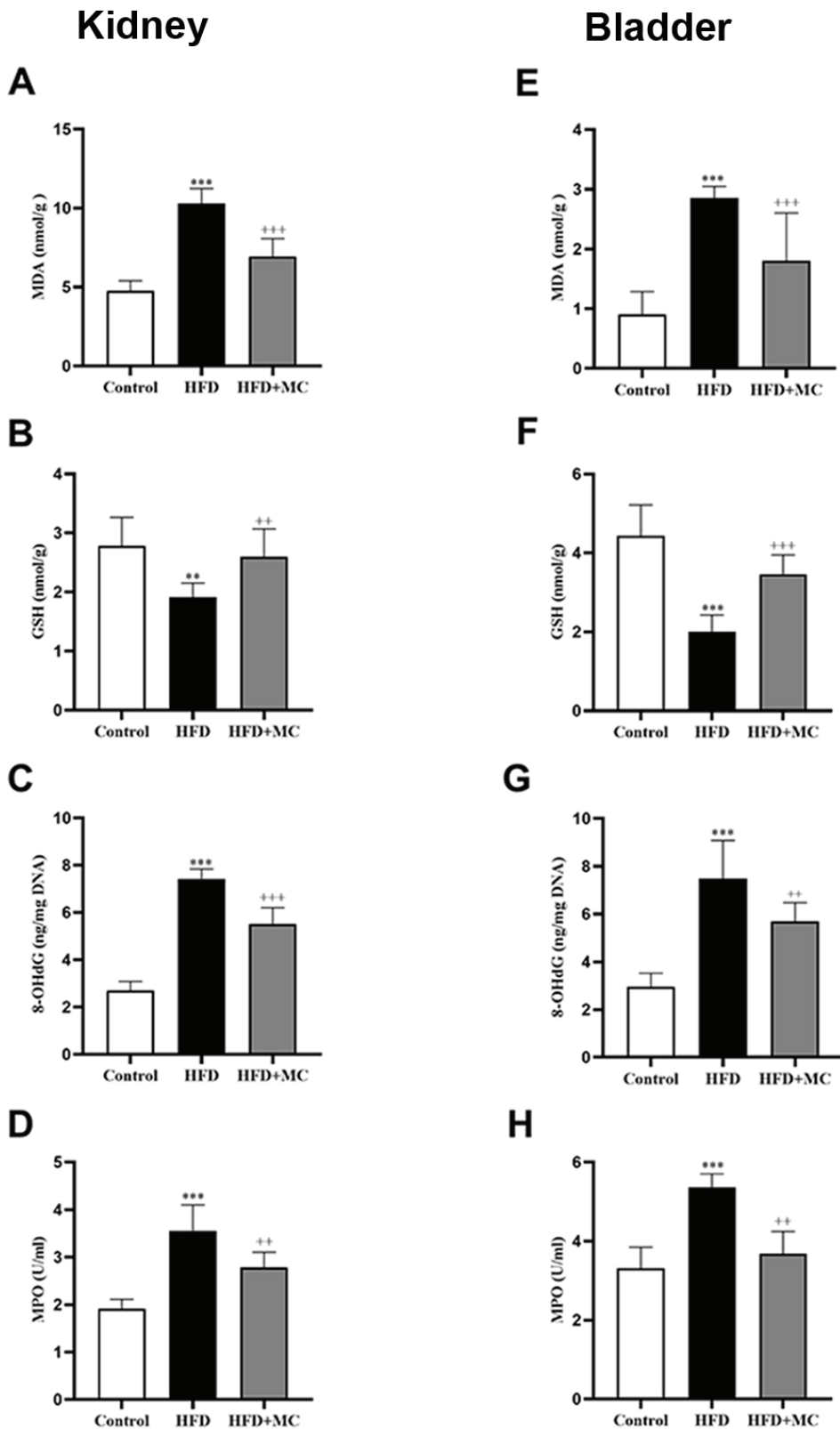


Figure 3. MDA (A, E), GSH (B, F), 8-OHdG (C, G) and MPO (D, H) levels in kidney and bladder homogenates of the experimental groups.

p<0.01 and *p<0.001 compared to the control group. ++p<0.01, +++p<0.001 compared to the HFD group.

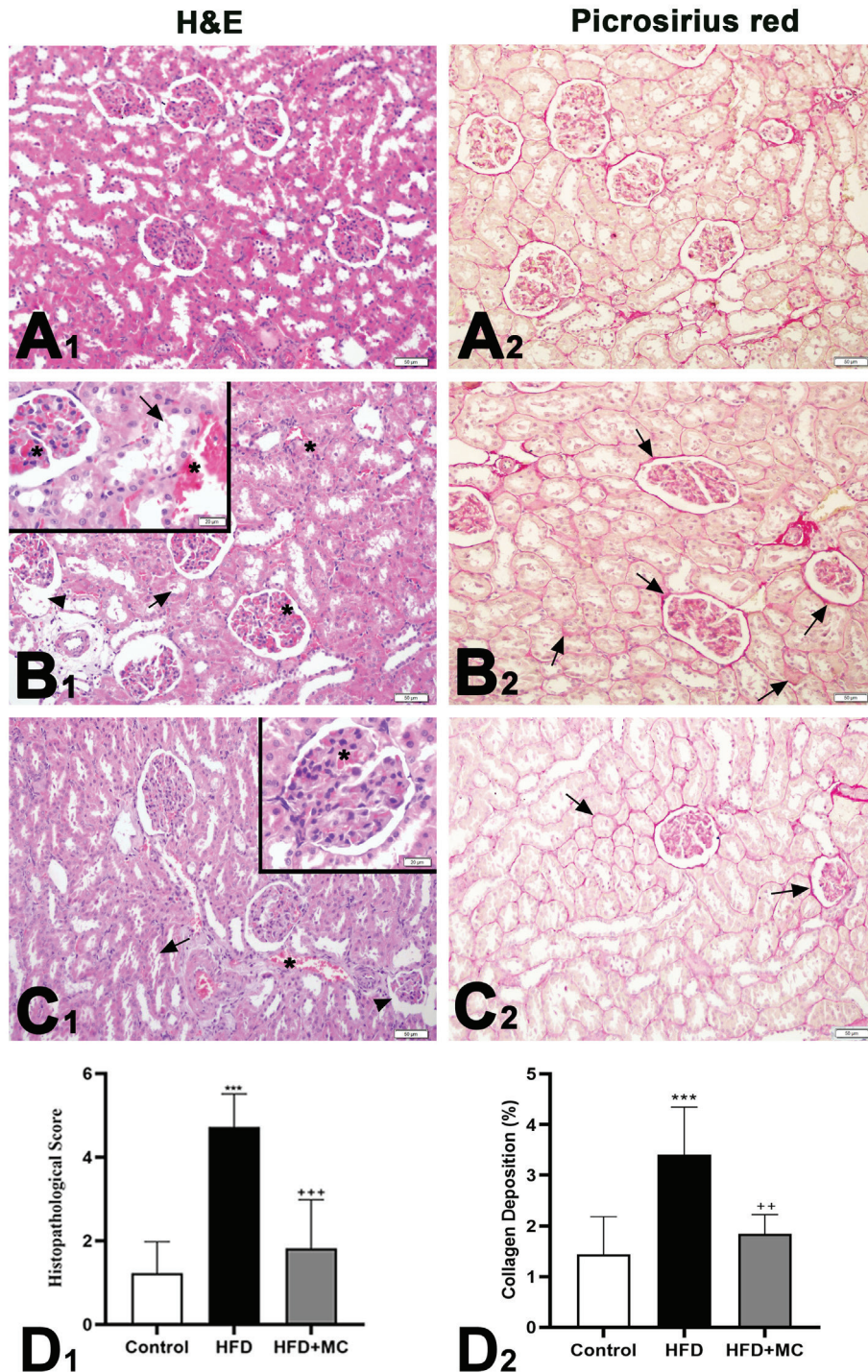


Figure 4. Representative H&E (A₁-C₁) and picrosirius red (A₂-C₂) stained light micrographs, histopathological score (D₁) and collagen deposition (D₂) of kidney in the experimental groups.

Regular renal corpuscles, and proximal and distal tubuli (A₁) and interstitial connective tissue with collagen distribution (A₂) are seen in the control group. Degenerated renal corpuscles with dilatation of Bowman space (arrowhead), glomerular and vascular congestion (*), degenerated proximal and distal tubuli (arrow) with luminal cellular debris (B₁) and increase of collagen deposition (B₂) are seen in the HFD group. Decrease of degenerated renal corpuscles with dilatation of Bowman space (arrowhead), glomerular and vascular congestion (*) and degenerated proximal and distal tubuli (arrow, C₁) and collagen deposition (C₂) are seen in the HFD+MC group. ***p<0.001 compared to the control group. **p<0.01 and ***p<0.001 compared to the HFD group. Scale bar: 50 μm, insets in B₁ and B₂: 20 μm.

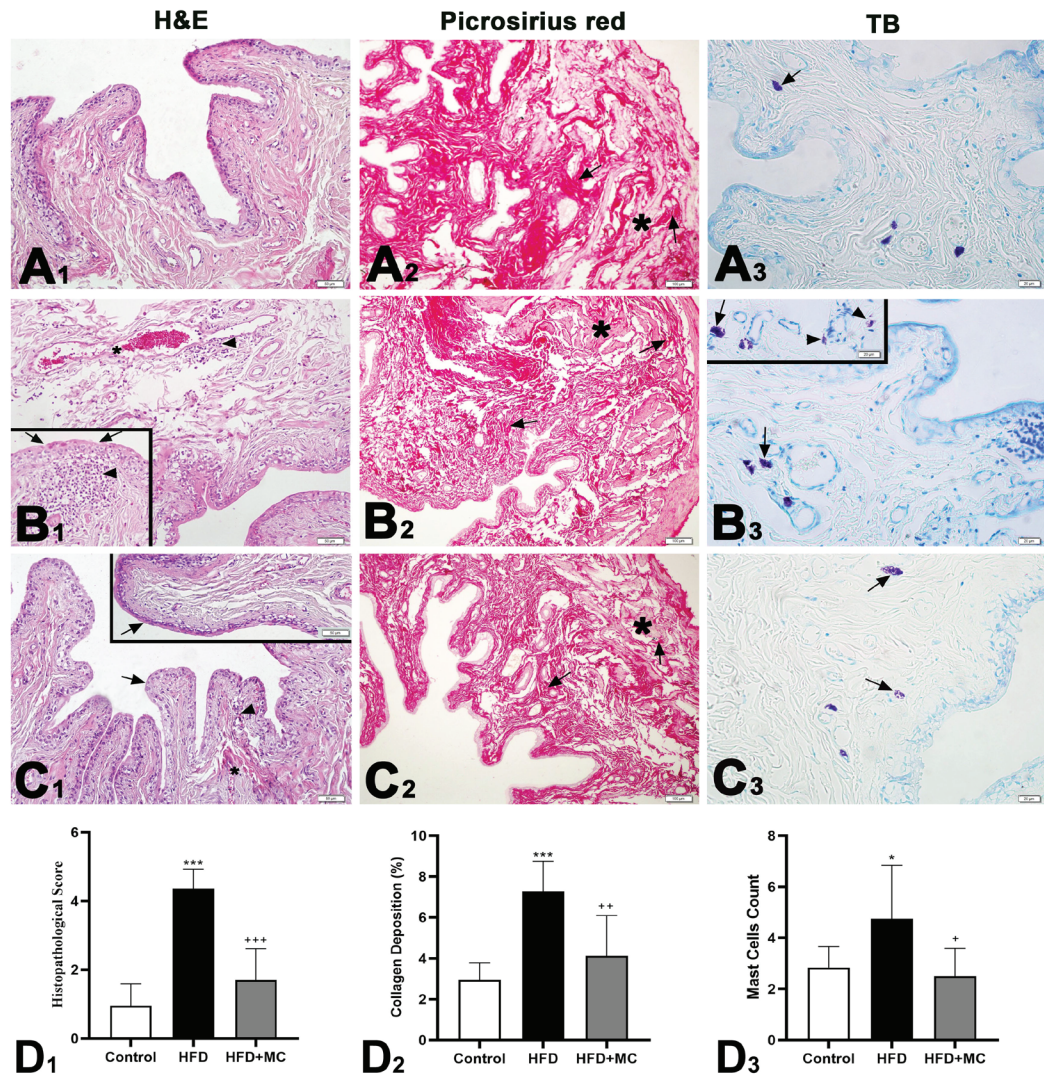


Figure 5. Representative H&E (A₁-C₁), picrosirius red (A₂-C₂) and TB (A₃-C₃) stained light micrographs, histopathological score (D₁), collagen deposition (D₂) and mast cell count (D₃) of bladder in the experimental groups.

Regular mucosal layer with urothelium and muscular layer (A₁), collagen distribution (A₂) in both mucosa and muscular layers and a few number of mast cells (A₃) in mucosa are seen in the control group. Degenerated urothelium in local area (arrow), vascular congestion (*) and inflammatory cell infiltration (arrowhead) in mucosa (B₁), increase of collagen deposition in mucosa (arrow) and around the muscle bundles (*, B₂) and increased granulated (arrow) and degranulated (arrowhead) mast cells (B₃) were observed in the HFD group. Quite regular urothelium (arrow), decreased inflammatory cells (arrowhead) and vascular congestion (*) in mucosa (C₁), decreased collagen distribution in mucosa (arrow) and around muscle bundle (*, C₂) and decreased mast cells (arrow) in mucosa (C₃) are seen in the HFD+MC group. *p<0.05 and ***p<0.001 compared to the control group. *p<0.05, **p<0.01 and ***p<0.001 compared to the HFD group. Scale bar: A₁-C₂: 50 μm; A₃-C₃ and inset in B₁ and C₁: 20 μm.

cells in the control group. However, NOX-2 and NFκB-immunostained urothelial cells, inflammatory cells, blood vessels and smooth muscle cells increased in the HFD group. NOX-2 and NFκB-immunostained cells decreased in the MC-treated HFD group. The percentage of NOX-2 (p<0.05) and NFκB (p<0.05) ir area increased in the bladder of the HFD group compared to the control group. However, percentage of NOX-2 (p<0.05) and NFκB (p<0.01) ir area increased in the bladder of the HFD+MC group compared to the HFD group (Figure 7).

TUNEL Analysis Results

A small number of TUNEL-positive cells in the kidney and the bladder were present in the control groups. TUNEL-positive cells increased in the kidney (p<0.05) and the bladder (p<0.001) of the HFD group compared to the control group. MC treatment in the HFD-fed rats reduced the TUNEL-positive cell number in the kidney (p<0.05) and the bladder (p<0.001) compared to the HFD group (Figure 8).

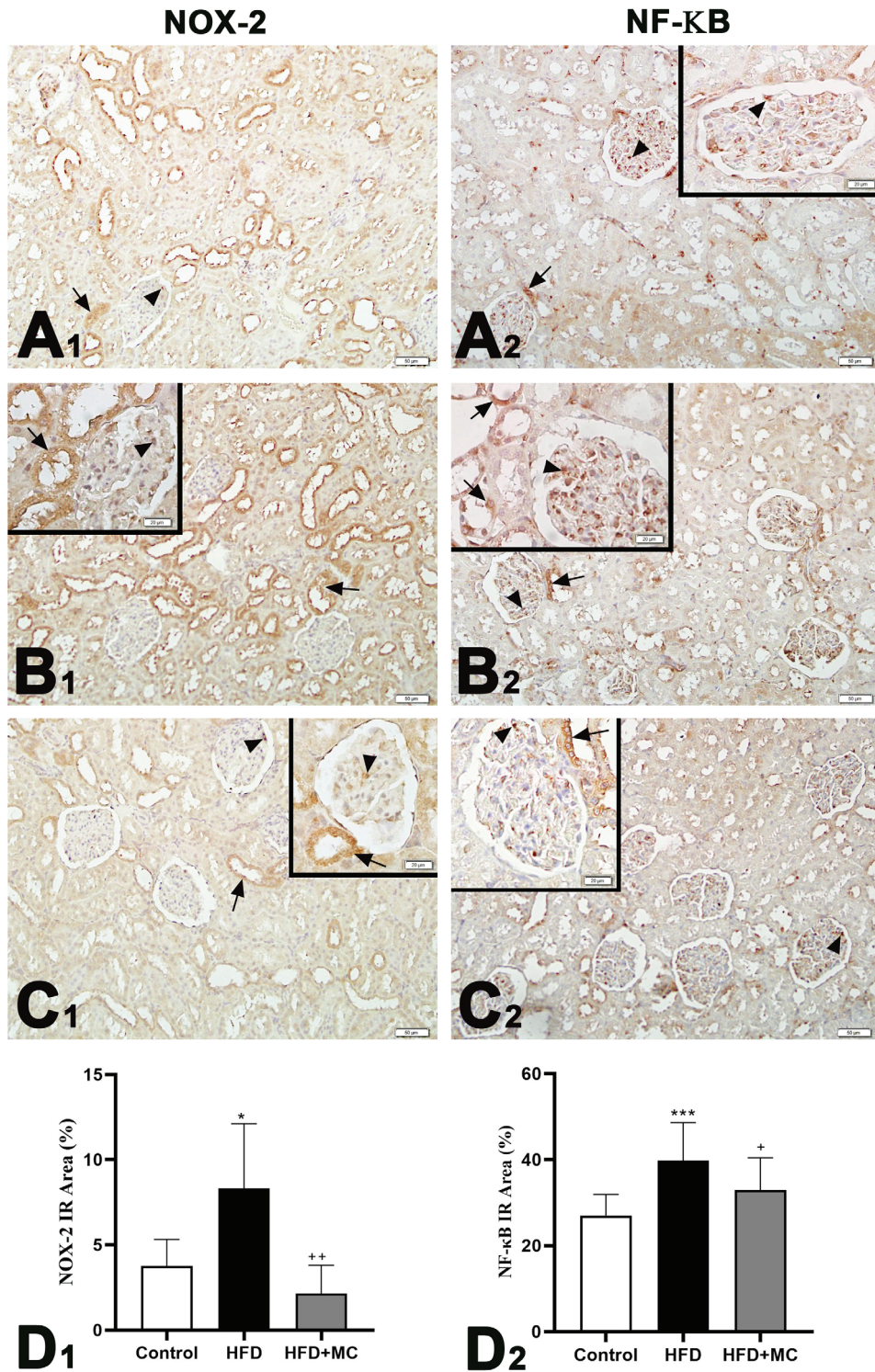


Figure 6. Representative NOX-2 (A₁-C₁) and NF-κB (A₂-C₂) immunostained light micrographs, percentage of NOX-2-ir area (D₁) and percentage of NF-κB-ir area (D₂) of kidney in the experimental groups.

NOX-2 (A₁) and NF-κB (A₂) immunopositive glomerular (arrowhead) and tubular (arrow) cells are seen in the control group. Increased NOX-2 (B₁) and NF-κB (B₂) immunopositive glomerular (arrowhead) and tubular (arrow) cells are seen in the HFD group. Decreased NOX-2 (C₁) and NF-κB (C₂) immunopositive glomerular (arrowhead) and tubular (arrow) cells are seen in HFD+MC group. *p<0.05 and ***p<0.001 compared to the control group. *p<0.05 and **p<0.01 compared to the HFD group. Scale bar: A₁-C₂: 50 μm; inset in B₁- C₂: 20 μm.

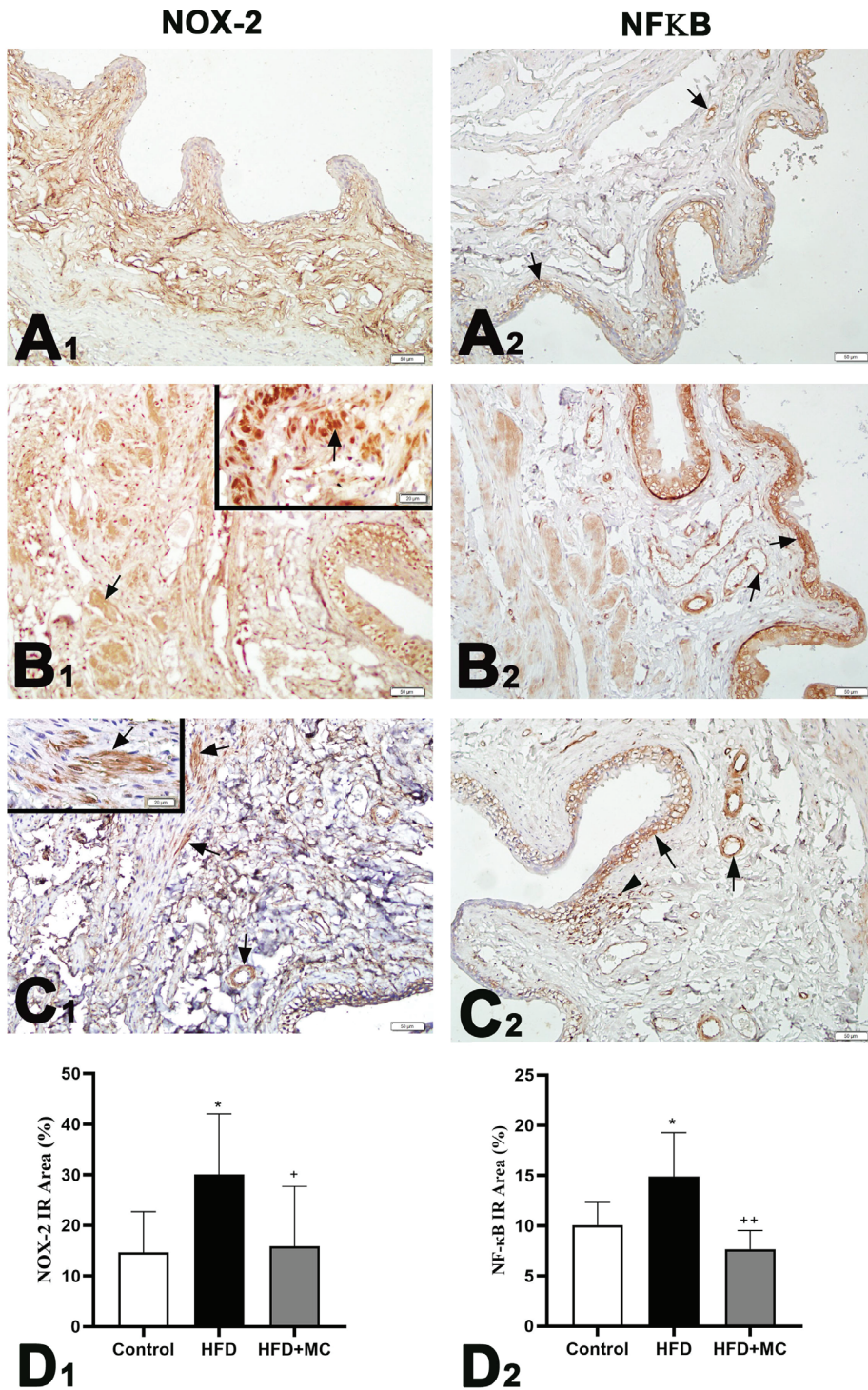


Figure 7. Representative NOX-2 (A₁-C₁) and NF-κB (A₂-C₂) immunostained light micrographs, percentage of NOX-2-ir area (D₁) and NF-κB-ir (D₂) area of bladder in the experimental groups.

NOX-2 (A₁) and NF-κB (A₂) immunopositive cells (arrow) are seen in the control group. Increased NOX-2 immunopositive muscle cells (arrow) and inflammatory cells (inset arrow, B₁) and NF-κB (B₂) immunostained (arrow) urothelial cells and blood vessels are seen in the HFD group. Decreased NOX-2 immunostained (arrow) blood vessels and smooth muscle cells (inset, C₁) and NF-κB immunostained (C₂) urothelial cells and blood vessels (arrow) and inflammatory cells (arrowhead) are seen in the HFD+MC group. *p < 0.05 compared to the control group. *p < 0.05 and **p < 0.01 compared to the HFD group. Scale bar: A₁-C₂: 50 μm; inset in B₁ and C₂: 20 μm.

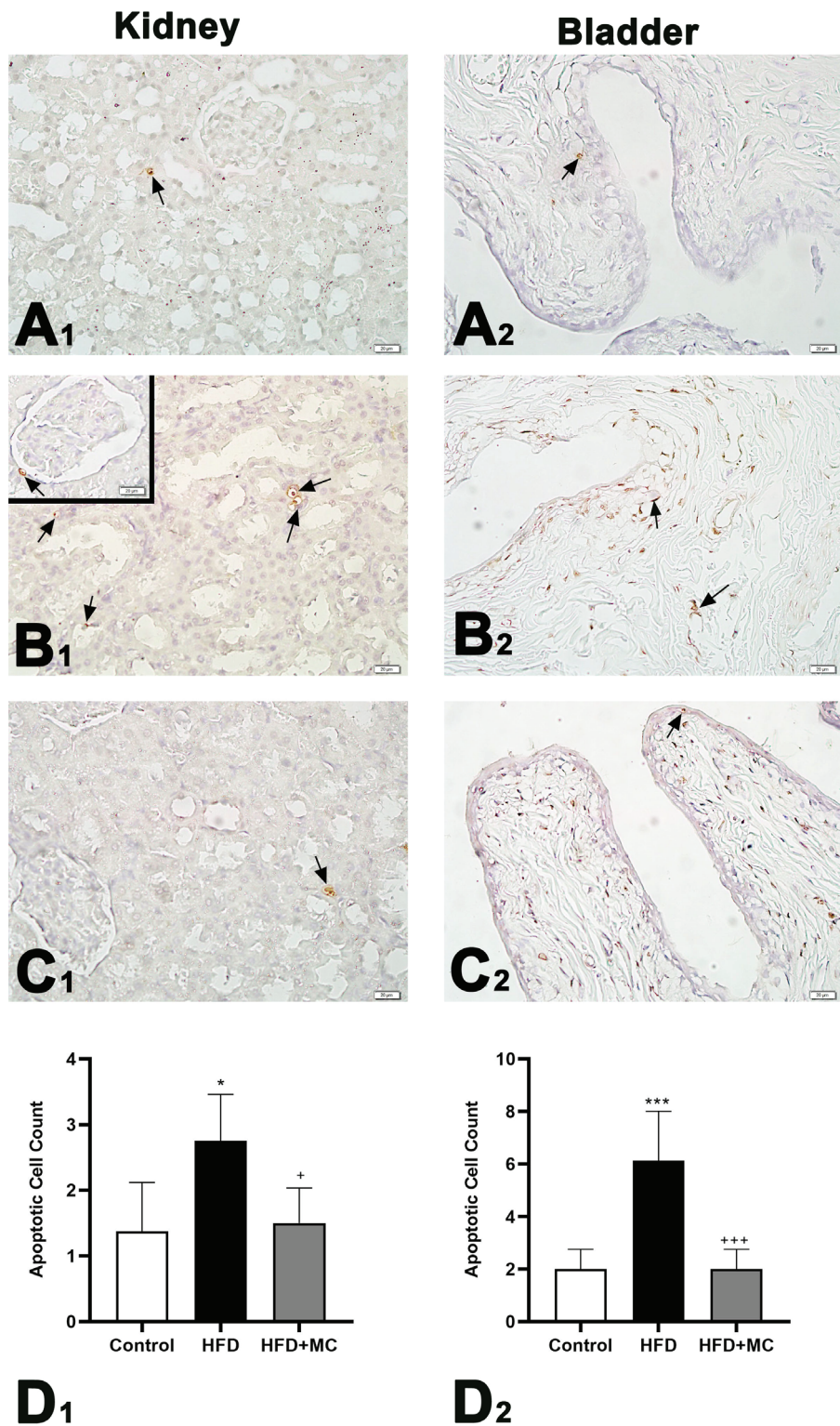


Figure 8. Representative TUNEL stained (A₁-C₂) light micrographs, apoptotic cell count of kidney (D₁) and bladder (D₂) in the experimental groups.

TUNEL positive cells (arrow) are seen in kidney (A₁) and bladder (A₂) of the control group. Increased TUNEL-positive cells (arrow) are seen in kidney (B₁) and bladder (B₂) of the HFD group. Decreased TUNEL-positive cells (arrow) are seen in kidney (C₁) and bladder (C₂) of the HFD+MC group. *p<0.05 and ***p<0.001 compared to the control group. +p<0.05 and ***p<0.001 compared to the HFD group. Scale bar: A₁-C₂: 20 μm

DISCUSSION

According to the findings of this study, increased body weight, hyperlipidemia and hyperleptinemia were observed in the HFD group. Additionally, increased renal and bladder MDA, 8-OHdG and MPO levels and decreased antioxidant GSH level were found in the HFD group. Parallel with the biochemical results, increased renal and bladder histopathological damage with the increase of NOX-2 and NF- κ B-positive cells and apoptotic cells were observed in this group. However, all these HFD-associated changes of serum lipid parameters, leptin level, renal and bladder histopathological damage and oxidative stress parameters were ameliorated by the MC extract treatment.

A body mass index over 30 kg/m² in adults is defined as obese. Obesity is the underlying cause of many diseases such as metabolic syndrome, type 2 diabetes, cardiovascular diseases, non-alcoholic fatty liver disease, CKD, overactive bladder and various cancers (2,4-7). Studies in rodents have shown that body weight increases as a result of HFD feeding (19,38-42). For controlling body weight and to prevent obesity related diseases, it is recommended to change lifestyle through physical activity and eating a low calorie diet containing more vegetables and fruits (2). Parallel to the previous studies that have shown the anti-obesity activity of MC extract (40,43), our study showed that body weight increased in HFD-fed rats and MC administration reduced body weight in the HFD-fed rats.

Increased free fatty acids in the blood and accumulation of white adipose tissue are associated with obesity (6). Adipose tissue accumulates fatty acid level increased in the blood and as a result, hypertrophy and hyperplasia of adipose tissue appear. Studies have revealed that serum cholesterol and triglyceride levels increase and HDL level decrease due to HFD feeding (38-40,42). CD36 receptor was also shown to accompany lipid uptake in the kidney. It was stated that no lipid accumulation occurred in mice with CD36 mutation and that no mitochondrial ROS form due to lipid accumulation in the kidney tubule epithelium and podocyte, thus apoptosis was not observed (8,44). In another study, it was found that free fatty acids in the human detrusor muscle cell line have a negative effect on the M3 receptor in these cells, causing a decrease in the contraction force of the bladder muscle (21). These studies demonstrate that the urinary system is sensitive to lipid toxicity. It has been shown that essential oils of MC have positive effects for the reduction of the total cholesterol and antioxidant capacity in most organs including kidney (25), and polyphenolic components (myricetin-3-O-rham, myricetin-3-O-gallac, miricetin, 5-O-galloyl quinic acid and etc.) of MC aqueous extract (100mg/kg) have positive effects on rat health by increasing the Lactobacilli and Bifidobacteria colonies and antioxidative activity (27). Moreover, hypolipidemic effects of MC fruits in streptozotocin-induced diabetic rats (45) and MC L. extract in HFD-fed rats (40) have been revealed. Parallel to the previous studies, increase of serum cholesterol and triglyceride levels and decrease of HDL level as well as renal and bladder damage were observed in the HFD group, however MC administration ameliorated serum lipid profiles and tissue damage.

Obesity has been shown to be a state of hyperleptinemia (46). Leptin, one of the adipokines secreted by hypertrophic adipose tissue, binds directly to the leptin receptor (OB-R) in the central nervous system and peripheral tissue. Although the main function of leptin is appetite control, it has been shown that it has receptors in peripheral tissues such as kidney and bladder, and it activates NF- κ B with a paracrine effect (47). Elevated serum leptin levels have been known to cause mesangial cell activation and tubular inflammation via the NOX-2 dependent pathway in HFD-induced non-alcoholic fatty liver disease. It was also shown that there is no renal inflammation in leptin and NOX-2 knockout mice (11). Body weight gain, hyperlipidemia and elevated serum TNF- α levels associated with increased bladder protein kinase C ζ phosphorylation, NF- κ B nuclear migration and impaired muscle contractility have been demonstrated in HFD-fed mice (39). In this study, in addition to the increase in serum leptin level, increased NOX-2 and NF- κ B immunopositive cells and MPO level in kidney and bladder were also observed. MC administration reduced the leptin level in blood serum as well as inflammatory markers in both kidney and bladder.

It has been reported that as a result of an excessively lipid-rich diet, free fatty acids in the circulation cause the capacity of adipose tissue to be exceeded and accumulate in ectopic organs such as kidney (48,49). Studies have shown that free fatty acids found in high levels in the serum and the tissues are important as they may cause oxidative stress in the body. In addition, it has been established that kidney tubule epithelial cells rich in mitochondria and bladder muscle cells are sensitive to oxidative stress (49,50). HFD-induced obesity leads to kidney and bladder damage and increase of MDA, IL-6 and TNF- α levels and decrease of GSH and superoxide dismutase levels (51). Furthermore, a high-fat/high-sugar diet has been shown to induce metabolic syndrome, a decrease in glomerular filtration rate, renal tubular injury and increased oxidative stress in the renal cortex (48). In another study, MC treatment reduced the MDA level and increased GSH level and superoxide dismutase and catalase activities in the kidney of animals with renovascular hypertension (32). In this study, an increase of MDA and decrease of endogenous GSH levels in the kidney and the bladder in the HFD group were noted. On the other hand, MC administration decreased the oxidative stress parameters in both renal and bladder homogenates due to the strong antioxidant compounds content.

As a result of DNA damage, which becomes another target in the increase of ROS, mutation, misreplication, apoptosis or cancer formation are observed (52). The oxidative DNA damage was determined by the measurement of 8-OHdG level (53). It has been stated that the increased level of 8-OHdG in the HFD-induced obesity triggers apoptosis (8,42,51,54). Additionally, it was observed that as a result of 23-month-long high fat/high sucrose intake, GSH level and proliferative cells decreased, and TNF- α , NF- κ B, caspase-3 and apoptotic cells increased in kidney together with high serum lipids in Bama minipigs (55). Moreover, tubular degeneration with degenerated mitochondria in the kidney of the HFD-fed mice (54) and glomerular basement

membrane thickening and podocyte degeneration with fusion of foot processes in HFD-fed rats (42) have been shown. In this study, we observed histopathological damage with glomerular and tubular degeneration in the kidney, urothelial degeneration and increase of inflammatory cells in the bladder, and increase of 8-OHdG level and apoptosis in renal and bladder samples of rats with four months of HFD feeding. Additionally, an increase of MDA and MPO levels and NF- κ B-positive cells in both kidney and bladder samples in this group were observed. However, MC treatment reversed the oxidative stress, apoptosis and inflammation in the HFD-fed rats.

It has been shown that oxidative stress causes damage not only by stimulating the inflammatory response but also by stimulating the inflammatory response in the formation of organ damage seen in obesity (56). MPO, a heme protein produced by neutrophils, is a chlorinating enzyme that initiates the response in acute inflammation and plays a role in the spread of chronic inflammation through the production of ROS such as NOX (57). It was shown that neutrophils infiltrate into adipose tissue in the early stage of HFD, and release of oxidant and inflammatory substances such as ROS, TNF- α and MPO occur (58). Increase of neutrophils in obese people and type 2 diabetic patients is also shown. Furthermore, it was stated that there was a positive correlation between MPO activation and metabolic disorders and MPO plasma level was higher in obese patients (59). NF- κ B is a family of inducible transcription factors that mediate signal-induced expression of several genes involved in immunity, inflammation, and cell growth. NF- κ B is shown to be activated by pathophysiological processes in TNF- α and angiotensin II cascades in kidney and is associated with experimental and human kidney disorders. NF- κ B inhibitors have been reported to prevent renal inflammation in experimental animals. Additionally, NF- κ B inhibitors have been reported to prevent renal inflammation in experimental animals (60). It has been established that elevated serum leptin causes inflammation in mesangial cells in HFD-induced kidney damage (11). Increased oxidative stress, NF- κ B activation and elevated inflammatory response were observed in HFD-induced nephropathy of mice (61). In another study, it was shown that NF- κ B expression and fibrosis in the bladder were increased in mice of cyclophosphamide-induced chronic cystitis model as a result of inflammation (17). It has been stated that the increase in ROS in the heart and aorta of HFD-induced obese rats contributes to inflammation by causing high MPO levels. Also, increased mast cell activation in the heart was observed in the HFD-fed rats (38). It has been found that HFD feeding increases mast cell infiltration in the rat mesentery (62). In another study, increased apoptotic and mast cells in the bladder of diabetic patients with overactive bladder were shown (63). Activated mast cells release many chemokines, histamine and proteases as well as proinflammatory cytokines, which activate the ROS formation. Parallel with the previous studies, the increase of MPO level and NF κ B-positive cells in both kidney and bladder and increase of mast cells in bladder of the HFD group were observed. MC treatment reduced these inflammatory markers in both kidney and bladder of the HFD-fed rats by inhibition of ROS generation.

Long-chain saturated fatty acids accumulate in various cells in the kidney, causing an increase in the production of ROS, which triggers glomerular mesangial cell inflammation through proinflammatory cytokines such as TNF- α , IL-6 and NF- κ B and causes interstitial matrix fibrosis by TGF- β 1 signaling (8,41). It has been revealed that free fatty acids trigger fibrosis in the detrusor muscle cell line and cause a decrease in the contraction force of the bladder muscle (21). It has been shown that there is an increase in glomerular and interstitial collagen in the kidney as a result of NOX-2-related oxidative damage (64). In another study, increase of collagen has been noted between muscle bundles of the bladder in HFD-induced obesity (19). Parallel with the previous studies, increase of collagen in interstitial connective tissue and around the glomeruli in kidney and between the muscle bundles in bladder and increase of MDA level and NOX-2 positive cells in both kidney and bladder were observed in the HFD group. MC treatment ameliorated the fibrosis in both kidney and bladder samples via the inhibition of ROS formation.

CONCLUSION

HFD-induced obesity causes hyperlipidemia and hyperleptinemia, renal and bladder fibrosis, increased oxidative, inflammatory and apoptotic activities and decreased endogenous antioxidant activity. However, MC administration improved serum lipid and leptin levels, fibrosis, oxidative damage via the reduction of MDA and 8-OHdG levels and NOX-2-immunopositive cells, elevation of endogenous antioxidant GSH level, inflammatory activity via the reduction of MPO activity and NF- κ B-immunopositive cells and apoptotic activity in both kidney and bladder samples. The antioxidative and anti-inflammatory activity of MC treatment appear to be important for the protective effects of MC on HFD-induced renal and bladder injury, however, defining these effects of MC requires further studies with advanced molecular and biochemical techniques to show possible therapeutic use.

Acknowledgement: The authors would like to thank Dr. Gizem Emre for her help in identification of the plant material.

Ethics Committee Approval: This study was approved by the Marmara University Animal Research Local Ethics Committee (10.2020.mar).

Informed Consent: Written consent was obtained from the participants.

Peer Review: Externally peer-reviewed.

Author Contributions: Conception/Design of Study- F.K.M., F.E.; Data Acquisition- F.K.M., B.E., A.S., D.A., G.Ş., F.E.; Data Analysis/Interpretation- F.K.M., B.E., D.A., G.Ş., F.E.; Drafting Manuscript- F.K.M., D.K., F.E.; Critical Revision of Manuscript- F.K.M., B.E., A.S., D.A., G.Ş., F.E.; Final Approval and Accountability- F.K.M., B.E., A.S., D.A., G.Ş., F.E.

Conflict of Interest: Authors declared no conflict of interest.

Financial Disclosure: This study was financially supported

by Marmara University, Scientific Research Project Committee (SAG-C-DRP-250919-0292).

REFERENCES

- Stein CJ, Colditz GA. The epidemic of obesity. *J Clin Endocrinol Metab* 2004; 89(6): 2522-5.
- World Health Organization. Obesity and overweight. 2021 June 9 (cited 2022 March 12). Available from: <https://www.who.int/news-room/fact-sheets/detail/obesity-and-overweight>
- Ding S, Fan Y, Zhao N, Yang H, Ye X, He D, et al. High fat aggravates glucose homeostasis by chronic exposure to bisphenol A. *J Endocrinol* 2014; 221: 167-79.
- Ejerblad E, Forel CM, Lindblad P, Fryzek J, McLaughlin JK, et al. Obesity and risk for chronic renal failure. *J Am Soc Nephrol* 2006; 17(6): 1695-702.
- Lin Y, Wang Y, Wu Q, Jin H, Ma G, Liu H, et al. Association between obesity and bladder cancer recurrence: A meta-analysis. *Clin Chim Acta* 2018; 480: 41-6.
- Manna P, Jain SK. Obesity, oxidative stress, adipose tissue dysfunction, and the associated health risks: causes and therapeutic strategies. *Metab Syndr Relat Disord* 2015; 13(10): 423-44.
- Kovesdy CP, Furth S, Zoccali C; World Kidney Day Steering Committee. Obesity and kidney disease: Hidden consequences of the epidemic. *Physiol Int* 2017; 104(1): 1-14.
- Hua W, Huang HZ, Tan LT, Wan JM, Gui HB, Zhao L, et al. CD36 mediated fatty acid-induced podocyte apoptosis via oxidative stress. *PLoS One* 2015; 10(5): e0127507.
- Lakkis JI, Weir MR. Obesity and Kidney Disease. *Prog Cardiovasc Dis* 2018; 61(2): 157-67.
- Powers SA, Ryan TE, Pak ES, Fraser MO, McClung JM, Hannan JL. Chronic high-fat diet decreased detrusor mitochondrial respiration and increased nerve-mediated contractions. *NeuroUrol Urodyn* 2019; 38(6): 1524-32.
- Alhasson F, Seth RK, Sarkar S, Kimono DA, Albadrani MS, Dattaroy D, et al. High circulatory leptin mediated NOX-2-peroxynitrite-miR21 axis activate mesangial cells and promotes renal inflammatory pathology in nonalcoholic fatty liver disease. *Redox Biol* 2018; 17: 1-15.
- Jiang F, Liu GS, Dusting GJ, Chan EC. NADPH oxidase-dependent redox signaling in TGF- β -mediated fibrotic responses. *Redox Biol* 2014; 2: 267-72.
- Yu J, Cui PJ, Zeng WL, Xie XL, Liang WJ, Lin GB, et al. Protective effect of selenium-polysaccharides from the mycelia of *Coprinus comatus* on alloxan-induced oxidative stress in mice. *Food Chem* 2009; 117: 42-7.
- Fujisaka S, Usui I, Bukhari A, Ikutani M, Oya T, Kanatani Y, et al. Regulatory mechanisms for adipose tissue M1 and M2 macrophages in diet-induced obese mice. *Diabetes* 2009; 58: 2574-82.
- Hotamisligil GS, Shargill NS, Spiegelman BM. Adipose expression of tumor necrosis factor- α : direct role in obesity-linked insulin resistance. *Science* 1993; 259: 87-91.
- Liu Y, Wang L, Luo M, Chen N, Deng X, He J, et al. Inhibition of PAI-1 attenuates perirenal fat inflammation and the associated nephropathy in high-fat diet-induced obese mice. *Am J Physiol Endocrinol Metab* 2019; 316: 260-7.
- Lai J, Ge M, Shen S, Yang L, Jin T, Cao D, et al. Activation of NF κ B-JMJD3 signaling promotes bladder fibrosis via boosting bladder smooth muscle cell proliferation and collagen accumulation. *Biochim Biophys Acta Mol Basis Dis* 2019; 1865(9): 2403-10.
- Meng R, Zhu DL, Bi Y, Yang DH, Wang YP. Apocynin improves insulin resistance through suppressing inflammation in high-fat diet-induced obese mice. *Mediators Inflamm* 2010; 2010: 858735.
- de Souza AC, Gallo CBM, Passos MCF, Crocchia C, Miranda GL, Sampaio FJB, et al. Effect of a high-fat diet on the rat bladder wall and bioactive action of Brazil nut oil. *Int Braz J Urol* 2019; 45(1): 161-8.
- Aizawa N, Homma Y, Igawa Y. Influence of high fat diet feeding for 20 weeks on lower urinary tract function in mice. *Low Urin Tract Symptoms* 2013; 5: 101-8.
- Oberbach A, Schlichting N, Heinrich M, Kullnick Y, Lehmann S, Adams V, et al. Hochfetttdiät induziert molekulare und physiologische Dysfunktionen der Harnblase (High fat diet-induced molecular and physiological dysfunction of the urinary bladder). *Urologe A* 2014; 53(12): 1805-11.
- Gomez CS, Kanagarajah P, Gousse AE. Bladder dysfunction in patients with diabetes. *Curr Urol Rep* 2011; 12: 419-26.
- Mafra D, Borges NA, Lindholm B, Shiels PG, Evenepoel P, Stenvinkel P. Food as medicine: targeting the uraemic phenotype in chronic kidney disease. *Nat Rev Nephrol* 2021; 17(3): 153-71.
- Aleksic V, Knezevic P. Antimicrobial and antioxidative activity of extracts and essential oils of *Myrtus communis* L. *Microbiol Res* 2014; 169(4): 240-54.
- Odeh D, Oršolić N, Berendika M, Đikić D, Drozdek SD, Balbino S, et al. Antioxidant and anti-atherogenic activities of essential oils from *Myrtus communis* L. and *Laurus nobilis* L. in *Rat*. *Nutrients* 2022; 14(7): 1465.
- Tuzlacı E. Türkiye'nin geleneksel ilaç bitkileri. İstanbul: İstanbul Tıp Kitabevi; 2016.
- Berendika M, Domjanić Drozdek S, Odeh D, Oršolić N, Dragičević P, Sokolović M, et al. Beneficial effects of laurel (*Laurus nobilis* L.) and myrtle (*Myrtus communis* L.) extract on rat health. *Molecules* 2022; 27(2): 581.
- Hennia A, Miguel M, Nemmiche S. Antioxidant activity of *Myrtus Communis* L. and *Myrtus Nivellei* Batt. & Trab. extracts: A brief review. *Medicines (Basel)* 2018; 5(3): 89.
- Rosa A, Deiana M, Casu V, Corona G, Appendino G, Bianchi F, et al. Antioxidant activity of oligomeric acylphloroglucinols from *Myrtus communis* L. *Free Radic Res* 2003; 37(9): 1013-19.
- Rossi A, Di Paola R, Mazzon E, Genovese T, Caminiti R, Bramanti P, et al. Myrtucommulone from *Myrtus communis* exhibits potent anti-inflammatory effectiveness in vivo. *J Pharmacol Exp Ther* 2009; 329(1): 76-86.
- Aidi Wannes W, Mhamdi B, Sriti J, Ben Jemia M, Ouchikh O, Hamdaoui G, et al. Antioxidant activities of the essential oils and methanol extracts from myrtle (*Myrtus communis* var. *italica* L.) leaf, stem and flower. *Food Chem Toxicol* 2010; 48(5): 1362-70.
- Arslan S, Ozcan O, Gurel-Gokmen B, Cevikelli-Yakut ZA, Saygi HI, Sen A, et al. Myrtle improves renovascular hypertension-induced oxidative damage in heart, kidney, and aortic tissue. *Biologia* 2022; 77: 1877-88.
- Sen A, Ozkan S, Recebova K, Cevik O, Ercan F, Demirci EK, et al. Effects of *Myrtus communis* extract treatment in bile duct ligated rats. *J Surg Res* 2016; 205 (2): 359-67.
- Aykac A, Ozbeyli D, Uncu M, Ertas B, Kilinc O, Şen A, et al. Evaluation of the protective effect of *Myrtus communis* in scopolamine-induced Alzheimer model through cholinergic receptors. *Gene* 2019; 689: 194-201.
- Sen A, Yuksel M, Bulut G, Bitis L, Ercan F, Ozyilmaz-Yay N, et al. Therapeutic potential of *Myrtus communis* subsp. *Communis* extract against acetic acid-induced colonic inflammation in rats. *J Food Biochem* 2017; 41 (1): e12297.
- Atici AE, Arabacı Tamer S, Levent HN, Peker Eyüboğlu İ, Ercan F, Akkiprik M, et al. Neuropeptide W attenuates oxidative multi-organ injury in rats induced with intra-abdominal sepsis. *Inflammation* 2022; 45(1): 279-96.

37. Koca O, Gokce AM, Akyuz M, Ercan F, Yurdakul N, Karaman MI. A new problem in inflammatory bladder diseases: use of mobile phones! *Int Braz J Urol* 2014; 40(4): 520-5.
38. Acikel Elmas M, Cakıcı SE, Dur IR, Kozluca I, Arınc M, Binbuga B, Bingol Ozakpınar O, Kolgazi M, Sener G, Ercan F. Protective effects of exercise on heart and aorta in high-fat diet-induced obese rats. *Tissue Cell* 2019; 57: 57-65.
39. Fan EWC, Chen LJ, Cheng JT, Tong YC. Changes of urinary bladder contractility in high-fat diet-fed mice: the role of tumor necrosis factor- α . *Int J Urol* 2014; 21(8): 831-5.
40. Kuru Yaşar R, Kuru D, Şen A, Şener G, Ercan F, Yarat A. Effects of *Myrtus communis* L. extract and apocynin on lens oxidative damage and boron levels in rats with a high fat-diet. *Turk J Ophthalmol* 2021; 51(6): 344-50.
41. Qiu S, Sun G, Zhang Y, Li X, Wang R. Involvement of the NF- κ B signaling pathway in the renoprotective effects of isorhamnetin in a type 2 diabetic rat model. *Biomed Rep* 2016; 4(5): 628-34.
42. Zhang L, Yang Z, Zhao Y, Yang X, Meng X, Liu J, et al. Renoprotective effects of Gushen Jiedu capsule on diabetic nephropathy in rats. *Sci Rep* 2020; 10(1): 2040.
43. Ahmed AH. Flavonoid content and antiobesity activity of leaves of *Myrtus Communis*. *Asian J Chem* 2013; 25(12): 6818-22.
44. Susztkat K, Ciccone E, McCue P, Sharma K, Böttinger EP. Multiple metabolic hits converge on CD36 as novel mediator of tubular epithelial apoptosis in diabetic nephropathy. *PLoS Med* 2009; 2(2): e45.
45. Tas S, Tas B, Bassalat N, Jaradat N. In-vivo, hypoglycemic, hypolipidemic and oxidative stress inhibitory activities of *Myrtus communis* L. fruits hydroalcoholic extract in normoglycemic and streptozotocin-induced diabetic rats. *Biomed Res* 2018; 29 (13): 2727–34.
46. Margetic S, Gazzola C, Pegg GG, Hill RA. Leptin: a review of its peripheral actions and interactions. *Int J Obes Relat Metab Disord* 2002; 26(11): 1407-33.
47. Kashiwagi E, Abe T, Kinoshita F, Ushijima M, Masaoka H, Shiota M, et al. The role of adipocytokines and their receptors in bladder cancer: expression of adiponectin or leptin is an independent prognosticator. *Am J Transl Res* 2020; 12(6): 3033-45.
48. García-Arroyo FE, Gonzaga-Sánchez G, Tapia E, Muñoz-Jiménez I, Manterola-Romero L, Osorio-Alonso H, et al. *Osthol* ameliorates kidney damage and metabolic syndrome induced by a high-fat/high-sugar diet. *Int J Mol Sci* 2021; 22(5): 2431.
49. Yamamoto T, Takabatake Y, Takahashi A, Kimura T, Namba T, Matsuda J, et al. High-fat diet-induced lysosomal dysfunction and impaired autophagic flux contribute to lipotoxicity in the kidney. *J Am Soc Nephrol* 2017; 28(5): 1534-51.
50. Li N, Ding H, Li Z, Liu Y, Wang P. Effect of high-fat diet-induced obesity on the small-conductance Ca²⁺-activated K⁺ channel function affecting the contractility of rat detrusor smooth muscle. *Int Urol Nephrol* 2019; 51(1): 61-72.
51. Lee M, Zhao H, Liu X, Liu D, Chen J, Li Z, et al. Protective effect of hydroxysafflor yellow A on nephropathy by attenuating oxidative stress and inhibiting apoptosis in induced type 2 diabetes in rat. *Oxid Med Cell Longev* 2020; 11: 7805393.
52. Suzuki S, Arnold LL, Pennington KL, Kakiuchi-Kiyota S, Cohen SM. Effects of co-administration of dietary sodium arsenite and an NADPH oxidase inhibitor on the rat bladder epithelium. *Toxicology* 2009; 261(1-2): 41-6.
53. Wu LL, Chiou CC, Chang PY, Wu JT. Urinary 8-OHdG: a marker of oxidative stress to DNA and a risk factor for cancer, atherosclerosis and diabetics. *Clin Chim Acta* 2004 Jan; 339(1-2): 1-9.
54. Takagi S, Li J, Takagaki Y, Kitada M, Nitta K, Takasu T, et al. Ipragliflozin improves mitochondrial abnormalities in renal tubules induced by a high-fat diet. *J Diabetes Investig* 2018; 9(5): 1025-32.
55. Li L, Zhao Z, Xia J, Xin L, Chen Y, Yang S, et al. A long-term high-fat/high-sucrose diet promotes kidney lipid deposition and causes apoptosis and glomerular hypertrophy in Bama minipigs. *PLoS One* 2015; 10(11): e0142884.
56. Gregor MF, Hotamisligil GS. Inflammatory mechanisms in obesity. *Annu Rev Immunol* 2011; 29: 415-45.
57. Brovkovych V, Gao XP, Ong E, Brovkovych S, Brennan ML, Su X, et al. Augmented inducible nitric oxide synthase expression and increased NO production reduce sepsis-induced lung injury and mortality in myeloperoxidase-null mice. *Am J Physiol Lung Cell Mol Physiol* 2008; 295(1): L96-103.
58. Elgazar-Carmon V, Rudich A, Hadad N, Levy R. Neutrophils transiently infiltrate intra-abdominal fat early in the course of high-fat feeding. *J Lipid Res* 2008; 49(9): 1894-903.
59. Wiersma JJ, Meuwese MC, van Miert JN, Kastelein A, Tijssen JG, Piek JJ, et al. Diabetes mellitus type 2 is associated with higher levels of myeloperoxidase. *Med Sci Monit* 2008; 14(8): CR406-10.
60. Zhang H, Sun SC. NF- κ B in inflammation and renal diseases. *Cell Biosci* 2015; 5: 63.
61. Chenxu G, Xianling D, Qin K, Linfeng H, Yan S, Mingxin X, et al. Fisetin protects against high fat diet-induced nephropathy by inhibiting inflammation and oxidative stress via the blockage of iRhom2/NF- κ B signaling. *Int Immunopharmacol* 2021 Mar; 92: 107353.
62. Fodor J, Fabry P, Lojda Z. The effect of long-term administration of diet with high fat content on the number of mast cells in the rat mesentery. *Virchows Arch Pathol Anat Physiol Klin Med* 1960; 333: 582-6.
63. Wang CC, Kuo HC. Urothelial dysfunction and chronic inflammation in diabetic patients with overactive bladder. *Low Urin Tract Symptoms* 2017; 9(3): 151-6.
64. Djamali A, Reese S, Hafez O, Vidyasagar A, Jacobson L, Swain W, et al. Nox2 is a mediator of chronic CsA nephrotoxicity. *Am J Transplant* 2012; 12(8): 1997-2007.

Effects of Apocynin against Monosodium Glutamate-Induced Oxidative Damage in Rat Kidney

Merve Acikel Elmas¹ , Gokcen Ozgun¹ , Ozlem Bingol Ozakpinar² , Zozan Guleken³ , Serap Arbak¹ 

¹Acibadem Mehmet Ali Aydinlar University, School of Medicine, Department of Histology and Embryology, Istanbul, Turkiye

²Marmara University, Faculty of Pharmacy, Department of Biochemistry, Istanbul, Turkiye

³Uskudar University, Faculty of Medicine, Department of Physiology, Istanbul, Turkiye

ORCID IDs of the authors: M.A.E. 0000-0002-5992-8191; G.O. 0000-0002-4866-619X; O.B.O. 0000-0002-8852-7733; Z.G. 0000-0002-4136-4447; S.A. 0000-0001-6279-9602

Please cite this article as: Acikel Elmas M, Ozgun G, Bingol Ozakpinar O, Guleken Z, Arbak S. Effects of Apocynin against Monosodium Glutamate-Induced Oxidative Damage in Rat Kidney. Eur J Biol 2022; 81(2): 231-239. DOI: 10.26650/EurJBiol.2022.1148934

ABSTRACT

Objective: Monosodium glutamate causes oxidative stress that affects a variety of organ systems, along with the kidney. The aim of this study was to evaluate the protective role of apocynin in kidney degeneration caused by monosodium glutamate using biochemical and histological methods.

Materials and Methods: Sprague-Dawley rats (n=32) were used for this study. Four experimental groups were randomly formed: the Control (Cont), Apocynin (APO), Monosodium Glutamate (MSG), and MSG+APO groups. The MSG group received oral administration of MSG (120 mg/kg) for 28 days. The MSG+APO and APO groups received apocynin (25 mg/kg) during the last 5 days of the experiment. Kidney tissue was processed for biochemical and microscopic analyses. Biochemical methods were used to examine the levels of malondialdehyde (MDA) and glutathione (GSH) in the tissue and the activities of myeloperoxidase (MPO) and superoxide dismutase (SOD). Light and electron microscopy were also used to examine for histological changes in kidney tissue.

Results: The MSG group was compared with the Cont and APO groups; it was found that MDA and MPO levels were elevated, whereas GSH and SOD activity were decreased. In contrast to the Cont and APO groups, the MSG+APO group showed higher GSH levels, lower MPO activities and increased MDA levels. While apocynin treatment improved renal tissue histology, MSG-induction led to deterioration of renal morphology.

Conclusion: The study revealed that MSG increased oxidative damage and renal tissue degeneration. Moreover, apocynin reduced renal damage by modulating the ratio of antioxidants to oxidants.

Keywords: Monosodium glutamate, Apocynin, Kidney, Galectin

INTRODUCTION

The flavor of food is improved by the use of monosodium glutamate (MSG), a common additive in prepared foods. However, various animal studies have shown that consumption of MSG is hazardous to a number of organs, including the liver, brain, thymus, and kidneys (1,2). Previous studies showed an association between renal fibrosis and chronic MSG consumption (3) and

that oxidative stress was the main reason for kidney injury (4). The main factor of oxidative stress is free radicals. The primary causes of a reactive oxygen species (ROS) and oxygen radicals in cells are increased formation or decreased elimination of these radicals (5). Studies showed that the metabolism of nutritional factors, intracellular or extracellular factors, or detoxification processes could be caused by oxidative stress (6). Con-



Corresponding Author: Merve Acikel Elmas

E-mail: merve.elmas@acibadem.edu.tr, acikelmerve@gmail.com

Submitted: 29.07.2022 • **Revision Requested:** 07.09.2022 • **Last Revision Received:** 23.09.2022 •

Accepted: 31.10.2022 • **Published Online:** 15.12.2022

Content of this journal is licensed under a Creative Commons Attribution-NonCommercial 4.0 International License.



sequently, increased glutamate metabolism in the kidneys, as seen with chronic MSG consumption, may contribute to ROS formation. Thus, excessive glutamate metabolism in the kidneys, as seen with chronic MSG consumption, was a source of ROS that could contribute to kidney disease.

The NADPH oxidase (Nox) complex is inhibited by apocynin (APO, 4-hydroxy-3-methoxyasetophenan) isolated from the medicinal plant *Picrorhiza kurroa*. The enzyme Nox is in charge of the production of ROS (7). APO is known as a selective Nox inhibitor in activated human neutrophils. It prevents its activity and the accompanying ROS production (7). In recent years, APO was the subject of experimental studies due to its anti-inflammatory activity. It was observed that APO induced the antioxidant defense system by increasing glutathione (GSH) and reduced cellular stress caused by ischemia (8). APO has become an especially important and widely used experimental agent to affect Nox activity. In addition, recent animal studies demonstrated the protective effects of APO on the kidneys in a model of induced nephrotoxicity (9).

Galectin-3 belongs to a family of soluble beta-galactoside-binding proteins found in many vertebrate epithelial and myoid cell types (10). Because of its ability to bind carbohydrates, it regulates cell growth, differentiation, and inflammation. It also plays a complicated, content-dependent function in the kidneys. During development, it supports the formation of kidney tissue (nephrogenesis). Its expression level is quite high in the ureteric bud and the structures derived from this bud (11). Elevated plasma galectin-3 levels are associated with the risk of recurrent renal dysfunction, chronic kidney disease, infections leading to cardiovascular problems, and renal dysfunction leading to death (11). In a study with rats, Nishiyama et al. showed that galectin-3 expression increased in acute renal failure due to ischemia and toxic damage and emphasized that galectin-3 could be important in acute tubular injury and in the subsequent recovery period (12). The researchers immunohistochemically detected the development of galectin-3 in proximal convoluted tubules two hours after reperfusion. In the later stages of regeneration period, they confirmed the presence of galectin-3 in the proximal and distal tubules (12). Chronic kidney disease is a global health problem, so the use of galectin-3, which is associated with kidney development in many studies and serves as a biomarker in this and related diseases, is important for early diagnosis of the disease (11).

In this study, we investigated the ameliorative effect of APO on kidneys, as a possible antioxidant effect, against MSG-induced kidney degeneration using biochemical, light, fluorescence and electron microscopic methods.

MATERIALS AND METHODS

Animals

Sprague-Dawley rats (n:32, 250-300 g) were housed in wire-bottomed individual cages (at 22±2°C) and relative humidity and fed pelleted laboratory chow on a 12-h/12-h light-dark cycle. The Animal Care and Use Committee of Acibadem University,

Istanbul, Turkey (ACU HADYEK -2021/63) approved the experimental protocols. The animals were randomly divided into four groups: (1) The Cont group was administered 120 mg/kg distilled water for 28 days with oral gavage, (2) the APO group was administered 120 mg/kg distilled water for 23 days, and APO 25 mg/kg was administered for 24 to 28 days. (3) The MSG group, which received MSG (120 mg/kg/day) for 28 days. (4) The MSG + APO group received MSG (120 mg/kg) during the experiment and APO (25 mg/kg) was given during the last 5 days of the experiment. All treatments continued for 28 days at the same hour (at 10 o'clock). At the end of the experiment, animals were immediately sacrificed, and kidney tissues were removed. For biochemical analysis, tissue samples were homogenized with ice-cold 150 mM KCl for the determination of MDA, MPO, SOD and GSH levels. Kidney tissues were also prepared for histological, immunohistochemical, and transmission electron microscopical analyzes to evaluate the morphological and ultrastructural changes.

Biochemical Analysis

Measurements of Kidney Tissue MDA Level

A commercially available kit (E-BC-K025-M, Elabscience, Houston, TX, USA) was used to determine the MDA levels. Thiobarbituric acid (TBA), one of the degradation products of lipid peroxidation, was used in the procedure to measure the intensity of the pink complex formed by MDA at a wavelength of 532 nm. The MDA levels in tissue were calculated in nmol/g.

Measurements of Kidney Tissue of MPO Activity

The MPO activity was determined using a commercially available kit (MBS704859, MyBioSource, CA, USA) Standard solutions were prepared according to the kit instructions. The solution was added after each application, and the plate was measured at 450 nm with a spectrophotometer (13).

Measurements of Kidney Tissue GSH Activity

GSH plays a role as an antioxidant molecule in the structural and functional protection of the integrity of cells, tissue, and organ systems. GSH analysis in testicular tissues was performed according to the Beutler method (13). The principle of the method is based on the fact that the GSH in the analysis tube reacts with 5,5'-dithiobis 2-nitrobenzoic acid (DTNB) to give a yellowish color and the light intensity of this color was read in the spectrophotometer at a wavelength of 410 nm. Tissue homogenates were centrifuged, and 10% TCA solution was added to the obtained supernatant, mixed, and centrifuged again to allow the proteins to precipitate. Light-colored supernatant samples were used for GSH analysis. The intensity of the color formed in the samples kept at room temperature for 5 minutes was read at 410 nm in the spectrophotometer and GSH levels in µmol/g tissue were found by using the glutathione standard graph.

Measurements of Kidney Tissue SOD Activity

SOD activity was determined with the Sigma SOD Determination Kit (E-BC-K019-M, Elabscience, Houston, TX, USA). The absorbance values were read at 450 nm after the SOD activity was incubated using an enzyme working solution.

Microscopical Analysis

Light Microscopical Preparation

Kidney tissue samples were fixed in a 10% neutral buffered formalin solution for 72 hours. After fixation, tissues were dehydrated with ethyl alcohol series (70%, 90%, 96%, 100%) and cleared with xylene. The tissues were embedded in paraffin. Sections (at 5 μ m) were then stained with hematoxylin-eosin (H&E) for general histopathologic assessment of renal tissue and with Periodic Acid-Schiff Reaction (PAS) to assess changes in the basement membrane and tubule brush border (14). The H&E-stained sections were semi-quantitatively scored for proximal and distal tubule damage, inflammatory cell infiltration, and vascular congestion (15). Sections were scored between 0 and 3 (0:none, 1:mild, 2:moderate, 3:severe) for each criterion. The total score was 9.

Galectin-3 Immunofluorescence Analysis

Paraffin tissue sections were taken on positively charged slides. The sections were rehydrated with decreasing ethyl alcohol (100%, 96%, 90%, 70%) series. Then the slides were placed in citrate buffer and kept in the microwave. The sections were then cooled, rinsed with phosphate-buffered saline (PBS), and treated with 5% bovine serum albumin (BSA). After rinsing with PBS, the slides were treated with goat anti-rabbit galectin-3 primary antibody (1:200, Cedarlane Laboratories Burlington, ON, Canada). The sections were stored (at +4°C, overnight) in the dark. The sections were washed with PBS (containing %1 BSA) and then treated with the secondary antibody conjugated

with Alexa Flour 488 (1:1000, Thermo Fisher Scientific, USA) for 1 hour and then washed with PBS (at room temperature) (16). Subsequently, the sections were incubated with 4'-6-diamidino-2-phenylindole (DAPI) in the dark and examined with a confocal microscope (Zeiss LSM 700).

Transmission Electron Microscopical Preparation

Kidney tissue samples were fixed with 2.5% glutaraldehyde solution and then postfixed in 1% osmium tetroxide. They were then processed for routine electron microscopic analysis (17). Uranyl acetate and lead citrate were used to contrast sections before being evaluated with a transmission electron microscope (Thermo Scientific TALOS L 120 C, The Netherlands).

Statistical Analysis

GraphPad Prism 4.0 was used for statistical analysis (GraphPad Software, San Diego, CA, USA). All data were expressed as means \pm SD. An analysis of variance (ANOVA) and Tukey's multiple comparison tests were used to compare the data sets. It was stated that $p < 0.05$ was statistically significant.

RESULTS

Biochemical Results

MDA concentration in kidneys was significantly ($p < 0.01$) higher in the MSG group (41.52 \pm 12.9) than in the Cont group (18.75 \pm 2.59) and the APO group (14 \pm 7.08). The APO treatment tended to reduce the MDA concentration in the MSG+APO group (16.79 \pm 7.57) compared with the MSG group (Figure 1a).

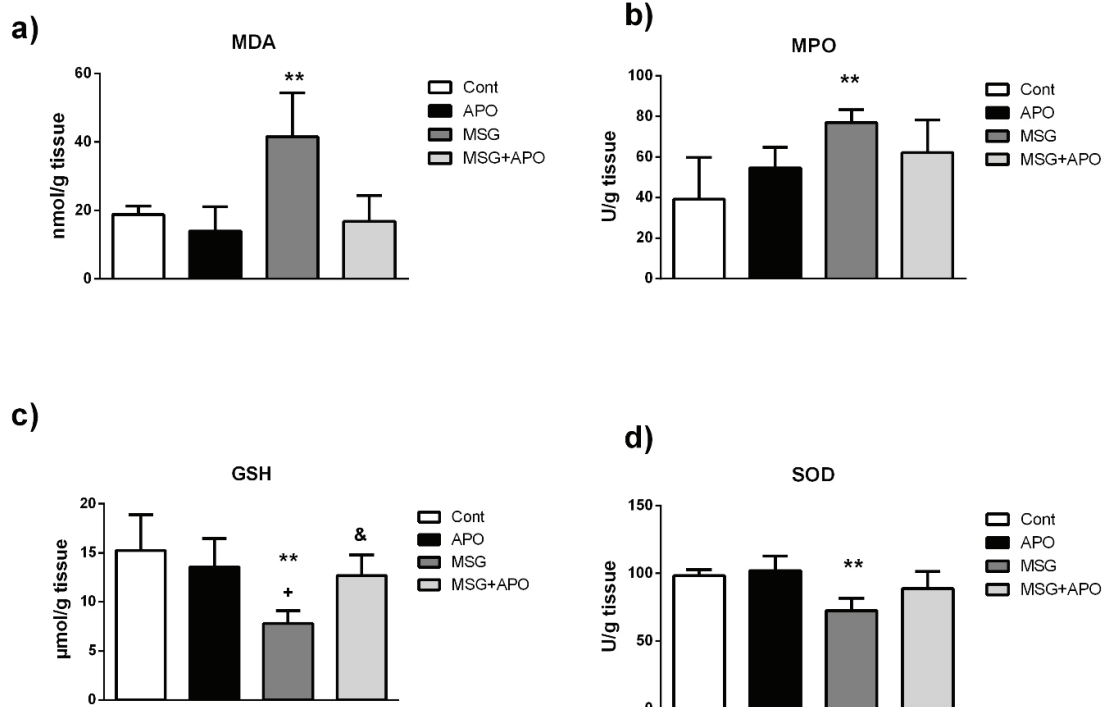


Figure 1. (a) Malondialdehyde (MDA) levels, (b) myeloperoxidase (MPO) activities, (c) glutathione (GSH) levels and (d) superoxide dismutase (SOD) activities in the kidney tissues. Values are represented as mean \pm SD. ** $p < 0.01$ versus control group; + $p < 0.001$ versus APO, & $p < 0.05$ versus MSG group.

It was found that MPO activity was significantly ($p < 0.01$) increased in the MSG group (76.97 ± 6.35) as compared to the Cont (39.21 ± 20.52) and APO (54.53 ± 10.18) groups, while the APO treatment tended to increase in the MSG+APO group (62.17 ± 16.19), but this increase was not statistically significant. (Figure 1b).

GSH levels in the MSG group (7.80 ± 1.30) renal tissue showed a significant ($p < 0.01$, $p < 0.001$, respectively) decrease compared to the Cont (15.26 ± 3.62) and APO (13.58 ± 2.87) groups, while the MSG+APO (12.68 ± 2.12) group showed increased GSH levels ($p < 0.05$) compared to the MSG group (Figure 1c).

SOD activity was significantly ($p < 0.01$) decreased with MSG administration in the MSG group (72.75 ± 9.03) as compared to the Cont (98.32 ± 4.60) group. The SOD activity also decreased in the APO (102 ± 10.94) group. Additionally, the MSG+APO group (88.766 ± 12.52) tended to increase, but this was not statistically significant (Figure 1d).

Light Microscopical Results

Normal kidney morphology was observed in the Cont and APO groups. Light micrographs showed that the ingestion of MSG affected the morphology of the nephrons. Thus, in the MSG group, a relative increase in Bowman's spaces, congestion of

glomerular capillaries, and thickening of the basement membrane were observed. In the APO group, an improvement in morphology was observed. In the MSG+APO group, there was less vascular congestion, tubular damage, and a reduction in Bowman's space observed (Figure 2). PAS positivity was seen in the proximal and distal tubules. PAS positivity was higher in the Cont and APO groups, but this positivity was decreased in the MSG group (Figure 3). Proximal and distal tubule PAS positivity was higher in the MSG+APO group than the MSG group (Figure 3).

Galectin-3 Immunofluorescence Results

Galectin-3 (Gal-3) immunoreactivity (IR) was observed predominantly in the proximal tubules of renal tissue in the experimental groups. The cytoplasm of proximal tubule cells had significantly higher IR, but glomerular Gal-3 expression was very low in the experimental groups. Gal-3 IR was similar in the Cont and APO groups, but Gal-3 IR was higher in the MSG group than in the other experimental groups. Gal-3 IR in the MSG+APO group was lower than in the MSG group (Figure 4). The fluorescence intensity of Gal-3 was highest in the MSG group as compared with the other experimental groups. The fluorescence intensity of the MSG+APO group was lower as compared to the MSG group (Figure 5).

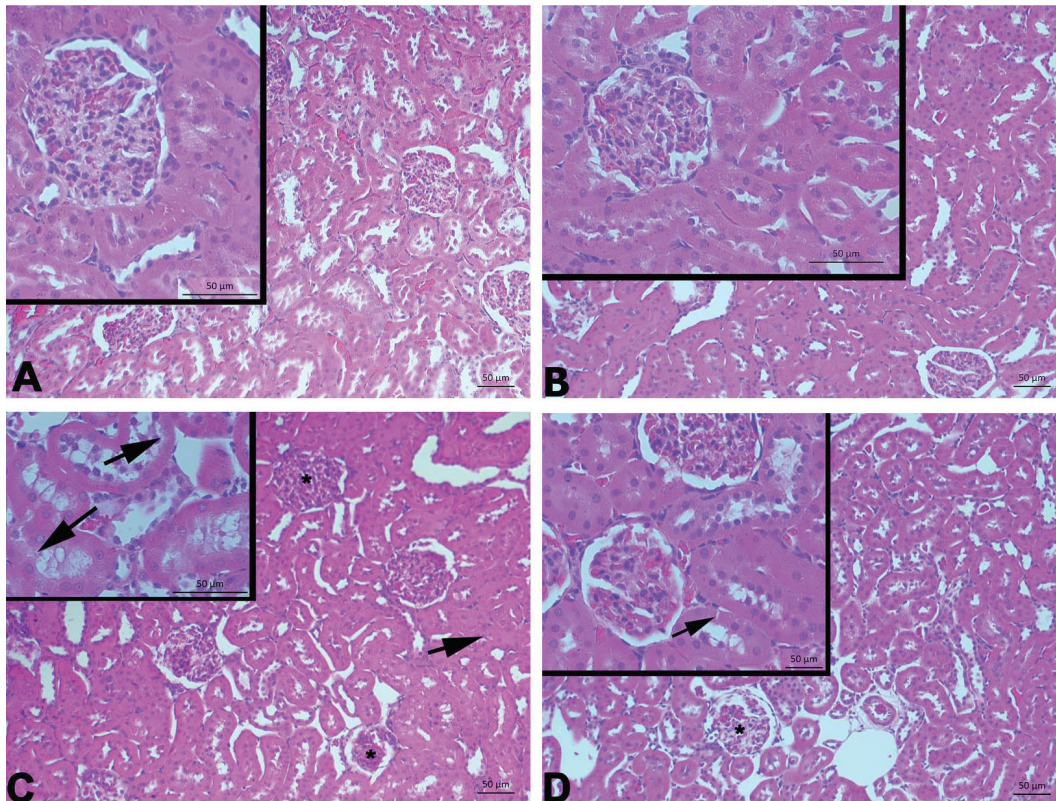


Figure 2. Normal kidney morphology in the Cont (A) and APO (B) groups. Severe tubular (arrow) and glomerular (*) degenerations were observed in the MSG group (C) and mild tubular (arrow) and glomerular (*) degenerations in the MSG+APO group (D). H&E staining.

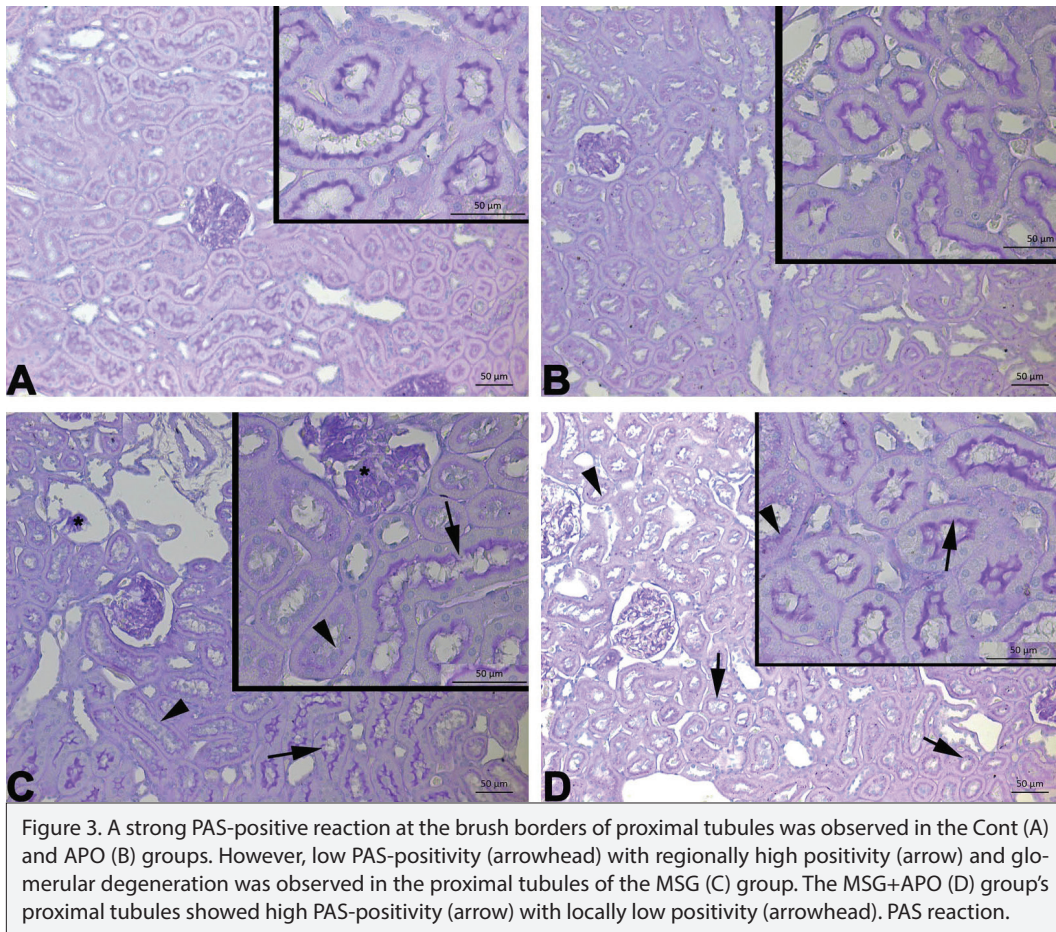


Figure 3. A strong PAS-positive reaction at the brush borders of proximal tubules was observed in the Cont (A) and APO (B) groups. However, low PAS-positivity (arrowhead) with regionally high positivity (arrow) and glomerular degeneration was observed in the proximal tubules of the MSG (C) group. The MSG+APO (D) group's proximal tubules showed high PAS-positivity (arrow) with locally low positivity (arrowhead). PAS reaction.

Electron Microscopy Results

Normal glomerulus and proximal tubule morphology were observed in the Cont and APO groups (Figures 6 a and b). Degeneration of podocyte structure, vacuoles and lipid droplets in the cytoplasm of proximal tubules were seen in the MSG group (Figure 6c). Ameliorated glomerular and tubular morphology were seen in the MSG+APO group (Figure 6d).

DISCUSSION

This study showed that MSG leads to oxidative stress by altering biochemical parameters. In the MSG group, both MDA levels and MPO activities increased, while GSH levels and SOD activities decreased. As for histopathological changes, degeneration of proximal and distal tubules, inflammatory cell infiltration, and vascular edema in renal tissue were also detected in the MSG given group. The APO treatment enhanced this biochemical and histopathological degeneration.

As well as ischemia and other toxic insults, chemicals can greatly damage the kidneys. Therefore, both direct and indirect disruptions of renal cell energy metabolism can lead to cell damage and acute renal insufficiency (15). MPO can also alter inflammatory responses by affecting multiple signaling pathways involved in cell signaling and cell-cell interactions (18). As

a result, MSG induced renal degeneration and oxidative stress could be related to an increase in MPO activity (19). In addition, APO as a Nox inhibitor requires activation by MPO (20). A significant factor in the nephrotoxic consequences was the exposure of the kidney to MSG, which led to the formation of ROS (21,22). By consuming MSG, ROS levels are elevated, leading to a reduction in antioxidant enzymes while an increase in oxidative stress, which results in tubulointerstitial fibrosis, thus giving rise to structural damage to kidneys.

The administration of MSG either intravenously or orally has been shown to affect both lipid peroxidation by products and renal function in rats (23). Following administration of MSG to rats, Paul et al. reported decreased SOD, catalase, glutathione-S-transferase, and GSH activities in the kidney (23). MDA and conjugated dienes, which are markers for lipid peroxidation, were also found to be increased in renal tissue treated with MSG. Furthermore, MSG treatment resulted in an increase in heat shock cognate 70, which is an indication of oxidative stress, and a reduction in glutathione-S-transferase (4). A few studies demonstrated the ameliorative effects of vitamin C, E, and quercetin on kidneys treated with MSG, however, the mechanisms of how these antioxidants work remain obscured (2). These antioxidants appeared to play a significant role in reducing renal

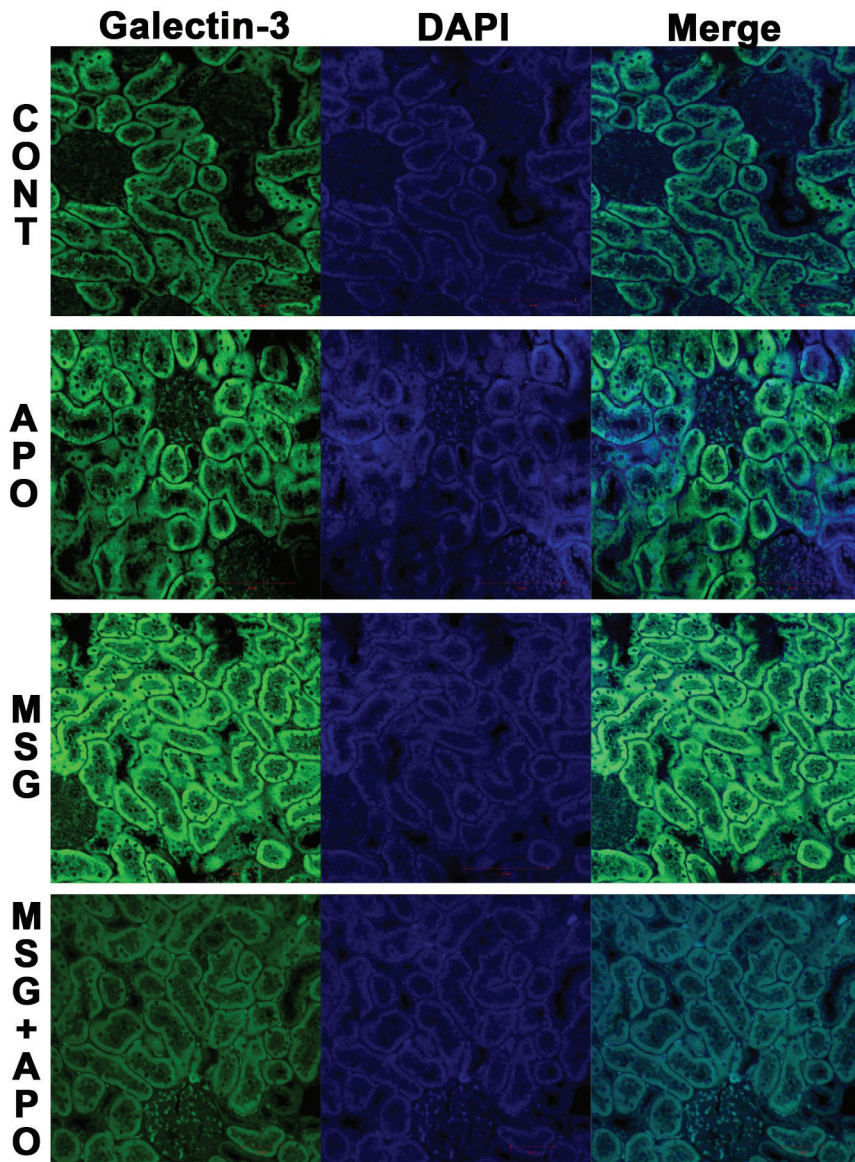


Figure 4. Galectin-3 (Gal-3) immunofluorescence staining in the experimental groups. Immunoreactivity (IR) of Gal-3 was similar in the Cont and APO groups. Gal-3 IR higher in the MSG group. Gal-3 IR in the MSG +APO group was lower than in the MSG group.

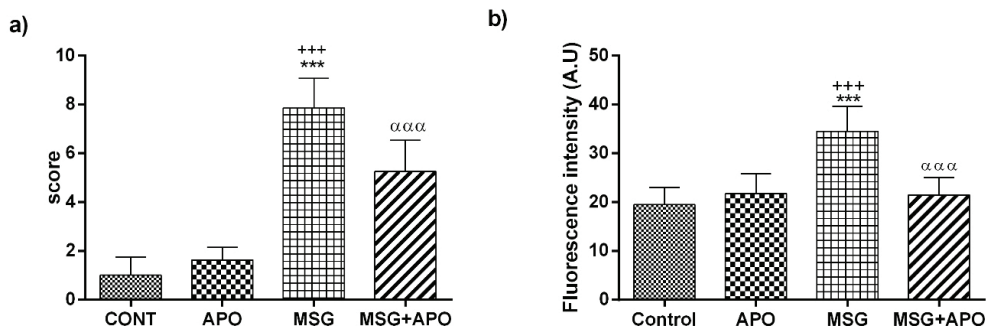


Figure 5. Histopathological score (a) and anti-Galectin-3 fluorescence intensity (b) graphs. Values are represented as mean±SD. ***p<0.001 versus control group; +++p<0.001 versus APO group, αααp<0.001 versus MSG group.

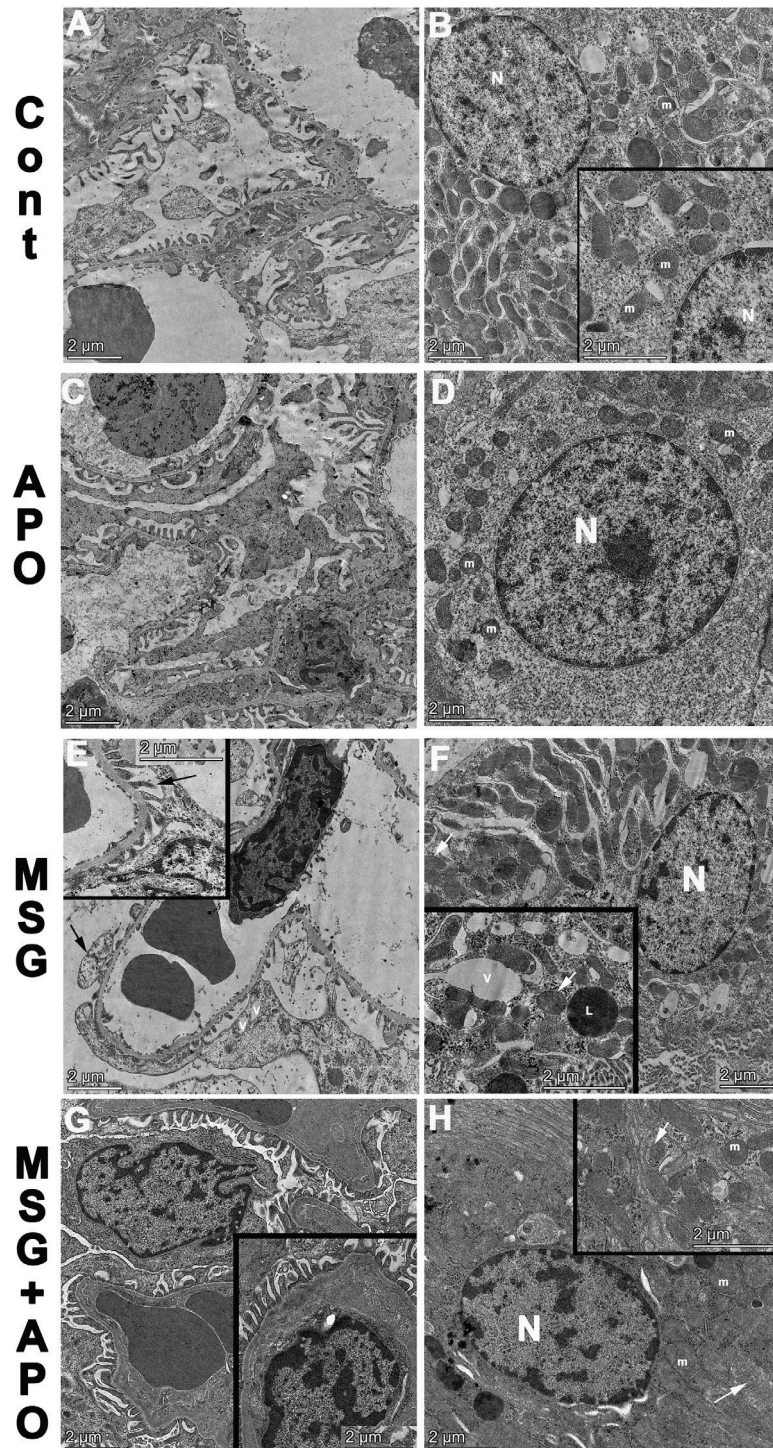


Figure 6. Electron micrographs of the experimental groups. Glomerulus (A, C) and proximal tubule (B, D) morphology is normal in the control and APO groups. Degenerated podocytes (black arrow) in the glomerulus (E), vacuoles (v), lipid droplets (L), degenerated mitochondria (white arrow) in the cytoplasm of proximal tubules were observed in the MSG group (F). Improved morphology of glomerulus (G), slightly degenerated morphology of proximal tubules with normal morphology of mitochondria (m) and degenerated mitochondria (white arrow) were observed in the MSG+APO group (H). Nucleus: N, electron micrographs contrasted with uranyl-acetate-lead citrate.

inflammatory responses through a reduction of inflammatory enzyme expressions and cytokine production (24) or inhibiting Nuclear Factor kappa B activity (25). Similar to previous studies, we observed that MDA level and MPO activity were higher in the MSG group than in the control and APO groups. In addition, GSH levels and SOD activity were lower in the MSG group than in the other experimental groups. APO treatment had a positive effect on these markers of oxidative stress in renal tissue.

Recent experimental studies showed that consumption of MSG altered kidney histopathology. Thus, swollen tubular morphology and infiltration of inflammatory cells were observed in rat kidneys (23,26). Experimental studies revealed that MSG-induced kidney deterioration was accompanied by cytoplasmic and nuclear degenerations of the proximal tubules (27). The studies also showed that several cells exhibited splitting and thickening of the basement membrane, partial loss of the brush border, and loss of the majority of cytoplasmic organelles. The nuclei of podocytes and endothelial cells typically exhibited chromatin condensation adjacent to the nuclear membrane, giving them an atypical appearance (28). The development of vascular problems linked to renal impairments is significantly influenced by oxidative stress, and the protective benefits of antioxidants could be explained by an increase in ROS degradation (29). APO is a Nox inhibitor and one of its positive effects could be a decrease in oxidative stress (30,31). Although the specific process of inhibition is not known, APO appears to be related to the ability of the cytosolic Nox complex component p47phox to translocate the membrane (20). In this study, renal pathophysiology was improved by APO treatment. Thus, it is thought that APO simultaneously improves kidney function. This effect is probably related to the different modes of action of the antioxidant used (32). In this study, renal morphology was degenerated in the MSG group. However, APO improved renal degeneration in the MSG+APO group. This effect might be related to the inhibition of Nox. Thus, renal morphology could be improved by the antioxidant effect of APO.

A member of the galectin family of beta-galactoside-binding lectins, galectin-3 has a carbohydrate recognition domain and is between 32 and 35 kDa in size. It controls cell proliferation, differentiation, and inflammation by binding to carbohydrates (11). The expression of galectin-3 was significantly increased in both ischemia and toxicity, suggesting that it may be crucial for acute tubular injury and subsequent regeneration (11). The kidneys of galectin-3 knockout mice were examined morphologically, and the results showed severe glomerular sclerosis, PAS-positive deposits in the mesangium, thickening of the glomerular basement membrane, and Bowman's capsule (33). Galectin-3 is connected with the onset of renal fibrosis in animal models (34). In this study, it was found that galectin-3 IR was higher in the MSG group. Thus, the toxicity of MSG could cause an increase in this immunoreactivity. APO treatment could also lead to a decrease in this immunoreactivity. The expression of galectin-3 could be useful for the evaluation of morphological degeneration parameters.

CONCLUSION

In the last decade, it has become clear that continuous intake of MSG has the potential to negatively affect peripheral organs, including the kidneys. In addition, antioxidants such as APO could be helpful in renal injury. Our biochemical and histological results suggest that APO could ameliorate the kidney injury induced by MSG through inhibition of Nox activity by improved biochemical and histopathological degenerations.

Acknowledgement: The authors would like to thank Dr. Selcuk Birdogan for his assistance with electron microscopic imaging.

Ethics Committee Approval: This study was approved by the ethics committee of Acibadem Mehmet Ali Aydinlar University 06.10.2021, 21/63.

Informed Consent: Written consent was obtained from the participants.

Peer Review: Externally peer-reviewed.

Author Contributions: Conception/Design of Study- M.A.E.; Data Acquisition- M.A.E., O.B.O., G.O.; Data Analysis/Interpretation- M.A.E., O.B.O., Z.G.; Drafting Manuscript- M.A.E., Z.G.; Critical Revision of Manuscript- M.A.E., S.A.; Final Approval and Accountability- M.A.E., S.A., G.O., O.B., Z.G.

Conflict of Interest: Authors declared no conflict of interest.

Financial Disclosure: Authors declared no financial support.

REFERENCES

1. Diniz YS, Fernandes AA, Campos KE, Mani F, Ribas BO, Novelli EL. Toxicity of hypercaloric diet and monosodium glutamate: oxidative stress and metabolic shifting in hepatic tissue. *Food Chem Tox* 2004; 42(2): 313-19.
2. Farombi EO, Onyema OO. Monosodium glutamate-induced oxidative damage and genotoxicity in the rat: modulatory role of vitamin C, vitamin E and quercetin. *Hum Exp Toxicol* 2006; 25(5): 251-9.
3. Sharma A, Prasongwattana V, Cha'on U, Selmi C, Hipkaew W, Boonnate P, Pethlert S, Titipungul T, Intarawichian P, Waraasawapati S, Puapiroj A, Sitprijia V, Reungjui S. Monosodium glutamate (MSG) consumption is associated with urolithiasis and urinary tract obstruction in rats. *PLoS One* 2013; 8(9): e75546.
4. Sharma A, Wongkham C, Prasongwattana V, Boonnate P, Thanan R, Reungjui S, Cha'on U. Proteomic analysis of kidney in rats chronically exposed to monosodium glutamate. *PLoS One* 2014; 9(12): e116233.
5. Bashan N, Kovsan J, Kachko I, Ovadia H, Rudich A. Positive and negative regulation of insulin signaling by reactive oxygen and nitrogen species. *Physiol Rev* 2009; 89(1): 27-71.
6. Stankiewicz A, Skrzydlewska E, Makiela M. Effects of amifostine on liver oxidative stress caused by cyclophosphamide administration to rats. *Drug Metabol Drug Interact* 2002; 19(2): 67-82.
7. Simons JM, Hart BA, Ip Vai Ching TR, Van Dijk H, Labadie RP. Metabolic activation of natural phenols into selective oxidative burst agonists by activated human neutrophils. *Free Radic Biol & Med* 1990; 8(3): 251-8.
8. Liu PG, He SQ, Zhang YH, Wu J. Protective effects of apocynin and allopurinol on ischemia/reperfusion-induced liver injury in mice. *World J Gastroenterol* 2008; 14(18): 2832-7.

9. Tan YC, Abdul Sattar M, Ahmeda AF, Abdul Karim Khan N, Murugaiyah V, Ahmad A, Hassan Z, Kaur G. Apocynin and catalase prevent hypertension and kidney injury in Cyclosporine A-induced nephrotoxicity in rats. *PLoS One* 2020; 15(4): e0231472.
10. Bao Q, Hughes RC. Galectin-3 expression and effects on cyst enlargement and tubulogenesis in kidney epithelial MDCK cells cultured in three-dimensional matrices in vitro. *J Cell Sci* 1995; 108 (Pt 8): 2791-800.
11. Chen SC, Kuo PL. The Role of Galectin-3 in the Kidneys. *Int J Mol Sci* 2016; 17(4): 565.
12. Nishiyama J, Kobayashi S, Ishida A, Nakabayashi I, Tajima O, Miura S, Katayama M, Nogami H. Up-regulation of galectin-3 in acute renal failure of the rat. *Am J Pathol* 2000; 157(3): 815-23.
13. Beutler E, Duron O, Kelly BM. Improved method for the determination of blood glutathione. *J Lab Clin Med* 1963;61:882-8.
14. Abd-Elkareem M, Soliman M, Abd El-Rahman MAM, Abou Khalil NS. Effect of *Nigella sativa* L. Seed on the Kidney of Monosodium Glutamate Challenged Rats. *Front Pharmacol* 2022; 13: 789988.
15. Omurtag GZ, Güranlıoğlu FD, Sehirli O, Arbak S, Uslu B, Gedik N, Sener G. Protective effect of aqueous garlic extract against naphthalene-induced oxidative stress in mice. *Journal Pharm Pharmacol* 2005; 57(5): 623-30.
16. Besler C, Lang D, Urban D, Rommel KP, von Roeder M, Fengler K, Blazek S, Kandolf R, Klingel K, Thiele H, Linke A, Schuler G, Adams V, Lurz P. Plasma and Cardiac Galectin-3 in Patients With Heart Failure Reflects Both Inflammation and Fibrosis: Implications for Its Use as a Biomarker. *Circ Heart Fail* 2017; 10(3).
17. Acikel Elmas M, Cakici SE, Dur IR, Kozluca I, Arinc M, Binbuga B, Bingol Ozakpinar O, Kolgazi M, Sener G, Ercan F. Protective effects of exercise on heart and aorta in high-fat diet-induced obese rats. *Tissue Cell* 2019; 57: 57-65.
18. Van der Veen BS, de Winther MP, Heeringa P. Myeloperoxidase: molecular mechanisms of action and their relevance to human health and disease. *Antioxidants & Redox Signaling* 2009; 11(11): 2899-937.
19. Kisc B, Miric D, Dragojevic I, Rasic J, Popovic L. Role of Myeloperoxidase in Patients with Chronic Kidney Disease. *Oxidative Medicine and Cellular Longevity* 2016; 1069743.
20. Stefanska J, Pawliczak R. Apocynin: molecular aptitudes. *Mediators Inflamm* 2008; 106507.
21. Ortiz GG, Bitzer-Quintero OK, Zárate CB, Rodríguez-Reynoso S, Laris-Arceo F, Velázquez-Brizuela IE, Pacheco-Moisés F, Rosales-Corral SA. Monosodium glutamate-induced damage in liver and kidney: a morphological and biochemical approach. *Biomed Pharmacother* 2006; 60(2): 86-91.
22. Pfaller W, Gstraunthaler G, Willinger CC. Morphology of renal tubular damage from nephrotoxins. *Toxicol Lett* 1990; 53(1-2): 39-43.
23. Paul MV, Abhilash M, Varghese MV, Alex M, Nair RH. Protective effects of α -tocopherol against oxidative stress related to nephrotoxicity by monosodium glutamate in rats. *Toxicology Mech Methods* 2012; 22(8): 625-30.
24. Ozaki M, Yamada Y, Matoba K, Otani H, Mune M, Yukawa S, Sakamoto W. Phospholipase A2 activity in ox-LDL-stimulated mesangial cells and modulation by α -tocopherol. *Kidney Int Suppl* 1999; 71: S171-3.
25. Bowie AG, O'Neill LA. Vitamin C inhibits NF-kappa B activation by TNF via the activation of p38 mitogen-activated protein kinase. *J Immunol* 2000; 165(12): 7180-8.
26. Sharma A. Monosodium glutamate-induced oxidative kidney damage and possible mechanisms: a mini-review. *J Biomed Sci* 2015; 22(1): 93.
27. Afeefy A, Mahmoud M, Arafa M. Effect of Honey on Monosodium Glutamate Induced Nephrotoxicity (Histological and Electron Microscopic Studies). *J Am Sci* 2012; 8: 146-56.
28. El-Mawla AMAA, Osman HEH. HPLC analysis and role of the Saudi Arabian propolis in improving the pathological changes of kidney treated with monosodium glutamate. *Spatula DD* 2011; 1: 119-27.
29. Sinha N, Dabla PK. Oxidative stress and antioxidants in hypertension-a current review. *Curr Hypertens Rev* 2015; 11(2): 132-42.
30. Deng W, Abliz A, Xu S, Sun R, Guo W, Shi Q, Yu J, Wang W. Severity of pancreatitis-associated intestinal mucosal barrier injury is reduced following treatment with the NADPH oxidase inhibitor apocynin. *Molecular Med Rep* 2016; 14(4): 3525-34.
31. Impellizzeri D, Esposito E, Mazzon E, Paterniti I, Di Paola R, Bramanti P, Cuzzocrea S. Effect of apocynin, a NADPH oxidase inhibitor, on acute lung inflammation. *Biochem Pharmacol* 2011; 81(5): 636-48.
32. Ciarcia R, Damiano S, Florio A, Spagnuolo M, Zacchia E, Squillaciotti C, Mirabella N, Florio S, Pagnini U, Garofano T, Polito MS, Capasso G, Giordano A. The Protective Effect of Apocynin on Cyclosporine A-Induced Hypertension and Nephrotoxicity in Rats. *J Cell Biochem* 2015; 116(9): 1848-56.
33. Iacobini C, Menini S, Oddi G, Ricci C, Amadio L, Pricci F, Olivieri A, Sorcini M, Di Mario U, Pesce C, Pugliese G. Galectin-3/AGE-receptor 3 knockout mice show accelerated AGE-induced glomerular injury: evidence for a protective role of galectin-3 as an AGE receptor. *FASEB J* 2004; 18(14): 1773-5.
34. Henderson NC, Mackinnon AC, Farnworth SL, Kipari T, Haslett C, Iredale JP, Liu FT, Hughes J, Sethi T. Galectin-3 expression and secretion links macrophages to the promotion of renal fibrosis. *Am J Pathol* 2008; 172(2): 288-98.

Epibrassinolide Triggers Apoptotic Cell Death in SK-N-AS Neuroblastoma Cells by Targeting GSK3 β in a ROS Generation-Dependent Way

Pinar Obakan Yerlikaya^{1,2} , Shafaq Naxmedova³ 

¹Istanbul Medeniyet University, Faculty of Engineering and Natural Sciences, Department of Molecular Biology and Genetics, Uskudar-Istanbul, Turkiye

²Istanbul Medeniyet University, Science and Advanced Technology Research Center, Uskudar-Istanbul, Turkiye

³Istanbul University, Aziz Sançar Institute of Experimental Medicine, Department of Genetics, Istanbul, Turkiye

ORCID IDs of the authors: P.O.Y. 0000-0001-7058-955X; S.N. 0000-0002-2288-8296

Please cite this article as: Obakan Yerlikaya P, Naxmedova S. Epibrassinolide Triggers Apoptotic Cell Death in SK-N-AS Neuroblastoma Cells by Targeting GSK3 β in a ROS Generation-Dependent Way. Eur J Biol 2022; 81(2): 240-250.
DOI: 10.26650/EurJBiol.2022.1191701

ABSTRACT

Objective: Epibrassinolide (EBR), a biologically active member of the brassinosteroids plant hormone family, has been recently indicated as an apoptotic inducer in various cancer cells without affecting non-tumor cell proliferation. Glycogen synthase kinase 3 β (GSK3 β) was the first identified molecule that acts as a critical mediator of glycogen metabolism and insulin signaling mechanism. GSK3 β has been described as an essential factor for tumor progression by phosphorylating and inactivating the pro-apoptotic family member of the Bcl-2 family, Bax. It was recently shown to regulate cell division, differentiation, and adhesion.

Materials and Methods: To investigate the relative cell viability affected by EBR treatment and the preventive effect of N-acetyl cysteine (NAC) we performed MTT assay and FACS analysis, respectively. Colony formation and soft agar techniques were used to understand the inhibitory effect of EBR on colony formation and diameters. Annexin V-PI analysis by flow cytometry was performed for the measurement of the apoptotic cell percentages. Fluorescence microscopy was performed for the determination of mitochondria membrane potential following DiOC6 staining. The expression profiles of apoptotic proteins, as well as GSK3 β and β -catenin were investigated by immunoblotting.

Results: Our results indicated that EBR induced mitochondria-mediated apoptosis by inducing ROS generation which can be prevented by NAC, a reactive oxygen species scavenger. EBR-induced apoptosis can influence the inhibitory phosphorylation of GSK3 β by Ser9 and prevents the translocation of the down-stream target, β -catenin.

Conclusion: This study evaluated EBR as a potential apoptotic inducer in neuroblastoma cell line SK-N-AS and investigated the GSK3 β involvement.

Keywords: Neuroblastoma, epibrassinolide, GSK3 β , reactive oxygen species

INTRODUCTION

Neuroblastoma is a common extracranial solid tumor in childhood formed due to the neoplastic transformation of neural crest cells. Tumors are present in the tissues that form the sympathetic nervous system, mainly the adrenal gland (1). The cancer staging varies between

the regressing tumors to highly metastatic and mortal ones due to poor prognosis and molecular signatures, including the *MYCN* gene, the most critical genetic marker of neuroblastoma aggressiveness (2). Treatment strategies mostly require chemotherapy, especially for the high-risk group, consisting of platinum derivatives, alkylating, and topoisomerase-inhibitor agents. In ad-



Corresponding Author: Pinar Obakan Yerlikaya

E-mail: pinar.obakan@medeniyet.edu.tr

Submitted: 19.10.2022 • **Accepted:** 22.11.2022 • **Published Online:** 15.12.2022



dition, in the case of ALK tyrosine kinase mutation in existing tumors, ALK inhibitor crizotinib is usually preferred (3). In recent years, glycogen synthase kinase 3 (GSK3) inhibitors have been used to reduce neuroblastoma cell growth and markers (4). Even ALK and GSK3 kinase inhibitors showed promising results in inducing apoptosis in neuroblastoma cell lines and in vivo mice models (5). Besides its role in glycogen synthesis, GSK3 performs critical functions in various cellular processes, including apoptosis, cell growth, invasion, and metastasis. Therefore, aberrant GSK3 activity is associated with many diseases, such as cancer (6). Several GSK3 inhibitors have been developed and are being tested in clinical trials (7).

Brassinosteroids (BRs) were first obtained from plant pollen of the genus *Brassica*. The first identified member of BRs, brassinolide, was isolated from pollen in the form of crystals and was the first plant component in steroid structure (8). BRs are natural polyhydroxy steroids found in vertebrates and insects, similar to steroid hormones (9). Their roles, such as embryonic and post-embryonic development and maintaining the organism's homeostasis, have been identified in animals. In plants, BRs control many physiological events. It has been shown that BRs are essential in regulating many events in plant development, especially in seed germination, root and stem development, vascular differentiation and fertility, and salinity and metal stress management (10). Recent studies have shown that Epibrassinolide (EBR) has the potential to induce apoptotic cell death in cancer cells (11). Due to the structural similarity, the first studies focused on the nuclear hormone receptor (NHR) action during cancer cell apoptosis (12). However, our group has shown that EBR-induced apoptosis occurred in NHR-expressing and non-expressing cell lines (13,14).

In this study, we showed that EBR induced pGSK3 β phosphorylation by Ser9 and inhibited the translocation of its downstream target β -catenin. EBR treatment triggered cell viability loss via mitochondria-mediated and caspase-dependent apoptosis in SK-N-AS cells. Moreover, we showed that EBR-induced apoptosis mainly occurs due to endoplasmic reticulum stress induction. Our recent findings also suggested that EBR is a candidate GSK3 β inhibitor in a low concentration and induces apoptosis in SK-N-AS cells and GSK3 β inhibition acting on the Ser9 phosphorylation domain may be important for this phenomenon.

MATERIALS AND METHODS

Drug and Antibodies

24-epibrassinolide was purchased from Apollo Scientific (Stockport, Cheshire, UK), dissolved in DMSO to make a 10 mM stock solution, and stored at -20°C. Bax, Bcl-2, Puma, Bid, cleaved caspase 3, cleaved caspase 7, pro-caspase 9, cleaved poly (ADP-ribose) polymerase (PARP), GSK3 β , phospho-GSK3 β Ser9, and β -catenin Histone H3 rabbit primary antibodies (each diluted 1:1,000) were purchased from Cell Signaling Technology (CST, Danvers, MA, USA). Horseradish peroxidase (HRP)-conjugated secondary anti-rabbit antibodies (diluted 1:3,000) were from CST.

Cell Culture

SK-N-AS cell line was obtained from American Type Tissue Culture Collection and was grown in DMEM medium supplemented with 10% fetal bovine serum, 1% 10 U/ml penicillin/streptomycin, and 1% non-essential amino acids. Cells were kept in a 5% CO₂ incubator at 37 °C (Heracell 150; Thermo Electron Corporation, Waltham, MA, USA).

MTT Assay

The effect of EBR on cell viability was determined by colorimetric 3-(4,5-dimethylthiazol-2-yl)-2,5-diphenyl-tetrazolium bromide (MTT; Roche, Indianapolis, IN, USA) assay. Cells were seeded at a density of 1x10⁴ cells/well in 96-well plates, allowed to attach overnight, and treated with the increasing concentrations of EBR (0-30 μ M) for 24 h. After the treatment, 10 μ l of MTT reagent (5 mg/ml) was added to the cell culture medium for 4 h. Following the removal of media, 200 μ l DMSO was added to dissolve the formazan crystals. The absorbance of the suspensions was determined at 570 nm with a microplate reader (Bio-Rad, Hercules, CA, USA).

Trypan Blue Dye Exclusion Assay

Cells were seeded on 6-well plates (5x10⁴ cells/well) and treated with increasing doses of EBR (0-10 μ M) for 96 h. Every 24 h, the cells were trypsinized and stained with trypan blue. Data were plotted on a graph indicating the number of cells (y-axis) vs time (x-axis). Viable and dead cells were counted under light microscopy.

Colony Formation Assay

SK-N-AS cells were seeded at a density of 5x10³/well in a 6-well petri dish. Following overnight attachment, cells were treated with 1 and 10 μ M EBR for 24 h. The drug-containing media were removed, and cells were allowed to form colonies in complete media for 10 days. The colonies were fixed with a solution of acetic acid and methanol (1:3) for 5 min. The supernatant was removed. Later, cells were stained with 0.5% crystal violet for 30 min at room temperature. Finally, the dye was washed away with distilled water, and the colonies were visualized under the light microscope.

Soft Agar Colony Formation Assay

5% agarose was first prepared and autoclaved. For the bottom agar, 500 μ l of 5% agarose and 500 μ l of DMEM medium containing 20% fetal bovine serum (FBS) were mixed and poured into a 6-well petri dish. The agar was kept in laminar flow until polymerization. 3% agarose was mixed with media containing 20% FBS and pipetted. The medium containing 10% FBS and 2500 cells were added to the mixture, pipetted, and poured into Petri dishes. For treated samples, a drug was added to this mixture. The petri dish was kept in a 5% CO₂ incubator at 37°C for 10 days. After 10 days, colonies were examined under a light microscope.

Fluorescence Microscopy

Propidium Iodide Staining

1x10⁴ cells were seeded in 6-well petri dishes and allowed to adhere overnight. 1 and 10 μ M EBR was applied for 24 h. After the

incubation period, the medium was discarded, and the cells were incubated with a DMEM medium containing propidium iodide (PI) for 30 min. At the end of this period, the medium containing PI was discarded, and cells were washed with 1x PBS. After adding 500 μ l of 1x PBS to each well, cells were examined under a fluorescent microscope (Excitation: 536 nm, Emission: 617 nm).

3,3'-Dihexyloxacarbocyanine Iodide (DiOC6) Staining

SK-N-AS (1×10^5) cells were seeded into 12-well plates. Following exposure of cells to EBR (1 and 10 μ M), they were washed once with 1X PBS and then stained with 4 nM 3,3'-dihexyloxacarbocyanine iodide (DiOC6) (40 nM stock concentration in DMSO; Calbiochem, La Jolla, CA, USA) fluorescent probe. The disruption of mitochondrial membrane potential (MMP) was visualized by fluorescence microscopy (excitation: 488 nm, emission: 525 nm).

4',6-diamidino-2-phenylindole (DAPI) Staining

The cells were seeded in 12-well plates at a density of 1×10^5 cells/well and treated with increasing concentrations of EBR for 24 h. Cells were stained with 1 μ l/ml DAPI (1 mg/ml stock concentration in 1X PBS) fluorescent probe and were incubated for 10 min in the dark. Nuclear DNA fragmentation was visualized using fluorescence microscopy (excitation: 350 nm emission: 470 nm).

2',7'-dichlorofluorescein-diacetate (DCFH-DA) Staining

DCFH-DA was used to monitor reactive oxygen species (ROS) production in EBR-treated cells. SK-N-AS cells were seeded at a density of 1×10^4 cells/well in a 6-well petri dish. 1 and 10 μ M EBR were applied for 24 h. 1 μ M DCFH-DA in fresh media were added to each well following the incubation period and washing step with 1x PBS. Cells were kept dark for 5'. After the washing step with 1x PBS, 500 μ l of PBS was added to each well, and the oxidized form of DCFH-DA was examined under the fluorescence microscope at 480 nm excitation and 500 nm emission wavelengths.

Immunoblotting

SK-N-AS cells were treated with the appropriate concentrations of EBR in a time-dependent manner. First, all the samples were washed with ice-cold PBS and lysed on ice in a solution containing 20 mM Tris-HCl (pH 7.5), 150 mM NaCl, Nonidet P-40 0.5%, (v/v), 1 mM EDTA, 0.5 mM PMSF, 1 mM DTT, and protease inhibitor cocktail (Complete, Roche). After cell lysis, the cell debris was removed by centrifugation for 15 min at 13,200 rpm, and protein concentrations were determined by the Bradford protein assay (BioRad). ProteoJET protein isolation kit was used for cytoplasmic and nuclear protein isolation. Cells were seeded in 100 mm Petri dishes at a density of 3×10^6 cells. Following EBR treatment for 24 h, cells were trypsinized and centrifuged at 600 g for 5 min. The nuclear and cytoplasmic protein isolation was performed according to the manufacturer's instructions. Samples were kept in the -80° freezer until use. Total, nuclear, and cytoplasmic protein lysates were separated on a 12% SDS-PAGE and transferred onto PVDF membranes (Roche). The membranes were then blocked with 5% milk blocking solution in Tris buffer saline-Tween 20 and incubated with appropriate primary and HRP-conjugated secondary antibodies (CST) in antibody buffer containing 5% (v/v) milk blocking solution. Following a gentle

washing step with 1X TBS-Tween 20, the proteins were analyzed using an enhanced chemiluminescence detection system.

Flow Cytometry

Determination of Apoptotic Cell Death by Annexin V and Propidium Iodide Staining

Apoptotic cell death was detected following EBR treatment by annexin V-PI staining (B.D. Biosciences). The protocol was performed according to the manufacturer's instructions. Briefly, cells were mixed in 500 μ l annexin V binding buffer, then incubated with 5 μ l annexin V-FITC and 5 μ l PI. (50 μ g/ml) for 10 minutes after centrifugation in the dark and at room temperature. 1×10^4 cells per sample were analyzed by flow cytometry. Cells are presented as dots in a rectangular plot, with annexin V fluorescence in the x- and PI fluorescence on the y-axis. The numbers in each panel of the quadrant represent the % of the cell population as healthy (lower-left), early apoptotic (lower-right), late apoptotic (upper-right), and necrotic (upper-left) populations. The analysis of the obtained data was carried out using the BD Accuri C6 program.

Determination of the ROS Generation by DCFH-DA Staining

SK-N-AS cells were seeded in 6-well plates (1×10^5 cells/well). Cells were trypsinized, resuspended in 1X PBS, and stained with DCFH-DA (1 μ M) (Molecular Probes, Inc., Eugene, OR, USA) for 15 min in a 5% CO₂ incubator. After the incubation period, DCFH-DA was added and flow cytometry analysis was performed (B.D. Biosciences, Accuri C6). Following exposure of cells to EBR for 24 h, media was carefully discarded.

Cell Cycle Analysis by PI Staining

Cells at a density of 2×10^5 cells/well were seeded in 6-well plates and then treated with EBR. Both floating and adherent cells were collected and fixed with 70% ethanol. After incubation on ice for 30 min, the cells were diluted with 1X PBS. Samples were then centrifuged at 1,200 rpm for 5 min. Pellets were resuspended in 1X PBS, RNase (100 μ g/ml), and PI solution (40 μ g/ml). Samples were kept for 30 min at 37°C in the dark. Cell cycle distribution was analyzed by Accuri C6 (B.D. Biosciences, Oxford, U.K.). 10,000 events/samples were acquired and evaluated using BD Accuri C6 software (B.D. Biosciences).

Statistical Analysis

All the experiments were statistically analyzed by two-way ANOVA using GraphPad Prism 9 (GraphPad Software, La Jolla, CA, USA). Error bars in the graphs were generated using \pm standard deviation (S.D.) values. Statistically significant results by ANOVA were further analyzed by Bonferroni posthoc analysis. A $p < 0.05$ was considered to indicate a statistically significant result.

RESULTS

EBR Treatment Diminished the SK-N-AS Cell Viability

The MTT test determined the effect of EBR on SK-N-AS cell viability. As seen in Figure 1A, the relative viability percentages of EBR-treated cells decreased dose-dependent. The percentage of relative viability after 24 h of 1 μ M EBR treatment was 67.7%.

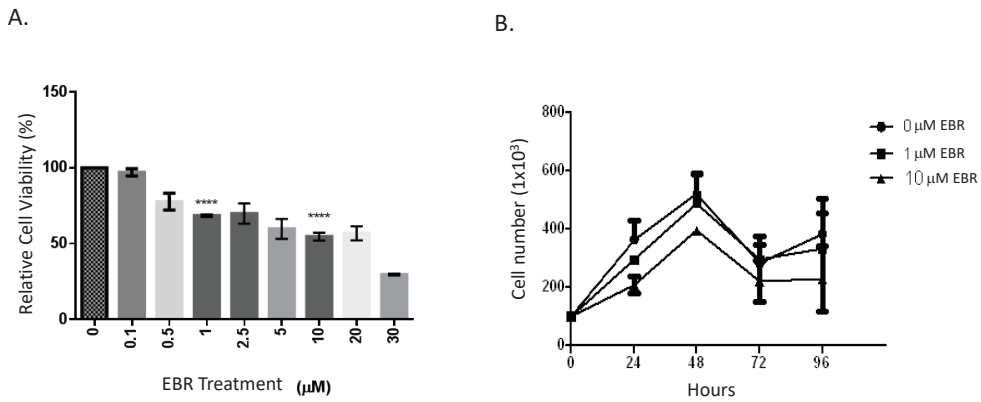


Figure 1. **A.** Investigation of dose-dependent cell viability of EBR in SK-N-AS cells by MTT method. **** $p < 0.00001$. **B.** Determination of the effect of EBR on cell survival in SK-N-AS cells. Cells were treated with 1 and 10 μM EBR for 24-96 h, and after staining with trypan blue, the cells were counted under a light microscope with the help of a Neubauer hemocytometer.

After 10 μM EBR treatment, the viability percentage dropped to 50.3%. (**** $p < 0.00001$). In addition, the effect of EBR on the SK-N-AS cell survival was also examined by trypan blue dye exclusion assay. Figure 1B indicates that EBR exerted a cytostatic effect rather than a cytotoxic one in concentrations 1 and 10 μM, time-dependently. 48 h EBR treatment dramatically prevented the survival of SK-N-AS cells.

EBR Inhibited the Clonogenic Potential of SK-N-AS Cells

A clonogenic assay was performed to determine the effect of EBR on colony formation in SK-N-AS cells. The colony formation potential of SK-N-AS cells was prevented in EBR-treated cells in a dose-dependent manner compared to control samples (Figure 2A). In addition, a soft agar colony formation test was also performed. As shown in Figures 3 and 4, the diameter of the col-

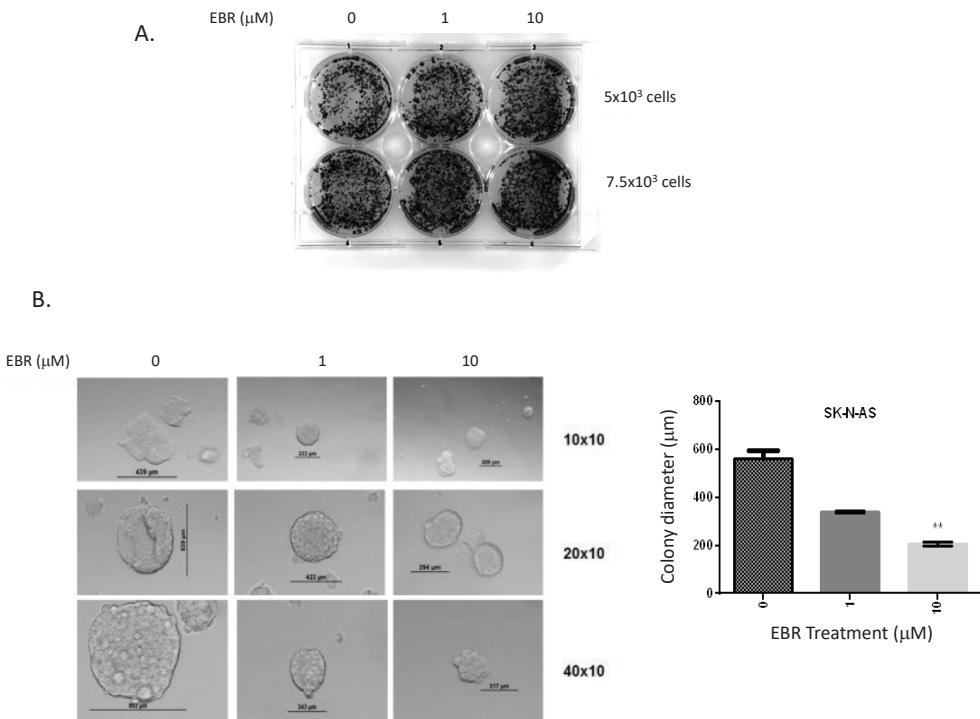


Figure 2. Investigation of the effect of EBR on colony formation in SK-N-AS cells. **A.** SK-N-AS cells were seeded in Petri dishes at 5x10³ and 7.5x10³ cells/well, 1 and 10 μl of EBR were applied for 24 h, and the cells were incubated for 14 days. After 14 days, it was fixed and stained with crystal violet and images were taken under a light microscope. **B.** Investigation of colony formation on soft agar in SK-N-AS cells to which EBR had been applied. Cells incubated on soft agar for 10 days were examined under a light microscope at the end of 10 days, and colony diameters were measured. ** $p < 0.01$

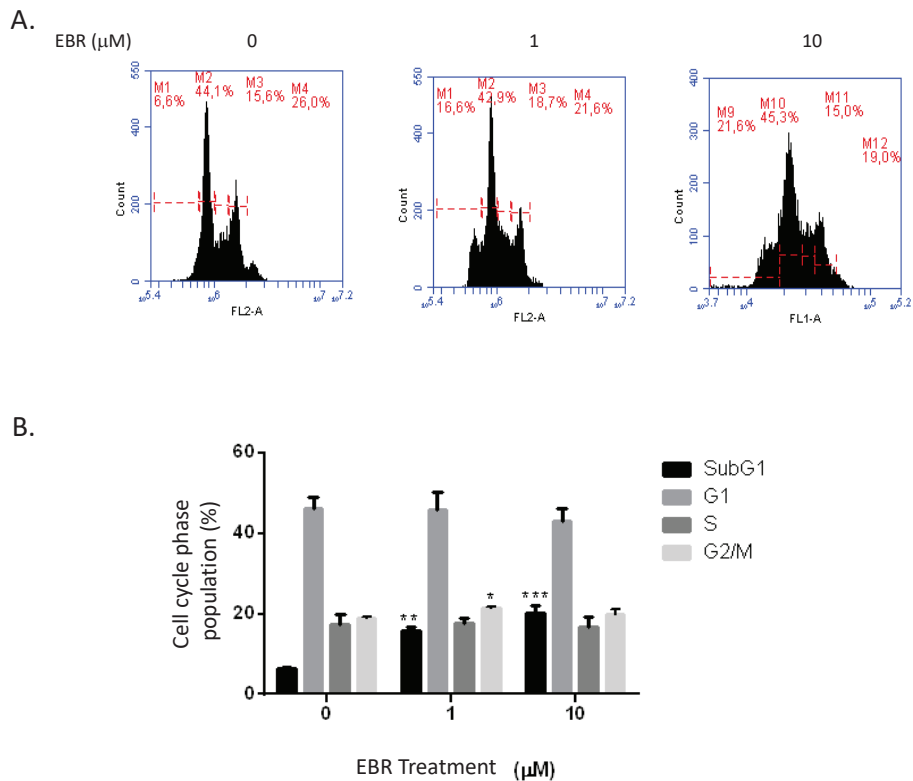


Figure 3. Flow cytometry analysis of cell cycle phases following exposure of SK-N-AS cells to EBR. **A.** Cells were incubated with EBR for 24 h, fixed with ethanol, and stained with PI. Flow cytometry was used for cell cycle analysis (Ex: 535 nm and Em: 617 nm). **B.** The number of cells in different cell cycle phases was determined after at least 3 repetitions of the experiment. Cell cycle distribution was analyzed by two-way ANOVA and Tukey's multiple comparisons test. * $p < 0.05$, ** $p < 0.01$ and *** $p < 0.001$

onies formed by the EBR-treated cells decreased depending on the dose. As seen in Figure 2B, a significant reduction in colony diameter was observed after 10 μM EBR treatment.

EBR Triggers Cell Cycle Arrest and Induced Apoptosis in SK-N-AS Cell Line

As seen in Figure 3A, an approximately 3-fold increase in the SubG1 population as a result of 24 h 1 μM EBR treatment was obtained in SK-N-AS cells, and an approximately 4-fold increase, as a result of 10 μM EBR application. This result shows that EBR activates the apoptotic mechanism in SK-N-AS cells. In addition, the percentage of G2/M phase cells decreased by 25% with exposure of cells to 10 μM EBR (Figure 3B). Annexin V and PI staining were performed to determine whether apoptotic cell death was triggered in EBR-treated SK-N-AS cells. As seen in Figure 4, an approximately 15 fold higher total early and late apoptotic cell population was observed in cells treated with 1 μM EBR for 24 h, compared to the untreated control group. Cells treated with 10 μM EBR also exhibited an increased apoptotic population percentage, approximately 25 fold compared to the untreated samples. No significant change was found in the necrotic population. This result shows that EBR activates the apoptotic mechanism in SK-N-AS cells. Later, DiOC6 staining was performed to show mitochondria-mediated apoptotic cell death

in the cell. Mitochondrial membrane potential is impaired in apoptotic cell death. For this reason, the dye cannot be retained in cells with the induction of apoptotic cell death. We found that both concentrations cause a decrease in the DiOC6 stained cell population, however, 10 μM EBR application was more effective to decrease DiOC6 staining compared to the 1 μM dose (Figure 5A). DAPI is a nucleic acid dye, which marks DNA fragmentation. Figure 5A clearly demonstrated the increase in DAPI staining inside the nucleus more specifically after 10 μM EBR treatment. We next checked the expression profiles of caspase and Bcl-2 family proteins playing a role in apoptosis induction using the immunoblotting technique. The changes in pro- and anti-apoptotic Bcl-2 family members, which have an essential role in mitochondria-mediated apoptotic cell death pathway, were investigated following EBR application. As seen in Figure 5B, Bid expression increased after 10 μM EBR treatment in SK-N-AS cells. Caspase-8 causes the proteolytic cleavage of Bid and causes Bid to migrate to mitochondria. Bid can bind to both Bax and Bcl-2, and it was observed that Bax expression increased as a result of 10 μM EBR application (Figure 5B). Bax resides in the cytosol and, upon apoptotic stimulation, binds to the mitochondrial membrane and induces pore formation. In addition, it was determined that the expression of PUMA protein increased

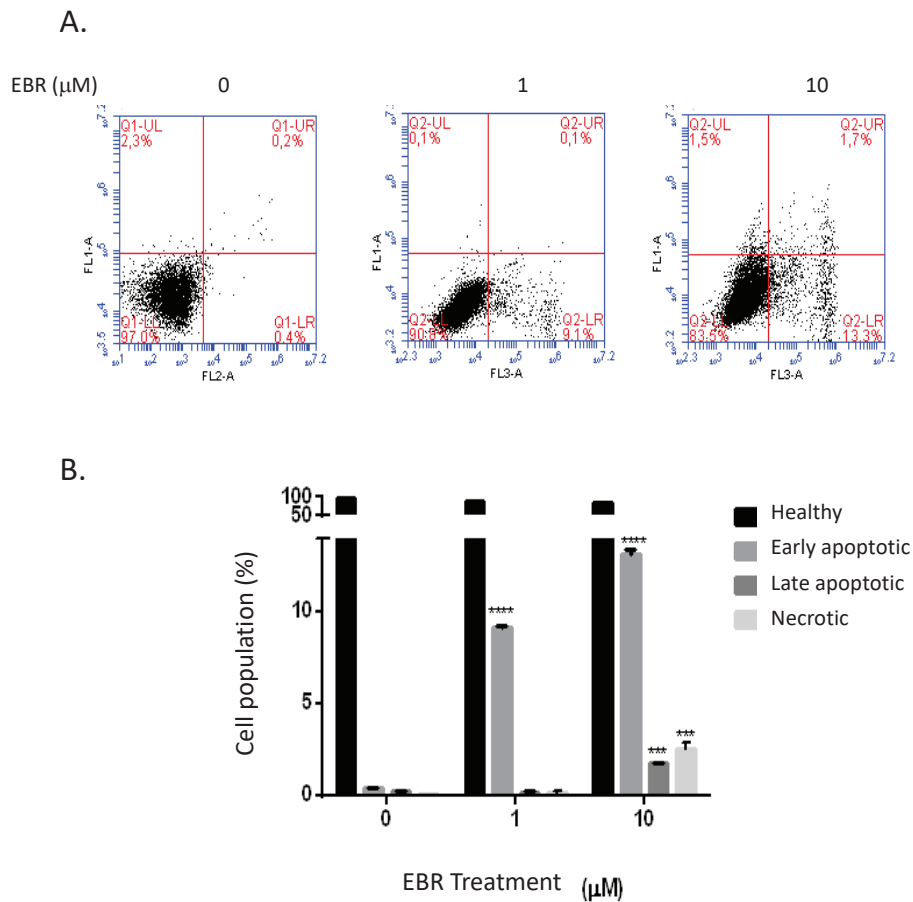


Figure 4. EBR induced apoptosis in SK-N-AS cells. **A.** After incubation with increasing concentrations of EBR for 24 h, cells were stained with Annexin V and PI and analyzed with FACS flow using the BD Bioscience Accuri C6 program. **B.** Percentages of early apoptotic, late apoptotic, and necrotic populations were determined after at least three independent experiments. *** $p < 0.001$ and **** $p < 0.0001$.

in SK-N-AS cells treated with 1 and 10 μM EBR for 24 h (Figure 5B). Puma stimulates apoptosis by binding to Bcl-2, promoting migration to mitochondria and releasing cytochrome c. It is seen in the data that the expression of the anti-apoptotic protein Bcl-2 protein is increased. As a result of 1 and 10 μM EBR application, no significant change was detected in the expression of Bcl-2 (Figure 5B). β -actin was used as a loading control.

Effective caspases cleave PARP, which is involved in DNA repair, causing apoptotic cell death. In addition to the Bcl-2 protein family, caspase family expressions in the apoptotic pathway were also investigated following EBR treatment in SK-N-AS neuroblastoma cells. The initiator caspase, procaspase-9, and the effective caspase-3 and caspase-7 expressions were determined. We found that the expression of the cleaved active form of PARP increased significantly in SK-N-AS cells after 1 and 10 μM EBR for 24 h (Figure 5B). Dose-dependent EBR treatment decreased procaspase-9 expression in the SK-N-AS cell line at 24 h. As a result of 1 and 10 μM EBR application, it was observed that the expression of cleaved caspase-3 and cleaved caspase-7

increased in SK-N-AS cells, confirming the apoptosis cell death (Figure 5B).

EBR Triggered ROS Generation Related to the Apoptotic Process in SK-N-AS Cells

To determine whether EBR affected ROS generation during the apoptotic induction in the SK-N-AS cell line, cells were treated with 1 and 10 μM EBR for 24 h and examined in flow cytometry following DCFH-DA staining. After diffusion into the cell, DCFH-DA is deacetylated by cellular esterases and then oxidized by ROS. As seen in Figure 5C, there was a significant increase in ROS in SK-N-AS cells treated with 1 and 10 μM EBR compared to control cells. N-acetyl cysteine (NAC), an agent that prevents the destructive effect of toxic agents in the apoptotic process triggered by EBR, was applied to SK-N-AS cells simultaneously with 10 μM EBR for 24 h, and changes in cell viability were observed. As seen in Figure 5D, NAC prevents the negative effect of EBR on cell viability in the SK-N-AS cell line and reverses the toxic effect of EBR (Figure 5D). In addition, NAC co-treatment also prevents EBR-induced ROS generation detected with DCFH-DA staining (Figure 5E).

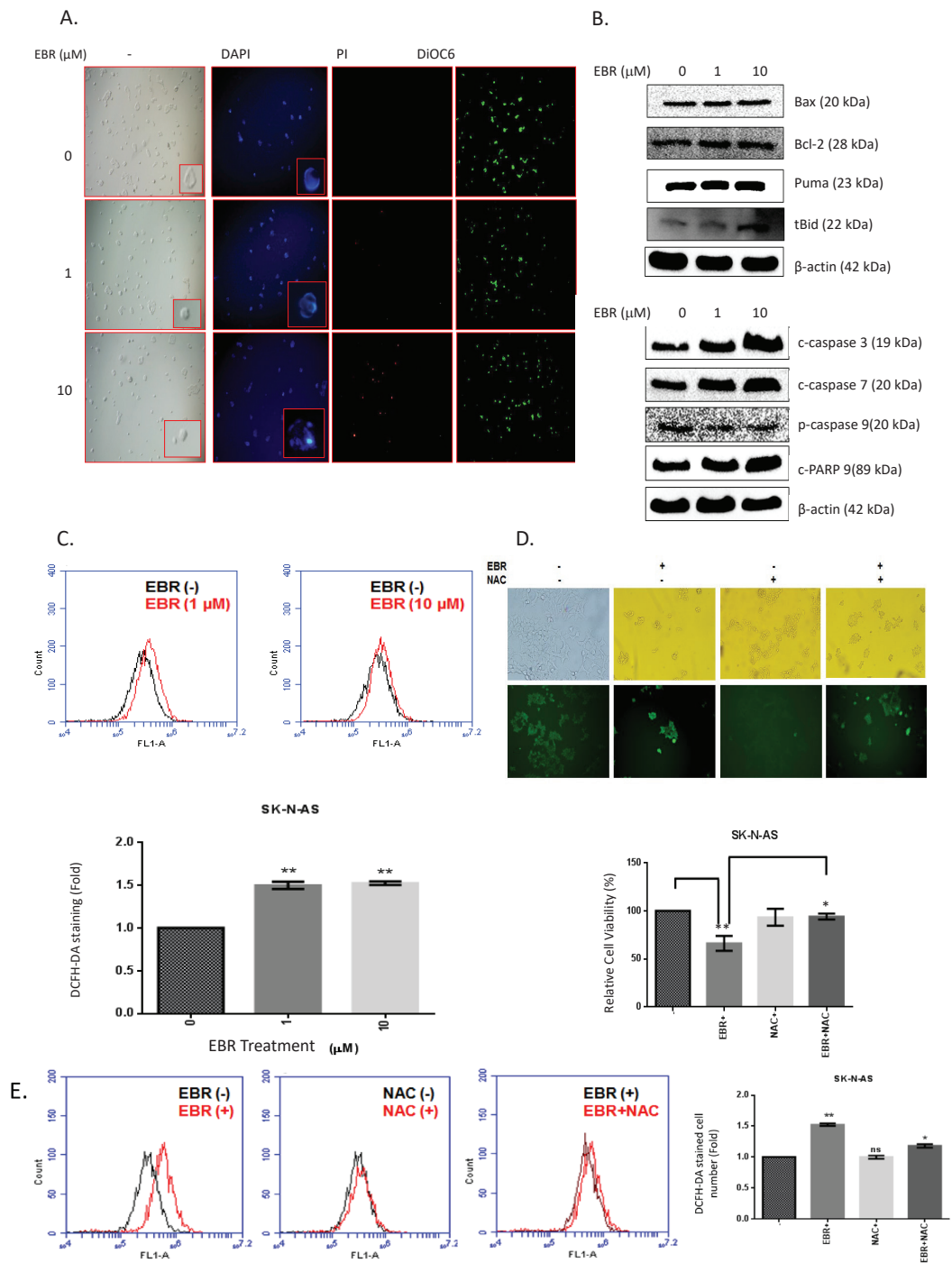


Figure 5. EBR-induced cell death was determined in SKNAS cells by fluorescent dyes. **A.** Cells treated with EBR for 24 h were later stained with DAPI, PI, and DiOC6, and examined under fluorescence microscopy (400x). **B.** 1 and 10 μM EBR was applied to SK-N-AS cells for 24 h. The immunoblotting method was used to determine the effects of EBR application on the pro- and anti-apoptotic Bcl-2 family, caspases, and PARP cleavage. After total protein isolation, 30 μg of protein was separated by 12% SDS-PAGE for each sample. The bands of the relevant proteins were determined based on the chemiluminescent feature. Beta-actin was used as the loading control. **C.** The effect of EBR treatment on ROS generation was determined after DCFH-DA staining. Cells were treated with 1 and 10 μM EBR for 24 h and then were stained with DCFH-DA. After 15 min of incubation, cells were analyzed by flow cytometry. **D.** The effect of NAC co-treatment with EBR on ROS generation was determined under fluorescence microscopy and by examining the cell viability loss with MTT assay. **E.** Co-treatment of NAC with EBR prevented ROS generation measured following FACS flow analysis. *p<0.05 and **p<0.01

Epibrassinolide Altered Wnt Signaling in SK-N-AS Cell Line

Wnt pathway proteins were examined in the SK-N-AS cell line. As seen in Figure 6A, a decrease was observed in the expression of GSK3 β protein in SK-N-AS cells after 1 μ M EBR for 24 h, in contrast, increased protein expression was observed following exposure of 10 μ M EBR to the cell line (Figure 6A). We also detected the increased expression profile of the phosphorylated form of GSK3 β by Ser9 residue, which indicates its inhibition after both 1 and 10 μ M EBR treatments. The downstream target of GSK3 β is β -catenin, an important transcription factor regulating various cellular processes including cell proliferation and cell cycle. As seen in Figure 6A, a decrease in the expression of the β -catenin protein was determined in SK-N-AS cells treated with 1 and 10 μ M EBR for 24 h. In addition, the nuclear localization of β -catenin was also prevented more specifically following the exposure of cells to 10 μ M EBR (Figure 6B).

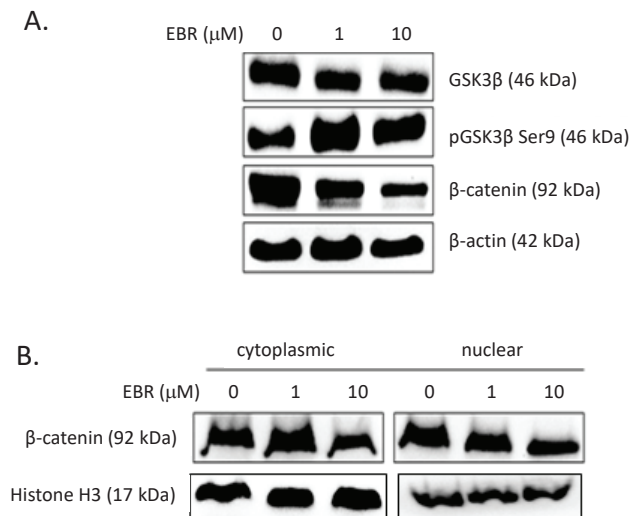


Figure 6. The effects of EBR were determined on GSK3/ β -catenin pathway. After **A.** total and **B.** nuclear-cytoplasmic protein isolation, 30 μ g of protein was separated by 12% SDS-PAGE for each sample. After the immunoblotting procedures, the bands of the relevant proteins were determined based on the chemiluminescent feature. Beta-actin was used as the loading control.

DISCUSSION

Neuroblastoma, one of the deadliest tumors of infancy, is the malignancy of neural crest cells. The heterogeneity of the tumor-forming cells causes resistance to treatment, leading to metastatic spread and poor survival (15). Despite new interventions in therapeutic approaches, the current therapies are not effective and new treatment options are urgently needed since the overall survival rate is less than 10%. Previous studies have shown that GSK3 β inhibition has been shown to reduce proliferation and increase apoptosis in neuroblastoma cells (4,5). The cell cycle arrest induced by lithium treatment has been shown to reduce cell proliferation in vitro in the B65 neuroblastoma cell line (4). Most importantly, similar effects were also observed in in vivo experimental set-ups, delayed tumor growth, and cell cycle arrest (16).

A potential GSK3 inhibitor EBR, similar to mammalian steroid hormones, belongs to the plant BR family, which has a vital role in plant growth and development. The cytotoxic effect of EBR was first identified in mammalian cancer cells. Later, the effect of EBR on nuclear hormone receptor (NHR) expressing cell lines was investigated, and it was concluded that EBR is a candidate for NHR expressing cells (12, 17). In this study, it was shown that EBR inhibited the cell cycle in the G1 phase in the estrogen-dependent MCF-7 breast cancer cell line, affecting the expression of CDKs (p21, p27, p53) and cyclins, which regulate the cycle and induced apoptosis (17). In 2014, our group demonstrated that EBR induced apoptosis in a p53-independent and caspase-dependent manner in both NHR expressing and non-expressing cancer cell lines, which pointed out another shared target between these cells (14). Intracellular proteomic changes were determined for this purpose by our group using the SILAC (stable isotope-labeled amino acid in cell culture) method (18). As a result of the study, our laboratory showed that many proteins related to cell survival, apoptosis, endoplasmic reticulum (ER) stress, and ubiquitination in cells exposed to EBR application were significantly altered compared to untreated control cells. Among these proteins, the most significant change was observed for calreticulin, which is a chaperone having a role in protein folding in the ER lumen and Ca²⁺ ion buffering (18). ER stress is defined as the accumulation of un/misfolded proteins in the ER lumen and the stress is often transmitted to the nucleus to start the cellular adaptation processes, including the induction of the transcription of chaperone proteins, or autophagy to eliminate misfolded proteins (19,20). However, ER stress can also initiate apoptosis if the recovery of cells in terms of protein folding is not achieved. The regulation of ER stress-induced apoptosis has been shown to involve GSK3 (21). GSK3 has two Ser/Thr kinase isoforms (GSK3 α and GSK3 β) with distinct roles and they are controlled by the inhibitory phosphorylations through Ser21 and Ser9, respectively (22). Following the activation of the Wnt signaling pathway, GSK3 associates with Axin to phosphorylate β -catenin and prepare it for proteasomal degradation (23). On the other hand, PI3K/Akt pathway activation can also lead to the inhibition of GSK3 β , which in turn can influence the downstream target's (β -catenin) translocation to the nucleus (24). β -catenin was the first identified molecule having a role in cell-cell adhesion, in collaboration with E-cadherin (25). A significant relationship was shown between β -catenin activity and apoptosis (26). According to previous studies, caspases target β -catenin during apoptotic events and cause the dismantling of the cell adhesion. On the other hand, the decrease of β -catenin nuclear translocation following inhibited Wnt signaling has been suggested as a marker of cell survival loss for several cells, including cancer and neuronal cells (27,28). Several studies suggested that GSK3 has an obligatory role in CHOP activation leading to ER stress-induced apoptosis by activating caspases (29). According to our previous results, EBR can act as a GSK3 β inhibitor in low concentrations (30). Therefore, we investigated the possible outcomes of GSK3 β inhibition in neuroblastoma cells in this study. We found that EBR treatment caused cell viability

loss and survival in SK-N-AS cells. The colony-forming potential of the cell was also prevented by EBR treatment at low concentrations of 1 and 10 mM. Like our previous findings, the apoptotic potential of EBR was also visualized in the neuroblastoma cell line. The cytostatic effect of EBR has been demonstrated in prostate and colon cancer cells at 10 and 20 μ M doses. A dose of 30 μ M EBR produced a cytotoxic effect in these cells. The effect on the clonogenic potential of SK-N-AS cells was not observed, although steroid-derived drugs, including bicalutamide, have been shown to inhibit colony formation in various cancer cell lines (31, 32). A significant increase in the early and late apoptotic population percentage was observed, confirming our recent results indicating EBR is an apoptotic inducer in different cancer cell lines. Apoptotic markers were investigated to understand whether the loss of cell viability induced by EBR is due to apoptotic cell death. Several studies also indicate that steroid-derived chemotherapeutics could cause DNA damage or DNA fragmentation (33). Similar to our previous results, in which EBR caused DNA fragmentation in prostate and colon cancer cells, EBR was also able to induce DNA fragmentation in SK-N-AS cells (13,14). EBR treatment also induced mitochondrial membrane potential loss and cell death. These results indicated the anti-cancer properties of EBR in neuroblastoma cells.

In the next stage of our study, SK-N-AS cells were examined in flow cytometry to determine whether EBR affects the formation of ROS in the apoptotic process. According to our results, ROS generation was significantly increased following each concentration of EBR treatment compared to control samples. These results suggest that cell death in EBR-treated SK-N-AS cells occurs by mitochondrial pathway-mediated apoptosis. When EBR was combined with N-acetyl cysteine (NAC) in SK-N-AS cells, its effect on ROS generation and cell viability was determined. Compared to EBR alone, the combination of EBR and NAC inhibited ROS generation and loss of cell viability in SK-N-AS cells. Based on this, it was concluded that EBR is an agent that causes the formation of ROS. NAC is an agent that plays a vital role in detoxifying glutathione and xenobiotics. It can detoxify free radicals and reactive electrophiles. In the study by Olivieri et al., it was stated that NAC protects cells from oxidative stress and cytotoxic-stimulating compounds in the SH-SY-5Y neuroblastoma cell line (34). In our study, although no cytotoxic effect of NAC on SK-N-AS cells was observed, it was observed that NAC reversed the cytotoxic effect of EBR when applied together with the drug. The EBR-induced cell death mechanism was identified as mitochondria-mediated apoptosis since we observed significant expression changes in pro- and anti-apoptotic protein levels. It was observed that the expression levels of Bax, truncated Bid, and Puma were increased in SK-N-AS cells compared to control cells following EBR treatment. Deprivation of pro-apoptotic proteins is one of the causes of drug insensitivity. Bax and Puma are pro-apoptotic proteins located in the cytosol that translocate to mitochondria with the induction of apoptosis. Bax and Puma are under the direct transcriptional control of p53 through their respective binding sites. They have been shown to increase cytochrome c release and caspase cleavage in vitro and in vivo. In

this respect, the increase in the expression of both pro-apoptotic proteins was necessary for the apoptotic effect of EBR in SK-N-AS cells. Studies have also shown the effect of EBR on Bax and Puma in colon, prostate, and breast cancer cells (35). In addition, Bid protein is another pro-apoptotic protein that is induced by caspase 8 activation via the external apoptotic pathway and effective on the mitochondrial pathway. Studies in the literature have not shown any effect of EBR on the extrinsic apoptotic pathway. This effect is specific to SK-N-AS cells, and the activation of this pathway needs to be clarified in the future. This study also examined Bcl-2 expression as an anti-apoptotic Bcl-2 family member. No significant changes in Bcl-2 protein expression were found in SK-N-AS cells. In the study by Obakan et al., it was shown that the expression of pro-apoptotic proteins Bax, Puma, Bak, and Bim in the PC3 prostate cancer cell line increased with EBR treatment, while the expression of anti-apoptotic proteins Mcl-1 and Bcl-2 decreased (14). In the study by Steigerova et al., it was shown that the expression of anti-apoptotic proteins Bcl-X_L and Bcl-2 decreased, and the expression of Bax and Bid pro-apoptotic protein decreased with time-dependent EBR treatment in MCF-7 breast cancer cell line (17). It has been shown that the expression of the anti-apoptotic proteins Bcl-2 and Mcl-1 did not change in the MDA-MB-438 breast cancer cell line, the Bid pro-apoptotic protein was cleaved, and the expression of Bax pro-apoptotic protein decreased. We also evaluated the effect of EBR on caspase cleavage in the SK-N-AS cell line. The cleaved and active forms of caspase-3, caspase-7, and PARP in the SK-N-AS cell line were found upregulated, and decreasing pro-caspase-9 expression was observed. Although the effect of EBR on neuroblastoma cells is not known in the literature, caspase-3, -7, -9 and PARP cleavage was observed in DU145 prostate and MDA-MB-231 breast cancer cells in other studies conducted with cancer cells that do not express functional steroid hormone receptors (14,17).

It is well known that GSK3 β can have a tumor-promoting or a tumor-inhibiting role, depending on the cancer cell type. The previous study by Dickey A. et al. showed that the inhibition of GSK3 β can increase apoptosis by decreasing the expression of the anti-apoptotic proteins XIAP and Bcl-2 (5). The same study also suggested that a decrease in cell viability was determined by inhibiting GSK3 β in Neuro-2A neuroblastoma cells, with the induction of apoptosis and cell cycle arrest. The conflicting effects of GSK3 β on apoptosis are known; it inhibits extrinsic death receptor-mediated apoptosis while promoting the mitochondrial intrinsic apoptotic pathway. In a study by Petit-Paitel et al. in 2009, it was shown that inhibition of GSK3 β activity in mouse TSM1 neuron cells prevents cell death by inhibiting mitochondrial membrane potential changes and subsequent caspase-9 and caspase-3 activation (36). In another study it was stated that overexpression of GSK3 β induced a caspase-dependent apoptosis in neuronal cells via Nuclear Factor κ B (NF κ B) Signaling inhibition. Kotliarova et al. also determined that the inhibition of GSK3 β causes the activation of oncogenic transcription factor c-myc, thus apoptosis and ultimately cytotoxicity, by stimulating pro-apoptotic factors such as Bax, Bim, and

tumor-necrosis-factor-associated apoptosis-stimulating ligand (TRAIL) (37). In our study, when cells are exposed to EBR, a decrease in the expression of GSK3 β and subsequent increase in the phosphorylated form of GSK3 β by Ser9 were observed, suggesting that EBR could inhibit GSK3 β activity. Despite the inhibition of GSK3 β , we found that β -catenin levels are downregulated in SK-N-AS cells after EBR treatment, especially with 10 mM EBR. Similarly, a decrease in expression of both cytoplasmic and nuclear β -catenin was observed in 10 μ M EBR treated cells. Studies showed that inhibition of GSK3 β leads to transcriptional activation of different target genes via β -catenin activation. For example, the activity of β -catenin has been shown related to increasing the number of neurons differentiating from neurospheres (38). The aberrant accumulation of β -catenin in tumors is considered associated with p53 inactivation, an important tumor suppressor. Sadot et al have shown that the overexpression of wild-type p53 down-regulated β -catenin in cancer cells is accompanied by the inhibition of its transactivation potential (39). They suggested that the link between p53 and β -catenin requires an active GSK3 β and the down-regulation of β -catenin is mediated by the ubiquitin-proteasome system. In addition, various recent studies also indicated that the down-regulation of β -catenin is an important phenomenon to decrease tumorigenicity, however, it can promote epithelial-mesenchymal transition, which occurs during metastasis (40,41). Therefore, the possible effects of EBR on epithelial-mesenchymal transition and metastasis could be examined in future experiments.

CONCLUSION

The data obtained from this study clearly showed for the first time that EBR can act on GSK3 β signaling and downstream targets, including β -catenin, and promote apoptosis in SK-N-AS neuroblastoma cells. The epithelial-mesenchymal transition and metastasis processes activated in response to EBR related to Wnt and β -catenin signaling are worth clarifying in the future. The obtained data also provides a basis for future studies regarding the therapeutic efficacy of EBR and its use in *in vivo* trials related to Wnt signaling.

Acknowledgements: We are thankful to Berkay Gurkan for technical assistance.

Ethics Approval Statement: All the experiments were performed using a commercially available cell line from ATCC. Neither human nor animal samples were used in this research.

Peer Review: Externally peer-reviewed.

Author Contributions: Conception/Design of Study- P.O.Y.; Data Acquisition- P.O.Y., S.N.; Data Analysis/Interpretation- P.O.Y., S.N.; Drafting Manuscript- P.O.Y., S.N.; Critical Revision of Manuscript- P.O.Y., S.N.; Final Approval and Accountability- P.O.Y., S.N.

Conflict of Interest: Authors declared no conflict of interest.

Financial Disclosure: We are thankful to Istanbul Kultur University Scientific Projects Support Center for supporting this study.

REFERENCES

1. Qiu B and Matthay KK. Advancing therapy for neuroblastoma. *Nat Rev Clin Oncol* 2022; 1-19.
2. Otte J, Dyberg C, Pepich A, and Johnsen JI, MYCN Function in Neuroblastoma Development. *Front Oncol* 2021; 10: 3210.
3. Foster JH, Voss SD, Hall DC, Minard CG, Balis FM, Wilner K, et al. Activity of Crizotinib in Patients with ALK-Abrerrant Relapsed/Refractory Neuroblastoma: A Children's Oncology Group Study (ADVL0912). *Clin Cancer Res* 2021; 27(13): 3543-8.
4. Carter YM, Kunnimalaiyaan S, Chen H, Gamblin TC, Kunnimalaiyaan M. Specific glycogen synthase kinase-3 inhibition reduces neuroendocrine markers and suppresses neuroblastoma cell growth. *Cancer Biol Ther* 2014; 15(5): 510-5.
5. Dickey A, Schleicher S, Leahy K, Hu R, Hallahan D, Thotala DK. GSK-3 β inhibition promotes cell death, apoptosis, and *in vivo* tumor growth delay in neuroblastoma Neuro-2A cell line. *J Neurooncol* 2011; 104(1): 145-53.
6. Augello G, Emma MR, Cusimano A, Azzolina A, Montalto G, McCubrey JA, Cervello M. The Role of GSK-3 in Cancer Immunotherapy: GSK-3 Inhibitors as a New Frontier in Cancer Treatment. *Cells* 2020; 9(6): 1427.
7. Arciniegas Ruiz SM, Eldar-Finkelman H. Glycogen Synthase Kinase-3 Inhibitors: Preclinical and Clinical Focus on CNS-A Decade Onward. *Front Mol Neurosci* 2022; 14: 792364.
8. Peres ALGL, Soares JS, Tavares RG, Righetto G, Zullo MAT, Mandava NB, Menossi M. Brassinosteroids, the Sixth Class of Phytohormones: A Molecular View from the Discovery to Hormonal Interactions in Plant Development and Stress Adaptation. *Int J Mol Sci* 2019; 20(2): 331.
9. Thummel CS, Chory J. Steroid signaling in plants and insects-common themes, different pathways. *Genes Dev* 2002; 16(24): 3113-29.
10. Manghwar H, Hussain A, Ali Q, Liu F. Brassinosteroids (BRs) Role in Plant Development and Coping with Different Stresses. *Int J Mol Sci* 2022; 23(3): 1012.
11. Kaur Kohli S, Bhardwaj A, Bhardwaj V, Sharma A, Kalia N, Landi M, Bhardwaj R. Therapeutic Potential of Brassinosteroids in Biomedical and Clinical Research. *Biomolecules* 2020; 10(4): 572.
12. Steigerova J, Rarova L, Oklestkova J, Krizova K, Levkova M, Svachova M, et al. Mechanisms of natural brassinosteroid-induced apoptosis of prostate cancer cells. *Food Chem Toxicol* 2012; 50(11): 4068-76.
13. Coskun D, Obakan P, Arisan ED, Çoker-Gürkan A, Palavan-Ünsal N. Epibrassinolide alters PI3K/MAPK signaling axis via activating Foxo3a-induced mitochondria-mediated apoptosis in colon cancer cells. *Exp Cell Res* 2015; 338(1): 10-21.
14. Obakan P, Arisan ED, Calcabrini A, Agostinelli E, Bolkent S, Palavan-Ünsal N. Activation of polyamine catabolic enzymes involved in diverse responses against epibrassinolide-induced apoptosis in LNCaP and DU145 prostate cancer cell lines. *Amino Acids* 2014; 46(3): 553-64.
15. Johnsen JI, Dyberg C, Wickström M. Neuroblastoma-A Neural Crest Derived Embryonal Malignancy. *Front Mol Neurosci* 2019; 12: 9.
16. Gao Y, Tan L, Yu JT, Tan L. Tau in Alzheimer's Disease: Mechanisms and Therapeutic Strategies. *Curr Alzheimer Res* 2018; 15(3): 283-300.
17. Steigerova J, Oklestkova J, Levkova M, Rarova L, Kolar Z, Strnad M. Brassinosteroids cause cell cycle arrest and apoptosis of human breast cancer cells. *Chem Biol Interact* 2010; 188 (3): 487-96.
18. Obakan P, Barrero C, Coker-Gurkan A, Arisan ED, Merali S, Palavan-Ünsal N. SILAC-Based Mass Spectrometry Analysis Reveals That Epibrassinolide Induces Apoptosis via Activating Endoplasmic Reticulum Stress in Prostate Cancer Cells. *PLoS One* 2015; 10(9): e0135788.

19. Bravo R, Parra V, Gatica D, Rodriguez AE, Torrealba N, Paredes F, et al. Endoplasmic reticulum and the unfolded protein response: dynamics and metabolic integration. *Int Rev Cell Mol Biol* 2013; 301: 215-90.
20. Adams CJ, Kopp MC, Larburu N, Nowak PR, Ali MMU. Structure and Molecular Mechanism of ER Stress Signaling by the Unfolded Protein Response Signal Activator IRE1. *Front Mol Biosci* 2019; 6: 11.
21. Nie T, Yang S, Ma H, Zhang L, Lu F, Tao K, et al. Regulation of ER stress-induced autophagy by GSK3 β -TIP60-ULK1 pathway. *Cell Death Dis* 2016; 7(12): e2563.
22. Beurel E, Grieco SF, Jope RS. Glycogen synthase kinase-3 (GSK3): regulation, actions, and diseases. *Pharmacol Ther* 2015; 148: 114-31.
23. Wu D, Pan W. GSK3: a multifaceted kinase in Wnt signaling. *Trends Biochem Sci* 2010; 35(3): 161-8.
24. Zhang C, Su L, Huang L, Song ZY. GSK3 β inhibits epithelial-mesenchymal transition via the Wnt/ β -catenin and PI3K/Akt pathways. *Int J Ophthalmol* 2018; 11(7): 1120-8.
25. Kourtidis A, Lu R, Pence LJ, Anastasiadis PZ. A central role for cadherin signaling in cancer. *Exp Cell Res* 2017; 358(1): 78-85.
26. Donmez HG, Demirezen S, Beksac MS. The relationship between beta-catenin and apoptosis: A cytological and immunocytochemical examination. *Tissue Cell* 2016; 48(3): 160-7.
27. Martinez-Font E, Pérez-Capó M, Ramos R, Felipe I, Garcías C, Luna P, et al. Impact of Wnt/ β -Catenin Inhibition on Cell Proliferation through CDC25A Downregulation in Soft Tissue Sarcomas. *Cancers (Basel)* 2020; 12(9): 2556.
28. Lee Y, Lee JK, Ahn SH, Lee J, Nam DH. WNT signaling in glioblastoma and therapeutic opportunities. *Lab Invest* 2016; 96(2): 137-50.
29. Mearns GP, Mines MA, Beurel E, Eom TY, Song L, Zmijewska AA, Jope RS. Glycogen synthase kinase-3 regulates endoplasmic reticulum (ER) stress-induced CHOP expression in neuronal cells. *Exp Cell Res* 2011; 317(11): 1621-8.
30. Obakan Yerlikaya P, Arisan ED, Coker Gurkan A, Okumus OO, Yenigun T, Ozbey U, Kara M, Palavan Unsal N. Epibrassinolide prevents tau hyperphosphorylation via GSK3 β inhibition in vitro and improves *Caenorhabditis elegans* lifespan and motor deficits in combination with roscovitine. *Amino Acids* 2021; 53(9): 1373-89.
31. Liao Y, Sassi S, Halvorsen S, Feng Y, Shen J, Gao Y, Cote G, et al. Androgen receptor is a potential novel prognostic marker and oncogenic target in osteosarcoma with dependence on CDK11. *Sci Rep* 2017; 7: 43941.
32. Wang Y, Mikhailova M, Bose S, Pan CX, deVere White RW, Ghosh PM. Regulation of androgen receptor transcriptional activity by rapamycin in prostate cancer cell proliferation and survival. *Oncogene* 2008; 27(56): 7106-17.
33. Bhutani KK, Paul AT, Fayad W, Linder S. Apoptosis inducing activity of steroidal constituents from *Solanum xanthocarpum* and *Asparagus racemosus*. *Phytomedicine* 2010; 17(10): 789-93.
34. Olivieri G, Baysang G, Meier F, Müller-Spahn F, Stähelin HB, Brockhaus M, Brack C. N-acetyl-L-cysteine protects SHSY5Y neuroblastoma cells from oxidative stress and cell cytotoxicity: effects on beta-amyloid secretion and tau phosphorylation. *J Neurochem* 2001; 76(1): 224-33.
35. Obakan P, Arisan ED, Coker-Gurkan A, Palavan-Unsal N. Epibrassinolide-induced apoptosis regardless of p53 expression via activating polyamine catabolic machinery, a common target for androgen sensitive and insensitive prostate cancer cells. *Prostate* 2014; 74(16): 1622-33.
36. Petit-Paitel A, Brau F, Cazareth J, Chabry J. Involvement of cytosolic and mitochondrial GSK-3beta in mitochondrial dysfunction and neuronal cell death of MPTP/MPP-treated neurons. *PLoS One* 2009; 4(5): e5491.
37. Kotliarova S, Pastorino S, Kovell LC, Kotliarov Y, Song H, Zhang W, et al. Glycogen synthase kinase-3 inhibition induces glioma cell death through c-MYC, nuclear factor-kappaB, and glucose regulation. *Cancer Res* 2008; 68(16): 6643-51.
38. Kuwahara A, Sakai H, Xu Y, Itoh Y, Hirabayashi Y, Gotoh Y. Tcf3 represses Wnt- β -catenin signaling and maintains neural stem cell population during neocortical development. *PLoS One* 2014; 9(5): e94408.
39. Sadot E, Geiger B, Oren M, Ben-Ze'ev A. Down-regulation of beta-catenin by activated p53. *Mol Cell Biol* 2001; 21(20): 6768-81.
40. Jang GB, Kim JY, Cho SD, Park KS, Jung JY, Lee HY, et al. Blockade of Wnt/ β -catenin signaling suppresses breast cancer metastasis by inhibiting CSC-like phenotype. *Sci Rep* 2015; 5: 12465.
41. Zhang L, Cheng H, Yue Y, Li S, Zhang D, He R. H19 knockdown suppresses proliferation and induces apoptosis by regulating miR-148b/WNT/ β -catenin in ox-LDL-stimulated vascular smooth muscle cells. *J Biomed Sci* 2018; 25(1): 11.

Anti-Cancer Effects of *Trigonella foenum* in Neuroblastoma Cell Line

Irem Urkmez¹ , Hatice Ilayhan Karahan Coven² , Asli Eldem² , Melek Pehlivan³ 

¹Izmir Katip Celebi University, Faculty of Medicine, Izmir, Turkiye

²Izmir Katip Celebi University, Medical Biology and Genetics, Izmir, Turkiye

³Izmir Katip Celebi University, Vocational School of Health Services, Izmir, Turkiye

ORCID IDs of the authors: I.U. 0000-0002-5466-3323; H.I.K.C. 0000-0002-3371-7345; A.E. 0000-0003-3510-6748; M.P. 0000-0001-8755-4812

Please cite this article as: Urkmez I, Karahan Coven HI, Eldem A, Pehlivan M. Anti-Cancer Effects of *Trigonella foenum* in Neuroblastoma Cell Line. Eur J Biol 2022; 81(2): 251-256. DOI: 10.26650/EurJBiol.2022.1167842

ABSTRACT

Objective: Current approaches focus on the use of natural compounds in plants in the treatment of cancer. *Trigonella foenum* (Fenugreek) is mainly used in medicine, food, and cosmetics due to its bioactive and aromatic compounds. Many compounds with medicinal effects are found in Fenugreek seeds. These compounds have been demonstrated to be effective on numerous cancer cells. Neuroblastoma is one of the most common extracranial solid malignancies in children. In our study, the effects of Fenugreek on cell cytotoxicity, cell damage, migration, and sphere formation in neuroblastoma cells were investigated.

Materials and Methods: The powder extract was dissolved in DMEM and filtered to prepare a stock solution of Fenugreek. We used MTT assay for the detection of cytotoxic effects of Fenugreek on SH-SY5Y cells, crystal violet staining for the analysis of morphological change in cells, wound healing test for the cell migration analysis, and agarose gel electrophoresis for detecting DNA damage. We created a spheroid to test the effect we observed in 2D culture, in 3D culture as well.

Results: The findings of our study showed that Fenugreek treatments caused significant reductions in cell proliferation and migration capacities in 2D neuroblastoma cells at IC₅₀ (1500 µg/ml) doses, respectively. In addition Fenugreek changed cell morphology and increased DNA fragmentation. Furthermore, Fenugreek caused disruption of 3D spheroid formation of SHSY-5Y cells in a dose- and time-dependent manner.

Conclusion: The determination of the anti-cancer effect of Fenugreek on neuroblastoma cancer may be a useful and feasible intervention in neuroblastoma patients in the light of further studies and with the help of new nano drug delivery systems.

Keywords: Fenugreek, neuroblastoma, proliferation, spheroid

INTRODUCTION

An increasing number of research studies are now focusing on investigations of the anti-cancer potential of plants. Because bioactive chemicals in plants have been shown to have a variety of biological and pharmacological effects, natural products are regarded as powerful sources for new drug discovery and development. The various medicinal effects of natural compounds in traditional medicine have sparked interest in their use in cancer treatment (1,2).

The annual plant Fenugreek (*Trigonella foenum graecum*) belongs to the Leguminosae family. Fenugreek is one of the oldest medicinal herbs known as an aromatic legume plant native to many Asian, Middle Eastern and European countries due to its therapeutic and medicinal properties and is recognized by the FDA (American Food and Drug Administration) (3). The antioxidant and anti-inflammatory properties of Fenugreek that has rich content of Diosgenin, Apigenin, Luteolin, and Kaempferol have been reported. Although there are studies on



Corresponding Author: Melek Pehlivan

E-mail: pehlivanmlk@gmail.com

Submitted: 30.08.2022 • **Revision Requested:** 16.09.2022 • **Last Revision Received:** 24.09.2022 •

Accepted: 21.10.2022 • **Published Online:** 20.12.2022

Content of this journal is licensed under a Creative Commons Attribution-NonCommercial 4.0 International License.



the antiproliferative effects of Fenugreek on cancer cells such as breast and colon cancers, there is no comprehensive study that has reported its potential therapeutic efficacy against SH-SY5Y cells (4).

Neuroblastoma accounts for 10% of pediatric cancers and is characterized with a high risk of death due to its strong metastatic potential. Neuroblastoma is a very variable and difficult-to-treat tumor that can range from spontaneous remission to tumor development to aggressive malignancy. It is known to develop from embryonic neural crest cells, which play a critical role in the development of the sympathetic nervous system (5). The molecular mechanisms underlying the development and progression of neuroblastoma are unknown (6).

In this study, we aimed to detect the cytotoxic effect of Fenugreek, which is utilized in traditional medicine and widely used in Turkish cuisine, on SH-SY5Y cells. In addition its potential effects on cell migration and DNA damage were investigated. The effects of Fenugreek on SH-SY5Y cells generated as two-dimensional (2D) and three-dimensional (3D) spheroid models were examined.

MATERIALS AND METHODS

Preparation of Fenugreek Extract

Fenugreek extract was donated by INDUS BIOTECH, INDIA. Before use it was dissolved in Dulbecco's Modified Eagle Medium (DMEM) (Gibco, Waltham, MA, USA).

Culture of The Neuroblastoma Cell Line 'SH-SY5Y'

The SH-SY5Y cell line from the American Type Culture Collection (ATCC) was cultured in DMEM (Gibco, Waltham, MA, USA) with 10% fetal bovine serum (FBS) (Serox GmbH, Mannheim, Germany), 2 mM L-glutamine (Sigma-Aldrich), 100 U/ml penicillin, and 100 g/ml streptomycin (Sigma-Aldrich). Cells were incubated in a 95% humidity and 5% CO₂ atmosphere at 37°C.

The Cytotoxic Effect of Fenugreek in SH-SY5Y Cells: MTT Assay

The cytotoxic effect of the plant extract was assessed using the MTT (3-[4,5-dimethylthiazol-2-yl]-2,5-diphenyltriazolium bromide) (BioFroxx, Germany) assay. In a 96-well plate, SH-SY5Y cells were seeded at 5x10³ cells/well and allowed to attach to the surface for 24 h. The cells were exposed to 100 µg/ml, 500 µg/ml, 750 µg/ml, 1000 µg/ml, and 1500 µg/ml concentrations of plant extract for 24 h and incubated for 4 h by adding 5 mg/mL of MTT. To each well, 100 µl dimethyl sulfoxide (DMSO) (Merck) was added to reduce formazan crystals. Absorbance at 570 nm was measured by a multiplate reader (BioTek™ Synergy™ HTX). The mean absorbance of the control cells was accepted as 100% viable. The effective dose (IC₅₀) value was calculated.

The Effect of Fenugreek on Morphological Changes in SH-SY5Y Cells: Crystal Violet Staining

SH-SY5Y cells were seeded at a density of 25x10⁴ cells per well in a 6-well plate and allowed to adhere to the surface for 24 h. After exposing the cells to the plant extract (750 µg/ml, 1500

µg/ml (IC₅₀), 3000 µg/ml for 24 h, the morphology of the cells was assessed using crystal violet staining. Phosphate buffered saline (PBS):methanol was added in a 1:1 ratio and maintained at +4°C for 3 h. After that, a solution of 0.1 % crystal violet and 5% methanol was added and incubated for 15 min at room temperature. The dye in the well was removed after the plate had been incubated. After waiting for the well to dry for 1-2 min, it was examined under a microscope (Olympus CKX53, 10X).

The Effect of Fenugreek on Cell Migration in SH-SY5Y Cells: The *In Vitro* Wound Healing Model

SH-SY5Y cells were seeded at 5 x 10⁵ cells/well in a 24-well plate and allowed to adhere to the surface for 24 h. A sterile plastic pipette tip was used to make a linear wound pattern on the sheet at once. Cells were exposed to Fenugreek at doses of 750 µg/ml, 1500 µg/ml (IC₅₀) and, 3000 µg/ml and compared to the control group. All of the samples were visualized using an inverted microscope (Olympus CKX53,10X) at 0th, 24th, 48th, 72th h.

The Effect of Fenugreek on DNA Damage in SH-SY5Y Cells: Electrophoretic Analysis

SH-SY5Y was seeded at 10⁶ cells/well in a 6-well plate. The cells were allowed to adhere to the 6-well plate overnight and exposed to the plant extract (750 µg/ml, IC₅₀, 3000 µg/ml) for 24 h. The cells were then scraped into a sterile tube, centrifuged for 5 min at 900 rpm, and resuspended in 1 ml of ice-cold PBS. DNA was extracted from the cell suspension using a commercial DNA isolation kit according to the manufacturer's instructions (Geneall, Korea). The concentrations and purity of the DNA samples were assessed in the Nanodrop. In the gel electrophoresis, DNA samples were run in 1% agarose at 140 V for 3 h. A UV Transilluminator was used for determination of the bands (Wealtec, USA).

The Effect of Fenugreek on *In Vitro* 3D SH-SY5Y Cells: The Agarose Matrix Spheroid Model

A sterile 1.5 % agarose coating was applied to the 96-well plate. SH-SY5Y cells were seeded at 2x10³ cells/well in agarose matrix and cultured for 10 days to generate a spheroid model. SH-SY5Y cells were exposed to Fenugreek (750 µg/ml, 1500 µg/ml (IC₅₀) and, 3000 µg/ml) for 24 h after sphere formation. The results were evaluated by using a microscope (Olympus CKX53, 10X).

Statistical Analysis

MTT assay results in order to determine the IC₅₀ value of Fenugreek were calculated with GraphPad Prism software v9. Non-linear regression analysis was performed for IC₅₀ calculations. p<0.05 was considered significant.

RESULTS

Fenugreek Induced Cytotoxicity in SH-SY5Y

The MTT assay was used to study the cytotoxic effect of different doses of Fenugreek (0-1000 µg/ml) on SH-SY5Y cells. After 24 h of treatment with various doses of plant extract, a dose-dependent decrease in cell viability was seen (Figure 1). After analyzing all of the concentrations with the GraphPad, the IC₅₀ dose was calculated to be 1500 µg/ml (p<0.05).

**Cytotoxic Effect of Fenugreek in SH-SY5Y Cells:
 MTT Assay**

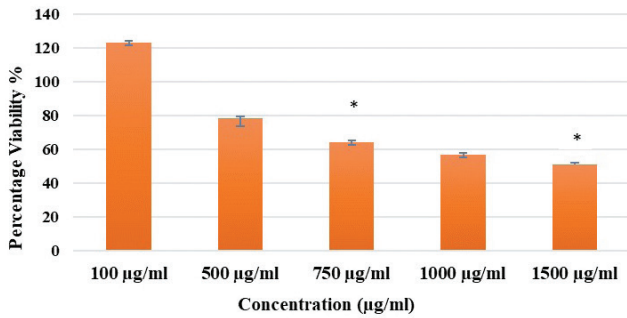


Figure 1. The cytotoxic effect of Fenugreek extract with different concentrations (100 µg/ml, 500 µg/ml, 750 µg/ml, 1000 µg/ml, 1500 µg/ml) on SH-SY5Y cells at 24th h. Experiments were carried out in triplicate. Data are expressed as mean±standard deviation (S.D.). *p<0.05.

The Effects of Fenugreek on the Cell Morphology

An inverted microscope was used to assess the effect of Fenugreek treatment on cell morphology. The results of the micro-

scope examination revealed that cell viability had decreased, which was consistent with the MTT test results. Crystal violet dye was used to stain the cells after they had been morphologically examined (Figure 2). The increasing changes in the morphology of SH-SY5Y cells were observed in a dose-dependent manner. In comparison to the control group, cell viability was reduced in the wells given varying doses of Fenugreek in microscopic examination. More than half of the cells treated with 750 µg/ml Fenugreek survived, but around half of the cells treated with the IC₅₀ dose died. Almost all of the cells died at the toxic dose of 3000 µg/ml.

Fenugreek Induced the Inhibition of Cell Migration

In order to evaluate the metastatic feature of the tumor, it is important to demonstrate its invasion and migration capabilities at the first stage. To investigate the effect of Fenugreek on cell migration in SH-SY5Y, a wound healing model, which is an in vitro approach, was established. The cells of control groups were migrated to the wound area after 24 h. When compared to the control group, the cell migratory capacity of the groups exposed to Fenugreek at 750 µg/ml, 1500 µg/ml (IC₅₀) and 3000 µg/ml concentrations decreased (Figure 3).

**Effect of Fenugreek on Morphological Changes in SH-SY5Y Cells:
 Crystal Violet Staining**

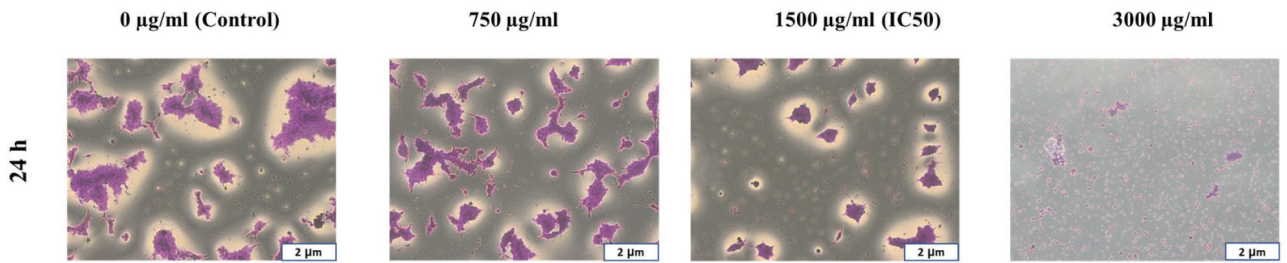


Figure 2. Crystal violet assay was performed in SH-SY5Y at 750 µg/ml, IC₅₀ (1500 µg/ml) and 3000 µg/ml doses.

**Effect of Fenugreek on Cell Migration in SH-SY5Y Cells:
 In Vitro Wound Healing Model**

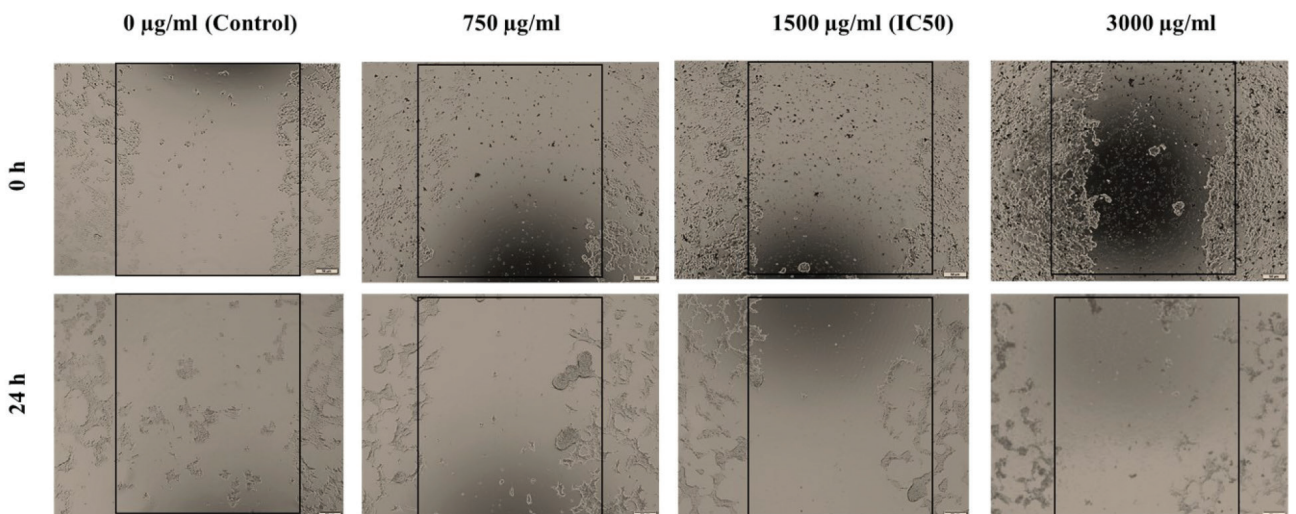


Figure 3. Cell migration was analyzed by wound-healing assay. Scale bar 50 µm.

The Effects of Fenugreek on the DNA Fragmentation

DNA fragmentation was studied using the traditional “DNA ladder” method, which involves extracting DNA from apoptotic cells and separating it on an agarose gel. In cells exposed to Fenugreek, chromosomal DNA was fragmented into short internucleosomal fragments, as illustrated in Figure 4, a biochemical

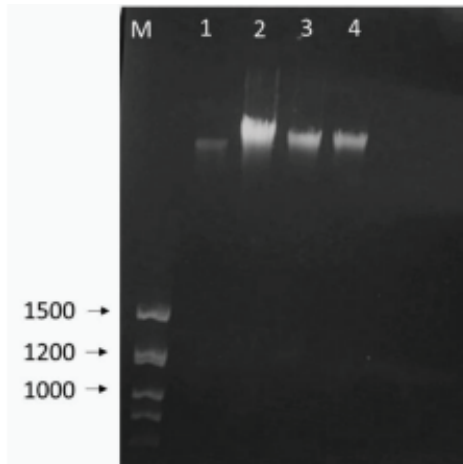


Figure 4. DNA Damage was examined with agarose gel electrophoresis in SH-SY5Y Cells. M:Marker, 1:Control (Untreated) 2: 3000 µg/ml, 3:1500 µg/ml, 4:750 µg/ml.

hallmark of cells undergoing apoptosis. Longer DNA fragmentation was observed when higher Fenugreek concentrations were applied.

The Effects of Fenugreek on Spheroid Forming Ability

We investigated the effect of Fenugreek extract on spheroid formation of SH-SY5Y cells in 3D culture. In each well of a 96-well round bottom extra low attachment plate, 2000 cells were planted. When compared to the control group, the internal structure of the spheroid was more scattered in the IC₅₀ treated group after 24 h. In comparison to the control group, the spheroid structure in the 3000 µg/ml applied group began to dissolve dramatically after 24 h (Figure 5).

DISCUSSION

Natural components make up a portion of the chemotherapeutic and chemopreventive medications, which can be used alone or in combination with other cancer treatment methods (7). Medicinal plants containing natural components have been shown to be effective and versatile chemopreventive agents against cancer types such as lung, breast, and liver cancer (8). The Fenugreek plant from the Leguminosae family has antioxidant and immunostimulatory properties that make it interesting for its use in cancer treatment. In particular, Fenugreek seeds and leaves that contain flavonoids and alkaloids offer a wide range of therapeutic uses (9,10).

Effect of Fenugreek on In vitro 3D SH-SY5Y Cells: Agarose Matrix Spheroid Model

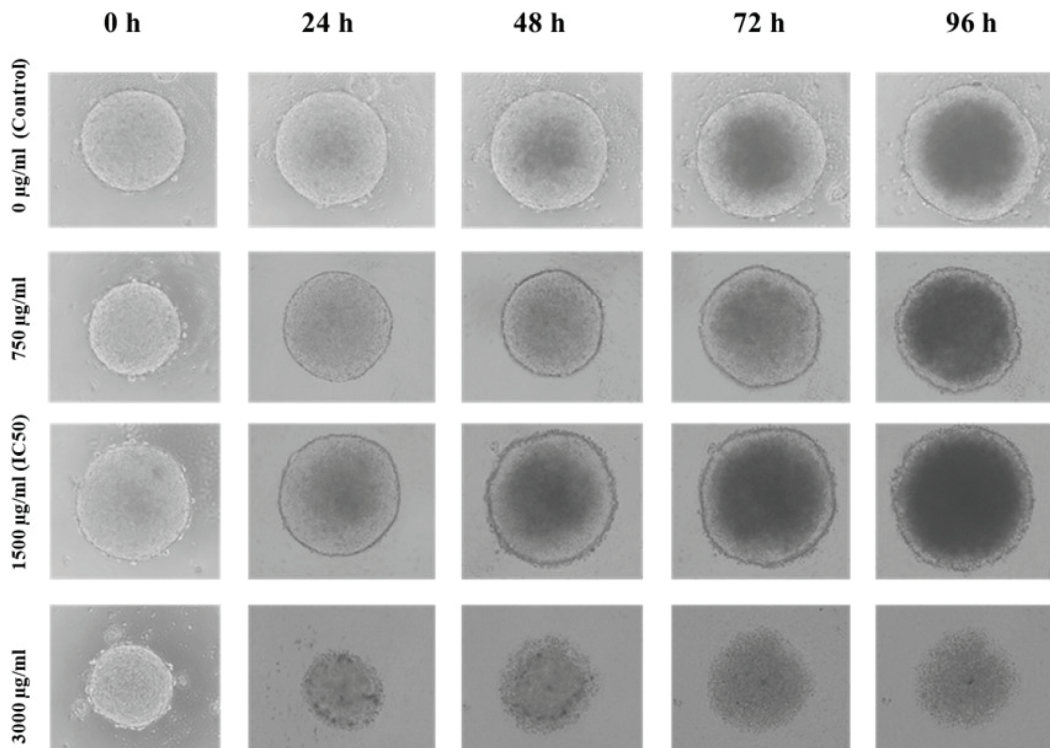


Figure 5. SH-SY5Y spheroids macroscopic aspect after Fenugreek extract treatment. Scale bar 50 µm.

Fenugreek seeds have been shown to have anti-oxidant, anti-diabetic and anti-nociceptive qualities, as well as hypocholesterolemic and anti-cancer capabilities (11). Furthermore Fenugreek constituents are beneficial to neurological health and its constituents have been shown to have hypolipidemic, hypoglycemic, antioxidant, and immunomodulatory effects, as well as a potential role in a variety of neurological disorders (12). With these known effects, we aimed to investigate the effects of Fenugreek extract on neuroblastoma cell viability in our study.

Several studies have focused on the cytotoxic effects of Fenugreek extract on cancer cells. Sebastian et al. showed that Fenugreek ethanolic extract reduced cell viability and triggered early apoptotic changes such as phosphatidylserine reversal and reduced mitochondrial membrane potential on the breast cancer cell line MCF-7 (13). In a different study, it was shown that both MeOH extracts from Fenugreek sprouts were more effective than those from seeds (14,15). Kaviarasan et al. found that Fenugreek had a cytoprotective effect against ethanol-induced cytotoxicity in human liver cells (16). Furthermore, Fenugreek whole plant extract has been also shown to be cytotoxic in vitro against a variety of cancer cell lines, including A549, HepG2, colon cells (502713, HT29), and IMR-32 (17).

Studies determining the effects of Fenugreek on neuroblastoma are few. Syed et al. used brain-derived fibroblast neuroblastoma cells in their study and they reported that IMR-32 neuroblastoma cell lines showed cytotoxic inhibition by Fenugreek extracts (18). We investigated its effect on the bone marrow-derived epithelial neuroblastoma cell line (SH-SY5Y) in our study. We discovered that cytotoxic activity of Fenugreek extract increased in the neuroblastoma cell line in a dose dependent manner.

Moreover, migration studies have been performed to detect the effect of Fenugreek on metastasis. Migration is one of the most important challenges in controlling the cancer process. Metastasis, or the migration of cells in cancer, has a negative impact on the treatment process in patients. As a result, it is critical to identify compounds that inhibit tumor cell migration. In the wound healing model created with SH-SY5Y cells, Fenugreek extract inhibited cell migration (19). In a study with breast cancer cell lines, they reported that the anti-metastatic effect of Fenugreek extract against breast cancer (20). In our study, which is similar to this publication, it was observed that applying Fenugreek extract to SH-SY5Y neuroblastoma cells had a dose-dependent anti-metastatic effect.

Plant extracts containing phenolic compounds can cause DNA damage. Several studies have shown that these compounds can cause mutagenic effects by intercalating with DNA (21). In the literature, it has been shown that Fenugreek extract may be associated with DNA damage in different cancer cells (3,22). Our results show that exposure to Fenugreek extract causes damage to the DNA of SH-SY5Y cells. We also showed that DNA fragmentation increased in a dose-depen-

dent manner in Fenugreek-treated cells compared to the control.

In summary, the Fenugreek plant had an anti-cancer effect on neuroblastoma cells. Taking advantage of the current breakthroughs in 3D spheroid technology for disease research and drug development, we wanted to validate the results we obtained in 2D culture in 3D culture as it more closely reflects the in-vivo tumor microenvironment. We observed the effects of dose application depending on time in the microscopic observation we made by applying the cytotoxic effects obtained with the two-dimensional cell culture to the 3D culture. Our results showed that Fenugreek content caused the deterioration of the spheroid structures of the cells in a 3D structure and reduced cell viability in SH-SY5Y cells.

In order for Fenugreek to be included in neuroblastoma treatment strategies studies, it is very important to thoroughly examine the Fenugreek content and evaluate the activity of the individual compounds of this herb. Although there are numerous published studies on the chemistry and bioactivity of Fenugreek seeds, Fenugreek sprouts and components and their effects in mediating changes in cell viability and cell proliferation in various other cancer cells, this study is the first to investigate the anti-cancer effects of Fenugreek in SH-SY5Y cells.

CONCLUSION

Fenugreek extract showed anti-cancer activity on the human neuroblastoma cancer SH-SY5Y cell line. Further studies are still needed to understand the cell viability inhibition mechanism. These positive results in the SH-SY5Y cell line indicate that Fenugreek extract may be a potential agent as an additive to widely used anticancer drugs for neuroblastoma cancer treatment.

Peer Review: Externally peer-reviewed.

Author Contributions: Conception/Design of Study- I.U., M.P.; Data Acquisition- I.U., M.P., H.I.K.C., A.E.; Data Analysis/Interpretation- I.U., M.P., H.I.K.C., A.E.; Drafting Manuscript- I.U.; Critical Revision of Manuscript- M.P.; Final Approval and Accountability- I.U., M.P., H.I.K.C., A.E.

Conflict of Interest: Authors declared no conflict of interest.

Financial Disclosure: Our study was approved and supported by The Scientific and Technological Research Institution of Turkey Projects 2209-A by the Project number of 1919B012004906.

REFERENCES

1. Chanchal DK, Alok S, Rashi S, Bijauliya RK, Yadav RD, Sabharwal M. Various medicinal plants used in the treatment of anticancer activity. *Int J Pharm Sci Res* 2018; 9(4): 1424-9.
2. Ohiagu FO, Chikezie PC, Chikezie CM, Enyoh CE. Anticancer activity of Nigerian medicinal plants: a review. *Futur J Pharm Sci* 2021; 7: 70.
3. Khalil MIM, Ibrahim MM, El-Gaaly GA, Sultan AS. *Trigonella foenum(Fenugreek)* Induced Apoptosis in Hepatocellular Carcinoma Cell Line, HepG2, Mediated by Upregulation of p53 and Proliferating Cell Nuclear Antigen. *BioMed Res Int* 2015; 2015: 914645.

4. Al-Oqail MM, Farshori NN, Al-Sheddi ES, Musarrat J, Al-Khedhairi AA, Siddiqui MA. In vitro cytotoxic activity of seed oil of fenugreek against various cancer cell lines. *Asian Pac J Cancer Prev* 2013; 14(3): 1829-32.
5. Marshall GM, Carter DR, Cheung BB, Liu T, Mateos MK, Meyerowitz JG et al. The prenatal origins of cancer. *Nat Rev Cancer* 2014; 14(4): 277-89.
6. Li J, Pang J, Liu Y, Zhang J, Zhang C, Shen G et al. Suppression of RRM2 inhibits cell proliferation, causes cell cycle arrest and promotes the apoptosis of human neuroblastoma cells and in human neuroblastoma RRM2 is suppressed following chemotherapy. *Oncol rep* 2018; 40(1): 355-60.
7. Cortelo PC, Demarque DP, Dusi RG, Albernaz LC, Braz-Filho R, Goncharova EI et al. A Molecular Networking Strategy: High-Throughput Screening and Chemical Analysis of Brazilian Cerrado Plant Extracts against Cancer Cells. *Cells* 2021; 10(3): 691.
8. Aydemir EA, Simsek E, Imir N, Göktürk RS, Yesilada E, Fiskin K. Cytotoxic and apoptotic effects of *Ebenus boissieri* Barbey on human lung cancer cell line A549. *Pharmacogn Mag* 2015; 11(42): 37-45.
9. Khoja KK, Howes MJR, Hider R, Sharp PA, Farrell IW, Latunde-Dada GO. Cytotoxicity of Fenugreek Sprout and Seed Extracts and Their Bioactive Constituents on MCF-7 Breast Cancer Cells. *Nutrients* 2022; 14(4): 784.
10. Wani SA, Kumar P. Fenugreek: A review on its nutraceutical properties and utilization in various food products. *J Saudi Soc Agric Sci* 2018; 17(2), 97-106.
11. Rahmati-Yamchi M, Ghareghomi S, Haddadchi G, Milani M, Aghazade M, Daroushnejad H. Fenugreek extract diosgenin and pure diosgenin inhibit the hTERT gene expression in A549 lung cancer cell line. *Mol Biol* 2014; 41: 6247-52.
12. Zameer S, Najmi AK, Vohora D, Akhtar M. A review on therapeutic potentials of *Trigonella foenum graecum* (fenugreek) and its chemical constituents in neurological disorders: Complementary roles to its hypolipidemic, hypoglycemic, and antioxidant potential. *Nutr Neurosci* 2018; 21(8): 539-45.
13. Sebastian KS, Thampan RV. Differential effects of soybean and fenugreek extracts on the growth of MCF-7 cells. *Chem Biol Interact* 2007; 170(2): 135-43.
14. Khoja KK, Howes MJR, Hider R, Sharp PA, Farrell IW, Latunde-Dada GO. Cytotoxicity of Fenugreek Sprout and Seed Extracts and Their Bioactive Constituents on MCF-7 Breast Cancer Cells. *Nutrients* 2022; 14(4): 784.
15. Khoja KK, Shaf G, Hasan TN, Syed NA, Al-Khalifa AS, Al-Assaf AH, Alshatwi AA. Fenugreek, a naturally occurring edible spice, kills MCF-7 human breast cancer cells via an apoptotic pathway. *Asian Pac J Cancer Prev* 2011; 12(12): 3299-304.
16. Kaviarasan S, Ramamurty N, Gunasekaran P, Varalakshmi E, Anuradha CV. Fenugreek (*Trigonella foenum graecum*) seed extract prevents ethanol-induced toxicity and apoptosis in Chang liver cells. *Alcohol & Alcoholism* 2006; 41(3): 267-73.
17. Syed QA, Rashid Z, Ahmad MH, Shukat R, Ishaq A, Muhammad N, et al. Nutritional and therapeutic properties of fenugreek (*Trigonella foenum-graecum*): a review. *Int J Food Prop* 2020; 23: 1777-91.
18. Verma KS, Singh KS, Mathur A. In vitro cytotoxicity of *Calotropis procera* and *Trigonella foenum-graecum* against human cancer cell lines. *J Chem Pharm Res* 2010; 2(4): 861-5.
19. Nelson VK, Sahoo NK, Sahu M, Sudhan HH, Pullaiah CP, Muralikrishna KS. In vitro anticancer activity of *Eclipta alba* whole plant extract on colon cancer cell HCT-116. *BMC Complement Med Ther* 2020; 20(1): 355.
20. Alrumaihi FA, Khan MA, Allemailem KS, Alsahli MA, Almatroudi A, Younus H, et al. Methanolic fenugreek seed extract induces p53-dependent mitotic catastrophe in breast cancer cells, leading to apoptosis. *J Inflamm Res* 2021; 16(14): 1511-35.
21. Sitarek P, Kowalczyk T, Santangelo S, Bialas JA, Toma M, Wieczfinska J. The Extract of *Leonurus sibiricus* transgenic roots with AtPAP1 transcriptional factor induces apoptosis via DNA damage and down regulation of selected epigenetic factors in human cancer cells. *Neurochem Res* 2018; 43: 1363-70.
22. Alshatwi AA, Shafi G, Hasan TN, Syed NA, Khoja KK. Fenugreek induced apoptosis in breast cancer MCF-7 cells mediated independently by fas receptor change. *Asian Pac J Cancer Prev* 2013; 14(10): 5783-8.

In silico Evaluation of *WWC1* in Melanoma Using Bioinformatic Analyses

Dilara Kamer Colak^{1*} , Ufuk Unal^{1*} , Sema Bolkent¹ 

¹Istanbul University-Cerrahpaşa, Faculty of Cerrahpasa Medicine, Department of Medical Biology, Istanbul, Türkiye

ORCID IDs of the authors: D.K.C. 0000-0003-4968-2826; U.U. 0000-0003-4913-3616; S.B. 0000-0001-8463-5561

Please cite this article as: Colak DK, Unal U, Bolkent S. *In silico* Evaluation of *WWC1* in Melanoma Using Bioinformatic Analyses. Eur J Biol 2022; 81(2): 257-266. DOI: 10.26650/EurJBiol.2022.1168881

ABSTRACT

Objective: It is suggested that *WWC1* has an active role in melanoma progression. Therefore, it was aimed to evaluate the *WWC1* gene expression profiles in melanoma, an aggressive malignant skin tumor.

Materials and Methods: Quantitative data from melanoma samples (n=592) were clinically evaluated using cBioPortal. Gene expression (GSE65904 and GSE22155) and gene methylation datasets (GSE120878) were retrieved from the Gene Expression Omnibus (GEO) database. Using the GeneMANIA database, the functions of given genes and pathways were evaluated. The STRING database achieved a protein-protein interaction (PPI) network was used to visualize it.

Results: Mutations in the *WWC1* were found in 6.7% of all melanoma samples, 8% of skin cutaneous melanoma, and 2.8% of metastatic melanoma. When the GeneMANIA platform was used to analyze gene interactions, it was determined that the *WWC1* gene shared common protein domains with three genes, was co-expressed with five genes, and interacted with 17 other genes. According to the function analysis results, the most effective of the ten functions of *WWC1* was Hippo signaling, with a coverage value of 0.16 (p=0.009). In addition, it then played a role in Notch signaling and organ growth. When the protein-protein interactions were examined, it was determined that it interacted with ten proteins and was co-expressed with nine.

Conclusion: The findings demonstrated the potential of *WWC1* to be effective in the progression of melanoma. Further research is needed to provide a more accurate analysis of *WWC1* expression and methylation.

Keywords: Melanoma, *WWC1*, KIBRA, Bioinformatic mining, GEO

INTRODUCTION

The skin is the body's biggest organ that serves as a protective barrier, regulating body temperature and preventing fluid loss. The epidermis, the outer layer of the skin, and the dermis underneath are the two main layers of the skin. It contains four main types of cells: keratinocytes (squamous cells, basal cells), Langerhans cells, Merkel cells, and melanocytes (1). The malignant form of melanocytes is called melanoma. Melanoma constitutes around 2% of all malignant skin cancers but is the deadliest (2). Studies show that melanoma incidence rises yearly as UV radiation exposure increases

(3,4). Even though surgery may be the only curative option for the majority of patients with early-stage cutaneous melanoma, it is ineffective for those with metastatic melanoma (5). Most research is moving in this direction as preventive and predictive biomarkers, and drug targets are needed to improve the accuracy of melanoma diagnosis and treatment.

Differentially expressed genes are identified during the progression of melanoma (6). Genes that are variably expressed during melanoma progression are thought to be targets. As a result of the bioinformatics analyses applied to the microarray datasets taken from the Gene Ex-

*Authors contributed equally to the writing of this paper.



Corresponding Author: Sema Bolkent

E-mail: bolkent@iuc.edu.tr

Submitted: 31.08.2022 • **Accepted:** 25.11.2022 • **Published Online:** 29.12.2022



pression Omnibus (GEO) database, 142 differentially expressed genes were detected in melanoma by Xia et al (7). In addition, epigenetic regulation of genes expressed differently in melanoma was also obtained through bioinformatic analysis. Moreover, it was concluded that the expression change of interleukin 27 (IL-27) in melanoma may be effective on cytokine-based immune therapy (8). Li et al. (9) detected 266 miRNAs that expressed differently in melanoma and emphasized the possibility of miRNA and target genes as prognostic and therapeutic biomarkers. On the other hand, frequently mutated genes, such as *BRAF*, are therapeutic targets for melanoma.

The Hippo signaling pathway is an effective regulator of cell proliferation and differentiation (10). Dysregulation of the Hippo pathway can cause tumorigenesis (11,12). The mammalian Hippo pathway includes two major effectors containing WW domain such as Yes Associated Protein (YAP) and transcriptional co-activator with PDZ-binding motif (TAZ) (13). It has been reported that WW and C2 domain-containing (WWC) protein family (*WWC1*, *WWC2*, *WWC3*) regulate the Hippo pathway (14–17). Overexpression of *WWC1*, also called KIBRA (Kidney and BRAin) because of its high expression in kidney and brain, increases the phosphorylation of YAP/TAZ. It has been shown both *in vitro* and *in vivo* that the Hippo pathway supports melanoma invasion by increasing YAP activity (18,19). Considering the role of *WWC1* in the Hippo pathway, no research was found regarding its relationship with melanoma. This study aimed to evaluate *the WWC1*, one of the regulator of the Hippo pathway, in melanoma by *in silico* analysis methods.

MATERIALS AND METHODS

Datasets Used for Gene-based Identification and Analysis of Clinical Data

Quantitative data from a total of 592 melanoma samples (S), including metastatic melanoma (MM) (DFCI, Nature Medicine 2019; n=144) and skin cutaneous melanoma (SCM) (TCGA, Pan-Cancer Atlas; n=448), were evaluated by using cBioPortal for Cancer Genomics (<https://www.cbioportal.org/>) in the study. The GEO2R analysis tool provided by The National Center for Biotechnology Information (NCBI) was used to evaluate data sets [GSE65904 (10,11), GSE22155 (12), and GSE120878 (13)] from GEO database to determine whether *WWC1* was associated with melanoma carcinogenesis and progression.

The cBioPortal was used to access the clinical information of patients. A total of 15 separate datasets were identified by the “melanoma” search in cBioPortal. As a result of the examination, two datasets were included in the study. Clinical data from 592 melanoma samples without any parameter distinction, including metastatic melanoma (DFCI, Nature Medicine 2019; n=144) and skin cutaneous melanoma (TCGA, Pan-Cancer Atlas; n=448), were analyzed using Graphpad 8.

Identifying RNA-seq Based Datasets

In the analyzes obtained from the all results of the study, repeated readings were combined in to single data, and their averages were included.

Analysis of Mutation Data

The sequence data of 592 patients collected through cBioPortal was compared to the reference genome. Two sets of melanoma (MM and SCM) data were examined for the mutation pattern of *WWC1*. Genomic alteration analysis was used to identify the genes that interact with *WWC1*.

Analysis of Expression Data

Firstly, the menu “resources” then the “gene and expressions” tab and the Gene Expression Omnibus database tab were switched on in NCBI. The keyword “melanoma” was searched in the GEO database. The results were scanned with “Expression profiling by array” and “Methylation profiling by array” sub-filters. GSE65904, GSE22155, and GSE120878 datasets were found suitable for the study. The raw file formats of GSE65904, GSE22155, and GSE120878 datasets were downloaded (10-13). The expression data were analyzed using GraphPad Prism 8. The *WWC1* expression data were analyzed along with all genes considered to be involved. Finally, the possible role of *WWC1* in the diagnosis was investigated due to the ROC curve analysis performed.

WWC1 Network Analysis

The *WWC1* was examined regarding gene interaction and functional relationships on the GeneMANIA platform (www.genemania.org), and proteins associated with the *WWC1* (KIBRA) protein, and their degree of association were determined via the STRING database (www.string-db.org).

Statistical Analysis

The data obtained from all analyzes were accepted as significant in the 95% confidence interval, $p < 0.05$ conditions. Normality, ANOVA, the Mann-Whitney U, the Wilcoxon Test and, Student t-test were used to compare numerical values of GSE65904, GSE22155, and GSE120878 datasets, respectively. To find statistical differences between categorical variables, the Chi-square test was utilized. The ROC curve analysis was used to analyze the expression coefficient. The Log-rank (Mantel-Cox) method was used to calculate the survival curves.

RESULTS

Results from cBioPortal

The study included two datasets containing 592 patients according to the determined keywords. Statistically significant results were obtained in 14 of 79 clinical parameters examined in patients with the *WWC1* mutations (n=39) of total melanoma samples (n=592). The samples with the *WWC1* mutations in mutation counts ($p < 0.001$) and total mutations ($p = 0.020$) were found to be significantly higher than samples without the *WWC1* mutations ($p < 0.001$), (Figures 1a and 1b). When all samples were evaluated according to their histological classification, it showed that the LMM (Lentigo malignant melanoma) and NOS (Not otherwise specified) structures were high in samples with the *WWC1* mutations ($p < 0.001$) by cBioPortal. The UV-induced mutations in patients with *WWC1* mutations were observed significantly more than in patients without *WWC1* mutations ($p = 0.035$), (Figure 1c). The mutation that is

present in a subset of tumor cells is defined as subclonal. The subclonal mutation development in samples with *WWC1* mutations was significantly high ($p=0.010$). It was determined that there was a significant difference in the early diagnosis of the disease in patients with *WWC1* mutations ($p=0.036$). When the expression correlation between genes that play an important role in melanoma progression was evaluated, it was determined that *WWC1* was significantly associated with *BRAF*. The relationship based on the amount of mutation was

similar to that shown in the gene expression data ($r=-0.12$; $p=0.012$), (Figure 1d and Table 1).

Results from GEO2R

When the GSE22155 (including 18 patients with lymph node metastases and 38 patients with subcutaneous metastases) dataset, the *WWC1* expression was evaluated in terms of clinical parameters. These parameters were sex, age at metastases, type of metastases, age at primary diagnosis, localization of primary melanoma, Breslow, Clark, stage, *BRAF/NRAS*, *CDKN2A*, homo-

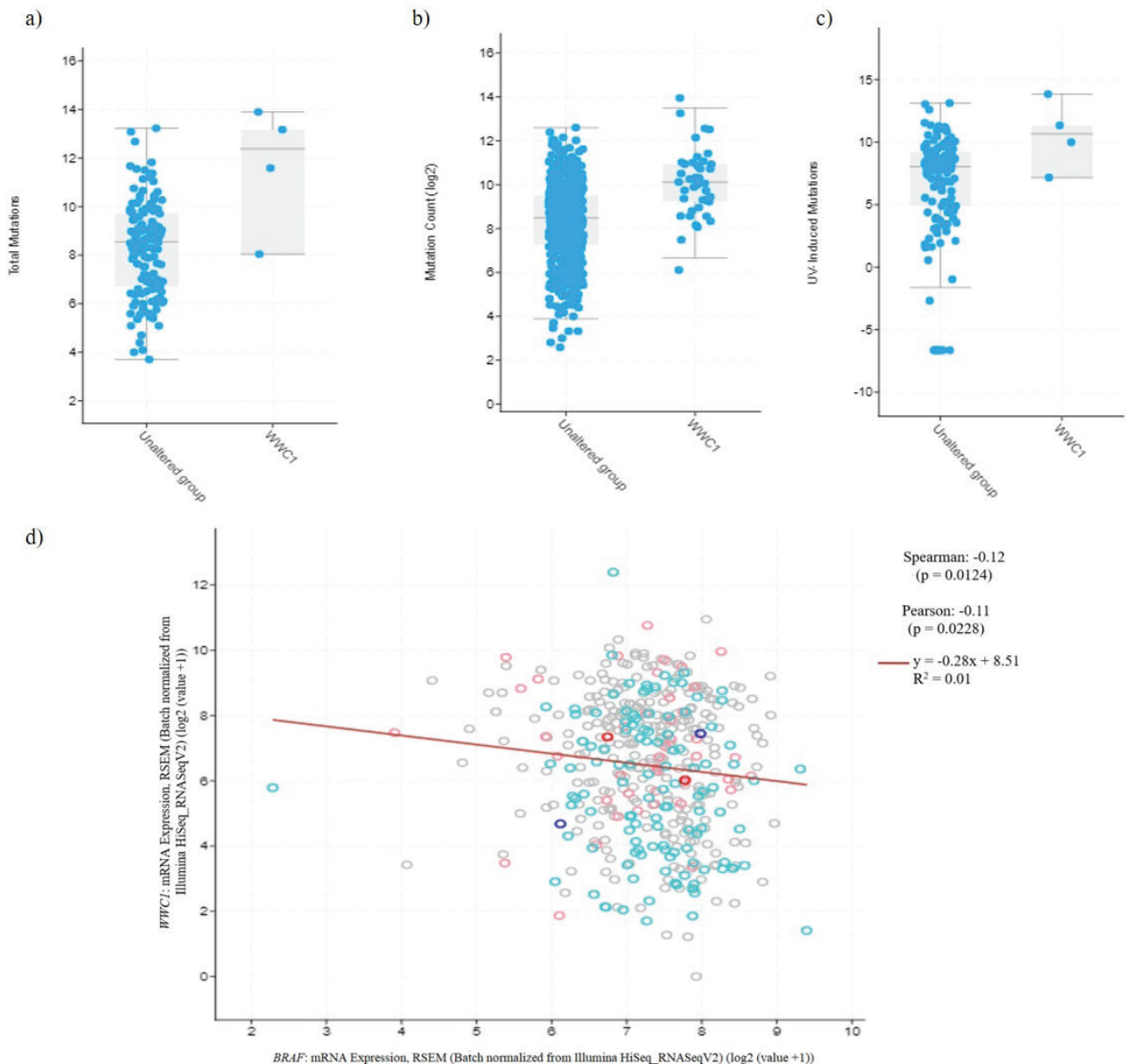


Figure 1. Alterations of *WWC1* determined with cBioPortal. a) Total mutations in all melanoma samples with *WWC1* mutations and unaltered group, b) Mutation count in all melanoma samples with *WWC1* mutations and unaltered group, c) UV-induced mutations in patients with *WWC1* mutations and unaltered group, d) Correlation analysis between *BRAF* and *WWC1*. Graphs through cBioPortal database.

Table 1. Clinical data were obtained from cBioPortal.

Clinical Attribute	Attribute Type	Statistical Test	p-Value
MUTATION STATUS			
Total mutations	• Sample	Wilcoxon Test	0.020
Mutation count	• Sample		<0.001
Tumor mutational burden, nonsynonymous	• Sample		<0.001
Mutation sub-clonal	• Sample		0.010
Mutation clonal	• Sample		0.003
UV-induced mutations	• Patients		0.035
CLASSIFICATION			
Histology	• Sample	Chi-squared Test	<0.001
International classification of diseases for oncology, Third Edition ICD-O-3 Histology code	• Patient		<0.001
Oncotree code	• Sample		0.026
Cancer type detailed	• Sample		0.026
DIAGNOSIS AND TREATMENT			
Immunotherapy	• Patient	Chi-squared Test	0.010
Prior diagnosis	• Patient		0.036

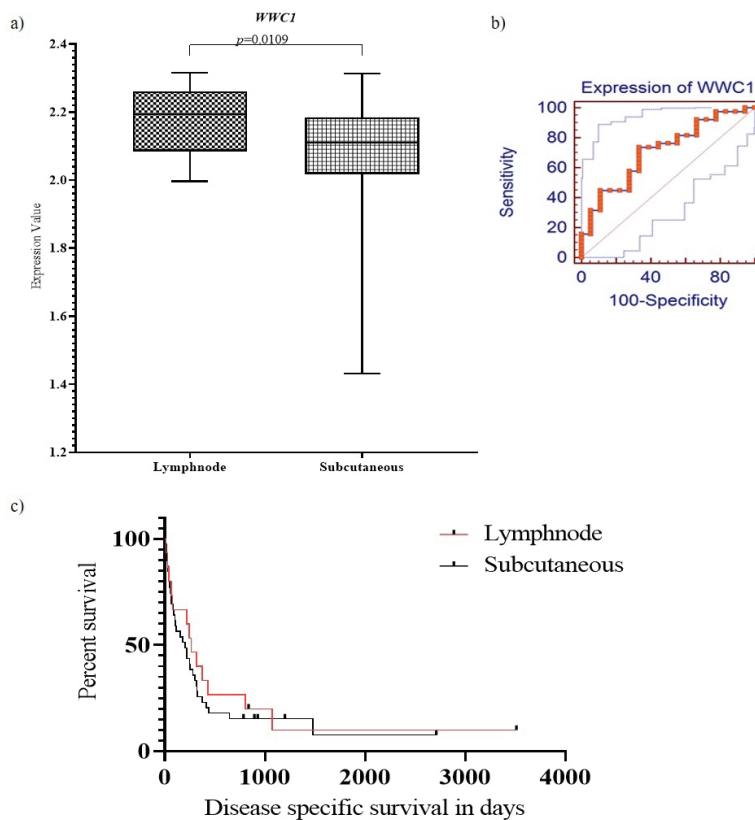


Figure 2. a) The statistical analysis of *WWC1* expression in lymph node and subcutaneous, b) ROC curve analysis of *WWC1* expression in lymph node and subcutaneous, c) *WWC1* expression effect on survival of the lymph node and subcutaneous metastasis groups. Values represent the mean \pm SD, $p < 0.05$. Graphs through GEO2R.

zygous deletion, germline, molecular subtype, *CD3*, *CD20*, and *Ki67*. A statistically significant difference was found only in the type of metastases parameter ($p=0.010$), (Figure 2a). As a result of the ROC curve analysis performed for the type of metastasis, the threshold value for *WWC1* expression of the subcutaneous group was found to be below 2.15 (73.68% sensitivity; 63.16% specificity), ($p=0.004$), (Figure 2b). The *WWC1* expression in the lymph node and subcutaneous metastasis groups did not have significant effect on survival ($p=0.547$), (Figure 2c).

As a result of the analysis of the GSE65904 dataset, a statistically significant difference was found between the *WWC1* expression of patients with regional lymph node metastases and the general patient group, including more than 50% of patients with metastases to internal organs (Figure 3a). It was determined that the *WWC1* expression of patients with regional lymph node metastases was less than 2.13 (sensitivity 47.8%, 90.7% specificity), and the general group was found to be more than 2.13 by ROC curve analysis ($p<0.001$), (Figure 3b). Because there were more than 50% of patients with internal organ metastases, the survival analysis revealed that the group labeled "General" had statistically significantly lower survival than the group with metastasis to the regional lymph node [Log-rank (Mantel-Cox) test], ($p<0.001$), (Figure 3c). A statistically significant difference was found in the *WWC1* expression between the cutaneous and lymph node locations of melanoma ($p=0.023$), (Figure 3d). The threshold value determined for *WWC1* expression at the tumor

localization was determined as 2.08 (52.2% sensitivity; 72.7% specificity) ($p=0.018$), (Figure 3e). If the *WWC1* expression was higher than 2.08, the tumor was located in the cutaneous layer, and if it was below 2.08, lymph node metastasis was detected. No statistically significant effect of *WWC1* on survival was found between cutaneously located tumor samples and lymph node metastasis samples [Log-rank (Mantel-Cox)] test, ($p=0.114$), (Figure 3f).

As a result of the analysis of the GSE120878 dataset, it was determined that *WWC1* methylation expression was significantly different between invasive localized melanoma samples and nevus samples ($p<0.001$), (Figure 4a). As a result of the ROC curve analysis, it was determined that ≤ 0.618 *WWC1* methylation amount was the threshold value between invasive localized melanoma samples and nevus samples (84.93% sensitivity; 75.28% specificity), ($p<0.001$), (Figure 4b).

Results of *WWC1* Network Analysis

Using the GeneMANIA platform to analyze the gene interactions, it was determined that the gene shared protein domains with three genes and physically interacted with 17 other genes in addition to being co-expressed with five other genes. In light of these findings, the three genes with the highest co-expression relationship with *WWC1* are *RBM47* (RNA Binding Motif Protein 47), *SH3YL1* (SH3 domain-containing YSC84-like protein 1), and *CLDN7* (Claudin-7) respectively. When evaluating phys-

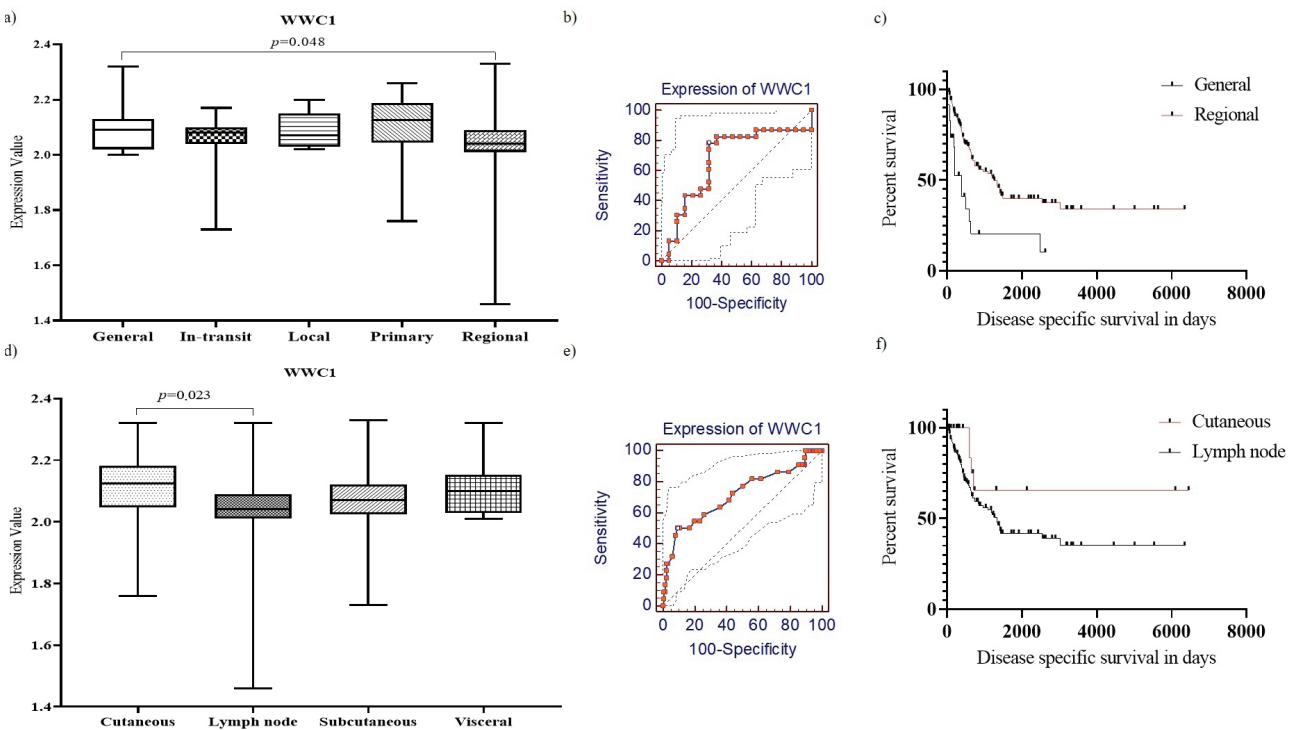


Figure 3. a) The statistical analysis of *WWC1* expression in tissues, b) ROC curves analysis of *WWC1* expression in tissues, c) *WWC1* expression effect on survival of the tissues. d) The statistical analysis of *WWC1* expression in tumor localization, e) ROC curve analysis of *WWC1* expression in tumor localization, f) *WWC1* expression effect on survival of the patients with different localized tumors. The graphs were performed through the GSE65904 dataset. Values represent the mean \pm SD, $p<0.05$.

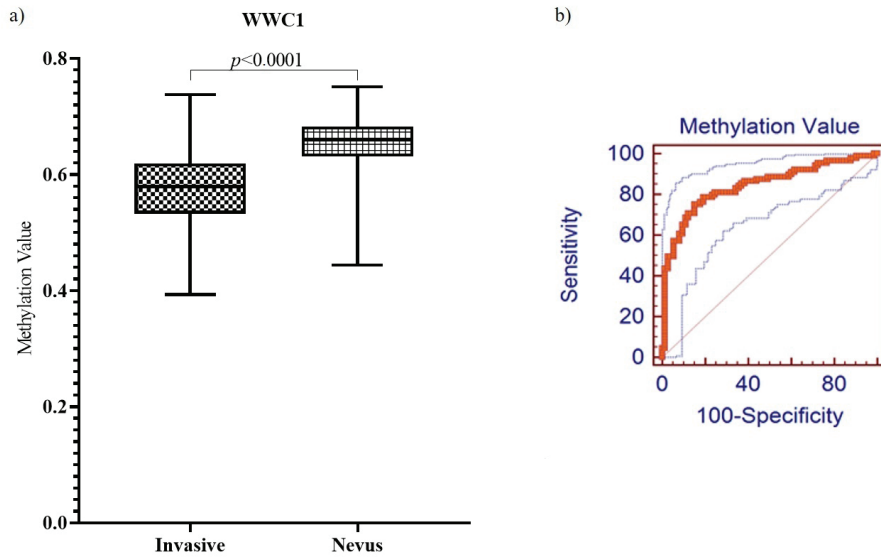


Figure 4. Analysis from GSE120878 dataset. a) The statistical analysis of *WWC1* expression in invasive tumor samples and nevus samples, b) ROC curve analysis of *WWC1* expression in invasive tumor samples and nevus samples. Values represent the mean \pm SD*, $p < 0.0001$.

ical interactions, it was determined that the highest were *NF2* (Moesin-Ezrin-Radixin Like (MERLIN) Tumor Suppressor), *SNX4* (Sorting nexin-4), and *DDR1* (Discoidin Domain Receptor Tyrosine Kinase 1) respectively. *YAP1* (Yes1 Associated Transcription-

al Regulator), *WWC2* (WW and C2 domain containing 2), and *NEDD4* (NEDD4 E3 Ubiquitin Protein Ligase) are the three proteins that share the most protein domains with *WWC1* (Figure 5 and Table 2).

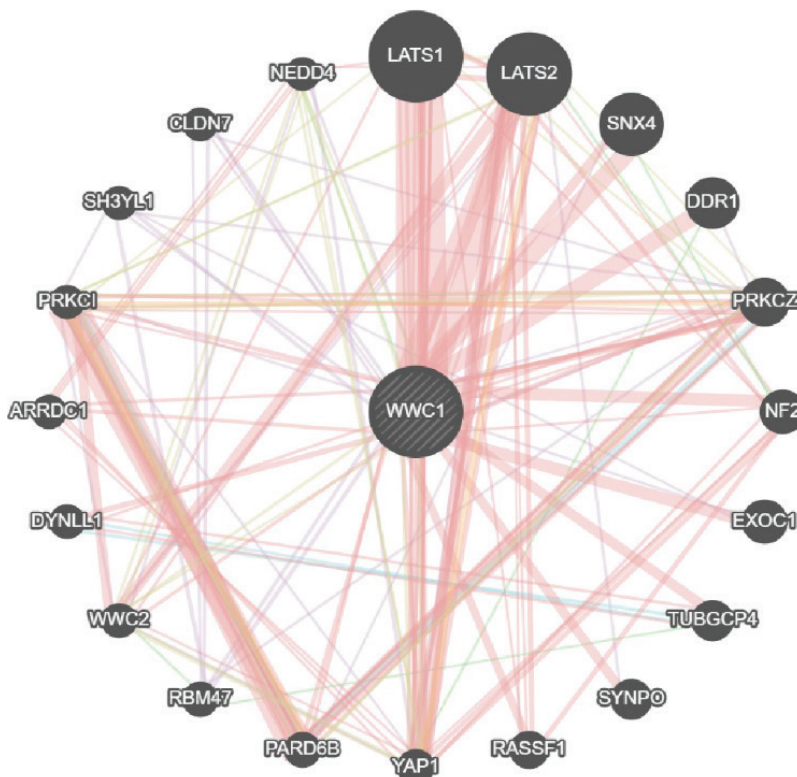


Figure 5. Gene interaction of *WWC1* diagram from GeneMANIA. *WWC1* most interacts with *LATS1* and *LATS2* in the diagram. The diagram shows physical interactions, co-expressions, genetic interactions, co-localizations, and shared of genes.

Table 2. Proteins that co-expressed with *WWC1* that obtained from STRING (Clustering Method: Kmeans).

Cluster Number	Cluster Color	Gene Count	Protein Name	Protein Identifier	Protein Description
1	Red	3	LATS1	ENSP00000437550	Serine/threonine-protein kinase LATS1 and LATS2; Negative regulator of YAP1 in the Hippo signaling pathway.
1	Red	3	LATS2	ENSP00000372035	
1	Red	3	NF2	ENSP00000344666	Along with <i>WWC1</i> can function in the regulation of the Hippo/SWH (Sav/Wts/Hpo) signaling pathway.
2	Green	7	DDN	ENSP00000390590	Dendrin; Promotes apoptosis of kidney glomerular podocytes.
2	Green	7	FRMD6	ENSP00000343899	Ferm domain-containing protein 6; upstream regulator of the Hippo signaling.
2	Green	7	INADL	ENSP00000360200	InaD-like protein; Scaffolding protein that may bring different proteins into adjacent positions at the cell membrane.
2	Green	7	PTPN14	ENSP00000355923	Tyrosine-protein phosphatase non-receptor type 14; Acts as a negative regulator of the oncogenic property of YAP.
2	Green	7	SNX4	ENSP00000251775	Sorting nexin-4; May be involved in several stages of intracellular trafficking.
2	Green	7	SYNPO	ENSP00000377789	Synaptopodin; Actin-associated protein that may play a role in modulating actin-based shape and motility of dendritic spines.
2	Green	7	<i>WWC1</i>	ENSP00000427772	Protein KIBRA; Probable regulator of the Hippo/SWH signaling pathway.
3	Blue	1	FRMD1	ENSP00000283309	Ferm domain-containing protein 1; May be a regulator of hippo signaling.

Table 3. Functions of *WWC1* (Table from GeneMANIA).

Function	FDR (False Discovery Rate)		Genes in Network	Genes in Genome	Coverage
Organ growth	0.007	0.77%	4	58	0.07
Hippo signaling	0.009	0.99%	3	19	0.16
Notch signaling pathway	0.025	2.59%	4	103	0.04
Regulation of developmental growth	0.100	10.04%	4	156	0.03
Apical junction assembly	0.152	15.23%	3	68	0.04
Tight junction organization	0.152	15.23%	3	73	0.04
Regulation of Notch signaling pathway	0.152	15.23%	3	73	0.04
Tight junction assembly	0.152	15.23%	3	69	0.04
Regulation of protein localization to nucleus	0.205	20.55%	3	91	0.03
Intracellular steroid hormone receptor signaling pathway	0.205	20.55%	3	95	0.03

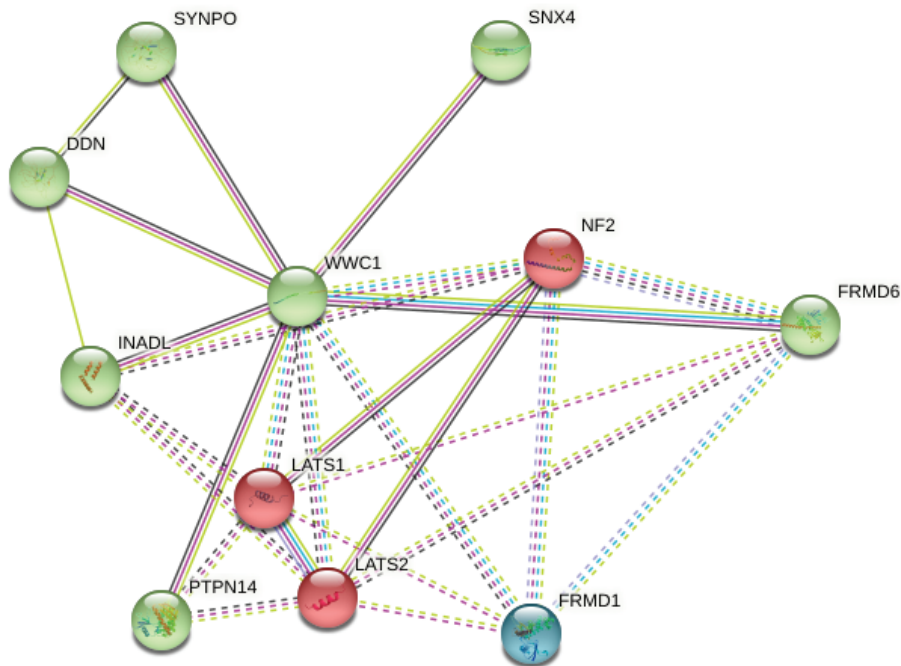


Figure 6. Protein interactions of *WWC1* diagram from STRING. *WWC1* interacted with ten proteins and co-expressed nine-tenths except for *SNX4*.

The *WWC1* had ten separate functions, and the function analysis results showed that it provided the most effective Hippo signaling, with a coverage value of 0.16 (FDR=0.009, Table 3). After that, it contributed to Notch signaling and organ development. It was discovered through protein-protein interactions that it interacted with ten proteins and co-expressed with nine of them (Figure 6).

DISCUSSION

The incidence of melanoma increases each year with increased exposure to sunlight. Following the increasing incidence, melanoma studies interested in melanoma etiology, pathogenesis, new diagnostic techniques, and potential therapeutic approaches are developing rapidly. However, the addition of unpredictable environmental factors that increase oncogenic activity factors such as tumor heterogeneity and drug resistance limit treatment options, shorten patient survival, and adversely affect the stability of treatment. Oncogenomics has advanced thanks to recent developments in high-throughput genome analysis tools, including next-generation sequencing (NGS) and microarray-based techniques (20). These resources are essential for the growth of cancer genomic projects including the International Cancer Genome Consortium (ICGC; <https://icgc.org/>) and The Cancer Genome Atlas (TCGA; <http://cancergenome.nih.gov/>). These projects have made it possible to evaluate the genetic, epigenetic, and omic information of cancer patients from around the world. The main aims of the programs are to advance personalized treatment, better under-

stand the molecular pathways of complex diseases like cancer and communicate the consequences on clinical phenotypes as datasets available to all researchers (21). Several oncogenic websites have been developed to help access the numerous cancer datasets in response to this aim. The cBioPortal website includes genomic information for several cancer types, such as copy number variations, mRNA and microRNA expression, DNA methylation, and protein.

The analysis performed on the cBioPortal platform revealed a positive correlation between the accumulation of mutations and the *WWC1* mutation. Knight et al. reported that 5q deletion on tumor development and metastatic progression were significantly affected by *KIBRA* (22). As a result of our analysis, the *WWC1* mutations showed a statistically significant increase in LMM, one of the histological subclasses of melanoma. There are molecular differences between melanoma and histological subclasses, and the molecular differences are consistent with our findings (23). Tumor heterogeneity, as with all malignancies, is one of the limitations of treatments. One of the significant sources of heterogeneity, sub-clonal mutation, causes the intercellular genomic sequence to vary from one another.

Additionally, *WWC1* mutations were seen, particularly during subclonal development. It is assumed that *WWC1* may facilitate subclonal formation (24). The changes that affect gene expression such as transcript levels and protein expression may accompany *WWC1* mutations. A study revealed a correlation between the *BRAF* expressions and *WWC1*, which actively

contributed to the growth of melanoma (23). Changes in the expression of many genes occurred in the onset and progression of melanoma (6). Detecting these changes will benefit both early diagnosis and narrow the treatment options according to the needs of the patient (25,26). Results obtained from the GSE65904 dataset showed that the expression of the *WWC1* gene helped to know whether the tumor was located cutaneously or in the regional lymph node. Patients who have metastasized to internal organs were approximately 50% of the general patient population as described by the GSE65904 dataset. Compared to the general patient population, patients with regional lymph node metastases displayed higher levels of the *WWC1* gene, demonstrated a tumor suppressor characteristic in melanoma. *WWC1* has also been a tumor suppressor in triple-negative breast cancer, clear cell renal cell carcinoma, and hepatocellular carcinoma studies (17,22,27).

Interestingly, when the GSE22155 dataset was analyzed, it was found that the *WWC1* expression was increased in melanoma patients with stage 4 lymph node metastases when compared to those with subcutaneous metastases. In previous studies, conflicting results regarding the tumor suppressor property of *WWC1* expression were presented, and that it could exhibit different behaviors in different cancer types (17,28,29). In addition, it was observed that its epigenetic regulation played an active role in cancer progression. Studies showed that the tumor suppressor property of *WWC1* was inhibited by silencing through methylation in the promoter region. Therefore, *in vitro* and *in vivo* analyzes are needed to determine its characteristic feature in melanoma.

KIBRA (*WWC1*), one of the proteins of the Hippo pathway, which has an important role in tumorigenesis, was reported to interact with both genes and proteins in cancers (30). As a result of the analysis using GeneMANIA, the *WWC1* was co-expressed with genes that supported the migration, proliferation, and development of cancer cells (31,32). In addition, it was found that *WWC1* in melanoma exhibited co-expression with *CLDN-7*, the seventh member of the claudin family, in which expression dysregulation was associated with cell migration (33,34). Murray et al. (35) showed that increased merlin (*NF2*) expression has a suppressive role in the development of melanoma both *in vitro* and *in vivo*. It was determined that increased *NF2* expression suppressed proliferation, migration and invasion in melanoma cells, and tumor volume and invasion in the *in vivo* melanoma model (35). In the study, it was determined that there was a physical interaction between *WWC1* and *NF2*, which played a role in activating the Hippo pathway. The significant suppression of melanoma cell proliferation by a *DDR* tyrosine kinase inhibitor (*DDR1-IN-1*) *in vitro*, *ex vivo*, and in tumor xenografts highlighted the potential of *DDR1* inhibition in melanoma. The interaction of *WWC1* with the protein products of the same genes was determined by the STRING database. Other genes (*DDR1*, *YAP1*, and *NEDD4*), which were found to interact physically with *WWC1* in our study, and were also shown to be the genes involved in the development of melanoma in previous studies (18,36,37).

CONCLUSION

It is the first study to show that *WWC1* may have an impact on the progression of melanoma. The effects of changes in the *WWC1* and *WWC1*-related genes in melanoma are predicted to become clear in the future.

Acknowledgements: Author Dilara Kamer COLAK is supporting by 100/2000 The Council of Higher Education (CoHE) Ph.D. Scholarship and The Scientific and Technological Research Council of Türkiye (TÜBİTAK) 2211-A National Ph.D. Scholarship Program.

Peer Review: Externally peer-reviewed.

Author Contributions: Conception/Design of Study-S.B., U.U., D.K.C.; Data Acquisition- U.U., D.K.C.; Data Analysis/Interpretation- S.B., U.U., D.K.C.; Drafting Manuscript- S.B., U.U., D.K.C.; Critical Revision of Manuscript- S.B.; Final Approval and Accountability- S.B., U.U., D.K.C.

Conflict of Interest: Authors declared no conflict of interest.

Financial Disclosure: Authors declared no financial support.

REFERENCES

1. Kolarsick PAJ, Kolarsick MA, Goodwin C. Site-specific cancer series: Skin cancer. 1st ed. Pittsburgh, PA: Oncology Nursing Society; 2009.
2. Linares MA, Zakaria A, Nizran P. Skin cancer. Prim Care Clin Off Pract 2015; 42(4): 645-59.
3. Ahmed B, Qadir MI, Ghafoor S. Malignant melanoma: Skin cancer-diagnosis, prevention, and treatment. Crit Rev Eukaryot Gene Expr 2020; 30(4): 291-7.
4. Henley SJ, Ward EM, Scott S, Ma J, Anderson RN, Firth AU, et al. Annual report to the nation on the status of cancer, part I: National cancer statistics. Cancer 2020; 126(10): 2225-49.
5. Davis LE, Shalin SC, Tackett AJ. Current state of melanoma diagnosis and treatment. Cancer Biol Ther 2019; 20(11): 1366-79.
6. Xu Y, Mu Y, Wang L, Zhang X. Detailed analysis of molecular mechanisms in primary and metastatic melanoma. J Comput Biol 2020; 27(1): 9-19.
7. Xia Y, Xie J, Zhao J, Lou Y, Cao D. Screening and identification of key biomarkers in melanoma: Evidence from bioinformatic analyses. J Comput Biol 2021; 28(3): 317-29.
8. Dong C, Dang D, Zhao X, Wang Y, Wang Z, Zhang C. Integrative characterization of the role of IL27 in melanoma using bioinformatics analysis. Front Immunol 2021; (18)12: 713001.
9. Li Q, Zhang L, Wu S, Huang C, Liu J, Wang P, et al. Bioinformatics analysis identifies microRNAs and target genes associated with prognosis in patients with melanoma. Med Sci Monit 2019; 25: 7784-94.
10. Maugeri-Saccà M, De Maria R. The Hippo pathway in normal development and cancer. Pharmacol Ther 2018; 186: 60-72.
11. Shen H, Huang C, Wu J, Li J, Hu T, Wang Z, et al. SCRIB promotes proliferation and metastasis by targeting Hippo/YAP signalling in colorectal cancer. Front Cell Dev Biol 2021; 9: 656359.
12. Kubelac P, Braicu C, Raduly L, Chiroi P, Nutu A, Cojocneanu R, et al. Comprehensive analysis of the expression of key genes related to Hippo signaling and their prognosis impact in ovarian cancer. Diagnostics 2021; 11(2): 344.
13. Chen Y-A, Lu C-Y, Cheng T-Y, Pan S-H, Chen H-F, Chang N-S. WW domain-containing proteins YAP and TAZ in the Hippo pathway as key regulators in stemness maintenance, tissue homeostasis, and tumorigenesis. Front Oncol 2019; 9: 60.

14. Wennmann DO, Schmitz J, Wehr MC, Krahn MP, Koschmal N, Gromnitza S, et al. Evolutionary and molecular facts link the WWC protein family to Hippo signaling. *Mol Biol Evol* 2014; 31(7): 1710-23.
15. Baumgartner R, Poernbacher I, Buser N, Hafen E, Stocker H. The WW domain protein Kibra acts upstream of Hippo in *Drosophila*. *Dev Cell* 2010; 18(2): 309-16.
16. Xiao L, Chen Y, Ji M, Dong J. KIBRA regulates Hippo signaling activity via interactions with large tumor suppressor kinases. *J Biol Chem* 2011; 286(10): 7788-96.
17. Höffken V, Hermann A, Pavenstädt H, Kremerskothen J. WWC proteins: Important regulators of Hippo signaling in cancer. *Cancers (Basel)* 2021; 13(2): 1-15.
18. Zhang X, Yang L, Szeto P, Abali GK, Zhang Y, Kulkarni A, et al. The Hippo pathway oncoprotein YAP promotes melanoma cell invasion and spontaneous metastasis. *Oncogene* 2020; 39(30): 5267-81.
19. Nallet-Staub F, Marsaud V, Li L, Gilbert C, Dodier S, Bataille V, et al. Pro-invasive activity of the Hippo pathway effectors YAP and TAZ in cutaneous melanoma. *J Invest Dermatol* 2014; 134(1): 123-32.
20. Chin L, Hahn WC, Getz G, Meyerson M. Making sense of cancer genomic data. *Genes Dev* 2011; 25(6): 534-55.
21. Klonowska K, Czubak K, Wojciechowska M, Handschuh L, Zmienko A, Figlerowicz M, et al. Oncogenomic portals for the visualization and analysis of genome-wide cancer data. *Oncotarget* 2016; 7(1): 176-92.
22. Knight JF, Sung VYC, Kuzmin E, Couzens AL, de Verteuil DA, Ratcliffe CDH, et al. KIBRA (*WWC1*) is a metastasis suppressor gene affected by chromosome 5q loss in triple-negative breast cancer. *Cell Rep* 2018; 22(12): 3191-205.
23. Bastian BC. The molecular pathology of melanoma: An integrated taxonomy of melanocytic neoplasia. *Annu Rev Pathol Mech Dis* 2014; 9(1): 239-71.
24. Lin Z, Meng X, Wen J, Corral JM, Andreev D, Kachler K, et al. Intratumor heterogeneity correlates with reduced immune activity and worse survival in melanoma patients. *Front Oncol* 2020; 10: 596493.
25. Cirenajwis H, Ekedahl H, Lauss M, Harbst K, Carneiro A, Enoksson J, et al. Molecular stratification of metastatic melanoma using gene expression profiling: Prediction of survival outcome and benefit from molecular targeted therapy. *Oncotarget* 2015; 6(14): 12297-309.
26. Regad T. Molecular and cellular pathogenesis of melanoma initiation and progression. *Cell Mol Life Sci* 2013; 70(21): 4055-65.
27. Schelleckes K, Schmitz B, Ciarimboli G, Lenders M, Pavenstädt HJ, Herrmann E, et al. Promoter methylation inhibits expression of tumor suppressor KIBRA in human clear cell renal cell carcinoma. *Clin Epigenetics* 2017; 9(1):109.
28. Stauffer S, Chen X, Zhang L, Chen Y, Dong J. KIBRA promotes prostate cancer cell proliferation and motility. *FEBS J* 2016; 283(10): 1800-11.
29. Zhou P-J, Xue W, Peng J, Wang Y, Wei L, Yang Z, et al. Elevated expression of Par3 promotes prostate cancer metastasis by forming a Par3/aPKC/KIBRA complex and inactivating the Hippo pathway. *J Exp Clin Cancer Res* 2017; 36(1): 139.
30. Han Y. Analysis of the role of the Hippo pathway in cancer. *J Transl Med* 2019; 17(1): 116.
31. Kobayashi M, Harada K, Negishi M, Katoh H. Dock4 forms a complex with SH3YL1 and regulates cancer cell migration *Cell Signal* 2014; 26(5): 1082-8.
32. Jiang Q-Q, Liu W-B. miR-25 promotes melanoma progression by regulating RNA binding motif protein 47. *Med Sci* 2018; 34: 59-65.
33. Escudero-Esparza A. The claudin family and its role in cancer and metastasis. *Front Biosci* 2011; 16(1): 1069.
34. Morita K, Morita NI, Nemoto K, Nakamura Y, Miyachi Y, Muto M. Expression of claudin in melanoma cells. *J Dermatol* 2007; 35(1): 36-8.
35. Murray LB, Lau YK, Yu Q. Merlin is a negative regulator of human melanoma growth. *Plos One* 2012; 7(8): e43295.
36. Reger de Moura C, Battistella M, Sohail A, Caudron A, Feugeas JP, Podgorniak M, et al. Discoidin domain receptors: A promising target in melanoma. *Pigment Cell Melanoma Res* 2019; pcmr.12809.
37. Kito Y, Bai J, Goto N, Okubo H, Adachi Y, Nagayama T, et al. Pathobiological properties of the ubiquitin ligase Nedd4L in melanoma. *Int J Exp Pathol* 2014; 95(1): 24-8.

Personalized Medicine: A Solution for Today and Tomorrow

Basak Dalbayrak¹ , Mustafa Dogukan Metiner¹ 

¹Institute of Biotechnology, Gebze Technical University, Kocaeli, Turkiye

ORCID IDs of the authors: B.D. 0000-0002-0863-4257; M.D.M. 0000-0003-0382-6652

Please cite this article as: Dalbayrak B, Dogukan Metiner M. Personalized Medicine: A Solution for Today and Tomorrow. Eur J Biol 2022; 81(2): 267-273. DOI: 10.26650/EurJBiol.2022.1110344

ABSTRACT

Personalized medicine is a multidisciplinary area that contains several techniques to provide patients with more efficient, cheaper, and fewer side effects treatment strategies. In customized medicine, each patient is viewed individually in order to provide more specific and efficient treatment. Using liquid biopsy, pharmacogenetics, point-of-care-testing, multi-omic-based technologies, wearable technologies, organoids, and 3D printers are some of the strategies covered in this review. Omics technology is promising for data collection, and management is vital for health records to combine complete information in one single platform. 3D printer technologies give opportunities to produce multi-drug tablets with controlled and targeted drug release. Additionally, organoids are the other biomaterial approaches to mimic the tumoroid microenvironment to develop new treatment strategies. Increasing demand for personalized medicine affects the improvement scope of this technology; personalized medicine is a vital and urgent area to improve.

Keywords: Personalized medicine, Liquid biopsy, Point-of-care-testing, Pharmacogenetic, Wearable devices, biomaterials, organoids/spheroids

INTRODUCTION

The starting point of personalized medicine is to eliminate the understanding of "one-size-fits-all" (1). Personalized medicine or P4 (predictive, preventive, personalized, and participatory) contains prevention, diagnostic, and treatment conditions depending on an individual's characteristics, such as transcriptomics, metabolomic markers, epigenetics, and genetic profiles (2,3). As a result, personalized medicine provides patients with fewer side effects, more efficacy, and lower cost of health (4). Nowadays, personalized medicine is a vital approach in the healthcare industry because personalized medicine is a form of medical intervention that enables the development of patient-specific treatment methods and drugs based on an individual's genomic, epigenomic, and proteomic information (5).

Therefore, developing treatment or disease prevention strategies according to the patient's genetic background, environmental factors, and geographical con-

ditions will be a more effective treatment method. In addition to treating disease, personalized medicine is also of great importance in preventing disease (6) as personalized medicine aims to administer the correct prediction, diagnosis, therapeutics, and drug to the right patient at the right time (7). The development of personalized medicine allows for the development of targeted therapeutic drugs as well as combination therapies and optimized use of already existing drugs (8). In this way, optimal drug administration is realized, and a practical result is obtained for the patient. The presence of diagnostic methods and diagnostic kits required for these procedures is an excellent criterion for personalized medicine (9). Although personalized medicine is considered a groundbreaking innovation, it is also known to have some limitations caused by a misunderstanding of the molecular mechanisms of some diseases. These difficulties may arise from insufficient genetic markers due to an inadequate understanding of the molecular mechanisms of some diseases.



Corresponding Author: Basak Dalbayrak

E-mail: bdalbayrak@gmail.com

Submitted: 28.04.2022 • **Revision Requested:** 28.05.2022 • **Last Revision Received:** 31.05.2022 •

Accepted: 05.08.2022 • **Published Online:** 02.12.2022

Content of this journal is licensed under a Creative Commons Attribution-NonCommercial 4.0 International License.



The global market size of personalized medicine was 14.4 billion dollars in 2021 in Europe, and it is estimated that this number will increase up to 27.3 billion dollars (10), as it is promising to reduce general public health expenses. For example, adequate treatment balances the health system's cost and reduces hospital stays. Furthermore, in drug development, clinical trials seem to increase efficiency by optimizing phase trials through a personalized medicine approach, and we can reduce the number of thousands of people used in phase 3 trials and reduce the cost of these trials (11). The following parts of this review will describe the diagnostic techniques, advantages, and disadvantages to explain today's needs and tomorrow's expectations.

The Advantages of Personalized Medicine

The advantages of personalized medicine could be collected briefly under three subtopics: 1) better treatment methods for patients, 2) better outcomes for every individual and health system, and 3) development of more efficient medicines. Advances in patient health demonstrate the benefits of personalized medicine. As it could be understood from the name of personalized medicine, individuality is the main point of this field, and these three advantages are the main scope of personalized medicine. Furthermore, providing advanced treatment to patients, enhanced drug efficacy, and changing health systems increase treatment efficiency with improved therapeutic strategies. Considering with advantages of the personalized medicine, this review will cover sections represented in Figure 1.

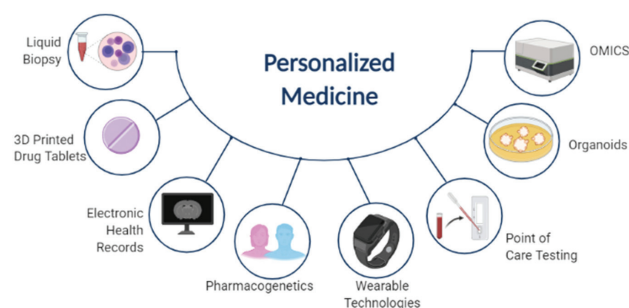


Figure 1. Summary of personalized medicine mentioned in this article (Created with BioRender.com).

Liquid Biopsy

Comparative research is generally carried out parallel with solid biopsy in the current liquid biopsy studies. Although liquid biopsies are not currently available for clinical use, they can be applied to monitor the progress of certain types of diseases. It might be used to diagnose and track the progress of diseases in future research. It is highly preferred because of its accessibility and low-cost method for patients and clinicians compared to solid biopsy. However, before reaching this level, extensive research should be done on the biomarkers of diseases. The liquid biopsy includes different soluble factors, such as hormones, circulating tumor cells, proteins, tumor markers, miRNA, and circulating cell-free nucleic acids (Figure 2) (12). Therefore, it provides detailed biological information about a patient who has genetic differences. The liquid biopsy may soon have clinical

uses for diagnosing and following certain disease types. Therefore, a liquid biopsy will be a helpful technology that holds promise for the future.

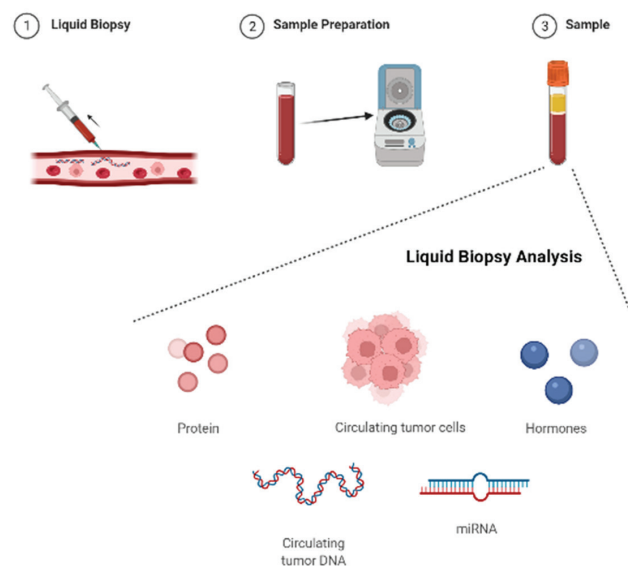


Figure 2. Schematic summary of liquid biopsy sample preparation and usage areas (Created with BioRender.com).

Liquid biopsy has plenty of advantages as much as disadvantages; in many patients, early-stage cancer and advanced disease may not be detected. Small amounts of ctDNA (circulating tumor DNA) and CTC (circulating tumor cell) and insufficient biomarkers may cause problems in diagnosis (13). The main difficulty in CTCs is the identification and characterization of cells. It is challenging to identify early-stage diseases because it is low in concentration and rare. Therefore, compassionate methods must be developed to collect and analyze CTC (14). In addition, the same gene variations can be present in several tumor types, so testing must be done in conjunction with other diagnostic tools to diagnose and prognosis accurately. In order to prevent these problems, it is necessary to develop biomarkers for the diseases to be investigated and fully clarify the different localizations at different stages of the disease.

Moreover, it is required to develop biomarkers for different mutations that cause diseases. In addition to these, there are FDA-approved liquid biopsy usage examples. For instance, CellSearch is the only FDA-approved EpCAM-based test, and it is also considered the "gold standard" for CTC detection. As mentioned, the primary purpose of this technique is to count epithelial CTC biomarkers such as CD45-, EpCAM+, CK 8+, and 19+ in whole blood. This kit defines CTC in cancer patients (15). In many studies on breast cancer and prostate cancer, positive results have been obtained by looking at the presence of CTC (16).

Another example is, in 2016, the FDA approved the cobas® epithelial growth factor receptor (EGFR) Mutation Test v2 to determine the eligibility of non-small cell lung cancer patients to receive specific EGFR tyrosine kinase inhibitors (17). In addition to

blood samples, there are diagnostic methods in different body fluid samples, one of which is urine used in bladder cancer. Various biomarkers are also present in urine samples (18,19).

Most physicians do not consider patients as individuals during prescriptions in clinical practice, but the applied treatment could be effective for some patients while not affecting others. Thus, it is essential to evaluate patients as individuals, and it is necessary to accept every individual as unique to increase the effectiveness of the treatment efficiency. Biomarkers are critical for predicting the disease pathway and selecting the appropriate treatment with the highest response (20,21). Not all but common diseases could be detected using a newly developed technique using the patient's blood called serum proteome, with the advantages of using the patient's blood rapidly and cheap compared with other omic-based methods (20). Depending on the serum protein detection techniques, the drug screening and treatment strategies could be arranged by serum proteome technique (20).

Pharmacogenetics

Pharmacogenomics deals with how patients respond to drugs based on their genetic background and treats drug therapy following the patient's genotype. Differences in drug response are due to inter-patient variability because all patients do not respond to the same drug in the same way (22).

The disease that has seen the most successful results in pharmacogenomics is cancer. For example, researchers have discovered many single nucleotide polymorphisms, variations in a single base pair in a DNA sequence that lead to breast cancer, and can prescribe the best treatment (23). Apart from giving the best results in the treatment of patients, pharmacogenomics has other benefits, such as saving time and costs. To protect

patients from the side effects of drugs, pharmacogenomics does not work by using a single medicine; instead patients try many drugs until they find which medication works best for them (23). Moreover, there are various limitations in applying pharmacogenetic tests: validated markers, validated tests, dosing algorithms, and laboratories with good laboratory practice (24). Therefore, to increase the usage of pharmacogenetics, it is of great importance to find new pharmacogenetic markers, increase the number of approved tests, and control and follow up the tests distributed for their clinical applications. Moreover, there are many biomarkers approved by the FDA, such as HLA-B, ESR, EGFR and HER2 (24–26). In addition, drugs and many possible gene interactions might be applied to enhance the usage of pharmacogenetics (27).

Point-of-Care Testing

Laboratory analyses play a significant role in diagnosing diseases and monitoring drug therapy. Following the importance of laboratory analysis, point-of-care testing (POCT), inpatient beds and operating rooms are developing rapidly. POCT aims to provide low-cost care close to patients' homes, reducing the time between sampling and analysis (28). Point-of-care testing is a laboratory-medical discipline that is rapidly emerging in clinical practice. POCT is characterized by outcome-based therapeutic actions with the aid of pre-prepared reagents.

Biosensors are generally used in POCT devices, and various POCT analyzers are available to protect against the adverse effects caused by physiological factors, storage environment, and sampling techniques. Additionally, the contents of the drugs used by the patient may have an effect on the test results (29,30). These devices are grouped according to practical uses by measurement mode, sensor characteristics, and complexity criteria (31). Commonly used POCT tests are reviewed in Table 1. In addition, POCT

Table 1. Commonly used point-of-care testing (POCT) applications.

Common Point-of-Care Tests			
Test	Clinical Setting	Markers	References
Blood gases	ICU settings, emergency rooms, operating rooms	tetralogy of Fallot (TOF), acute exacerbation COPD (AECOPD)	(32,33)
Cardiac markers	Emergency rooms	Troponin, CKMB, NTproBNP, D-Dimer	(34)
Creatinine	Radiology suites before contrast administration	KIM-1, MCP-1	(35)
Diabetes (glucose, HbA1c)	Home monitoring for patients with diabetes, inpatient monitoring for glycemic control	Hemoglobin A1c, FA, GA, OGTT, Adiponectin	(36)
hCG (pregnancy)	Emergency rooms, ICU settings	hCG	(37,38)
Infectious diseases	Outpatient and emergency settings for treatment decisions and cohorting or isolation	CRP, RSV, IL-1, IL-6	(39,40)
PT/INR	Coagulation clinics, cardiology practices, home monitoring	PT/INR	(41)
Urinalysis	Physician offices	interleukin-18 (IL-18), plasma neutrophil gelatinase-correlated lipocalin (NGAL), kidney injury molecule-1 (KIM-1), liver-type fatty acid-binding protein (L-FABP)	(42)

HbA1c: hemoglobin A1c, hCG: human chorionic gonadotropin, HIV: human immunodeficiency virus, ICU: intensive care unit, INR: international normalized ratio, PT: prothrombin time, RSV: respiratory syncytial virus.

devices have some required features such as easy to use, safe to use, easy to store, long-lasting, and consistent results with laboratories (28).

Biological Databases (Omic data) and Electronic Health Records

Big data, which is mainly the visualization of data (43,44), has changed the biomedical research pathway since it was first introduced in 1997. Collecting data is much faster than analyzing the data; therefore, molecular integration is essential when considering electronic health records (43,45). Data collection and analysis are crucial for identifying electronic health records and for drug and biomarker improvements of neurodegenerative diseases, cancers, cardiovascular diseases, and other critical or noncritical diseases (44). The first human genome sequence got the door to customizing the medicine in 2008 (46,47). Genomic data gives information about predicting and preventing disease with more targeted therapy options. More than 5,000 single-gene disorders could be recently treated (46). On the other hand, genetic test centers are increasing in demand, with over 55,000 centers. Moreover, the other important part of these genetic test centers is to help with diagnosis and detection of cancer, neurodegenerative diseases, and cardiovascular and other diseases (46). Additionally, personalized medicine promises the correct dosing of drugs. Knowing the patient's characteristics prevents adverse effects from the drugs and increases their efficacy.

Metabolomics is metabolites profiling of biological organisms, and biomarker of diseases in personalized medicine is the crucial concept of metabolomics. With other omics (transcriptomics, proteomics, and genomics), a disease's mechanism and pathophysiology could be analyzed in more detail, and with this advantage, the treatment strategies could be applied to the patient more efficiently (48). Determination of a target in biological organisms like small molecule quantification or identification is the critical point of omic-based technologies with computational techniques.

The relevance of genomic testing affects the individualizing of healthcare, and electronic health records have become an integral approach to collecting all data (diagnosis, medications, allergies, results, reports, etc.) from a patient in a single platform (46).

The central concept of personalized medicine is to customize health care, and for that reason collecting and analyzing data are two essential components of personalized medicine (49). Although data collection resources could be variable, like wearable devices, clinical trials, video streams found in elders' houses to detect falls, imaging tools, and genomic services, there could be some security risks with noise, missing data, or artifacts (50). In the field, there are some genome projects such as Baseline Study, Genome Atlas, 100,000 Genome Project, Encyclopedia of DNA Elements, 1,000 Genome Project, the UK Biobank Exome Sequencing Consortium, and SHGP (Saudi Human Genome Project) (50,51). The variety of countries with different genome

projects provides a variety of detection of rare diseases with high impact; thus, artificial intelligence becomes a step forward to analyze and determine rare diseases with genome sequencing by analyzing genome databases (51).

When we talk about databases, the data collection capacity is enormous; for example, only neuroimaging produces 10 petabytes every year (43). In addition, data collection favors genomics complementary to liquid biopsy results (43). Finally, using artificial intelligence with collected data gives another opportunity for personalized medicine to interpret the results from data (4).

Radiomics are the medical imaging part of omic-based technologies, and it is vital to diagnosis and clinical decisions (52). Furthermore, radiomics are like a bridge between imaging and personalized medicine; giving more attention to radiomics could provide a more proper response in terms of treatment technology (52).

Wearable Technologies

Wearable devices have revolutionized the field of continuous patient follow-up outside the clinic. It is provided regularly to the patient through mobile applications or digital health. Real-time monitoring can take patient care and follow-up out of hospital rooms so that it follows patients wherever they go. Many wearable devices are used in medical research that can be classified into three main categories: mechanical, physiological, and biochemical (53).

The developing wearable technology provides people with a healthier lifestyle, metabolic status, diagnosis, and treatment opportunities. These wearable devices include smartwatches, wristbands, hearing aids, tattoos, subcutaneous sensors, and electronic textiles (54).

Distinguishing health-related and actionable data from the data density of wearables is a significant challenge. Algorithms are being developed to overcome this difficulty in analyzing various data. Based on the data from wearable devices, digital biomarkers of the disease have emerged (55). Another positive aspect of patient follow-up in wearable devices is that they can be used in drug development. The physiological data collection can be used in drug development, dosage determination, and dosing frequency adjustment. However, some problems arise in the use of this technology. These issues include scientific, regulatory, ethical, legal, data management, infrastructure analysis, and security issues (56).

Organoids

Personalized medicine is an urgent area for modern oncological treatments because biomarkers for diagnostic approaches become essential instead of tumor site detection. In addition, determining the molecular feature of the tumor and treating that feature could be easier than treating the whole tumor by mimicking tumor structure in vitro with organoids (57).

The other crucial personalized medicine strategy for cancer or tumoroid tissue treatment is to create spheroids or organoids

from the patient's tumor cells to examine drug efficacy, determine disease progression, and develop a treatment (3). Understanding the tumoroid microenvironment is possible *in vitro* 3D platforms like spheroids and organoids for drug testing and new treatment strategies. The best perspective is to recapitulate the tumor tissue in a 3D environment from the patient's tumor cells, most probably cancer stem cells. 3D tumor spheroids or organoids give information on the intercellular interactions and morphology of the tumor, and this knowledge improves the best treatment strategies with appropriate screening techniques (3,58).

Besides the treatment strategies, it is possible to use organoids/spheroids for drug testing to observe the efficacy of the drugs on the patients *in vitro*. Halfter and colleagues used spheroids obtained from the tissue and the cell line to compare the effectiveness of the therapeutics (59). This study is the only one strategy to understand the spheroid's chemotherapeutic efficacy, which could be improved with organoid banks not only for drug testing, but also for developing treatment strategies to understand disease progression.

3D Printed Drug Tablets

The other important concept for personalized medicine is materials and techniques to produce drug tablets for different types of diseases with high drug release controllability. The shape and the size of the drug can be arranged using the software of 3D printers (49,60). The biomaterial used to create a drug ought to be biocompatible with FDA approval. Moreover, the production techniques should be FDA-approved as well. The drugs to treat patients could be a part of the population, but not for everybody; therefore, customized drug tablets become a step forward for specific patient groups who are tested and decided after physician examination. Customized drug tablets are potentially simple, inexpensive, much more effective, and could be multiple drugs in a tablet. Depending on the fabrication technique, the dosage, carriers, release period, and several drugs could be arranged in a tablet utilizing 3D printing technology (49).

The challenges of 3D printed drugs are caused mainly by 3D printer technology, dosage formulations, safety, regulations, and quality controls (60).

Future Aspects

Personalized medicine's market size is estimated at \$87 billion in 2023 (1), and the prediction of the genetic testing market for 2024 will be over \$22B, and the genomics will be in patients' hands (46).

The increasing need and demand for personalized medicine show that the disease pathophysiology and biomarkers are related to each other. Therefore, collecting data and analyzing the data could possibly be reached as an effective treatment with fewer side effects and more efficacy (61).

The multi-omic approach will be vital to improving personalized medicine; the concept of multi-omic is basically combin-

ing DNA and RNA alterations, metabolomics, and proteomics. Data analysis combined with artificial intelligence will make personalized medicine more precious in the future (4). Moreover, using *in vitro* studies with organoids is the other necessity for personalized medicine approaches due to the high capability of recognition and targeted drug release abilities (1), (57). From this perspective, we reviewed recent technologies such as wearable technologies, organoids, and 3D-printed drug tablets. These technologies possess a critical market share in the current medical monitoring, diagnosis, and treatment modalities by providing personalized solutions for everyone. Especially wearable technologies promise to promote point-of-care technologies with accurate and sustainable data providing capacity.

CONCLUSION

The use of personalized medicine in clinical practice is expected to increase. It is thought that the interest in this field will grow as health technology progresses. All of the various methods used for personalized medicine mentioned above can potentially create significant changes in the field of health by using them for drug development, diagnostic kit development, and data collection. The main goal of personalized medicine should be better to define disease development, have more effective treatment responses, and reduce health costs. For this purpose, it is necessary to inform pharmaceutical companies, insurance companies, researchers, and society. In this way, interest and knowledge in this crucial field in health technology should be increased, and this area should benefit from both work areas and treatment methods.

Informed Consent: Written consent was obtained from the participants.

Peer Review: Externally peer-reviewed.

Author Contributions: Conception/Design of Study- B.D., M.D.M.; Data Acquisition- B.D., M.D.M.; Data Analysis/Interpretation- B.D., M.D.M.; Drafting Manuscript- B.D., M.D.M.; Critical Revision of Manuscript- B.D., M.D.M.; Final Approval and Accountability- B.D., M.D.M.

Conflict of Interest: Authors declared no conflict of interest.

Financial Disclosure: Authors declared no financial support.












REFERENCES

1. Aguado BA, Grim JC, Rosales AM, Watson-Capps JJ, Anseth KS. Engineering precision biomaterials for personalized medicine. *Sci Transl Med* 2018;10(424).
2. Franssen FME, Alter P, Bar N, Benedikter BJ, Iurato S, Maier D, et al. Personalized medicine for patients with COPD: Where are we? *Int J COPD* 2019;14:1465-84.
3. Gilazieva Z, Ponomarev A, Rutland C, Rizvanov A, Solovyeva V. Promising applications of tumor spheroids and organoids for personalized medicine. *Cancers (Basel)* 2020;12(10):1-19.
4. Fröhlich H, Balling R, Beerenwinkel N, Kohlbacher O, Kumar S, Lengauer T, et al. From hype to reality: Data science enabling personalized medicine. *BMC Med* 2018;16(1):1-15.

5. Mathur S, Sutton J. Personalized medicine could transform health-care (Review). *Biomed Reports* 2017;7(1):3-5.
6. Vogenberg FR, Barash CI, Pursel M. Personalized medicine - Part 1: Evolution and development into theranostics. *PT* 2010;35(10).
7. Papassotiropoulos A. The potential and limits of personalized medicine. 2012;1-10.
8. Dall'Erà MA, Davies BJ, Eggen S. Active surveillance for prostate cancer. *Transl Androl Urol* 2018;7(2):195-6.
9. Sadée W, Dai Z. Pharmacogenetics/genomics and personalized medicine. *Hum Mol Genet* 2005;14(2):207-14.
10. Arciniegas Paspuel, O. G., Álvarez Hernández, S. R., Castro Morales, L. G., & Maldonado Gudiño CW. *Europe Precision Medicine Market*. Graphical Research. 2021. p. 6.
11. Goetz LH, Schork NJ. Personalized medicine: motivation, challenges, and progress. *Fertil Steril* 2018;109(6):952-63.
12. Merker JD, Oxnard GR, Compton C, Diehn M, Hurley P, Lazar AJ, et al. Circulating tumor DNA analysis in patients with cancer: American society of clinical oncology and college of American pathologists joint review. *J Clin Oncol* 2018;36(16):1631-41.
13. Ignatiadis M, Sledge GW, Jeffrey SS. Liquid biopsy enters the clinic — implementation issues and future challenges. *Nat Rev Clin Oncol* 2021;18(5):297-312.
14. Marrugo-Ramírez J, Mir M, Samitier J. Blood-based cancer biomarkers in liquid biopsy: A promising non-invasive alternative to tissue biopsy. *Int J Mol Sci* 2018;19(10):1-21.
15. Hardingham JE. Detection of circulating tumor cells using Immunobead-PCR. *Clin Appl PCR* 2003;2014:225-32.
16. Bidard FC, Fehm T, Ignatiadis M, Smerage JB, Alix-Panabières C, Janni W, et al. Clinical application of circulating tumor cells in breast cancer: Overview of the current interventional trials. *Cancer Metastasis Rev* 2013;32(1-2):179-88.
17. Torres S, González Á, Cunquero Tomas AJ, Calabuig Fariñas S, Ferrero M, Mirda D, et al. A profile on cobas® EGFR Mutation Test v2 as companion diagnostic for first-line treatment of patients with non-small cell lung cancer. *Expert Rev Mol Diagn* 2020;20(6):575-82.
18. Ferro M, La Civita E, Liotti A, Cennamo M, Tortora F, Buonerba C, et al. Liquid biopsy biomarkers in urine: A route towards molecular diagnosis and personalized medicine of bladder cancer. *J Pers Med* 2021;11(3):1-17.
19. Gadalla AAH, Friberg IM, Kift-Morgan A, Zhang J, Eberl M, Topley N, et al. Identification of clinical and urine biomarkers for uncomplicated urinary tract infection using machine learning algorithms. *Sci Rep* 2019;9(1):1-11.
20. Lamb JR, Jennings LL, Gudmundsdottir V, Gudnason V, Emilsson V. It's in Our Blood: A Glimpse of Personalized Medicine. *Trends Mol Med* 2021;27(1):20-30.
21. Schork NJ. Time for one-person trials.:3-5.
22. Mini E, Nobili S. Pharmacogenetics: Implementing personalized medicine. *Clin Cases Miner Bone Metab* 2009;6(1):17-24.
23. Sauna ZE, Kimchi-Sarfaty C, Ambudkar SV, Gottesman MM. Silent polymorphisms speak: How they affect pharmacogenomics and the treatment of cancer. *Cancer Res* 2007;67(20):9609-12.
24. Marsh S, Van Rooij T. Challenges of incorporating pharmacogenomics into clinical practice. *Gastrointest Cancer Res* 2009;3(5):206-7.
25. Ventola CL. The role of pharmacogenomic biomarkers in predicting and improving drug response. *PT* 2013;38(10):624-7.
26. FDA. *Drugs Table of Pharmacogenomic Biomarkers in Drug Labeling* 2014;1-15.
27. Dere WH, Suto TS. The role of pharmacogenetics and pharmacogenomics in improving translational medicine. *Clin Cases Miner Bone Metab* 2009;6(1):13-6.
28. John AS, Price C. Existing and emerging technologies for point-of-care testing. *Clin Biochem Rev* 2014;35(3):155-67.
29. Nichols JH, Street C. Management of point-of-care testing. 1999;1-13. Available from: <https://acutecaretesting.org/en/articles/management-of-pointofcare-testing>
30. Lewis K, Joyce-Nagata B, Gilmore Fite E. The Effect of time and temperature on blood glucose measurements. *Home Healthc Nurse* 1992;10(3):56-61.
31. Luppá PB, Müller C, Schlichtiger A, Schlebusch H. Point-of-care testing (POCT): Current techniques and future perspectives. *TrAC - Trends Anal Chem* 2011;30(6):887-98.
32. Bhardwaj V, Kapoor P, Irapachi K, Ladha S, Chowdhury U. *Thailand Blood Gas Analyzer and Cardiac Biomarker Market Outlook to 2025 - Thailand's growing number of heart disease patients with improving healthcare facilities will drive the industry growth in long term*: Ken Research. *Ann Card Anaesth* 2017;20(1):67-71.
33. Çaltekin I, Gökçen E, Albayrak L, Atik D, Savrun A, Kuşdoğan M, et al. Inflammatory markers and blood gas analysis in determining the severity of chronic obstructive pulmonary disease. *Eur J Critic Care* 2020;2(2):187-92.
34. Research K. *Thailand blood gas analyzer and cardiac biomarker market outlook to 2025 - thailand's growing number of heart disease patients with improving healthcare facilities will drive the industry growth in long term*: Ken Research. 2021; Available from: <https://www.prnewswire.com/news-releases/thailand-blood-gas-analyzer-and-cardiac-biomarker-market-outlook-to-2025---thailands-growing-number-of-heart-disease-patients-with-improving-healthcare-facilities-will-drive-the-industry-growth-in-long-term-ken-res>
35. de Oliveira Vilar Neto J, da Silva CA, Meneses GC, Pinto DV, Brito LC, da Cruz Fonseca SG, et al. Novel renal biomarkers show that creatine supplementation is safe: a double-blind, placebo-controlled randomized clinical trial. *Toxicol Res (Camb)* 2020;9(3):263-70.
36. Dorcelly B, Katz K, Jagannathan R, Chiang SS, Oluwadare B, Goldberg IJ, et al. Novel biomarkers for prediabetes, diabetes, and associated complications. *Diabetes, Metab Syndr Obes Targets Ther* 2017;10: 345-61.
37. Memtsa M, Jurkovic D, Jauniaux ERM. Diagnostic biomarkers for predicting adverse early pregnancy outcomes: Scientific impact paper no. 58. *BJOG An Int J Obstet Gynaecol* 2019;126(3):e107-13.
38. Cho SI, Goldman MB, Ryan LM, Chen C, Damokosh AI, Christiani DC, et al. Reliability of serial urine HCG as a biomarker to detect early pregnancy loss. *Hum Reprod* 2002;17(4):1060-6.
39. Hwang H, Hwang BY, Bueno J. Biomarkers in infectious diseases. *Dis Markers* 2018;2018:2-3.
40. Zandstra J, Jongerius I, Kuijpers TW. Future biomarkers for infection and inflammation in febrile children. *Front Immunol* 2021;12:1-14.
41. Zermatten MG, Fraga M, Calderara DB, Aliotta A, Moradpour D, Alberio L. Biomarkers of liver dysfunction correlate with a prothrombotic and not with a prohaemorrhagic profile in patients with cirrhosis. *JHEP Reports* 2020;2(4).
42. Nadkarni GN, Coca SG, Meisner A, Patel S, Kerr KF, Patel UD, et al. Urinalysis findings and urinary kidney injury biomarker concentrations. *BMC Nephrol* 2017;18(1):1-6.
43. Cirillo D, Valencia A. Big data analytics for personalized medicine. *Curr Opin Biotechnol* 2019;58:161-7.
44. Hassan M, Awan FM, Naz A, Enrique J, Alvarez O, Cernea A, et al. Innovations in genomics and big data analytics for personalized medicine and health care: A review. *Int J Mol Sci* 2022;23(9):4645.
45. Hulsen T, Jamuar SS, Moody AR, Karnes JH, Varga O, Hedensted S, et al. From big data to precision medicine. *Front Med* 2019;6:1-14.

46. Abul-Husn NS, Kenny EE. Personalized medicine and the power of electronic health records. *Cell* 2019;177(1):58-69.
47. Phillips KA, Deverka PA, Hooker GW, Douglas MP. Genetic test availability and spending: Where are we now? Where are we going? *Health Aff* 2018;37(5):710-6.
48. Jacob M, Lopata AL, Dasouki M, Abdel Rahman AM. Metabolomics toward personalized medicine. *Mass Spectrom Rev* 2019;38(3):221-38.
49. Tan YJN, Yong WP, Kochhar JS, Khanolkar J, Yao X, Sun Y, et al. On-demand fully customizable drug tablets via 3D printing technology for personalized medicine. *J Control Release* 2020;322:42-52.
50. Reza Soroushmehr SM, Najarian K. Transforming big data into computational models for personalized medicine and health care. *Dialogues Clin Neurosci* 2016;18(3):339-43.
51. Alrefaei AF, Hawsawi YM, Almaleki D, Alafif T, Alzahrani FA, Bakhrebah MA. Genetic data sharing and artificial intelligence in the era of personalized medicine based on a cross-sectional analysis of the Saudi human genome program. *Sci Rep* 2022;12(1):1-10.
52. Guiot J, Vaidyanathan A, Deprez L, Zerka F, Danthine D, Frix AN, et al. A review in radiomics: Making personalized medicine a reality via routine imaging. *Med Res Rev* 2022;42(1):426-40.
53. Tamsin M. Wearable biosensor technologies. *Int J Innov Sci Res* 2015;13(2):697-703.
54. Yetisen AK, Martinez-Hurtado JL, Ünal B, Khademhosseini A, Butt H. Wearables in medicine. *Adv Mater* 2018;30(33):e1706910.
55. Dunn J, Runge R, Snyder M. Wearables and the medical revolution. *Per Med* 2018;15(5):429-48.
56. Izmailova ES, Wagner JA, Perakslis ED. Wearable devices in clinical trials: Hype and hypothesis. *Clin Pharmacol Ther* 2018;104(1):42-52.
57. Hoeben A, Joosten EAJ, van den Beuken-Van Everdingen MHJ. Personalized medicine: Recent progress in cancer therapy. *Cancers (Basel)* 2021;13(2):1-3.
58. Takahashi T. Organoids for drug discovery and personalized medicine. *Annu Rev Pharmacol Toxicol* 2019;59:447-62.
59. Halfter K, Hoffmann O, Ditsch N, Ahne M, Arnold F, Paepke S, et al. Testing chemotherapy efficacy in HER2 negative breast cancer using patient-derived spheroids. *J Transl Med* 2016;14(1):1-14.
60. Vaz VM, Kumar L. 3D Printing as a promising tool in personalized medicine. *AAPS PharmSciTech* 2021;22(1):49.
61. Sharpton SR, Schnabl B, Knight R, Loomba R. Current concepts, opportunities, and challenges of gut microbiome-based personalized medicine in nonalcoholic fatty liver disease. *Cell Metab* 2021;33(1):21-32.

Thioredoxin-Interacting Protein: The Redoxissome Complex in Glomerular Lesion

**Gabriel Pereira¹ , Emily Pereira dos Santos² , Maria Augusta Ruy-Barbosa² ,
Sofia Tomaselli Arioni² , Thabata Caroline de Oliveira Santos² ,
Débora Tavares de Resende e Silva³ , Juan Sebastian Henao Agudelo⁴ ,
Maria do Carmo Pinho Franco¹ , Ricardo Fernandez² , Rafael Luiz Pereira² ,
Danilo Cândido de Almeida¹ **

¹Federal University of São Paulo, School of Medicine, Nephrology Division, São Paulo, Brazil

²Federal University of Paraná, Department of Physiology, Curitiba, Brazil

³Federal University of Fronteira Sul, Campus Chapecó, Chapecó, Santa Catarina, Brazil

⁴Central Unit of Valle del Cauca, Faculty of Health Sciences, Valle del Cauca, Tuluá, Colombia

ORCID IDs of the authors: G.P. 0000-0002-7836-4280; E.P.S. 0000-0002-2026-7250; M.A.R.B. 0000-0002-4195-6186; S.T.A. 0000-0001-8079-3191; T.C.O.S. 0000-0002-7770-8758; D.T.R.S. 0000-0002-3813-7139; J.S.H.A. 0000-0003-4123-6741; M.C.P.F. 0000-0003-0604-7689; R.F. 0000-0002-6760-3952; R.L.P. 0000-0002-6056-724X; D.C.A. 0000-0003-3661-2124

Please cite this article as: Pereira G, Pereira dos Santos E, Ruy-Barbosa MA, Tomaselli Arioni S, Caroline de Oliveira Santos T, Tavares de Resende e Silva D, et al. Thioredoxin-Interacting Protein: The Redoxissome Complex in Glomerular Lesion. Eur J Biol 2022; 81(2): 274-280. DOI: 10.26650/EurJBiol.2022.1163544

ABSTRACT

Chronic Kidney Disease (CKD) affects millions of people worldwide and is a global health problem with few treatment options. The mechanisms underlying the pathogenesis of CKD include oxidative damage and inflammation. Damage to the glomeruli may be observed during the course of co-associated diseases such as diabetes, but also in specific conditions such as focal segmental glomerulosclerosis. During its early manifestation, podocyte's damage and death are key factors to glomerulopathies and its protection may represent an important therapeutic approach. Importantly, podocytes pathology involves inflammation and cellular damage, principally due to excessive oxidative stress. Underlying mechanisms associated to both inflammation and oxidative stress during the course of a renal lesion must be elucidated for the development of better clinical and research approaches to kidney physiology. Thus, here we discuss the role of the Thioredoxin system, an antioxidant mechanism, and TXNIP, a thioredoxin inhibitor linked to NRLP3 inflammasome activation, as a pivotal axis in the pathophysiology of glomerular lesions.

Keywords: Oxidative stress, Inflammasome, Thioredoxin, TXNIP, Podocytes, Focal Segmental Glomerulosclerosis

GLOMERULAR LESIONS, OXIDATIVE STRESS, REDOX SYSTEM AND INFLAMMATORY MECHANISMS OF RENAL DAMAGE

Chronic kidney disease (CKD) is estimated to affect roughly 13.4% of the world's population (1). Damage to renal tissue can occur from different underlying conditions and mechanisms, including infections, hemodynamic changes, and direct injury to renal components.

Glomeruli damage currently accounts for 25% of the total kidney lesions observed in the adult population, with a higher incidence among the young population (2).

Focal Segmentar Glomerulosclerosis (FSGS) is a histologic pattern of lesion of the glomeruli characterized by the focal manifestation of sclerotic lesions in some glomeruli, and segmental fibrosis observed in portions



Corresponding Author: Gabriel Pereira

E-mail: pereira.gabriel18@unifesp.br

Submitted: 30.08.2022 • **Accepted:** 19.10.2022 • **Published Online:** 21.12.2022



of the affect glomeruli. It is believed that FSGS manifestation begin with damage to podocytes, a highly specialized cell that composes the glomerular filtration barrier, causing its death and detachment from the glomerular basal membrane. This process exposes the basal membrane and scar formation initiates from the contact of the basal membrane and parietal epithelial cells (3).

The manifestation of FSGS is highly correlated with the expression of inflammation markers. The analysis of gene expression profile of FSGS patients after renal transplant, revealed a differential expression of genes primarily involved with inflammation process, such as nuclear factor- κ B (NF- κ B) and cytokines (IL-1 β), which could be related with the organ reperfusion process considering the contact of the allograft with the serum of the patient (4).

Besides the role of inflammation in the pathogenesis of FSGS and glomerular damage, oxidative stress has also been observed as a major factor present in the initial manifestation of glomerular damage.

One mechanism of podocyte injury can occur after cellular stimuli and crosstalk between podocyte and glomerular endothelial cells. The paracrine communication mediated by molecules secreted by podocytes such as Endothelin-1, induces mitochondrial stress causing dysfunction of endothelial glomerular cells, leading to later mechanisms of podocyte apoptosis (5). Hence, the understanding of the cellular oxidation process can be a strategy for alternative treatments in FSGS.

Faced with oxidative insult, the cell normally activates its redox system where the "thioredoxin axis" is a powerful reductor agent acting in the oxidated protein, decreasing the cellular stress signaling and activation. Here we discuss the role of the Thioredoxin system, an antioxidant mechanism, and TXNIP, an endogenous thioredoxin inhibitor, as a pivotal axis in the pathophysiology of glomerular lesion.

THIOREDOXIN

Thioredoxin (Trx) proteins are part of a key antioxidant system highly preserved in many organisms, ranging from archaea to mammals (6). Trx was firstly described as an electron donor for ribonucleotide reductase, with subsequent roles discovered as in redox control, growth factor and inflammatory response activity (6). In mammals, two isoforms of Trx are present and distinguish between its location. Thioredoxin-1 (Trx1) is located mainly in the cytosol, but is also present in the nuclei, plasma membrane and has extracellular activity, while Thioredoxin-2 (Trx2) is located in the mitochondria (7,8).

Trx is induced by metabolic components such as estrogen, prostaglandins and cAMP, and different stimuli, such as virus infection, ischemia reperfusion and hydrogen peroxide (7). Nuclear factor erythroid 2 like 2 (NRF2) is a master antioxidant pathway activated upon reactive oxygen species (ROS) production that promotes the upregulation of over 250 genes involved in

processes of redox homeostasis, carbohydrate and lipid metabolism, DNA repair and more, including Trx (9).

Trx reductase activity is performed by reaction with thiol-oxidized proteins where Trx constantly alternates between reduced and oxidized forms and is reduced back by thioredoxin reductase, an enzyme that catalyzes the electron transport from the reduced form of nicotinamide adenine dinucleotide phosphate (NADPH) to the oxidized Trx (6,8). Furthermore, Trx1 is capable of binding and modulation of proteins such as Nf κ B, p53, glucocorticoid receptor, estrogen receptor and others by its thiol-disulfide reaction, with a reported anti-inflammatory response in both intra and extracellular environments (7) and it seems to be involved in responses of cellular growth and cell death, with increased levels in tumoral cells (10).

Thioredoxin Interaction Protein and Redoxosome Complex Signaling

Firstly described as Thioredoxin Binding Protein 2 (TBP-2), a molecule identical to a protein previously named Vitamin D-up-regulated protein 1 (VDUP-1), the Thioredoxin interaction protein (TXNIP) is an oxidant, apoptotic molecule and endogenous Trx inhibitor (11) that binds to the reduced form of both Trx isoforms, in a disulfide exchange reaction with the reduced Trx that is unique to the TXNIP (7). When translocated to the mitochondria, TXNIP interaction with Trx2 causes mitochondrial dysfunction, since Trx2 inhibits apoptosis signal regulation kinase 1 (Ask1), while TXNIP translocation also results in increased reactive oxygen species (ROS) accumulation and increases NLRP3 inflammasome activation in the mitochondria (7). In response to endoplasmic reticulum stress, TXNIP favors the paths of programmed cell death due to unbalance and accumulation of the unfolded protein response (8). While Trx is upregulated in many human tumors, TXNIP acts as a tumor suppressor and is downregulated in many cancers (10). This relation illustrates the complex mechanisms of Trx/TXNIP interaction in homeostasis and diseases status, since the regulation of Trx components may protect against oxidative damage and inflammation in several pathologies while the opposite could be observed in the tumoral tissue.

Thus, considering the involvement of Trx/Txnip axis during mechanisms related to cellular environment and diseases, Yoshihara *et al.* suggested that this signaling complex composed by Trx and Txnip should therefore be called "Redoxosome" (7).

TXNIP as an Inflammation Component

Currently, TXNIP response in different mechanisms vary from oxidative stress and inflammation. One function attributed to TXNIP is the activation of NOD-like receptor protein-3 (NLRP3) inflammasome in a redox dependent manner. This multi-protein complex, composed of NLRP3 oligomers, caspase-1, apoptosis-associated speck-like protein containing caspase recruitment domain (ASC), regulates the innate immune response causing the activation of caspase-1 and further activation of interleukin(IL)-1 β . These complexes detect and trigger respons-

es over stimuli as cellular damage and stress, where TXNIP is suggested as playing the communication from the redox disturbance present in the latter to the activation of inflammasome (8,10)

Upon oxidative stress, the increase in ROS causes the oxidation of the disulfide bond between TXNIP and the reduced Trx, leading to the dissociation of the TXNIP/Trx complex (10). As a consequence and response to ROS, Trx may act in its antioxidant pathway, and TXNIP is now available to turn in its inflammatory responses, such as directly interacting with NLRP3 inflammasome (8).

Interestingly, Yoshihara *et al.* highlight conflicting reports over NLRP3 activation by TXNIP (7). While some suggest an increase in TXNIP-NLRP3 interaction under oxidative stress, the authors suggest the existence of another component involved in the Trx response that is also necessary in the NLRP3 response to oxidative stress, emphasizing the existence of a redoxosome complex composed by molecules that participate in the Trx reducing process.

While still in debate, early studies had suggested that TXNIP is the mediator of the NLRP3 inflammasome activation. This is supported by results showing that the products of NLRP3, activation of caspase-1 and secretion of mature IL-1 β were less present when ablation of TXNIP was promoted together with use of the inflammasome activators (12). This interaction of TXNIP and the activation of NLRP3 response is implicated to be present in different diseases such as obesity-induced insulin resistance, metabolic disorders in ischemic heart and type 1 and type 2 diabetes (8).

Interestingly, TXNIP also activates NF- κ B. NF- κ B is a transcriptional factor involved in the inflammatory response that leads to the expression of pro-inflammatory genes. Human macrophages (U937) transfected with a siRNA for TXNIP expressed reduced levels of both: i) phosphorylated nuclear factor inhibitor alpha (pI κ B α), crucial component of NF- κ B activation, and ii) phosphorylated-NF- κ B after inflammatory stimuli, as well as attenuated cytokines and inflammatory molecules (13).

The Glomerular Lesion and TXNIP

TXNIP has been associated with processes of inflammation, fibrosis and ROS lesion in diabetic nephropathy (14) along with damage and apoptosis in podocytes (15). TXNIP is induced by hyperglycemia, thus its role in the development of diabetic nephropathy is remarkable for its impairment of thioredoxin activity in a glucosis-induced manner.

Markers of renal injury present in diabetic nephropathy such as albuminuria, proteinuria and serum creatinine were not increased in response to TXNIP knockout in a streptozotocin diabetic mice model, along with lesser histological manifestation of renal lesions due to the absence of TXNIP (16). The inhibition of TXNIP gene expression results in reduced renal interstitial collagen deposition induced by diabetes and reduced type I collagen of interstitial areas of diabetic rat kidneys (17). Further-

more, TXNIP silencing in podocytes reduced apoptosis via interaction with the mTOR pathway and could reduce renal damage by modulation of p38 MAPK phosphorylation (15). Additionally, TXNIP knockout mitigated podocyte foot process effacement and contributed to the maintenance of glomerular barrier membrane thickness in the diabetic nephropathy model (16).

Moreover, the role of TXNIP in glomerular injury was verified by the direct interaction found between TXNIP and NLRP3 inflammasome activation in cultured human podocytes (18). In response to advanced-glycation end products, compounds resulting from the process of ageing as well as inflammation and hyperglycemia, TXNIP was highly expressed in glomerulus and podocyte, where the epigenetic machinery of pos-translational histone modifications are reported to be regulators of TXNIP expression under hyperglycemia and advanced-glycation products exposure (19). In the context of FSGS patients, increased TXNIP level was detected in urinary sediments when compared to healthy individuals, while the same occur in diabetic nephropathy patients (20). Further involvement of TXNIP in cellular components of renal physiology are shown in Table 1.

These evidences suggest that TXNIP is an important factor in inflammatory and oxidative response for its capability of reducing Trx activity and promoting key inflammatory agents such as NLRP3 inflammasome and NF- κ B activation. Consequently, further interventions that result in a regulatory response decreasing TXNIP levels, resulting in increased Trx activity could lead to interesting therapeutic approaches.

For its activity in several physiological responses, systemic inhibition of TXNIP could be useful beyond promoting moderate risk including dysregulation of its proapoptotic activity. In this sense, the use of antioxidants, including natural pharmacological active compounds, have been shown to modulate TXNIP and NLRP3 inflammasome together with its antioxidant activity. In this manner, modulation of TXNIP expression may result in interesting pharmacological responses. Known mechanisms of TXNIP synthesis promotion includes vitamin D₃, hence the previous name of the identical described protein vitamin D-upregulated protein-1 (VDUP-1), heat shock protein and PPAR α and γ . Although many different molecules interact with the TXNIP gene promoter region, one of the main stimuli for its synthesis is the raise in glucose concentration (21).

On the other hand, inhibitory effects on TXNIP expression and augment of TXNIP clearance are promoted by pharmacological hypoglycemic compounds. Administration of insulin or Metformin suppresses TXNIP expression while also accelerating TXNIP degradation in different tissues (21). While this suggests a significant role of TXNIP in diabetes and its associated pathologies, interaction between TXNIP and pathological mechanisms independent of glucose disturbances or compounds not related to glucose metabolism found in different studies highlights the many capabilities of TXNIP.

As discussed by Mohamed *et al.* (2021), the use of traditional medicine compounds such as Taohong Siwu decoction, Z-Gug-

Table 1. Kidney cellular components responses over TXNIP modulation.

Cell	Mechanism	Effect on TXNIP	Cellular response	Reference
Podocyte	Inhibition of S-adenosylhomocysteine hydrolase promotes inhibition of EZH2 and reduction in H3K27me3 and upregulates TXNIP.	↑	↑ NLRP3 activation ↑ ROS ↑ Podocyte cell death	(26), (27)
	Activators of AMPK suppress TXNIP expression levels.	↓	↑ AMPK ↑ Thioredoxin reductase activity	(28)
	gp91 ^{phox} overexpression is induced by TXNIP in high-glucose exposed podocytes; inhibition of TXNIP reduced F-actin fibers loss from high-glucose exposure in podocytes.	↓	↓ gp91 ^{phox} ↑ F-actin fibers, otherwise reduced during the lesion model	(29)
	Silencing of TXNIP in high-glucose induced podocytes reduced NLRP3, caspase-1 and IL-1β production/activity.	↓	↓ NLRP3 activation ↓ caspase-1 activity ↓ IL-1β production ↑ F-actin fibers, otherwise reduced during the lesion model	(18)
	Knockdown of TXNIP in murine podocyte suppresses the activation of mTORC1 and mTORC2, downregulates Nox1 and Nox4 expression and prevents p38 MAPK phosphorylation.	↓	↓ Epithelial-to-mesenchymal transition ↓ ROS ↓ Podocyte cell death	(30), (15)
	H ₂ S promote binding disruption of Trx from TXNIP in mouse podocyte.	-	↑ Trx availability; prevention of oxidative podocyte injury	(31)
Glomerular mesangial cells	Inhibition of S-adenosylhomocysteine hydrolase promotes inhibition of EZH2 upregulates TXNIP in rat mesangial cell.	↑	↑ TXNIP mRNA levels	(27)
	Exposure to high glucose and LPS increased expression of mRNA and protein of TXNIP and NLRP3 inflammasome.	↑	↑ NLRP3 ↑ procaspase-1 ↑ IL-1β	(32)
	Silencing of TXNIP inhibits expression of NLRP3, ASC and caspase-1.	↓	↓ Cell proliferation ↑ SOD activity ↓ Collagen IV	(33)
	Silencing of TXNIP suppressed high-glucose induced ASK1 phosphorylation and cleaved caspase-3 expression in mouse mesangial cells.	↓	↓ ASK1 phosphorylation ↓ cleaved caspase-3	(34)
	Absence of TXNIP protein inhibited Collagen IV deposition and ROS after 24h-treatment in high-glucose exposure of mouse mesangial cells.	↓	↓ Collagen IV ↓ ROS	(35)
	Silencing of TXNIP and activation of AMPK further inhibited TXNIP mRNA expression levels.	↓	↓ ROS ↑ SOD activity ↑ CAT activity ↑ Cell viability	(36)
Tubular renal cells	Inhibition of S-adenosylhomocysteine hydrolase promotes inhibition of EZH2 upregulates TXNIP in NRK-52E and MDCK cells.	↑	↑ TXNIP mRNA levels	(27)
	IL-1β induces expression of TXNIP and Nox4 in HK-2 tubular cells.	↑	↑ ROS	(37)

Table 1. Kidney cellular components responses over TXNIP modulation. (continued)

Cell	Mechanism	Effect on TXNIP	Cellular response	Reference
	TRPV4 agonists increases TXNIP level in NRK-52E cells through increase of intracellular Ca ²⁺ .	↑	↑ Cell injury	(38)
	Knockdown of TXNIP on NRK-E52 tubular cells protected the cells over ADR administration.	↓	↑ Cellular viability ↑ p-P38	(28)
	Silencing of TXNIP reduces mitophagy regulator protein BNIP3 and suppress phosphorylation of mTOR by high glucose.	↓	↓ ATP production impairment ↓ mitochondrial ROS ↓ mitophagy	(17)

Differential responses of kidney cellular components to modulations of TXNIP and its effects. ADR: Adriamycin. AMPK: 5'-AMP-activated protein kinase. ASK1: Apoptosis signal-regulating kinase 1. CAT: Catalase. EZH2: enhancer of zeste homolog 2. FN: Fibronectin. H₂S: Hydrogen sulphide. H3K27me3: trimethylation of histone 3 lysine 27. IL: interleukin. LPS: lipopolysaccharide. MAPK: p38 mitogen-activated protein kinase. mTOR: mammalian target of rapamycin complex. NLRP3: nod-like receptor protein 3. p-P38: phosphorylated P-38. ROS: Reactive oxygen species. SOD: superoxide dismutase. Trx: Thioredoxin. TXNIP: Thioredoxin-interacting protein

gulsterone, an herbal steroid, Umbelliferone, natural antioxidant, Curcumin, antioxidant extracted from *Curcuma longa*, and other pharmacological therapies as Verapamil and Metformin; all together can promote modulation of TXNIP activity and TXNIP-NLRP3 inflammasome activation in severe disease models. Some of the reported effects include attenuation of ischemic brain injury, prevention of fatty liver, improvement of hyperglycemic stroke damage, and several diabetes-related complications via TXNIP and TXNIP-NLRP3 inflammasome activation (22).

For instance, use of curcumin in a model of ischemic reperfusion leads to a decrease in Nf-κB expression, while also reducing

TXNIP protein and mRNA levels present in tubules during the renal ischemic reperfusion injury, promoting cytoprotective effects against oxidative stress (23). Furthermore, curcumin also presents modulation of TXNIP in neurotoxicity (24) and promotion of Trx1 during prostate cancer (25). Not only acting as a regulator of TXNIP, curcumin also has an important antioxidant activity by activation of Nuclear factor erythroid 2-related factor 2 (NRF2), promoting the expression of many others antioxidants enzymes, such as Heme Oxygenase-1 and superoxide dismutase (24), indicating that modulation of TXNIP is included in its functional activity. A brief overview and mechanisms of TXNIP activity over inflammation and oxidative stress are summarised in Figure 1.

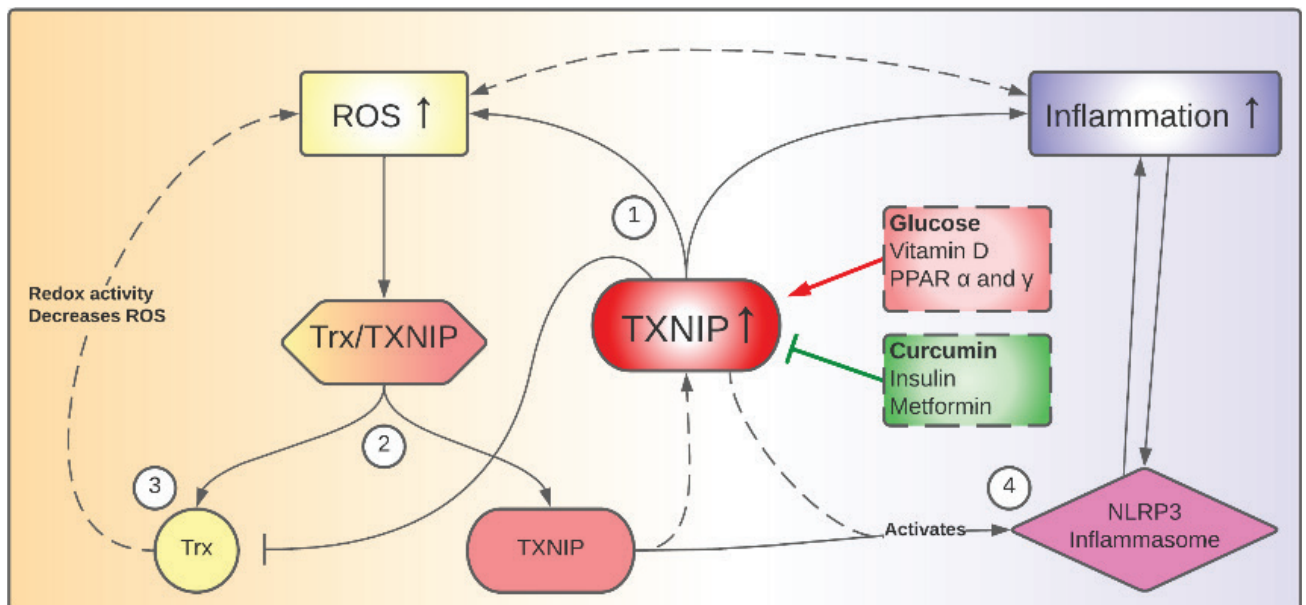


Figure 1. TXNIP acting as a link between inflammation and oxidative stress. (1) Increased TXNIP leads to ROS by inhibition of Trx redox activity. (2) Increased ROS causes dissociation of Trx/TXNIP complex. This dissociation frees (3) Trx to its antioxidant response and (4) TXNIP to act as an activator of NLRP3 in a ROS-dependent response.

CONCLUSION

In summary, Trx and TXNIP are involved in the mechanisms of homeostasis and progression of a variety of diseases, ranging from cancer to diabetes and kidney disease, and are highly expressed in damage tissues by inflammation and/or oxidative stress. Being involved in both mechanisms of glomerular lesions, TXNIP is a molecule of high importance in the pathogenesis of several diseases and may represent a key factor and a link for the oxidative response and inflammatory mechanisms. While overexpressed, TXNIP may contribute to the progression of different pathologies, however, its downregulation can contribute to cancer growth and migration, due to its role in cell apoptosis, while also improving the redox mechanism. Therefore, the elucidation of TXNIP axis role in diseases such as its modulation in FSGS could contribute to the understanding of the global pathophysiology of most chronic kidney diseases, as well as others related to renal disfunctions.

Acknowledgement: We would like to thank the Coordenação de Aperfeiçoamento de Pessoal de Nível Superior (Capes) and the Conselho Nacional de Desenvolvimento Científico e Tecnológico (CNPq) for the financial support and scholarships

Peer Review: Externally peer-reviewed.

Author Contributions: Conception/Design of Study- G.P., D.C.A., D.T.R.S., J.S.H.A., M.C.P.F., R.L.P., R.F.; Data Acquisition- G.P., E.P.S., M.A.R.B., S.T.A., T.C.O.S.; Data Analysis/Interpretation- G.P., D.C.A.; Drafting Manuscript- G.P., E.P.S., M.A.R.B., S.T.A., T.C.O.S.; Critical Revision of Manuscript- D.C.A., D.T.R.S., J.S.H.A., M.C.P.F., R.L.P., R.F.; Final Approval and Accountability- G.P., E.P.S., M.A.R.B., S.T.A., T.C.O.S., D.T.R.S., J.S.H.A., M.C.P.F., R.L.P., D.C.A.

Conflict of Interest: Authors declared no conflict of interest.

Financial Disclosure: We emphasize the important contribution of Coordenação de Aperfeiçoamento de Pessoal de Nível Superior (Capes) and Conselho Nacional de Desenvolvimento Científico e Tecnológico (CNPq).

REFERENCES

- Hill NR, Fatoba ST, Oke JL, Hirst JA, O'Callaghan CA, Lasserson DS, et al. Global prevalence of chronic kidney disease – A systematic review and meta-Analysis. *PLoS One* 2016; 11: e0158765. <https://doi.org/10.1371/journal.pone.0158765>.
- KDIGO. Kidney Disease: improving global outcomes (kdigo) glomerular diseases work group. KDIGO 2021 Clinical practice guideline for the management of glomerular diseases. *Kidney Int* 2021; 100: S1–276.
- Campbell KN, Tumlin JA. Protecting podocytes: A key target for therapy of focal segmental glomerulosclerosis. *Am J Nephrol* 2018; 47: 14-29.
- Otalora L, Chavez E, Watford D, Tueros L, Correa M, Nair V, et al. Identification of glomerular and podocyte-specific genes and pathways activated by sera of patients with focal segmental glomerulosclerosis. *PLoS One* 2019; 14: e0222948. <https://doi.org/10.1371/journal.pone.0222948>.
- Daehn I, Casalena G, Zhang T, Shi S, Fenninger F, Barasch N, et al. Endothelial mitochondrial oxidative stress determines podocyte depletion in segmental glomerulosclerosis. *J Clin Invest* 2014; 124: 1608-21.
- Collet J-F, Messens J. Structure, function, and mechanism of thioredoxin proteins. *Antioxid Redox Signal* 2010; 13: 1205-16.
- Yoshihara E, Masaki S, Matsuo Y, Chen Z, Tian H, Yodoi J. Thioredoxin/Txnip: Redoxosome, as a redox switch for the pathogenesis of diseases. *Front Immunol* 2014; 4.
- Cao X, He W, Pang Y, Cao Y, Qin A. Redox-dependent and independent effects of thioredoxin interacting protein. *Biol Chem* 2020; 401: 1215-31.
- Jaganjac M, Milkovic L, Sunjic SB, Zarkovic N. The NRF2, Thioredoxin, and glutathione system in tumorigenesis and anticancer therapies. *Antioxidants (Basel)* 2020; 9: 1151.
- Hwang J, Suh H-W, Jeon YH, Hwang E, Nguyen LT, Yeom J, et al. The structural basis for the negative regulation of thioredoxin by thioredoxin-interacting protein. *Nat Commun* 2014;5:2958.
- Nishiyama A, Matsui M, Iwata S, Hirota K, Masutani H, Nakamura H, et al. Identification of thioredoxin-binding protein-2/vitamin D3 up-regulated protein 1 as a negative regulator of thioredoxin function and expression. *J Biol Chem* 1999;274:21645–50.
- Zhou R, Tardivel A, Thorens B, Choi I, Tschopp J. Thioredoxin-interacting protein links oxidative stress to inflammasome activation. *Nat Immunol* 2010; 11: 136-40.
- Kim S-K, Choe J-Y, Park K-Y. TXNIP-mediated nuclear factor- κ B signaling pathway and intracellular shifting of TXNIP in uric acid-induced NLRP3 inflammasome. *Biochem Biophys Res Commun* 2019; 511: 725-31.
- Wu M, Li R, Hou Y, Song S, Han W, Chen N, et al. Thioredoxin-interacting protein deficiency ameliorates kidney inflammation and fibrosis in mice with unilateral ureteral obstruction. *Lab Invest* 2018; 98: 1211-24.
- Song S, Qiu D, Wang Y, Wei J, Wu H, Wu M, et al. TXNIP deficiency mitigates podocyte apoptosis via restraining the activation of mTOR or p38 MAPK signaling in diabetic nephropathy. *Exp Cell Res* 2020; 388: 111862.
- Shah A, Xia L, Masson EAY, Gui C, Momen A, Shikatani EA, et al. Thioredoxin-Interacting Protein Deficiency Protects against Diabetic Nephropathy. *JASN* 2015; 26: 2963-77.
- Huang C, Zhang Y, Kelly DJ, Tan CYR, Gill A, Cheng D, et al. Thioredoxin interacting protein (TXNIP) regulates tubular autophagy and mitophagy in diabetic nephropathy through the mTOR signaling pathway. *Sci Rep* 2016; 6: 29196.
- Gao P, Meng X-F, Su H, He F-F, Chen S, Tang H, et al. Thioredoxin-interacting protein mediates NALP3 inflammasome activation in podocytes during diabetic nephropathy. *Biochim Biophys Acta-Mol Cell Res* 2014; 1843: 2448-60.
- Thieme K, Pereira BMV, da Silva KS, Fabre NT, Catanozi S, Passarello M, et al. Chronic advanced-glycation end products treatment induces TXNIP expression and epigenetic changes in glomerular podocytes in vivo and in vitro. *Life Sci* 2021; 270: 118997.
- Monteiro MB, Santos-Bezerra DP, Thieme K, Admoni SN, Perez RV, Machado CG, et al. Thioredoxin interacting protein expression in the urinary sediment associates with renal function decline in type 1 diabetes. *Free Radic Res* 2016; 50: 101-10.
- Chong C-R, Chan WPA, Nguyen TH, Liu S, Procter NEK, Ngo DT, et al. Thioredoxin-Interacting Protein: Pathophysiology and Emerging Pharmacotherapeutics in Cardiovascular Disease and Diabetes. *Cardiovasc Drugs Ther* 2014; 28: 347-60.
- Mohamed IN, Li L, Ismael S, Ishrat T, El-Remessy AB. Thioredoxin interacting protein, a key molecular switch between oxidative stress and sterile inflammation in cellular response. *World J Diabetes* 2021; 12: 1979-99.

23. Rogers N, Stephenson M, Kitching A, Horowitz J, Coates P. Amelioration of renal ischaemia–reperfusion injury by liposomal delivery of curcumin to renal tubular epithelial and antigen-presenting cells. *Br J Pharmacol* 2012; 166: 194-209.
24. Li Y, Li J, Li S, Li Y, Wang X, Liu B, et al. Curcumin attenuates glutamate neurotoxicity in the hippocampus by suppression of ER stress-associated TXNIP/NLRP3 inflammasome activation in a manner dependent on AMPK. *Toxicol Appl Pharmacol* 2015; 286: 53-63.
25. Rodriguez-Garcia A, Hevia D, Mayo JC, Gonzalez-Menendez P, Coppo L, Lu J, et al. Thioredoxin 1 modulates apoptosis induced by bioactive compounds in prostate cancer cells. *Redox Biol* 2017; 12: 634-47.
26. Dai X, Liao R, Liu C, Liu S, Huang H, Liu J, et al. Epigenetic regulation of TXNIP-mediated oxidative stress and NLRP3 inflammasome activation contributes to SAHH inhibition-aggravated diabetic nephropathy. *Redox Biol* 2021; 45: 102033.
27. Siddiqi FS, Majumder S, Thai K, Abdalla M, Hu P, Advani SL, et al. The histone methyltransferase enzyme enhancer of zeste homolog 2 protects against podocyte oxidative stress and renal injury in diabetes. *JASN* 2016; 27: 2021-34.
28. Gao K, Chi Y, Sun W, Takeda M, Yao J. 5'-AMP-Activated Protein Kinase Attenuates Adriamycin-Induced Oxidative Podocyte Injury through Thioredoxin-Mediated Suppression of the Apoptosis Signal-Regulating Kinase 1–P38 Signaling Pathway. *Mol Pharmacol* 2014; 85: 460-71.
29. Gao P, He F-F, Tang H, Lei C-T, Chen S, Meng X-F, et al. NADPH oxidase-induced NALP3 inflammasome activation is driven by thioredoxin-interacting protein which contributes to podocyte injury in hyperglycemia. *J Diabetes Res* 2015; 2015: 504761.
30. Song S, Qiu D, Shi Y, Wang S, Zhou X, Chen N, et al. Thioredoxin-interacting protein deficiency alleviates phenotypic alterations of podocytes via inhibition of mTOR activation in diabetic nephropathy. *J Cell Physiol* 2019; 234: 16485-502.
31. Mao Z, Huang Y, Zhang Z, Yang X, Zhang X, Huang Y, et al. Pharmacological levels of hydrogen sulfide inhibit oxidative cell injury through regulating the redox state of thioredoxin. *Free Radic Biol Med* 2019; 134: 190-9.
32. Feng H, Gu J, Gou F, Huang W, Gao C, Chen G, et al. High Glucose and Lipopolysaccharide Prime NLRP3 Inflammasome via ROS/TXNIP Pathway in Mesangial Cells. *J Diabetes Res* 2016; 2016: 6973175.
33. Wang S, Zhao X, Yang S, Chen B, Shi J. Salidroside alleviates high glucose-induced oxidative stress and extracellular matrix accumulation in rat glomerular mesangial cells by the TXNIP-NLRP3 inflammasome pathway. *Chem Biol Interac* 2017; 278: 48-53.
34. Shi Y, Ren Y, Zhao L, Du C, Wang Y, Zhang Y, et al. Knockdown of thioredoxin interacting protein attenuates high glucose-induced apoptosis and activation of ASK1 in mouse mesangial cells. *FEBS Letters* 2011; 585: 1789-95.
35. Shah A, Xia L, Goldberg H, Lee KW, Quaggin SE, Fantus IG. Thioredoxin-interacting protein mediates high glucose-induced reactive oxygen species generation by mitochondria and the NADPH oxidase, Nox4, in Mesangial Cells. *J Biol Chem* 2013; 288: 6835-48.
36. Xu W, Wang L, Li J, Cai Y, Xue Y. TXNIP mediated the oxidative stress response in glomerular mesangial cells partially through AMPK pathway. *Biomed Pharmacother* 2018; 107: 785-92.
37. Wu M, Han W, Song S, Du Y, Liu C, Chen N, et al. NLRP3 deficiency ameliorates renal inflammation and fibrosis in diabetic mice. *Mol Cell Endocrinol* 2018; 478: 115-25.
38. Zhang X, Mao Z, Huang Y, Zhang Z, Yao J. Gap junctions amplify TRPV4 activation-initiated cell injury via modification of intracellular Ca²⁺ and Ca²⁺-dependent regulation of TXNIP. *Channels* 2020; 14: 246-56.